Geochemistry of metalliferous sediments from the northern Oman ophiolite

Wilson, Robin A.

Geochemistry of metalliferous sediments from the northern Oman ophiolite

Robin A. Wilson BSc. (Hons)

A Thesis submitted in partial fulfilment of the requirements for the degree of Doctor of Philosophy

Department of Geological Sciences
University of Durham

March 1997

Sonnets from the Portuguese VI: Go from me

Go from me. Yet I feel that I shall stand
Henceforward in thy shadow. Nevermore
Alone upon the threshold of my door
Of individual life, I shall command
The uses of my soul, nor lift my hand
Serenely in the sunshine as before,
Without the sense of that which I forbore,
Thy touch upon the palm. The widest land
Doom takes to part us, leaves thy heart in mine
With pulses that beat double. What I do
And what I dream include thee, as the wine
Must taste of its own grapes. And when I sue
God for myself, He hears that name of thine,
And sees within my eyes, the tears of two.

Browning, E.B, 1856

To my parents and family

ABSTRACT

Geochemistry of metalliferous sediments of the northern Oman ophiolite.

A range of siliceous, ferruginous and ferromanganiferous deposits are intercalated with, and overlie the lavas of the Late Cretaceous northern Oman ophiolite. Most of the deposits lie on the upper surface of the spreading event lavas; spreading event magmatism and later seamount-building events are coeval to relatively small metalliferous sediment deposits.

The mineralogical and geochemical characteristics of these sediments are a function of the interaction between local hydrothermal systems, the marine depositional environment, and early diagenetic transformations. Various techniques are employed to objectively determine the actual end-member component compositions from which the metalliferous sediments formed. The sediments are a mixture of primary biosiliceous oozes and hydrothermal metallic components which were deposited at or near a marginal ocean-basin spreading axis during Cenomanian time.

Factor analysis, selective acid leaching experiments and linear programming modelling identify six geologically reasonable end-members, which represent biosiliceous sediment, carbonate sediment, detrital sediment, hydrogenous sediment, and hydrothermal sediment. The techniques show that the sediments have a complicated hydrothermal history which is associated with the evolution of the Oman ophiolite. The hydrothermal component is sub-divided into high temperature and low temperature end-members which are characteristic of the proto-seamount and proto-rift event environments respectively. Vent proximal and vent-distal facies are described. The geochemistry of the deposits provides evidence for calcareous pelagic dissolution by hydrothermal fluids, which resulted in the relative concentration of a hyaloclastic component. The deposits which were not early-lithified are epidotized. Metamorphic transformation of the primary sediment occurred prior to eruption of the upper lava unit.

The techniques which have been used to describe the range, composition and distribution of the end-member components provide a flexible framework for the characterisation of geological mixing in all marine metalliferous sediments.

Declaration

I declare that this thesis, which I submit for the degree of Doctor of Philosophy at the University of Durham, is my own work and is not substantially the same as any which has previously been submitted for a degree at this or another University,

Robin Alexander Wilson

University College, University of Durham

March, 1997

Acknowledgements

This work was made possible by the financial support of the Natural Environmental Research Council, which the writer gratefully acknowledges. I would like to thank my principal supervisor Dr. Julian Pearce for his initial stimulus and timely inputs of advise over the course of the project. Thanks also to Professors Howard Colley and Derek Ellwood for providing enthusiastic motivation, research facilities and occasional lunches. My special thanks also go to Dr. Amanda Bird, who has provided a constant source of scientific knowledge and played the enthusiastic assistant throughout the project: and for all the present semicolons and commas.

Numerous members of the Department have provided assistance and interesting discussions, including Dr. Grenville Holland, Mr. Dave Astberry, Mr. Dave Stephenson, and Karen. In particular, I am very grateful to Mr. Ron Hardy, *the* unpaid alternative supervisor, who made up at random all the numbers in this project, off the top of his head, during a lunch-break in Waterstone's. I would like to take this opportunity to utterly condemn, in print, Mr. Hardy's outrageous touting of crime (so-called) fiction and the building material known as "Fablon". I also wish to thank Dr. Chris Ottley for his patience with the HPLC and my subsequent ICP-MS work. Thanks also to Parky, Mark, Mehmet, Nurdane, Erchan, for odd bits of geochemical advise, and also to Sarah and Vicky for all the stationary. Thanks to Toby for destroying the printer at the very last possible hour, just to add that extra excitement. Many thanks to the notorious anthropologist, Professor C. Bruce Scruttucks of ANU, for the months of entertainment he provided.

Without the following people, I should have finished much much sooner. Mostly these are rowers, and the rest think that they might be on good days, if its not raining or cold, or early. First, the lovely Karina, who consumed most of my sanity, time and cash; and Jon Freemoon (the dewy-eyed grandfather of rowing) who not only provided pukka geochemical chat, but also entertained the masses with his amorous endeavours and unending attempts at recapturing the his lost youth using heart rate monitors and young females. Thanks also to Hollie and the Maroon. Hollie provided the cash input and gourmet meals while her monkey broke things up. Big Ruth Moody has been most fab during my stresses, as has Agent Chunder and Mrs. Kate Thompson. The later have also unfortunately assisted in the fall from moral grace of the boy Pinner.

In the past, this thesis has also suffered from the following unruly influences: Inmark Sareen, (plus his dad and O.J. Simpson), hippie Alex, The Mistress, Chris-T-Gin-ger, Tartan Temptress, the Crow (you still owe me for the undergrad. dissertation), Fat Al (of vegan turd fame), Mad Chris (ta for the rowing kit), Nasty Mr. Brown, the Phantom and Beth. Also V.C. Bob Peel, Rich, Big Ted and the Burford Bros. from St. Leonards, Dawn the Dwaff (I'm catching you up), (Dr.) Gareth Stansfield in Iraq, and Fossie. The above have added uncounted months to the time this thesis has taken me. DARC, UCBC, Klute and Rixies are responsible for the rest of the lost time.

Finally, many thanks to my parents, Great Aunt Ellen and the rest of my large family, for all their support and help, during my protracted (and continuing) education.

GEOCHEMISTRY OF METALLIFEROUS SEDIMENTS FROM THE NORTHERN OMAN OPHIOLITE

List of Figures

CHAPTER 1

CHAPTER 2

CHAPTER 3

CHAPTER 4

CHAPTER 5

APPENDIX A

List of Tables

CHAPTER 2

CHAPTER 3

CHAPTER 1

Introduction

1.1 Aims and objectives of the project

The overall objective of this project is to produce a detailed geochemical model of the metalliferous sediments of the Oman ophiolite. The Oman ophiolite is now widely accepted as a type-locality for the study of metalliferous deposits formed by hydrothermal precipitation and pelagic sedimentation at a sea-floor spreading centre. The aims of this project are: (1) to present a precise and accurate geochemical data-set; (2) to examine the spatial and temporal variation in bulk-rock geochemistry; (3) to investigate the possible sediment sources, including detrital, hydrothermal, hydrogenous, and biogenic contributions; (4) to examine the hydrothermal system in detail, and the relationship of the sediments to it; and (5) to develop a model which can explain the geochemical variation in terms of the evolution of the ophiolite.

The samples used in this study were collected by Dr Julian Pearce from the northern Oman ophiolite. A total of 250 whole-rock samples of metalliferous sediment were available for the purposes of this project, none of which had been pre-analysed or pre-prepared. The sample preparation techniques employed are described in Appendix A. Sample location sketch maps were also available.

1.2 Methodology

Recent attempts, based on the "geosphere of origin" model (Goldberg, 1954), have concentrated on quantifying the sources of the elements which are found in marine sediments. The specific combinations of elements which make up each sample of metalliferous sediment are derived from various sources and have been transported as particulate or dissolved components to the site of sediment deposition. In this study, the inter-element associations which characterise the contribution of each source will be termed a *component,* and the methods will all focus on the sediment-forming components: (1) by identifying the components and calculating their composition; (2) by calculating the proportion of each

component in each sample; and (3) by calculating the regional variation in sediment component *distribution* and variation in component *composition.* Because the numerical techniques that this project employs rely heavily on the quality of the whole-rock data, one of the primary requirements of the methodology will be that it produces precise and accurate data to ensure the reliability of the subsequent modelling.

This project is based on the data obtained by analysing metalliferous sediments using: X-ray Fluorescence Spectrometry (XRF), Inductively-Coupled Mass Spectrometery (ICP-MS), X-ray Diffraction Spectrometry (XRD), and Atomic Absorption Spectrometry (AA). The sample preparation techniques, accuracy, precision and error control are fully explained in Appendix A. The full results of all of the techniques are listed in Appendix B.

Factor analysis is the first method which will be applied to allow end-member component compositions to be extracted from whole-rock geochemical data. The technique works by reducing the measured set of variables to a simpler set of inter-element relationships (i.e., the components) which are not directly measurable. Previous geological applications of factor analysis, in seeking to quantify admixtures of fixed end-member components, have previously been applied to modern carbonate sediments, ferromanganese nodules, marine plate-surface sediments and recent rise-crest sediments (Dymond *et al.,* 1976; Full *et al.,* 1981; Leinen and Pisias, 1984; Full and Ehrlich, 1986; Leinen, 1986). The usefulness of the technique depends on the quality of the whole-rock data, the rotation procedure used to extract the factors, and the quality of the interpretation placed on the factors which emerge. The results which factor analysis produces will be used to calculate the approximate composition of the end-member components, and the approximate quantities of each end-member component in each sample in the study.

The Dymond (1981) study is the second numerical model which will applied to the whole rock data. Again, this technique is based on the assumption that physical mixing of the following components may be quantified: biogenic, detrital, hydrothermal, hydrogenous, and dissolution residue. Linear programming using a series of linear equations dealing with known elemental ratios and measured whole rock data will be used to calculate a number of

unknown values. In the Dymond (1981) study, these unknown values relate to the proportions of the set of end-member components that made-up each sample. The simplified end-members, which were used by Dymond (1981) were as follows: (1) detrital weathering products; (2) hydrothermal precipitates; (3) biogenic precipitates; (4) hydrogenous ferromanganese precipitates; and (5) residue remaining after the dissolution of planktonic organisms. One of the drawbacks of the Dymond (1981) technique is that it has previously only applied to recent plate-surface sediments for which the end-member component compositions had been directly measured. One of the aims of this project will be to evaluate the adaptability of the technique in order to apply it to sediments from a different geological period and environment, especially those for which directly measured end-member components are not available.

An important technique which has been used in the literature to refine the linear programming model is carried out using calculated, rather than measured, end-member components. For example, Leinen and Pisias (1984) have used factor analysis to calculate the end-member composition necessary to the linear programming model. Although this was previously only applied for comparative purposes (Leinen and Pisias, 1984) to the same recent plate-surface sediments studied by Dymond (1981), this study is proposing to apply the technique to ancient sediments. Linear programming using directly measured components will be compared to linear programming using components calculated by factor analysis. This technique is ideally suited to ancient sediments, such as those from Oman. This is because, despite their geochemical similarity to modern rise-crest sediments (Fleet and Robertson, 1980; Karpoff *et al.*, 1988), ancient sediments suffer from the effects of diagenesis, poor exposure or dissolution with the result that it is not possible to directly measure the end-member components.

This project proposes physically separating the sediment into a number of fractions in order to directly analyse the phases making up the sediments. Separating a sediment into fractions, which represent the constituent phases, is carried out in three stages by using three acids, of increasing strength, on different aliquots of each sample (Balistieri and Murray, 1986; Miller and Cronan, 1994). The acid leaching solutions which are used are as follows: (1) 25% acetic acid; (2) 3:7 mixture of 35% nitric acid and 25% hydroxylamine hydrochloride; and (3) 50% hot hydrochloric acid. The previous use of chemical separation techniques to determine the composition of pelagic sediment-forming

phases is well documented (Chester and Hughes, 1967; Aplin, 1983; Lyle *et al.*, 1977; Aplin and Cronan, 1985; Balistrieri and Murray, 1986; Miller and Cronan, 1994). In this study, the purpose of using physical separation and analysis of the phases, is to determine the chemistry of the sediment-forming components. This data provides information on end-member compositions which is independent of the information which is derived from whole-rock data.

Finally, having calculated the composition of each component and the proportions of each component in each sample, the geological processes will be inferred from the temporal and spatial variations of the components and their compositions. The results will finally be used to compare metalliferous sedimentation in Oman with previous studies of ancient and modern metalliferous sediments and with the most recent findings from active hydrothermal systems (Barrett, 1992; Feely *et al,* 1994, 1996; Anshutz and Blanc, 1995; Herzig and Hanning, 1995; Edmond *et al.*, 1996).

1.3 The field area

The samples in this study are metalliferous sediments taken from the Semail ophiolite of northern Oman. The Semail nappe (Figure 1.1) is a thrust sheet over 600 km long and 150 km wide, covering an area of over 20,000 km2, which has been broken up during emplacement, into a number of major blocks (Glennie *et al.*, 1974; Reuber, 1988). At the base of the ophiolite sequence is a serpentinized harzburgite mantle sequence, passing up into layered cumulate gabbro and peridotite, to "high level" gabbro. The high level gabbro is though to have formed in axial magma chambers which fed overlying sheeted dykes and pillow lavas (Axis Unit) (Alabaster and Pearce, 1985; Ernewein *et al.*, 1988). A later series of off-axis lavas (Lasail Unit and Alley Unit) were related to ultramafic to acidic late-intrusive complexes (Alabaster and Pearce, 1985).

The Oman metalliferous sediments are interbedded within the successive lava flows of the extrusive sequence, schematically summarised overleaf (Figure 1.2). The earliest sediments are taken from the lowest pillow lavas which formed above an active spreading ridge. The greatest number of samples in this study are taken from metalliferous deposits which occur in the volcanic sequence

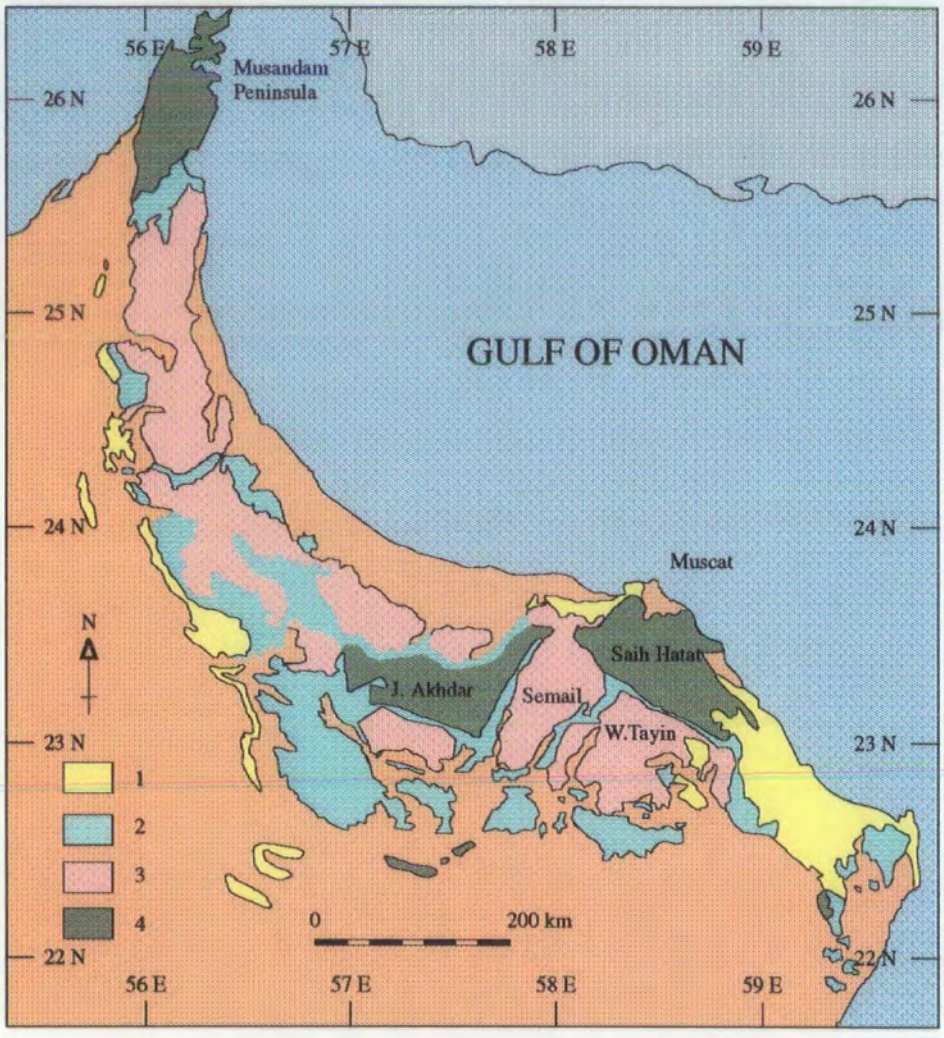

Map of the Oman ophiolite (after Glennie et al., 1974). 1= Maastrichtian and Tertiary; 2= ophiolite; 3 = allochthonous sediments (Hawasina nappes); 4 = autochthonous units of the Arabian paltform

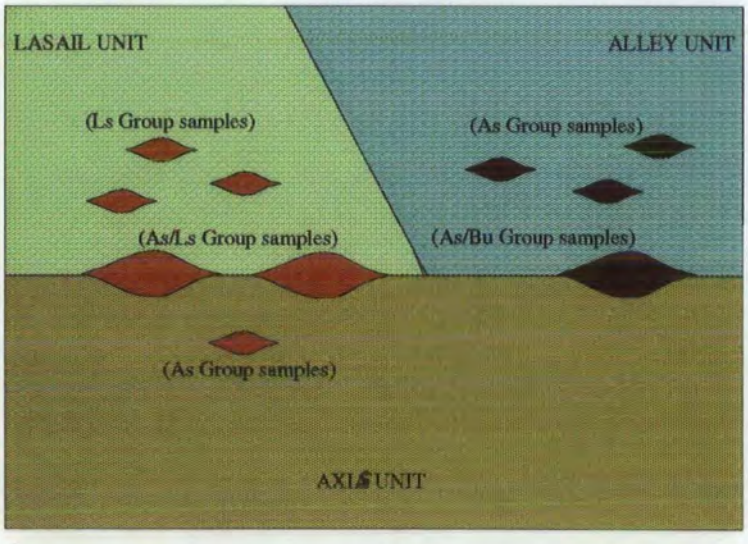

Figure 1.2 Schematic horizontal position of the studied metalliferous sediment deposits within the Axis Unit, Lasail Unit and Alley Unit.

above the spreading centre lavas but prior to the overlying "off-axis" volcanic sequence. Evidence cited in the literature (e.g., plastic deformation of layering in the host gabbros near to the contact with late intrusives) supports a very narrow time interval between axis and off-axis volcanism during which these sediments formed (Tippet *et al.,* 1981; Beurrier *et al.,* 1987; Ernewein *et al.,* 1988). A small number of samples are taken from deposits which are interbedded in the off-axis lavas representing sedimentation associated with the latest magmatic episodes. The period of active spreading-centre volcanism has been dated from radiolaria microfauna as Albo-Cenomanian, and the subsequent off-axis magmatism is dated, using the same method, as Cenomanian to Early Turonian time (Tippet *et al.,* 1981; Blome and Irwin, 1985; Bourdillion de Grissac *et al.,* 1987). Thus, the metalliferous sediments may represent a period of up to approximately 18 m.y.

This study proposes an objective examination of the geochemical and mineralogical compositions of marine sediments through conceptually simplifying sediment-forming processes into the mixing of limited numbers of components (Chester and Hughes, 1967, 1969; Chester and Messiha-Hanna, 1970; Cronan, 1976; Krishnaswami, 1976; Dymond, 1981; Leinen and Pisias, 1984). This approach, which has been adopted by most recent workers, only requires a limited number of elements to summarise the components and thereby infer the major sediment-forming processes. A common feature of previous studies has been to attempt to differentiate or quantify physical, biological and chemical processes from the bulk chemical composition of the sediments. In the past, a number of specific techniques were employed to explain sediment bulk-composition in terms of a number of *building block* components (Cronan, 1976; Dymond *et al.,* 1976; Dymond, 1981; Dymond *et al.,* 1984; Cronan *et al.,* 1981; Leinen and Pisias, 1984).

1.4 Thesis description

A brief outline of the following chapters is presented below;

CHAPTER 2: This chapter summarises, from the literature, the basalt-sediment relationships and the magmatic ore-forming processes in the ophiolite of northern Oman. The chapter goes on to describe the geographical and geological setting of the sediments which are analysed in this study. After summarising the

whole-rock data in tabular form, chapter 2 discusses the major and trace element geochemistry. The bulk-rock data is then be presented on comparative diagrams, with the aim of placing the Oman sediments in the context of other, known, metalliferous deposits. For the same purpose, Chapter 2 also includes the mineralogy of the sediments as defined by X-Ray diffraction data.

CHAPTER 3: This chapter briefly summarises the previous applications of factor analysis to sedimentary environments and describes in detail the factor analysis methodology. The chapter then uses the factor analysis to calculate and statistically evaluate the end-member sediment-forming components from the whole-rock data. The aim of this chapter is to use factor analysis to quantify the distribution pattern of the elements, thereby defining the composition of each component. The chapter concludes by summarising the regional variation in component compositions and the variation in importance of each component according to spatial and temporal differences.

CHAPTER 4: This chapter applies a selective chemical leaching technique to a representative subset of the metalliferous sediments for the purpose of comparability with the numerical methods based on whole-rock data. Linear programming is then explained and applied to the whole-rock data and the results summarised. The chapter presents a statistical evaluation of the linear programming output. An attempt is made to modify, using factor analysis data, the *general* linear programming method to the *specific* end-member compositions which are relevant to the Oman rise-crest environment in the Cretaceous period. The chapter concludes by summarising and evaluating the results of the modified linear programming method.

CHAPTER 5: The aim of this chapter is to produce a geological interpretation on the basis of the results of the various techniques that have been employed. In the course of discussing the statistical validity and significance of the results, a unified geological model is put forward for sediment formation during the evolution of the Oman ophiolite during Cretaceous times.

CHAPTER 2

Ferromanganoan sediments: major and trace element geochemistry

2.1 Introduction

The aim of this chapter is to introduce the large geochemical data set and to examine the variation in bulk-rock geochemistry. The basalt-sediment relationships of the Oman ophiolite are briefly summarised and then the major, trace and rare earth element geochemistry of the Oman ferromanganoan samples is described. This Chapter also introduces the process of end-member component mixing and assesses the applicability of this type of modelling to the undestanding of ancient metalliferous deposits. Also, this Chapter investigates the relationship of major and trace element behaviour to volcanic stratigraphic location of the deposits. An account of the mineralogy of the samples determined by XRD analysis is also included. The framework put forward by this Chapter is the basis from which chemical leaching experiments, factor analysis and linear programming analyses will be used to help understand the geological processes behind the whole-rock data.

The samples in this study are of ferromanganoan-type from various locations within the lava pile of the Semail nappe (Figure 2.1). Metalliferous sediments of this type are predominantly the product of sea-floor hydrothermal mineralization resulting from exchange of heat and chemicals which occurs between the lithosphere and the oceans at divergent plate boundaries at mid-ocean ridges (MORs), at intra-plate volcanic centres and within or behind volcanic island arcs (Rona, 1993).The relative importance of hydrothermal processes in the oceans began to be appreciated only after the discovery of ferromanganese and trace-metal enriched sediments on the flanks of the EPR. Recent studies of ocean ridge processes have increased understanding of hydrothermal systems and of the processes by which metalliferous sediments are generated in the spreading centre tectonic environment of the Oman ridge (e.g. Dymond *et al.*,1973; Fleet and

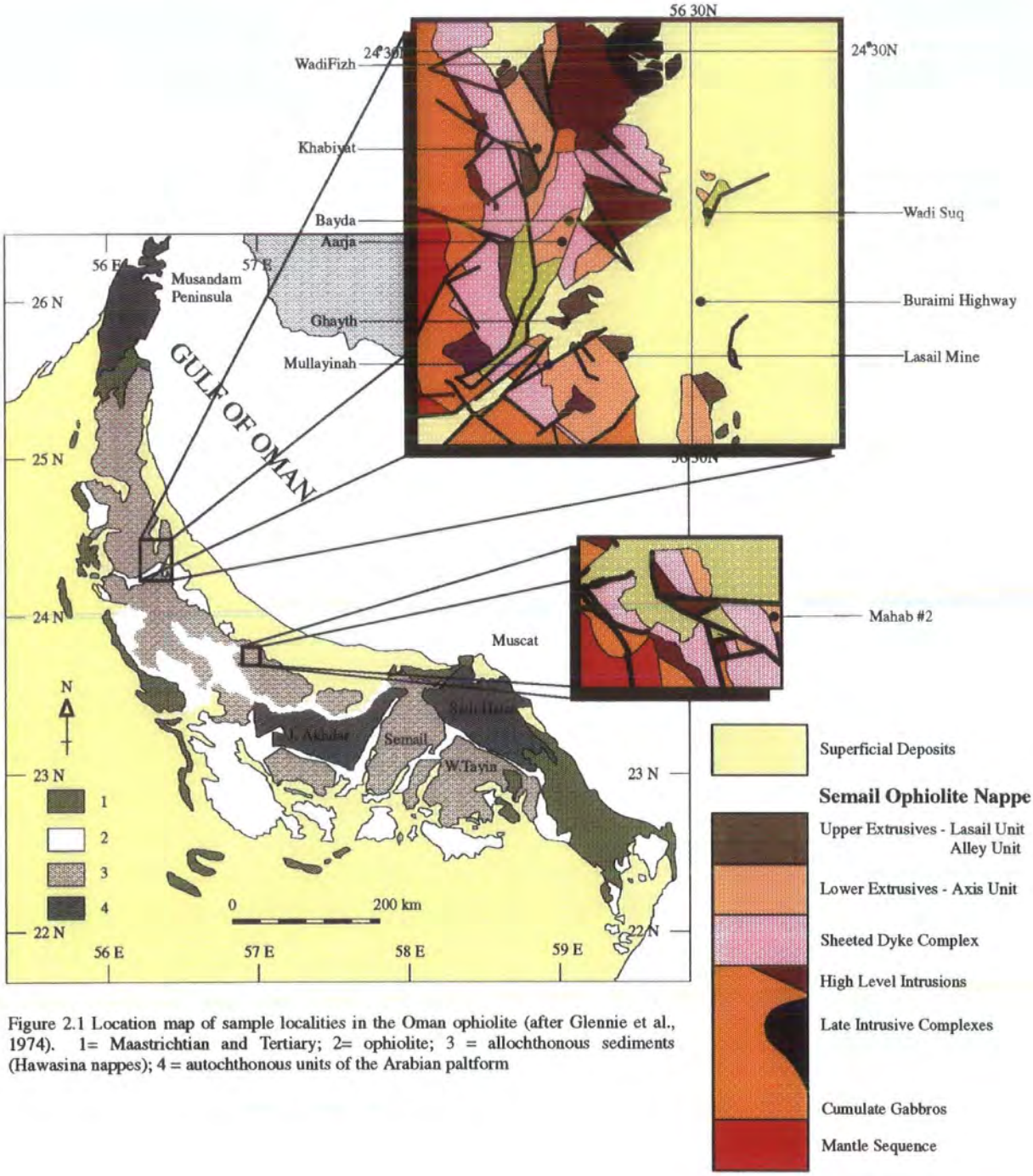

Figure 2.1 Location map of sample localities in the Oman ophiolite (after Glennie et al., 1974). 1= Maastrichtian and Tertiary; 2= ophiolite; 3 = allochthonous sediments (Hawasina nappes); 4 = autochthonous units of the Arabian paltform

Robertson, 1980; Alabaster and Pearce, 1985; Robertson *et al.*, 1987; Hall *et al.*, 1988; Boyle, 1990; Mills and Elderfield, 1995).

In using ophiolites as ancient analogues to modern hydrothermal systems, the Oman ophiolite has been chosen because it is one of the better studied. The reason for this is because it has not been deformed by any subsequent collision since its obduction onto the Arabian continental platform in late Campanian to Early Maastrichtian time except for slight tilting due to a post-Cretaceous tectonic event, (Perrin *et al.*, 1993). Samples in this study are from the exposed magma-hydrothermal system interface have therefore been subjected to minimal overprinting by subsequent processes involved in crustal generation. The data provided in this Chapter may provide useful constraints for mineral exploration both in other ophiolite complexes and in deep sea environments, (Nehlig, 1993).

Analytical data used in this chapter have been obtained by the following techniques:
(1) X-Ray Fluorescence (XRF) was used to determine the major elements and to determine the trace elements Sc, V, Cr, Co, Ni, Cu, Zn, Rb, Sr, Y, Zr, Nb, Cs, and Ba.
(2) Inductively-Coupled Plasma Mass Spectrometry (ICP-MS) at BNFL's Westlakes Industrial Research Laboratories, Cumbria, and ICP-MS at the Department of Geological Sciences, at the University of Durham were used to determine the Rare Earth Elements (REEs).
(3) X-Ray diffraction (XRD) was carried out on selected samples at the University of Durham.

The techniques used to prepare and analyse samples are given in Appendix A and the full dataset is listed in Appendix B.

2.2 Basalt-sediment relationships in the arc-basin environment

In this Section the relevant lava units of the Oman ophiolite are briefly described for the purpose of providing a framework for discussing the relationship between volcanic stratigraphic position and sediment geochemistry. In Section 2.3, the sample localities will be discussed in more detail and the geographical and geological setting of the sediment in this study will be contrasted to that of analogous recent and ancient sediments.

The magmatic history of the Semail ophiolite of Oman has already been well documented (eg., Pearce *et al.*,1981; Alabaster, *et al.*, 1982; Alabaster and Pearce, 1985; Ernewein, *et al.*, 1988; Nehlig, *et al.*, 1994). The lava sequence (Figure 2.2) of the ophiolite is currently classified into five major lava units (Alabaster and Pearce, 1985). This replaces a classification system which used two units, the "Lower" and the "Upper" lava units (Fleet and Robertson 1980). The five lava units which are referred to in this study are (in order of eruption from oldest to youngest), the *Geotimes* unit, the *Lasail* unit, the *Alley* unit, the *Clinopyroxene-phyric* unit, and the *Salahi* unit. Following extrusion of the Semail pre-emplacement Mesozoic sediments known as the *Suhaylah* Formation of Upper Cretaceous to Tertiary age were deposited. A more recent study using different terminology for the same lava units (Ernewein *et al.*, 1988) will also be mentioned in this Chapter.

Classification into three main magmatic episodes is common to both models. In the terminology of Ernewein *et al.*, (1988) these are referred to as V1, $V2_{primitive}$, and $V2_{evolved}$; and in the terminology of Alabaster and Pearce (1985) these are referred to as the "Geotimes" (Spreading axis event) unit, the "Lasail" (Seamount building event) unit and the "Alley" (Rifting event) unit respectively. With respect to this study of the Oman metalliferous sediments, it is sufficient that the V1 unit approximates to the Geotimes unit, and the V2 to the Alley and Lasail units. For the purposes of this study, the Alabaster and Pearce (1985) classification system will be used.

2.2.1 The Alabaster and Pearce (1985) Classification System

Five lava units are referred to in the Alabaster and Pearce (1985) classification system (Figure 2.2): (1) *Geotimes* unit; (2) *Lasail* unit; (3) *Alley* unit; (4) *Clinopyroxene-phyric* unit; and (5) *Salahi* unit. The ferromanganoan sediments in this study are only associated with the first three lava units. The distinctive field characteristics of the units, in particular their colour, has ensured that the sample locations of the ferromanganoan deposits in the Oman ophiolite are accurate. The three relevant lava units are described in the following sub-sections.

2.2.1.1 "Geotimes" unit (As)

The earliest volcanic event, which is termed the "Geotimes" unit or Axis (As) unit (Pearce *et al.*, 1981; Alabaster and Pearce, 1985), represents submarine volcanism at a fast-spreading ridge-crest. The unit is characteristically reddish-

brown in colour as a result of brownstone facies metamorphism (Alabaster *et al.*, 1982). The Geotimes unit is classified as basaltic andesite of MORB affinity plotted on Zr/Y-Zr and Cr-Y diagrams (Figure 2.3). The importance of this unit

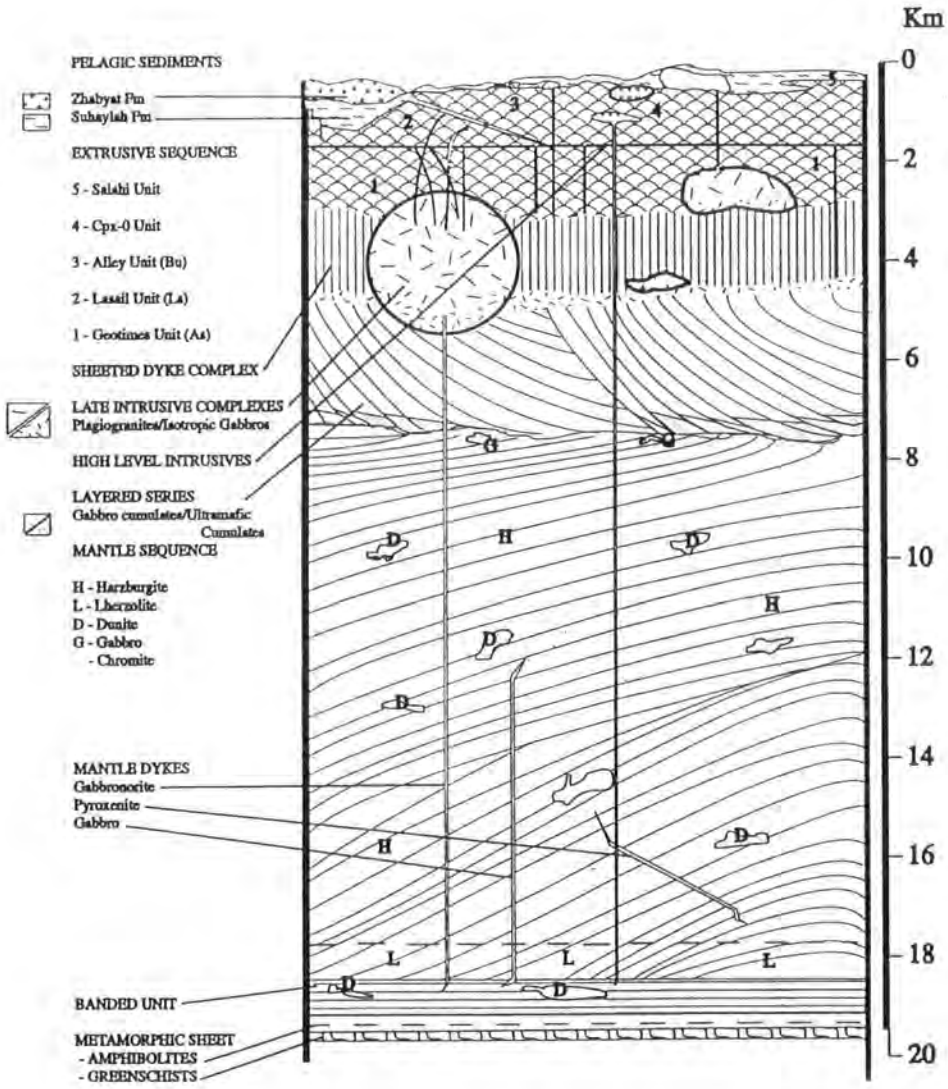

Figure 2.2 Schematic cross-section of the ophiolite of northern Oman (after Pearce et al., 1982; Alabaster and Pearce, 1985)

with regard to the location and formation of hydrothermal deposits is that it is formed of basaltic pillow lavas in sections up to 1.5 km thick with an undulating upper surface upon which all successive lava units were emplaced. The upper surface of the unit is the volcanic stratigraphic position of the following sample localities: Wadi Suq, Aarja mine, Bayda mine, Khabiyat, Wadi Fizh, Huwayl, Lasail mine and Mahab #2.

2.2.1.2 "Lasail" Unit (Ls)

The "Lasail" Unit (Ls) is distinct both in the field, and geochemically, from the underlying basaltic pillow lavas of the Geotimes Unit.

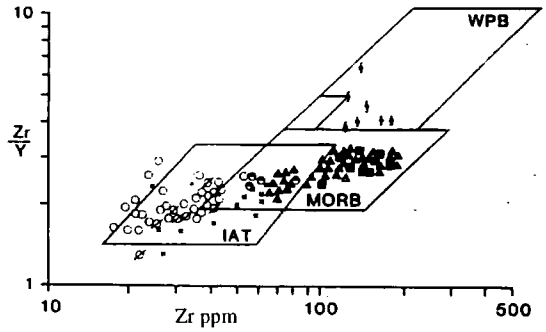

Figure 2.3 (a) Zr/Y versus Zr diagram to show the island arc affinity of the Lasail and Alley Units (open symbols) and the Mid-ocean affinities of the Axis Unit lavas (closed symbols). Discriminant boundaries (after Pearce, 1980) enclose fields occupied by non-cumulate basalts of mid-ocean ridge basalt (MORB), island arc tholeiites (IAT), and within-plate basalts (WPB) affinities. After: Alabaster *et al.*, 1982.

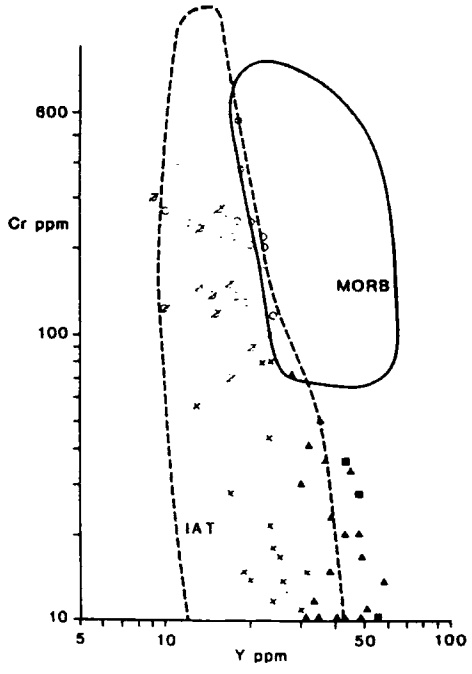

Figure 2.3 (b) Cr versus Y plot showing that the Alley and Lasail lava plot entirely within the volcanic arc field (Pearce, 1980)

The geochemical association of the Lasail Unit with sheeted dykes that cross-cut the main sheeted dyke complex is evidence that the lavas erupted off-axis, this evidence is summarised in Pearce *et al.*, (1981) and Alabaster *et al.*, (1982). Because the occurrence of this Unit is discontinuously distributed as centres of

activity spaced along the north-south strike of the complex the Lasail lavas are though to represent discrete volcanic seamounts (Alabaster *et al.,* 1982).

The geochemical evidence of TiO_2/Zr plots (Figure 2.4) supports the seamount hypothesis in that the Lasail unit is intermediate in composition more Island Arc-like than MORB-like (Pearce and Norry, 1979). In the field, the unit is grey-green in colour as a result of prehnite-pumpellyite facies metamorphism. The whole unit has undergone intense hydrothermal alteration and contains ferromanganoan deposits from Huwayl.

The most important sample locations of the Lasail unit to this study occur at the contact of its lower surface with the upper surface of the Geotimes unit. At this volcanic stratigraphic position, occur the major ferromanganoan deposits of the Lasail mine and Mahab #2.

2.2.1.3 "Alley" unit (Bu)

The "Alley" unit which is also known as the Basal Upper unit (Bu) occurs along NW-SE faults and is thought to represent magmatic eruptions in a submarine graben setting.

The Bu (Alley) lava unit overlies the Ls (seamount) lava, where the Ls unit is present, otherwise it occurs directly in contact with the As (Axis) unit. The Alley unit is a brownish-green colour as a result of zeolite facies metamorphism (Alabaster *et al.,* 1982).

A large number of samples in this study are taken from the basal contact of this unit with the Axis unit. In addition, samples from Wadi Fizh, Semdah West and Ghayth samples are taken exclusively from within the unit rather than from its upper or lower boundary.

2.2.2 The Ernewein *et al.,* (1988) Classification System

Ernewein, *et al.,* (1988) proposed a three episode model of magmatism which essentially uses different terminology to explain lava units subdivided as described above. Using the terminology of Ernewein *et al.,* (1988) the "V1" is equivalent to the "Geotimes" unit, the "$V2_{Primitive}$" equivalent to the "Lasail" unit and the "$V2_{Evolved}$" equivalent to the "Alley" unit.

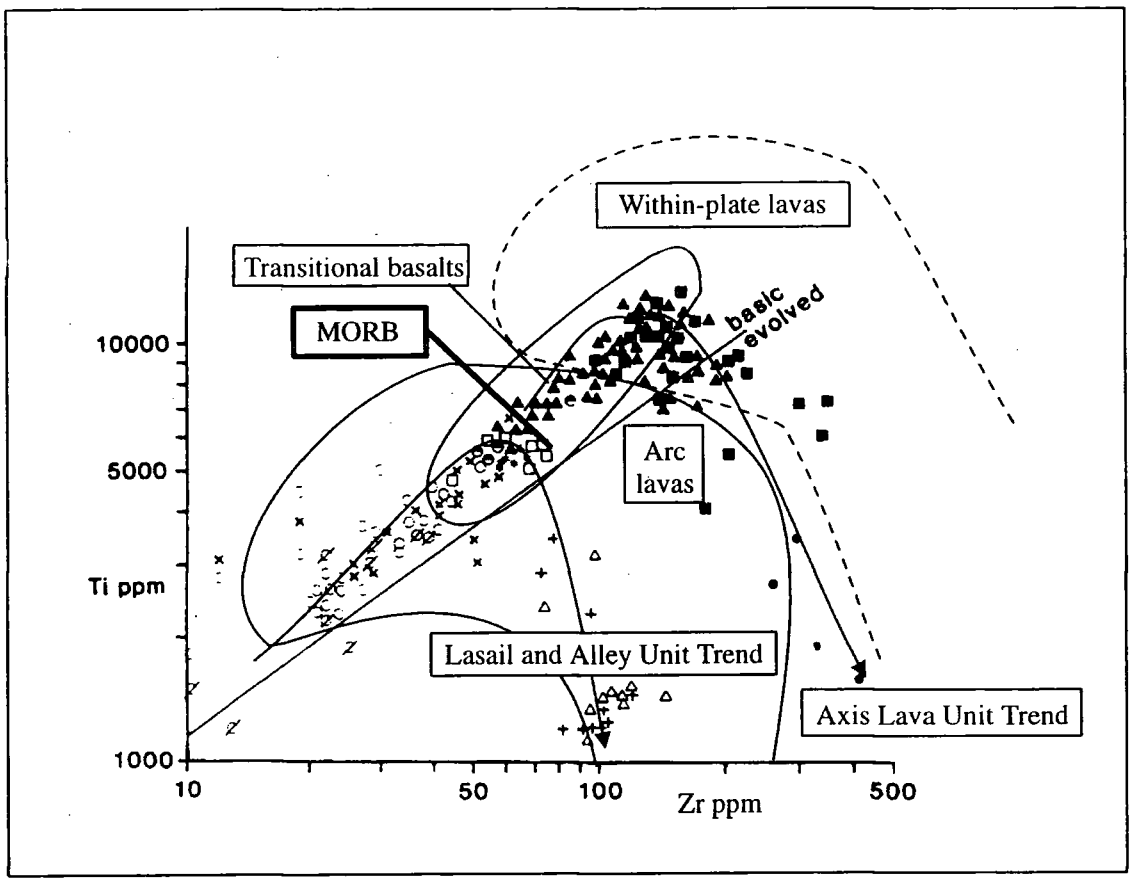

Figure 2.4 Ti versus Zr diagram for the Oman lavas and shallow intrusives. The As Unit (solid symbols) contrast with the overlying lava units (open symbols). Because the As Unit lavas are the only unit to to belong to the same fractionation trend as the more evolved compositions of the main intrusive complex and therefore represent formation due to sea-floor spreading processes. The Ls and Bu Units follow a volcanic arc fractionation trend. (After: Pearce, 1980; Alabaster *et al.*, 1982)

2.2.3 Summary of terminology

For the purposes of this study, the Ernewein *et al.*, (1988) and Alabaster *et al.*, (1982) models both suggest a similar magmatic history of the ophiolite complex. Both models use geochemical evidence which suggest: (1) that the Geotimes/V1 unit lava was erupted above a back-arc spreading centre in a marginal ocean basin during the Cenomanian period (Upper Cretaceous); and (2) that the Lasail/V2 $_{\text{Primitive}}$ and Alley/V2 $_{\text{Evolved}}$ units were erupted off-axis above an active oceanward subduction zone immediately prior to intra-oceanic detachment and obduction. The contrast between the two models, which centres on whether the ophiolite was produced by normal sea-floor spreading (Ernewein *et al.*, 1988) or by back-arc crust forming processes (Pearce *et al.*, 1981; Alabaster *et al.*, 1982), does not affect the principal conclusions of this chapter with respect to the

sediment-forming processes. The terminology which will be used in this Chapter is derived from Alabaster *et al.*, (1982) and is as follows:

As unit - denotes the spreading event lava unit known as "Axis", "Geotimes" or "V1"
As Group - denotes ferromanganoan sediment obtained from the above lava unit
Ls unit - denotes the seamount event lava unit known as "Lasail" or "$V2_{Primitive}$"
Ls Group - denotes ferromanganoan sediment obtained from the above lava unit
Bu unit - denotes the rifting event lava unit known as "Alley", "Basal Upper" or "$V2_{Evolved}$"
Bu Group - denotes ferromanganoan sediment obtained from the above lava unit

N.B. As/Ls and As/Bu denotes the boundary between the lava units or the Group of ferromanganoan sediment obtained from the boundary.

The location of most metalliferous sedimentation in the Oman metalliferous sediments is at, or close to, the boundaries between the distinct periods of magmatism outlined above.

Three major massive sulphide mines (Bayda, Aarja, Lasail) are found at the upper boundary of the As unit with overlying Ls unit or Bu unit lavas overlying. The following Sections describe briefly the localities from which sediment used in this study has been sampled

2.2.4 Relationship of the metalliferous sediment-forming processes to magmatism

2.2.4.1 Axis unit intralava sediment

The intra-lava sediment from within the As unit is rare and the samples provided do not represent a major proportion of the total number of samples in this study. Where samples are obtained from Wadi Suq, these are from locations at least 300m beneath the Wadi Suq gossan that crop out close to the As/Bu contact. Samples from *within* the lava pile are not sub-metalliferous sediment veining, but mark time intervals when metalliferous sediment accumulated in the lava surface during localised quiescence in magmatism.

2.2.4.2 Axis unit lava surface sediment

Metalliferous sediments including massive sulphide deposits first begin to appear in the volcanic stratigraphic pile towards the final stages of Axis unit volcanism.

Massive sulphide deposits and oxidized gossans are not directly or genetically related to metalliferous sediments according to field relationships (See Section 2.3) and geochemistry (Boyle, 1990). Each of the three principal mines of the Semail ophiolite is located at the volcanic stratigraphic upper surface of the As unit (See Section 2.3): the Lasail and Bayda mines are located at the As/Ls boundary and the Aarja mine is located at the As/Bu boundary. The greatest thickness of ferromanganese sediment marks the unconformably overlain upper surface of the Axis lava unit. Alabaster *et al.,* (1982) suggest that the magma chambers feeding Upper Lava unit volcanism either set up or rejuvenated hydrothermal convection.

The locations that have been sampled from the upper boundary of Axis unit *Geotimes* lava with *Lasail* lava are the Lasail mine, Huwayl gossan (core and outcrop), and the Mahab N°2 gossan. The Lasail mine location has a large gossan, and samples of metalliferous sediment are located in veins 0.25 - 1.00 m thick and as close as 25 m from the mineralization. The samples taken from Mahab are associated with another similar but smaller gossan which is 200 m by 5 m in size, outcrops over a distance of 50 m, and is approximately 0.50 m thick. The Huwayl samples represent samples taken from core and outcrop. No outcrops of metalliferous sediment have been reported or found in the Lasail unit other than at or proximal to its lower boundary.

The Bu unit is in contact both with Ls unit lava and with the earlier As unit spreading event lava. The relatively young Bu lava unit contains thin intercalated metalliferous sediment-like sediment. The sample location for Bu Group samples is the fault-bounded structure north of the Lasail area that is termed the "Alley", (Coleman, 1981). The Alley lava units represent fissure eruptions along graben faults and metalliferous samples represent the hydrothermal system active immediately prior to the volcanism associated with graben formation.

High level felsite and rhyolite magma chambers emplaced in the Axis unit are thought to have been responsible for setting up hydrothermal activity (Alabaster *et al.,* 1982). Thus, As/Bu and As/Ls metalliferous sediments are the products of off-axis magmatism related to intra-oceanic detachment above an oceanward subduction zone, during a period of time following the cessation of spreading centre magmatism (Pearce *et al.,* 1982; Alabaster *et al.,* 1982; Ernewein *et al.,* 1988).

The close relationship of ferromanganoan sediment to waning magmatism is also characteristic of analogous metalliferous sediments from Cyprus (Constantinou and Govett, 1972; Robertson, 1975; Karpoff *et al.*, 1988; Robertson and Varnavas, 1993). Evidence from Cyprus further suggests that thin lava breccias sometimes underlying metalliferous sediments occurred only in the early stages associated with the initial emergence of the hydrothermal fluid so that quiescent discharge dominated the subsequent sediment-forming hydrothermal system (Constantinou and Govett, 1972; Robertson, 1975; Karpoff *et al.*, 1988).

2.2.4.3 Alley unit intralava sediment

Ferromanganoan sediment within the Bu unit lava is common in contrast to the relative absence of hydrothermal sediment in the seamount (Ls unit) lava or in the basement spreading event (As) lava.

2.3 Geographical and geological setting of the metalliferous sediments

All the sediments sampled are located in the eastern foothills of the Oman mountains west of Sohar. The location map (Figure 2.1) shows the sample locations and outcrop of metalliferous sediment and their associated sulphide ore deposit. The study area extends from Khabiyat and Wadi Fizh in the north to the Mahab #2 mine at Wadi Sarami. The sample locations are given in Table 2.1, and are described below, listed according to their position in the ophiolite lava pile.

2.3.1 South of Bayda

2.3.1.1 Bayda mine

One horizon of metalliferous sediment is present at a distance of 300 m from the Bayda mine located at 26937N 4410E. An outcrop of 0.75 m thickness and 25 m in length is exposed at the As/Bu boundary.

2.3.1.2 Aarja mine

One horizon of metalliferous sediment is exposed at a distance of 300 m from the large Aarja gossan, located at 26928N 4400E. The thickness of outcrop is 0.75 m and the actual length exposed is 100 m. Of the eight samples collected, all are from the As/Bu boundary, but there is a wide compositional range present represented by the wide range in colours from blackish-red (U80) to light to moderate or greyish brown (U81, U82).

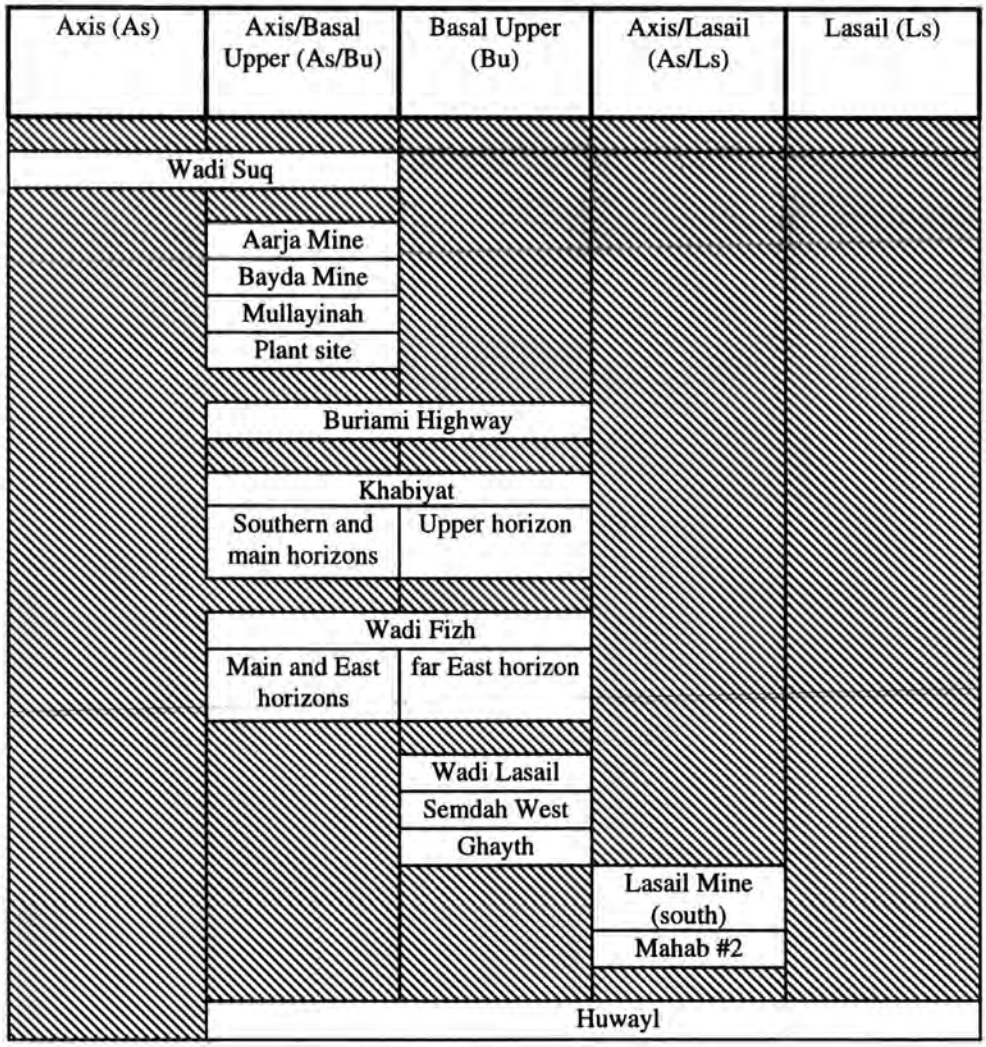

Table 2.1 Sample localities by volcanic statigraphic location

2.3.1.3 Ghayth

At Ghayth, two metalliferous sediment horizons are exposed 1.5 km from the gossan which is located at Ghayth #31 (Grid reference: 206910N 4445E). The samples are located within the Basal Upper lava unit and the thickness of outcrop is 0.25 m which is exposed for a distance of 60 m. Five samples have been collected of which the more Mn-rich samples are dusky brown in colour and the relatively Mn-poor samples are greyish red in colour.

2.3.1.4 Wadi Suq

The Wadi Suq locality, at 26925N 4515E, contains an exposure of the boundary of the As/Bu lava units. Here, and in the Axis lava unit, there is exposure of

sediment. At a distance of 300 m from the gossan, which outcrops as three small hillocks at the boundary of the lava units, four intra-lava sediments from within the Axis sequence have been sampled: the Mn-poor sample is greyish red, the remainder are brown. Two samples represent the As/Bu boundary. The outcrop exposed at Wadi Suq is 300 m in length and ±1m in thickness but between 2 km to 3 km length of outcrop may be inferred. Sample 20655 was taken from 2 km north along strike of the main outcrop.

2.3.1.5 Wadi Lasail and Lasail mine

The Lasail Mine is located at Grid reference 26845N 4423E. At a distance of 25m from the large gossan 50m of metalliferous sediment is exposed in a horizon 0.5 m thick at the As/Ls boundary. Thirty-one samples have been taken from this exposure. At Wadi Lasail, Grid Reference 26859N 4429E, 3 km west of the Lasail Mine, samples represent the 100 m length outcrop of 1 m thickness.

2.3.1.6 Mulayyinah

Mulayyinah occurs at the As/Bu boundary (Grid Reference: 26855N 4394E) where a single horizon 0.75 m thick is exposed for 10 m. The distance of the sample location from the gossan is 50 m, and the size of the gossan is 20 m x 5 m. Only one sample was taken.

2.3.1.7 Huwayl

Two sediment horizons are present at Huwayl (26825N 440E) at the boundaries of the As/Ls and the As/Bu lava units. The lower horizon is 1.0 m thick and the upper horizon up to 0.2 m in thickness, 500 m actual outcrop is exposed. There is no evidence of a gossan close to this location but malachite has been found in the immediate vicinity. The following colours typify the samples from Huwayl:

Brownish grey	-	Siliceous calcareous sediment, but Mn-poor
Dark grey	-	Calcareous, but Mn-poor
Dusky red	-	Siliceous calcareous sediment but FeMn-poor
Greyish brown	-	Siliceous sediment
Greyish red	-	Siliceous, but Mn-poor

2.3.1.8 Mahab #2

The Mahab #2 area located at 26545N 4727E differs from the other locations in that it is in the Sarami Block rather than the Salahi or Fizh Blocks from which all

of the other samples are taken. Four samples from the As/Ls boundary represent the single horizon which is exposed for 50 m, 0.5 m thick. The sedimentation is exposed 500 m south east of the Mahab #2 (200 m x 5 m) gossan. These samples are greyish-red and contains remarkably high MnO content for samples for samples belonging to the As/Ls Group.

2.3.1.9 Buraimi Highway

Two small exposures of metalliferous sediment were taken from exposure on the Buraimi Highway at 20 km and 22 km west of Sohar. In each outcrop, only 10m length was exposed but up to 200 m could be inferred. The thicknesses of the exposures is 0.75 m and 0.25 m respectively. There is no known gossan or mineralization in the localities, the country rock in each location being As/Bu.

2.3.2 North of Bayda

2.3.2.1 Khabiyat

The three horizons exposed at Khabiyat were extensively sampled. Although only a 400 m length is continuously exposed it is possible to infer that up to 1.5 km length of metalliferous sediment is present. The thickness of the three horizons varies between 0.8 m and 3.0 m. All of the samples except two occur at the As/Bu boundary which is 1.5 km from numerous small gossans. The two samples, 20648 and 20647, were found approximately 100 m from the As/Bu contact within the Basal Upper unit. The samples from Khabiyat are of the following colours and types:

Greyish-Dusky brown	-	manganiferous, but Fe-poor
Greyish red	-	manganiferous, but Fe-Si-poor

2.3.2.2 Wadi Fizh

The area around Wadi Fizh (Grid Reference 27100N 4390E) contains three outcrops of metalliferous sediment, each separated from the others by approximately 500 m of lava. The three horizons are 100 m, 25 m and 300 m in length, being 0.75 m, 0.5 m and 1 m thick respectively. Twenty-one samples in total were taken from at this locality from the As/Bu boundary and the Bu unit. The samples from the Wadi Fizh are uniformly greyish brown and Mn-rich.

2.3.2.3 Semdah West

The samples from Semdah West were taken from two localities. At locality No.1 (Grid Reference: 27198N 4390E), 0.3 m thickness of sediment is exposed for 25 m and, at locality No.2 (Grid Reference: 27170N 4375E), 1m thickness of sediment is exposed for 150 m. At locality No.1, all of the sediment present appears to be exposed whereas, at the second locality, it is possible to infer a total of 300 m possible metalliferous sediment deposit. Ten samples were taken from these localities representing intra-lava sediment from the Basal Upper lava unit. There is no gossan in the vicinity of the sediment. Samples range from moderate to greyish-brown and are ferromanganoan in character. Those samples are blackish red to very dusky red in colour.

2.3.3 Recent and ancient analogues

Ancient and modern metalliferous sediments will be summarised briefly in order to place the samples in this study into the context of analogous marine sediments. By identifying the contrasts and similarities of Oman metalliferous sediments, the significance of the geochemical data may be applied more widely.

Lalou (1983) lists 70 locations at which contemporary marine hydrothermal precipitation of ferromanganoan sediment is currently occurring and, of these, 6 sites are relatively well studied in the literature. Because ophiolites represent allochthonous fragments of ocean lithosphere, they all are likely to contain metalliferous sediment of the type described in this study. However, some ophiolites have been studied better than others. These include the Oman ophiolite, the Troodos ophiolite (Cyprus) and the Othris and Pindos ophiolites (Greece). Data from the six sites of active hydrothermal ferromanganoan sedimentation and from the relevant ophiolites are summarized briefly below (Table 2.2 and Table 2.3).

2.3.3.1 Recent marine hydrothermal ferromanganese deposits

The East Pacific Rise (EPR) represents open ocean hydrothermal deposits which are found on the ridge crest separating the Nazca and Pacific Plates from 21°N to 20°S. The complete range of marine hydrothermal deposits have been found at the various sites along the EPR ranging from massive sulphide beds, Fe silicates, and Fe, Mn and ferromanganese oxyhydroxides (Hekinian *et al.*, 1980; Zierenberg *et al.*, 1984; Hekinian and Fouquet, 1985).

The Bauer Deep is a small basin located between the Galapagos Rise and the EPR in the south-east Pacific. A summary of the mineralogy and geochemistry of the Bauer deep metalliferous sediments may be found in Dymond *et al.* (1984).

The Galapagos region is one of the most extensively surveyed parts of the ocean floor. The hydrothermal activity includes the white smoker type low-temperature activity which produces solutions rich in Mn relative to high temperature black smokers.

	1	2	3	4	5	6	7	8	9	10
Mn wt%	6.0	4.6	2.9	43.0	55.0	47.0	4.0	27.9	41.0	38.0
Fe wt%	18.00	14.10	0.06	0.16	0.20	0.66	22.29	1.05	0.80	2.70
Al wt%	0.50	2.30	-	0.18	-	0.20	0.79	1.27	0.90	0.69
Ti wt%	0.02	-	-	-	-	0.00	-	-	0..04	0.11
Co ppm	105	64	19	24	39	13	10	82	33	30
Ni ppm	430	820	353	880	180	125	80	371	310	400
Cu ppm	730	910	43	450	50	80	76	206	120	80
Zn ppm	380	330	-	540	2020	90	35	83	400	310
Mo ppm	30	-	-	-	-	540	-	-	900	-
V ppm	450	-	-	-	-	110	152	214	110	-

Table 2.2 Average compositions of recent ferromanganoan deposits. Data from: (1) Metalliferous sediment EPR rise-crest, Bostrom and Peterson, 1966; (2) Metalliferous sediment Bauer Deep, Dymond *et al.*, 1984; (3) Hydrothermal deposit TAG area, Scott *et al.*, 1974; (4) Hydrothermal deposit TAG area, Toth, 1980; (5) Hydrothermal deposits Galapagos, Moore and Vogt, 1976; (6) Hydrothermal deposits Galapagos, Moorby and Cronan, 1983; (7) Hydrothermal clay-rich deposit FAMOUS Area, Hoffert *et al.*, 1978; (8) Hydrothermal FeMn deposit, Hoffert *et al.*, 1978; (9) Hydrothermal deposit S.W. Pacific Island Arc system, Moorby *et al.*, 1984; (10) Hydrothermal deposit Gulf of Aden, Cann and Strens, 1982.

The metalliferous hydrothermal sediment of the Atlantis II deep of the Red Sea has been extensively studied in terms of chemical components. The principal component sources are thought to be of biogenic and detrital particles, authigenic minerals and element supply by hot hydrothermal brine (Bischoff, 1969; Hartmann, 1980 and 1985; Anschutz and Blanc, 1995).

The TAG area (Trans-Atlantic Geotraverse) at 26°N on the MAR is one of the largest known active hydrothermal deposits at a sediment-free spreading ridge (Thompson *et al.*, 1988; Tivey *et al.*, 1995). Samples of sulphide from black and white smoker chimneys, sulphides, oxides and ochres have also now been sampled from active mounds (Rona *et al.*, 1986; Mills and Elderfield, 1995; Tivey *et al.*, 1995).

The FAMOUS Area (French-American Mid-Ocean Undersea Study) at 37°N on the MAR has provided samples of hydrothermal green clay-rich minerals and black ferromanganese concretions (Hoffert *et al.*, 1978).

2.3.3.2 Ophiolite terrains associated with ferromanganoan deposits

Other than from Oman, metalliferous ferromanganoan sediments have also been reported in detail from the Troodos ophiolite of Cyprus and the Subpelagonian, Othris and Pindos ophiolites of Greece. The classic studies of metalliferous sediments from the Troodos ophiolite defined the basic terminology used in this study (Constantinou and Govett, 1972; Robertson and Hudson, 1973; Robertson, 1975; Robertson, 1976).

	1	2	3	4	5	6	7	8
Mn wt%	1.6	11.2	12.5	2.4	2.9	2.4	2.4	10.9
Fe wt%	44.0	30.7	28.6	11.0	5.3	32.5	37.7	35.3
Al wt%	2.0	1.0	1.7	6.2	6.6	1.0	1.2	1.0
Ti wt%	0.1	1.0	0.1	0.4	0.4	0.1	0.9	0.2
Co ppm	129	133	104	74	57	76	145	85
Ni ppm	336	368	335	152	100	163	130	164
Cu ppm	803	1400	1180	421	280	1180	1200	1180
Zn ppm	467	381	404	414	306	289	386	301
V ppm	886	689	613	152	189	1493	1490	597

Table 2.3 Average compositions of Tethyan ferromanganoan deposits. Data: (1) Basal pale brown metalliferous sediment; (2-3) Dark metalliferous sediment; (4-5) Uppermost grey metalliferous sediment; (6-7) Brown metalliferous sediment; (8) Dark metalliferous sediment (Robertson and Hudson, 1973)

The Cyprus metalliferous ferromanganoan sediment has been classified under the general headings of umber and ochre (Table 2.3). Although these terms are generic, the difference between the two is that ochre is thought to form by subaerial weathering of sulphide ore bodies whereas umber is thought to be a primary pricipitate formed by late stage hydrothermal systems and normal ocean-ridge depositional processes (Constantinou and Govett, 1972; Boyle, 1990). Oman sediments are comparable to the Cyprus metalliferous sediments in their relationship to sulphide ore-bodies: they are located on the upper surface of the volcanic basement which formed at a Tethyan ocean spreading ridge system at some distance from the closest ore-bodies which may or may not be genetically related to them. The Cyprus evidence suggests that metalliferous sediment is the product of the last stages of sea-floor spreading-related volcanism (Robertson and Hudson, 1973; Robertson, 1975). The Cyprus metalliferous sediment is also commonly found in hollows and voids in the top surface of lower lavas beneath the upper pillow lavas, suggesting that formation of the Cyprus metalliferous sediment postdated the final spreading event volcanic stages (Robertson, 1975). This is entirely consistent with the evidence presented in this study of the Oman sediments.

2.3.4 End-member component mixing

It will be assumed that the bulk composition of metalliferous sediments, such as those described above, can be regarded as the sum of the contributions of a metalliferous sediment of individual *fractions* (Krisnaswami, 1976). It is one of the stated aims of this project to determine whether this is a valid assumption or not. Each fraction may be further subdivided into a number of sediment-forming *components* which are represented as inter-element relationships or *chemical signals.* By adopting this framework, this study proposes to relate bulk metalliferous sediment geochemistry to multi-source chemical signals. This technique has previously been adopted in studies of recent metalliferous sediments formed at rise-crest and off-axis locations (e.g., Krisnaswami, 1976; Dymond, 1981; Leinen and Pisias, 1983; Cronan *et al.,* 1991), but has not previously been applied to ancient metalliferous sediments.

Broad compositional ranges of metalliferous sediments have been explained as a function of contributions from individual fractions by Krishnaswami (1976). From studies of recent metalliferous sediments, and studies at active seafloor

hydrothermal sites, it is thought that the fractions result from mixing of elements from at least five different sources at or near to the lava-seafloor interface (Dymond, 1981). Using whole-rock chemistry, end-member component models have been successfully applied to recent metalliferous sediment data (Dymond, 1981; Leinen and Pisias, 1984; Miller and Cronan, 1994).

The basic end-members which will be considered are as follows: (1) detrital weathering products, primarily from continental erosion; (2) hydrothermal precipitates from solutions produced by interaction of sea-water and the recently emplaced oceanic crust; (3) biogenic precipitates produced by planktonic organisms fallen to the sea floor; (4) hydrogenous ferromanganese precipitates which are accumulating everywhere in the ocean at very slow rates; (5) Ba-rich dissolution residue remaining from the dissolution of planktonic organisms (Dymond, 1981; Leinen and Pisias, 1984).

2.4 Mineral paragenesis: X-Ray Diffraction analysis

X-Ray Diffraction (XRD) analysis has been carried out for selected bulk rock samples (Table 2.4). By using this technique it is intended to clarify the basis of the sediment building blocks which will be identified using the chemical leaching experiment and numerical modelling techniques in the following Chapters. Using XRD, the lithogenous components are particularly well differentiated from the Fe-oxides which comprise the bulk of the sediments.

Two minerals characterises every metalliferous sediment sample, regardless of volcanic stratigraphic location, these are: (1) α-quartz, identified by its strong peaks at 2.326Å and 4.230Å and weaker at1.817Å and 2.455Å; and (2) hematite, with strong peaks at 2.691Å and 1.692Å and weak at 2.515Å and 1.841Å.

Goethite is present in only two of the samples examined, which is comparable to the findings of Karpoff *et al.* (1988). Goethite and Fe-oxyhydroxides are both found in modern pelagic metalliferous sediments, and therefore are to be expected in ancient analogues. Previous studies of metalliferous sediment from Oman have identified greater abundance of goethite than in this study (Robertson and Fleet, 1986). The XRD evidence of this study suggests that goethite has been largely converted to hematite by burial diagenesis and oxidative metamorphism. The two samples in which goethite is found probably represent recent subaerial

weathering of the ancient deposits which has resulted in a "reconstructive dissolution re-precipitation" reaction (Schwertman and Taylor, 1977).

Sample	1	2	3	4	5	6	7	8	9	10	11	12	13	14	15	16	17
α-Quartz	☑	☑	☑	☑	☑	☑	☑	☑	☑	☑	☑	☑	☑	☑	☑	☑	☑
Hematite	☑	☑	☑	☑	☑	☑	☑	☑	☑	☑	☑	☑	☑	☑	☑	☑	☑
Goethite	☑										☑	☑					
Pyrite														☑	☑	☑	
Nontronite			☑	☑		☑	☑					☑					
Mn oxyhydroxides																	
Lithiophorite	☑	☑		☑	☑	☑	☑		☑	☑	☑			☑			
Cryptomelane			☑	☑													
Manganite	☑					☑	☑										
Carbonates																	
Calcite	☑	☑	☑	☑	☑	☑	☑	☑	☑	☑	☑			☑			
Huntite	☑	☑		☑		☑	☑					☑	☑				
Ankerite	☑	☑				☑		☑						☑			
Volcanic minerals																	
Pyroxene		☑	☑														
Plagioclase	☑			☑	☑	☑	☑										
Epidotes																	
Peimontite			☑								☑			☑			
Epidote			☑	☑	☑	☑	☑										
Clinozoisite			☑			☑											
Apatites																	
Apatite														☑			
Carbonate-apatite			☑		☑												

Table 2.4 Mineralogy of selected subset of Oman metalliferous sediments using XRD analysis. ***Samples: (1-8) As/Bu - 20635, 20641, 20643, 20654, 20668, 20669, U82, 20662; (9-12) Bu - 20660, 20691, 20694, 20695; (13-17) As/Ls - 20601, 20602, 20680, U11, U55.***

The manganese minerals detected by XRD are commonly cryptomelane or lithiophorite. These are found mainly in the samples taken from the As/Bu boundary, but only in three of the samples from As/Ls boundary. The Mn

mineral is manganite in three of the As/Bu Group samples, (20635, 20669 and 20662).

Three carbonate minerals have been detected: calcite $CaCO_3$, ankerite, $Ca(Fe, Mg)(CO_3)_2$, and huntite, $Mg_3Ca(CO_3)_4$. Calcite dominates the samples taken from the As/Bu boundary. Of five of the samples especially enriched in calcite, one is from the As/Ls boundary and four are from the As/Bu boundary. The Fe and Mg rich carbonates are more commonly found at the As/Ls boundary.

Metasomatic events which have affected the lava sequence have resulted in metamorphic mineral phases in the metalliferous sediments. Epidotization throughout the sample set is the result of metasomatism of the whole lava sequence. Apart from one example of piedmontite (Sample: 20643), the Fe-Mn rich epidote, the metamorphic minerals are either epidote or clinozoicite. The occurence of piedmontite has been shown by SEM-Tracor determination to infill the internal moulds of radiolarians in lower lava of the Oman ophiolite (Karpoff, *et al.,* 1988). Of the eight samples analyzed from the As/Bu boundary, seven are found to be epidotized, compared to two of the six taken from the As/Ls boundary. The difference may indicate greater protection from circulating metasomatic fluids by early lithification as a consequence of more rapid baking by fresh overlying lava of the As/Ls compared to As/Bu boundary deposits.

Possible volcaniclastic input is evident in a small number of samples from the presence of pyroxene or plagioclase which may have originated from submarine erosion of the the local lava rather than from terrestrial detritus.

Accessory phases present include scarce apatites and even less commonly, pyrites. In samples, 20601, 20602 and U80 from the As/Ls boundary, accessory pyrites is detected. The presence of pyrites indicates either that unusually anoxic or reducing conditions prevailed which prevented the oxidization of the sediments; or that the sediments were formed in closer proximity to hydrothermal vents. The apatites and carbonate-apatites, seen in three of the samples, may be detrital or due to hydrothermal input or may imply that the phosphates were introduced into the sediments by their interaction with interstitial waters and lava under reducing conditions (Karpoff, *et al.,* 1988).

Difficulties remain in X-Ray diffraction analysis of these samples. For example, the metalliferous sediments consist of high but variable amounts of amorphous iron and manganese which cause the background diffraction level to rise sharply

and remain high. To examine the apparently amorphous Fe and Mn material, the colloidal portion causing the analytical problems must be separated off and discarded, allowing for the remainder to be reanalysed. To do this, samples have been placed in a 100ml beaker of distilled water, agitated, and the water decanted off, the denser material having settled out. The water containing the remainder of the sample in suspension was then evaporated off leaving particles of sample on a glass slide previously placed in the bottom of the beaker. X-Ray analysis of this material showed some samples contained nontronite ($Na_{0.3}Fe_2SiO_4O_{10}(OH)_2.xH_2O$) which was identified by its main peaks at 15.2Å and 4.48Å and by its high background values.

In summary, the X-Ray Diffaction (XRD) analysis identifies silica, haematite, nontronite and Mn-oxides plus a mixture of minor lithogenous and carbonate minerals.

2.5 Major Element Geochemistry

This section uses 14 selected bivariate and ternary plots of major element data to place the Oman sediments in the context of previous classification schemes. The framework on which this interpretation of marine sediment is based is that they represent the sum of contributions from a number of different but identifiable "building blocks". This technique is developed in this study from the successive studies of recent pelagic sediment (Chester and Messiha-Hanna, 1970; Krishnaswami, 1976; Dymond, 1981; Li, 1981; Leinen and Pisias, 1984; Chester, 1990). So long as the original source components were not in themselves of variable composition, inter-element correlation may be interpreted in terms of variation of a small number of measureable components (Toth, 1980; Dymond, 1981; Marchig *et al.,* 1982; Leinen and Pisias, 1984; Boyle, 1990). Pelagic sediments are thought to consist of authigenic and detrital components which may be recognized using whole-rock data as multiple-component signals. Hydrothermal input and incorporation of a biogenic component are considered in addition to the authigenic and detrital components.

The major element chemistry of the inter-lava sediments from Oman is comparable to metalliferous sediments from the Oman and other ophiolite terrains (Fleet and Robertson, 1976; Lippard *et al.,* 1976; Karpoff *et al.,* 1988). The metalliferous sediments have previously been classified on the basis of their field relationships, ore mineralogy and the Fe, Mn and Al content. Al_2O_3, Fe_2O_3

and MnO are summarized below (Table 2.5) with comparable analyses of ochre and metalliferous sediments from the Troodos ophiolite.

The data above show: (1) the geochemical similarity of the Oman ferromanganoan sediment to the Cyprus metalliferous sediment; and (2) the distinction of both types of metalliferous sediment from ochre and the other oceanic sediments. Despite this, the data also show that there are geochemical differences between the two ophiolites and between samples from different volcanic stratigraphic locations within the Oman lava pile. The average Cyprus composition is higher in Fe and Mn content then the Oman metalliferous sediment in this study whereas Al contents are similarly low in both cases.

		Al_2O_3	Fe_2O_3	MnO
1.	Axis	2.16	29.28	8.92
	Axis/Lasail	2.96	33.03	1.44
Oman	Lasail	4.68	36.85	0.58
metalliferous	Basal Upper	4.52	22.10	7.65
sediment	Axis/Basal Upper	4.25	22.58	8.47
	Average	4.11	28.97	5.41
2. Cyprus metalliferous sediment		2.80	46.30	12.60
3. Cyprus metalliferous sediment		2.87	40.00	21.00
4. Brown ochre		2.38	49.40	1.79
5. Orange-yellow ochre		1.72	62.20	1.28
6. Red-yellow ochre		2.19	78.00	0.60
7. Red hematitic ochre with suphides		0.62	54.30	0.06
8. Iron-rich Cyprus mudstone		4.35	39.89	9.18
9. Radiolarian mudstone		9.45	7.29	1.66
10. Average deep-sea clay		15.87	9.29	1.06
11. Average deep-sea carbonate		2.78	1.29	0.16
12. Average Pacific clay		-	7.29	0.76

Table 2.5 Average Al_2O_3, Fe_2O_3 and MnO contents in ferromangoan sediments. Data: (1) this study; (2-7). Constantinou and Govett, (1972); (8-12) Robertson and Hudson, (1972).

A basic twofold subdivision of the dataset by volcanic-stratigraphic position is apparent from Fe and Mn contents (Table 2.5) and in the whole-rock data (Appendix B). The Bu and As/Bu samples are characterised by high MnO-

content (av.7.65 wt% and av.8.47 wt%) whereas Ls and As/Ls samples are characterised by low MnO-contents (av. 0.58 wt% and 1.44 wt%).

2.5.1 Frequency distribution of the elements Fe and Mn

The frequency distribution (Figure 2.5) of the two key elements, Fe and Mn, illustrate three aspects of the major element analyses. First, (Figure 2.5) the frequency distribution of Fe_2O_3 in the Bu and As/Bu samples shows a Gaussian distribution about the mean values of 22.1 wt % and 22.58 wt % respectively. This is in contrast with the asymmetry shown about the mean by the As/Ls and Ls samples. The As/Ls boundary, from which 87 samples are analysed, shows an asymmetric curve from its peak in the 20.00-20.99 wt% Fe_2O_3 category to a maximum value of 75.4 wt% in sample U12 from the Lasail mine (south). Second, the As/Ls and Ls sample have a different frequency distribution of MnO to Bu and As/Bu samples. The latter are normally distributed about the mean 6-10 wt% whereas the former have a secondary peak at between 8.00-10.00 wt% in addition to the distribution about the mean of 0.00 to 0.99 wt%. Third, the number of samples obtained from the Axis unit and from the Lasail unit are insufficient to allow statistically valid interpretation of average data. Despite this, the samples were obtained by systematic sampling of the location in the northern Oman mountains at which ferromanganoan sediment outcrops and the number of samples reflects the relative importance and volume of deposits.

The frequency plots overleaf suggest that the data may be split into two chemically distinct groups which are as follows:

FeMn-rich	-	to include As/Bu and Bu samples
Fe-rich, Mn-poor	-	to include Ls, As and As/Ls samples

2.5.2 Bivariate and Ternary Relationships

The aim of this Section is to categorise the sediments in relation to previous classification schemes and to suggest which end-member components may be applicable to test the proposed mixing models.

Figure 2.5 Frequency distribution Diagrams

Histograms of iron values showing frequency distribution of Fe_2O_3 in metalliferous sediments from Oman

Histograms of manganese values showing frequency distribution of MnO_2 in metalliferous sediments from Oman

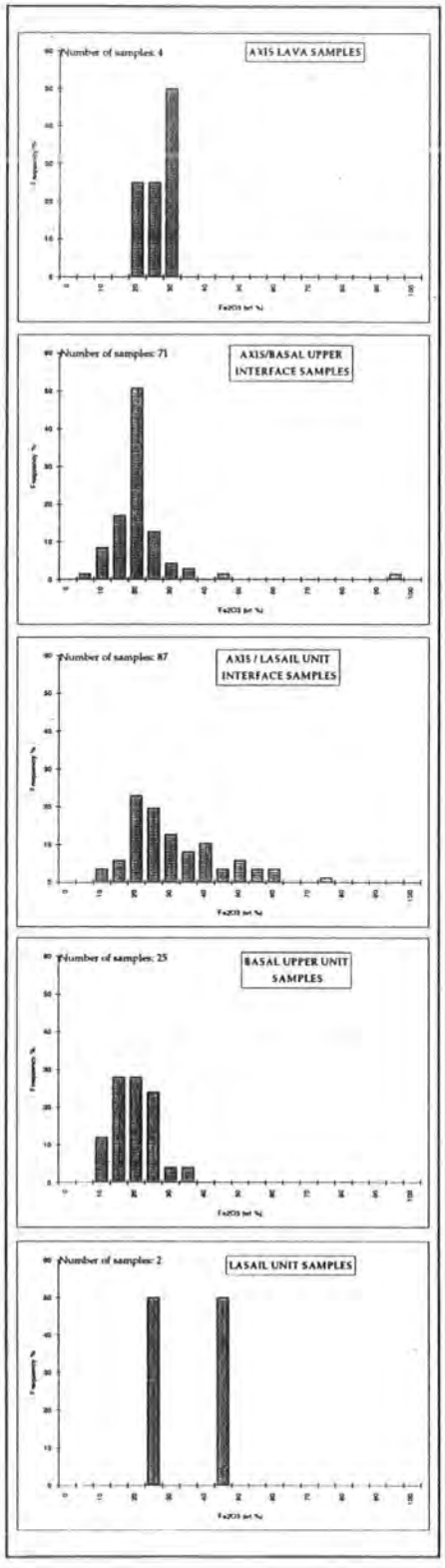

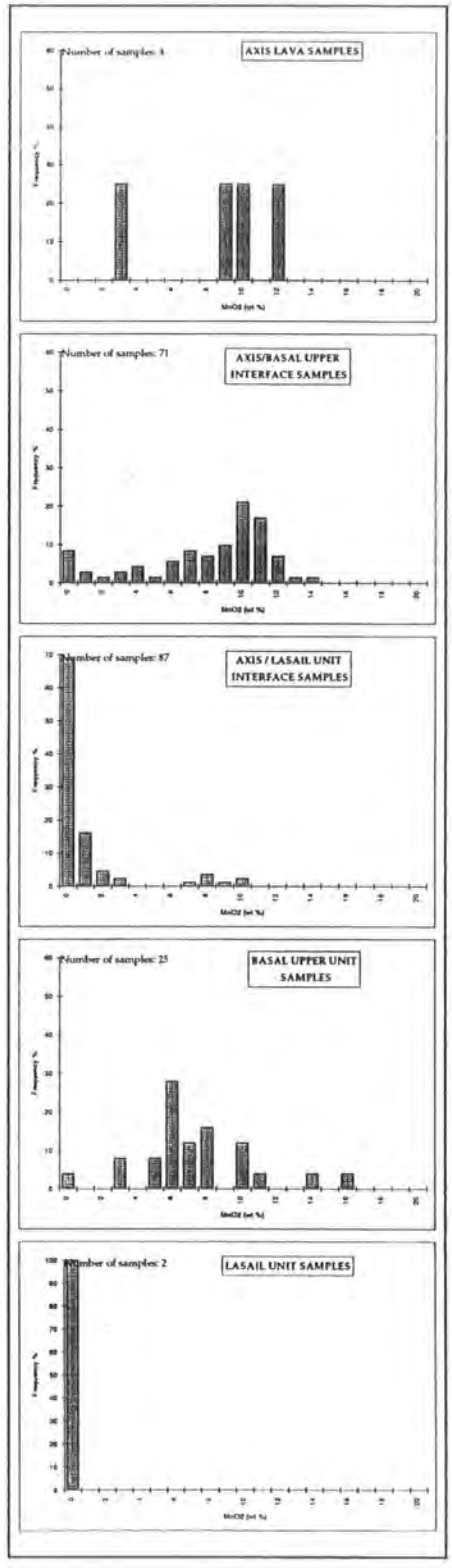

2.5.2.1 The Bonatti diagram

The ternary diagram of Fe_2O_3 - MnO - (Co + Ni + Cu), Figure 2.6, from Bonatti *et al.,* (1972), is frequently used in the literature to distinguish between hydrothermal and hydrogenous sediments. This diagram operates on the principle that hydrothermal sediments are trace element depleted relative to hydrogenous sediments. The Oman samples plot entirely within the defined hydrothermal field and outside of the field into which hydrogenous samples, Fe-Mn crusts or Mn nodules appear (Bonatti *et al.,* 1972; Toth, 1980; Robertson and Varnavas, 1992). Despite plotting within the hydrothermal field, the details of the origin of the Oman samples remain unclear from this diagram. The reason for this is that, on the Bonatti diagram, the Mn-apex is occupied by both hydrothermal and diagenetic deposits, (Cronan *et al.,* 1991). Nevertheless, Figure 2.6 suggests that the mixing of two components on the dilution line connecting the Fe-apex to a Mn-rich end-member.

2.5.2.2 Fe_2O_3-SiO_2-MnO ternary relationships

The data are plotted to show ternary relationships between Fe, Si and Mn for the purpose of comparison with (1) analogous ancient deposits from Cyprus (Figure 2.7) and (2) modern analogues from Galapagos and EPR (Figure 2.8). This diagram has also been used previously to evaluate compositional variability of sediment-forming components, particularly of hydrothermal components.

2.5.2.2.1 Ancient analogues

Figure 2.7 shows the relative content of Fe, Si and Mn of the deposits. Superimposed onto the plot are a number of fields defined from ancient sea-water hydrothermal systems. The two trend lines expressed on Figure 2.7 confirm the bimodal subdivision of the Oman data according to volcanic stratigraphic position: As, Bu and As/Bu samples plot on a linear trend from the Si-apex to an Fe-Mn component whereas Ls and As/Ls samples plot solely on a mixing line between Fe and Si components.

There is a continuous range of Fe/Mn variation between samples falling on the Fe-Si mixing line and those falling on the $Fe\text{-}Si_{55} : Mn_{45}$ mixing line, thus:

(1) The As/Ls samples are principally compositions between a Si-rich end-member and an Fe-rich end-member.

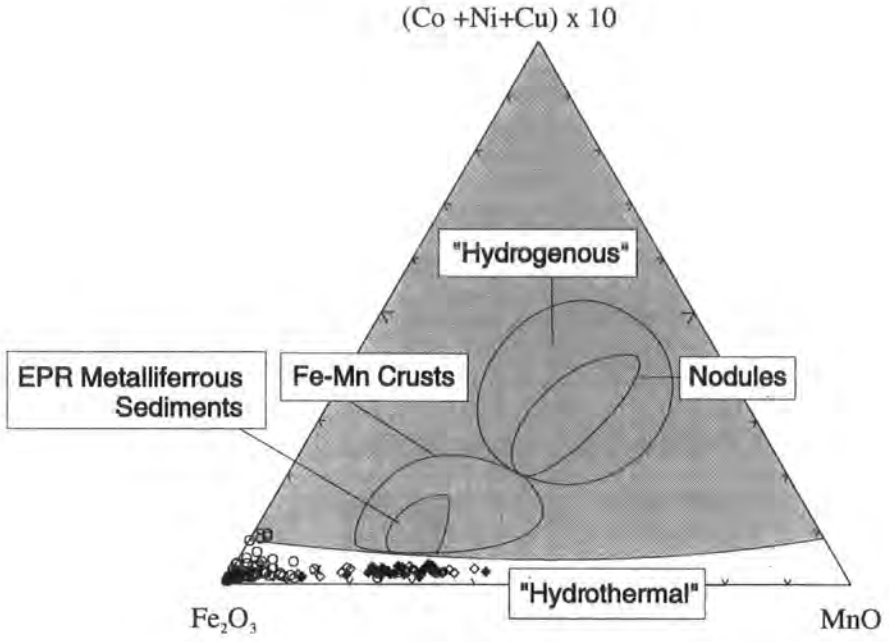

Figure 2.6 Ternary diagram of Fe2O3 versus MnO versus (Co+Ni+Cu)x10. "Hydrogenous " and "Hydrothermal" fields defined by Bonnatti et al., (1972), EPR metalliferous sediment field by Corliss and Dymond, 1975, and Fe-Mn nodules field by Toth, 1980.

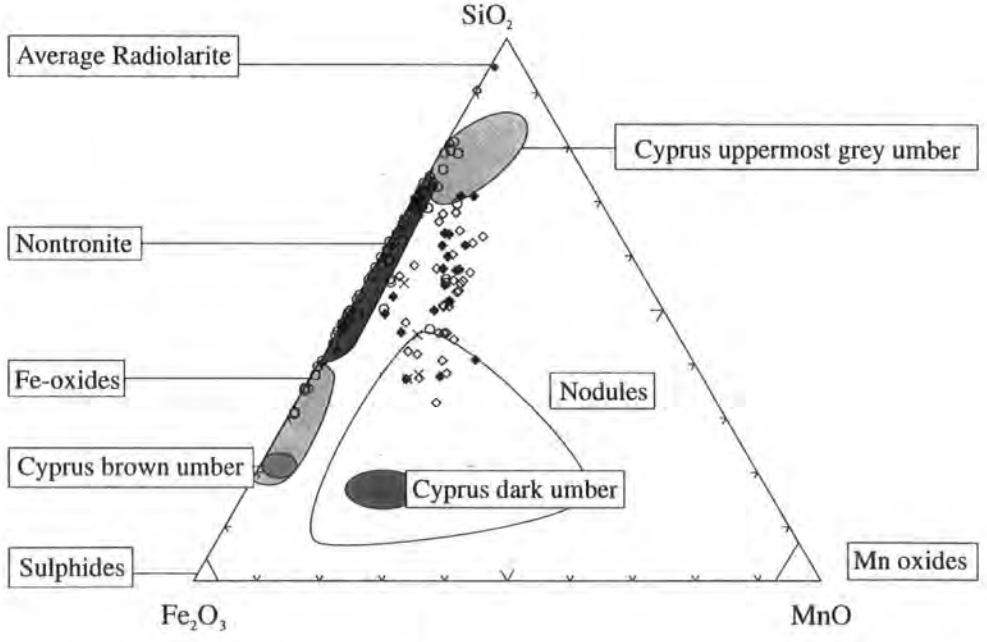

Figure 2.7 Ternary Fe_2O_3-SiO_2-MnO plot of Oman metalliferous sediment. Cyprus data: Robertson and Hudson (1973); Nodule data: Toth (1980)

(2) The As/Bu group represents mixing between a Si-rich end-member and either an Fe-Mn component of relatively fixed proportions or with a Fe-component and Mn-component. If the latter is the case the straight mixing-line indicates that the relative proportions of the three components varied only in (Fe + Mn)/Si.

(3) The As and Bu groups exhibit variable Fe/Mn ratios between the other two trend-lines on the diagram.

Mean compositional values of the Cyprus metalliferous sediments fall on the two mixing trends set by the Oman sediment. All but one Cyprus locality (Boyle, 1990) fall on the similar Mn-rich trend as the As/Bu and Bu Group Oman sediments. Metalliferous sediment from Skouriotissa, Kambia, Margi, Mathiati, Analiondas, Dhrapia, and Kalavasos follow the mixing line between SiO_2 and a mixed Fe-Mn component. In contrast, the samples from Mangaleni (Cyprus) plot on the mixing line between SiO_2 and a pure end-member Fe_2O_3 component. This is similar to the As and As/Ls data in this study.

In the Oman data, the Fe-Mn end-member is geochemically different to the Fe-Mn end-member of the Cyprus data (Figure 2.8). The difference between Cyprus data (Boyle, 1990) and the Oman sediment is in the higher ratio of Mn:Fe in the Mn-rich sediment of Oman:

Cyprus - mix between SiO_2 and $Fe_{70}Mn_{20}$ to $Fe_{90}Mn_{10}$ component
Oman - mix between SiO_2 and $Fe_{80}Mn_{20}$ to $Fe_{60}Mn_{40}$ component

Data from this study overlaps the Cyprus-defined (Boyle, 1990) mixing line but also this study includes more Mn-rich deposits. This is significant because of the trace metal association with the Mn-component. The early published data (Robertson and Hudson, 1973) defined the fields of *brown umber* and *dark umber* which fall on the Si-Fe and Si-Mn mixing lines respectively. In contrast with Oman sediments, the Cyprus metalliferous sediment has a more restricted compositional range. This is especially true of the Si content. The brown and dark umber fields are lower in Si content than any examples of metalliferous sediment from Oman.

The range in Si-content of the Oman sediments is probably explained by variation in the abundance of biogenic opal, or hydrothermal Si input. Cyprus

metalliferous sediments characteristically have SiO_2 values of less than half those contained in the Oman sediments, (Varnavas, 1981; Boyle, 1990).

2.5.2.2.2 Modern analogues

The Oman data may be compared with modern metalliferous ferromanganoan sediments on the Fe-Si-Mn ternary diagram (Figure 2.8) (data from: Bonatti *et al.*, 1971; Dymond *et al.*, 1973; Robertson and Hudson, 1973; Corliss *et al.*, 1978; Toth, 1980; Dymond, 1981).

In Figure 2.8 mixing between pure-Fe and pure-Si end members explains the sulphide, Fe-oxide and nontronite fields. Mixing between pure-Si and an Fe-Mn component results in Fe-oxyhydroxides, notably in modern samples from Famous, NAZCA surface rise crest, Galapagos mound Fe-oxides, and the ancient average Cyprus metalliferous sediment.

The As/Bu and Bu samples fall almost exactly on the field of the Nazca rise-crest samples (Dymond, 1981), the average Galapagos Mound Fe-oxides and the average FAMOUS trend. This represents mixing between pure Si and an FeMn-component. The variability of Si content shown by the Oman data is comparable to that of Nazca plate metalliferous sediments.

The As/Ls and Ls samples fall within the nontronite field which represents mixing between pure silica and pure iron components. None of the samples in this study is sufficiently rich in Fe to fall within the Fe-oxide field defined by Dymond (1981).

The pattern described above reflects bimodality in the data. Samples may be subdivided as follows: (1) those similar to nontronites; and (2) those similar to Nazca rise crest samples. The suggested subdivision also coincides with the subdivision by volcanic stratigraphic position. The implication is that the geochemical differences between Mn-rich and Mn-poor samples result from spatial or temporal differences in the relationship of the sediment to the vent during their formation. A few exceptions are observed which may be used to infer that the processes governing the type of deposit was produced overlapped in some way. The As/Ls (Lasail Mine) samples U56C, U73, U75, U76, U77 and U79 and (Mahab #2) samples 20641, 20642, 20643 and 20644 are atypically Mn-rich and the As/Bu samples (Khabiyat) 20669, (Aarja Mine) U80 and U81 and (Huwayl) 20682, 20683 and 20684 are atypically Mn-poor.

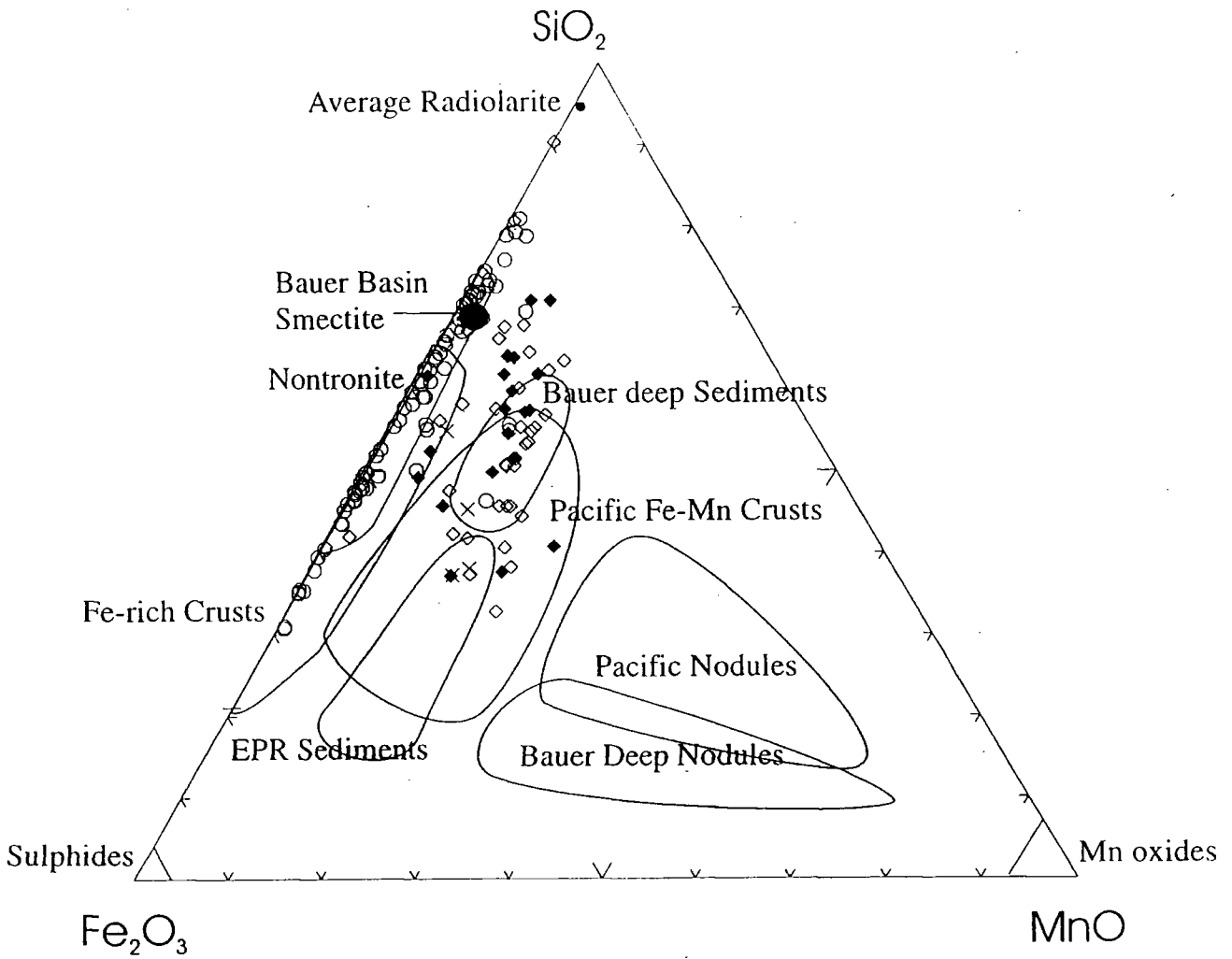

Figure 2.8 Ternary Fe_2O_3-SiO_2-MnO plot of Oman metalliferous sediment. Including fields for recent ferromanganoan sediments (After: Toth, 1980; Karpoff *et al.*, 1988)

2.5.2.2.3 Nazca surface rise-crest trend: Mn-rich metalliferous sediment

The mixing line of the Mn-rich trend following the Nazca surface rise-crest trend (Dymond, 1981); and that of the Dark umber (Robertson and Hudson, 1973) represent the variable mixing of a pure siliceous component with a component of relatively constant Fe-Mn ratio. The source of Mn in marine sediments may be inferred from the concentrations of that element in deep-sea deposits (Chester and Aston, 1976):

The average Mn-contents from recent marine sediments (Table 2.6) suggest that hydrothermal active ridge sediments and ferromanganese nodules are the most important Mn-sources, i.e., hydrothermal activity and hydrogenous precipitation from sea water are the most important means of incorporating Mn into the sediment. Consequently, the Mn-rich metalliferous sediment probably differs from the Mn-poor metalliferous sediment as a result of differences either in hydrothermal or hydrogenous processes. It is possible to suggest that the typical Mn-rich metalliferous sediment differs from the Mn-poor metalliferous sediment because of: (1) proximity to venting; (2) the existence of two different hydrothermal systems; (3) different sedimentation rates causing differences in hydrothermal : hydrogenous input. Because the sediments are thought to be dominantly hydrothermal in origin, it is unlikely that deposition rates vary sufficiently to affect the relative proportions of hydrogenous input. Variation in the intensity of the hydrothermal input is the most likely means by which sediments are more or less Mn-enriched.

	Mn ppm
Near shore mud	850
Deep-sea carbonate	1000
Atlantic deep-sea clay	4000
Pacific deep-sea clay	12,500
Active ridge sediment	60,000
Ferromanganese nodules	220,000

Table 2.6 Average Mn-content of recent marine sediments (Chester & Aston, 1976)

2.5.2.2.4 Nontronite trend: Mn-poor metalliferous sediment

The mixing line between pure Fe and pure Si results in an elongate field along the Fe-Si base line corresponding to Mn-poor metalliferous sediments. On this mixing line are located those deposits with low abundance of Mn and other transition elements, including: nontronite and iron-montmorillonites, (e.g. in Red sea brine deposits, (Bischoff, 1969); and "mound" deposits from Galapagos, (Corliss *et al.*, 1972)). The Fe-sulphides of sea water hydrothermal origin which are characteristic of ophiolite terrains within the basaltic crust appear at the Fe-apex (Dymond, 1981).

Mn-poor samples from Oman demonstrate the variable dilution of pure hydrothermal Fe-sulphide by Si (probably biogenic opal or hydrothermal silica) and also overlap the nontronite field. In Section 2.4, XRD analysis showed that all samples contained a small quantity of nontronite ($Na_{0.3}Fe_2SiO_4O_{10}(OH)_2.H_2O$). In all of the Mn-poor metalliferous sediment samples, hematite and quartz are the dominant phases present. Nontronite formation has been experimentally determined to occur in slightly acidic, mildly reducing conditions with moderate concentrations of Fe (4 to 7.5 ppm) and Si (20 ppm) in solution, (Harder, 1976). In more oxidizing conditions or at higher concentrations of Fe and Si goethite and quartz were found to precipitate. This fits in well with the XRD finding that all the samples analysed from the Si-Fe trend contain quartz and hematite. Although goethite is present in sample U51, it is likely that primary goethite found in analogous modern metalliferous sediments has been converted by burial diagenesis and oxidative metamorphism to hematite in a "*reconstructive dissolution-reprecipitation reaction*" (Schwertman and Taylor, 1977).

It is likely that Mn-poor samples are mixtures of at least two end members, one being pure Si, the other being pure Fe, and that there was variability in the Fe and Si concentrations, temperature and pH during formation of the samples from hydrothermal fluids. The high SiO_2 content relative to the Cyprus metalliferous sediments may reflect greater hydrothermal input of that element in addition to the incorporation of biogenic silica. The pure Fe-component is likely to be the result of precipitation of Fe as sulphides, nontronite and oxyhydroxides due to sub-sea floor mixing of the hydrothermal fluid with cooler oxygenated bottom water. The result of this is that unmixed hot solutions do not vent directly into sea water so that pure Fe-sulphides are not found (Dymond, 1981).

2.5.2.2.5 Summary: Fe_2O_3-SiO_2-MnO ternary plot

A number of possible processes are suggested which may result in the two mixing lines (Oman and Cyprus metalliferous sediments): (1) that there were primary differences in the composition of the hydrothermal fluid; (2) that there is more than one hydrothermal system present; (3) that proximity to venting causes differences in sediment chemistry.

Evidence from active systems and experimental work supports the first proposition that there were primary differences in the hydrothermal fluid. Temperature change controls the relative proportion of transition metals in hydrothermal solutions, e.g., the Fe/Mn ratio experimentally changes from 1 : 1 at 350° C to 5 : 1 at 500° C, (Biscoff and Rosenbauer, 1989). The primary hydrothermal fluid chemistry is also modified by sub-sea floor mixing of sea water with cooler oxygenated bottom water and by venting of hydrothermal fluids directly into bottom waters (Chester, 1990). Iron sulphides may result from venting of unmixed solutions straight into cooler sea water at the sea floor-sea water interface (e.g., EPR sulphides), whereas sub-sea floor mixing of the hydrothermal fluid will result in precipitation of sulphides, nontronite and oxyhydroxides prior to reaching the vent leading to increasing Mn precipitation and the production of todorokite and birnessite crusts (e.g., in the TAG mounds of the Galapagos). Thus, variation in temperature, pH and mixing of hydrothermal solution may produce the observed differences without evoking end-member component mixing or seperate hydrothermal systems.

The proximity of each Mn deposit to vent areas is known because the distance between the metalliferous sediment to the proximal sulphide ore deposits can be measured. However, there is no evidence to suggest that specific metalliferous sediments are genetically related specifically to any of the gossans. The Axis/Basal Upper sediments often demonstrate the association with numerous small gossans. Whereas the Aarja and Bayda deposits, which have been collected 300m from large gossans. The Axis/Lasail samples also tend to be collected away from the immediate vicinity of large ore deposits. The Aarja and Bayda deposits suggest that the differences between the two mixing trends do not only represent the effects of vent proximity.

Samples from the As/Bu Group on the Si - (Fe + Mn) trend may represent the physical mixing of the nontronite, sulphides, Fe-oxides and Mn-Oxides. This could occur by the dispersal of fine particulate and absorption of Mn on the

surfaces of oxidising dispersing sulphide particles. Physical reworking of sulphide chimneys with pure Mn-oxide (birnessite and todorokite) and other Fe and Mn precipitates followed by redeposition is probably the mechanism to explain homogenisation of a sediment with heightened Mn : Fe ratio. There is strong evidence to suggest that that metalliferous sediments represent physically reworked and redeposited sediments so physical homogenization of the minerals formed by hydrothermal vents is most probable (Robertson, 1975).

Homogenization of the sediments would also explain the presence of the well defined Mn-rich and Mn-poor trends with very few intermediate compositions. Had samples not been reworked, then each deposit ought to contain the compositional aureoles similar to those found in the Atlantis II Deep: sulphides $\Rightarrow$ Fe-silicates $\Rightarrow$ Fe-oxides $\Rightarrow$ Mn-oxides (Cronan, 1976). This is not observed in data from the Oman deposits. The absence of the full compositional range at each locality could be produced by two processes: (1) physical reworking of sediments, or (2) large-scale post-burial metamorphism or remobilization of the transition elements affecting entire deposits.

The physical mixing of the nontronites, sulphides, Fe-oxides and Mn-oxides is suggested by field evidence and by geochemical patterns. Oman and Cyprus metalliferous sediments have well-documented internal laminations and unconformability with underlying basalts (Constantinou and Govett 1972; Robertson and Hudson 1972; Robertson 1975; Robertson 1976). The geochemical pattern suggests that two end-member physical environments co-existed, represented by the As/Ls (Seamount) boundary and the As/Bu (Rifting) boundary. The physical reworking of these sediments has removed the fine-scale spatial compositional zoning around vents, or between vents of slightly different temperatures, resulting in two "average" compositional trends.

The trend of the As/Ls samples suggests that this location may be vent-proximal and have greater hydrothermal-Fe content. Greater Mn-content implies that the As/Bu samples formed at a vent-distal location. Proximal sediments probably result from the mixing of sulphide chimneys with Fe-silicates, nontronite and goethite. Whereas distal sediments may be mixtures of Mn-Oxides (birnessite and todorokite) with Fe-oxides. This model fits in with seamount areas being the centre of hydrothermal activity (Pearce and Norry, 1979; Pearce *et al.*, 1981; Alabaster *et al.*, 1982; Alabaster and Pearce, 1985).

The differences in the Fe:Mn ratio which produce the two trends cannot be due to large-scale post-burial metamorphism or remobilization of the transition elements affecting entire deposits. The reason for this is that in many of the mine locations a number of typical Mn-rich metalliferous sediment samples will be present when the rest of the samples from that horizon in that mine are Mn-poor. For example, samples U76, U77, and U79 from the Lasail Mine (As/Ls) and U75 from Huwayl plot in the metalliferous sediment-group rather than the ochre-group to which the rest of the As/Ls samples from these locations belong. The reverse also occurs: e.g., in Wadi Fizh, the siliceous sample, 20714 plots on the Mn-poor mixing line whereas the rest of the mine belongs to the Mn-rich typical Mn-rich metalliferous sediment trend. In the former, vent-proximal samples seem to show localized characteristics of the distal facies and, in the latter the more distal facies appears to retain some localized evidence of vent processes. This may reflect incomplete homogenization of the sediments.

The variability of the Si-content is also significant on the Fe-Si-Mn diagrams (Figures 2.7 and 2.8). Variability in Si-content is much greater than in Cyprus metalliferous sediments but closely follows the field defined by the NAZCA surface, rise crest samples (Dymond, 1981). This is hard to explain solely using the Fe-Si-Mn diagram since in the case of NAZCA sediments, the variability is thought to represent systematic decrease in Si content away from the equatorial zone of high productivity. This is unlikely to explain SiO_2 variability in Oman metalliferous sediment, which currently is thought to have formed above a mantle-anchored hotspot in the paleolatitude of 10° N (Perrin *et al.*, 1993).

In Figure 2.9, Fe-Si-Mn is plotted by mine location. Where there are sufficient samples to show a pattern, i.e. Huwayl, Wadi Fizh, Khabiyat, Semdah West and Lasail Mine, the full range of SiO_2 variation is present in each mine. The evidence indicates that the distance from a hypothetical high productivity zone cannot a geologically reasonable mechanism for SiO_2 variation. The variation must therefore represent either variable hydrothermal input or variable biogenic Si-input for some reason other than latitudinal variation.

The distribution of opaline Si in deep-sea sediments depends upon different productivities of Si-secreting organisms in the overlying surface waters. Silicate concentration increases by shell dissolution down the water column until it reaches a maximum at c.1000m. This suggests that the Si-component is likely to be added in similar absolute amounts to all areas of the off-axis environment in which the sediments formed. The Si-variability shown

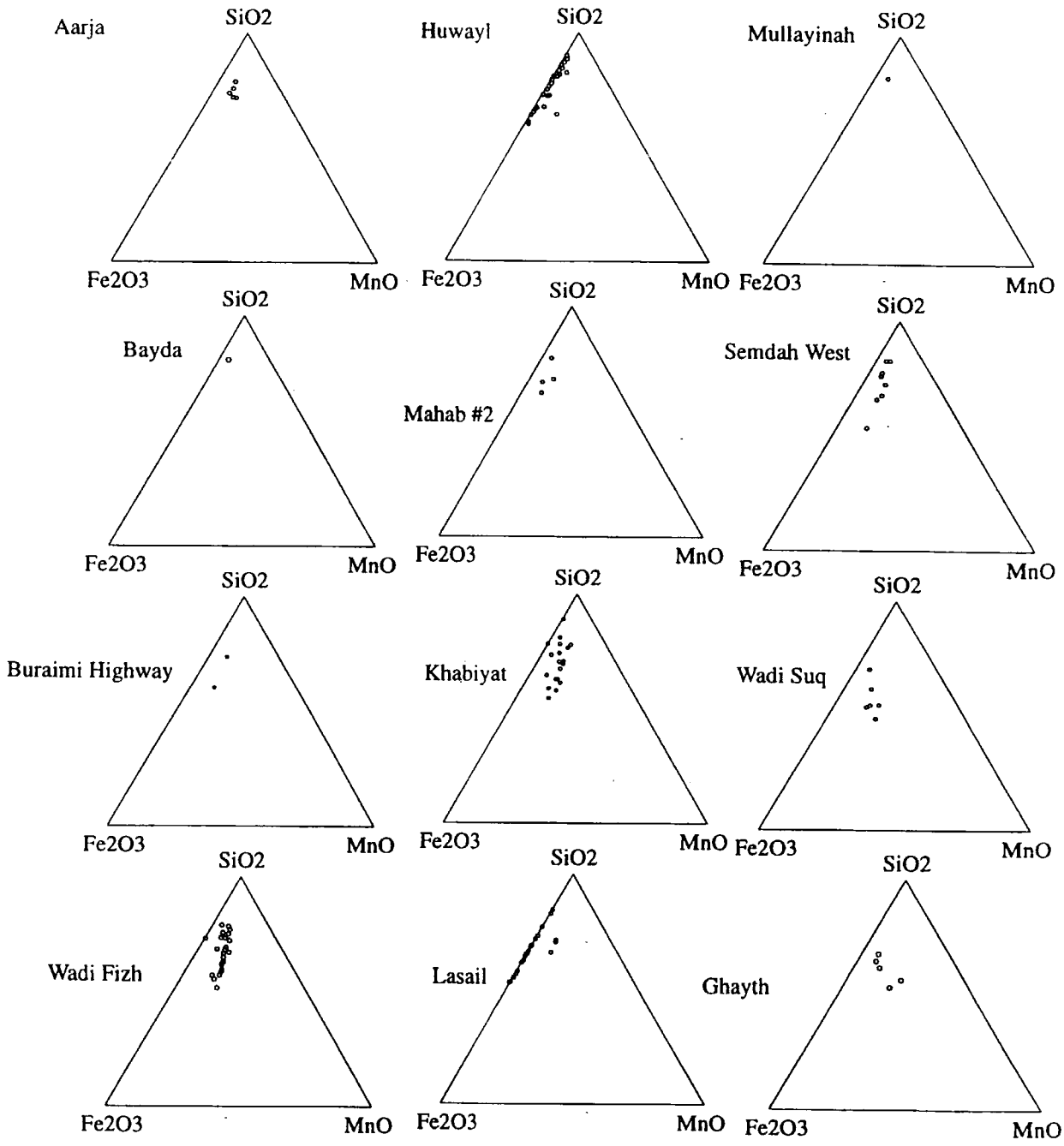

Figure 2.9 Fe_2O_3-MnO-SiO_2 plot of Oman metalliferous sediments by sample location

is likely to be dependent on variations in the proportions of hydrothermal-Fe and hydrothermal-Mn which dilute the Si content.

2.5.2.3 Fe_2O_3-Al_2O_3-MnO ternary relationships

On the Fe_2O_3-Al_2O_3-MnO ternary diagram the Mn-poor group fall on an elongate trend parallel to the Fe-Al axis. An elongate trend exist along the zero Mn base-line and so there is variation in the Fe_2O_3:Al_2O_3 ratio between $Detrital_0$:$Fe\text{-}Oxide_{100}$ and $Detrital_{26}$:$Fe\text{-}Oxide_{74}$. Also, the Mn-rich group plot away from the Fe-Al mixing line in a field of variable Mn-enrichment and variable detrital enrichment. The proportion of Al_2O_3 never exceeds 8.7 wt%. Finally, an intermediate group is present which overlaps the Mn-rich and Mn-poor groups.

The Oman sediment overlaps (Figure 2.10) the Cyprus inter-lava clay-rich umber field (Boyle, 1990). However, this field was not previously subdivided as the Oman data suggests it should be. None of the Oman samples resemble either the high-Al supra-lava clay-rich umber of Skouriotissa, Margi or Kalvasos, or the relatively Al-depleted supra-lava umber from Dhrapia, Analiondas or Skouriotissa.

In this study, the XRD analysis revealed the minor presence of crystalline aluminosilicate minerals (plagioclase, pyroxene and clays commonly kaolinite, illite, chlorite or montmorillonite) which is probably derived from submarine volcanoes, land erosion or submarine weathering. Al is therefore taken as a representative major element of the detrital component.

Rock detritus and the common rock-forming minerals are represented on the AFM diagram by the Al-apex (Figure 2.10). This indicates the relative scarcity of detrital input which either results from deposition in an open ocean environment or by the swamping of detrital input by other components.

Of the sediment included in this study, the As/Ls Group is closest to the Fe-apex. Furthermore, the As/Ls Group are (1) more Fe-rich than any of the Cyprus sediments; and (2) according to the recent classification of Cyprus sediments (Boyle, 1990), dissimilar to any of the Cyprus metalliferous sediments.

The elongate trend, which is apparent at all of the locations, is an indication that relative detrital input varies even within a single sediment horizon from a single sample locality. Using this diagram (Figure 2.10), it is geologically reasonable

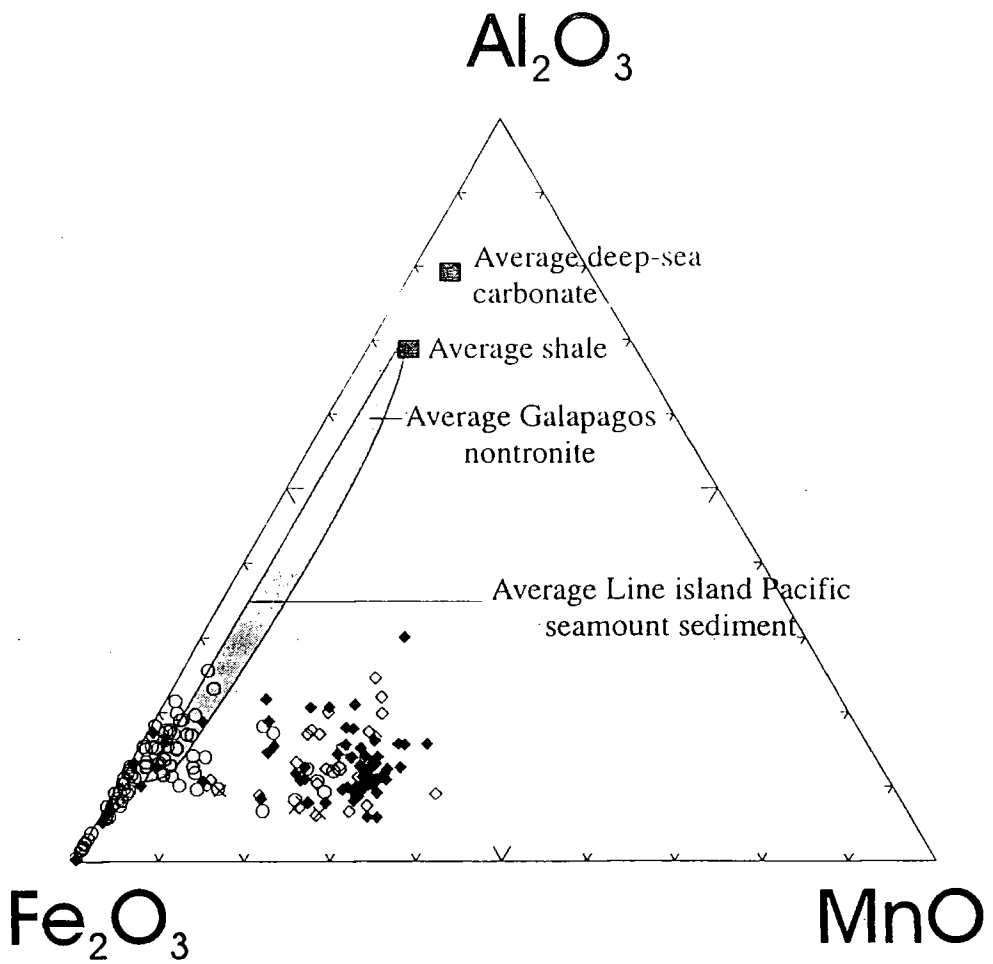

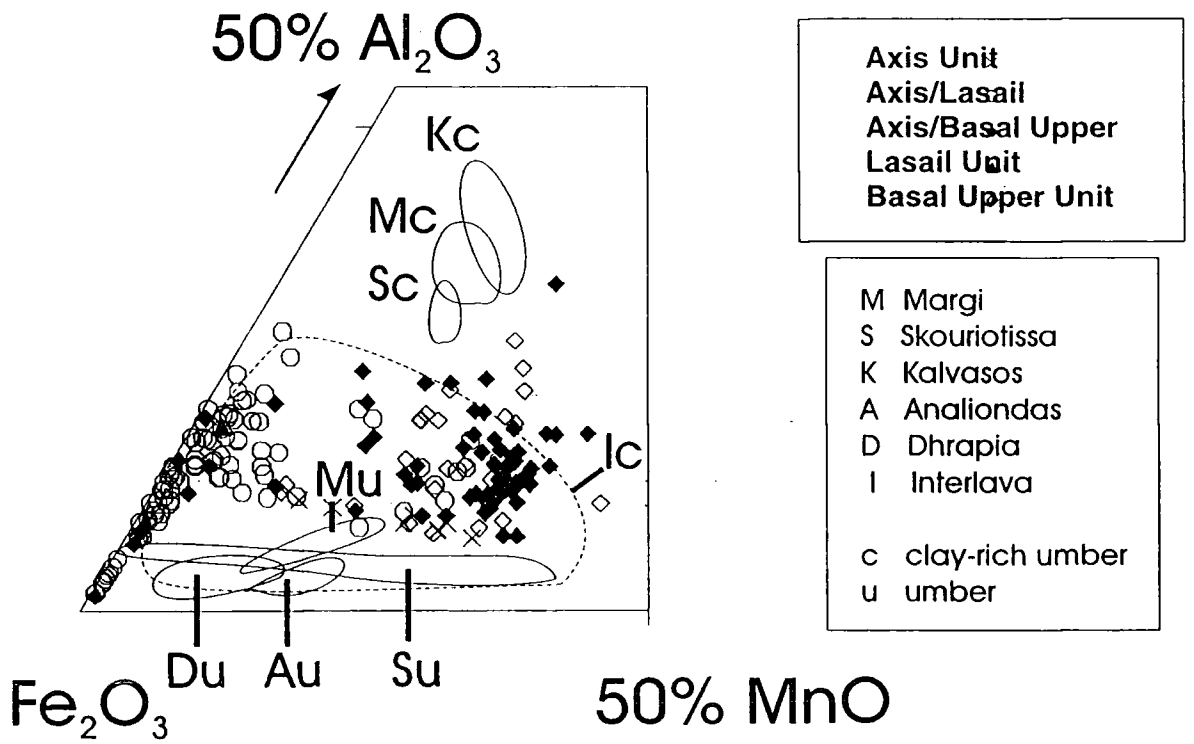

Figure 2.10 Fe_2O_3-Al_2O_3-MnO plot to Compare Oman metalliferous sediments and other ferromanganoan deposits, data from: Robertson & Hudson, 1973; Robertson, 1976; Boyle, 1990; Robertson & Varnavas, 1992)

that variable hydrothermal input is responsible for swamping detrital grains. In all locations and volcanic stratigraphic positions the detrital input forms a small proportion of the sediment. This suggests (1) that Al is supplied to the sediment largely by detrital components; and (2) that Al content directly reflects hydrothermal variations.

2.5.4 Inter-element correlations

The bivariate plots described in this section are intended to illustrate the complexity of the interrelationships between the elements as a result of contributions from individual fractions and mixing of components from at least five different sources at or near to the lava-seafloor interface, (Dymond, 1981; Leinenn and Pisias, 1984; Miller and Cronan, 1994).

2.5.4.1 Hydrothermal element associations

Studies have shown that the major elements Fe, Si and Mn are associated with hydrothermal activity at active ridge environments and that metalliferous sediments are enriched in the elements Fe, Si and Mn relative to deep sea clays (Chester and Aston, 1976; Barrett, 1992; Herzig and Hannington, 1995; Stepanova *et al.*, 1996) (Table 2.7). End-member fluid values for different hydrothermal vents have also now been directly sampled and studied (Table 2.8) (e.g., von Damm *et al.*, 1983, 1985; Rudnicki and Elderfield, 1992; Feely *et al.*, 1996).

On the bivariate plot of Fe_2O_3 versus MnO (Figure 2.11), there is a different correlation between Fe and Mn according to location. This may reflect different hydrothermal processes or systems and affects all of the other interelement relationships. A significant positive relationship exists between Mn and Fe for Mn-rich metalliferous sediment samples, which is in contrast to the negative relationship between Mn and Fe for Mn-poor metalliferous sediment samples (Figure 2.11).

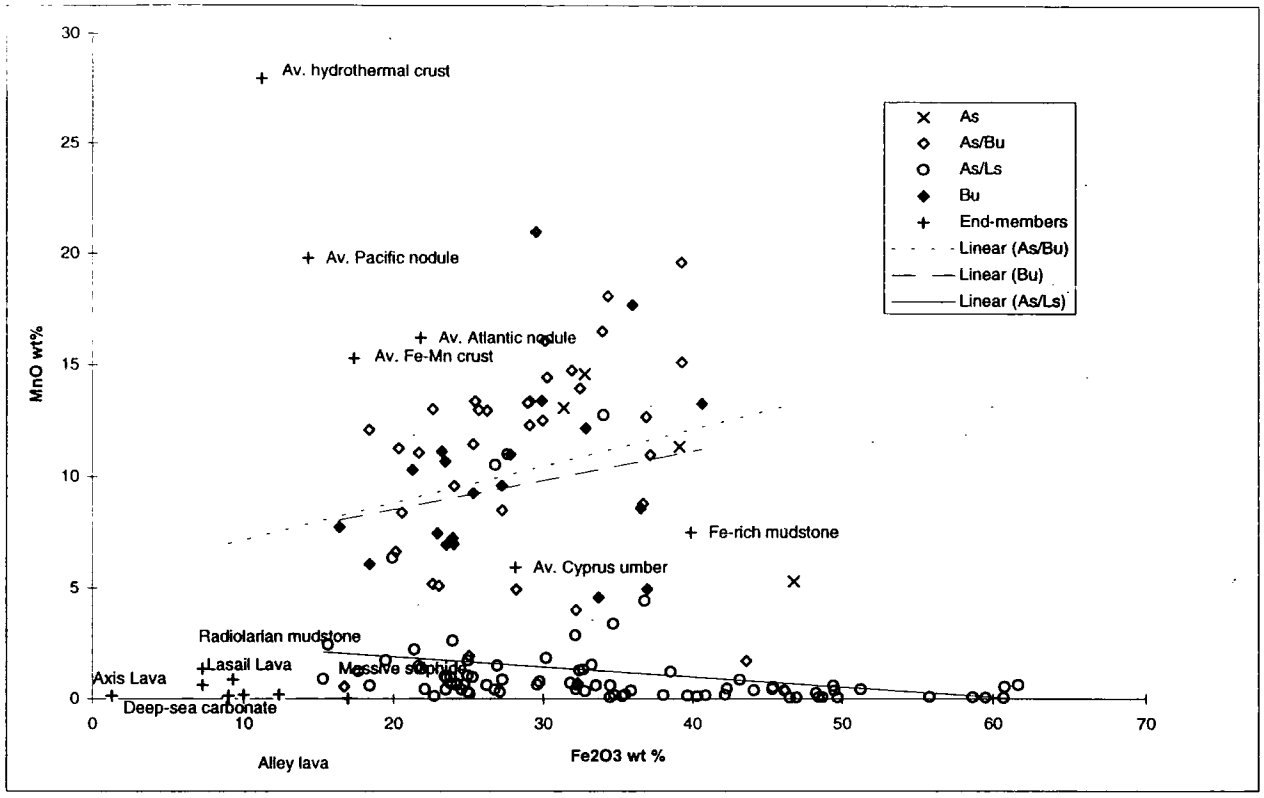

Figure 2.11 Fe2O3 versus MnO diagram. Data from: this study; Alabaster et al., 1982; Boyle, 1990; Chester, 1990

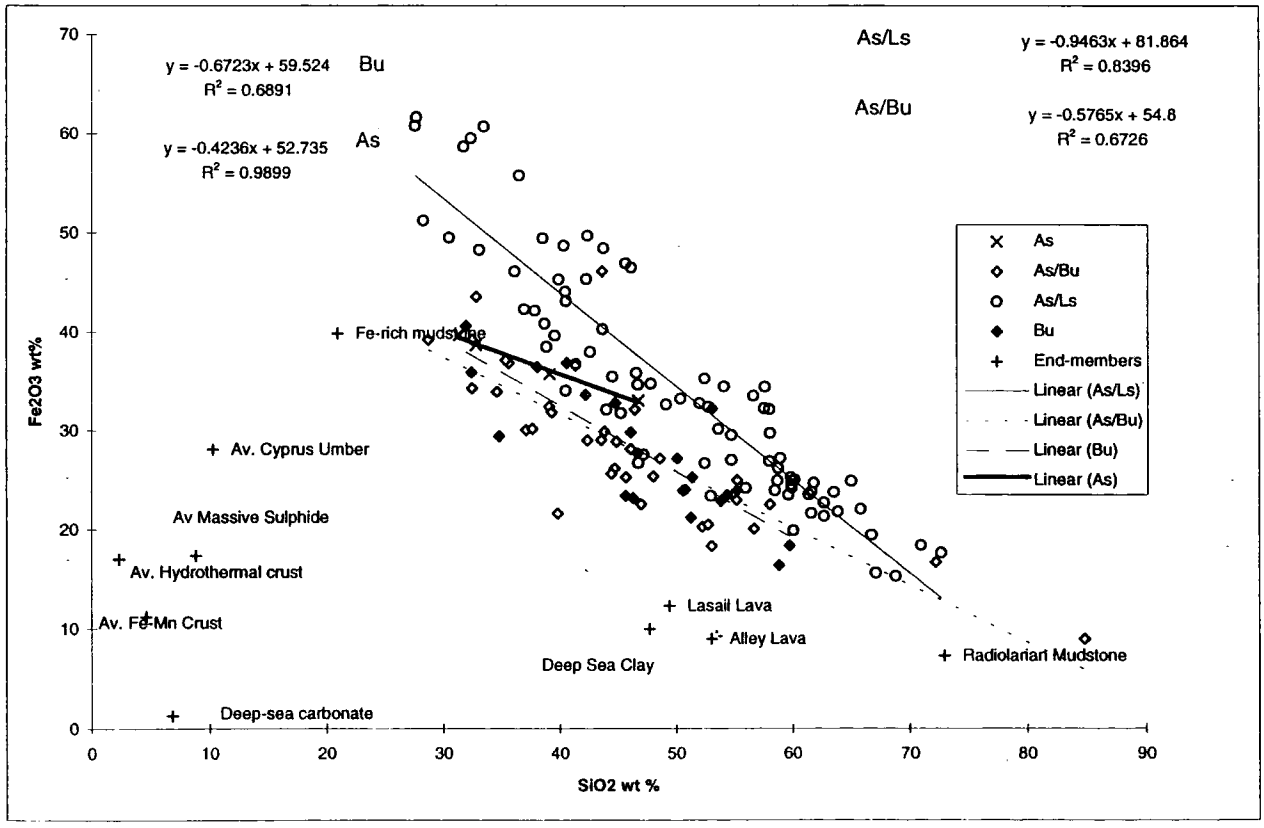

Figure 2.12 Fe2O3 versus SiO2 diagram. Data from: this study; Alabaster et al., 1982; Boyle, 1990; Chester, 1990

	Mn ppm	Fe ppm
Near shore mud	850	69,000
Deep-sea carbonate	1,000	9,000
Atlantic deep-sea clay	4,000	82,000
Pacific deep-sea clay	12,500	65,000
Active ridge sediment	60,000	180,000
Ferromanganese nodules	220,000	140,540

Table 2.7 Mn and Fe content of marine sediments. Data: Chester and Aston, 1976

	Mn ppm	Fe ppm
Standard seawater	<0.01	<0.01
EPR 13°N-21°S	3,610 - 29,320	6,000 - 101,000
Guayamas	1,280 - 2,360	80 - 1,800
Juan de Fuca Ridge (S)	26,100 - 44,800	103,000 - 187,000
MAR 23°N-26°N	4,430 - 10,000	16,400 - 21,800
Lau Basin	58,000 – 71,000	12,000 - 29,000

Table 2.8 Mn and Fe content of hydrothermal fluids. Data: von Damm *et al.*, 1985.

The inference is that the hydrothermal component in As, As/Bu and Bu samples is ferromanganoan whereas the hydrothermal component in As/Ls samples is ferrous. The negative relationship between Mn and Fe in Mn-poor metalliferous sediment not only suggests that the hydrothermal component is Fe-oxide, but also that the source of Mn is diluted by increased hydrothermal input. This makes geological sense if the Mn input to Mn-poor metalliferous sediment were to be from a hydrogenous rather than hydrothermal source. This interpretation also explains the elevated Mn-content when the Mn source is hydrothermal and why low Mn-contents occur when hydrogenous processes control Mn input. Because the sediment is predominantly hydrothermal, the background hydrogenous, detrital and biogenic signals are swamped by hydrothermal precipitation in rise crest sediments of this type (Dymond, 1981).

The Si-content of the samples may reflect aluminosilicate detritus, hydrothermal precipitation or siliceous biogenic ooze. The negative mixing lines between Fe_2O_3 and SiO_2 (Figure 2.12) may either imply that the siliceous and ferrous components are separate or that closure exists in the data. Fe_2O_3 and SiO_2 covary regardless of volcanic stratigraphic position (Figure 2.12) whereas MnO and SiO_2 do not (Figure 2.13). The bivariate plots confirm that in the As/Ls samples the source of MnO is either hydrogenous or of a different hydrothermal source to Fe_2O_3.

The Fe_2O_3 - SiO_2 mixing line falls into the field defined by the mixing of opaline silica $\rightarrow$ nontronite $\rightarrow$ iron oxide $\rightarrow$ iron sulphide. The range of Fe_2O_3/SiO_2 ratios is compatible with nontronite deposition which, in samples containing higher Si-content, are likely to contain a significant biohydrothermal silica input. None of the samples fall in the Fe-oxide field which lies to the Fe-rich end of the mixing line. The evidence may be interpreted in terms of admixing of hydrothermal iron silicate hydroxide (nontronite) with pure biogenic opal, and that as consequence of closure of the data, the Fe-Si mixing line is displaced to lower absolute values as a result of dilution by a separate Mn-oxide component.

The positive correlation between P_2O_5 and Fe_2O_3 (Figure 2.14) supports the hydrothermal origin of P_2O_5 which is present in the solid solution of iron oxyhydroxides with $CaHFe(PO_4)_2$ present in active hydrothermal systems (Fox, 1991).

2.5.4.2 Detrital element associations

Positive correlations between Al, Mg and Si are characteristic of all the metalliferous sediments from Oman (Figure 2.15). Because, by definition, the detrital component is crystalline and unchanged by transportation, the Al_2O_3/TiO_2 (Figure 2.15) ratios remain unchanged and therefore reflect the original ratios of the lithogenous source. The average Al_2O_3/TiO_2 ratios of the lava groups are tabulated overleaf (Table 2.9).

Also included on Figure 2.15 are the average values for recent transitional sediments of the Galapagos hydrothermal system, average calcareous ooze and average granular nontronite (Moorby, 1983). All of the samples have

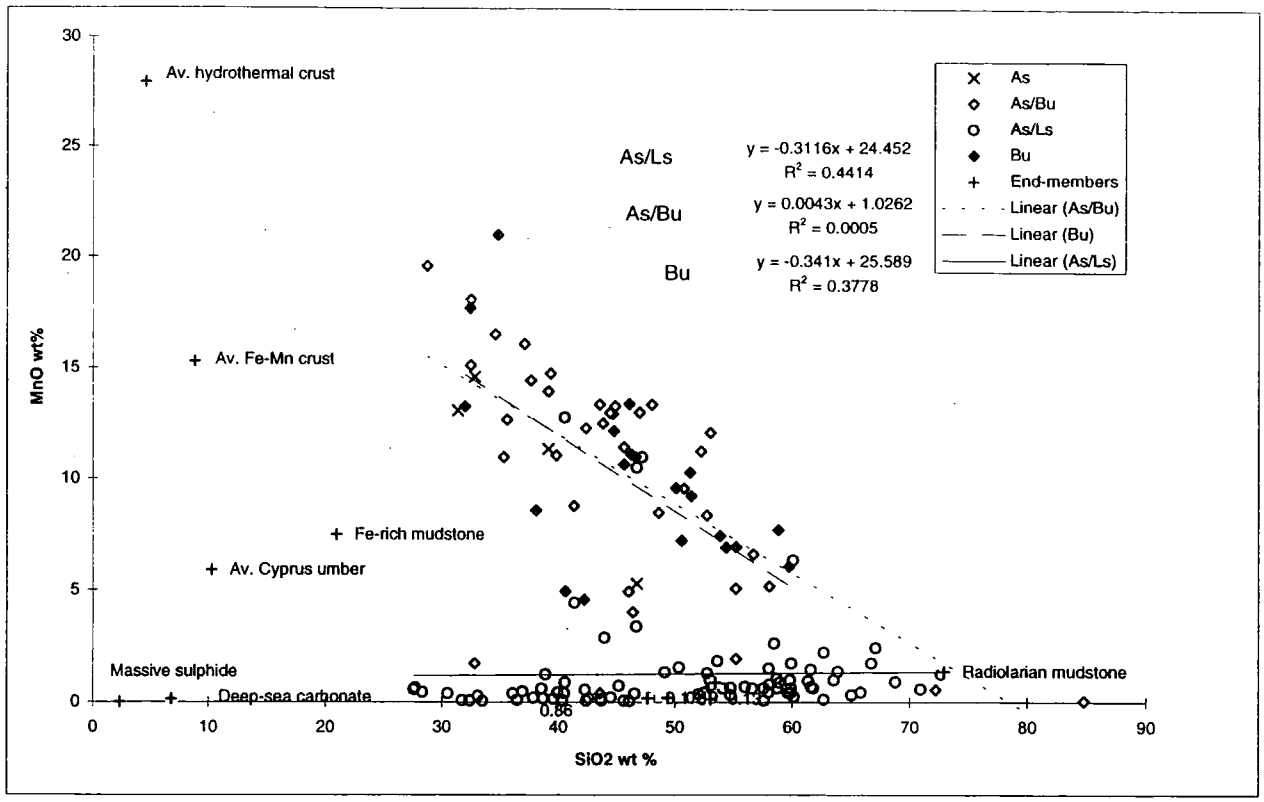

Figure 2.13 MnO versus SiO2 diagram. Data from: this study; Alabaster et al., 1982; Boyle, 1990; Chester, 1990

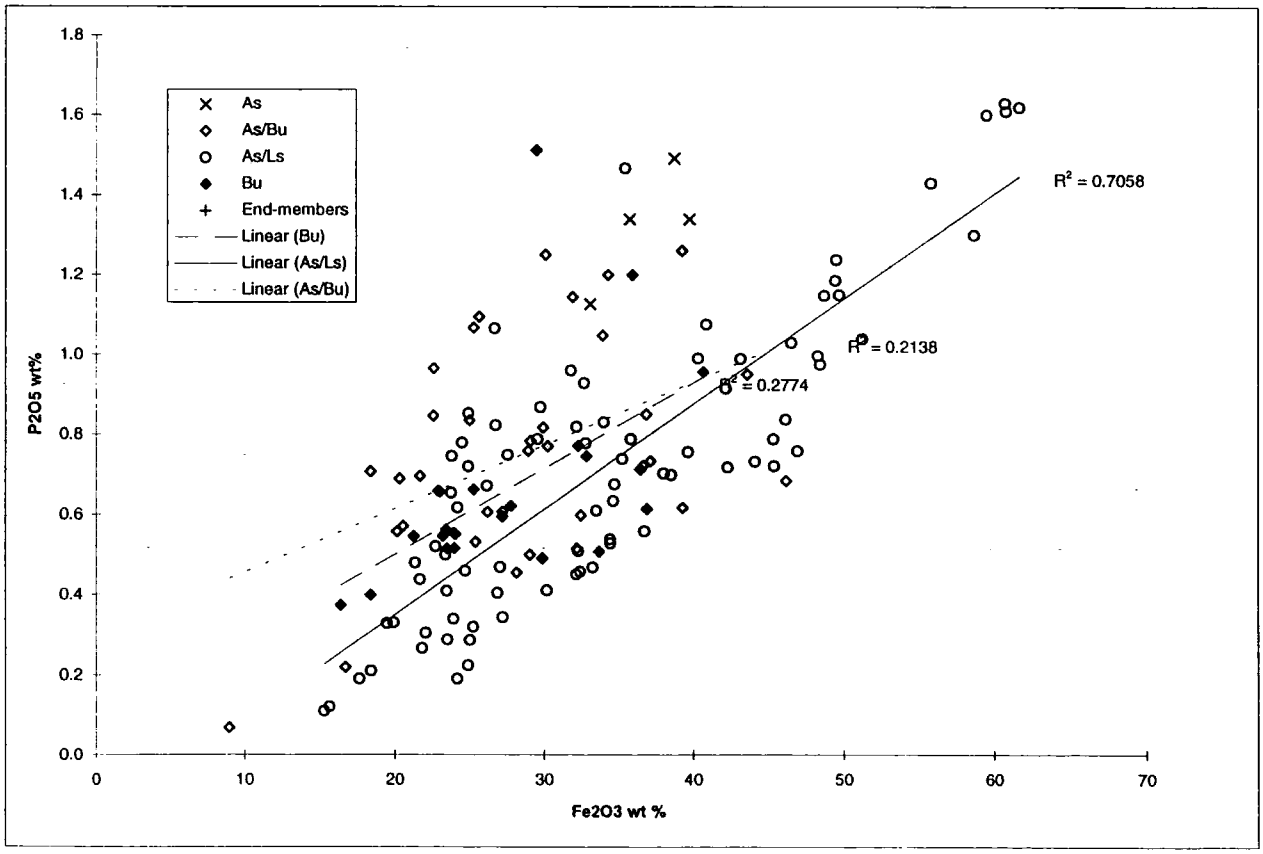

Figure 2.14 P2O5 versus Fe2O3 diagram. Data from: this study; Alabaster et al., 1982; Boyle, 1990; Chester, 1990

approximately constant Al_2O_3/TiO_2 ratios corresponding to those of calcareous ooze. The Al_2O_3 and TiO_2 content of calcareous ooze probably result from a small component of detrital clay in the form of Al-bearing smectite (Migdisov *et al.*, 1983). Thus, the evidence indicates that the detrital component was inherited from the background content of the ooze by processes comparable to those forming modern Galapagos mound nontronites and transitional sediments (Barrett, 1992). This also indicates that Al_2O_3 and TiO_2 behaviour was conservative during the formation of the Oman hydrothermal sediments.

Table 2.9 Average TiO_2/Al_2O_3 ratio (Data: Alabaster *et al.*, 1982)

Lava unit	**Al_2O_3/TiO_2**
Geotimes (Axis) Lava	0.1147
Axis Metalliferous Sediment	0.0514
Lasail (Seamount) Lava	0.0408
Lasail Metalliferous Sediment	0.0342
Axis/Lasail Metalliferous Sediment	0.0400
Basal Upper (Rifting) Lava	0.0387
Basal Upper Metalliferous Sediment	0.0377
Axis/Basal Upper Metalliferous Sediment	0.0428

The linear spread of the data (Figure 2.15) may result from a number of processes: (1) the loss or gain of mobile elements during sediment transformation during hydrothermal activity; or (2) variable detrital versus calcareous source input. In the former process, the apparently anomalous gain in Al_2O_3 and TiO_2 above the level found in the precursor calcareous ooze is explained by variable carbonate removal. Conversely the spread of data towards the origin is caused by the mass addition of other components to the sediment, presumably from hydrothermal solutions. The group of 17 samples which requires dilution by other components includes all 7 samples which are characterised as ochre (Constaninou and Govett, 1972) plus 9 further samples from the As/Ls group (Ochre: U2, U3, U7, U8, U10, U11; Metalliferous sediment: U4, U5, U41A, U47, U64, U72, U74, U82, 20669, 20661). In the second proposed process, in which calcareous and detrital input are not as intimately related as studies of recent hydrothermal sediments suggest (MacLean and Kranidiotis, 1987; Barret and MacLean, 1991; Barrett, 1992), it is possible that variable detrital component

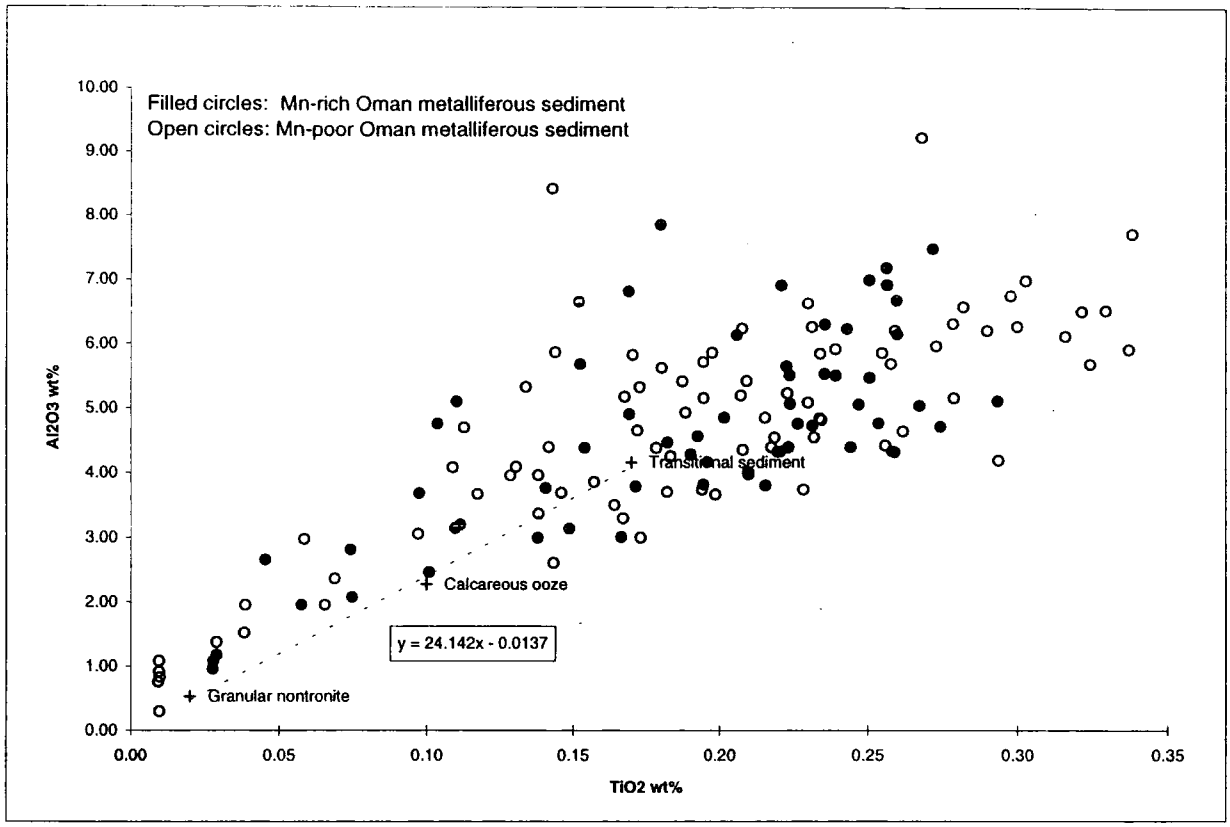

Figure 2.15 Al2O3 versus TiO2 diagram. Data from: this study; Moorby, 1983.

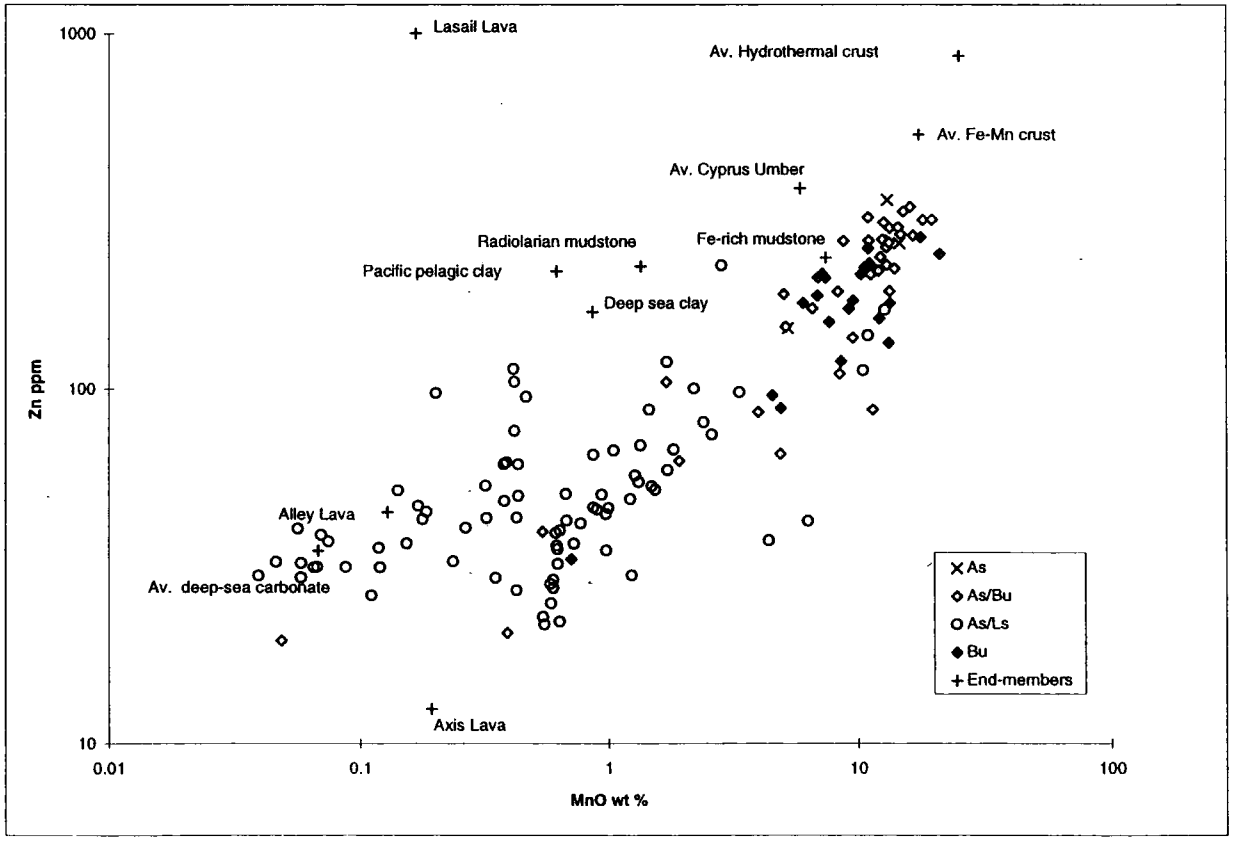

Figure 2.16 Zn versus MnO diagram. Data from: this study; Alabaster et al., 1982; Boyle, 1990; Chester, 1990

input compared to the background formation of calcareous ooze has resulted in the spread of data along the mixing line.

When plotted with the average values for the local lava series, (Figure 2.15) the possible lithogenous sources may be inferred: (1) the Al_2O_3/TiO_2 ratio of Bu corresponds to that of Bu lava; (2) the Al_2O_3/TiO_2 of As samples does not correspond to incorporation of Axis lava derived detritus; (3) the Al_2O_3/TiO_2 of As/Ls and As/Bu samples are both compatible with detritus derived from Lasail or Basal Upper lava; and (4) the Ls samples have an average ratio of 0.0342 which is within the field defined by the Lasail lava.

The suggested interpretation of the data (Figure 2.15) is that the local volcanic lava provided the lithogenous component to the intra-lava sediments of the Bu and Ls Groups. Similarly, the lithogenous contribution to sediments, which formed on the surface of the axial lava, is compatible with the post-spreading event lava units (i.e. Ls or Bu lavas). The important departure from what may be expected, is that it is necessary to incorporate post-spreading event detrital products in the As group samples: if Axis lava hosted sediment requires incorporation of Bu or Ls lava, then it is suggested that seamount volcanism had begun in some areas while in others basement (As) lava were still forming. This confirms the work by Pearce *et al.,* (1981) which described a model in which Lasail magma was injected into the "still-hot" Axis lava but is contradictory to the proposition by Ernewein, *et al.,* 1988 that the upper surface of the Axis lava represent a significant break in volcanism.

2.5.4.3 Biogenic element associations

In the Goldberg (1954) classification, the biogenic component of marine sediments included both organic matter and inorganic shell material. The principal biogenic components are carbonate and opaline shell material, and relatively minor sources include skeletal apatite (phosphates) and barite (sulphates). In the previous Section, the Oman data demonstrated that the process of carbonate removal resulted from hydrothermal precipitation. In Section 2.5.4.1 it was demonstrated that total silica content is likely to be the product of Si Detrital < Si Biogenic < Si Hydrothermal.

The major elements, Si and Ca, are concentrated in calcareous and siliceous marine sediments of biological origin. The wide spread of Si/Fe and Si/Mn ratios

in the data resembles that of recent Nazca Plate rise-crest samples (Figure 2.8), and has been explained as variation in the abundance of biogenic opal in a systematic manner away from an equatorial high productivity zone (Dymond, 1980). It is more reasonable to suggest that the data reflect variable or non-uniform hydrothermal input to the sea floor. Although there is a close resemblance between the fields defined by the samples in this study and the Nazca Plate surface sediments, latitudinal variation cannot be evoked for Oman metalliferous sediments. The majority of the samples fall within the range of Si/Fe ratios, characteristic of the hydrothermal Fe-oxides and nontronites. However, the range in Si/Fe ratios also fall outside the Si-rich nontronite range impling that mixing occurred between the hydrothermal Fe-rich minerals and a pure Si-rich component. The pure Si-component is either hydrothermal or biogenic in origin since the detrital content of the sediments is uniformly low.

Pure Si is identified in analysis of buoyant and neutrally buoyant hydrothermal plumes (Rudnicki and Elderfield, 1992; Feely *et al.,* 1994; Feely *et al.,* 1996), but the significant negative correlation between Fe and Si (Figure 2.12) requires that Fe forms a separate component in the plume from Si. This would require the full admixing of Fe_2O_3:SiO_2 ratios from 0.22 to 2.23 independently of Mn-content or volcanic stratigraphic location. The major element diagrams do not allow discrimination between biogenic or hydrothermal origin for the pure-Si component. The sediments appear to be predominantly hydrothermal, the deposition rate was therefore likely to have been high. Consequently, it is also likely that background biogenic source input was swamped by hydrothermal precipitation close to the vent area and progressively less so with increasing distance from it.

2.6 Trace element geochemistry

The major element geochemistry has demonstrated that the metalliferous sediments are the product of at least three identifiable sources: (1) local high temperature hydrothermal vents, (2) local hyaloclastite and (3) external biogenic sediment. From the major element chemistry and the literature, the following eight components may also be suggested for further investigation:

(1) Hydrothermal Mn-oxide
(2) Hydrothermal Fe-oxide
(3) Hydrothermal Si-oxide
(4) Hydrothermal Ca-Fe phosphate
(5) Hydrogenous Mn-oxide
(6) Detrital Aluminosilicate
(7) Biogenic calcium carbonate
(8) Biogenic opal

Each component represents an association of elements, and each is derived from a different source. Possible sources are difficult to infer from simple bivariate and ternary plots. The hypothesis of this study is that a limited number of selected components may be used to describe the sediment-forming processes, and that various numerical and chemical techniques may be applied to quantify these end-members. In the previous section, major element chemistry was discussed with reference to potential sources. In the following discussion, the trace elements will also be assumed to be related to various end-member components. The trace elements which behave similarly will be grouped together for discussion.

2.6.1 Cu, Co, Pb and Zn

The elements Pb, Cu, Zn, and Co exhibit increasing concentration with increasing Mn concentration. This is represented by the plot of Zn versus MnO (Figure 2.16). The positive linear correlation of the trace elements versus Mn is in contrast to recent buoyant plume studies which have found that particulate Pb, Cu, Co and Zn positively correlate with particulate Fe concentration (Barrett, 1992; Rudnicki and Elderfield, 1992). Particulate Fe concentration has been previously used as a tracer for simple mixing and dispersal in geochemical analyses of hydrothermal plume samples. Evidence from plume studies also indicates that these trace elements are taken up by Fe-oxyhydroxides prior to their emplacement in the buoyant plume, and that once in the plume, their preferential removal to the neutrally buoyant plume occurs. The As/Ls samples do not show any significant correlation of Fe with Pb, Cu, Co or Zn. An hydrothermal Fe-oxide end-member may have lost these trace elements prior to settling from the plume.

Possible mechanisms for the removal of Pb, Cu, Co and Zn to the neutrally buoyant plume include preferential settling or oxidative dissolution of these elements (Garden, *et al.*, 1991).

The significant positive linear trend for Zn versus MnO may be used to infer that quantitative mixing of these elements occurred in the plume, possibly Zn was scavenged by adsorption to Mn-oxide surface sites (Figure 2.16). This is also the suggested mode of incorporation of Pb, Cu and Co into the hydrothermal component of the metalliferous sediments. The correlation between MnO and Fe_2O_3 in the As/Bu, Bu and As sediments (Figure 2.11) explains the positive correlation of the trace elements with Fe in these samples. Pb, Cu, Co and Zn scavenging in the plume may take place in the plume across the entire ridge segment which is Mn enriched due to slow scavenging of Mn in studies of modern hydrothermal systems. Mn precipitation may be induced by suspended hydrothermal Fe plume particles, Mn-precipitating bacteria and surficial sediments (Freely *et al.*, 1994). Fe-rich minerals are the only significant particulate plume phase, (Rudnicki and Elderfield, 1992), and their quantitative loss of trace elements probably provides the source for trace elements scavenged by Mn particles. Although this process may characterise the entire ridge segment, it would be masked by relatively high settling out rate of trace element-poor Fe-oxides in the vent proximal locations.

2.6.2 Ni

As predicted in studies of active hydrothermal systems, the behaviour of Ni in plume processes resembles in some ways that of Cu, Co and Zn (Kurnosov *et al.*, 1983; Freely *et al.*, 1994). There is a weak positive correlation between Ni, MnO and Fe_2O_3 in each sample Group except for the As/Bu samples (Figure 2.17). However, Ni also demonstrates a weak positive relationship with Al_2O_3, which suggests that it may also be incorporated into the aluminosilicate component (Figure 2.18). There is no positive correlation between Ba and SiO_2 which is consistent with a non-biological, Si-rich end-member.

In this study, Ni may be grouped with Mn, Co and Zn in terms of their hydrothermal source associations but Ni may also be derived from a detrital source component. Identical inter-element relationships are reported elsewhere for recent ferromanganoan sediments (Li, 1981; Thompson *et al.*, 1984; Balistreri and Murray, 1986). The consistency of the observations suggests that the Mn-

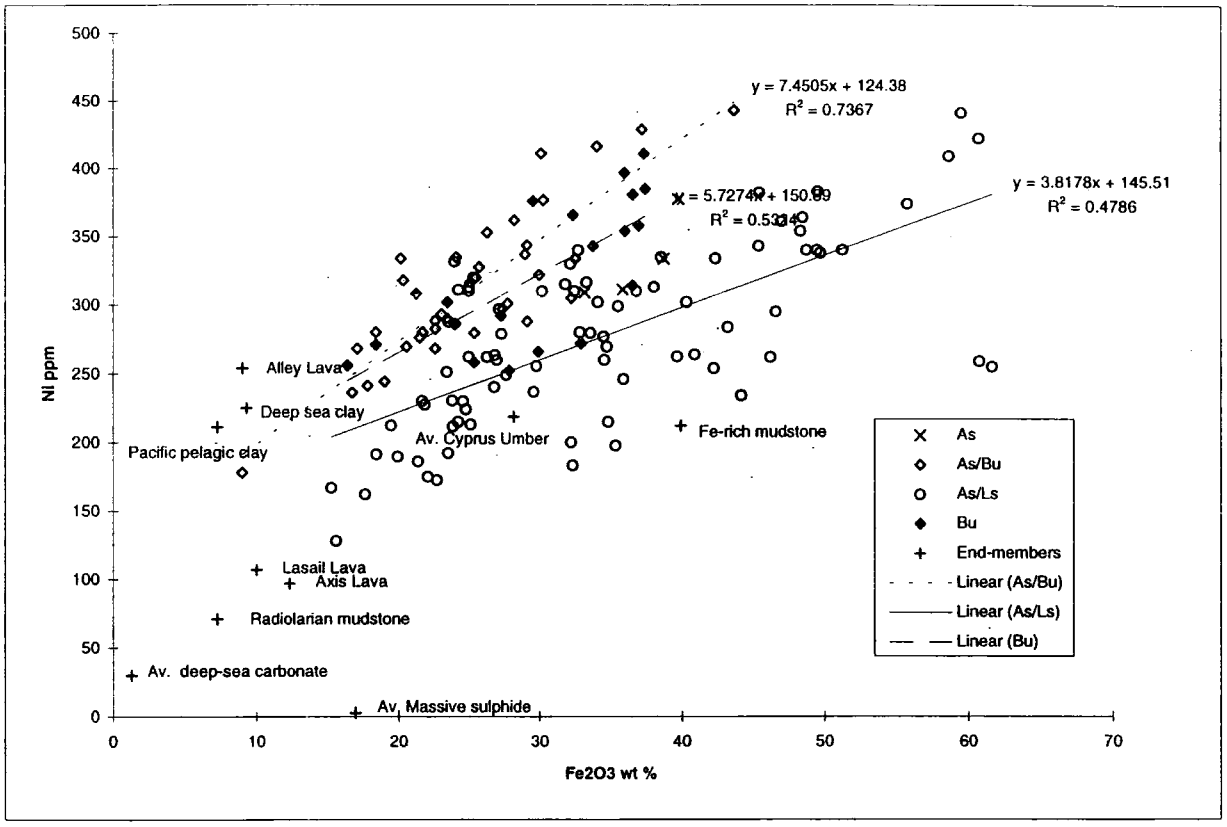

Figure 2.17 Ni versus Fe2O3 diagram. Data from: this study; Moorby, 1983.

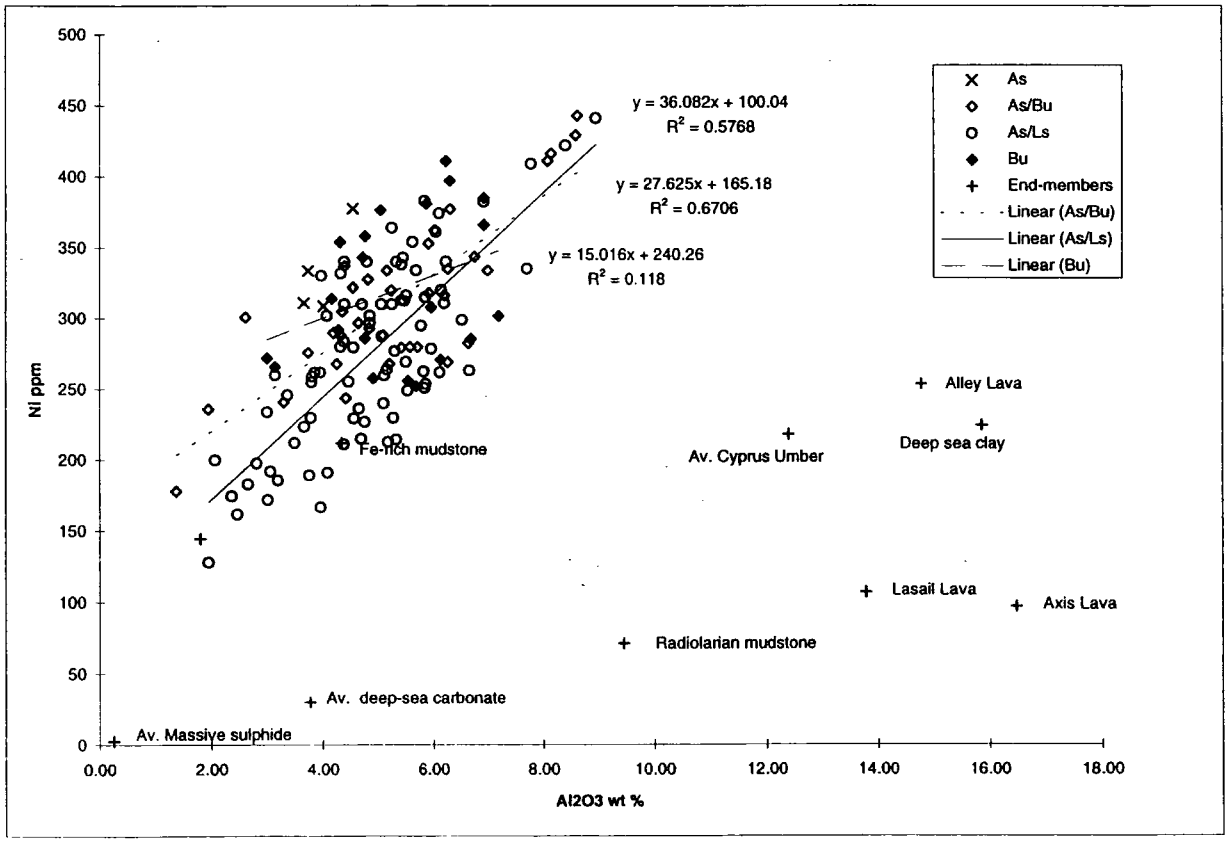

Figure 2.18 Ni versus Al2O3 diagram. Data from: this study; Alabaster et al., 1982; Boyle, 1990; Chester, 1990

content is the controlling factor in determining the binding ability of metals such as Cd, Ba, Co, Ni and Zn (Li, 1981). The control of trace metal content on samples in this study is directly related to the surface characteristics of particulates in suspension in the plume and particulate Mn has different binding abilities for metals to Fe oxyhydroxides.

2.6.3 Mo

Experimental evidence suggests that Mo forms oxyanions with Mn oxides (Li, 1981), but there is little evidence in this study to support that finding. The plot of Mo versus SiO_2 (Figure 2.19) illustrates a positive linear relationship between the two elements for As/Ls Group samples. SiO_2 is thought to be biogenic and hydrothermal in origin Different sources for the Si content of the vent proximal and vent distal samples may explain the the positive correlation of Mo and SiO_2 in As/Ls Group samples and the absence of correlation in the other samples.

2.6.4 Cr, V, As, and P

Positive linear conservative relationships (Figure 2.20) between the oxyanions (Cr, V, As and P) and Fe probably result from co-precipitation and may therfore preclude later scavenging or removal processes (Rudnicki and Eldefield, 1992). This is confirmed by other studies: hydrothermal plumes at TAG sites and the Juan de Fuca Ridge demonstrate positive relationships between the oxyanions and Fe which are controlled entirely by the precipitation of Fe oxyhydroxides in the earliest stages of the ascent of the buoyant plume (Feeley *et al.,* 1990; Rudnicki and Eldefield, 1992). However, recent studies of the EPR axis, Cr, V, As and P described the process of *scavenging* of these elements from sea water by Fe oxyhydroxides (Feely *et al.,* 1994). From the evidence in this study and the examples of previous studies, the precipitation of the oxyanions appears to be probably controlled by the precipitation of Fe-oxyhydroxides. The study of transects across the EPR show lowest concentrations of Cr, V, As and P in the plume above the vents, which indicates that the source from which these elements are scavenged to be sea water (Feely *et al.,* 1994).

The relationship of P_2O_5 with V (Figure 2.21) is identified in the Axis Group samples and may represent the formation of $CaHFe(PO_4)_2$ in solid solution with Fe Oxyhydroxides (Fox, 1991). Correlation of P_2O_5 with Fe_2O_3 (Figure 2.14)

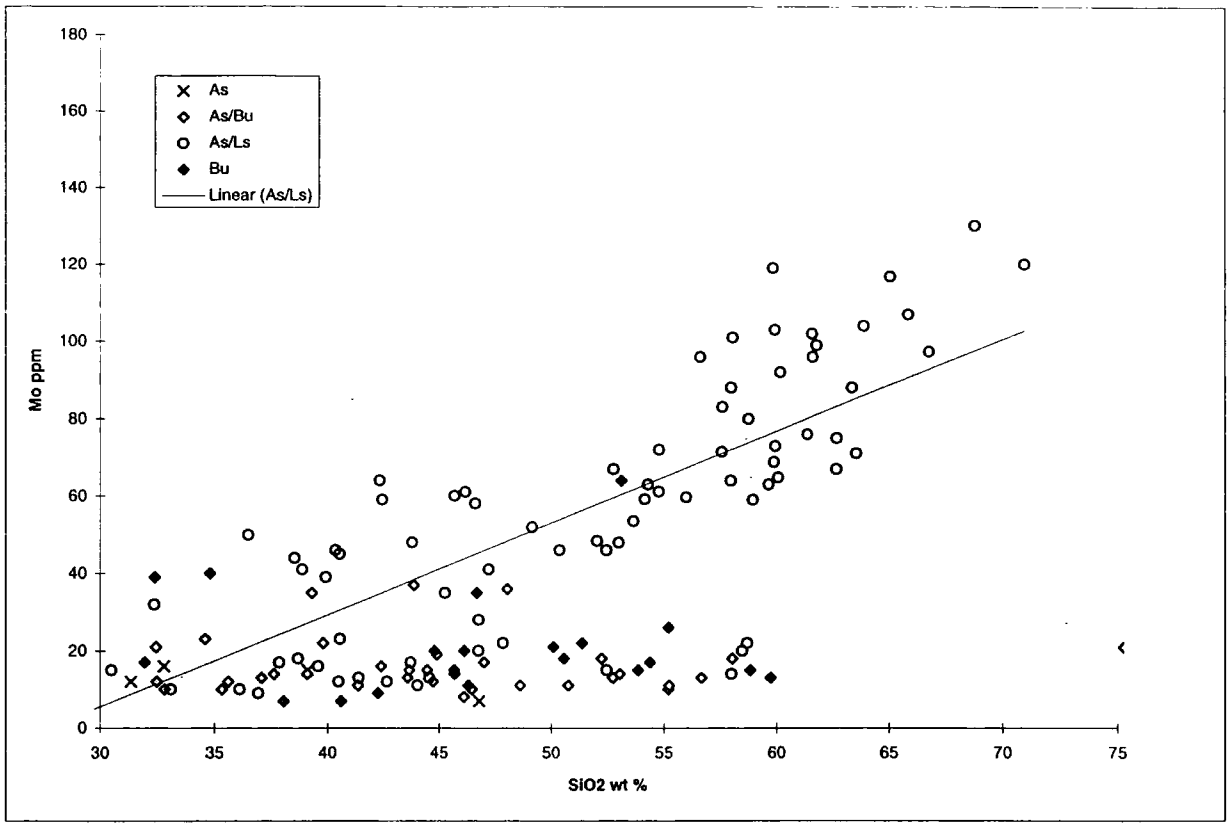

Figure 2.19 Mo versus SiO2 diagram. Data from: this study.

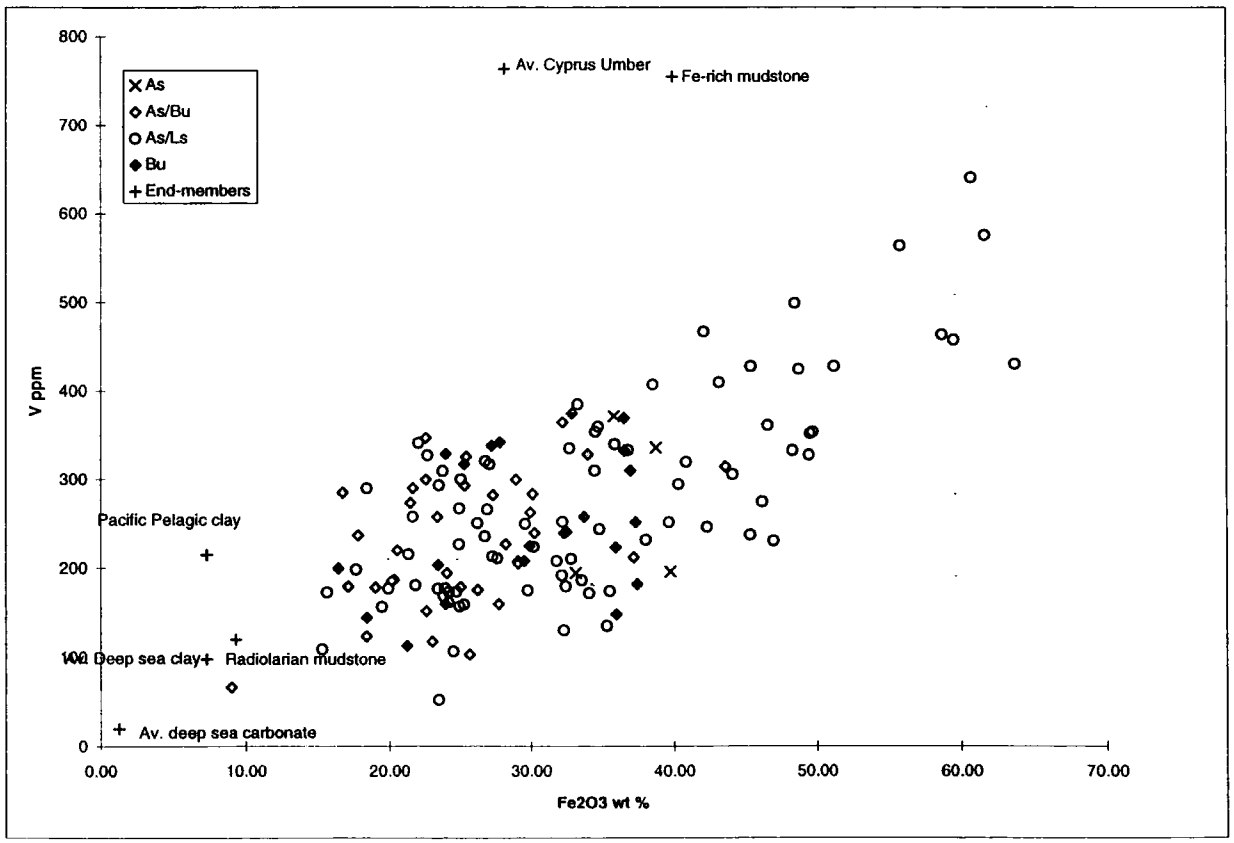

Figure 2.20 V versus Fe2O3 diagram. Data from: this study; Alabaster et al., 1982; Boyle, 1990; Chester, 1990

may account for the scarce apatite (of hydrothermal-hydrogenous origin) which has been identified using XRD analysis.

Lithogenous components may supply much of the the Cr content of normal deep-sea sediments and diagenetic sediments that have not been affected by hydrothermal sources. Supporting evidence for this is provided in other studies by data which shows the association of Cr with minor detrial impuritites in carbonates (Varnavas and Pangos, 1981). A statistically significant positive correlation between Cr and the immobile detrital elements Al, Ti, Mg, Zr and Rb is present in modern deep sea and diagenetic sediments (Marchig *et al.*, 1982). But because Cr is also partially mobilised in hydrothermal processes, it may also be scavenged by Fe oxyhydroxides in hydrothermal sediments (Figure 2.20). This explains why Cr enrichment is not followed by corresponding enrichment in the other terrigenous-derived elements in the samples in this study (Figure 2.22). The Oman metalliferous sediment data plot within the field defined by hydrothermal metalliferous deposits from the EPR, and Red Sea on the Cr/Zr diagram. Because diagenetic and hydrothermal sediments are both dark red-brown coloured fine grained mudstones, this method for distinguishing between two types of ancient metalliferous sediment may be a useful exploration tool (Marchig and Gundlach, 1982; Marchig *et al.*, 1982).

The element, As, shows positive linear correlation with Fe_2O_3 in As/Bu and Bu samples but not in Mn-poor As/Ls samples (Figure 2.23). This may reflect a seawater source of As in some sediments. The data are compatible with the more recent plume models (Freely *et al.*, 1994) which demonstrate that the lowest values of particulate As occur in the plume overlying the vents whereas, in the vent-distal plume, particulate As is at its highest level. In the vent-proximal locations, represented by the As/Ls and Ls samples, As has not been scavenged from sea water, is found at its lowest concentrations, and is derived by hydrogenous precipitation. In vent-distal locations, represented by As/Bu samples, the particulate Fe oxyhydroxides have remained suspended in the plume for a sufficient period of time to have scavenged As from sea water. Cr follows the same pattern as As and V correlates with As in As/Bu sediments.

2.6.5 Sc

Sc concentration shows a positive linear correlation with Al_2O_3 (Figure 2.24), which confirms the findings of other workers that Sc is concentrated in the aluminosilicate detrital fraction (Li, 1981). Sc is particularly concentrated in

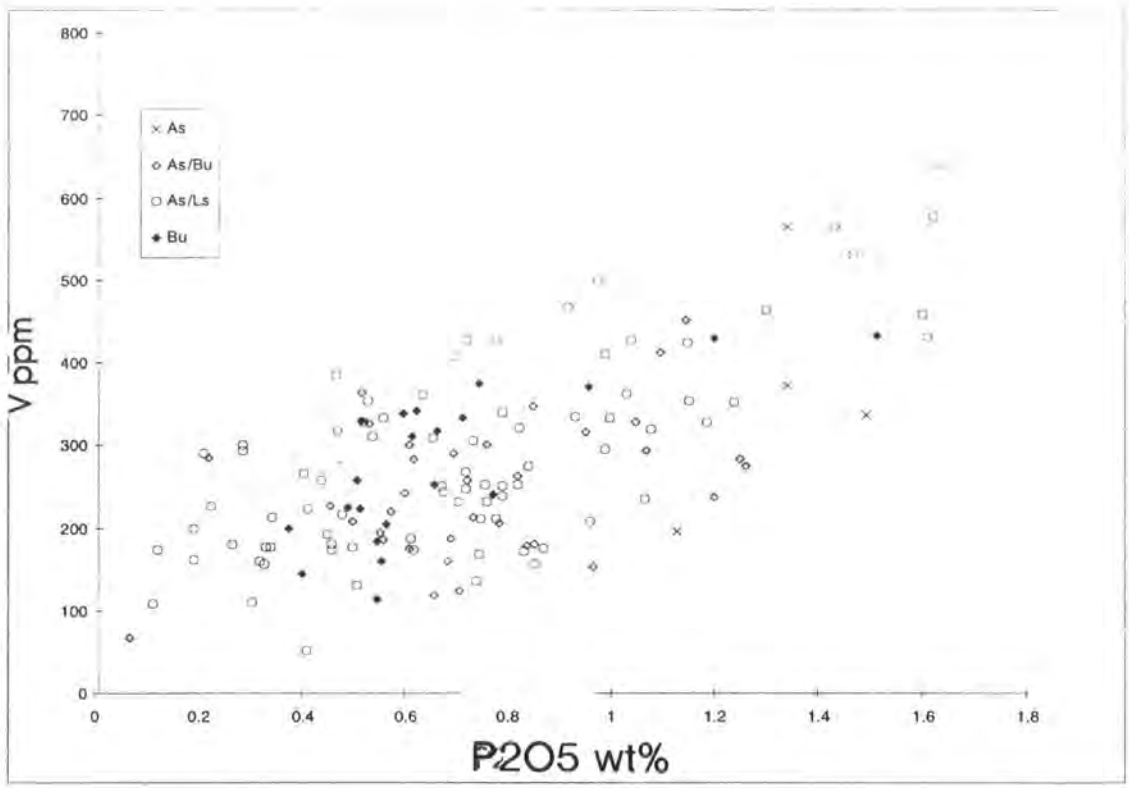

Figure 2.21 V versus P2O5.

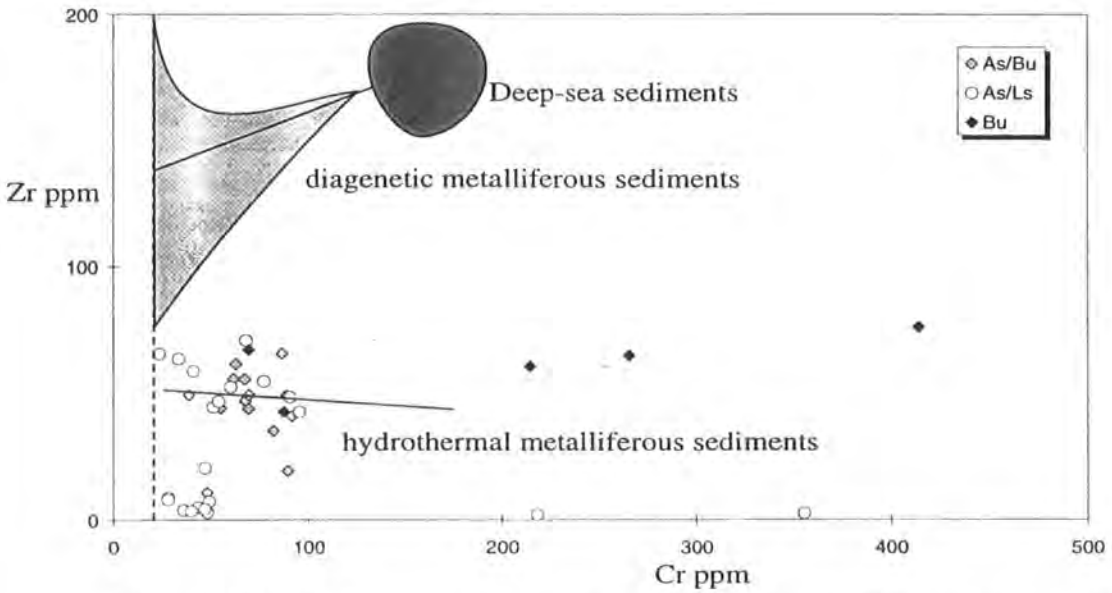

Figure 2.22 Zr versus Cr discrimination diagram for three groups of sediments with different genesis. (After: Marchig *et al.*, 1982).

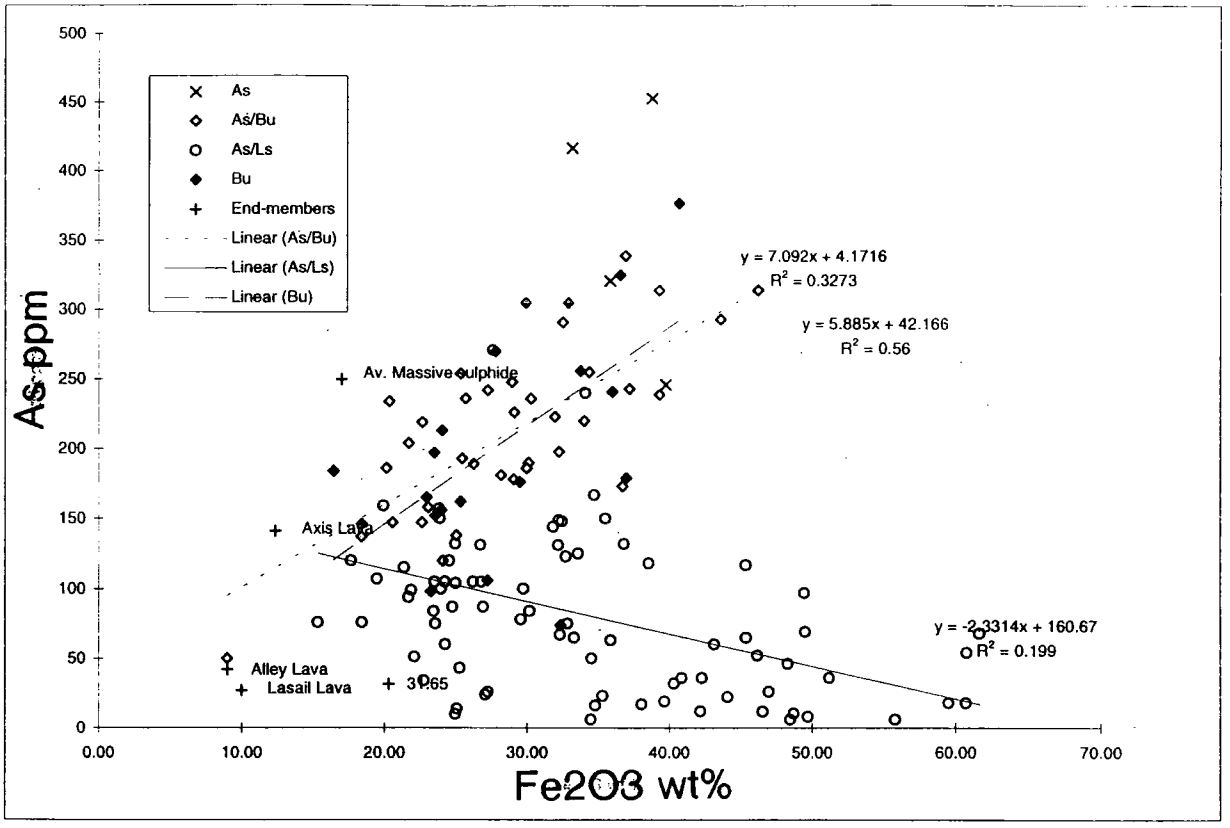

Figure 2.23 As versus Fe2O3 diagram. Data from: this study.

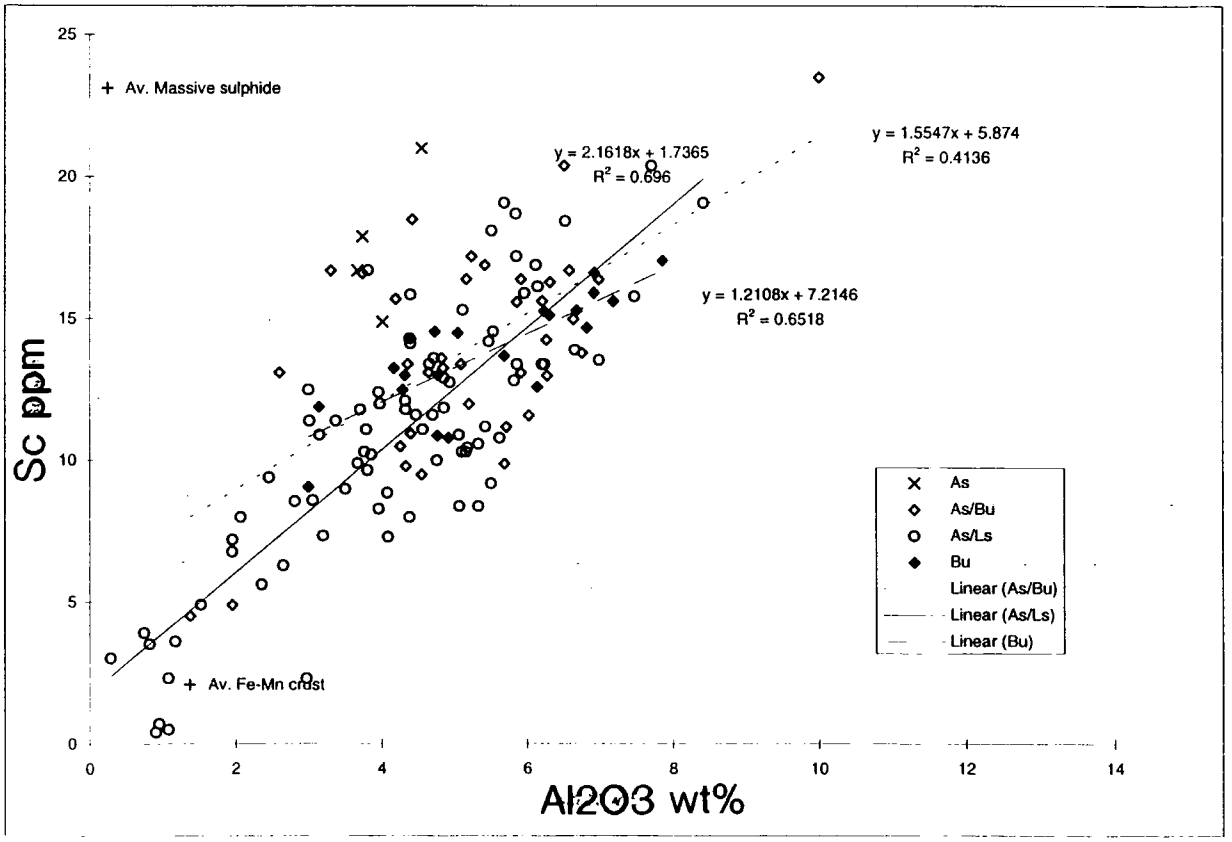

Figure 2.24 Sc versus Al2O3 diagram. Data from: this study; Alabaster et al., 1982; Boyle, 1990; Chester, 1990

clinopyroxene, which has been identified using XRD analysis in a small proportion of the samples (Section 2.4). The proposed detrital component is thought to have been concentrated in the hydrothermal sediments by the dissolution of carbonate during hydrothermal activity. The positive correlation between Sc and Al_2O_3 supports the evidence for incorporation of a detrital fraction in the carbonate component. Correlation between Al, Mg and Ti, could otherwise be taken to represent authigenic smectite clay minerals.

2.6.6 Lanthanide and actinide geochemistry

The object of determining REE data is to compare the Oman metalliferous sediment with similar ancient and modern deposits and to assess the rôle played by the hydrothermal system. Shale normalized rare earth element (REE) distribution patterns have been most frequently used to interpret the sediment-forming components making up marine sediments, (e.g., Toth, 1980; Marchig *et al.,* 1982; Barrett and Jarvis, 1988; Rudnicki and Elderfield, 1992; Mills and Elderfield, 1995).

All of the samples are enriched in LREE relative to HREE (Figure 2.25), which is generally comparable to Cyprus metalliferous sediment and ferromanganoan sediments (Robertson and Fleet, 1975). Comparison between the As/Ls Group samples and the As/Bu Group samples reveals that the REE content is independent of Mn:Fe ratio.

The abundance patterns of the REE in the metalliferous sediment samples are similar to that of sea water (Figure 2.26) and to the measured REE content of hydrothermal fluids (Mitra *et al.,* 1994; Klinkhammer *et al.,* 1994; Mills and Elderfield, 1995). Sea water and hydrothermal fluids are both LREE:HREE enriched and contrast markedly with the REE geochemistry of MOR basalt and pelagic clay. The REE content of pelagic ooze is of an order of magnitude higher than in the metalliferous sediments (Figure 2.26) but the patterns are dissimilar in that the Ce anomaly is characteristic of metalliferous sediments but not of ooze (Robertson and Fleet, 1975; Migdisova *et al.,* 1983).

In contrast to metalliferous sediment, typical hydrogenous manganese nodule data shows an inverse REE pattern, including a positive Ce anomaly. Despite the difference in magnitude of REE content, the abundance pattern of metalliferous sediment most closely resembles that of sea water, thus the major particulate

phases may scaveng the REE from seawater. The proposed method of REE incorporation is by rapid adsorption onto poorly crystalline colloidal ferromanganoan oxyhydroxides (Barrett and Jarvis, 1988).

If the samples were to have a significant diagenetic component, then smaller negative Ce anomalies and higher absolute REE concentration would be expected. Deep sea sediments (calcareous and siliceous ooze) exhibit the smallest Eu anomalies and REE concentrations lower than either hydrothermal or diagenetic sediment. The wide range of total REE content of the Oman samples suggest dilution by a REE-free component.

In natural systems, only Ce and Eu exist in anything other than a trivalent state: (1) Ce^{3+} may be oxidized to Ce^{4+}; and (2) Eu^{3+} may be reduced to divalent Eu2+ (e.g., Mills and Elderfield, 1995). The behaviour of Ce in this study is illustrated by the Ce/La ratio (Figure 2.27). Of the samples that plot on the sea water trend (Ce/La = 0.35), there are three separate groups: (1) a REE-depleted group containing samples U11, U12, 20662, and 20669; (2) a high Ce/La group ;and (3) a normal sea water trend group. Departure from the sea water trend occurs in two forms for two reasons: (1) samples with a ratio greater than that of sea water may result from mixing with a component of detrital derivation, (average Ce/La ratio for lava and dykes in the Semail ophiolite = 2.50) or (2) samples with Ce/La ratio less than sea water require a component derived from solutions with a lower ratio than that of sea water itself and, since ratios of river water, shallow ocean water (100m), and deep ocean water (2500m) have Ce/La ratios = 1.9, 1.29, and 0.89 respectively (Chester, 1990), the hydrothermal source must supply the sediment.

The variation Ce/La ratios and content (Figure 2.27) result from mixing seawater-derived REE with REE-bearing terrigenous detritus. The positive Ce/La anomaly of the ochre samples indicates that the REE content is associated more closely with derivation of REE from hydrothermal fluids than from seawater.

The three main features of the REE behaviour are: (1) that the chemical sediments reflect the composition of sea water; (2) that there is a wide range of REE content within each sample Group; and (3) that the trend of these patterns is also similar to that of typical hydrothermal sediments (i.e., depleted in Ce, relatively enriched in HREE, and relatively depleted compared to average deep sea sediments).

Figure 2.26 (a) Shale normalised REE abundance plot, and (b) Chondrite-normalised REE abundance plot. Data for marine plankton, seawater, hydrothermal metalliferous sediments, deep-sea sediments, nodules, and diagenetic sediments from: Lippard *et al.*, 1986; Mitra *et al.*, 1994; Klinkhammer *et al.*, 1994; Mills and Elderfield, 1995.

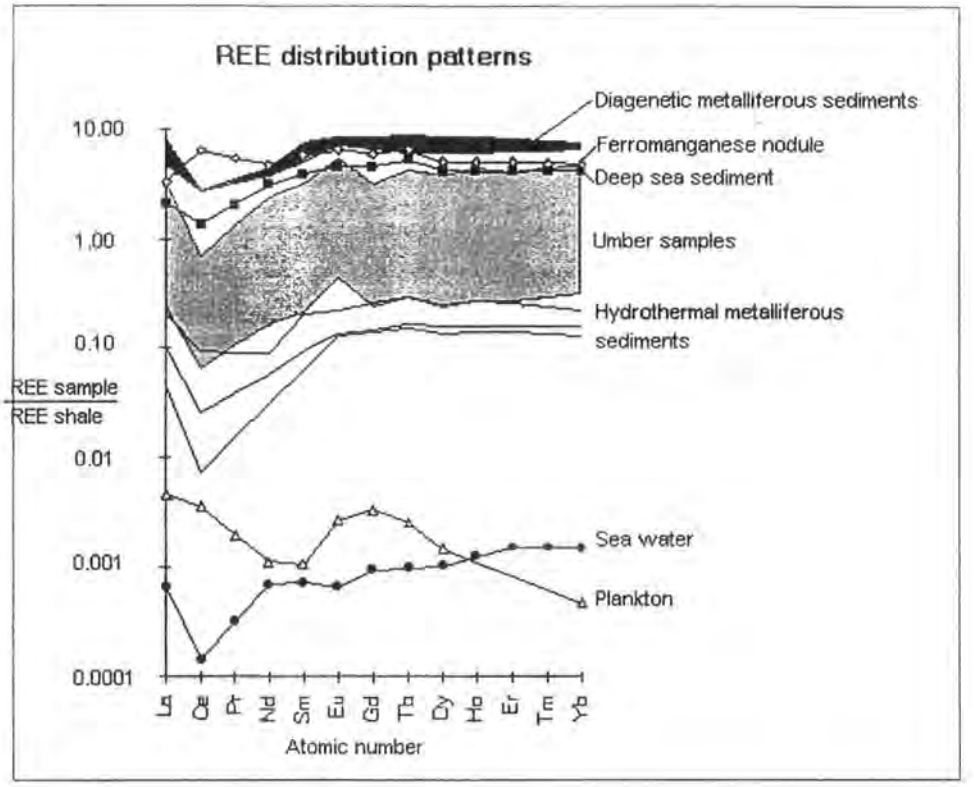

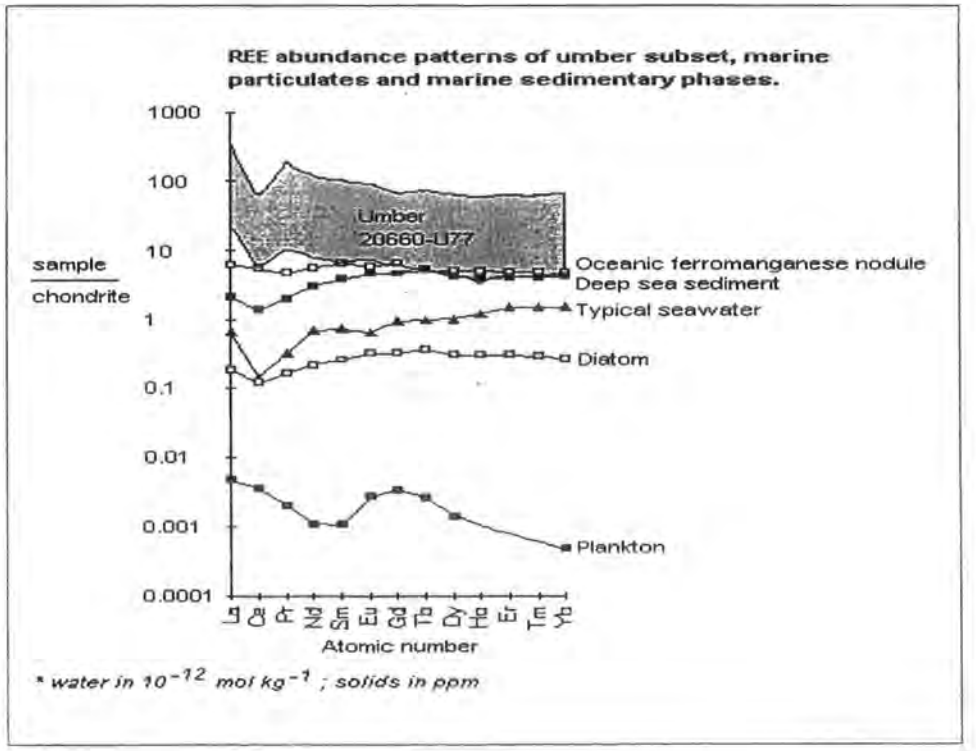

Figure 2.27 Ce versus La diagram

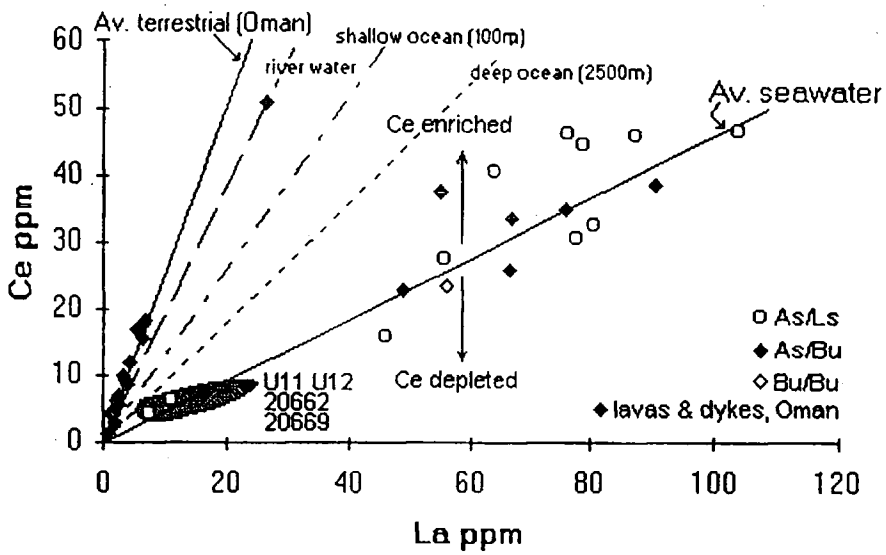

Average seawater Ce/La = 0.46 (Elderfield & Greaves, 1982)
Average (Oman) lavas & dykes Ce/La = 2.50 (Lippard, et al, 1986)
Average river waterCe/La = 1.9; shallow ocean Ce/La = 1.29; and deep ocean Ce/La = 0.89 (Elderfield & Greaves, 1983)

2.7 Summary

To help to summarise the complex interelment relationships, the Pearson product moment correlation coefficient, *r*, has been calculated (Table 2.10). The value of *r* reflects the numerical degree of association between the element data in terms of a linear relationship. The correlation coefficient is a dimensionless index that ranges from -1.0 to 1.0 inclusive. A hypothesis test of independence between the variables has also been applied to test for *significant* correlation between the variables. The correlation coefficient is only intended here to illustrate the gross features of the rise crest marine sediments.

The data (Table 2.10) may be interpreted in terms both of physical components made up of elemental associations and of the spatial variability in inter-element correlations. The inter-element associations indicate the major element composition of the physical components, which will be suggested as the hypothetical "building blocks" of rise-crest sediments. However, the major element associations are not constant throughout the ophiolite but instead reflect volcanic stratigraphic position.

Table 2.10 confirms that throughout the data, irrespective of location, is a positive Ti-Al-Mg relationship suggestive of a lithogenous component. The association of Ti, Al and Mg may be accounted for by clay minerals, feldspar or pyroxene which have been identified using XRD analysis. By definition, the lithogenous phase is part of the crystalline mineral matrix which has undergone no major changes during transportation (Goldberg, 1954), and in consequence, the ratios of major elements to one another would remain unchanged. The clay minerals which quantitatively make up the greatest proportion of lithogenous material (Chester 1990), structurally are stacked SiO_4 tetrahedra with one or two octahedral sheets of oxygen atoms or hydroxyl ions with Al, Mg or Fe cations between them (Chester, 1990). The principal sediment-forming minerals largely control the major element composition and it is demonstrable that Al is concentrated mainly in the clays since neither Al, Mg or Ti is positively correlated to any of the other major elements at any of the locations.

The principal negative correlations in the bivariate diagrams are between major elements and silica. Insignificant negative correlations (Figure 2.10) reflects the need to subdivide the data into geochemically alike subsets prior to calculating

correlation coefficients. This has been carried out in the next chapter as a preliminary to a comprehensive factor analysis study.

Correlation coefficient data (Table 2.10) does help to define the relationship between the major elements and the following minor elements: U, Th, Pb, Ta, Tm, Er, Ho, Dy, Eu, Sm, Nd, Pr, Y, Nb, La, Gd, Yb, Tb, Cs, Zr, Hf, Sr, Rb. The lanthanides show no statistically significant relationship, positive or negative, with CaO, P_2O_5 and Fe_2O_3. Positive correlations with Al and Mn confirm that the detrital aluminosilicate phase and the hydrothermal Mn-oxide phase are both important REE sources. U is positively correlated to the Fe-oxide phase. The behaviour of Th resembles the lanthanides in its affinity to the detrital phase. Cs correlates with the Mn-oxide phase.

The main conclusions of this Chapter are that: (1) the ancient metalliferous sediments of Oman closely resemble the recent EPR sediments in their geochemistry and environment of depoition; (2) that there was spatial variation in the hydrothermal system at the Oman rise-crest environment; and (3) that the complex interelement associations are most adequately summarised using correlation coefficient data. The possible presence of a number of recognisable sediment-forming components has been suggested, and these will be dealt with more comprehensively in the following chapters.

	Al	Ba	Ca	Ce	Co	Cr	Cs	Cu
Al	1.000							
Ba	0.215	1.000						
Ca	0.032	-0.237	1.000					
Ce	0.822	0.045	0.002	1.000				
Co	-0.262	0.034	0.274	-0.147	1.000			
Cr	0.142	0.847	-0.032	0.051	0.326	1.000		
Cs	-0.128	-0.052	0.176	-0.413	0.240	0.014	1.000	
Cu	-0.519	-0.050	-0.413	-0.421	0.180	-0.069	0.018	1.000
Dy	0.706	-0.156	0.194	0.859	-0.137	-0.074	-0.382	-0.518
Er	0.662	-0.105	0.259	0.785	-0.137	-0.016	-0.409	-0.551
Eu	0.709	-0.145	0.177	0.832	-0.114	-0.052	-0.362	-0.446
Fe	-0.282	-0.133	-0.619	-0.100	0.042	-0.207	-0.076	0.725
Gd	0.756	-0.099	0.157	0.899	-0.117	-0.017	-0.412	-0.485
Hf	0.421	0.297	0.371	0.515	0.072	0.257	-0.213	-0.121
Ho	0.682	-0.151	0.183	0.825	-0.151	-0.087	-0.380	-0.502
La	0.718	0.016	0.186	0.903	0.004	0.114	-0.442	-0.503
Mg	0.446	-0.043	-0.427	0.474	-0.540	-0.259	-0.300	-0.290
Mn	-0.032	0.156	0.536	-0.021	0.821	0.394	0.356	-0.105
Nb	0.650	0.029	0.258	0.873	-0.182	0.027	-0.437	-0.375
Nd	0.736	-0.070	0.222	0.898	-0.005	0.052	-0.344	-0.524
Ni	0.222	-0.040	0.020	0.378	0.052	-0.074	0.065	-0.507
P	0.315	-0.145	0.015	0.104	-0.133	-0.152	-0.086	-0.064
Pb	0.042	0.555	0.234	0.077	0.489	0.635	-0.172	-0.093
Pr	0.728	-0.092	0.200	0.905	0.003	0.024	-0.354	-0.509
Rb	0.280	0.697	-0.217	0.065	-0.023	0.424	-0.105	-0.096
Sc	0.757	-0.053	0.265	0.672	-0.009	-0.075	-0.065	-0.524
Si	0.141	0.052	-0.365	0.090	-0.671	-0.117	-0.220	-0.320
Sm	0.699	-0.205	0.188	0.829	-0.090	-0.105	-0.348	-0.480
Sr	0.440	0.120	-0.106	0.556	-0.141	0.080	-0.267	-0.303
Ta	0.059	0.023	0.628	0.148	0.001	0.028	-0.083	-0.066
Tb	0.692	-0.167	0.168	0.847	-0.132	-0.086	-0.375	-0.506
Th	0.721	0.138	-0.145	0.789	-0.162	0.120	-0.413	-0.462
Ti	0.881	0.096	-0.007	0.925	-0.143	0.048	-0.205	-0.520
Tm	0.688	-0.076	0.273	0.832	-0.037	-0.001	-0.379	-0.492
U	0.195	-0.015	-0.334	0.394	-0.128	-0.009	-0.421	0.347
V	-0.195	-0.093	0.240	-0.490	-0.098	-0.205	0.303	0.305
Y	0.706	0.013	0.320	0.848	0.006	0.106	-0.443	-0.586
Yb	0.687	-0.067	0.217	0.830	-0.130	0.016	-0.427	-0.523
Zn	0.119	0.258	0.506	0.031	0.672	0.468	0.453	-0.119
Zr	0.414	0.323	0.302	0.594	0.143	0.412	-0.534	-0.406

Table 2.10 Correlation coeffient (r) data for the Oman metalliferous sediments

	Dy	Er	Eu	Fe	Gd	Hf	Ho	La
Al								
Ba								
Ca								
Ce								
Co								
Cr								
Cs								
Cu								
Dy	1.000							
Er	0.951	1.000						
Eu	0.980	0.918	1.000					
Fe	-0.112	-0.262	-0.049	1.000				
Gd	0.989	0.937	0.978	-0.092	1.000			
Hf	0.244	0.233	0.260	-0.238	0.316	1.000		
Ho	0.993	0.953	0.977	-0.084	0.973	0.203	1.000	
La	0.945	0.892	0.925	-0.098	0.966	0.418	0.928	1.000
Mg	0.410	0.349	0.417	0.201	0.434	-0.039	0.412	0.409
Mn	-0.046	0.019	-0.076	-0.291	-0.034	0.289	-0.049	0.105
Nb	0.813	0.772	0.776	-0.101	0.847	0.655	0.787	0.881
Nd	0.958	0.897	0.947	-0.125	0.972	0.392	0.941	0.985
Ni	0.416	0.288	0.366	0.109	0.390	0.069	0.420	0.480
P	0.348	0.373	0.439	0.159	0.367	-0.057	0.363	0.278
Pb	-0.090	-0.012	-0.103	-0.212	-0.029	0.486	-0.092	0.161
Pr	0.959	0.889	0.941	-0.104	0.971	0.369	0.941	0.984
Rb	-0.262	-0.237	-0.254	-0.179	-0.197	0.413	-0.252	-0.076
Sc	0.716	0.668	0.729	-0.262	0.738	0.396	0.690	0.686
Si	0.000	0.094	-0.059	-0.361	-0.018	-0.246	-0.016	-0.119
Sm	0.985	0.911	0.971	-0.066	0.974	0.196	0.978	0.931
Sr	0.643	0.687	0.680	-0.101	0.632	0.086	0.656	0.561
Ta	0.073	0.089	0.070	-0.234	0.108	0.778	0.044	0.194
Tb	0.994	0.935	0.980	-0.074	0.982	0.217	0.990	0.946
Th	0.760	0.748	0.703	-0.071	0.776	0.260	0.748	0.789
Ti	0.790	0.733	0.761	-0.202	0.815	0.420	0.766	0.797
Tm	0.955	0.962	0.935	-0.222	0.942	0.343	0.950	0.902
U	0.366	0.292	0.392	0.536	0.406	0.087	0.369	0.419
V	-0.441	-0.436	-0.339	0.068	-0.433	0.131	-0.406	-0.468
Y	0.933	0.914	0.921	-0.238	0.944	0.461	0.919	0.965
Yb	0.957	0.981	0.935	-0.210	0.948	0.290	0.958	0.909
Zn	-0.096	-0.051	-0.124	-0.358	-0.056	0.416	-0.122	0.070
Zr	0.398	0.424	0.385	-0.481	0.449	0.701	0.355	0.546

Table 2.10

	Mg	Mn	Nb	Nd	Ni	P	Pb	Pr
Al								
Ba								
Ca								
Ce								
Co								
Cr								
Cs								
Cu								
Dy								
Er								
Eu								
Fe								
Gd								
Hf								
Ho								
La								
Mg	1.000							
Mn	-0.562	1.000						
Nb	0.372	0.044	1.000					
Nd	0.398	0.100	0.856	1.000				
Ni	0.373	0.117	0.371	0.478	1.000			
P	0.278	-0.233	0.128	0.314	0.082	1.000		
Pb	-0.209	0.646	0.168	0.061	0.062	-0.221	1.000	
Pr	0.401	0.096	0.851	0.997	0.480	0.278	0.042	1.000
Rb	0.073	0.143	-0.041	-0.134	0.021	-0.111	0.574	-0.146
Sc	0.215	0.113	0.590	0.745	0.384	0.537	-0.030	0.728
Si	0.377	-0.618	-0.092	-0.109	-0.166	-0.138	-0.413	-0.107
Sm	0.385	-0.035	0.767	0.954	0.402	0.371	-0.139	0.961
Sr	0.355	-0.197	0.427	0.586	0.165	0.305	-0.245	0.574
Ta	-0.200	0.258	0.526	0.175	0.009	-0.044	0.276	0.152
Tb	0.451	-0.060	0.800	0.965	0.432	0.357	-0.114	0.967
Th	0.467	-0.038	0.654	0.755	0.343	0.193	0.143	0.762
Ti	0.464	0.032	0.717	0.815	0.434	0.163	0.078	0.817
Tm	0.288	0.075	0.786	0.906	0.280	0.296	0.032	0.903
U	0.436	-0.260	0.441	0.382	-0.125	0.085	-0.089	0.405
V	-0.204	-0.014	-0.301	-0.421	-0.351	0.273	0.032	-0.452
Y	0.352	0.128	0.846	0.948	0.421	0.314	0.215	0.938
Yb	0.374	0.015	0.796	0.904	0.299	0.309	0.054	0.897
Zn	-0.514	0.930	0.096	0.077	0.032	-0.257	0.635	0.067
Zr	0.013	0.241	0.555	0.487	0.061	-0.208	0.593	0.475

Table 2.10

	Rb	Sc	Si	Sm	Sr	Ta	Tb	Th
Al								
Ba								
Ca								
Ce								
Co								
Cr								
Cs								
Cu								
Dy								
Er								
Eu								
Fe								
Gd								
Hf								
Ho								
La								
Mg								
Mn								
Nb								
Nd								
Ni								
P								
Pb								
Pr								
Rb	1.000							
Sc	0.093	1.000						
Si	0.054	-0.085	1.000					
Sm	-0.285	0.716	-0.063	1.000				
Sr	-0.141	0.495	0.328	0.588	1.000			
Ta	0.038	0.150	-0.329	0.043	-0.145	1.000		
Tb	-0.268	0.700	-0.015	0.991	0.646	0.057	1.000	
Th	0.135	0.531	0.138	0.743	0.410	-0.069	0.750	1.000
Ti	0.199	0.760	0.136	0.754	0.546	-0.031	0.769	0.745
Tm	-0.190	0.699	-0.007	0.921	0.684	0.114	0.933	0.761
U	-0.211	-0.074	-0.146	0.410	0.190	0.050	0.418	0.396
V	0.211	-0.057	-0.346	-0.410	-0.450	0.308	-0.431	-0.450
Y	-0.052	0.713	-0.102	0.902	0.569	0.244	0.920	0.776
Yb	-0.187	0.646	0.059	0.910	0.667	0.085	0.936	0.794
Zn	0.244	0.158	-0.537	-0.086	-0.291	0.353	-0.115	-0.023
Zr	0.363	0.327	0.055	0.331	0.264	0.356	0.360	0.415

Table 2.10

	Ti	Tm	U	V	Y	Yb	Zn
Al							
Ba							
Ca							
Ce							
Co							
Cr							
Cs							
Cu							
Dy							
Er							
Eu							
Fe							
Gd							
Hf							
Ho							
La							
Mg							
Mn							
Nb							
Nd							
Ni							
P							
Pb							
Pr							
Rb							
Sc							
Si							
Sm							
Sr							
Ta							
Tb							
Th							
Ti	1.000						
Tm	0.785	1.000					
U	0.144	0.301	1.000				
V	-0.418	-0.413	-0.167	1.000			
Y	0.768	0.939	0.289	-0.370	1.000		
Yb	0.770	0.978	0.325	-0.420	0.940	1.000	
Zn	0.091	0.007	-0.241	0.079	0.079	-0.046	1.000
Zr	0.508	0.507	-0.013	-0.297	0.626	0.493	0.257

Table 2.10

CHAPTER 3
Statistical inter-element correlation using factor analysis

3.1 Introduction

The purpose of this chapter is to evaluate the applicability and usefulness of the factor analysis procedure for analysing multivariate data in terms of linear combinations of end-members. The overall objective is to calculate the distribution pattern of the elements, thereby quantitatively defining the composition of each sediment-forming component. In a number of examples in the literature, factor analysis, using Varimax rotation, has produced meaningful geological information (Heath and Dymond, 1977; Full *et al.,* 1981; Leinen and Pisias, 1984; Full and Ehrlich, 1986). Although the technique has various strengths and weaknesses, the Varimax vectors will be assessed as a reasonable starting point for other techniques which are designed to extract end-member compositions for ancient sediment.

The correlation matrices, scree plots, factor pattern matrices and methods for factor extraction are discussed with specific reference to the results obtained in this study. The dataset from Oman subdivides geochemically by volcanic stratigraphic position into two broad groups of samples. The factor analysis is applied firstly to the whole dataset and then to the sample groups individually in an attempt to refine the output. Furthermore, the factor analysis technique may be used to calculate hypothetical "pure" end-members which ought to represent local element sources. In this way, the results of factor analysis may also be of comparative use in the assessment of existing numerical source models which may be applied to metalliferous sediments. Factor analysis was also carried out for the purpose of deriving geologically reasonable local end-member components to use in linear programming techniques in Chapter 4.

3.2 Previous applications of Factor Analysis

In previous studies, it has been common practice to describe metalliferous sediments in terms of admixtures of fixed-composition end-components

(Dymond, 1981). Goldberg (1954) and Krishwasnami (1976) first defined the framework for interpretation of sediment whole-rock data in terms of the sum of the contributions of different components. Using their method, sediment samples which are thought to form from variable mixtures of end-member components can be presented as plots on mixing diagrams showing theoretical dilution lines between the suggested end-members. The assumption that fixed composition end-members do exist and do combine in variable amounts to form the sediments in Oman is demonstrated below by using factor analysis with Varimax solution. Most recently, partitioning according to their sources using Varimax rotation has helped to characterise geologic mixtures in sediments by determining the actual composition of end-member sources (Full *et al.*, 1981; Leinen and Pisias, 1984; Full and Ehrlich, 1986). Meaningful geological application of factor analysis has been applied to modern carbonate sediments, ferromanganese nodules, marine plate-surface sediments and recent rise-crest sediments which are analogous to Oman umbers (Dymond *et al.*, 1976; Full *et al.*, 1981; Leinen and Pisias, 1984).

Previous studies have concluded that the main contribution of factor analysis is to the understanding of the association of variance in data sets. Because of the extremely variable absolute values of variables in Oman umber, and because the variables are commonly associated with more than one end-member, factor analysis may be a particularly useful tool. When studying ancient sediment for which direct analysis of end-members may not be possible due to poor exposure, factor analysis may be particularly useful (Leinen and Pisias, 1984; Full and Ehrlich, 1986).

This study applies a version of factor analysis known as *principal-axis factoring* which is a method similar to principal components analysis: the first stage is that the squared multiple correlation coefficients are used as initial estimates of communalities; based on these estimates a number of factors are extracted, communalties are estimated from factor loadings, and new estimates extracted, the new communality estimates replacing the old. The method used in principal-axis factoring continues until negligible change occurs in the communality estimates.

The other methods which could possibly have been used to extract factors are as follows: (1) *Unweighted Least Squares Method,* (2) *Generalised Least Squares Method,* (3) *Maximum Likelihood Method,* (4) *Alpha Method* and (5) *Image Factoring*. The first three methods listed above all consider the cases to be a

sample from some population and consider the variables to be fixed. The Unweighted Least Squares Method (1) and the Generalised Least Squares Method (2) are very similar to each other in that a factor pattern matrix is produced for a fixed number of factors to minimise the sum of the squared differences between the observed and the reproduced correlation matrices. The two methods differ in that the latter weights correlation inversely by the uniqueness of the variables. The Maximum Likelihood Method (3) uses a similar inverse correlation weighting to derive parameter estimates that are most likely to have produced the observed correlation matrix given that the sample is from a multivariate normal distribution. The fourth method, the Alpha Method, differs from the principals unifying the first three methods in that variables in a particular analysis are considered to be a sample from the universe of potential variables. The four methods above are similar to one another in that they all determine the common part of the variable as a function of hypothetical factors, and all four methods differ from the Image Factoring Method (5) that determines the common part of the variable as its linear regression on remaining variables. In the factor extraction phase, which ever method is used, the number of factors required to describe the data adequately is determined.

The technique applied in this chapter adopts the general principals outlined by the previous studies cited above. The hypothesis is that, if the same *Factors* emerge from each of the three volcanic stratigraphic positions in the lava pile, then variability in the dataset may be explained in terms of admixtures of fixed composition end-members. Alternatively, the model can also show variability in end-member components should they exist.

The factor analysis technique reduces an observed set of relationships between many interrelated variables to a simpler set of relationships between fewer variables which are termed *clusters* or *factors*. The output is in the form of "unifying constructs" which represent the geological end-member element associations. The artificial inter-element associations are derived from measurement of directly observable variables that otherwise are not measurable other than by chemical separation techniques which also have drawbacks. The calculation is based upon measured bulk-rock data obtained by X-ray Fluorescence (XRF) analysis.

The associations between the original variables are measured by correlation coefficients and pairs of correlations are expressed by the *correlation matrix*. Correlation matrices showing inter-element relationships are calculated using

trace element and major element bulk-rock analysis and used to illustrate significant correlated element pairs.

3.3 Applying factor analysis to geochemical data

The procedure which transforms whole rock XRF data to meaningful factor analysis output will be presented in Section 3.4 in the following order:

(1) The algorithms used are briefly outlined and explained.

(2) A correlation matrix for all variables is explained and then calculated from XRF whole-rock data (73 As/Bu samples; 88 As/Ls samples; and 25 Bu samples) using the formulae described in Section 3.4.1.

(3) Factor extraction is explained and carried out. The number of factors necessary to represent the data and the method for calculating them is assessed.

(4) Varimax rotation is applied to the extracted factors, thus transforming the factors to make them more understandable by producing a best-fit of the factor axes to the variables in vector-space.

3.4 The Factor Analysis model

The basic assumption in the factor analysis evaluation of geochemical datasets is that underlying dimensions, or *factors*, can be used to explain complex phenomena. The observed correlation between variables result from their sharing these factors. The factor analysis does provide results which show complex inter-element associations but it does not explain these associations. For example, in this study, correlation between elements may be attributable to the hydrothermal, biogenic, detrital or hydrogenous components suggested in the previous chapter. Thus the aim of factor analysis is to identify the non-directly-observable factors which are artificial constructions based on individual measurable variables.

3.4.1 Algorithms

The proposed factor analysis model is based on the Pearson product-moment coefficient of linear correlation in which the numerical values are termed the *correlation coefficient, r.* Correlation coefficients quantify the interdependence

of two variables on one another based on measurement of a number of individuals.

The equation used in this study to obtain a factor analysis solution (Equation 3.1) mathematically resembles the multiple regression equations (Equation 3.2). The first equation is a hypothetical expression of metalliferous sediment in terms of a sediment of multi-component origin. The second equation assumes that **y** is a function of a series of independent variables. The equations resemble one another in that they both represent a matrix equation where metalliferous sediment (**y**) = **[element 1, element 2, ..., element 20]** and **a, b, ..., x** represent the properties of the components.

Eqn 3.1 **Metalliferous sediment = a(*hydrothermal*) + b(*hydrogenous*) + c(*biogenic*)+ d(*detrital*) + ... + x(n)**

Eqn 3.2 $y = f(x_n) = a + b_1x_1 + b_2x_2 + ... + b_nx_n$

The results of applying the equation above to multivariate geochemical data is that groups of variables emerge which then are interpreted as end-member components which are neither pre-known nor pre-selected. The factors representing end-members must then be labelled in a geologically meaningful way according to which variables are interrelated.

The method which has been adopted uses the equation below (Equation 3.3) which includes the general model for the *i*-th standardized variable and which includes an expression **U** termed a *Unique factor*. The Unique factor in the case of the metalliferous sediments is that part which cannot be explained by the other factors. The Unique factors are those unrelated to each other as well as unrelated to the common factors. Thus, the general model is written as Equation 3.3:

Eqn 3.3 $X_i = A_{i1}F_1 + A_{i2}F_2 + ... + A_{ik}F_k + U_i$

where the **F**'s are the common factors, **U**, the Unique factor and the **A**'s the coefficients used to combine the k factors.

The factors are determined from the measured variables (XRF whole-rock data) and are estimated as being linear combinations of the variables. Thus, for example, a factor proposed to represent the "detrital component" could be expressed as Equation 3.4:

Eqn 3.4 $\textbf{Detrital} = C_1(Al) + C_2(As) + C_3(Ba) + ... + C_{20}(Zr)$

where the C_1 to C_{20} are coefficients.

Although it is statistically possible and physically likely that all of the variables contribute in some way to the proposed detrital factor, it is preferable that a restricted number of variables characterize detrital input. To decide which variables contribute to each factor, coefficients scores are used. The general expression (Equation 4.5) for the estimate of the *j*-th factor is:

Eqn 3.5 $F_j = \Sigma^{p}_{i=1} W_{ji}X_i = W_{ji}X_1 + W_{ji}X_2 + ... + W_{jp}X_p$

where the W_{ji} to W_{jp} are the factor score coefficients, and **p** the number of variables. The total number of possible correlation between the original variables is quantified by the correlation coefficients and expressed in the *correlation matrix*.

3.4.2 Correlation matrices

Correlation matrices estimate the correlation which exists between each element for a total population of which only a sub-set has been measured. If the correlation between variables are small it is unlikely that they share common factors. The values represent the correlation coefficient, ***r***, which has been produced by the Pearson product-moment coefficient of linear correlation described above. The statistical significance of each value representing the relationship between element *x* and element *y* is calculated for each of the sample groups. The values of ***r*** presented in the correlation matrices vary between +1 and -1. A perfect linear relationship in which element *x* is in perfect sympathy with element *y* receives an ***r***-value of +1. Perfect antipathy between a pair of elements receives an ***r***-value of -1 and no relationship between a pair produces ***r*** = 0. The value of r^2 is equal to the total variance explained by the linear relationship for the pair of elements, for example ***r*** = 0.77 between Co and MnO (Table 3.2: Axis/Basal Upper boundary), whereas r^2 = 0.593; i.e. 59.3% of Co and MnO is explained by the linear relationship.

Table 3.4a: Correlation Coefficient Matrix (Bu)

	AL2O3	AS	BA	CAO	CO	CR	CU	FE2O3	MGO	MNO	MO	NI	P2O5	PB	SC	SIO2	SR	TIO2	V	ZN	ZR
AL2O3	1.000																				
AS	0.075	1.000																			
BA	0.547	-0.145	1.000																		
CAO	-0.369	-0.093	-0.448	1.000																	
CO	-0.530	0.169	-0.198	-0.106	1.000																
CR	0.177	-0.163	0.070	0.471	-0.209	1.000															
CU	0.136	-0.088	0.120	0.079	-0.034	0.425	1.000														
FE2O3	-0.361	0.062	-0.300	-0.379	0.455	-0.489	-0.410	1.000													
MGO	0.228	0.287	0.227	-0.227	-0.223	-0.100	-0.247	0.171	1.000												
MNO	-0.486	0.155	-0.140	0.099	0.840	-0.071	0.106	0.046	-0.283	1.000											
MO	0.138	-0.233	-0.333	-0.243	0.058	-0.116	0.163	0.342	-0.343	-0.093	1.000										
NI	-0.501	0.208	-0.355	0.177	0.648	-0.114	-0.154	0.600	0.209	0.494	-0.097	1.000									
P2O5	-0.266	0.104	-0.215	-0.019	0.178	-0.318	-0.581	0.659	0.412	-0.157	-0.162	0.549	1.000								
PB	0.302	0.197	0.367	0.187	-0.182	0.400	0.555	-0.774	-0.247	0.174	-0.240	-0.421	-0.669	1.000							
SC	0.063	0.171	-0.343	0.361	0.078	0.051	-0.013	0.146	-0.226	0.024	0.205	0.258	0.131	-0.124	1.000						
SIO2	0.607	-0.050	0.531	-0.765	-0.452	-0.228	0.073	-0.119	0.113	-0.512	0.169	-0.712	-0.278	0.082	-0.402	1.000					
SR	0.160	-0.274	-0.190	0.116	-0.387	-0.009	0.299	-0.063	-0.278	-0.222	0.402	-0.172	-0.233	-0.021	0.447	0.063	1.000				
TIO2	0.476	0.215	0.375	-0.361	0.036	0.001	-0.114	0.231	0.518	-0.043	0.025	0.345	0.202	-0.096	0.161	0.065	-0.025	1.000			
V	0.066	-0.170	-0.101	-0.054	-0.139	-0.271	-0.032	-0.004	-0.452	-0.280	0.125	-0.307	0.092	-0.073	0.007	0.279	0.113	-0.556	1.000		
ZN	-0.080	0.202	0.137	0.309	0.280	0.261	0.416	-0.534	-0.219	0.682	-0.230	0.051	-0.533	0.751	-0.041	-0.352	-0.050	-0.043	-0.334	1.000	
ZR	0.078	0.086	0.577	-0.064	0.222	0.183	0.076	-0.280	-0.127	0.383	-0.371	0.043	-0.196	0.420	-0.142	0.014	-0.319	0.272	-0.243	0.420	1.000

Table 3.4b: 1-tailed significance correlation matrix (Bu)

	AL2O3	AS	BA	CAO	CO	CR	CU	FE2O3	MGO	MNO	MO	NI	P2O5	PB	SC	SIO2	SR	TIO2	V	ZN
AL2O3	.																			
AS	0.367	.																		
BA	0.003	0.255	.																	
CAO	0.042	0.336	0.016	.																
CO	0.005	0.220	0.182	0.315	.															
CR	0.210	0.228	0.375	0.012	0.169	.														
CU	0.267	0.344	0.293	0.360	0.440	0.021	.													
FE2O3	0.045	0.389	0.082	0.037	0.015	0.009	0.026	.												
MGO	0.147	0.092	0.149	0.149	0.153	0.325	0.128	0.218	.											
MNO	0.009	0.240	0.262	0.327	0.000	0.375	0.316	0.418	0.096	.										
MO	0.264	0.142	0.060	0.132	0.396	0.299	0.228	0.055	0.054	0.337	.									
NI	0.007	0.170	0.048	0.209	0.000	0.302	0.241	0.001	0.169	0.008	0.330	.								
P2O5	0.110	0.319	0.163	0.466	0.208	0.070	0.002	0.000	0.025	0.238	0.230	0.003	.							
PB	0.080	0.184	0.042	0.196	0.203	0.029	0.003	0.000	0.128	0.214	0.135	0.023	0.000	.						
SC	0.387	0.218	0.055	0.045	0.361	0.409	0.477	0.253	0.150	0.457	0.174	0.117	0.276	0.286	.					
SIO2	0.001	0.411	0.005	0.000	0.015	0.148	0.371	0.294	0.304	0.006	0.221	0.000	0.099	0.355	0.028	.				
SR	0.232	0.103	0.192	0.299	0.034	0.483	0.083	0.388	0.100	0.154	0.028	0.217	0.142	0.462	0.016	0.387	.			
TIO2	0.011	0.163	0.039	0.045	0.435	0.498	0.302	0.145	0.006	0.423	0.455	0.053	0.178	0.331	0.232	0.385	0.454	.		
V	0.383	0.218	0.324	0.404	0.263	0.106	0.443	0.493	0.015	0.098	0.285	0.077	0.338	0.371	0.488	0.099	0.303	0.003	.	
ZN	0.358	0.177	0.267	0.075	0.098	0.114	0.024	0.004	0.158	0.000	0.145	0.409	0.004	0.000	0.426	0.050	0.411	0.424	0.060	.
ZR	0.362	0.348	0.002	0.385	0.154	0.202	0.365	0.098	0.282	0.035	0.041	0.422	0.185	0.023	0.259	0.475	0.069	0.105	0.132	0.023

Determinant of correlation matrix+A78 = 0

Kaiser-Meyer-Olkin measure of sampling adequacy = 0.1694

Bartlett test of sphericity = 506.4

Table 3.3a: Correlation Coefficient Matrix (As/Ls)

As/Ls	AL2O3	AS	BA	CAO	CO	CR	CU	FE2O3	MGO	MNO	MO	NI	P2O5	PB	SC	SIO2	SR	TIO2	V	ZN	ZR
AL2O3	1.000																				
AS	0.184	1.000																			
BA	0.114	0.437	1.000																		
CAO	0.089	0.475	0.223	1.000																	
CO	-0.046	0.303	0.232	0.004	1.000																
CR	-0.109	0.037	0.227	0.481	-0.051	1.000															
CU	-0.198	-0.035	-0.023	-0.136	0.024	0.065	1.000														
FE2O3	-0.297	-0.541	-0.306	-0.563	0.359	-0.201	0.107	1.000													
MGO	0.477	-0.146	-0.106	-0.248	-0.062	-0.198	-0.159	0.107	1.000												
MNO	0.089	0.695	0.598	0.486	0.572	0.115	-0.070	-0.366	-0.223	1.000											
MO	0.026	-0.001	0.044	-0.012	-0.235	0.025	0.004	-0.263	-0.260	-0.072	1.000										
NI	0.486	0.416	0.113	0.115	0.164	-0.158	-0.303	-0.126	0.412	0.181	-0.162	1.000									
P2O5	0.052	0.273	-0.152	0.022	-0.034	-0.023	0.110	0.030	0.075	-0.087	-0.094	-0.029	1.000								
PB	0.109	0.642	0.515	0.342	0.572	0.064	-0.009	-0.344	-0.270	0.925	0.017	0.094	0.001	1.000							
SC	0.570	0.351	0.126	0.354	0.184	0.124	-0.217	-0.125	0.113	0.245	-0.229	0.538	0.200	0.163	1.000						
SIO2	0.009	-0.026	-0.013	-0.303	-0.565	-0.142	0.044	-0.538	-0.057	-0.251	0.384	-0.132	-0.159	-0.157	-0.351	1.000					
SR	-0.300	-0.015	0.228	-0.061	0.233	0.224	0.116	0.275	-0.224	0.180	-0.031	-0.204	-0.061	0.127	-0.082	-0.233	1.000				
TIO2	0.821	0.225	0.107	0.126	0.020	-0.103	-0.229	-0.228	0.365	0.106	-0.066	0.618	-0.064	0.062	0.712	-0.042	-0.210	1.000			
V	-0.097	-0.251	0.007	-0.157	0.058	0.230	-0.069	0.301	0.027	-0.090	-0.071	-0.179	0.076	-0.093	-0.030	-0.136	0.180	-0.206	1.000		
ZN	0.193	0.577	0.643	0.289	0.372	0.041	0.043	-0.321	0.150	0.750	-0.062	0.245	-0.052	0.669	0.197	-0.146	0.158	0.256	-0.164	1.000	
ZR	0.557	0.580	0.333	0.473	-0.148	0.116	-0.136	-0.823	-0.019	0.431	0.173	0.375	-0.072	0.378	0.399	0.350	-0.201	0.604	-0.270	0.429	1

Determinant of correlation matrix = 0
Kaiser-Meyer-Olkin measure of sampling ade = 0.6154
Bartlett test of sphericity = 1450.7

Table 3.3b 1-tailed significance correlation matrix (As/Ls)

	AL2O3	AS	BA	CAO	CO	CR	CU	FE2O3	MGO	MNO	MO	NI	P2O5	PB	SC	SIO2	SR	TIO2	V	ZN
AL2O3	.																			
AS	0.048	.																		
BA	0.152	0.000	.																	
CAO	0.212	0.000	0.021	.																
CO	0.340	0.003	0.017	0.485	.															
CR	0.164	0.372	0.020	0.000	0.323	.														
CU	0.036	0.378	0.420	0.110	0.415	0.279	.													
FE2O3	0.003	0.000	0.002	0.000	0.000	0.034	0.168	.												
MGO	0.000	0.093	0.170	0.012	0.287	0.037	0.076	0.167	.											
MNO	0.211	0.000	0.000	0.000	0.000	0.149	0.266	0.000	0.022	.										
MO	0.408	0.495	0.345	0.458	0.016	0.412	0.486	0.008	0.009	0.259	.									
NI	0.000	0.000	0.155	0.151	0.069	0.076	0.003	0.128	0.000	0.051	0.071	.								
P2O5	0.321	0.006	0.085	0.422	0.381	0.417	0.161	0.394	0.251	0.217	0.198	0.397	.							
PB	0.164	0.000	0.000	0.001	0.000	0.282	0.469	0.001	0.007	0.000	0.441	0.199	0.496	.						
SC	0.000	0.001	0.128	0.001	0.048	0.131	0.024	0.129	0.154	0.013	0.019	0.000	0.035	0.071	.					
SIO2	0.467	0.407	0.452	0.003	0.000	0.101	0.345	0.000	0.303	0.011	0.000	0.118	0.076	0.078	0.001	.				
SR	0.003	0.447	0.019	0.291	0.017	0.021	0.148	0.006	0.021	0.051	0.390	0.032	0.291	0.126	0.230	0.017	.			
TIO2	0.000	0.021	0.167	0.128	0.428	0.177	0.019	0.019	0.000	0.170	0.278	0.000	0.282	0.289	0.000	0.354	0.028	.		
V	0.191	0.011	0.476	0.079	0.301	0.018	0.268	0.003	0.403	0.210	0.261	0.053	0.248	0.201	0.393	0.110	0.052	0.031	.	
ZN	0.041	0.000	0.000	0.004	0.000	0.357	0.351	0.002	0.088	0.000	0.288	0.013	0.321	0.000	0.037	0.093	0.077	0.010	0.069	.
ZR	0.000	0.000	0.001	0.000	0.092	0.148	0.111	0.000	0.432	0.000	0.059	0.000	0.259	0.000	0.000	0.001	0.034	0.000	0.007	0.000

Table 3.2a: Correlation Coefficient Matrix (As/Bu)

As/Bu	AL2O3	AS	BA	CAO	CO	CR	CU	FE2O3	MGO	MNO	MO	NI	P2O5	PB	SC	SIO2	SR	TIO2	V	ZN	ZR
AL2O3	1.000																				
AS	-0.033	1.000																			
BA	-0.120	0.384	1.000																		
CAO	0.154	0.523	0.032	1.000																	
CO	-0.098	0.551	0.444	-0.004	1.000																
CR	0.032	0.255	0.562	0.188	-0.027	1.000															
CU	0.108	0.224	0.162	-0.022	0.508	0.110	1.000														
FE2O3	-0.113	0.024	-0.113	-0.440	0.387	-0.106	0.343	1.000													
MGO	0.488	-0.187	-0.353	-0.234	-0.215	-0.076	0.242	0.302	1.000												
MNO	-0.065	0.686	0.464	0.281	0.774	0.070	0.432	-0.021	-0.371	1.000											
MO	-0.354	-0.527	0.083	-0.408	-0.231	0.006	-0.146	-0.199	-0.295	-0.300	1.000										
NI	0.134	0.447	-0.027	0.149	0.551	-0.084	0.482	0.581	0.350	0.368	-0.618	1.000									
P2O5	-0.209	0.216	-0.020	0.111	0.103	0.059	0.089	0.258	0.097	0.121	-0.264	0.340	1.000								
PB	-0.061	0.545	0.324	0.183	0.626	0.081	0.437	-0.087	-0.321	0.734	-0.309	0.267	-0.085	1.000							
SC	0.185	0.284	0.112	0.124	0.340	0.053	0.505	0.359	0.151	0.239	-0.325	0.437	0.237	0.141	1.000						
SIO2	-0.183	-0.736	-0.133	-0.695	-0.509	-0.142	-0.400	-0.220	0.027	-0.603	0.704	-0.671	-0.340	-0.384	-0.473	1.000					
SR	0.012	0.213	0.096	0.155	0.212	0.134	0.214	0.050	-0.206	0.325	0.095	0.122	-0.035	0.229	0.307	-0.245	1.000				
TIO2	0.425	0.029	0.000	-0.292	0.300	-0.175	0.338	0.370	0.469	0.153	-0.484	0.480	-0.041	0.297	0.419	-0.131	-0.094	1.000			
V	0.066	0.489	0.265	-0.019	0.218	0.254	0.256	0.202	0.134	0.231	-0.188	0.233	0.099	0.128	0.151	-0.238	0.139	0.000	1.000		
ZN	0.058	0.629	0.467	0.256	0.760	0.082	0.513	0.019	-0.219	0.901	-0.326	0.486	0.162	0.711	0.222	-0.599	0.249	0.192	0.257	1.000	
ZR	0.382	0.289	0.062	0.088	0.251	-0.030	0.273	-0.104	0.309	0.381	-0.567	0.289	-0.032	0.500	0.112	-0.247	-0.027	0.702	0.128	0.311	1.000

Determinant of correlation matrix = 0.000

Kaiser-Meyer-Olkin measure of sampling adequacy = 0.468

Bartlett test of sphericity = 723.2 Significance

Table 3.2b: 1-tailed significance correlation matrix (As/Bu)

	AL2O3	AS	BA	CAO	CO	CR	CU	FE2O3	MGO	MNO	MO	NI	P2O5	PB	SC	SIO2	SR	TIO2	V	ZN
AL2O3																				
AS	0.421																			
BA	0.234	0.008																		
CAO	0.175	0.000	0.423																	
CO	0.276	0.000	0.002	0.490																
CR	0.423	0.058	0.000	0.126	0.435															
CU	0.257	0.085	0.163	0.446	0.000	0.253														
FE2O3	0.247	0.443	0.247	0.003	0.007	0.261	0.016													
MGO	0.001	0.127	0.014	0.076	0.094	0.323	0.069	0.031												
MNO	0.348	0.000	0.001	0.041	0.000	0.335	0.003	0.449	0.010											
MO	0.014	0.000	0.309	0.005	0.078	0.486	0.187	0.112	0.034	0.032										
NI	0.207	0.002	0.435	0.183	0.000	0.306	0.001	0.000	0.014	0.011	0.000									
P2O5	0.101	0.093	0.451	0.251	0.266	0.361	0.296	0.057	0.279	0.231	0.052	0.017								
PB	0.355	0.000	0.022	0.132	0.000	0.311	0.003	0.300	0.023	0.000	0.028	0.050	0.304							
SC	0.129	0.040	0.249	0.225	0.017	0.373	0.001	0.012	0.180	0.071	0.022	0.003	0.073	0.195						
SIO2	0.132	0.000	0.210	0.000	0.000	0.195	0.006	0.089	0.435	0.000	0.000	0.000	0.017	0.008	0.001					
SR	0.470	0.097	0.280	0.173	0.097	0.209	0.095	0.382	0.104	0.022	0.282	0.231	0.417	0.081	0.029	0.067				
TIO2	0.003	0.431	0.500	0.035	0.032	0.143	0.018	0.010	0.001	0.177	0.001	0.001	0.403	0.033	0.004	0.214	0.284			
V	0.345	0.001	0.052	0.454	0.092	0.060	0.058	0.109	0.208	0.079	0.126	0.077	0.274	0.219	0.179	0.073	0.199	0.499		
ZN	0.364	0.000	0.001	0.058	0.000	0.309	0.000	0.455	0.090	0.000	0.021	0.001	0.162	0.000	0.087	0.000	0.063	0.121	0.057	
ZR	0.008	0.037	0.355	0.297	0.062	0.428	0.046	0.264	0.028	0.008	0.000	0.037	0.424	0.001	0.249	0.065	0.434	0.000	0.219	0.027

Table 3.1a: Correlation Coefficient Matrix (full dataset)

	AL2O3	AS	BA	CAO	CO	CR	CU	FE2O3	MGO	MNO	MO	NI	P2O5	PB	SC	SIO2	SR	TIO2	V	ZN	ZR
AL2O3	1.000																				
AS	0.074	1.000																			
BA	0.161	0.165	1.000																		
CAO	0.063	0.435	0.024	1.000																	
CO	-0.100	0.506	0.142	0.219	1.000																
CR	0.032	0.052	0.241	0.301	0.005	1.000															
CU	-0.158	-0.019	-0.005	-0.094	0.042	0.050	1.000														
FE2O3	-0.270	-0.386	-0.236	-0.585	0.047	-0.223	0.100	1.000													
MGO	0.431	-0.182	-0.072	-0.320	-0.213	-0.124	-0.129	0.220	1.000												
MNO	-0.004	0.632	0.271	0.520	0.819	0.131	-0.008	-0.387	-0.335	1.000											
MO	-0.016	-0.201	-0.116	-0.186	-0.261	-0.051	0.011	-0.091	-0.162	-0.269	1.000										
NI	0.339	0.372	-0.002	0.239	0.381	-0.059	-0.223	-0.074	0.286	0.354	-0.253	1.000									
P2O5	-0.068	0.142	-0.133	-0.010	0.031	-0.130	0.070	0.160	0.113	-0.084	-0.059	0.068	1.000								
PB	0.078	0.601	0.399	0.474	0.598	0.258	0.034	-0.454	-0.342	0.830	-0.235	0.237	-0.190	1.000							
SC	0.433	0.360	0.041	0.372	0.340	0.094	-0.154	-0.127	0.019	0.336	-0.281	0.540	0.170	0.280	1.000						
SIO2	0.005	-0.366	-0.029	-0.574	-0.598	-0.154	0.014	-0.186	0.098	-0.578	0.449	-0.378	-0.149	-0.446	-0.458	1.000					
SR	-0.179	0.067	0.052	0.087	0.216	0.112	0.110	0.118	-0.252	0.232	-0.043	-0.077	-0.082	0.226	0.054	-0.258	1.000				
TIO2	0.722	0.179	0.117	0.054	0.142	-0.020	-0.179	-0.165	0.331	0.158	-0.127	0.582	-0.055	0.167	0.630	-0.102	-0.151	1.000			
V	-0.031	-0.039	0.010	-0.101	0.074	-0.007	-0.030	0.214	-0.002	-0.005	-0.055	-0.088	0.093	-0.011	0.004	-0.090	0.145	-0.175	1.000		
ZN	0.083	0.597	0.312	0.492	0.714	0.165	0.052	-0.390	-0.188	0.907	-0.273	0.382	-0.106	0.852	0.323	-0.548	0.231	0.216	-0.018	1.000	
ZR	0.458	0.470	0.337	0.436	0.251	0.169	-0.093	-0.725	-0.090	0.524	-0.041	0.390	-0.110	0.532	0.384	-0.028	-0.084	0.597	-0.148	0.500	1.000

Table 3.1b: 1-tailed significance correlation matrix (full dataset)

	AL2O3	AS	BA	CAO	CO	CR	CU	FE2O3	MGO	MNO	MO	NI	P2O5	PB	SC	SIO2	SR	TIO2	V	ZN
AL2O3	.																			
AS	0.191	.																		
BA	0.027	0.024	.																	
CAO	0.227	0.000	0.388	.																
CO	0.116	0.000	0.045	0.004	.															
CR	0.352	0.269	0.002	0.000	0.478	.														
CU	0.029	0.409	0.475	0.131	0.308	0.277	.													
FE2O3	0.001	0.000	0.002	0.000	0.289	0.004	0.115	.												
MGO	0.000	0.015	0.196	0.000	0.005	0.069	0.062	0.004	.											
MNO	0.483	0.000	0.001	0.000	0.000	0.058	0.462	0.000	0.000	.										
MO	0.425	0.008	0.082	0.013	0.001	0.273	0.449	0.140	0.027	0.001	.									
NI	0.000	0.000	0.490	0.002	0.000	0.240	0.004	0.189	0.000	0.000	0.001	.								
P2O5	0.211	0.045	0.057	0.451	0.356	0.060	0.202	0.027	0.088	0.157	0.240	0.208	.							
PB	0.175	0.000	0.000	0.000	0.000	0.001	0.341	0.000	0.000	0.000	0.002	0.002	0.011	.						
SC	0.000	0.000	0.312	0.000	0.000	0.130	0.033	0.064	0.410	0.000	0.000	0.000	0.021	0.000	.					
SIO2	0.476	0.000	0.363	0.000	0.000	0.033	0.435	0.013	0.122	0.000	0.000	0.000	0.037	0.000	0.000	.				
SR	0.016	0.211	0.269	0.150	0.005	0.090	0.096	0.080	0.001	0.003	0.303	0.179	0.165	0.003	0.259	0.001	.			
TIO2	0.000	0.016	0.081	0.261	0.045	0.407	0.016	0.024	0.000	0.029	0.064	0.000	0.255	0.023	0.000	0.112	0.035	.		
V	0.355	0.321	0.451	0.113	0.189	0.467	0.359	0.005	0.491	0.474	0.254	0.147	0.134	0.446	0.480	0.143	0.042	0.018	.	
ZN	0.160	0.000	0.000	0.000	0.000	0.024	0.267	0.000	0.012	0.000	0.000	0.000	0.103	0.000	0.000	0.000	0.003	0.005	0.413	.
ZR	0.000	0.000	0.000	0.000	0.001	0.021	0.134	0.000	0.141	0.000	0.314	0.000	0.095	0.000	0.000	0.367	0.158	0.000	0.038	0.000

Determinant of correlation matrix = 0.000

Kaiser-Meyer-Olkin measure of sampling adequacy = 0.674

Bartlett test of sphericity = 2259

Correlation matrices have been calculated from the entire dataset (Table 3.1), the Axis/Basal Upper boundary (Table 3.2), the Axis/Lasail boundary (Table 3.3) and the Basal Upper Unit (Table 3.4). All of the matrices show that at least half of the coefficients are greater than 0.3 in absolute value. A 1-tailed significance correlation matrix accompanies each correlation coefficient matrix (Tables 3.1 to 3.4).

In As/Bu Group samples (Table 3.2), for example, all of the elements except for P show a large correlation with at least one other variable in the dataset from the Basal Upper lava unit. The statistical significance (t) of each correlation coefficient (r) is tabulated on the 1-tailed significance matrix that accompanies each correlation matrix. Values of t which must be exceeded are tabulated for a t-distribution with v degrees of freedom (Appendix A.5). There is only *significant* positive correlation between pairs of elements (at the 5 % significance level), when the calculated t values (Tables 3.1 to 3.4) are in excess of the following tabulated t values:

(1)	As/Ls	$v = 81$	$t = 1.671$
(2)	As/Bu	$v = 46$	$t = 1.684$
(3)	Bu	$v = 21$	$t = 1.721$
(4)	Full data-set	$v = 148$	$t = 1.658$

In Table 3.2, all of the elements except Sr show a large correlation with at least one other variable from the As/Bu boundary. In Table 3.3, all but P show a large correlation with at least one other variable.

3.4.3 Method for factor extraction

The factor extraction process is the most efficient technique for extracting a simpler set of relationships among fewer variables from the 20 elements considered in the analysis (it is also possible to extract clusters from correlation matrices by the Ramifying Linkage Method which is far simpler but less informative). In geology two techniques of factor analysis are commonly used, these are the *R-mode* technique and the *Q-mode* technique. The Q-mode technique correlates *two individual samples* on the basis of a large number of measured variables and is used mainly in palaeontology to extract the factors necessary to distinguish and define species from one another. The R-mode technique, which is more commonly used in geochemistry, correlates *pairs of*

variables for a large number of samples and is consequently more applicable to the type of data used in this study.

The R-mode technique used in this study uses a *principal component solution* which is obtained by the extraction of *eigenvalues* from the correlation matrix. Factors are extracted by several different methods, using a series of matrix and vector operations, from the correlation matrix. The difference between the methods used to determine what is a "good fit" and the reason for the choice of Principal Axis Factoring have been outlined briefly in Section 3.4

R-mode factor analysis technique correlates pairs of variables for a large number of samples to produce a principal component solution by the extraction of eigenvalues from the correlation matrix. The principal components results (Tables 3.1, 3.2, 3.3, 3.4) are solutions in which the maximum possible fraction of the total variance of the data is accounted for by first factor, the maximum remaining variance on the second factor, and so on. The first and second factors are mutually exclusive, i.e., are uncorrelated with each other. Successive components explain progressively smaller proportions of the total variance and none of the factors correlates with any of the others.

In each sample Group, six factors have been necessary to represent the data. To decide this it was necessary to examine the percentage of total variance represented explained by each. The total variance is the sum of the variance of each variable (all factors have a mean = 0 and standard deviation = 1 for simplicity). In this study there are 20 variables since 20 elements have been analysed and are considered, and each is standardized to have a variance of 1. Hence the total variance is 20.

The total variance that is explained by each factor is known as the *eigenvalue* (Table 3.5, all samples; Table 3.6, As/Bu; Table 3.7, As/Ls; Table 3.8, Bu). In conjunction with tabulated eigenvalues, the percentage of variation attributed to each factor and the cumulative percentages are given. Looking, for example, at Table 3.7, the data for the Axis/Lasail boundary, the first factor has a variance of 5.44 which is 25.9% of the total variance of 21. The second factor has a variance of 3.11 which is 15.8 % of the total variance of 21, and so on. The factors have been arranged in descending order of variance. The cumulative data shows that, in this example, the first two factors alone account for 41.7% of the total variance of the data and that the first six factors account for 74.1% of the total variance. The remaining 15 factors account for only 25.9% of the variance. Hence a six

Table 3.5: Final Statistics (full dataset)					
Variable	Communality	Factor	Eigenvalue	%var	cum%
AL2O3	0.7629	1	6.0929	29	29
AS	0.6744	2	2.9151	13.9	42.9
BA	0.6366	3	2.2791	10.9	53.7
CAO	0.8740	4	1.3203	6.3	60
CO	0.8329	5	1.2006	5.7	65.8
CR	0.7113	6	1.0332	4.9	70.7
CU	0.6445	7	1.0017	4.8	75.4
FE2O3	0.8887				
MGO	0.6496				
MNO	0.9307				
MO	0.5190				
NI	0.7050				
P2O5	0.8232				
PB	0.8506				
SC	0.6911				
SIO2	0.8633				
SR	0.4293				
TIO2	0.8283				
V	0.8112				
ZN	0.8674				
ZR	0.8493				

Table 3.6: Final Statistics (As/Bu)					
Variable	Communality	Factor	Eigenvalue	%var	cum%
AL2O3	0.7477	1	6.4439	30.7	30.7
AS	0.8235	2	3.2629	15.5	46.2
BA	0.7678	3	2.0866	9.9	56.2
CAO	0.9273	4	1.9216	9.2	65.3
CO	0.8587	5	1.5129	7.2	72.5
CR	0.7503	6	1.2213	5.8	78.3
CU	0.6386				
FE2O3	0.8437				
MGO	0.8098				
MNO	0.9023				
MO	0.8652				
NI	0.8186				
P2O5	0.5786				
PB	0.8055				
SC	0.6453				
SIO2	0.9423				
SR	0.6919				
TIO2	0.8656				
V	0.5265				
ZN	0.8243				
ZR	0.8158				

Table 3.7: Final Statistics (As/Ls)					
Variable	Communality	Factor	Eigenvalue	%var	cum%
AL2O3	0.7886	1	5.4480	25.9	25.9
AS	0.8201	2	3.3110	15.8	41.7
BA	0.7006	3	2.7469	13.1	54.8
CAO	0.8491	4	1.6428	7.8	62.6
CO	0.7978	5	1.3283	6.3	68.9
CR	0.7741	6	1.0879	5.2	74.1
CU	0.4916				
FE2O3	0.9276				
MGO	0.6572				
MNO	0.9331				
MO	0.3750				
NI	0.6612				
P2O5	0.7983				
PB	0.8341				
SC	0.7709				
SIO2	0.8503				
SR	0.5008				
TIO2	0.8291				
V	0.5277				
ZN	0.7921				
ZR	0.8856				

Table 3.8: Final Statistics (Bu)					
Variable	Communality	Factor	Eigenvalue	%var	cum%
AL2O3	0.8716	1	4.7184	22.5	22.5
AS	0.9080	2	4.0692	19.4	41.8
BA	0.9002	3	3.1794	15.1	57
CAO	0.9628	4	2.0795	9.9	66.9
CO	0.9231	5	1.8841	9	75.9
CR	0.6995	6	1.2102	5.8	81.6
CU	0.6439	7	1.0520	5	86.6
FE2O3	0.9142				
MGO	0.9124				
MNO	0.9282				
MO	0.8145				
NI	0.8870				
P2O5	0.8534				
PB	0.9094				
SC	0.9026				
SIO2	0.9672				
SR	0.6995				
TIO2	0.9401				
V	0.8186				
ZN	0.8858				
ZR	0.8512				

factor model appears to be appropriate for the As/Ls boundary samples. Similarly, Table 3.8 shows that the first 6 factors account for 86.6% of the total variance in samples from the Basal Upper unit, and Table 3.6 shows that the first 6 factors account for 78.3% of the total variance at the Axis/Basal Upper boundary.

The determination of the six or seven factor model in all cases has been adopted on the criterion that only factors accounting for variances greater than 1 should be included. This is because an eigenvalue less than 1 is of greater significance than a single variable since each variable has a variance of 1.

3.4.4 Scree plots

The total variance associated with each factor may be plotted on a *Scree Plot*, for all samples (Figure 3.1), Axis/Basal Upper boundary samples (Figure 3.2), Axis/Lasail boundary samples (Figure 3.3), and Basal Upper Unit samples (Figure 3.4). On each plot, there is a distinct break between the steep slope of the large factors and the gradual trailing off of the rest of the factors. In Figure 3.1 and Figure 3.2, the tailing off occurs at six factors, and in Figure 3.3 a less clear tailing off occurs after 5 factors. The break in slope of the line and the gradual tailing off visually resembles the debris at the base of a mountain or cliff, this has caused it to be termed "scree". Scree has been experimentally determined to begin at the k-th factor where k is the true number of factors. From the three scree plots it appears that a six-factor model adequately explains the metalliferous sediment data.

3.4.5 The factor pattern matrix

Each row of the factor pattern matrix contains the coefficients used to express a standardised variable in terms of the factors. These coefficients are called factor loadings since they indicate how much weight is assigned to each factor, and the matrix is termed the *Factor Pattern Matrix.* Tables 3.9, 3.10, 3.11 and 3.12 contain the data for the *Factor Pattern Matrices* obtained from the metalliferous

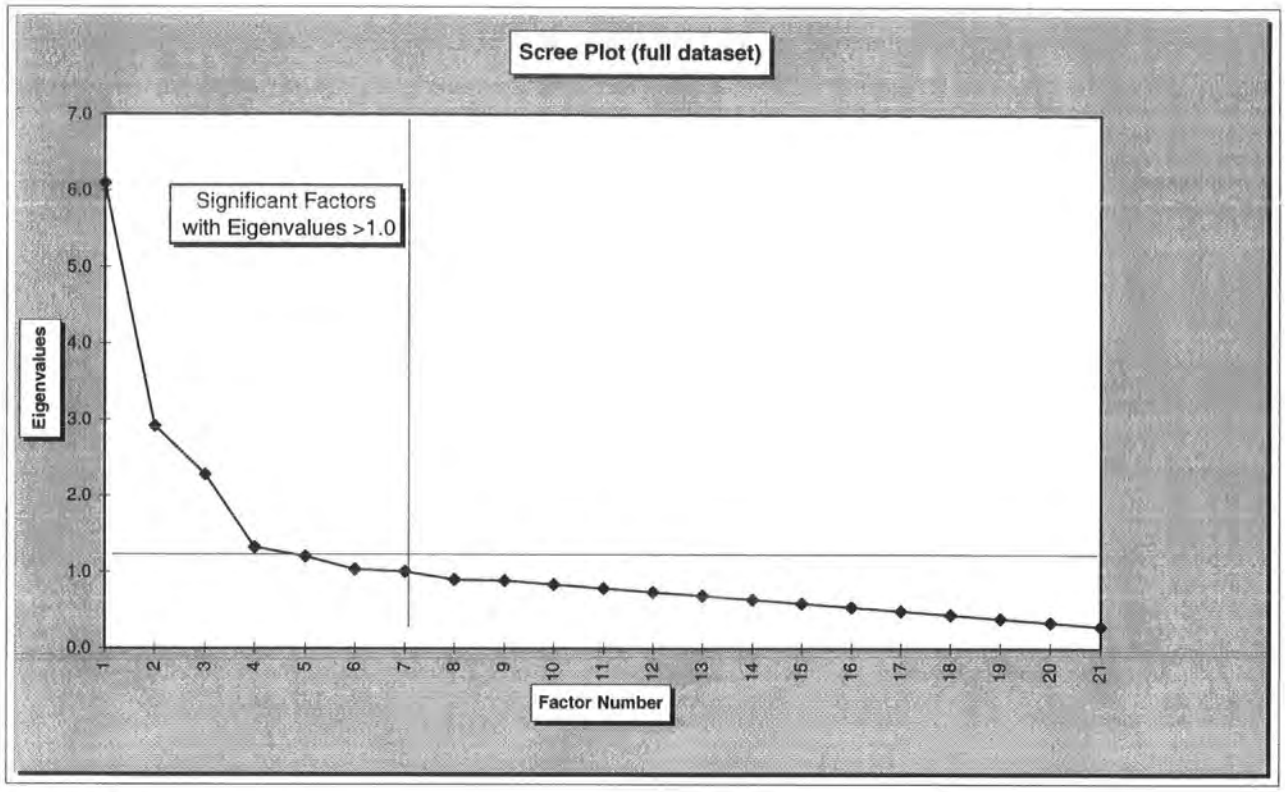

Figure 3.1

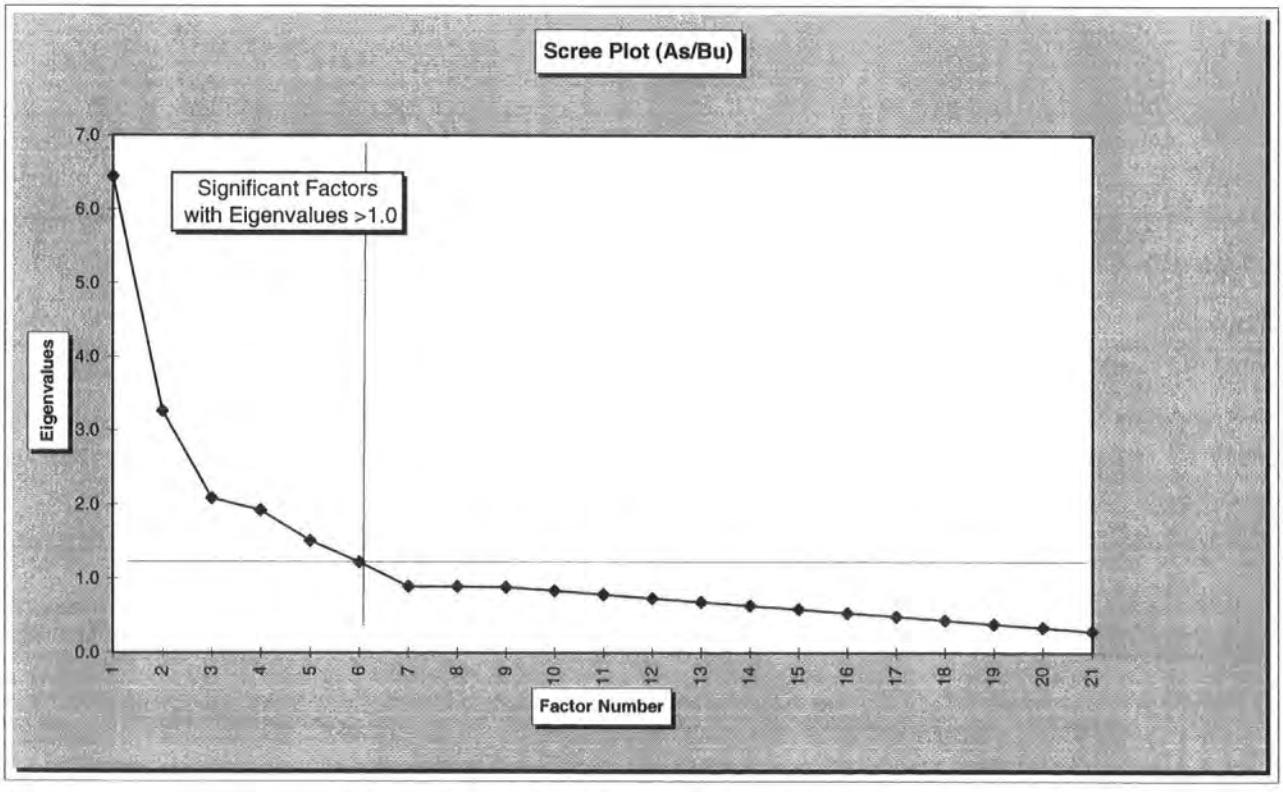

Figure 3.2

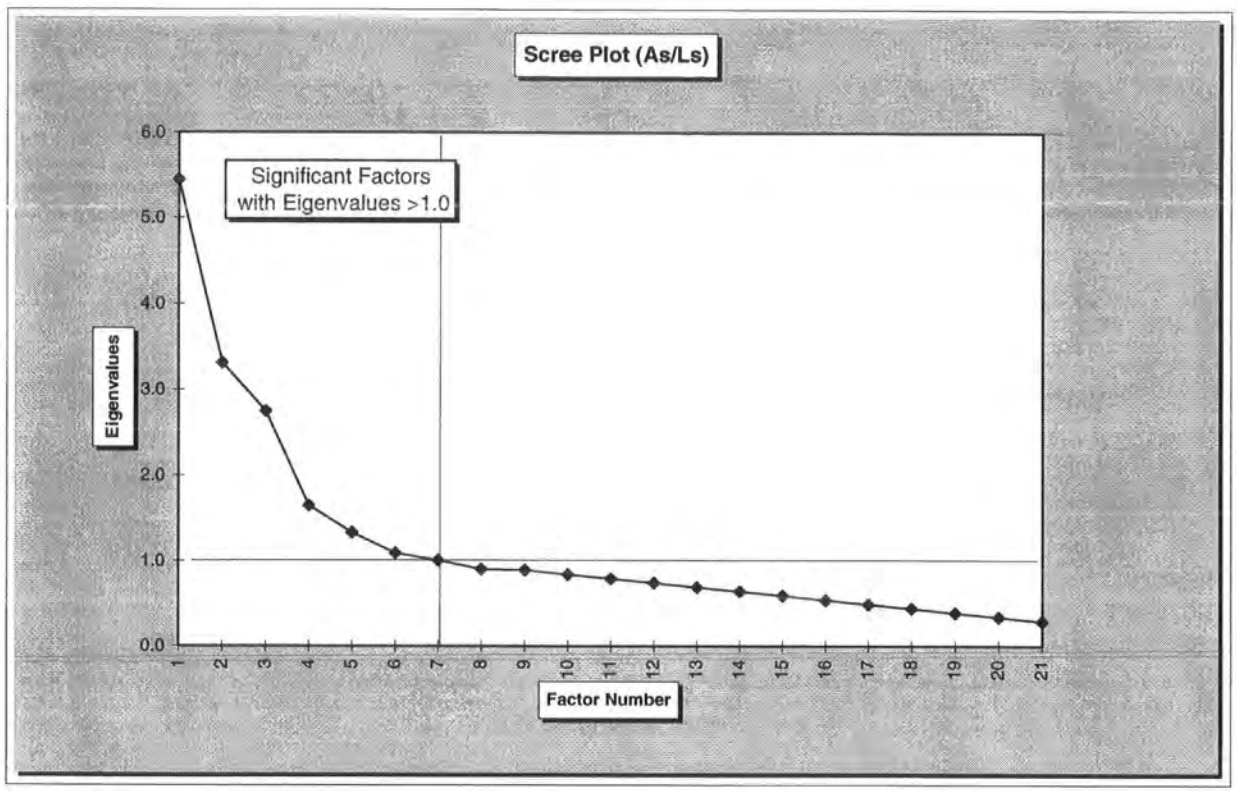

Figure 3.3

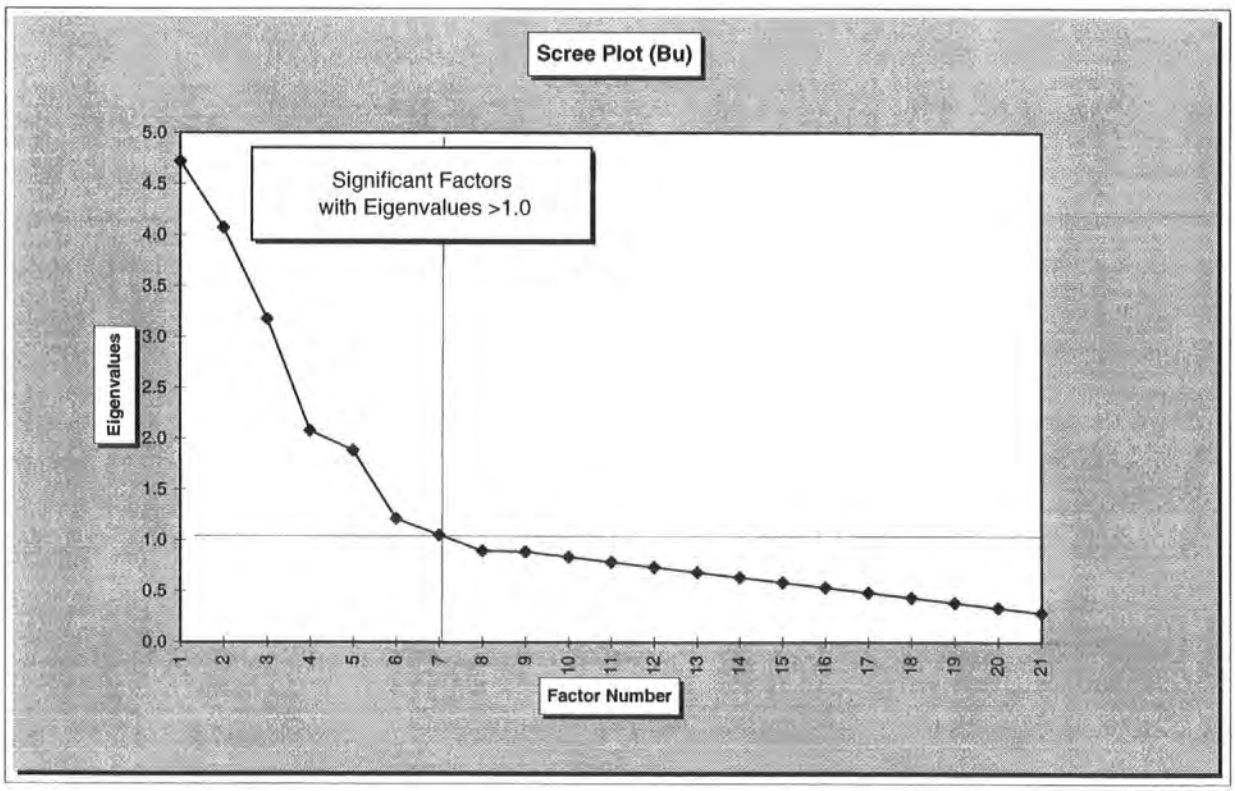

Figure 3.4

sediments. For example, the iron component index for the As/Bu Group can be expressed as:

Eqn 3.6 Fe component = $0.257F_1 + 0.508F_2 + 0.623F_3 - 0.353F_4 - 0.021F_5 - 0.064F_6$

and the Mn component index as:

Eqn 3.7 Mn component = $0.826F_1 - 0.382F_2 + 0.074F_3 + 0.194F_4 - 0.170F_5 - 0.003F_6$

Factors with large absolute value coefficients are closely related to the variable, for example Factor 1 in the As/Ls Group (Table 3.11) is the factor with the largest loading for MnO Pb, Zn, Ba and As.

A further interpretation can be made from factor loading data because the values are equal to the standardized regression coefficients in the multiple regression equation. The implication is that original variable acts as the dependent variable and the factors as the independent variables. Because the factors are uncorrelated, the values of the coefficients are not dependent upon each other and so represent the correlation between the factors and the variables, i.e. the unique contribution of each variable. Furthermore, because the factors are uncorrelated, the sum of the variance proportions explained by each factor is equal to the total proportion of the variance. For example, for the Mn-component at the Axis/Basal Upper boundary, Factor 1 explains 68.2% of the variance for this variable. This is the correlation coefficient for Factor 1 squared $(0.826)^2$. Similarly Factor 2 explains 14.5%, Factor 3 explains 0.5%, Factor 4 explains 3.76%, Factor 5 explains 1.15% and Factor 6 explains 0.001% of the variance of this variable. The total percentage of the variance of Fe accounted for by the 6-Factor model is therefore 84.3%.

The proportion of variance explained by the common factors is called the *communality* of the variable. The last column of Tables 3.9, 3.10, 3.11 and 3.12 reproduce the communalities for the variables. Communalities range from 0 to 1. A value of 0 indicates that the common factors explain none of the variance and a value of 1 indicates that all the variance is explained by the (six or seven) common factors. Variance not explained by common factors is attributable to the Unique factor discussed above, and may be termed the uniqueness of the variable.

Table 3.9: Unrotated factor scores matrix - Full dataset

	Factor 1	Factor 2	Factor 3	Factor 4	Factor 5	Factor 6	Factor 7
MNO	0.8963	-0.2889	0.0152	0.0331	0.1937	-0.0703	-0.0021
ZN	0.8816	-0.2105	0.0023	0.1298	0.1619	0.0070	-0.0516
PB	0.8451	-0.2566	-0.1795	0.1760	0.0859	0.0073	0.0017
AS	0.7206	-0.0706	0.0133	-0.2348	0.2184	0.1456	0.1610
CO	0.6967	-0.3003	0.3686	0.1139	0.3211	-0.0722	-0.0136
ZR	0.6943	0.3798	-0.4376	-0.0186	0.1059	0.0666	0.1247
CAO	0.6554	-0.1218	-0.1707	-0.4620	-0.4250	-0.0551	-0.0579
SIO2	-0.6152	0.2421	-0.5614	0.0759	0.2938	0.0265	0.1352
SC	0.5865	0.3981	0.3239	-0.1274	-0.2366	-0.0122	0.1064
NI	0.5405	0.4737	0.3746	-0.0849	0.1089	-0.1356	-0.1033
AL2O3	0.2582	0.7840	-0.0786	0.2122	-0.1167	0.0497	0.1195
TIO2	0.4267	0.7815	0.0839	0.1477	0.0552	-0.0348	-0.0490
MGO	-0.2148	0.6337	0.3366	0.2305	-0.0002	0.1489	-0.1151
SR	0.1730	-0.4603	0.1383	0.2753	-0.1856	-0.2299	0.0731
FE2O3	-0.4917	-0.1585	0.7365	0.2566	0.0354	-0.0453	-0.1013
MO	-0.3469	0.0026	-0.4497	-0.1545	0.2345	-0.2048	0.2751
BA	0.3339	-0.0092	-0.3127	0.5805	-0.0076	0.2719	0.1276
CR	0.2380	-0.1311	-0.2948	0.1829	-0.6827	0.2002	-0.1046
CU	-0.0742	-0.3269	-0.0228	0.1142	0.1625	0.6687	-0.2120
P2O5	-0.0558	0.0338	0.4194	-0.4568	0.0174	0.5352	0.3842
V	-0.0612	-0.1912	0.2798	0.2874	-0.1806	-0.0681	0.7568

Table 3.10: Unrotated factor scores matrix - As/Bu

As/Bu	Factor 1	Factor 2	Factor 3	Factor 4	Factor 5	Factor 6
ZN	0.8368	-0.2763	0.0856	0.1683	-0.1065	-0.0297
MNO	0.8269	-0.3821	0.0747	0.1944	-0.1708	-0.0036
SIO2	-0.8246	0.0019	0.3009	0.3914	0.0986	-0.0939
AS	0.7873	-0.2915	-0.2129	-0.1873	0.0582	-0.1870
CO	0.7844	-0.1349	0.4211	0.1287	-0.1704	-0.0482
NI	0.7153	0.4440	0.1076	-0.2767	-0.1407	-0.0434
PB	0.6999	-0.2811	0.0316	0.4504	-0.1807	-0.0112
MO	-0.6282	-0.4114	0.4741	0.1221	0.1107	0.2220
CU	0.6115	0.2005	0.3444	0.0744	0.1715	0.2663
SC	0.5214	0.2927	0.1515	-0.2480	0.1521	0.4244
MGO	-0.0189	0.8441	-0.0963	-0.0281	0.2902	-0.0514
TIO2	0.4164	0.6916	0.0832	0.4532	0.0059	-0.0392
BA	0.3785	-0.5186	0.2033	0.1963	0.4760	-0.2217
CAO	0.3515	-0.3286	-0.7408	-0.3186	-0.1063	0.1848
FE2O3	0.2575	0.5089	0.6236	-0.3534	-0.0216	-0.0643
AL2O3	0.1473	0.4793	-0.4880	0.2658	0.3208	0.2907
P2O5	0.2505	0.1045	0.0615	-0.6192	-0.1166	-0.3226
ZR	0.5034	0.3470	-0.3223	0.5568	0.0115	-0.1670
CR	0.1531	-0.3380	-0.1003	-0.1236	0.7596	-0.1015
V	0.3837	-0.0178	0.1053	-0.1658	0.5333	-0.2367
SR	0.2961	-0.2521	0.1393	-0.1061	0.1113	0.7054

Table 3.11: Unrotated factor scores matrix - As/Ls

As/Ls	Factor 1	Factor 2	Factor 3	Factor 4	Factor 5	Factor 6
AS	0.8052	0.1617	-0.0942	-0.0486	-0.3627	0.0534
MNO	0.8017	0.5111	0.0351	-0.1407	0.0112	-0.0894
ZR	0.7795	-0.3366	-0.3949	0.0479	0.0579	0.0570
ZN	0.7372	0.2836	0.0722	-0.3101	0.1005	0.2381
PB	0.7227	0.5045	-0.0181	-0.2237	-0.0750	-0.0354
BA	0.5846	0.3538	-0.1007	-0.1503	0.3687	0.2551
SC	0.5749	-0.3184	0.4296	0.3906	-0.0447	-0.0003
NI	0.5182	-0.4639	0.3853	-0.0976	0.0182	-0.1383
AL2O3	0.5111	-0.6547	0.1982	-0.0094	0.1374	0.2015
TIO2	0.5636	-0.6387	0.2724	0.0104	0.1677	0.0326
SR	-0.0572	0.5675	0.1455	0.0484	0.3284	0.2101
MGO	0.0133	-0.5521	0.4382	-0.2073	0.1354	0.3143
SIO2	-0.1086	-0.3503	-0.7591	-0.3226	0.0874	0.1666
FE2O3	-0.6175	0.2147	0.6968	-0.1036	0.0536	-0.0327
MO	-0.0252	-0.0467	-0.5823	-0.1083	0.1459	-0.0125
CO	0.3141	0.5226	0.5820	-0.2456	-0.0418	-0.1589
CR	0.1387	0.2915	-0.1770	0.7205	0.2962	0.1783
CAO	0.5902	0.1538	-0.1970	0.5997	-0.1105	-0.2578
P2O5	0.0052	-0.0313	0.1612	0.2616	-0.6959	0.4676
V	-0.2593	0.1971	0.2274	0.3049	0.3849	0.3589
CU	-0.1831	0.2787	-0.1344	-0.1225	-0.3166	0.4971

Table 3.12: Unrotated factor scores matrix - Bu

	Factor 1	Factor 2	Factor 3	Factor 4	Factor 5	Factor 6	Factor 7
FE2O3	-0.8487	-0.2905	0.0752	-0.1641	0.2625	-0.0881	-0.0193
PB	0.7946	0.4571	0.0940	-0.0110	0.0043	0.2444	-0.0180
NI	-0.7789	0.4074	0.2217	0.1684	0.1642	-0.0953	0.0272
P2O5	-0.7741	-0.2686	0.1788	0.1897	-0.2643	0.0018	0.2101
AL2O3	0.5941	-0.4829	0.2527	0.2642	0.3109	0.1615	0.1704
CU	0.5409	0.3108	-0.2066	-0.0089	0.3537	-0.1175	-0.2703
ZN	0.3893	0.8131	0.1490	-0.0642	0.1277	0.1403	-0.1039
MNO	-0.2299	0.8040	0.1696	-0.3902	0.2183	0.0102	-0.0147
SIO2	0.5035	-0.7320	0.1830	-0.3513	0.0986	0.0795	-0.0695
CAO	-0.0223	0.5776	-0.4668	0.5114	-0.3699	-0.0283	0.1070
CO	-0.5465	0.5467	0.1943	-0.4711	0.2517	-0.0309	0.0394
TIO2	-0.0996	-0.1584	0.6725	0.4030	0.5165	-0.0956	0.1208
MGO	-0.1842	-0.3318	0.6366	0.4447	-0.1671	0.0143	-0.3705
BA	0.5582	-0.1975	0.6240	-0.1320	0.0108	-0.2235	0.3047
SR	0.1665	-0.1700	-0.5792	0.2713	0.4771	-0.0101	0.0779
ZR	0.3043	0.4033	0.5539	-0.1858	0.0209	-0.1422	0.4838
V	0.0552	-0.3415	-0.5089	-0.4161	-0.2554	0.2670	0.3611
CR	0.4373	0.3552	-0.0923	0.4774	-0.0754	-0.3732	-0.0256
SC	-0.2482	0.1428	-0.3460	0.4721	0.4260	0.3089	0.4485
MO	-0.0953	-0.2771	-0.4601	-0.1721	0.6662	-0.1209	-0.1701
AS	-0.1319	0.1627	0.3862	0.1259	0.0611	0.8159	-0.1721

Table 3.13: Rotated Factor Scores - Full dataset

	Factor 1	Factor 2	Factor 3	Factor 4	Factor 5	Factor 6	Factor 7
MNO	0.947	0.017	0.132	0.097	-0.079	-0.014	0.016
ZN	0.891	0.106	0.162	0.123	-0.113	0.092	-0.001
PB	0.853	0.053	0.033	0.251	-0.184	0.141	0.049
CO	0.803	-0.012	0.353	-0.230	-0.018	0.000	0.098
AS	0.749	0.123	-0.039	0.079	0.296	-0.028	-0.045
ZR	0.565	0.532	-0.380	0.293	-0.019	0.044	-0.123
TIO2	0.164	0.882	0.036	-0.032	-0.057	-0.067	-0.114
AL2O3	-0.033	0.853	-0.113	0.135	-0.038	0.025	0.044
NI	0.371	0.600	0.286	-0.140	0.083	-0.280	-0.141
MGO	-0.405	0.592	0.231	-0.249	0.049	0.123	-0.047
SC	0.328	0.563	0.297	0.206	0.231	-0.277	0.073
SIO2	-0.491	-0.004	-0.718	-0.196	-0.130	0.210	-0.086
MO	-0.180	-0.179	-0.648	-0.120	-0.052	-0.127	0.034
FE2O3	-0.415	-0.189	0.595	-0.521	0.003	0.033	0.234
CR	-0.001	-0.006	0.156	0.783	-0.162	0.202	0.080
CAO	0.488	-0.015	0.077	0.668	0.155	-0.359	-0.175
P2O5	-0.044	0.001	0.105	-0.076	0.889	0.040	0.115
CU	0.037	-0.286	0.127	-0.012	0.218	0.678	-0.195
BA	0.285	0.220	-0.122	0.218	-0.259	0.561	0.249
V	-0.020	-0.052	0.021	-0.045	0.143	-0.026	0.886
SR	0.223	-0.294	0.270	0.096	-0.273	-0.040	0.368

Table 3.14: Rotated Factor Scores - As/Bu

As/Bu	Factor 1	Factor 2	Factor 3	Factor 4	Factor 5	Factor 6
MNO	0.901	-0.016	0.052	0.230	0.110	0.151
PB	0.868	0.146	-0.128	0.098	0.021	0.060
ZN	0.847	0.066	0.123	0.204	0.150	0.156
CO	0.834	0.014	0.329	-0.089	0.063	0.205
AS	0.576	0.019	0.250	0.544	0.363	0.022
TIO2	0.270	0.816	0.197	-0.260	-0.133	0.054
ZR	0.426	0.765	-0.099	0.110	-0.001	-0.165
AL2O3	-0.188	0.748	-0.225	0.218	0.058	0.227
MGO	-0.427	0.711	0.323	-0.128	0.034	0.029
MO	-0.228	-0.575	-0.397	-0.555	0.020	0.129
FE2O3	0.016	0.094	0.797	-0.376	-0.032	0.238
NI	0.332	0.358	0.703	0.191	-0.054	0.215
P2O5	-0.017	-0.162	0.681	0.258	0.077	-0.124
CAO	0.097	-0.064	-0.123	0.943	0.028	0.096
SIO2	-0.408	-0.148	-0.424	-0.699	-0.090	-0.276
CR	-0.042	-0.059	-0.121	0.140	0.838	0.090
BA	0.484	-0.147	-0.142	-0.100	0.694	-0.004
V	0.125	0.115	0.278	0.023	0.646	0.054
SR	0.181	-0.175	-0.122	0.124	0.046	0.772
SC	0.121	0.246	0.377	0.109	0.073	0.641
CU	0.409	0.288	0.275	-0.148	0.152	0.517

Table 3.15: Rotated Factor Scores - As/Ls

As/Ls	Factor 1	Factor 2	Factor 3	Factor 4	Factor 5	Factor 6
MNO	0.913	0.010	0.136	0.262	-0.064	-0.088
PB	0.884	-0.053	0.084	0.171	-0.118	-0.001
ZN	0.856	0.226	-0.020	-0.042	0.063	0.047
BA	0.737	0.091	-0.174	0.039	0.328	-0.104
AS	0.702	0.193	-0.039	0.344	-0.308	0.276
TIO2	0.103	0.889	-0.033	0.063	-0.100	-0.118
AL2O3	0.084	0.872	-0.140	-0.002	-0.038	0.018
NI	0.167	0.716	0.180	0.017	-0.263	-0.139
SC	0.118	0.699	0.305	0.411	-0.002	0.074
MGO	-0.158	0.647	0.083	-0.439	0.082	0.083
SIO2	-0.105	-0.055	-0.875	-0.216	-0.153	-0.009
FE2O3	-0.333	-0.208	0.708	-0.472	0.218	-0.050
CO	0.567	-0.064	0.669	-0.119	-0.032	-0.099
MO	0.013	-0.182	-0.567	0.024	-0.037	-0.135
ZR	0.418	0.511	-0.525	0.380	-0.174	-0.021
CAO	0.269	0.077	0.002	0.876	-0.058	-0.024
CR	0.030	-0.085	-0.077	0.627	0.606	0.022
V	-0.145	-0.039	0.159	-0.043	0.691	0.034
SR	0.274	-0.296	0.200	-0.067	0.539	-0.060
P2O5	-0.090	0.076	0.184	0.130	-0.078	0.853
CU	0.099	-0.313	-0.102	-0.214	0.117	0.560

Table 3.16: Rotated Factor Scores - Bu

Bu	Factor 1	Factor 2	Factor 3	Factor 4	Factor 5	Factor 6	Factor 7
P2O5	-0.894	0.071	-0.147	0.114	-0.028	-0.040	0.107
PB	0.839	-0.095	-0.128	-0.081	0.329	-0.066	0.247
CU	0.755	0.027	0.035	0.083	-0.109	0.141	-0.181
ZN	0.733	0.423	-0.242	0.078	0.221	-0.057	0.229
FE2O3	-0.729	0.387	0.332	0.155	-0.275	0.139	-0.063
CO	-0.119	0.944	0.106	0.004	0.061	-0.020	0.057
MNO	0.254	0.909	-0.068	0.007	0.133	-0.050	0.108
NI	-0.437	0.670	-0.257	0.392	-0.065	0.123	0.089
AL2O3	0.223	-0.656	0.362	0.223	0.340	0.282	0.127
CAO	0.142	0.040	-0.944	-0.125	-0.133	0.128	-0.028
SIO2	0.113	-0.562	0.761	-0.129	0.133	-0.156	-0.030
CR	0.451	-0.188	-0.529	0.269	0.121	0.029	-0.305
V	-0.178	-0.219	0.144	-0.842	-0.029	0.097	-0.011
TIO2	-0.182	-0.029	0.245	0.789	0.364	0.279	0.111
MGO	-0.334	-0.309	0.042	0.700	-0.043	-0.366	0.279
ZR	0.216	0.267	-0.015	0.073	0.847	-0.101	-0.003
BA	0.176	-0.283	0.334	0.183	0.763	-0.217	-0.120
SC	-0.142	0.065	-0.299	-0.003	-0.022	0.863	0.206
SR	0.195	-0.250	0.019	-0.064	-0.286	0.680	-0.224
MO	0.077	0.077	0.473	-0.033	-0.463	0.506	-0.327
AS	0.022	0.112	0.050	0.167	-0.030	0.002	0.929

The relevance of the data presented in Tables 3.9, 3.10, 3.11 and 3.12 is that it enables the 6-Factor models to be assessed. However, the interpretation of the results, which are presented on the factor pattern matrix, is facilitated by rotation of the data which is a process of transforming the factors to make them more understandable by producing a best-fit of the factor axes to the variables in vector space.

3.4.6 The rotation phase

Having determined from the bulk rock data the Principal Factor solutions above, which are the unrotated co-ordinates of the variables relative to the factor axes, a rotation of the Factor Axes has been carried out for the purpose of transforming the initial matrix into one that is easier to interpret.

The problem that rotation overcomes is that in the Principal Factor matrix most Factors correlate with many variables. The process of rotation both reduces the number of distinct groups while also simplifying those groups by reducing the number of elements contained within each.

Table 3.17 Oman umber rotated factor scores

	UNROTATED FACTORS Table 3.9	ROTATED FACTORS Table 3.13
Factor 1	(i) MnO-Zn-As-Co-Ni-Pb-Cu-Sc-TiO_2-Zr (ii) SiO_2-Mo	(i) *MnO-Pb-Zn-Co-As-Zr-Ba-Cu*
Factor 2	(i) MgO-TiO_2-Fe_2O_3-Al_2O_3 (ii) Mo-Ba	(i) *TiO_2-Al_2O_3-MgO-Zr*
Factor 3	(i) CaO-Al_2O_3 (ii) Fe_2O_3	(i) *Fe_2O_3-Ni-P_2O_5*
Factor 4	(i) Pb-TiO_2-Zr (ii) P_2O_5	(i) *CaO-As* (ii) *SiO_2-Mo*
Factor 5	(i) Ba-Cr-V	(i) *Cr-Ba-V*
Factor 6	(i) Sr-Sc	(i) *Sc-Sr-Cu*

Rotation overcomes in two ways the problem that most factors correlate with many variables: (1) in the ideal rotated solution each factor contains values that are not zero for only a small number of variables, and (2) in the ideal rotated

solution each variable has non-zero values for only one (or very few) Factor. If the two above conditions are satisfied then a *simple structure* has been achieved. By rotating to a simple structure, the data is reduced to factors that are substantively meaningful.

By rotating the solution, neither the communalities nor the percentage of variance is changed. However, the percentage of variance accounted for by each factor is affected. There are a number of different rotation methods, but in this study, the Varimax method is used, which is an orthogonal rotation that is the most commonly used for geological data (Full *et al.,* 1981; Leinen and Pisias, 1984; Full and Ehrlich, 1986). The Varimax method attempts to minimize the number of variables that have high loading on a factor. The solution reached is a best-fit of the factor axes to the variables in vector space, produced by the pairs of factor axes remaining orthogonal during rotation with the result that in comparison with the principal component solution the variables are closer to the factor axes. The original Factor Matrices have been rotated using the Varimax method to produce the Rotated Factor Matrices (Tables 3.13, 3.14, 3.15 and 3.16) for the full dataset, the As/Bu, the As/Ls and the Bu samples respectively.

The effect of rotation on the calculated interelement relationships which make up the hypothetical components is summarised above (Table 3.17). The Factors are extracted from the matrix given that the inter-element correlations of >0.4 (Holland, 1996, pers.comms).

3.5 Factor Analysis Output: Major and Trace element data

By using the procedure outlined above, the samples in this study have been analyzed by factor analysis. In this Section, the output of the factor analysis is assessed. The discussion is based upon the Varimax rotated factor scores (Tables 3.13, 3.14, 3.15 and 3.16).

The interpretation of the rotated factor matrices will be carried out as follows: factor analysis of the dataset as a whole will be taken as first-estimates of the different components likely to comprise the sediments. The reason for then splitting up the samples to carrying out factor analysis is the geochemical bimodality identified in Chapter 3 from major element analyses. The groups that will be used are: (1) Axis/Lasail boundary samples, (2) Axis/Basal Upper boundary samples and (3) Basal Upper lava unit samples. The effect of this on the output is that clearer trends emerge from the data.

Table 3.18 Metalliferous sediment components - all samples (from Table 3.17)

FACTOR	ELEMENT ASSOCIATION	INTERPRETATION
FACTOR 1	(i) MnO-CaO-Zn-Pb-As-Co-Ni-Zr	Hydrothermal Mn-oxide
	(ii) Fe_2O_3-SiO_2	Hydrothermal Fe-Si oxide
FACTOR 2	(iii) Al_2O_3-TiO_2-MgO-Sc-Ni-Zr	Detrital aluminosilicate
FACTOR 3	(iv) SiO_2 - Mo	Hydrothermal Si
	(v) Fe_2O_3	Hydrothermal Fe-oxide
FACTOR 4	(vi) CaO - Cr	Biogenic calcareous ooze
FACTOR 5	(vii) P_2O_5	Apatite
FACTOR 6	(viii) Cu-Ba	-
FACTOR 7	(ix) V	-

The rotated factor matrix (Table 3.18) for the full dataset has produced a seven factor model. Each Factor may contain two end-member sediment forming components. The elements making up the groups are extracted on the basis of rotated factor scores >0.4 (Holland, 1996, pers.comms.).

Although the above results may represent end-member components, it was suggested in Chapter 2 that different component compositions were present at the different volcanic stratigraphic positions. To minimise the effect of diverse end-member compositional range, the Factors above must be considered to as representative of only the broadest elemental associations. The major element associations represent the sediment-forming minerals which, in marine sediments, includes the clays, biogenic opal and carbonates, and the hydrothermal precipitates. Without refining the input, the results of factor analysis (Table 3.18) are not sufficiently clear to define the components positively. In the following sub-sections, the components suggested above will de described and the variation by volcanic straitigraphic position assessed.

By plotting the rotated correlation scores by sample (from Table 3.19, 3.20, 3.21, 3.22) for the full dataset (Figure 3.5), a basic twofold pattern emerges which has been identified in Chapter 2: FACTOR 1 when plotted versus FACTOR 2 shows that the data are systematically separated on FACTOR 1 according to the volcanic stratigraphy. Positive Factor Scores are produced for the samples from the Axis Unit, the Basal Upper Unit and the Axis/Basal Upper boundary.

Figure 3.5 Rotated factor scores (by sample)

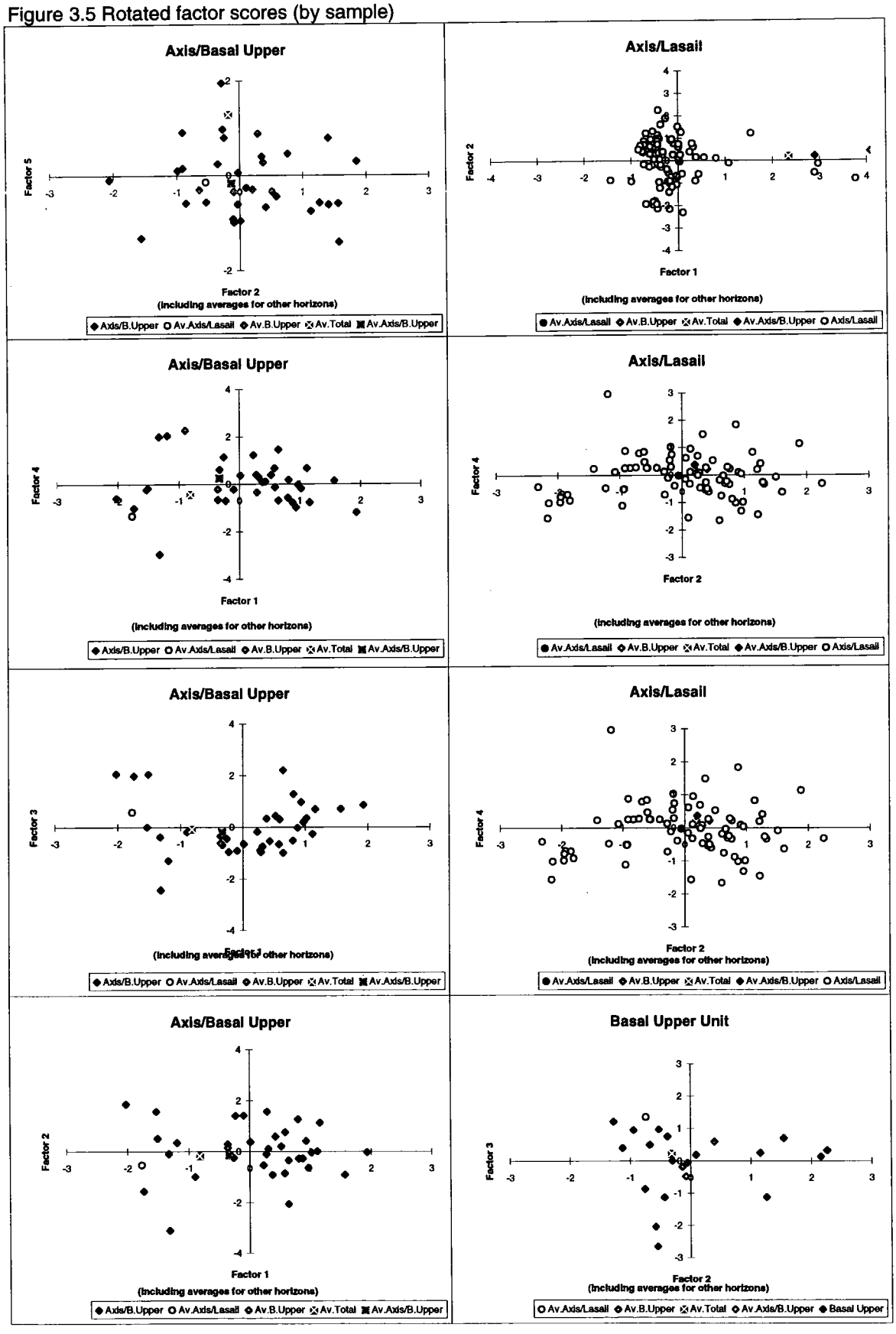

Figure 3.5 ctd. Rotated factor scores (by sample)

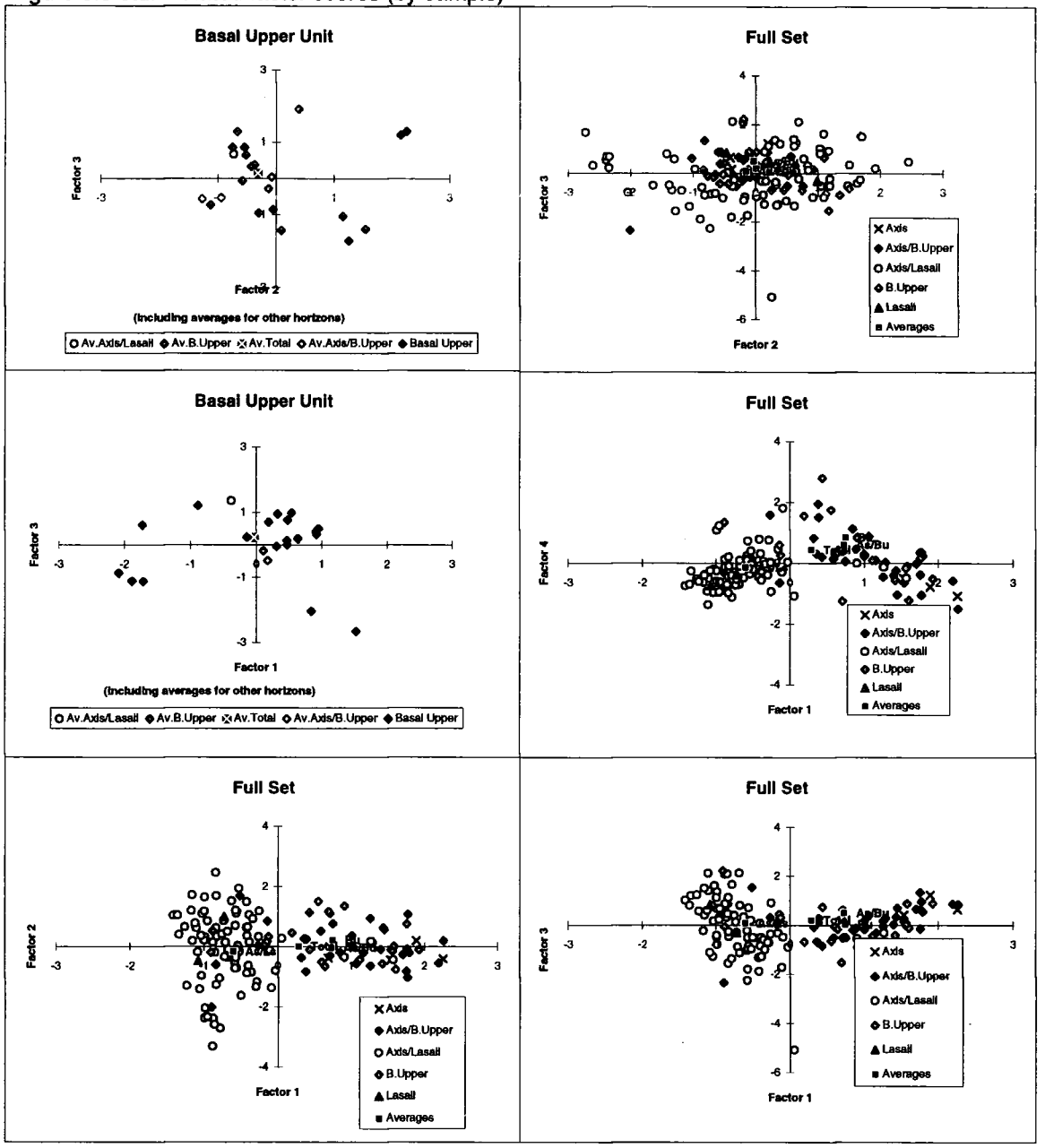

Negative scores on FACTOR 1 are taken by samples from the Lasail Unit and the Axis/Lasail boundary. The explanation of this is that FACTOR 1 contains the hydrothermal components, the differences between which controls the sediment geochemistry. Scree plots (Figures 3.2 and 3.3) suggest that As/Bu and As/Ls Group samples may each be described using six factors each with eigenvalues of >1. The contribution of each element variable to each of the Factors has been calculated (Tables 3.23, 3.24, 3.25, and 3.26) and shows that the total variance of the data is accounted for by first factor, the maximum remaining variance by the second factor (this being uncorrelated with the first), and successive components explaining progressively smaller proportions of the total variance. The Varimax rotation ensures that correlation between the factors is at a minimum.

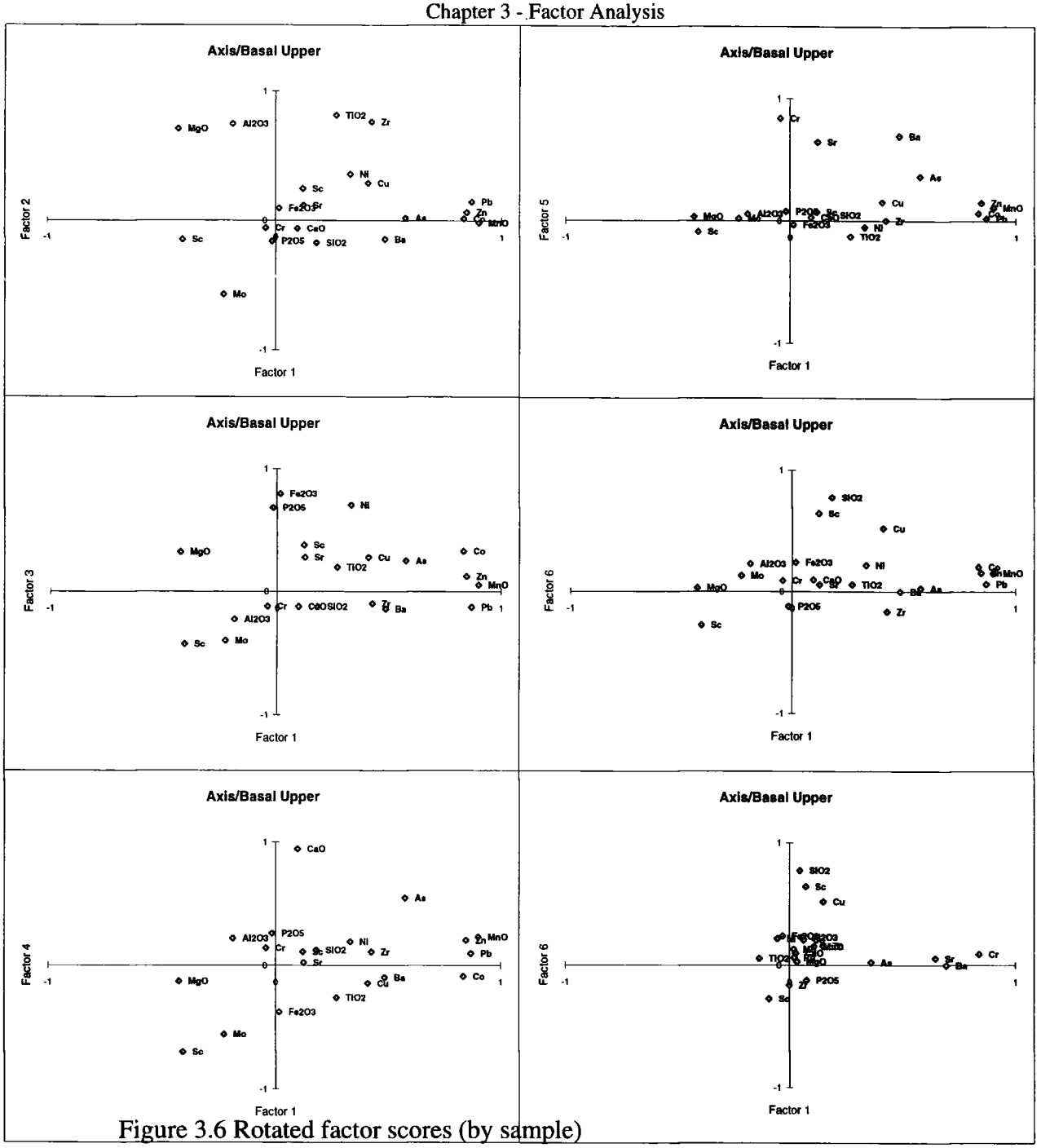

Figure 3.6 Rotated factor scores (by sample)

By plotting rotated factor scores by element, it is possible to summarise visually the inter-element relationships which constitute the sediment-forming components (Figure 3.6).

3.5.1 Hydrothermal Mn-Oxide Component

The Mn-oxide component (Table 3.18) is FACTOR 1 for As/Bu and As/Ls Group samples and FACTOR 2 for Bu Group samples. The elements associated with Mn are as follows:

Table 3.19 Factor scores (by sample)

Sample	Factor 1	Factor 2	Factor 3	Factor 4	Factor 5	Factor 6	Factor 7
Av As/B	0.1699	-0.0793	-0.4841	0.0432	-0.1723	2.1035	
Av As/L	-0.3766	-0.7333	1.3475	0.6655	-2.2224	-0.3190	
Av Bu	0.1060	-0.1341	-0.1837	-0.2815	0.2067	0.6634	0.2965
Av tota	-0.8192	-0.1755	-0.0767	-0.4344	1.2821	0.9398	

Table 3.20 Factor Score (by sample) - As/Bu

Sample	Factor 1	Factor 2	Factor 3	Factor 4	Factor 5	Factor 6
20617	-0.8975	-0.9882	-0.1868	2.2693	0.1018	-0.2161
20634	0.8145	-0.2821	1.2834	0.1743	1.9477	-1.0831
20635	1.9299	-0.0244	0.8555	-1.2015	0.0566	-0.1176
20636	-0.3582	0.2890	-0.3377	-0.6599	0.8813	-0.5325
20637	0.8024	1.2628	-0.5241	-0.5819	-0.5783	-0.1917
20638	0.3098	0.1022	-0.7522	0.3012	-0.2635	-0.1558
20639	0.5209	0.1987	0.4372	0.3869	-0.3038	-0.4344
20640	0.2759	-0.1059	-0.8967	0.3962	-0.9222	-0.5022
20641	0.5790	-0.8558	-0.6621	0.6637	-0.5867	3.3875
20642	1.1161	0.0096	-0.2693	0.6668	-0.9616	0.7878
20643	-1.1959	0.3490	-1.2964	2.0520	0.3937	1.0007
20644	0.4264	0.5821	-0.5409	0.1061	-0.4455	0.0096
20645	0.9709	-0.6441	0.1940	-0.0314	-0.3075	1.1402
20646	0.2295	-0.5331	-0.1841	1.2274	-0.5633	-0.2092
20649	1.0213	-0.0347	0.3497	-0.1909	-0.6102	-0.8316
20650	0.8770	-0.2643	-0.0313	-0.7889	0.9746	-0.5936
20651	0.9343	0.4106	0.9635	-0.9823	-0.6760	-0.0388
20652	0.5871	0.7623	0.3080	-0.1363	0.4550	0.3067
20653	0.6432	-2.0613	2.2038	1.4517	-0.0932	-0.6998
20654	1.5678	-0.9065	0.7054	0.1397	0.1492	0.1064
20659	1.1602	1.1279	0.6950	-0.7808	-0.7558	1.0438
20662	0.3780	-0.9084	0.3337	0.0916	0.9069	-0.4797
20663	-0.2593	-0.2441	-0.4500	1.1387	0.7943	-0.1344
20664	0.2877	1.5683	-0.9650	-0.3538	-1.4057	-0.5042
20665	0.0148	0.3713	-0.6580	0.3583	0.2686	-1.5752
20666	-0.0942	1.4063	-0.9057	-0.2325	-0.6228	-0.6842
20668	-1.3281	-0.0928	-0.3767	1.9965	-0.9960	-0.5728
U82	-1.3180	-3.1083	-2.4361	-2.9509	-0.6709	-0.3993
U83	0.6436	-0.3487	-0.9951	-0.6895	0.2404	0.6277
20671	-0.3297	-0.0967	-0.6951	0.6142	-0.3473	-1.2559
20682	-1.5322	1.5588	0.0018	-0.2283	-0.5968	-1.2596
20683	-2.0230	1.8508	2.0599	-0.5955	0.2936	2.2032
20684	-1.5113	0.5106	2.0487	-0.1730	-0.3440	-1.1072
20685	-1.7384	-1.5623	1.9857	-1.0130	-1.3208	-0.4166
20687	-0.2274	1.4039	-0.9551	-0.7065	0.7801	-0.3774

Table 3.21 Factor scores (by sample) - Bu

Sample	Factor 1	Factor 2	Factor 3	Factor 4	Factor 5	Factor 6	Factor 7
U22	-0.1459	1.1536	0.2425	-1.0432	0.3165	-0.9517	0.0766
U23	0.1939	1.5441	0.6990	-1.3935	-0.7935	-0.5458	-0.0342
U24	-1.8820	1.2568	-1.1212	-1.7249	1.2788	0.8365	0.8232
20648	0.6353	0.0891	0.1855	-1.4349	-0.8766	-0.4792	0.7114
20660	0.3059	-0.0519	-0.0531	-0.8576	-0.6033	-0.5499	-0.2028
20676	0.4678	-0.3013	0.0020	-0.9514	-0.9339	-0.7296	-0.1191
20686	-0.8831	-1.2718	1.2124	-0.5691	-0.2308	2.7259	-0.9534
20688	1.5224	-0.5479	-2.6528	0.8514	-0.0181	-0.4279	-1.4469
20689	0.8390	-0.5816	-2.0413	-0.0739	-0.0257	0.7382	0.4093
20690	0.4828	-0.3778	0.7564	0.3699	2.1070	0.0184	-0.2707
20691	0.5418	-0.5240	0.9759	0.6382	2.1111	-0.2444	-0.8055
20692	0.9114	-1.1272	0.3994	-0.7315	-0.0584	-1.0558	0.2203
20693	0.9558	-0.6725	0.4928	1.2846	-0.4280	0.3676	3.7055
20694	0.4653	2.1531	0.1359	1.2049	0.1587	0.5566	-0.6872
20695	0.9200	2.2603	0.3213	1.3079	-0.3394	0.1918	-0.2823
20696	-1.7258	0.3919	0.5977	1.9199	0.0868	-0.7270	0.4732
20697	-1.7120	-0.4316	-1.1332	0.3255	-0.0588	-0.7656	-0.3243
20698	-2.0853	-0.7555	-0.8727	0.8487	-0.3996	-1.1336	0.2783
20699	0.3271	-0.9435	0.9471	-0.5406	1.6245	-1.0885	-0.2178

Table 3.22 Factor scores (by sample) - As/Ls

Sample	Factor 1	Factor 2	Factor 3	Factor 4	Factor 5	Factor 6
20602	0.0990	-2.3158	1.0982	-0.4168	4.5320	0.1192
20679	-0.4219	0.4275	1.0693	-0.6120	-0.1804	-0.1931
20680	0.0116	0.5996	1.9730	-1.6639	0.1294	-0.7745
20681	-0.6740	1.2112	1.5555	0.1904	0.3399	0.4489
U1	0.0412	1.3227	0.4413	-0.3407	-0.8662	1.2332
U2	-0.4322	-2.1438	0.5198	-1.0146	0.1942	0.5195
U3	-0.6820	-1.9299	0.9962	-0.6968	0.3677	0.0198
U4	-0.9888	-0.9256	0.7684	-0.5096	0.5611	0.8080
U5	-0.4878	-1.7990	-0.7047	-0.9202	0.0390	-0.6426
U6	-0.0048	1.5097	-0.4913	-0.0876	0.0611	0.8739
U7	-0.5267	-1.9588	0.3401	-0.9852	0.4048	-0.3260
U8	-0.5245	-1.8413	0.6277	-0.7082	0.7113	0.5117
U9	0.8048	0.1030	-1.4825	-1.5638	0.1603	3.7312
U10	-0.4471	-1.9504	0.5333	-0.7845	-0.0460	0.3111
U11	-0.1838	-2.1639	1.1517	-1.5589	0.4535	1.8253
U13	-0.7398	0.3747	0.5600	-0.5450	0.7544	0.5315
U14	-0.5508	0.3659	0.7572	-0.4963	0.2191	-0.4185
U14A	-0.5733	0.9523	0.3058	-1.3179	0.3063	0.0330
U15	-0.7549	0.4032	0.6711	-0.5047	-0.3743	0.2669
U16	-0.7147	0.8639	0.3982	-1.0199	-0.2208	-0.0840
U17	-0.5899	0.6349	0.6758	-0.7665	-0.2344	0.3489
U19	-0.7165	0.6979	1.2978	-0.3139	-0.0153	0.0240
U20	-0.3593	1.6065	1.0060	-0.6366	0.3122	-0.1393
U21	-0.3371	0.2366	0.5777	0.0483	-0.2458	-0.5852
U25	-0.4275	1.1374	-0.6779	0.8271	1.2918	1.0770
U26	-0.4557	0.2815	-0.3687	0.0785	-0.3335	0.1319
U27	-0.2012	-0.5502	-0.7499	0.2509	-0.5003	1.4712
U28	-0.2329	-0.3980	-0.9806	0.2532	-0.7691	2.5620
U29	-0.4178	-0.1798	-1.1016	1.0224	0.3786	1.4850
U30	-0.2620	1.8822	1.0337	1.1277	0.3287	1.9209
U31	-0.4367	0.8086	0.1841	-0.8841	1.1962	-0.7687
U32	-0.1042	0.2590	-0.4718	-0.0165	0.0184	2.8946
U33	-0.4107	2.2480	0.5145	-0.3251	0.4532	0.4768
U34	-0.7972	0.6647	0.9763	-0.0348	-1.0441	-0.3565
U35	-0.3792	0.0546	-0.6528	-0.1584	-0.6585	-0.2079
U36	-0.3948	0.9823	-0.7467	-0.9984	1.0853	-1.1708
U47	-0.2122	-0.9392	-1.3436	-0.5241	0.1985	-0.8489
U48	-0.0885	0.7674	0.0469	0.2184	0.7030	0.1373
U59	0.0827	-0.5968	-0.9267	0.4691	-0.8700	0.7307
U75	3.7609	-0.8268	1.7320	0.2547	-1.9456	-0.5753
U37	-0.5917	0.2930	-1.2921	-0.4757	0.9781	-1.0339
U38	-0.1446	0.9106	-0.6295	0.0915	0.8998	-0.8901
U39	-0.4994	0.0620	1.3411	0.6142	-0.2009	0.4867
U40	0.0680	1.2610	-0.5143	0.4098	-0.4451	-0.0459
U41	-0.8363	0.4959	1.1402	0.5255	0.0934	-0.5129
U41A	-0.3813	-1.2237	-1.4521	-0.4855	-0.3417	-1.1778
U42	-0.5331	1.2966	-0.6817	-0.2707	-0.5835	-0.3191

Table 3.22 (ctd..) Factor scores (by sample) - As/Ls

Sample	Factor 1	Factor 2	Factor 3	Factor 4	Factor 5	Factor 6
U45	1.0781	-0.1162	-1.8656	-0.3964	0.0502	-1.1135
U46	-0.1435	-0.7345	-1.7965	0.2721	0.2928	-0.5196
U49	0.2501	0.3836	-1.2477	-0.2734	-0.5406	-1.1126
U50	0.5465	0.1273	-3.1078	-0.3239	0.0969	-1.3045
U51	0.3240	0.6071	-0.3447	-0.1892	0.1986	-0.5254
U52	-0.1282	0.9521	-0.6069	0.0366	-0.3584	-0.7131
U53	0.3661	-0.9093	-0.6412	0.8742	-0.3480	0.1115
U54	0.2979	0.7639	-0.6036	-0.3421	-0.9203	-1.1696
U55	-0.7240	-0.1725	2.2868	0.2884	-1.3266	-1.5352
U56A	-0.3579	-0.2809	2.3991	0.1235	-0.8765	-1.5850
U56B	-0.0333	-0.6845	-0.1347	0.7853	-0.2362	-0.9083
U56C	-1.4323	-0.8744	0.6414	5.7822	1.9329	-0.2991
U57	-0.3636	-0.1931	-0.5141	0.5395	-0.9050	-0.0970
U58	-0.4087	0.3351	-0.5293	1.4838	-0.7761	1.9008
U60	-0.1742	-0.9139	-1.3761	0.2502	-1.0663	-0.5720
U61	0.0105	0.1336	-0.9843	0.1022	-0.1778	-0.1609
U62	-0.4335	0.8710	-0.1013	1.8263	2.5620	-0.6894
U63	0.0082	0.7338	-0.6544	0.2855	-0.6175	-0.1013
U64	-0.3956	-0.9578	-0.1965	-1.1222	-0.6364	-1.0554
U65	-0.4301	0.7187	0.1772	-0.2426	-0.8750	-0.3864
U66	-0.5561	-0.2204	0.2229	-0.1129	0.1720	-0.7256
U67	-0.3215	0.3828	-1.1468	0.2668	-0.0058	-1.0752
U68	0.4322	-0.6069	-0.3739	0.8378	-1.8651	1.4105
U69	0.3831	0.1404	0.1700	0.9529	-0.2665	0.1346
U70	1.5465	1.2185	0.2087	-1.4534	-0.0413	-0.4600
U71	0.0485	0.2531	-0.1531	0.6884	-0.8444	-0.8818
U72	-0.0293	-1.0710	-0.1890	0.1155	-0.7777	1.4356
U73	-0.1246	-1.1850	0.3022	2.9607	-1.6127	-1.0208
U74	-0.1882	-1.4115	-0.2647	0.2295	-0.8456	-0.6991
U76	2.8899	-0.5607	0.6246	0.2577	-0.6554	-0.0074
U77	2.9701	-0.1636	1.4902	0.7411	-1.8379	0.5052
U78	-0.6050	-0.2735	-1.1594	-0.7268	-0.1035	-0.2809

Table 3.23 Distribution of element into each factor (%) - full dataset

	Factor 1 (%)	Factor 2 (%)	Factor 3 (%)	Factor 4 (%)	Factor 5 (%)	Factor 6 (%)	Factor 7 (%)
MNO	96.4	0.0	1.9	1.0	0.7	0.0	0.0
ZN	91.5	1.3	3.0	1.7	1.5	1.0	0.0
PB	85.6	0.3	0.1	7.4	4.0	2.3	0.3
CO	77.5	0.0	15.0	6.3	0.0	0.0	1.2
AS	83.3	2.2	0.2	0.9	13.0	0.1	0.3
ZR	37.5	33.3	17.0	10.1	0.0	0.2	1.8
TIO2	3.3	94.0	0.2	0.1	0.4	0.5	1.6
AL2O3	0.1	95.3	1.7	2.4	0.2	0.1	0.3
NI	19.6	51.1	11.6	2.8	1.0	11.2	2.8
MGO	25.2	53.9	8.2	9.6	0.4	2.3	0.3
SC	15.6	45.9	12.8	6.1	7.8	11.1	0.8
SIO2	27.9	0.0	59.8	4.4	2.0	5.1	0.9
MO	6.2	6.2	81.0	2.8	0.5	3.1	0.2
FE2O3	19.4	4.0	39.8	30.5	0.0	0.1	6.1
CR	0.0	0.0	3.4	86.3	3.7	5.7	0.9
CAO	27.2	0.0	0.7	51.0	2.8	14.8	3.5
P2O5	0.2	0.0	1.3	0.7	95.9	0.2	1.6
CU	0.2	12.7	2.5	0.0	7.4	71.3	5.9
BA	12.8	7.6	2.3	7.4	10.5	49.5	9.8
V	0.0	0.3	0.1	0.2	2.5	0.1	96.7
SR	11.6	20.1	16.9	2.1	17.4	0.4	31.5

Table 3.24 Distribution of element into each factor (%) - As/Bu

As/Bu	Factor 1 (%)	Factor 2 (%)	Factor 3 (%)	Factor 4 (%)	Factor 5 (%)	Factor 6 (%)
MNO	89.9	0.0	0.3	5.9	1.3	2.5
PB	93.6	2.6	2.0	1.2	0.1	0.5
ZN	86.9	0.5	1.8	5.0	2.7	2.9
CO	81.1	0.0	12.6	0.9	0.5	4.9
AS	40.4	0.0	7.6	36.0	16.0	0.1
TIO2	8.4	76.9	4.5	7.8	2.0	0.3
ZR	22.2	71.7	1.2	1.5	0.0	3.4
AL2O3	4.7	74.8	6.8	6.4	0.5	6.9
MGO	22.5	62.4	12.9	2.0	0.1	0.1
MO	6.0	38.2	18.2	35.7	0.0	1.9
FE2O3	0.0	1.1	75.3	16.8	0.1	6.7
NI	13.4	15.7	60.4	4.4	0.4	5.6
P2O5	0.0	4.5	80.2	11.5	1.0	2.7
CAO	1.0	0.4	1.6	95.8	0.1	1.0
SIO2	17.7	2.3	19.1	51.9	0.9	8.1
CR	0.2	0.5	2.0	2.6	93.7	1.1
BA	30.6	2.8	2.6	1.3	62.7	0.0
V	2.9	2.5	14.7	0.1	79.2	0.6
SR	4.7	4.4	2.2	2.2	0.3	86.2
SC	2.3	9.4	22.1	1.9	0.8	63.6
CU	26.2	13.0	11.9	3.4	3.6	41.8

Table 3.25 Distribution of element into each factor (%) - As/Bu

As/Ls	Factor 1 (%)	Factor 2 (%)	Factor 3 (%)	Factor 4 (%)	Factor 5 (%)	Factor 6 (%)
MNO	89.4	0.0	2.0	7.4	0.4	0.8
PB	93.6	0.3	0.8	3.5	1.7	0.0
ZN	92.5	6.4	0.0	0.2	0.5	0.3
BA	77.4	1.2	4.3	0.2	15.3	1.6
AS	60.0	4.5	0.2	14.4	11.6	9.3
TIO2	1.3	95.2	0.1	0.5	1.2	1.7
AL2O3	0.9	96.4	2.5	0.0	0.2	0.0
NI	4.2	77.5	4.9	0.0	10.4	2.9
SC	1.8	63.4	12.1	22.0	0.0	0.7
MGO	3.8	63.8	1.0	29.4	1.0	1.1
SIO2	1.3	0.4	90.1	5.5	2.7	0.0
FE2O3	11.9	4.7	54.0	24.0	5.1	0.3
CO	40.3	0.5	56.1	1.8	0.1	1.2
MO	0.0	8.8	85.8	0.2	0.4	4.9
ZR	19.7	29.5	31.1	16.3	3.4	0.1
CAO	8.6	0.7	0.0	90.3	0.4	0.1
CR	0.1	0.9	0.8	50.7	47.4	0.1
V	4.0	0.3	4.8	0.3	90.4	0.2
SR	15.0	17.5	8.0	0.9	57.9	0.7
P2O5	1.0	0.7	4.2	2.1	0.8	91.2
CU	2.0	20.0	2.1	9.3	2.8	63.8

Table 3.26 Distribution of element into each factor (%) - Bu

	Factor 1 (%)	Factor 2 (%)	Factor 3 (%)	Factor 4 (%)	Factor 5 (%)	Factor 6 (%)	Factor 7 (%)
P2O5	93.7	0.6	2.5	1.5	0.1	0.2	1.3
PB	77.4	1.0	1.8	0.7	11.9	0.5	6.7
CU	88.6	0.1	0.2	1.1	1.8	3.1	5.1
ZN	60.7	20.2	6.6	0.7	5.5	0.4	5.9
FE2O3	58.1	16.4	12.1	2.6	8.2	2.1	0.4
CO	1.5	96.5	1.2	0.0	0.4	0.0	0.3
MNO	7.0	89.1	0.5	0.0	1.9	0.3	1.3
NI	21.5	50.6	7.4	17.3	0.5	1.7	0.9
AL2O3	5.7	49.4	15.0	5.7	13.2	9.1	1.9
CAO	2.1	0.2	92.5	1.6	1.8	1.7	0.1
SIO2	1.3	32.7	59.9	1.7	1.8	2.5	0.1
CR	29.1	5.1	40.0	10.3	2.1	0.1	13.3
V	3.9	5.8	2.5	86.5	0.1	1.1	0.0
TIO2	3.5	0.1	6.4	66.3	14.1	8.3	1.3
MGO	12.2	10.4	0.2	53.7	0.2	14.7	8.5
ZR	5.5	8.4	0.0	0.6	84.3	1.2	0.0
BA	3.5	8.9	12.4	3.7	64.7	5.2	1.6
SC	2.2	0.5	9.9	0.0	0.1	82.6	4.7
SR	5.4	8.9	0.1	0.6	11.7	66.1	7.2
MO	0.7	0.7	27.5	0.1	26.3	31.5	13.1
AS	0.1	1.4	0.3	3.1	0.1	0.0	95.1

As/Bu	MnO - Pb - Zn - Co -As - Zr - Ba
As/Ls	MnO - Pb - Zn - Co - As - Zr - Ba
Bu	MnO - Fe_2O_3 - Co - Zn - Ni

The data above, and the comparability of the rotated factor matrices (Tables 3.14 and 3.15) for As/Bu Group and As/Ls Group samples, suggest that a single model can be proposed which will explain bulk sediment composition variation in terms of admixture of fixed composition end-members. In contrast, the Bu Group samples may be dealt with separately owing to the more complex inter-element relationships which have resulted in slightly modified end-member composition output.

Because almost exactly the same associations of elements emerge from As/Ls Group and As/Bu group samples, physical mixing of end-member components may be used to explain the variable composition of the sediments (Table 3.27). The compositions of the factors making-up the As/Bu and the As/Ls groups are listed below, (Table 3.27: elements common to both groups emboldened), showing that although factor analysis is capable of calculating inter-elemental associations it remains necessary to interpret the resulting factors in terms of end-member components.

Table 3.27 Factors extracted from Tables 3.24 and 3.25.

	Axis-Basal Upper	**Axis/Lasail**	**Interpretation of component**
FACTOR 1	**MnO-Pb-Zn-Co-As-Zr-Ba**	**MnO-Pb-Zn-Co-As-Zr-Ba**	(1) Hydrothermal Mn
FACTOR 2	**TiO_2-Al_2O_3-MgO-Zr**	**TiO_2-Al_2O_3-MgO-Zr**-Ni-Sc	(2) Detrital
	Mo		
FACTOR 3	**Fe_2O_3-P_2O_5**-Ni	**Fe2O3-Co**	(3) Hydrothermal Fe
	SiO_2-Mo	**SiO_2-Mo-Zr**	(4) Hydrothermal Si
FACTOR 4	**SiO_2-Mo**	Fe_2O_3-MgO	
	CaO-As	**CaO**-Cr-Sc	5) Biogenic carbonate
FACTOR 5	**Cr-V**-Ba	**Cr-V**-Sr	
FACTOR 6	Sr-Sc-Cu	P_2O_5-Cu	

Although FACTOR 1 is an artificial construct, rather than a measurable entity, it is representative of a physical component of the samples given that its presence is inferred in both types of Axis lava surface sediments. To use the output of factor analysis, it is necessary having defined an underlying concept to label it in a geologically meaningful way. A hydrothermal origin of Mn and the association of manganese with the trace elements Pb, Zn, Co, As and Zr is consistent with recent studies of active hydrothermal plumes (Kurnosov, *et al.*, 1983; Freely *et al.*, 1994).

FACTOR 1 is a Mn-component which is uncorrelated with the other factors and in the form of manganese-dioxide can be termed a *scavenger* in a chemical sense: surface adsorption of micro-component elements to precipitates of finely divided manganese dioxide, iron hydroxide, and aluminium hydroxide in laboratory studies are well documented (Li, 1981, Nyffeler *et al.*, 1984, Honeyman *et al.*, 1988, Jannasch *et al.*, 1988). The degree of adsorption which takes place depends on the relationship between the charge and size of the adsorbed ion and the charge and topographical character of the adsorbing surface (Goldberg, 1954). The presence of hydrated oxides of manganese (negatively charged sols) in ocean waters would be expected to give rise to adsorption, the species collected being positively charged ions. Listed below for comparison with this study, the *surface complex formation model* (summary by Li, 1981; Chester, 1990) for inorganic adsorption of ions at hydrous oxide surfaces and a factor analysis study of trace element enrichment in pelagic clays (Li, 1981).

(1)	Li (1981):	MnO + Ba, Co, Cu, Zn, Mg, Ca, Tl and Ni
(2)	Chester (1990):	MnO + Ba, Co, Cu, Zn, Mg, Ca, Sr and Ni

The association of Co, Cu and Zn with Mn is compatible with Mn-scavenging from the water column. The correlation of Ba and Mn may result from re-suspension of Mn- and Ba- rich bottom sediments followed by slow scavenging in the hydrothermal plume (Freely *et al.*, 1994). Although Mn is enhanced in pelagic clays relative to nearshore mud (Chester and Messiha-Hanna, 1970) and may represent an authigenic phase, (i.e. one which is non-lattice-held and derived from "solution"), the slow precipitation of Mn from hydrothermal solutions is characteristic of the hydrothermal sites at rise-crest sites (Freely *et al.*, 1994). Lalou (1983) suggests two models which explain ferromanganese metalliferous sediments in terms of hydrothermal and hydrogenous processes and, in Chapter 2, bivariate plots are used to suggest that, although some Mn may be hydrogenous, the majority is of hydrothermal affinity. The manganese-oxide

component is termed a precipitate rather than a halmyrolysate using the Elderfield *et al.*, (1976) classification, and may either be a hydrothermal precipitate or a hydrogenous precipitate using the Cronan (1990) refinement of the previous classification.

Table 3.28 Comparison of Axis Lava surface sediments and Basal Upper intra-lava sediments

	Axial lava surface sediments	Basal Upper Intra-lava sediments
FACTOR 1	**MnO - Pb - Zn - Co - As - Zr - Ba**	P_2O_5 - Fe_2O_3 - Ni
		Pb - Cu - Zn - Cr
FACTOR 2	TiO_2 - Al_2O_3 - MgO - Zr - (Ni - Sc)	**MnO - Fe_2O_3 - Co - Ni - Zn**
	Mo	Al_2O_3 - SiO_2
FACTOR 3	Fe_2O_3 - P_2O_5 - Ni	CaO - Cr
	SiO_2 - Mo - (Zr)	SiO_2 - Mo
FACTOR 4	Fe_2O_3 - MgO or Co	TiO_2 - MgO - Ni
	CaO - (As - Cr - Sc)	V
FACTOR 5	Cr- Ba - V *or* V - Sr - Cr	Mo
		Zr - Ba
FACTOR 6	Sr - Sc - Cu *or* P_2O_5 - Cu	Mo - Sr - Sc
FACTOR 7	Not applicable	As

The two possible sources of Mn in the study samples may be summarised as follows: (1) the one hundred fold enrichment of Mn and Co relative to crustal abundance (Cronan, 1976) in hydrogenous encrustations suggest that those elements are derived from the water column whereas (2) Red Sea studies (e.g. Cronan, 1980) suggest a hydrothermal precipitation sequence causing spatial separation of precipitates around the venting source. In the second possible Mn source the elements solubilized during hydrothermal activity, which include Mn, Co, Cu, and Ni, are subsequently removed from solution by precipitation of solid phases in the order (1) sulphides → (2) iron silicates → (3) iron oxides → (4) manganese oxides. Thus, iron and manganese oxides form separate haloes around the vent. Close proximity of the Oman sediments in this study to hydrothermal massive sulphide deposits and the voluminous work documenting the association of metalliferous sediments with massive sulphides, (e.g., *Troodos ophiolite, Cyprus* - Robertson and Hudson, 1973; Varnavas, 1981; Oudin and Constantinou, 1984; Boyle, 1990; *EPR* - Klein, 1991; *Othris and Pindos*

ophiolite - Robertson and Varnavas; 1993; *Oman ophiolite* - Fleet and Robertson, 1980; Robertson and Fleet, 1986; Haymon *et al.,* 1989 and 1990) suggest that much of the manganese represents an hydrothermal perturbation spike superimposed over a low background of authigenic manganese accumulation.

The elements associated with MnO in Bu Group samples differ from the other sample groups described above. The principle difference is that Bu Group samples contain a ferromanganoan component whereas the As/Ls and As/Bu Group samples contain a manganoan component which is distinctly separate from Fe (Table 3.28). Some of the trace metal associations are common to Axial surface sediment and Bu group samples.

MnO is seen to be most consistently associated with Co and the relationship of MnO with Fe_2O_3 explains the association of Ni with this component. For Bu Group samples, the trace elements Zr, Ba and As appear as elemental associations independent of major element components. The Bu Group data provide the clearest evidence for a distinct ferromanganese component rather than separate Fe and Mn phases.

Table 3.29 Average MnO content, Oman sediments (this study)

Group	**Average MnO content**
Total for all Groups	6.2 wt%
Lasail Unit	0.58 wt%
Axis Unit	8.92 wt%
Basal Upper Unit	6.65 wt%
Axis/Basal Upper	7.19 wt%
Axis/Lasail	3.34 wt%

The X-ray Diffraction analysis discussed in Section 2.4 identified lithiophorite, cryptomelane and manganite as Mn-oxyhydroxides that are present in the samples:

lithiophorite	(Co,Mn)O(OH)
cryptomelane	KMn_8O_{16}
manganite	γ-MnOOH

The mineral lithiophorite explains the incorporation of Co into the Mn-oxide phase, whereas the other trace elements are likely to be loosely adsorbed to the

oxide surfaces. The volumetric importance of this phase can be estimated from the MnO-content of the sample since no other major element forms part of this factor. The average MnO content (Table 3.29) for the sample groups varies between 0.58 wt% and 8.92 wt%, the average being 6.2 wt%:

3.5.2 Hydrothermal Fe-oxide Component

The factor analysis output suggests complexity in the hydrothermal component. The hydrothermal ferromanganoan end-member of the Bu Group samples was discussed in the previous Section. The identical Fe_2O_3 - P_2O_5 - Ni association reflects the similarity between the Bu and As/Bu Group samples and is consistent with hydrothermal origin of P_2O_5 which has been identified in solid solution with oxyhydroxides in active hydrothermal systems (Fox, 1991). There are apparently two hydrothermal Fe-oxide components to the As/Ls Group, and the inter-element relationships are very different to the other sample Groups.

The Fe-oxide inter-element associations are as follows:

As/Ls:	(1) Fe_2O_3 - Co
	(2) Fe_2O_3 - MgO
As/Bu:	(1)Fe_2O_3 - P_2O_5 - Ni
Bu	(1)Fe_2O_3 - P_2O_5 - Ni
	(2)Fe_2O_3 - MnO - Co - Zn - Ni

The association of the transition metals Co, Sc and Ni with Fe_2O_3 indicates that these are probably adsorbed onto the Fe-oxide surfaces. The relationship of Sc to the Fe-component is in both cases less close than that of Co because Sc is also intimately associated with the detrital phase in the As/Ls samples and with Cu and Sr in the As/Bu samples.

The behaviour of Co is interesting because of the difference in its behaviour pattern between As/Ls and As/Bu Group samples. Co associates strongly with the Fe-component in the As/Ls Group but strongly with the Mn-component in the As/Bu Group. In both examples, the transition metal is adsorbed onto OH ligands on the metal oxide surfaces. In the As/Bu samples, the greater abundance of Mn-oxide preferentially binds Co rather than Fe-oxide. Co binds to Fe_2O_3 in As/Ls Group samples in which the Fe-oxide component has swamped the Mn-oxide source.

3.5.3 Siliceous Components

The association of Si to the other elements is very consistent throughout the sample Groups. In each volcanic stratigraphic position, SiO_2 is associated with Mo in a separate phase. In addition, in As/Bu samples, SiO_2 is associated with MgO in a second phase which is probably due to epidotization.

The near pure Si-component either represents a hydrothermal Si-component or a biogenic Si-component. The presence of siliceous oozes formed by opal secreting organisms, which are trace element poor, is confirmed by presence of radiolarians from identical metalliferous sediments (umber and radiolarian mudstone) sampled from the Axial lava surface and used for biostratigraphic dating (Blome and Irwin, 1985; Beurrier *et al.,* 1987). Radiolarians and diatoms which contribute opaline skeletal material probably represent an important role in the incorporation of silica to metalliferous sediments.

If the siliceous component is hydrothermal, then it is unrelated to either hydrothermal Fe or Mn. In the previous Chapter, admixture of Fe and Si might be explained by the hydrothermal precipitation of nontronite and Fe-oxide and goethite, all of which contain silica, and which are recognized in XRD analysis. In support of the hydrothermal origin of the Si component, the output of factor analysis for all samples (Table 3.18) suggests that Si forms (1) one component which is pure Si and is associated with Mo, and (2) another component which is Fe_2O_3 - SiO_2. It is consistent with the interpretation of the previous chapter that SiO_2 is both hydrothermal and biogenic in origin. Possibly the Varimax rotation, in an attempt to simplify the factors, has been unable to detect the pattern which is apparent in the preliminary factor analysis output.

3.5.4 Detrital Al - Ti - Mg Silicate component

Having dealt with hydrothermal input which represents emanations closely associated with the ridge-crest environment, the remaining factors represent the *background* signal, i.e., the marine sediment-forming minerals which make up non-ridge crest deep-sea sediments. Marine sediments are principally of three sediment types: clays, siliceous oozes and carbonate oozes. The average major element composition of the three sediment types is listed in Table 3.30.

The composition As/Bu Group associations of FACTOR 2 (Table 3.28), are TiO_2 - Al_2O_3 - MgO - Zr plus Ni and Sc in the As/Ls Group samples. The Bu Group subdivides similar major element associations between FACTOR 2 (Al_2O_3 -

SiO_2) and FACTOR 4 (TiO_2 - MgO). The association of elements in FACTOR 2 correspond with those found in lithogenous crystalline material. The lithogenic inputs to oceans are dominated by the clay minerals and quartz, the most commonly found clays are as follows, (Chester, 1990):

Kaolinite	$Al_2SiO_5(OH)_4$
Illite	$KAl_2(Si_3AlO_{10})(OH)_2$
Chlorite	$MgAl(Si_3Al)O_{10}(OH)_8$
Montmorillonite	$Na(Al,Mg)_2Si_4O_{10}(OH)_2.xH_2O$

Using XRD analysis, none of the above clay minerals is identified in the samples. This may be due to the volumetric dominance of hydrothermal Fe-oxide which masks the detrital signal. Except for the Bu group samples, the factor analysis technique has not identified Si as correlating positively with the association of elements of detrital origin. Since the detrital component is made up of crystalline silicate minerals, the ability of factor analysis to evaluate Si-content of minor components accurately is clearly inadequate. However, there is an independent Si-rich factor for each sample group, including the Bu Group samples in which Si is identified as two separate components.

The Factors which appear consistently in all samples with the same element associations are the hydrothermal-Mn oxide component and the detrital Al-Mg-Ti component. The two components are made of two groups of elements: Mn-Oxides - MnO-Pb-Zn-Co-As-Ba; and aluminosilicates - TiO_2 - Al_2O_3 - MgO - (SiO_2) - Zr - (Ni) - (Sc) - (Mo). Since the elements in each Factor are interrelated as a single end-member component, it is possible to use a single element from each of the factors to represent that group on a bivariate plot. Neither Al_2O_3 nor MnO appears associated with any other component in the Factor Analysis model. The may be calculated from the square of the rotated factor score that:

(1) The hydrothermal-Mn component contains: 82.8% of the bulk Mn, and 0.02% of the bulk Al

(2) The detrital component contains: 0.64% of the bulk Mn, and 55.9% of the bulk Al

Consequently, since the major element composition of marine sediments appears to be controlled largely by the relative proportions of the sediment forming

minerals, the elements which be used to represent the two factors will be MnO and Al_2O_3 for FACTOR 1 and FACTOR 2 respectively. Either by plotting 82.8% of the bulk Mn-content versus 55.9 % of bulk Al-content by sample or by *defining detrital content = hydrothermal-Mn content* as $82.8/55.9 = 1.48$, it is possible to compare the relative proportions of each of the two end-members in each sample since Al_2O_3 and MnO are precisely equivalent to that component (Figure 3.5).

Table 3.30 (Data: El Wakeel and Riley, 1961)

Element	**Calcareous ooze**	**Lithogenous clay**	**Siliceous ooze**	**Oceanic Average**
SiO_2	26.96	55.34	63.91	42.72
TiO_2	0.38	0.84	0.65	0.59
Al_2O_3	7.97	17.84	13.30	12.29
Fe_2O_3	3.00	7.04	5.66	4.89
FeO	0.87	1.13	0.67	0.94
MnO	0.33	0.48	0.50	0.41
CaO	0.30	0.93	0.75	0.60
MgO	1.29	3.42	1.95	2.18
Na2O	0.80	1.53	0.94	1.10
K2O	1.48	3.26	1.90	2.10
P_2O_5	0.15	0.14	0.27	0.16
H2O	3.19	6.54	7.13	5.35
CaCO3	50.09	0.79	1.09	24.87
MgCO3	2.16	0.83	1.04	1.51
Org.C	0.31	0.24	0.22	0.27
Org.N	-	0.016	0.016	0.015
Total	100.0	100.0	100.0	100.0

The presence of epidote in some samples of the Bu Group may have complicated the relationship of Al to Si and separated it slightly in vector-space from Ti and Mg (Figure 5.6). Since it is likely that at least two hydrothermal systems produced the metalliferous sediments, it is possible that the difference between Axis sediments and inter-lava Bu sediments represents different metasomatic processes. The secondary pumpellyite-bearing facies produced by low

temperature oxidizing downward flowing sea water may be responsible for the differences noticed in this study.

In the same way that Mn-component content was estimated, so the detrital content can be estimated as $Al_2O_3 + TiO_2 + MgO$ to give an average of 6.8 wt.% for all of samples. This does not include Si, which in the factor analysis is not included in the silica component, but for comparative purposes this is irrelevant. The approximate detrital content calculated in this way is as follows (Table 3.31):

Table 3.31 Average approximate detrital content

	Average $Al_2O_3 + MgO + TiO_2$ (detrital) content
Total for all Groups	6.80 wt%
Lasail Unit	9.64 wt%
Axis Unit	5.57 wt%
Basal Upper Unit	6.77 wt%
Axis/Basal Upper	6.25 wt%
Axis/Lasail	7.99 wt%

Other than in intra-lava sediments from the Lasail Unit, for which there are very few available samples, the detrital content is consistently low for each of the groups. Such uniformly low incorporation of detritus may (a) explain why clay minerals are not easily detectable using XRD analysis, and (b) suggest that the samples formed either very quickly and/or in an environment devoid of clastic input. The trace elements, Zr, Ni and Sc, are associated with minerals of detrital origin.

3.5.5 Biogenic Carbonate Component

Table 3.30 illustrates the importance of aluminium in the clay, silicon in siliceous ooze, and calcium in the calcareous oozes. The Ca-rich component is principally carbonate shell material defined as a *biogenous component* in the first classification suggested by Goldberg, (1954). The source of this component is principally one of the three major carbonate secreting organisms of the oceans, i.e., coccolithophorids, foraminifera and pteropods. From factor analysis, the Ca component is associated only with Cr or As. The three carbonate minerals, calcite, huntite, and ankerite, were detected using XRD analysis. The control of the trace element-poor carbonate component is primarily related to water depth

and secondarily to primary productivity, shell dissolution and dilution of the component by other sediment-forming components. The topographic high of the Semail spreading ridge environment is typical of the environment in which calcareous oozes tend to be found, (Bostram, 1973).

An alternative assessment of the factor analysis could be that the Ca-rich inter-element associations represent pyroxene detritus, since Cr is particularly high in pyroxenes and the only trace element consistently associated with CaO in the factor analysis. In the minor element associations Cr and V appear in the same Factors for the As/Bu and As/Ls Group which confirms the likelihood that the Ca-rich component is pyroxene rather than carbonate since V is also concentrated in pyroxene. Evidence was also presented in the previous chapter for dissolution of the carbonate component and the relative enrichment of the detrital component. Moreover, the incorporation of minor detrital phases which are Cr-rich into the carbonate phase has also been established (Varnavas and Panagos, 1981).

A portion of the Ca-content of the As/Bu samples is also likely to be of hydrothermal origin, since it correlates with Mn-oxide in factor analysis output for the full data set.

3.5.6 Trace metal associations

FACTOR 5 and FACTOR 6 explain only 13.0% (As/Bu) and 11.5% (As/Ls) of the variance of the dataset respectively. The groups represent trace element associations unrelated exclusively to any of the major element components (Table 3.32). The groups are as follows:

Table 3.32 Trace element associations estimated by factor analysis

	Bu	**As/Bu**	**As/Ls**
FACTOR 1	Pb - Cu - Zn - Cr		
FACTOR 5	Zr - Ba	V-Cr-Ba	V-Cr-Sr
FACTOR 6	Sr - Sc - Mo	Sr-Sc-Cu	
FACTOR 7	As		

The Pb-Cu-Zn-Cr correlation of Bu Group results from complexity in the ferromanganoan component which does not arise in the other Groups. The

correlation between Cr and V probably results from the inclusion of pyroxene detrital grains within the background carbonate phase. The other associations probably deal with processes too complex for Factor Analysis to quantify. Because the trace elements are not always directly associated with any of the end-member components, the elements Cu, Sr, Sc, Cr, Ba and V will be thought of as having complex relationships involving multiple origins related to a number of marine processes.

3.5.7 Summary

At least eight geologically plausible end-member components have been identified using factor analysis, these are:

(1) Hydrothermal Mn oxide
(2) Hydrothermal Fe oxide
(3) Hydrothermal Fe-Si oxide
(4) Hydrothermal Fe-Mn oxide
(5) Hydrothermal Si
(6) Detrital aluminosilicate
(7) Biogenic carbonate
(8) Biogenic silica

Having carried out factor analysis on the major and trace element data, the next section contains the output of factor analysis when the major elements are excluded and only trace elements and the REE are used.

(1) Factor analysis does not consistently effectively explain the role of each element. Variability in the proportion of variance explained by the model ranges from 37.5% of Mo, the in As/Ls Group to 96.7 % of Si, in the Bu Group. Si, Mn and Ca are most consistently adequately explained of the major elements, P_2O_5 is most often least well explained. The variation in trace elements tends to explain between 70 % and 80 % of the data. Cu, V and Sr are least well explained.

(2) The seven factor model of the Basal Upper group best explains variance in the dataset. This is especially noticeable for the trace elements Pb, Co, Sc, As and Ba for each of which >90 % of variance is explained by the model.

(3) The Fe-oxide component is always associated with Co, Ni, Sc and V, commonly associated with Sc and also may contain As, Pb and Zn.

(4) The Mn-oxide component is always associated with Pb, Zn, Cu, Sr, Cr, As, Zr and Ba, commonly associated with Ni and Mo, and also may contain Sc, V and Co.

(5) The Mn-oxide component is associated with small amounts of Fe_2O_3 in the Bu group. 15% of the Fe_2O_3 in these samples is contained within the Mn-oxide component.

(6) The detrital component containing the Al_2O_3, TiO_2 and MgO is associated with 13% to 51% of the Ni present in the samples and 26% to 58% of the Zr. The detrital component may also be associated with minor Sc.

(7) The Ca-rich component contains 27% to 40% of the Cr present and may also contain Ni and As.

(8) The siliceous component is always associated only with Mo of which it contains between 22% and 32% of the total. Other than its association with Si, Mo is otherwise either poorly explained by the model (As/Ls) or associated only in the trace element groups.

(9) Epidote is recognised as a Ca-Al silicate in the As/Bu samples only and it is not associated with any significant trace elements.

(10) The remaining factors are made up of trace element associations and are best explained as being related to more than one major end-member component. Commonly found associated in significant amounts are Cr and V.

3.6 Factor Analysis Output: trace element and REE data

In this Section, the factor analysis technique has been applied again omitting the major element data for the purpose of clarifying the relationships outlined above. In this section, analysis is carried out on the trace elements using the trace elements only and the REE as variables. To ensure consistency with the previous

factor analysis the dataset is divided geochemically by volcanic stratigraphic position. The following Factor Analyses were undertaken:

(1) Full dataset (200 samples), trace elements only (Zn, Pb, Co, As, Zr, Cu, Ni, Sc, Ba, Cr, V, Sr, Mo)

(2) As/Bu subset, trace elements only (Zn, Pb, Co, As, Zr, Cu, Ni, Sc, Ba, Cr, V, Sr, Mo)

(3) As/Ls subset, trace elements only (Zn, Pb, Co, As, Zr, Cu, Ni, Sc, Ba, Cr, V, Sr, Mo)

(4) Bu subset, trace elements only (Zn, Pb, Co, As, Zr, Cu, Ni, Sc, Ba, Cr, V, Sr, Mo)

(5) Full dataset (30 samples), trace elements + REEs

(6) As/Bu subset, trace elements + REEs

(7) As/Ls subset, trace elements + REEs

(8) Bu subset, trace elements + REEs

3.6.1 Trace element factors

The groups that result are taken from the Factor Matrices and rotated to *simple structure* by the Varimax method. Table 3.33 summarizes the trace element output for comparison with the results of factor analysis on the entire dataset. The data in the **Trace Element** column (Table 3.33) below represents factor analysis output which has not been complicated by the inclusion of the major element patterns.

The trace elements behave in similar but not identical ways once the complications of the major element components have been eliminated from the Factor Analysis. From the above above (Table 3.33), the elements can be dealt with in groups which exhibit alike behaviour. The groups that emerge are:

(1) Pb-Zn-Ba-Co-As-(Zr-Cu)
(2) Sr-Sc-Ni

(3) Cr-V

The elements Mo, Zr, As, and Sr will be dealt with individually as their behaviour is inconsistent, suggesting that they are incorporated into the sediment in different ways.

Table 3.33 Factor Analysis Output

	Major and Trace element Groups	Trace Element Groups
(1) All		
	MnO-CaO-TiO_2-Zn-Pb-As-Co-Zr	Zn-Pb-Co-As-Zr
	Fe_2O_3-SiO_2	
	TiO_2-Al_2O_3-MgO-Ni-Sc	Ni-Sc
	Sr	
	P_2O_5-Fe_2O_3	
	Zr-Mo	Mo
	Cr	Cr
	Cu-P_2O_5	Cr-Ba
	V	V-Sr
(2) As/Bu		
	MnO-Zn-Pb-Co-As-Zr-(Cu-Ba)	Pb-Zn-Co-Ba
	TiO_2-Al_2O_3-MgO-Zr	Zr
	SiO_2-Mo	Mo
	Fe_2O_3-P_2O_5-Ni	
	Cr-Ba-V	Cr-V-As
	Sr-Sc-Cu	Sr-Sc-Cu-Ni
(3) As/Ls		
	MnO-Pb-Zn-Ba-As	Pb-Zn-As-Ba-Zr
	TiO_2-Al_2O_3-MgO-Ni-Sc	Sc-Ni-Cu
	SiO_2-Mo-Zr	Mo-Zr
	Fe_2O_3-Co	Co
	CaO-Cr	
	V-Sr	Cr-V-Sr
	P_2O_5-Cu	
(4) Bu		
	Fe_2O_3-P_2O_5	
	Pb-Cu-Zn	Pb-Zn-Cu
	MnO-Co-Ni-Zn	Ni-Co
	Al_2O_3-SiO_2	
	CaO-Cr	Cr
	V	V
	TiO_2-MgO	
	Ba-Zr	Ba-Zr
	Sc-Sr-Mo	Sc-Sr-Mo
	As	As-(Sr)

3.6.2 REE factors

The results of Varimax rotation for the REEs and Major Elements are summarized in Table 3.34 below. The purpose of this Factor Analysis was to

determine where the REEs reside in the sediments from their association with the major element components.

Table 3.34 REE associations

	Axis/Basal Upper	Axis/Lasail
FACTOR 1	(1) TiO_2-CaO-Al_2O_3-Nb-Y-Hf-Zr - (actinides) Th - U - (lanthanide) La to Yb (2) SiO_2-Cs-Co	(1) TiO_2-CaO-Al_2O_3-Nb-Y-Sc-Ni-Cu-Sr-Ta - (actinide) Th - (lanthanide) La - Yb
FACTOR 2	(1) MnO-Co-Zn-V-Cu-Cs (2) SiO_2-MgO-Zr	(1) Fe_2O_3-Cu-(actinide) U (2) SiO_2-CaO- (Er) - (Yb)
FACTOR 3	(1) Cr	(1) P_2O_5-V-Pb-Cr (2) Fe_2O_3 - P_2O_5 - Ba-Ni-Rb
FACTOR 4	(1) Al_2O_3-TiO_2-Sc-Rb	(1) TiO_2-Rb-Hf-Zr-Ba-Cs
FACTOR 5	(1) CaO-Hf-Ta	(1) MnO-Co-Z (2) SiO_2-MgO
FACTOR 6	(1) Ba-Zn	

The lanthanide elements behave uniformly throughout, associating with the major elements, TiO_2, CaO, and Al_2O_3 which represent the detrital and calcareous components. The elements, Sc, Rb, Hf and Zr, load with the same factor. The actinide elements (U and Th) both relate to the detrital/calcareous phases in the Mn-rich sediments whereas only Th does so in Mn-poor sediments. U associates with the Fe component in As/Ls samples. A Mg-silicate is identified using this Factor Analysis calculation but no REEs are associated with it.

3.7 Quantifying end-member components

In the previous Sections, the factor analysis output has been used to describe a range of end-member components qualitatively. In addition, the factor analysis results may be used to quantitatively determine the actual composition of end-member sources in the Oman sediments. The procedure in this study follows previous factor analyses for sediments (Full *et al.*, 1981, 1982; Full and Ehrlich, 1986) but by limiting the end-member contributions to zero or positive concentrations, the geologically reasonable implications of negative contributions, such as remobilization and redeposition of Mn, are not quantified by this method. The selection of the number of end-members used to model the data attempt to provide an objective solution to partitioning problems by choosing end-members in the following way (Leinen and Pisias, 1983):

(1) At least 95% of the variance in the data set must be explained by the sum of the squares of the end-members.

(2) All of the end-members that explained less than 2% of the total variance were rejected.

(3) All of the end-members which did not have a geologically reasonable explanation were rejected.

In practise, the factors in which a major element appeared all represented as end-members. Because the factors are uncorrelated, the product of the sum of the square of the variance and the bulk element composition equals the concentration of that element for each factor of a given sample. By using the major element bulk content for each sample, the concentration is calculated of each of the end-members in each sample. Using equation 3.8 below, it is possible to quantify the compositions of each of the components involved in the formation of the metalliferous sediments.

Eqn 3.8 $\text{"component } x\text{"} = C_1(\text{Al}) + C_2(\text{As}) + C_3(\text{Ba}) + \ldots + C_{20}(\text{Zr})$

where the $\mathbf{C_1}$ to $\mathbf{C_{20}}$ are coefficients. Thus, meaningful end-member components have been calculated using the equation above, substituting the values from the rotated factor matrix for the values of **C**. The factor analysis results have suggested slightly different end-members for each of the volcanic stratigraphic locations. The average values, which are calculated by sample Group from the contribution of components to each individual sample, are summarised below (Table 3.35) from the data in Appendix B:

The labels assigned to each of the elemental associations are those which have been described qualitatively in Section 3.5. Fe-oxide, which is a separate component in each of the sample Groups, contains a proportion of P_2O_5 in As/Bu and Bu Group samples (Section 3.5.2). A ferromanganoan component exists in Bu group samples in addition to the Fe-oxide component, and a manganoan component contributes to As/Bu and As/Ls Group samples. The siliceous component has been labelled hydrothermal, although it is certain that a portion of it is biogenic, but the factor analysis has failed to distinguish this possibility. Detrital and Biogenic Carbonate components are unambiguous in the results. A

phosphate component that is unrelated to Fe_2O_3 is present in As/Ls Group samples.

Table 3.35 Average end-member component contents

End-member Component	**As/Ls**	**As/Bu**	**Bu**
Hydrothermal Mn-Oxide	1%	11%	-
Hydrothermal Fe-(P)-Oxide	33%	21%	22%
Hydrothermal Fe-Mn-Oxide	-	-	11%
Hydrothermal/Biogenic Silica	51%	35%	41%
Total Hydrothermal Contribution	**86%**	**67%**	**75%**
Detritus	4%	12%	3%
Biogenic Carbonate	8%	19%	20%
Phosphate	0	-	-

Interpreting the Factors as end-members accounts for the very wide compositional range present in the samples taken from the Semail ophiolite, if the assumptions and simplifications indicated throughout the text are accepted.

3.8 Summary

The factor analysis of Oman ophiolite bulk sediment geochemical data has provided 7 end-member components with which to describe the sample-forming processes. Fixed-composition end-member component mixing cannot accurately be used for the Oman sediment because the application of factor analysis to subsets of the data did not, in each example, provide identical results. However, general similarities exist between the sub-sets of data, which suggest that admixtures of end-member components of similar compositions did provide the source of the elements. The results have shown that Fe-oxide is associated with P_2O_5 and Ni, and that MnO and Fe_2O_3 are not found in the same component except in the Bu samples. The association of Fe, Mn, Cu and Zn is comparable with earlier studies using factor analysis of similar recent sediments (Leinen and Pisias, 1983). Al, Mg and Ti are conservative elements associated with detritus. The element Si forms a separate component which constitutes between 35.5% and 51.7% of the samples. Since the samples are rise-crest samples of principally

hydrothermal origin, it is geologically unreasonable to term this component biogenic silica. It is notable that previous factor analysis studies find that Si is not related to Al in aluminosilicates (Leinen and Pisias, 1983). The inability of factor analysis to determine the origin of this component is one of the major drawbacks of its application.

The composition of the rotated components all represent geologically reasonable end-members. In order to compare and assess the results of this study, the components have been recalculated as elemental ratios (Figure 3.36).

Table 3.36 (a) Elemental ratio coefficients used in normative analysis, Nazca sediments (Dymond, 1981)

Element	(E/Al)D	(E/Fe)H	(E/Si)B	(E/Ni)A	(E/Ba)R
Al	1.0000	0.0060	0.002000	1.5	0.5000
Si	3.0000	0.1300	1.000000	4.5	0.0000
Mn	0.0160	0.2900	0.000023	30.0	0.0070
Fe	0.7000	1.0000	0.001000	15.0	0.3500
Ni	0.0015	0.0009	0.000040	1.0	0.0065
Cu	0.0012	0.0042	0.000050	0.5	0.0160
Zn	0.0014	0.0019	0.000080	0.1	0.0040
Ba	0.0120	0.0050	0.002000	0.2	1.0000

(b) Elemental ratio coefficients derived from factor analysis, Nazca sediments (Leinen and Pisias, 1983)

Element	(E/Al)D	(E/Fe)H	(E/Si)B	(E/Ni)A	(E/Ba)R
Al	1.000	0.005	0.011	2.0	0.522
Si	1.987	0.019	1.000	90.0	0.000
Mn	0.192	0.305	0.066	25.7	0.568
Fe	0.776	1.000	0.342	0	1.138
Ni	0.011	0.0021	0.000	1.0	0.018
Cu	0.0058	0.0043	0.0019	0.48	0.022
Zn	0.0020	0.0018	0.001	0.06	0.007
Ba	0.0012	0.0001	0.043	3.45	1.000

(c) Elemental ratio coefficients derived from factor analysis, Bu samples (this study)

Element	(E/Al)D	(E/Fe)H	(E/Si)H	(E/Fe)H2
Al	1.000	0.000	0.009	0.000
Si	2.033	0.015	1.000	0.000
Mn	0.200	0.002	0.004	1137
Fe	0.855	1.000	0.132	1.000
Ni	0.008	9.100	0.000	1.000
Cu	0.004	1.790	0.030	9860
Zn	0.000	0.168	0.000	19855
Ba	0.050	0.000	0.081	2648

The comparison between the end-members calculated for Nazca plate surface sediments and Oman rise-crest sediments reveals that for the detrital component, the resulting elemental ratio coefficients closely resemble those of the previous studies. Moreover, there is a close resemblance between ratios for the Si end-member which is termed biogenic in Nazca sediments but provisionally termed hydrothermal in Oman sediments. However, as a result of limiting the input of factor analysis to rise-crest samples, the details of the hydrothermal source has been obtained which prevoiusly have been ignored. The elemental ratios produced by this study do not closely resemble those of previous Nazca plate surface sediments. The reason for this is that this study effectively sought to subdivide into source component what had previously been taken to be a uniform hydrothermal end-member. The geological interpretation of the factor analysis output will be discussed in Chapter 5.

CHAPTER 4
Determination of end-member components using chemical partitioning experiments and linear programming

4.1 Introduction

This chapter presents an objective approach to identifying the principal sources of variation in a data set for the purpose of selecting geologically reasonable end-members. Linear programming uses a set of equations to represent source-element relationships to determine a set of unknowns; each unknown represents the percentage of a different source *component* in the sample. The technique has been previously used to determine recent plate surface sediment compositions (Dymond, 1981; Heath and Dymond, 1981; Leinen and Pisias, 1984). To interpret the results of linear programming, sediment-forming phases have also been chemically separated. The leaching experiment described in this chapter is used to provide independent comparative data to quantify the mode of incorporation of the elements into the sediments. By chemical partitioning of elements between the various constituent phases of the Oman rise-crest samples, this chapter aims to discuss the processes by which the elements have been incorporated into the sediments. The chemical separation technique used in this study was based on the classic method established by Chester and Hughes (1967) and follows modifications by Miller and Cronan (1994) and Rogers (1996, *pers. comms.)* detailed in Appendix A.3.2.

Previous applications of the linear programming technique have concentrated on large-scale source variations in plate surface sediments from a wide range of depositional environments (Heath and Dymond, 1977; Dymond, 1981; Heath and Dymond, 1981). Because this study concentrates on rise-crest sediments, it has been necessary to modify the original technique by emphasising different inter-element ratios and different end-member compositions.

First, using chemical leaching, it has been possible to physically separate a number of fractions, and then to individually analyse them directly. Previous leaching work on pelagic sediments (eg., Chester and Hughes, 1967; Chester and

Hughes, 1969; Chester and Messiha-Hanna, 1970; Cronan, 1976) has demonstrated meaningful relationships between element patterns and sediment supply mechanisms by separating ferromanganese minerals, carbonate minerals, and absorbed trace elements from the samples. The aim of conducting the leaching experiment, which is presented in this Chapter, was to establish the true nature of element partitioning for comparative purposes with the results of factor analysis and linear programming techniques. It is necessary to determine which elements are associated with which components because: (1) trace elements are not partitioned equally between the phases, and (2) the proportions in which the phases are present is variable.

Second, the original linear programming (Dymond, 1981) model has been applied to the large Oman data set for the purpose of comparison with previous studies, and the output is assessed to enable modification of the end-members. The element distribution pattern calculated by factor analysis has then been assessed with respect to the results of the leaching study which identifies how the elements are partitioned between the various phases.

Third, the original linear programming model is applied, in an adjusted form, to take into account end-members that are more geologically realistic for the rise-crest environment.

Finally, inter-element ratios which have been calculated from the factor analysis output (Chapter 3) are substituted into the linear programming equations. The purpose of this is to assess the sensitivity of the technique to the inclusion of local end-member compositions.

There are no previous studies in which end-member composition has been calculated by linear programming the ophiolite sediments of Oman. The procedure that is followed for the metalliferous sediments from Oman is, however, similar to that used previously for magma mixing, chemical mode, and liquid line of descent calculations, (Wright and Doherty, 1970), and follows the modifications proposed for recent Nazca plate surface sediments, (Heath and Dymond, 1981; Dymond, 1981).

4.2 Geochemical partition analysis

The procedure is designed to separate three different components and a residual fraction:

(1) The carbonate mineral constituents, the loosely sorbed ions, and the interstitial water evaporates soluble in the acetic acid.

(2) All of the above plus the ferromanganese oxide phases reducible by hydroylamine HCl.

(3) All of the above, plus the iron oxide minerals reducible by hot HCl.

(4) Bulkcontent, including the more resistant silicates and aluminosilicates which are insoluble in HCl.

Because the chemical attacks are on different sub-samples of the each sample, and not sequentially on individual samples, the portions of each element soluble in each phase are determined by subtraction (see Appendix A.3.2).

4.2.1 Methodology

A representative sub-set of samples has been selected from the data set for the purpose of chemical leaching experiments. The samples have been selected to cover the complete range of compositions exhibited by each of the sample Groups. This includes representatives of the ochres as well as the umbers. The samples chosen are the same ones as were chosen for REE analysis, since partition data has been obtained for the REEs as well as for the major elements (see Appendix B.6). The partition experiment methodology is described fully, in more detail in Appendix A.3.2.

Following bulk analysis using XRF, the samples are weighed accurately into three representative 1 g ± 0.001 g sub-samples of each sample. The first sub-sample is leached with 10% acetic acid which is added slowly until reaction ceases and stirred for twenty-four hours. The leachate is then filtered through previously weighed filter papers and the residue weighed. The leach solution is then transferred to 50 ml polyethylene bottles. The second sub-sample is leached with an excess of mixed acid-reducing agent consisting of acetic acid and hydroxylamine hydrochloride. This is then stirred for twenty-four hours. The solution is then filtered through (previously weighed) filter papers. The leach solution transferred to 50 ml polyethylene bottles. The third sub-sample is leached with hot 50% HCl and kept hot for twenty-four hours prior to filtration.

Figure 4.1 Element distribution pattern for the Oman metalliferous sediments: calculated by selective leaching experiments

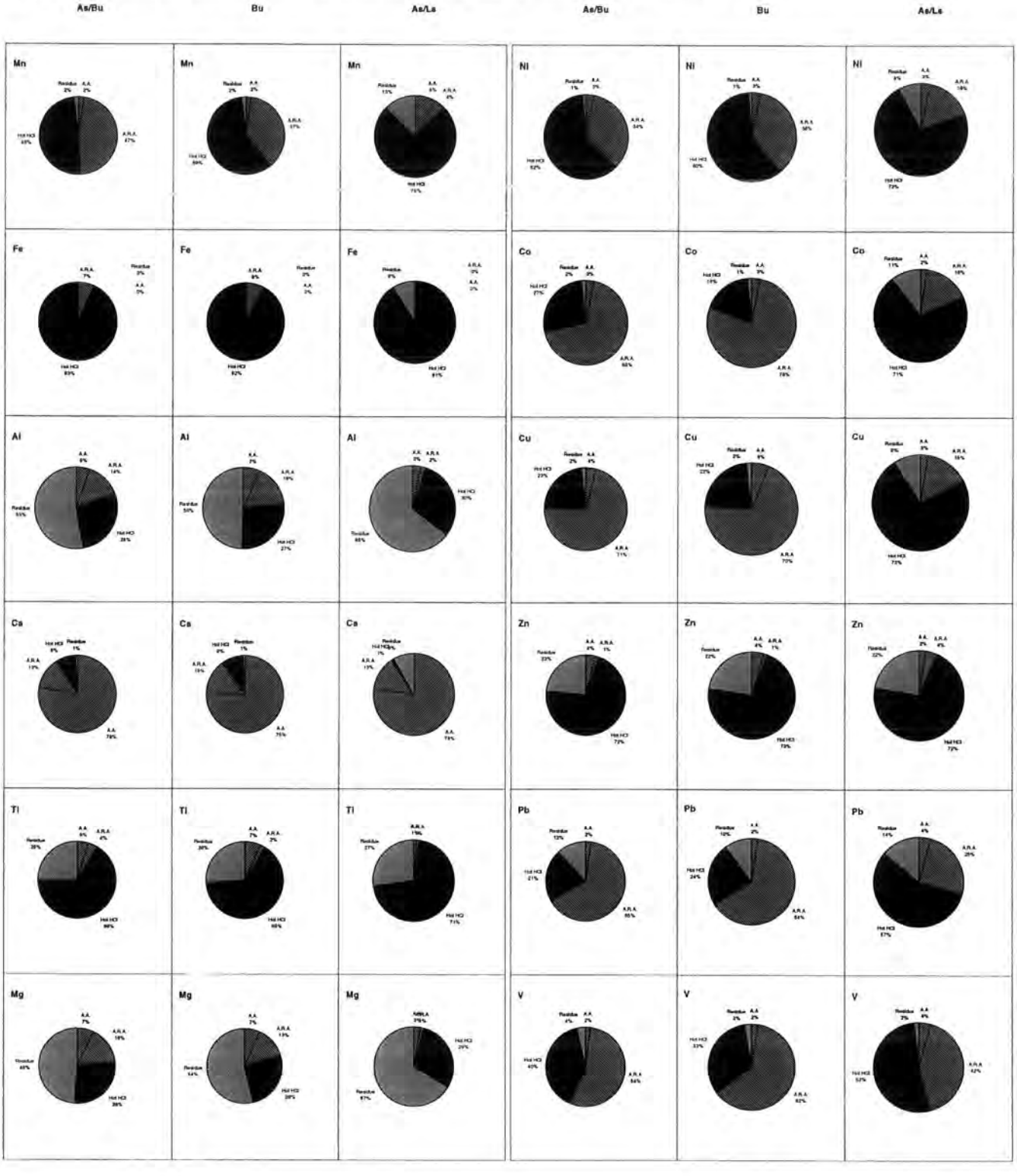

The solution is filtered through previously weighed filter papers and the residue weighed. The leach solution is transferred to 50ml polyethylene bottles.

Leach solutions are analysed for the Fe, Mn, Al, Ca, Ti, Mg, Ni, Co, Cu, Zn, Pb and V using atomic absorption spectrophotometry and for the REEs, La, Ce, Pr,

Nd, Sm, Eu, Gd, Tb, Dy, Ho, Er, Tm and Yb using ICP-MS at Durham University.

4.2.2 Previous studies

Chemical separation techniques have been widely used previously to determine the composition of pelagic sediment phases (e.g., Chester and Hughes, 1967; Aplin, 1983; Lyle *et al.*, 1984; Aplin and Cronan, 1985; Balistrieri and Murray, 1986; Miller and Cronan, 1994).

In previous applications of this methodology, the (hot) HCl-soluble leachate has been known as the "iron oxide" fraction. The HCl attack principally dissolves the major elements Fe, Zn, Cu, Pb, Mg, Al and Ba (Cronan, 1976). Consequently, the HCl soluble leachate contains both the iron phase with associated elements bound in its structure (which are not soluble in hydroxylamine HCl), and the iron stripped from the insoluble clay minerals. The insoluble residuum made up of clay minerals has been termed the "aluminosilicate" fraction and represents lava-derived lattice-held detrital clay minerals stripped of adsorbed trace elements and quartz.

4.3 Partitioning of elements between phases

The results of the atomic absorption and ICP-MS analyses are given in Appendix B.6 and the average concentrations of the sediments and average partition results in Table 4.1. The average values are for each of the samples Groups. The average composition of the sample Groups and the inter-element relationships are described in Chapter 2.

By comparing the compositions of the various chemical fractions of the sediment, it is possible to estimate the partitioning of elements between the constituent phases. The chemical fractions which will be referred to are as follows: (1) the *acetic acid-soluble fraction,* which refers to that part of the sample which is soluble in 10% acetic acid; (2) the *hydroxylamine-HCl-soluble fraction,* which refers to the part of the sediment which is soluble in the acid-reducing agent leach but not in acetic acid; (3) the *HCl-soluble fraction* which refers to that pert of the sample which is dissolved by hot 50% HCl but not by the acid reducing agent; and (4) the *detrital fraction* which is the HCl-insoluble residue.

Table 4.1 (a) Partition experiment results (Major elements as wt%, trace elements as ppm)

	As/Bu					Bu					As/Ls				
	A.A.	A.R.A.	Hot HCl	Residue	**Bulk**	A.A.	A.R.A.	Hot HCl	Residue	**Bulk**	A.A.	A.R.A.	Hot HCl	Residue	**Bulk**
Mn	0.20	4.03	4.22	0.16	**8.61**	0.23	4.56	7.25	0.24	**12.28**	0.06	0.03	0.57	0.10	**0.76**
Fe	0.00	1.44	20.45	0.02	**21.91**	0.00	1.97	24.06	0.00	**26.03**	0.00	0.00	34.21	3.35	**37.56**
Al	0.22	0.57	1.18	2.18	**4.14**	0.23	0.55	0.91	1.66	**3.36**	0.07	0.04	0.66	1.42	**2.19**
Ca	6.14	1.03	0.67	0.06	**7.91**	5.10	0.98	0.62	0.05	**6.74**	4.14	0.71	0.06	0.45	**5.36**
Ti	0.01	0.01	0.09	0.04	**0.14**	0.01	0.00	0.12	0.05	**0.18**	0.00	0.00	0.07	0.03	**0.09**
Mg	0.11	0.26	0.45	0.79	**1.62**	0.11	0.21	0.42	0.85	**1.59**	0.05	0.03	0.53	1.19	**1.79**
Ni	8.71	106.10	190.25	4.26	**309.32**	10.29	124.90	206.92	4.71	**346.82**	6.23	32.58	145.61	16.14	**200.57**
Co	3.11	72.80	28.77	1.63	**106.30**	7.06	171.54	40.52	2.81	**221.93**	2.80	19.16	85.55	12.80	**120.30**
Cu	12.81	227.10	74.66	5.06	**319.63**	26.46	295.12	94.87	7.38	**423.83**	22.38	132.17	650.03	80.87	**885.47**
Zn	6.90	2.75	132.92	43.71	**186.28**	9.48	3.01	152.33	47.65	**212.47**	1.04	1.94	33.51	10.40	**45.84**
Pb	2.02	58.16	19.27	10.80	**90.26**	2.56	74.84	27.54	12.15	**117.08**	0.30	1.78	4.04	0.98	**7.10**
V	3.89	107.31	78.31	7.37	**196.89**	2.91	78.64	41.19	3.19	**125.93**	12.62	129.20	162.31	5.26	**309.40**
La	98.20	319.07	5412.89	449.18	**6279.34**	105.28	425.11	6143.34	491.49	**7165.21**	62.37	127.63	3205.19	257.37	**3652.55**
Ce	42.17	137.98	2334.82	190.22	**2705.20**	53.95	213.39	3084.39	242.88	**3594.61**	28.05	60.35	1471.64	115.00	**1675.05**
Pr	1.73	5.49	91.72	7.52	**106.46**	1.84	6.98	98.43	7.85	**115.09**	1.28	2.63	68.61	5.48	**78.00**
Nd	35.74	112.05	1867.93	153.84	**2169.56**	41.12	152.74	2182.00	173.58	**2549.44**	26.83	53.50	1453.40	114.05	**1647.78**
Sm	5.41	17.08	280.51	23.22	**326.22**	5.52	21.20	296.29	24.30	**347.32**	3.48	6.98	194.46	15.24	**220.16**
Eu	1.07	3.30	55.53	4.59	**64.50**	1.04	4.00	55.61	4.63	**65.28**	0.67	1.35	38.30	3.00	**43.32**
Gd	3.50	10.93	182.03	14.89	**211.35**	3.75	14.48	200.06	16.54	**234.83**	2.17	4.50	125.74	9.70	**142.11**
Tb	0.60	1.84	31.12	2.59	**36.14**	0.60	2.32	32.38	2.70	**38.00**	0.35	0.70	20.30	1.56	**22.91**
Dy	3.45	10.69	178.74	14.88	**207.77**	3.45	14.11	192.39	15.88	**225.83**	2.17	4.30	121.95	9.50	**137.92**
Ho	0.56	1.75	29.06	2.42	**33.79**	0.57	2.37	30.80	2.59	**36.33**	0.36	0.70	20.35	1.59	**23.00**
Er	2.17	6.63	110.65	9.37	**128.83**	2.23	8.92	119.43	10.09	**140.67**	1.32	2.52	74.20	5.79	**83.84**
Tm	0.59	1.78	29.83	2.52	**34.71**	0.63	2.50	33.90	2.79	**39.83**	0.37	0.74	21.17	1.65	**23.93**
Yb	2.24	6.66	113.02	9.70	**131.62**	2.19	9.05	118.94	10.02	**140.20**	1.36	2.71	79.19	6.21	**89.48**
Shale Normalized															
La	3.16	10.26	174.05	14.44	**201.91**	3.39	13.67	197.53	15.80	**230.39**	2.01	4.10	103.06	8.28	**117.45**
Ce	0.63	2.07	35.00	2.85	**40.56**	0.81	3.20	46.24	3.64	**53.89**	0.42	0.90	22.06	1.72	**25.11**
Pr	1.73	5.49	91.72	7.52	**106.46**	1.84	6.98	98.43	7.85	**115.09**	1.28	2.63	68.61	5.48	**78.00**
Nd	1.18	3.69	61.45	5.06	**71.37**	1.35	5.02	71.78	5.71	**83.86**	0.88	1.76	47.81	3.75	**54.20**
Sm	0.90	2.86	46.91	3.88	**54.55**	0.92	3.55	49.55	4.06	**58.08**	0.58	1.17	32.52	2.55	**36.82**
Eu	0.91	2.80	47.06	3.89	**54.66**	0.88	3.39	47.13	3.92	**55.32**	0.57	1.14	32.46	2.54	**36.71**
Gd	0.64	1.99	33.10	2.71	**38.43**	0.68	2.63	36.37	3.01	**42.70**	0.39	0.82	22.86	1.76	**25.84**
Tb	0.70	2.17	36.61	3.04	**42.52**	0.70	2.73	38.09	3.18	**44.70**	0.41	0.83	23.88	1.83	**26.95**
Dy	0.62	1.93	32.26	2.69	**37.50**	0.62	2.55	34.73	2.87	**40.76**	0.39	0.78	22.01	1.71	**24.90**
Ho	0.56	1.75	29.06	2.42	**33.79**	0.57	2.37	30.80	2.59	**36.33**	0.36	0.70	20.35	1.59	**23.00**
Er	0.66	2.02	33.79	2.86	**39.34**	0.68	2.73	36.47	3.08	**42.95**	0.40	0.77	22.66	1.77	**25.60**
Tm	0.59	1.78	29.83	2.52	**34.71**	0.63	2.50	33.90	2.79	**39.83**	0.37	0.74	21.17	1.65	**23.93**
Yb	0.72	2.14	36.31	3.12	**42.28**	0.70	2.91	38.21	3.22	**45.04**	0.44	0.87	25.44	2.00	**28.74**

Table 4.1 (b) Partition experiment results - elemental distribution pattern (%)

	As/Bu				Bu				As/Ls			
	A.A. (%)	A.R.A. (%)	Hot HCl (%)	Residue (%)	A.A. (%)	A.R.A. (%)	Hot HCl (%)	Residue (%)	A.A. (%)	A.R.A. (%)	Hot HCl (%)	Residue (%)
Mn	0.02	0.47	0.49	0.02	0.02	0.37	0.59	0.02	0.08	0.04	0.75	0.13
Fe	0.00	0.07	0.93	0.00	0.00	0.08	0.92	0.00	0.00	0.00	0.91	0.09
Al	0.05	0.14	0.28	0.53	0.07	0.16	0.27	0.50	0.03	0.02	0.30	0.65
Ca	0.78	0.13	0.08	0.01	0.76	0.15	0.09	0.01	0.77	0.13	0.01	0.08
Ti	0.05	0.04	0.66	0.25	0.07	0.02	0.65	0.26	0.01	0.01	0.70	0.27
Mg	0.07	0.16	0.28	0.49	0.07	0.13	0.26	0.53	0.03	0.01	0.29	0.66
Ni	0.03	0.34	0.62	0.01	0.03	0.36	0.60	0.01	0.03	0.16	0.73	0.08
Co	0.03	0.68	0.27	0.02	0.03	0.77	0.18	0.01	0.02	0.16	0.71	0.11
Cu	0.04	0.71	0.23	0.02	0.06	0.70	0.22	0.02	0.03	0.15	0.73	0.09
Zn	0.04	0.71	0.23	0.01	0.04	0.72	0.22	0.01	0.04	0.73	0.23	0.02
Pb	0.02	0.64	0.21	0.12	0.02	0.64	0.24	0.10	0.04	0.25	0.57	0.14
V	0.02	0.55	0.40	0.04	0.02	0.62	0.33	0.03	0.04	0.42	0.52	0.02
La	0.02	0.05	0.86	0.07	0.01	0.06	0.86	0.07	0.02	0.03	0.88	0.07
Ce	0.02	0.05	0.86	0.07	0.02	0.06	0.86	0.07	0.02	0.04	0.88	0.07
Pr	0.02	0.05	0.86	0.07	0.02	0.06	0.86	0.07	0.02	0.03	0.88	0.07
Nd	0.02	0.05	0.86	0.07	0.02	0.06	0.86	0.07	0.02	0.03	0.88	0.07
Sm	0.02	0.05	0.86	0.07	0.02	0.06	0.85	0.07	0.02	0.03	0.88	0.07
Eu	0.02	0.05	0.86	0.07	0.02	0.06	0.85	0.07	0.02	0.03	0.88	0.07
Gd	0.02	0.05	0.86	0.07	0.02	0.06	0.85	0.07	0.02	0.03	0.88	0.07
Tb	0.02	0.05	0.86	0.07	0.02	0.06	0.85	0.07	0.02	0.03	0.89	0.07
Dy	0.02	0.05	0.86	0.07	0.02	0.06	0.85	0.07	0.02	0.03	0.88	0.07
Ho	0.02	0.05	0.86	0.07	0.02	0.07	0.85	0.07	0.02	0.03	0.88	0.07
Er	0.02	0.05	0.86	0.07	0.02	0.06	0.85	0.07	0.02	0.03	0.89	0.07
Tm	0.02	0.05	0.86	0.07	0.02	0.06	0.85	0.07	0.02	0.03	0.88	0.07
Yb	0.02	0.05	0.86	0.07	0.02	0.06	0.85	0.07	0.02	0.03	0.89	0.07
Shale Normalized												
La	0.02	0.05	0.86	0.07	0.01	0.06	0.86	0.07	0.02	0.03	0.88	0.07
Ce	0.02	0.05	0.86	0.07	0.02	0.06	0.86	0.07	0.02	0.04	0.88	0.07
Pr	0.02	0.05	0.86	0.07	0.02	0.06	0.86	0.07	0.02	0.03	0.88	0.07
Nd	0.02	0.05	0.86	0.07	0.02	0.06	0.86	0.07	0.02	0.03	0.88	0.07
Sm	0.02	0.05	0.86	0.07	0.02	0.06	0.85	0.07	0.02	0.03	0.88	0.07
Eu	0.02	0.05	0.86	0.07	0.02	0.06	0.85	0.07	0.02	0.03	0.88	0.07
Gd	0.02	0.05	0.86	0.07	0.02	0.06	0.85	0.07	0.02	0.03	0.88	0.07
Tb	0.02	0.05	0.86	0.07	0.02	0.06	0.85	0.07	0.02	0.03	0.89	0.07
Dy	0.02	0.05	0.86	0.07	0.02	0.06	0.85	0.07	0.02	0.03	0.88	0.07
Ho	0.02	0.05	0.86	0.07	0.02	0.07	0.85	0.07	0.02	0.03	0.88	0.07
Er	0.02	0.05	0.86	0.07	0.02	0.06	0.85	0.07	0.02	0.03	0.89	0.07
Tm	0.02	0.05	0.86	0.07	0.02	0.06	0.85	0.07	0.02	0.03	0.88	0.07
Yb	0.02	0.05	0.86	0.07	0.02	0.06	0.85	0.07	0.02	0.03	0.89	0.07

In the rise-crest sediments, major element data suggests that a number of phases are present, including, ferromanganese oxides, ferrous oxides, carbonate, silica, and detrital aluminosilicates. The variations within each sediment type (Figure 4.1) will be described by element and volcanic stratigraphic position.

4.3.1 Manganese

Manganese shows very similar partitioning between the fractions for all of the sediment types (Figure 4.1). However, sediments of the As/Ls Group have a lower bulk Mn-content and, as a result, there was less Mn to be acid reducible. This suggests that Mn is associated with the major iron phase in As/Ls Group samples, and that in contrast, Mn is divided between the ferromanganoan phase and the iron oxide phase in As/Bu and Bu Group samples.

4.3.2 Iron

The distribution of Fe is uniformly concentrated in the HCl-soluble fraction throughout the sediment types (Figure 4.1). Fe is also dissolved by the acid-reducing leach for As/Bu and Bu Group samples, which is in contrast to the 9% of Fe that is also concentrated in the detrital fraction of As/Ls Group samples. The Fe may be composed of the same phase because of the similarity between the proportions of Fe which are HCl-soluble. This is in contrast to Mn which behaves differently between sediment types.

4.3.3 Aluminium, Magnesium, Titanium and Zinc

The behaviour of Al, Mg, Ti and Zn is similar to Fe in that the distribution pattern is the same for all of the sediment sample Groups (Figure 4.1). Moreover, the distribution patterns of Al, Mg, Ti and Zn are also similar to one another. These elements are the only four which are significantly concentrated in the detrital fraction of those analyzed in this study. This represents the aluminosilicate detritus of local origin. Between 50% and 65% of Al is also concentrated in the HCl-soluble fraction as a result of the presence of minerals which are partially soluble in HCl, e.g., smectite clays. The distribution of Ti and V into the HCl-soluble fraction would support the presence of Fe-smectite, which may result from the reaction of Fe-oxyhydroxides with biogenic silica (e.g. Heath and Dymond, 1977; Moorby and Cronan, 1981). Zn is the only minor element not to be associated significantly with the ferromanganese phase.

4.3.4 Calcium

Because of the dissolution of $CaCO_3$, at least 75% of the Ca is concentrated in the acetic acid-soluble leach. None of the other elements is concentrated above 10% in the acetic acid-soluble phase. The most concentrated is Mg, with Cu, Co, Cu and Zn at approximately the same low level (3% - 4%).

4.3.5 Cobalt, Copper and Lead

The similarity of the distribution patterns of Co, Cu and Pb suggest that these elements are incorporated into the phases in similar ways (Figure 4.1). The partitioning of Co, Cu and Pb shows stratigraphic variation in that all three behave in an Mn-philic manner in As/Bu and Bu Group samples but partition into the Fe-oxide phase in As/Ls Group samples where the Fe content is higher (and Mn is significantly less abundant). Co, Cu and Pb are the most Mn-philic elements followed by V and Ni. The different element distribution patterns are evidence that the trace metals may form alternative associations in the absence or depletion of a major Mn-phase.

4.3.6 Vanadium

The distribution of V is similar to Co, Cu and Pb in that it is Mn-philic in As/Bu and Bu Group samples, but forms associations with Fe oxide in the absence of a major Mn phase in As/Ls Group samples (Figure 4.1). In contrast to Co, Cu and Pb, the distribution pattern of V is also significant in the HCl-soluble phase in As/Bu and Bu Group samples. This supports the view that V is associated with clays as well as the ferromanganoan component. There is only a slight difference in V partitioning between the sediment types as a result of the association of this element with Fe as well as with Mn.

4.3.7 Nickel

Ni is partitioned mainly into the HCl-soluble fraction. Consequently, there is less pronounced variation between As/Bu - Bu Group samples and As/Ls group samples than for the elements which are most Mn-philic. The association of Ni in the major iron phase is compatible with other studies of recent and ancient ferromanganese oxide deposits (Moorby and Cronan, 1981; Cronan *et al.*, 1991). Ni is also partitioned into the acid-reducing fraction confirming that it is associated with both Fe oxide and ferromanganese oxide phases.

4.3.8 REEs

The partitioning of the REEs is plotted for average values by volcanic stratigraphic position on shale-normalized REE plots (Figure 4.2). All of the REEs show significant concentration in the HCl-soluble fraction which reflects the process of adsorption of the REE from solution by Fe oxyhydroxides. A seawater-like pattern is present in each of the phases and no fractionation of the REE is observed. Relatively flat REE patterns are consistently present, which contrasts with recent studies of EPR metalliferous sediments (Barrett and Jarvis, 1988); these authors refer to metalliferous sediments which are consistently enriched in HREE relative to LREE. The strong correlation between ΣREE, P and Fe (Chapter 2) suggests that the REE which was originally associated with Fe oxyhydroxides may have been transferred to apatite during diagenesis. The partition data confirms that the REE are not associated with the manganiferous phases, which is consistent with previous studies of metalliferous sediments (e.g, Jarvis, 1995; Barrett and Jarvis, 1988).

4.4 The linear programming technique (Dymond, 1981)

This study develops a model by which measured bulk sediment composition is matched to calculated bulk sediment composition resulting from the summation of constituent end-member compositions by trial-and-error procedures. The computer method uses linear programming to calculate the blending of elements to match the elemental composition of each particular rock sample. A system of 8 equations and 5 unknowns selects one solution from an infinite number. Previous studies have used the process of solving a series of linear equations for the purpose of defining pure end-member compositions and to determine what mix of these sources best describes bulk sediment composition, (Bryan *et al.*, 1969; Dymond, 1981; Dymond and Heath, 1977, 1981). The procedure used in this study is modified from the Dymond (1981) study. The method used is outlined below.

4.4.1 Methodology

The Dymond (1981) study uses a normative calculation to account for the compositional variability of the Nazca plate surface sediments. The procedure assumes that mixing occurs between components from different sources; the results quantify the proportional mix of the user-defined components. Furthermore, the simple component framework has been restricted to only five end-members (Dymond, 1981). The end-members in the original study are as

Figure 4.2 Shale normalized REE pattern in reponse to selective chemical leaching experiments

(a) As/Bu Group Samples

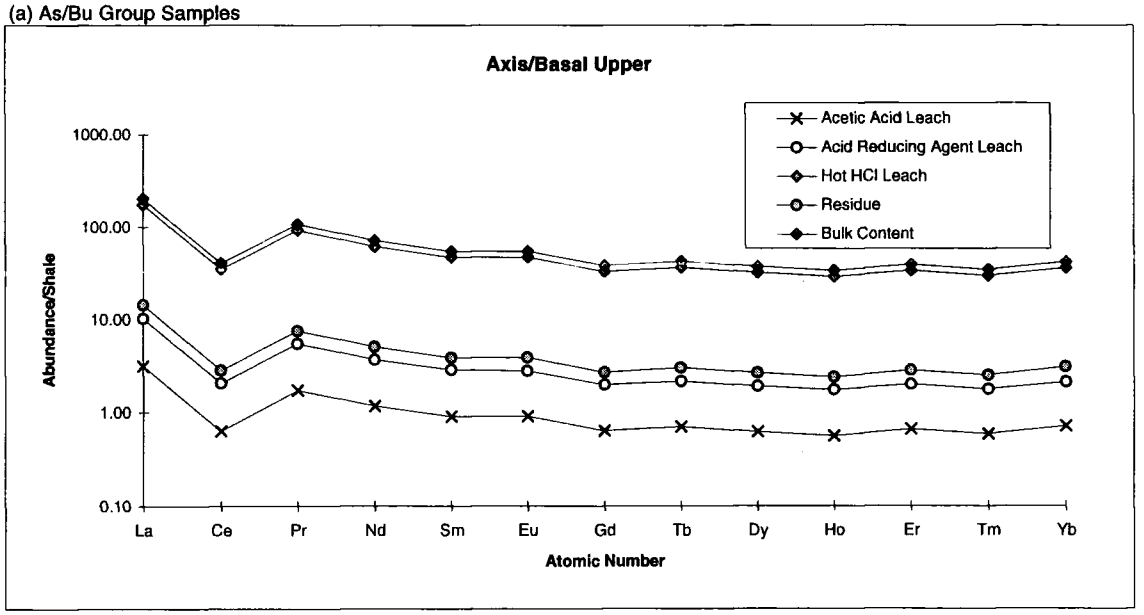

(b) Bu Group samples

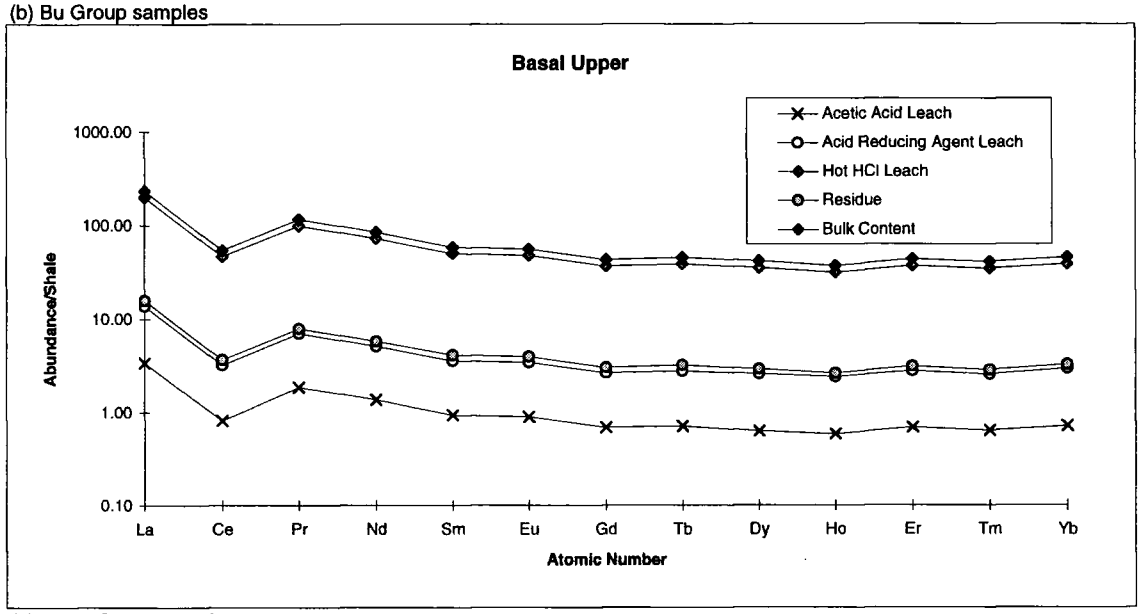

(c) As/Ls Group samples

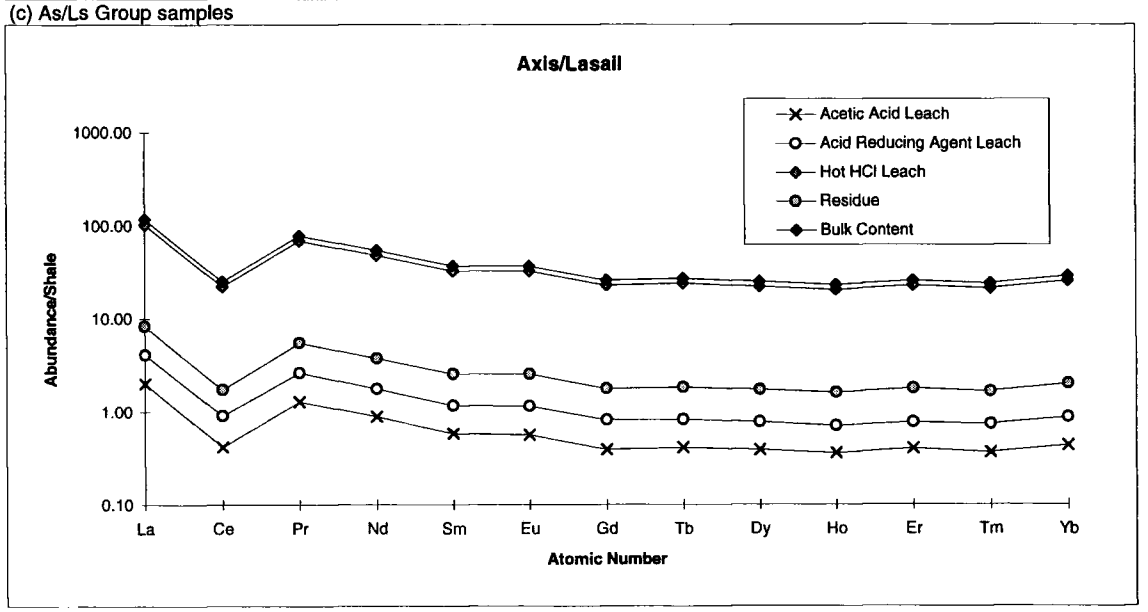

follows: (1) detrital weathering products, primarily from continental erosion; (2) hydrothermal precipitates from solutions produced by interaction of sea-water and the recently emplaced oceanic crust; (3) biogenic remains, perhaps planktonic organisms fallen to the sea floor; (4) hydrogenous ferromanganese precipitates which are accumulating in the ocean at very slow rates; (5) Ba-rich dissolution residue remaining from the dissolution of planktonic organisms.

Linear programming solves a system of equations using a mathematical procedure termed the *simplex algorithm* which selects one solution from an infinite number to best fit some a specified objective function. The two key features of the method are that: (i) all the unknowns take positive or zero values, and (ii) the objective function changes monotonically with each cycle of the algorithm until it reaches its minimum value in a finite number of steps, (Wright and Doherty, 1970). Two advantages of using this technique are that: (1) linear programming allows restrictions to be placed on the solutions; this is important because negative solutions have no physical meaning, i.e. it is meaningless to add a negative quantity of an element to a mixture of elements making up the bulk composition; and (2) linear programming allows specification of a minimised value for the sum of the squares of the residuals as the objective function.

The equations deal with known elemental ratios of 8 elements from five environments, and use the known bulk analysis of the 8 elements in the particular sample to calculate five unknowns. The five unknowns are the variables relating to the detrital Al, (D_{Al}), hydrothermal Fe, (H_{Fe}), biogenic Si, (B_{Si}), authigenic Ni, (A_{Ni}), and dissolution residue Ba, (R_{Ba}). Using this terminology, eight equations are defined below in an over-determined system of linear equations for which there are five unknowns:

Eqn 4.1 $Al_T = (Al/Al)_D D_{Al} + (Al/Fe)_H H_{Fe} + (Al/Si)_B B_{Si} + (Al/Ni)_A A_{Ni} + (Al/Ba)_R R_{Ba}$

Eqn 4.2 $Si_T = (Si/Al)_D D_{Al} + (Si/Fe)_H H_{Fe} + (Si/Si)_B B_{Si} + (Si/Ni)_A A_{Ni} + (Si/Ba)_R R_{Ba}$

Eqn 4.3 $Mn_T = (Mn/Al)_D D_{Al} + (Mn/Fe)_H H_{Fe} + (Mn/Si)_B B_{Si} + (Mn/Ni)_A A_{Ni} + (Mn/Ba)_R R_{Ba}$

Eqn 4.4 $Fe_T = (Fe/Al)_D D_{Al} + (Fe/Fe)_H H_{Fe} + (Fe/Si)_B B_{Si} + (Fe/Ni)_A A_{Ni} + (Fe/Ba)_R R_B$

Eqn 4.5 $Ni_T = (Ni/Al)_D D_{Al} + (Ni/Fe)_H H_{Fe} + (Ni/Si)_B B_{Si} + (Ni/Ni)_A A_{Ni} + (Ni/Ba)_R R_{Ba}$

Eqn 4.6 $Cu_T = (Cu/Al)_D D_{Al} + (Cu/Fe)_H H_{Fe} + (Cu/Si)_B B_{Si} + (Cu/Ni)_A A_{Ni} + (Cu/Ba)_R R_{Ba}$

Eqn 4.7 $Zn_T = (Zn/Al)_D D_{Al} + (Zn/Fe)_H H_{Fe} + (Zn/Si)_B B_{Si} + (Zn/Ni)_A A_{Ni} + (Zn/Ba)_R R_{Ba}$

Eqn 4.8 $Ba_T = (Ba/Al)_D D_{Al} + (Ba/Fe)_H H_{Fe} + (Ba/Si)_B B_{Si} + (Ba/Ni)_A A_{Ni} + (Ba/Ba)_R R_{Ba}$

In the above equations, the known values are the 40 elemental ratio coefficients for the five components (Table 4.2), and the values Al_T, Si_T, Mn_T, Fe_T, Ni_T, Cu_T,

Zn_T, and Ba_T are the measured bulk content of the element in each particular sample. For any element, the product of the variable and its elemental coefficient gives the concentration of that element from each of the sources (Dymond, 1981). For example, $(Fe/Al)_D$ x D_{Al} = concentration of detrital Fe in the sample.

In each of the eight equations, the left side is the measured concentration and the sum of the right side is the calculated model concentration. When the model has a perfect fit, the left side of the equation equals the right side of the equation. Linear programming will reach the best fit values for the five variables D_{Al}, H_{Fe}, Si_B, A_{Ni}, and R_{Ba} when the sum of the squares of the residuals is at a minimum. To carry out this operation, the following equations are used:

Eqn 4.9 $$E_T = (E/Al)_D D_{Al} + (E/Fe)_H H_{Fe} + (E/Si)_B B_{Si} + (E/Ni)_A A_{Ni} + (E/Ba)_R R_{Ba}$$

Eqn 4.10 $$E_T - ((E/Al)_D D_{Al} + (E/Fe)_H H_{Fe} + (E/Si)_B B_{Si} + (E/Ni)_A A_{Ni} + (E/Ba)_R R_{Ba}) = B^i$$

where equation 4.9 is the general form for the bulk content of any element in a given sample, and where B^i in equation 4.10 equals the value of the residual, i.e., the difference between the calculated and the measured bulk content. Where the value of B^i is a minimum for each of the 8 residuals, the algorithm has reached the best fit for the specified objective function. Since there are 8 equations:

Eqn 4.11 $$\Sigma(B^2)\ i = 1 \text{ to } 8 = \text{minimum}$$

The elemental ratio coefficients of the five components used in the normative analysis (Table 4.2) are attempts to define the elemental ratios characteristic of the five end-member sources used in the normative analysis (Dymond, 1981).

Table 4.2: Elemental ratio coefficients (Dymond, 1981)

Element	$(E/Al)_D$	$(E/Fe)_H$	$(E/Si)_R$	$(E/Ni)_A$	$(E/Ba)_R$
Al	1.0000	0.0060	0.002000	1.5	0.5000
Si	3.0000	0.1300	1.000000	4.5	0.0000
Mn	0.0160	0.2900	0.000023	30.0	0.0070
Fe	0.7000	1.0000	0.001000	15.0	0.3500
Ni	0.0015	0.0009	0.000040	1.0	0.0065
Cu	0.0012	0.0042	0.000050	0.5	0.0160
Zn	0.0014	0.0019	0.000080	0.1	0.0040
Ba	0.0120	0.0050	0.002000	0.2	1.0000

Methods were investigated to obtain an optimum solution that is influenced equally by the trace elements as well as the major elements. Problems arose in previous studies from using unmodified whole rock XRF data because of the difference by three orders of magnitude between the parts per million trace element from major element content. Consequently, the trace elements may not affect the solution unless the data is transformed or the calculations are weighted. In the original methodology, the trace element data was multiplied by a factor to obtain an optimum solution for the trace element equations.

The element concentrations (Al, Si, Fe, Mn, Ni, Cu, Zn and Ba) for each of the five sources equals the product of the appropriate coefficients and the unknown. For example, the contribution of copper from the hydrothermal sources equals $(Cu/Fe)_H$ multiplied by H_{Fe}. Furthermore, by assuming an absolute concentration of a representative element for each source (Table 4.3) the weight fraction of each of those sources may be calculated.

Table 4.3 element concentration in pure end-member source, (Dymond, 1981)

Element	End-member	Concentration in pure end-member
Al	Detrital	84,000 ppm
Fe	Hydrothermal	348,000 ppm
Si	Biogenic	360,000 ppm
Ni	Hydrogenous	10,000 ppm
Ba	Dissolution Residue	270,000 ppm

4.4.2 Modified Methodology

In this Section, the output is assessed which results from applying the Dymond (1981) methodology in an unmodified form to the data set. The calculations used to obtain the results are based on concentrations given in the literature from which the original (Dymond, 1981) elemental ratio coefficients are calculated. By repeating the original methodology, trace element scaling factors between 1 and 40 have also been investigated.

By direct application of the original model to ancient Oman ridge-crest samples, the Dymond (1981) model has been used to produce a set of results which are summarised below (Table 4.4):

Table 4.4 Oman Results using the Dymond (1981) methodology

Number of samples: 146	Total Average	Average As/Bu	Average As/Ls	Average Bu
Detrital Component (%)	44.0	29.5	55.5	24.6
Hydrothermal Component (%)	37.6	35.4	38.8	36.9
Biogenic Component (%)	11.2	20.0	3.6	24.5
Authigenic Component (%)	3.9	9.1	0.5	8.5
Dissolution Residue (%)	0.0	0.0	0.0	0.0

The unrefined linear programming calculation has resulted in geologically unrealistic sediment sources. The results suggest that the detrital component is equal or greater than the hydrothermal component contribution. This is unrealistic for two reasons: (1) the non-hydrothermal minerals comprise a relatively small proportion of the sediment compared with hydrothermal Fe-oxide in XRD analysis; and (2) the aluminosilicate elements are quantitatively relatively less abundant than hydrothermal Fe and Mn (Table 3.5). The dissolution residue does not account for any of the variation in the data set. This suggests that the Oman metalliferous sediments record preservation of biological debris rather than dissolution of biological remains. This would be expected in areas of rapid burial of biogenic debris, or rapid lithification due to relatively fast emplacment of lavas above the sediments. In the Nazca surface sediments, high biogenic sedimentation near the Equator preserves biogenic debris from dissolution (Dymond 1981). Dissolution of biogenic debris is also inhibited at the rise-crest because of relatively enhanced hydrothermal input.

By plotting the calculated bulk trace element content (E_T) versus measured trace element content it is possible to determine the scaling factor best suited to optimisation of the model. Comparably with previous work (Dymond, 1981), factors between 1 and 20 produced the closest fit of the model to measured concentrations. For Ni, Cu and Zn the best fit between the measured and calculated concentrations could be obtained without multiplied of the data. Minor-element weighting used as described above allows the elements Cu, Ni, Zn and Ba to influence the outcome of the calculation but at the same time without allowing these elements to outweigh the major element contribution.

This study found that the problems could be easily overcome by using the log of the data.

4.4.3 Modified end-member components

By experimentation with different hydrothermal end-members and repeated runs using different elemental ratios an optimal combination was determined. The criteria for selecting an optimal result were as follows:

(1) That the fit between calculated E_T and measured E_T for each element be statistically significant to the 5% significance level in a hypothesis test for the population correlation coefficient. No modelled results were considered for which the value of r was not significant to 5% on the basis of Pearson's Population Correlation Coefficient.

(2) That all of the five end-members appear in the results to the extent that none is excluded in a geologically unrealistic manner.

(3) That there is correlation between the results of the linear programming model and those of the factor analysis model, or that any discrepancy might be explained satisfactorily.

On the basis of numerous runs using different average elemental ratios for the hydrothermal end-member components, the majority were rejected on the basis of the first and second criteria above. From both the unmodified runs and the subsequent modified re-runs it is evident that the hydrothermal end-member originally used by Dymond (1981) was consistently included in the results and accurately portrays the iron-rich, manganese-poor hydrothermal component principally found in the As/Ls Group.

On the criteria set out above, the eventual best-fit scenario was achieved using average data for hydrothermal Mn-crusts documented from the Trans-Atlantic Geotraverse (TAG) hydrothermal area (Scott *et al* 1974; Toth 1980). The resulting model using the elemental ratios below (Table 4.5) fulfils best the necessary pre-conditions for accepting the model.

Without recourse to changing the basic structure of the model, the above elemental ratios satisfy all of the criteria listed above. Figure 4.3 is a comparison

between the measured XRF values of the 8 elements and the 8 values computed as the sum of the contributions of the five sources using the Dymond (1981) element ratio coefficients.

Table 4.5 Elemental ratio coefficients of the five components used in the successful normative analysis

	$(E/Al)_D$	$(E/Fe)_H$	$(E/Fe)_{H2}$	$(E/Si)_B$	$(E/Ni)_A$
Al	1.0000	0.0060	0.16200	0.002000	1.5
Si	3.0000	0.1300	1.00300	1.000000	4.5
Mn	0.0160	0.2900	0.60200	0.000023	30.0
Fe	0.7000	1.0000	1.00000	0.001000	15.0
Ni	0.0015	0.0009	0.00170	0.000040	1.0
Cu	0.0012	0.0042	0.00220	0.000050	0.5
Zn	0.0014	0.0019	0.00130	0.000080	0.1
Ba	0.0120	0.0050	0.00050	0.002000	0.2

From the evidence of Chapter 2 and Chapter 3, the Oman sediment formed from at least two hydrothermal sources: ferrous, ferromanganoan, and probably siliceous. The evidence suggests that one source is Fe-rich, Mn-poor (Chapter 2). This source is represented by the original hydrothermal component proposed by Dymond, (1981). The second hydrothermal source is Mn-rich and Fe-rich, and is represented by average hydrothermal ferromanganoan data (Toth, 1980). Because the Si-rich component is of indeterminate origin, it is represented by $(E/Si)_B$ ratios. The detrital ratios used are average values taken from Oman lavas (Pearce and Alabaster, 1982), and these differ little from the values used by Dymond (1981). The ferromanganoan source has been substituted for the dissolution residue source which does not contribute to the sediment.

For comparability, this study retains the original methodology based on calculation of end-members using compositional data which has been corrected to a carbonate-free basis. Having then computed the five end-member components, these were corrected for carbonate content which results in a six-fold source model.

4.5 Assessment of modified methodology

When summarized graphically in the scatter diagrams, the model accounts nearly perfectly for the major elements Fe, Mn, Si and Al and at the same time produces good linear positive trends for the four minor elements Ba, Cu, Ni and Zn (Figure 4.3). The degree of association of measured E_T versus calculated E_T is calculated

using the product moment correlation coefficient giving the following values for *r* all of which are significant at the 5% level (Table 4.6):

Table 4.6 *r* - values

Element	*r*
Al	0.937
Si	0.984
Fe	0.999
Mn	0.999
Cu	0.843
Ni	0.660
Zn	0.899
Ba	0.690

The higher the *r*-value, the more closely the model fits the measured data. The hydrothermal sources are statistically very well accounted for using the model, despite the fact that the scatter diagrams (Figure 4.3) show that the inaccuracies occur at the lower Mn concentrations (As/Ls Group) and in a limited number of samples on the Al and Si plots (As/Ls Group). Problems with accounting perfectly for Mn in the As/Ls Group indicates that there is some inaccuracy in modelling the ferromanganese source component.

Shortcomings in evaluating the hydrothermal components are all likely to result from problems in quantifying the role of Si. For example, in terms of calculated Si_{Total}, the As/Ls Group is poorly modelled, probably as a result of the major role of Si, in the biogenic, hydrothermal and detrital sources. This in turn accounts for the small number of irregularities in Al_T and the somewhat lower *r*-value of 0.937. Alternatively the model may be affected by variability in detrital elemental ratios for a selected number of samples from the As/Ls Group though this seems less likely given the constancy of Al/Ti ratio in the data (see Chapter 2).

4.5.1 Distribution Pattern of the elements

The element distribution pattern calculated by the model is summarised by Group to show the average contribution to each element from the five sources used in the model (Table 4.7, data from: Appendix B). The associations of elements which are used to define the components are assessed, below, on the basis of the results of the chemical leaching experiments. For the purpose of defining the

role of volcanic stratigraphic position, the data has been calculated for each sample Group.

4.5.1.1 Aluminium

Aluminium distribution patterns are typically thought to be intimately related to the lattice-held (detrital) source. The leaching study confirms that as much as 72% of the total concentration of this element is in the detrital fraction (Table 4.1). Comparable leaching studies report >70% of Al in the detrital component (e.g., Chester and Messiha-Hanna, 1970). The XRD analysis in this study has identified the presence of clinopyroxene and plagioclase. The significant positive correlation between Al, Mg, Ti and Si (Chapter 2) is therefore more likely to represent lithogenous detrital material than authigenic smectite clay. Irrespective of this, aluminium is predominantly associated with this fraction.

The linear programming data supports a detrital Al source in that it predicts that between 65.38% and 95.73% of the total Al content is associated with the detrital fraction. On average 78.47 ± 11% of the Al in the samples is detrital. Within the study area there is little variation between Groups of samples. This is comparable with the leaching study, in which 41% to 73% of the Al occurs in the detrital residue.

The comparison of linear programming with partitioning data, by sample, for Al (Table 4.8) illustrates the point that even a conservative element such as Al is partitioned between a number of phases, but that it may be more abundant in one phase than the others. Al is principally detrital. A hydrothermal-Al source is suggested despite the comparative data indicating that partition analysis and linear programming use different criteria to define the hydrothermal component. The main difference in the results is that some detrital material is partially soluble in As/Ls samples which is still identified as detrital using linear programming.

Figure 4.3 Measured versus calculated bulk element content (Using element ratio coefficients after: Dymond, 1981)

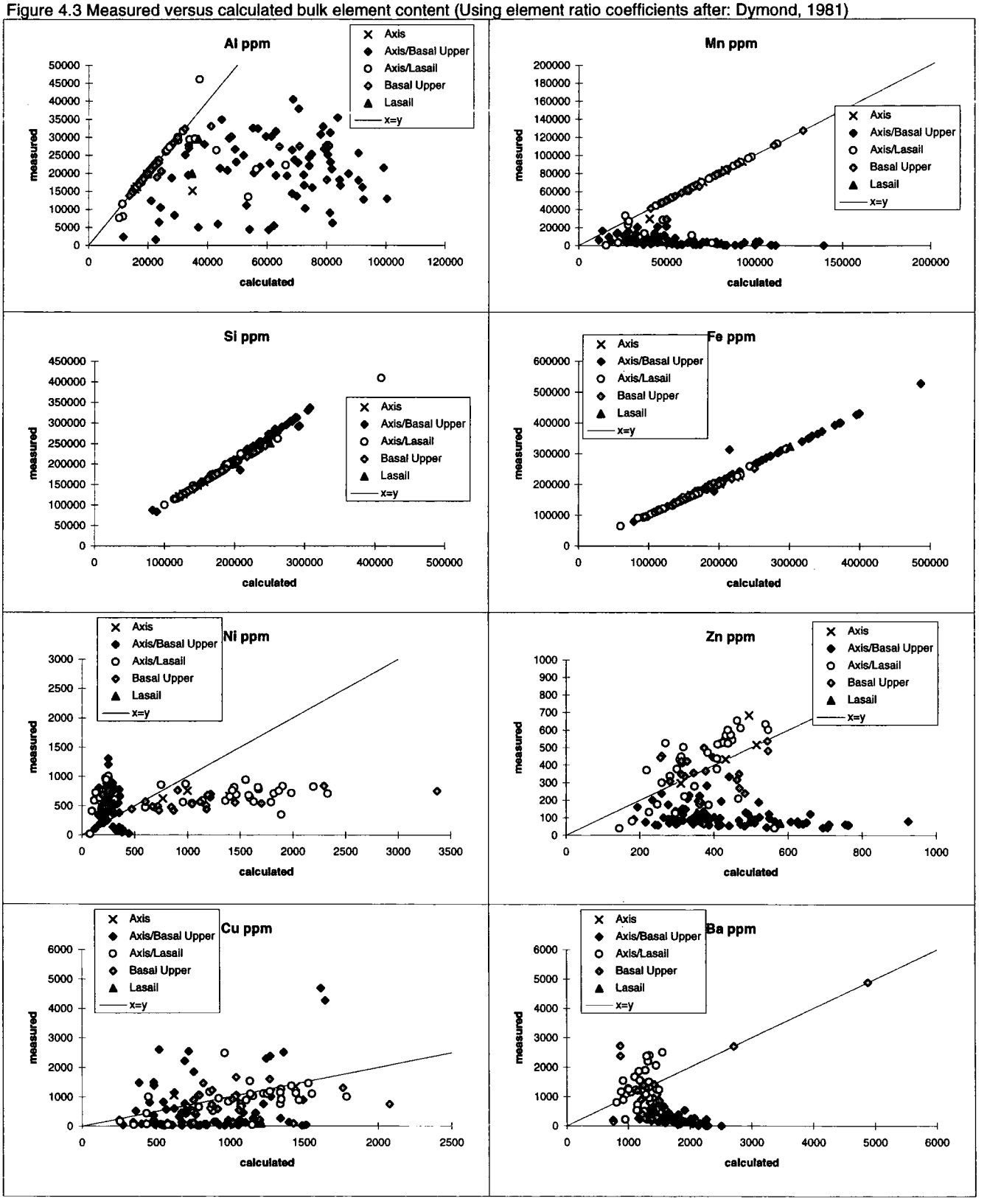

Table 4.4 Authigenic end-member content versus non authigenic components
(End-members calculated using Dymond (1981) element ratio coefficients

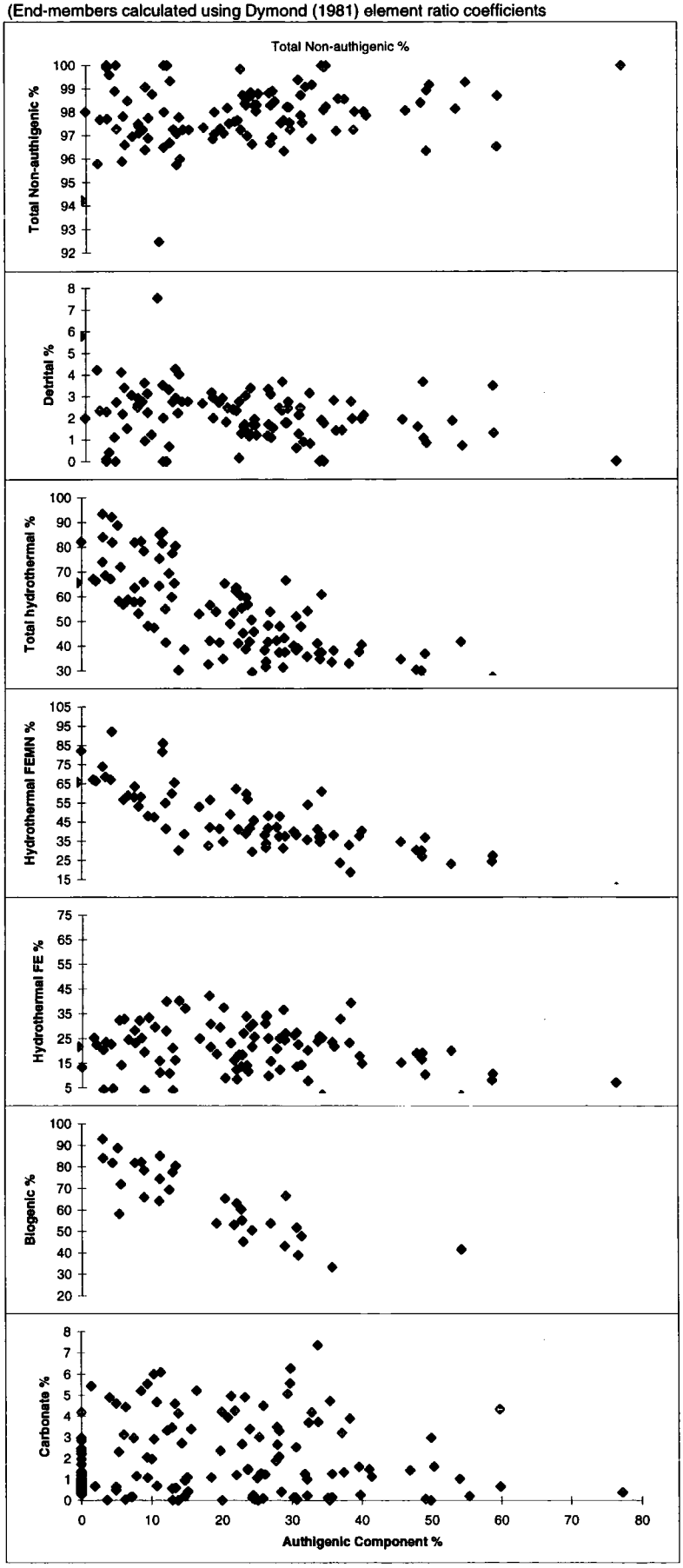

Table 4.7 Distribution of the elements calculated by linear programming

	Detrital	Hydrothermal Fe-rich	Hydrothermal FeMn-rich	Biogenic	Authigenic
Aluminium					
Average As	65.3	0.0	14.1	0.6	19.9
Average As/Bu	74.3	0.0	12.0	0.5	12.9
Average As/Ls	76.8	14.9	5.7	0.6	2.3
Average Bu	80.0	7.2	0.0	0.4	12.2
Average Ls	95.7	2.8	1.2	0.0	0.2
Silica					
Average As	14.0	0.0	37.8	40.2	7.8
Average As/Bu	26.7	0.3	29.9	37.8	5.1
Average As/Ls	25.2	39.6	4.0	30.4	0.5
Average Bu	31.3	34.2	0.0	29.6	4.7
Average Ls	31.7	26.1	1.9	40.0	0.1
Iron					
Average As	0.1	98.3	1.5	0.0	0.0
Average As/Bu	0.4	1.8	97.7	0.0	0.0
Average As/Ls	3.2	92.2	2.0	0.0	2.4
Average Bu	0.5	99.2	0.0	0.0	0.2
Average Ls	24.9	67.9	2.7	0.0	14.
Manganese					
Average As	2.6	75.7	0.0	0.0	21.5
Average As/Bu	6.4	0.6	75.1	0.0	17.7
Average As/Ls	5.9	82.0	10.0	0.0	1.9
Average Bu	7.8	75.0	0.0	0.0	17.0
Average Ls	22.2	70.7	6.3	0.0	0.6
Nickel					
Average As	0.3	45.0	4.2	0.0	45.3
Average As/Bu	1.8	0.0	50.2	0.3	47.5
Average As/Ls	0.1	38.4	16.6	1.3	43.4
Average Bu	2.6	41.5	0.0	0.1	55.7
Average Ls	4.8	46.6	15.0	0.0	33.4
Copper					
Average As	0.0	89.6	0.2	0.0	10.0
Average As/Bu	0.4	16.9	71.4	0.1	11.1
Average As/Ls	1.6	77.8	9.0	0.2	11.2
Average Bu	0.3	92.4	0.0	0.0	7.2
Average Ls	5.0	84.0	0.0	0.0	10.9
Zinc					
Average As	0.0	9025	4.7	1.6	3.3
Average As/Bu	0.0	5.2	83.4	2.1	9.0
Average As/Ls	2.7	40.4	36.4	6.9	13.4
Average Bu	4.8	82.0	0.0	1.8	11.3
Average Ls	9.5	77.1	0.4	0.0	12.9
Barium					
Average As	11.5	71.5	0.6	16.4	0.0
Average As/Bu	25.7	0.5	55.4	18.2	0.0
Average As/Ls	33.3	33.5	0.1	32.2	0.6
Average Bu	32.7	50.0	0.0	16.9	0.2
Average Ls	36.7	60.3	0.0	0.0	2.9

There is substantial evidence from recent metalliferous sediment studies that Fe-oxyhydroxides react with biogenic opal to produce Fe-smectite (e.g., Heath and Dymond, 1977; Cole, 1985; Jarvis, 1985; Barrett and Jarvis, 1988). A good correlation exists between linear programming data and partition analysis data for As/Bu and Bu samples.

A second source of Al is hydrothermal (7.27% and 20.12% of the total for the element is found), and this may be confirmed by the partition data which records Al in the ferromanganese oxide phase. In the previous section the evidence suggested that the As/Ls Group formed in the more active hydrothermal vent region, and at this point the evidence suggests that the As/Ls Group receives proportionally the greatest contribution of Al from a hydrothermal source. This supports the view that hydrothermal Al has diluted the detrital Al in the area in which hydrothermal input is greatest. This finding is compatible with the Dymond (1981) data for the "Rise Crest" samples in which on average 16% of total Al was hydrothermal. The modelled data is in keeping with studies of active hydrothermal systems in which enhanced Al levels are observed around hydrothermal vents (Dymond *et al* 1977; Haymon *et al* 1979).

4.5.1.2 Silica

The distribution of Si in the ancient deposits from Oman is governed by hydrothermal, detrital and biogenic sources (Table 4.7). The biogenic and the hydrothermal silica sources are approximately equivalent to one another, both being more significant than the detrital source of Si. No partition data are available for Si.

Si in the form of biogenic opal forms between 29.7% and 40.26% of the average total Si. Diatoms and radiolarians are the principal opal-secreting organisms, and also fossiliferous silica from hydrothermal vent worms have been identified in sediments from the Semail ophiolite (Haymon *et al.,* 1984).

As well as the preferential preservation of Si of biological origin, the samples in this study resemble those of the "Rise Crest" (Dymond, 1981) in that the hydrothermal source is a significant contributor of Si (28.08% to 43.7%). According to studies of the Red Sea system the general order in which metals are precipitated from hydrothermal solutions is as follows (Cronan, 1980): sulphides → iron silicates → iron oxides → manganese oxides. The association of silica

with the hydrothermal fraction is therefore to be expected in ridge-crest samples. As with the distribution of Al, the distribution of Si is relatively more important in the As/Ls Group hydrothermal source than to any of the other hydrothermal sources. The evidence suggests that, where the hydrothermal source is either closer or more vigorous, the Si from detrital and biogenic sources is swamped by hydrothermal Si. Evidence was presented, in the previous section, for the possible recrystallization of Fe oxyhydroxides as a result reaction with biogenic opal. The "hydrothermal" association of Si with Fe in the sediments may in fact be a secondary diagenetic reaction which is indistinguishable using linear programming alone. The evidence shows that Si in Fe phases may be partly derived from hydrothermal solutions and partly from the dissolution of biogenic siliceous component of calcareous ooze (Barrett, 1992):

$$4Fe_2^{+} + 8SiO_2 + 6H_2O + O_2 \rightarrow Fe_4Si_8O_{20}(OH)_4 + 8H^{+}$$

(e.g., formation of nontronite in oxidizing conditions from Si and Fe)

The detrital aluminosilicate source has already been well documented in this study from XRD analysis, which has identified detrital grains within the sediment and from Factor Analysis which has unequivocally identified aluminium-titanium-magnesium silicates. The detrital silica source has been well documented since the classic paper defining sedimentary building block components which identified the range of major and minor sources arising from land erosion, from submarine volcanoes and from underwater weathering (Goldberg, 1954).

4.5.1.3 Iron

The distribution of iron in the sediments is principally determined by the hydrothermal source which accounts for up to 99.86% of the total iron contribution (Table 4.7). The authigenic and detrital sources also contribute small proportions of iron to the bulk content: hydrogenous/lithogenous Fe input is predicted by the model in other studies for basin and for normal plate surface environments (Dymond, 1981; Leinen and Pisias, 1984). As the iron content in samples from non hydrothermal sources is relatively low (Table 4.8), their contribution is effectively swamped in the active ridge-crest environment where the Fe-rich hydrothermal source is predominant:

Table 4.8 (data: Chester and Aston, 1976)

	Near-shore muds	Deep-sea carbonate	Atlantic deep-sea clay	Pacific deep-sea clay	Active ridge sediment
Fe_2O_3	6.99 wt.%	0.90 wt.%	8.20 wt.%	6.50 wt.%	18.00 wt.%

The iron distribution pattern is compatible with the two previous studies in which, at the ridge crest environment, 91% of the total iron input to the sediment was attributed to the hydrothermal component (Dymond, 1981; Leinen and Pisias, 1984). The partition analysis confirms the predominance of Fe in the hydrothermal phases, but suggests that there is also a minor detrital Fe source for As/Ls Group samples (Table 4.8). The detrital Fe source is uniformly low in linear programming data. The only complication in this study is that, in using two hydrothermal components, the iron contribution is dominated by the iron-rich source for all the Groups except the As/Bu Group. This pattern replicates the dominance of the FeMn-rich source in the inter-seamount area and the predominance of the Fe-rich source elsewhere. The presence of a ferromanganese component is reflected in the partition data for the As/Bu sediments. The close similarity of partition data and linear programming data shows that particulate plume processes are dominated by Fe precipitation to the extent that all other possible sources are effectively masked. This study confirms that Fe may be used as tracer for simple mixing and dispersion from the plume and, consequently, that normalization to iron provides information relating to additional phases other than dispersion and dilution.

4.7.1.4 Manganese

In a similar manner to the distribution pattern of iron, that of manganese is determined by which of the hydrothermal sources predominated during formation of the sediment. Unlike the distribution pattern of iron, an important source of Mn is hydrogenous. The detrital source is also significant in all of the locations.

The hydrothermal source contributes 79.15% of the Mn present compared with 87% in the 1981 study of Dymond. In the As/Bu Group, which is notably higher in Mn than the other Groups, 75.19% of the Mn is found in the FeMn-rich Source

Figure 4.5 (a) Measured versus calculated bulk element content. Linear programming used elemental ratio coefficients Modified from Dymond (1981) - see text for modification

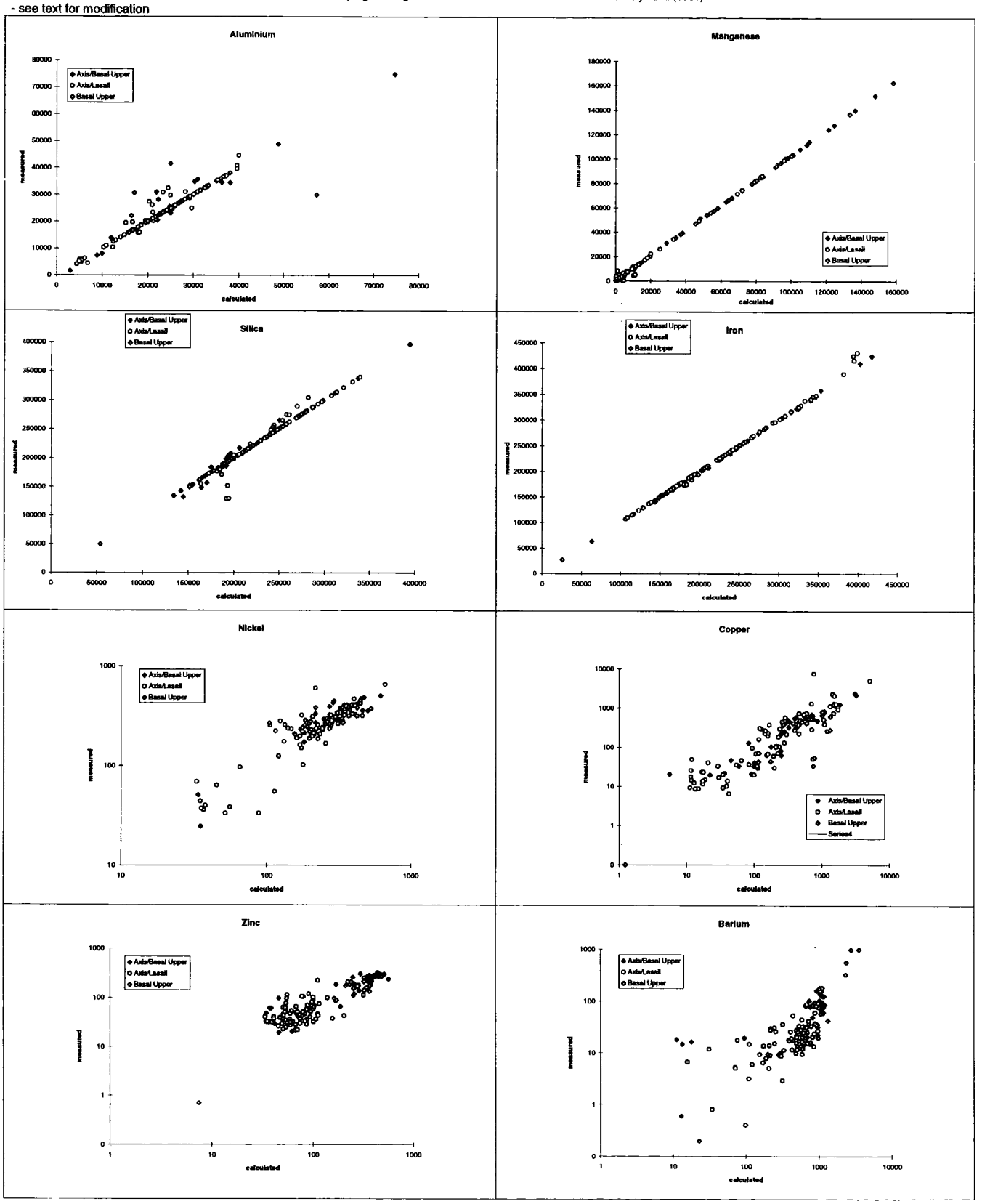

Figure 4.5 (b) Error versus elemental content. Linear programming used elemental ratio coefficients Modified from Dymond (1981) - see text for modification

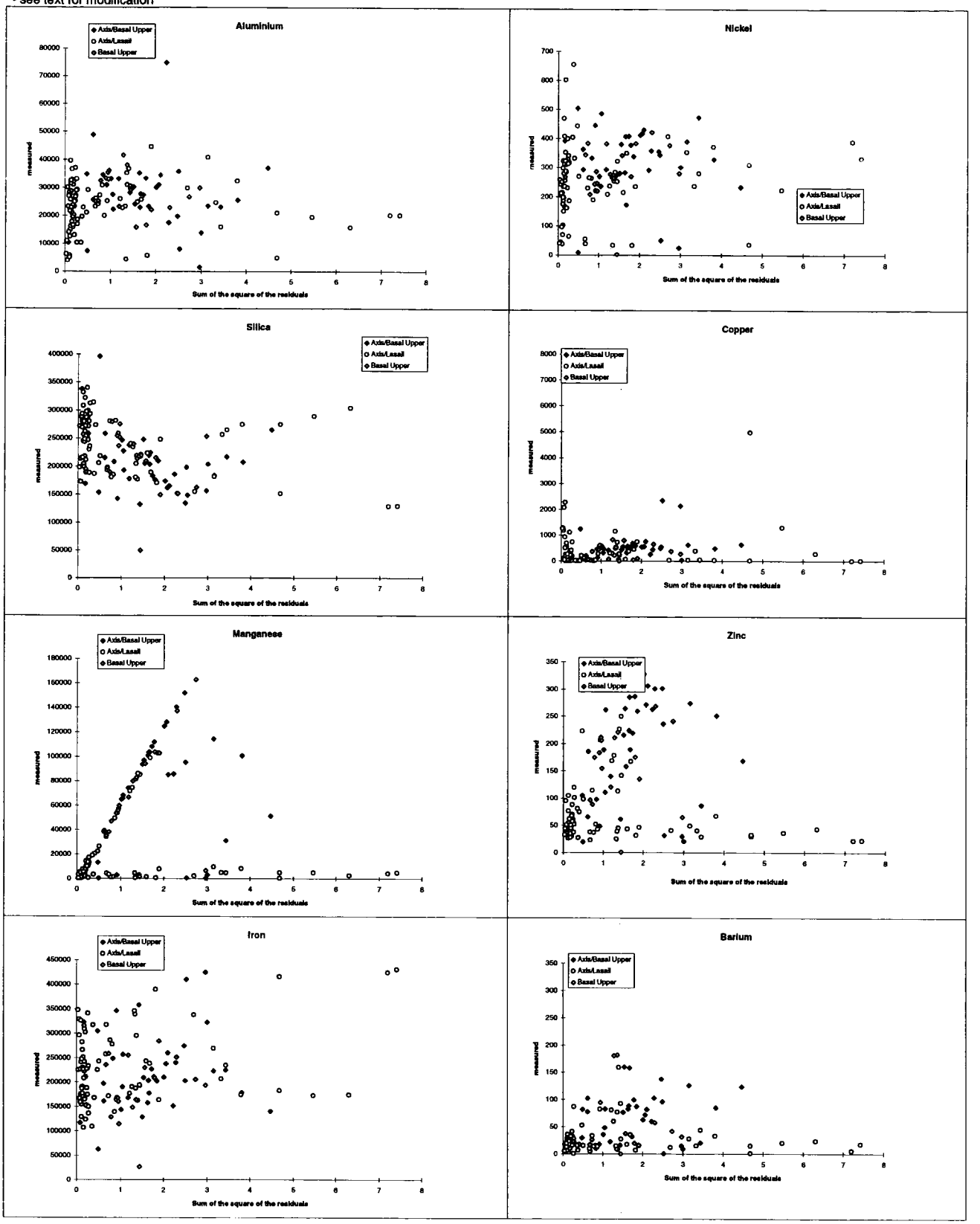

compared to 0.64% found in the Fe-rich Source. Despite the iron-rich source also containing Mn (the Fe:Mn ratios being 0.29 and 0.60 respectively for the Fe-rich and the FeMn-rich Sources), the predominance in the As/Bu Group of the FeMn-rich Source swamps any significant contribution of Mn by the Fe-rich Source to the sediment. The As/Ls Group is, significantly, not just the reverse of this situation since there existed a more effective contribution from both hydrothermal sources than occurred in the As/Bu Group (see Table 4.7). In consequence of the As/Ls Group being comprised of 7.6% FeMn-rich Component and 50.7% Fe-rich Component, the distribution pattern of Mn between the two sources is satisfactorily explained.

The contribution of the Mn from the hydrogenous component may also be explained from the classic studies of the mineralogy of open-ocean ferromanganese nodules and from subsequent modelling of iron and manganese sources in the oceans (Buser and Grutter, 1956; Lalou, 1983). The principal minerals found are δMnO_2, birnessite and toderokite. Relative to average crustal abundance, the elements Mn, Co, Mo and Th are 100-fold enriched and Fe is enriched by a factor of less than 10 (Cronan, 1976). The model in this study attributes significantly far less Mn to the seamount As/Ls Group (1.95%) than to any of the other Groups: As (21.54%), As/Bu 17.73%) and Bu (17.07%). The relatively high proportion of hydrogenous-Mn in the As/Bu Group is particularly significant since this Group is also the one dominated by the FeMn-rich hydrothermal component. These results can only suggest that the hydrothermal input from the As/Ls Group was sufficiently volumetrically high so as to mask the hydrogenous input. Table 4.9 shows that it is valid to suggest that the Oman sediment is dominantly of hydrothermal origin.

The non-hydrothermal Mn sources were more important further from the active vent field and a greater contribution of manganese from sea-water in the hydrogenous component. Diagenetic processes involving a sediment substrate might also produce enrichment in Mn indirectly from sea-water but this cannot be taken account of in the simplistic model used.

Detrital Mn forms a much less significant portion of the contribution of Mn to the sediment. The findings of this study suggest a slightly greater proportion of Mn of detrital origin (9.02%) compared to the original study (4.0%) by Dymond (1981). Thus, detrital Mn forms up to 78% of total Mn in the "Eastern Nazca Plate" area of the latter study and that estimated chemical compositions of the

detrital fraction of deep-sea sediment include significant Mn-content (Krishnaswami, 1976; Bacon and Rusholt, 1982; Thompson *et al.*, 1984).

The leaching experiment has partitioned Mn between the ferromanganese oxide phase and the iron oxide phase (As/Bu Group) whereas the linear programming has not. From this evidence, either linear programming has failed to distinguish between two different hydrothermal end-members, or partition data has only partially dissolved the ferro-manganese oxide component. It is more likely that linear programming has associated all of the Mn with the hydrothermal end-member that closely resembles "ferromanganoan sediment"; whereas the partition data is showing that a Mn oxide phase is physically mixing with Fe oxyhydroxide onto which MnO is adsorbed. Evidence from Troodos umbers with similar Fe/Mn compositions supports a similar two-fold hydrothermal source for the ferromanganoan sediments of the Oman ophiolite (Robertson and Hudson, 1973).

4.5.1.5 Nickel

The distribution pattern of nickel reflects predominantly the authigenic (45.1%) and the hydrothermal (50.6%) sources. In comparison, the Dymond (1981) study finds that Ni is authigenic in the "Basins" (70%) and "Northern Nazca Plate" (55%); detrital (73%) in the "Eastern Nazca Plate"; and a mixture of hydrothermal (39%) and authigenic (40%) in the "Rise Crest". The comparability between the modern "Rise Crest" samples and the ancient sediments is again particularly noticeable.

In both the ancient and recent deposits, the hydrothermal Ni is almost as important as the hydrogenous nickel, which would be expected since Ni is one of the elements enriched by between 50 and 100 times in ferromanganese nodules relative to average crustal abundance (Cronan, 1976). Previous partitioning data indicate that Ni is concentrated in authigenic fractions associated with Mn, Co and Cu, and is enriched in pelagic clays. The partition data in this study (Table 4.1) suggests that Ni is concentrated in Ferromanganese oxide and iron oxide phases which also suggests that Ni has been removed from solution to form the sediment (Chester and Messiha-Hanna, 1970).

The apparent hydrothermal Ni source in the Oman samples and in "Rise Crest" samples of the Dymond (1981) study cannot be explained by precipitation from hydrothermal solutions. Studies of hydrothermal solutions and of the sediment

precipitating from them indicate that hydrothermal fluid (e.g., from the high-temperature system at 21°N on the EPR) is an insignificant source of nickel (von Damm *et al.*, 1985). From Ni : Fe ratios in the fluids and sediments, it may be concluded that the Ni has been scavenged from seawater by hydrothermal ferromanganese precipitates. The linear programming model in this study and partition analysis suffer from the same drawback as the original linear programming model (Dymond, 1981), in that it is unable to distinguish between elements precipitated directly from hydrothermal solutions and those co-precipitated from sea water as a result of the precipitation of hydrothermal phases.

The detrital Ni source contribution (1.95%) is far less significant than the hydrogenous and "hydrothermal" contributions (Table 4.7). The study by Bacon and Rusholt (1982) found a 1 : 1 ratio of detrital : authigenic nickel in deep-sea clays. Similar Ni values in detrital fractions (ranging between 46 ppm to 92 ppm) have been obtained using various chemical separation and graphical techniques (Chester and Hughes, 1967; Krishnaswami, 1976; Bacon and Rusholt, 1982; Thompson *et al.*, 1984).

4.5.1.6 Copper

The copper distribution pattern reflects inputs from hydrothermal (90.3%) and hydrogenous (8.1%) sources. The average values for both are slightly higher than those predicted by Dymond (1981) for the "Rise Crest" locations (70% and 6% respectively) but this is explained by the presence in that study of the dissolution residue (16%) which is not computed in the model of this study. In comparison, the biogenic and detrital components are not significant contributors of Cu (0.8% and 1.4% respectively). The partitioning of Cu into the Fe-Mn fraction and Fe fraction during chemical leaching (Table 4.1) is comparable to the results of linear programming (Table 4.9). Leaching data suggests that Cu is Mn-philic when a Mn oxide phase is present, but that it is also adsorbed by the Fe oxide phase when Mn is less abundant.

Investigations of black smokers on the EPR have directly sampled the hydrothermal end-member solutions and the chimney precipitates surrounding the vents. These studies show that the chimney is composed of sulphides of Fe, Zn and Cu (Edmond *et al.*, 1982; Von Damm *et al.*, 1983), that Cu in vented solutions is present at up to 44 $\mu mol.kg^{-1}$ compared to 0.007 $\mu mol.kg^{-1}$ in average seawater (Von Damm *et al.*, 1985). Given the extreme enrichment of Cu in

Figure 4.6 Measured bulk content (Durham XRF) versus bulk content calulated from Factor analysis-derived elemental ratio coefficients and applied to linear programming

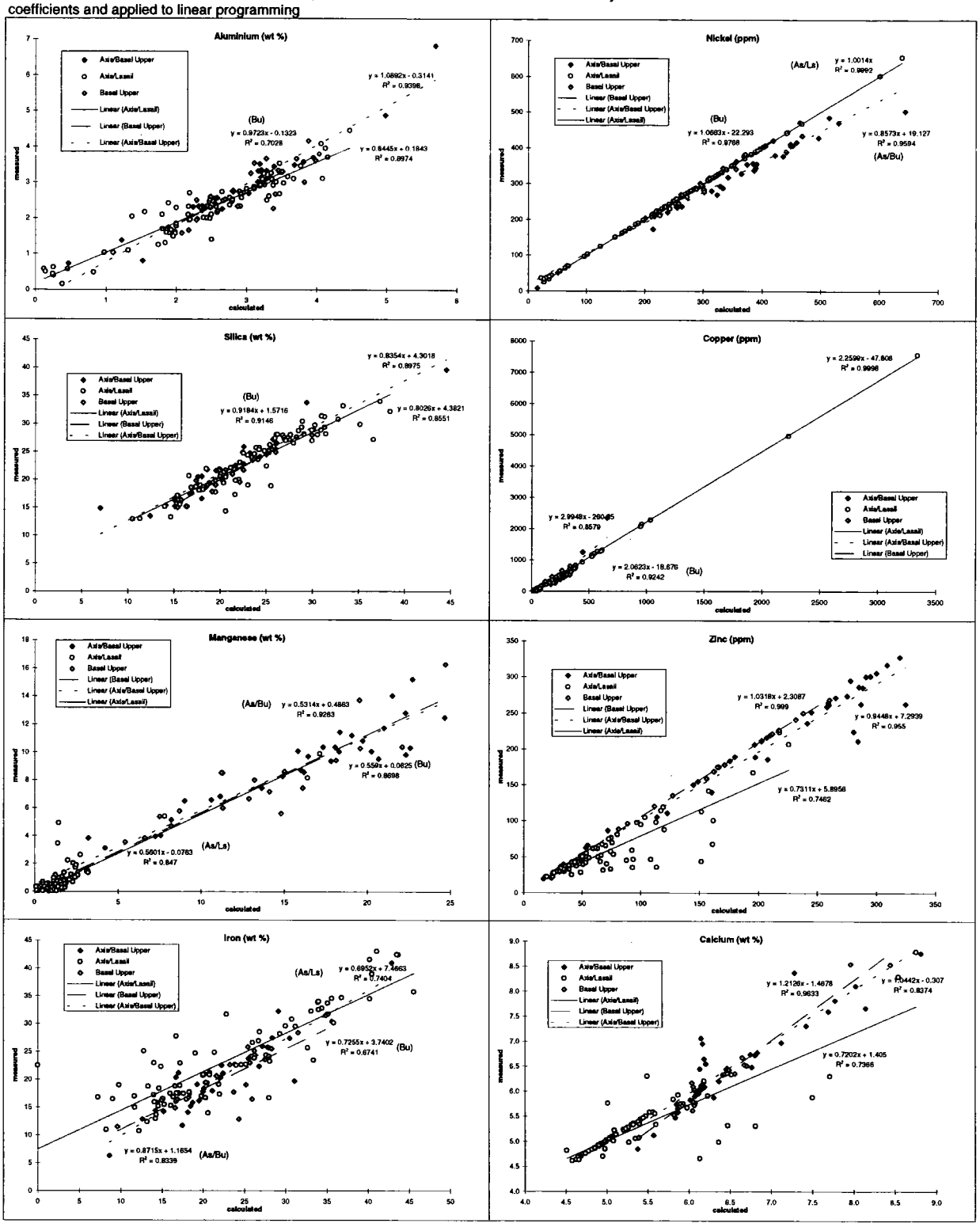

hydrothermal solutions relative to ambient sea water, the distribution pattern predicted by this study is expected. The association of Cu with the hydrothermal fractions, especially that of the FeMn component, is likely (comparably with Ni) to reflect very efficient scavenging from sea water by Mn hydroxide particles that

escape the immediate vent area to form the metalliferous sediments (Lalou, 1983).

The hydrogenous source of copper is of much less importance than the hydrothermal source in the rise crest location in which the Oman sediment formed. However, the hydrogenous proportion (8.1%) is likely to reflect the inclusion of hydrogenous Cu-, Ni-, Zn-rich mineral todorokite which is characteristic of ferromanganese nodules under non-hydrothermal conditions (Dymond *et al.*, 1984).

4.5.1.7 Zinc

The distribution pattern for Zn (Table 4.7) is very similar to that of Cu and in that closely resembles the original study of recent sediment (Dymond, 1981). The contribution of Zn from the hydrothermal source (84.0%) and the hydrogenous source (10.0%) resemble that of Cu because of the similar chemistries and behaviour patterns of the two elements. Similarly, there is a small detrital contribution (3.4%) to the total Zn content. The element : Fe ratios of both Zn and Cu in hydrothermal solutions are comparable to those in the sediments surrounding vents (Von Damm *et al.*, 1985), and studies suggest that both elements may remain in solution beyond the immediate vent area, so making them available for inclusion in the hydrothermal end-members contributing to metalliferous sediment of the type in this study.

Linear programming evidence supports partition analysis in suggesting similar detrital Zn source contribution. Partition analysis data (Table 4.1), calculates that between 22% and 23% of the Zn in each of the sample Group is of detrital origin.

4.5.1.8 Barium

The distribution pattern of Ba (Table 4.7) suggests that it is derived from biogenic (16.8%), hydrothermal (53.9%) and detrital sources (28.0%). The distribution of Ba represents the greatest departure of the model in this study from the original model on which it is based (Dymond 1981): the reason for the discrepancy is in the non-inclusion of the dissolution residue component in this study which in the earlier study accounts for 75% of "Rise Crest"-derived Ba.

Having found during the preliminary investigations in this study that the dissolution residue is an insignificant element sink, it is suggested that Ba is

introduced into the samples by the hydrothermal and biogenic sources in a manner described by other more recent investigations. Biogenic carriers for Ba include calcium carbonate and opal (Collier and Edmond, 1984). Hydrothermal-fluvial flux studies indicate that Ba may be leached effectively from basalt at high temperatures (Li, 1981; Thompson *et al.*, 1984; Von Damm *et al.*, 1985). With regard to Ba, the ineffectiveness of the earlier model runs which have led to the discarding of the dissolution residue source in favour of a second hydrothermal source, the model is less well able to predict accurately the distribution of the element than the original model.

4.5.2 Assessment of components

The results of the normative sediment calculations are reproduced in full for all samples in Appendix B.5. A representative subset of the data set summarises results for the each sample Group below (Table 4.9) together with the average results of each Group (Table 4.10).

Table 4.9 Results of Linear Programming: Representative samples

	20655	**20657**	**20646**	**20666**	**U13**	**U76**	**20693**	**U23**
	As	As	As/Bu	As/Bu	As/Ls	As/Ls	Bu	Bu
% Detrital	0.5	0.6	8.5	32.3	13.4	29.5	25.1	12.3
% Hydrothermal Fe	0.0	0.0	0.4	0.0	82.1	41.4	67.1	80.6
% Hydrothermal FeMn	82.3	81.9	63.2	58.1	0.0	0.0	0.0	0.0
% Biogenic	10.3	9.4	23.7	7.2	1.9	21.3	3.6	0.0
% Authigenic	0.9	2.6	2.8	2.2	2.0	2.9	4.2	4.1
% Carbonate	6.0	5.5	1.5	0.2	0.7	5.0	0.0	3.0

4.5.2.1 Detrital Component

Relative to the overall mean, the As/Bu Group samples are relatively depleted in the detrital content, the Bu Group are relatively enriched, and the As/Ls have detrital content similar to the mean. The As/Bu Group of samples have an average detrital contribution of 15.8% with variation between 0.0 and 63.0%. This Group demonstrates the greatest range of detrital component by sample location (Table 4.11) and the detrital source contribution is of less importance to this Group than it is to the Bu Group. The three principal sulphide deposits of the As/Bu Group, (Aarja, Khabiyat and Bayda), appear to have almost identical detrital contributions, both to each other and to the Lasail Mine of the As/Ls Group. The Wadi Suq samples have the lowest proportional detrital source

contribution reflecting the highest hydrothermal input, which is also responsible for the proportional dilution of the biogenic component.

Table 4.10 Results of Linear Programming: Averages by Group

	Average As	Average As/Bu	Average As/Ls	Average Bu	Average Total
Number of samples -	4	36	81	25	146
% Detrital	5.4	15.8	19.5	27.5	19.8
% Hydrothermal Fe	0.0	0.2	52.5	46.3	37.9
% Hydrothermal FeMn	75.3	62.4	7.0	1.4	20.4
% Siliceous	12.0	17.8	17.8	18.7	18.0
% Authigenic	2.1	2.4	1.4	2.9	1.9
% Carbonate	5.3	1.6	1.8	4.6	2.2

Table 4.11 Percentage of detrital component

Group	Location	Mean (%)	Standard deviation (%)	Range (%)
Average	All Groups	19.8	13.7	0.5 - 16.3
As	Wadi Suq	5.4	7.5	0.5 - 16.3
As/Bu	Wadi Suq	0.0	0.0	0.0
As/Bu	Buraimi Highway	12.5	-	12.5
As/Bu	Aarja	15.0	12.1	0.1 - 32.3
As/Bu	Khabiyat	17.7	13.9	2.1 - 63.0
As/Bu	Bayda	18.4	-	8.4
As/Bu	Huwayl	20.5	21.2	4.5 - 51.1
As/Ls	Lasail Mine	17.6	14.3	0.0 - 55.1
As/Ls	Huwayl	22.5	10.4	0.0 - 40.0
Bu	Ghayth	25.3	4.4	21.7 - 32.8
Bu	Semdah West	28.6	11.0	11.6 - 40.2

N.B. "-" denotes single sample

The As/Ls Group from the Lasail Mine and Huwayl locations are composed of detrital source contributions ranging between 0.0 to 55.1% and 0.0 to 40.0% respectively. Despite the greater variability from the Lasail mine, the average detrital source content from Huwayl is 5% greater.

The detrital input is relatively most important to the Bu Group. Unlike the other sample Groups, each sample of the Bu Group contain at least 10% of detrital component. The As Group of four samples has a range of detrital contribution between 0.5% and 16.3%. It is unlikely that volcanic stratigraphic position is a

major control on detrital content, given the range of values for each sample Group. Proximity to a detrital source cannot be the primary control of fluctuations in the relative importance of the detrital component for either the As/Ls or the As/Bu Group. Fluctuation in the hydrothermal source are thought to be the principal control on the contribution of the other components (Dymond, 1981; Chester, 1990)

However, the Bu Group does not exhibit the range of detrital content which is characteristic of the other sample Groups. The relative consistency of the detrital content in Bu Group samples probably results either from (1) consistency in hydrothermal input, or (2) physical homogenization of the sediment prior to final depositon.

4.5.3.2 The Hydrothermal Components

For consistency with the results of Chapter 2, this study has used two hydrothermal end-members, rather than one, to model ridge-crest processes that formed the ancient Oman deposits. The results of this are summarised in (Table 4.12)

The principal drawback of using two end-member hydrothermal sources is that linear programming is unable to quantify admixtures of the two. By defining two hydrothermal sources, this study enables the contribution of each to be modelled from the measure E_T. The ability to quantify, as below, the interplay between (1) the hydrothermal ferromanganese source and (2) the hydrothermal iron-rich manganese-poor source is the principal advantage of having modified the original normative model. In all of the average values calculated (Table 4.12), it is always true that one hydrothermal component dominates the other. The model output (Appendix B) shows a tendency to attribute the hydrothermal source to one or the two end-members rather than to a mixture of the two. Other than for the As/Ls mine, linear programming has allocated, to each sample, either one hydrothermal source or the other. In contrast, rare samples from the Lasail Mine often contain both of the hydrothermal end-members. This is atypical of the results of linear programming in this study.

Table 4.12 Percentage of hydrothermal components

Group	Location	Mean	Standard Deviation	Range	Mean	Standard Deviation	Range
		Hydrothermal FeMn-rich			Hydrothermal Fe-rich		
As	Wadi Suq	0	0	0	75.3	14.8	53.2-84.0
As/Bu	Buraimi H/way	0	0	0	66.6	-	66.6
As/Bu	Khabiyat	0	0	0	54.6	-	54.6
As/Bu	Bayda	0	0	0	55.2	-	55.2
As/Bu	Aarja	0	0	0	55.6	20.2	43.2-99.6
As/Bu	Wadi Suq	0	0	0	79.2	2.6	85.0-88.7
As/Bu	Huwayl	0	0	0	77.4	21.7	46.6-95.2
As/Ls	Huwayl	77.4	21.7	23.0-98.5	0	0	0
As/Ls	Lasail Mine	51.6	32.1	0.0-99.1	19.1	37.0	0.0-99.5
Bu	Semdah West	44.2	21.4	18.7-80.6	0	0	0
Bu	Ghayth	56.3	18.6	23.6-67.1	0	0	0

N.B. "-" denotes single sample

At every location, other than Semdah West, the average total hydrothermal component exceeds the average of the sum of the non-hydrothermal components. In a number of individual samples, the total calculated hydrothermal input is less than 50% of the total.

Bearing in mind the need to question the validity of model on the grounds of the proportions of each hydrothermal source, the basic pattern that results may be summarised as follows (Table 4.13):

Table 4.13 Ratio of Fe-rich to (Fe + Mn)-rich hydrothermal components

Group	Hydrothermal component	Fe/FeMn Ratio
As	Ferromanganese Source	0
As/Bu	Ferromanganese Source (+ very occasional Ferrous Source)	0.05 : 1
As/Ls	Ferrous Source and Ferromanganese Source	7.61 : 1
Bu	Ferrous Source	30.03 : 1

The Bu data consist almost entirely of the pure Fe-rich source and the As data consist almost entirely of the pure FeMn-rich source. In contrast, the sediment formed on the Axial lava surface contain contributions from both the hydrothermal sources: the As/Ls data demonstrate mixing of Fe-rich and FeMn-

rich sources whereas the As/Bu data are dominated by the FeMn-source source almost to the exclusion of the Fe-rich source.

The combined source contribution of the two hydrothermal components suggests that, as expected, the sediment is predominantly hydrothermal in origin (Table 4.14) except for the Bu Group samples from Semdah West. The pattern of the two sources suggests that there are processes which disperse the hydrothermal precipitates as well as there being different types of hydrothermal activity present at the ridge crest.

Table 4.14 Combined hydrothermal input

Group	Location	Mean	Standard Deciation	Range
As	Wadi Suq	75.3	14.8	97.4 - 99.1
As/Bu	Buraimi H/way	52.0	-	52.0
As/Bu	Khabiyat	58.7	15.6	15.1 - 88.7
As/Bu	Bayda	55.2	-	55.2
As/Bu	Aarja	65.6	20.2	43.2 - 99.6
As/Bu	Wadi Suq	79.2	2.6	85.0 - 88.7
As/Bu	Huwayl	77.4	21.7	46.6 - 89.6
As/Ls	Huwayl	53.0	19.4	24.2 - 98.5
As/Ls	Lasail Mine	70.7	23.1	27.4 - 99.5
Bu	Semdah West	44.2	21.4	18.7 - 80.6
Bu	Ghayth	56.3	21.5	23.6 - 67.1

From Red Sea studies, vent haloes have been discovered formed by the precipitation from hydrothermal solutions of solid phases in the following order (Cronan 1976; Cronan 1980):

(1) sulphides
(2) iron silicates
(3) iron oxides
(4) manganese oxides

This suggests that the linear programming data are describing the axial lava surface in terms of vent-proximal and vent-distal hydrothermal end-members. Those samples which are dominated by the iron-rich hydrothermal source

represent vent-proximal locations, whereas those dominated by the iron-manganese hydrothermal source represent vent-distal locations. The As/Ls Group represents the area closer to the vent-field (but not close enough to contain sulphides) and the As/Bu Group represents the area further from the vented hydrothermal solutions. Because both the As/Ls and As/Bu Group samples are taken from the axial lava surface, it is assumed that they are approximately contemporaneous. The earlier As Group appears only to contain a ferromanganese hydrothermal input indicating that the small-sized and rare deposits found within the lower (As) lavas are the product of distal vent. The youngest sediment, which is represented by samples of the Bu Group, is dominated by the Fe-rich hydrothermal source. The Fe-rich end-member shows that the samples are vent proximal (Cronan, 1976; Cronan, 1980), suggesting formation from a hydrothermal system driven by the active magmatism and rifting which produced the Alley lava.

4.5.3.3 The siliceous source

The variation in siliceous component source is very consistent, (see Table 4.10), the average values being as follows: As/Bu 17.9%, As/Ls 17.7% and Bu 18.0%. The variation in each Group is considerable (Table 4.15).

The conclusion that may be drawn from the data is that the processes controlling the siliceous source contribution acted uniformly in the study area throughout the period of formation of the samples. A similar distribution would be expected, according to the original model components (Dymond, 1981), if the siliceous component were of biogenic origin and if large-scale biogenic source pattern were to systematically reflect the latitude of formation. According to Dymond (1981), the latitudinal pattern found for Nazca plate sediments is only "slightly disturbed" at the ridge crest by hydrothermal activity and near the continental margin by detrital input. However, Oman sediments are of a single latitude, so that variation in the Si-rich component cannot be the result of latitudinal variation in biogenic input. The wide range in Si-input is also characteristic of other ancient metalliferous sediments formed at a single latitude, for example, the Cyprus umbers (Robertson, 1976; Varnavas, 1981; Boyle, 1984).

Table 4.15 Biogenic Source Contribution

Group	Location	Mean (%)	Standard Deviation (%)	Range (%)
As	Wadi Suq	12.0	7.9	4.9 - 23.3
As/Bu	Wadi Suq	11.3	4.2	7.0 - 13.0
As/Bu	Aarja	16.9	12.6	0.0 - 30.4
As/Bu	Khabiyat	18.4	15.1	0.0 - 55.4
As/Bu	Bayda	24.4	-	24.4
As/Bu	Buraimi Highway	30.2	-	30.2
As/Bu	Huwayl	0.0	-	0.0
As/Ls	Lasail Mine	9.9	15.4	0.0 - 59.9
As/Ls	Huwayl	22.5	17.3	0.0 - 59.8
Bu	Ghayth	11.1	15.4	1.4 - 38.3
Bu	Semdah West	19.6	2.7	0.5 - 39.7
Total		17.8	16.5	0.0 - 59.9

The average percent of the Si-rich component, if it is of biogenic origin, is consistent with sediment genesis at latitudes of between 18° and 38° as predicted by other studies to which this study is comparable in terms of the biogenic end-member (Dymond, 1981; Leinen and Pisias, 1983). This is consistent with the proposed palaeoposition of the ridge at 45°E and 10°N (Thomas *et al.*, 1988; Perrin *et al.*, 1993).

4.5.3.4 The Hydrogenous Source

The hydrogenous content of the Oman samples is uniformly low, forming only on average between 1.4% and 2.9% of the samples. The hydrogenous source, in the sense in which it is referred to in this study, is thought to be deposited at a uniform rate at any given location on the sea floor (Krishnaswami, 1976). If this assumption is true, the hydrogenous source is inversely proportional to accumulation rate since its abundance is directly controlled solely by the rate of accumulation of the other sources.

Figure 4.7 Linear programming results using Modified Dymond (1981) Element Ratio Coefficients for comparison with factor analysis output

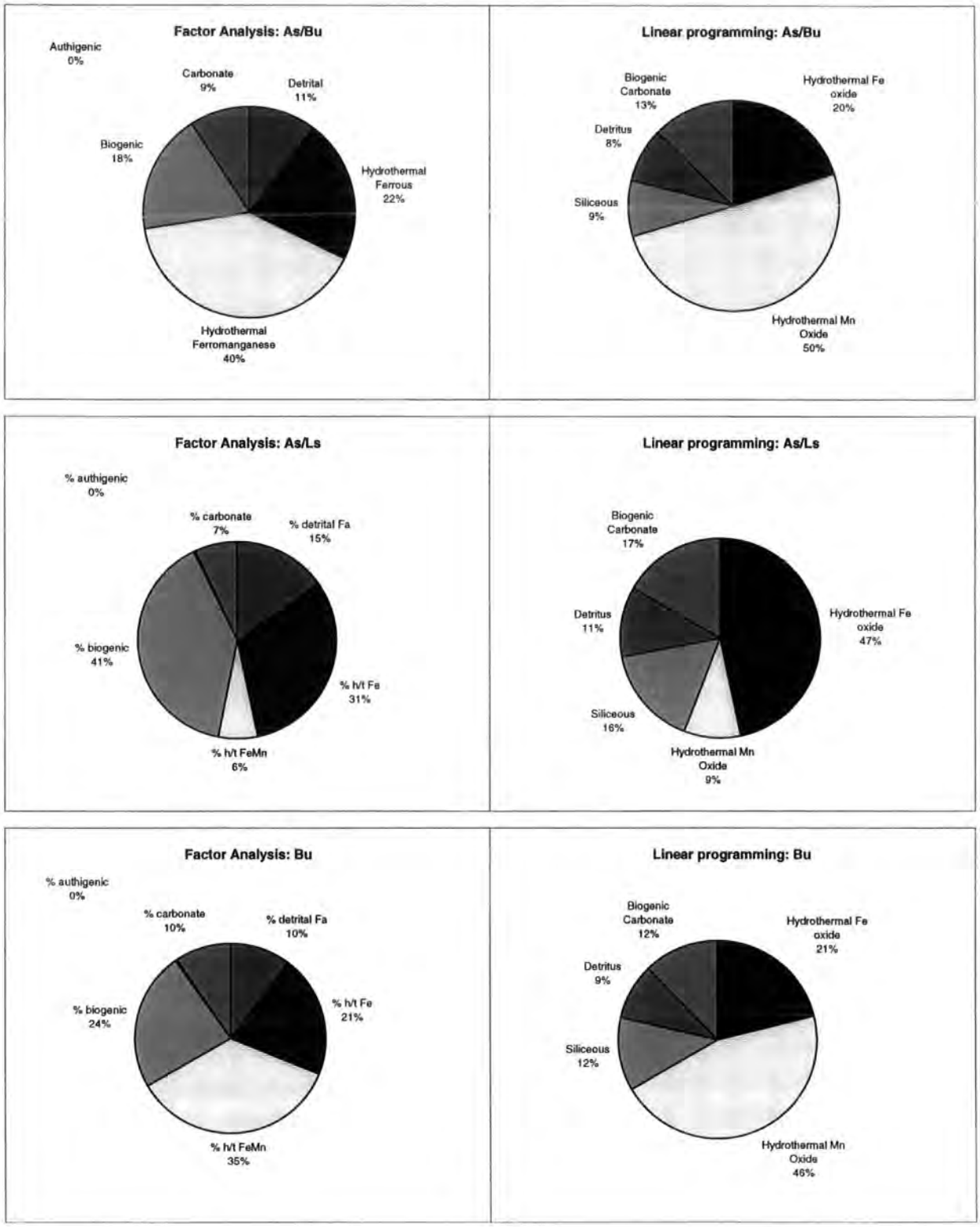

Using data from Table 4.10, the average authigenic source composition (%) is plotted versus each of the other components (Figure 4.4). The result shows: (1) the positive correlation between increasing authigenic source and increasing detrital, biogenic and carbonate sources; and (2) the negative correlation between hydrothermal source input and authigenic source input. Assuming hydrogenous

Figure 4.8 Factor Analysis Output versus Linear Programming (Modified Dymond, 1981, Components) Output

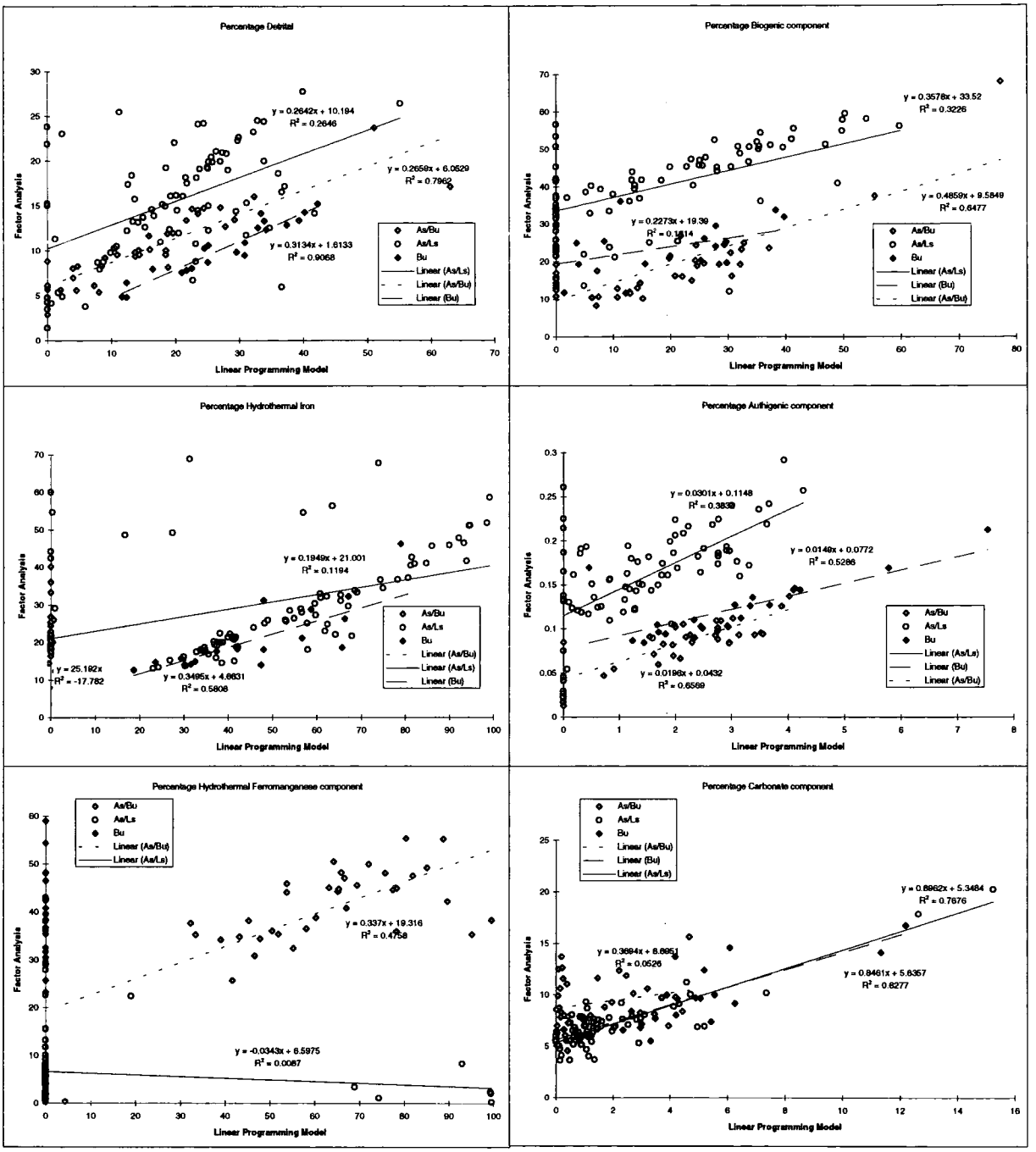

abundance to be inversely proportional to the total sedimentation rate, the trends that emerge are as follows:

(1) At high sedimentation rates (denoted by the lower values of authigenic abundance), the hydrothermal component forms a greater proportion of a given sample relative to its mean abundance, and the detrital, biogenic and carbonate sources all contribute low proportions relative to their mean abundance.

Figure 4.9 Factor Analysis Output versus Linear Programming (factor analysis-derived components) Output

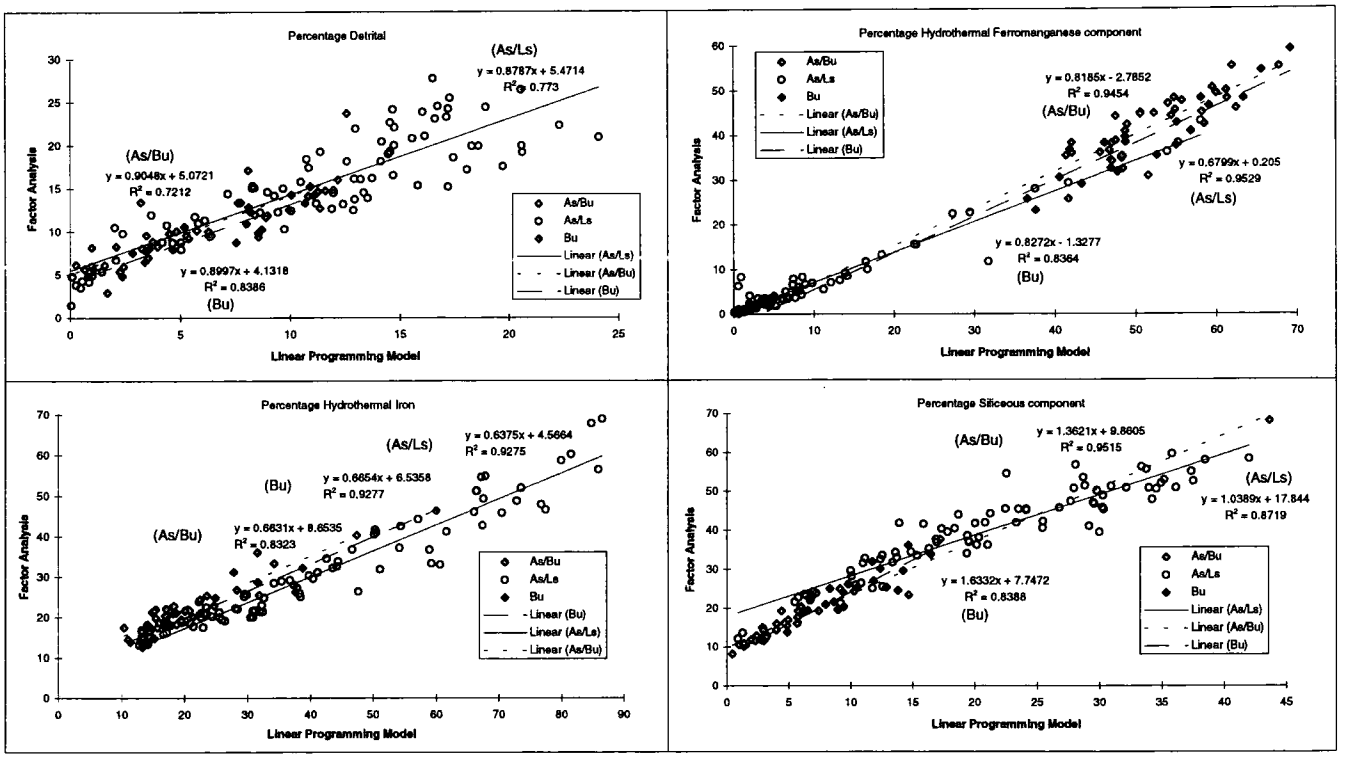

(2) At low sedimentation rates (denoted by the higher values of authigenic abundance), the reverse of the previous point is true.

This suggests that, when the sediment is being very rapidly deposited the sediment-forming processes are dominated by the hydrothermal source input to a greater extent when deposition is slower. Not unexpectedly, the data show that rapid sedimentation is the result of periods of greater hydrothermal activity which dilutes the other components, all of which must therefore accumulate at a relatively uniform rate. As this pattern is only clearly seen when using average data it suggests that the hydrogenous component, in its calculated form using this model, is only a very rough inverse indicator of sedimentation rate and that many factors control relative source contribution using more complex processes than those initially suggested.

The quantitative calculation of authigenic abundance suggests that, on average, it forms a slightly smaller proportion of the As/Ls group (1.4 ± 1.2%) than either the As/Bu Group (2.4 ± 1.1%) or the Bu Group (2.5 ± 1.6%). The authigenic abundance in As/Bu and Bu samples is approximately 1.7 times that of As/Ls Group samples, thus suggesting that the average rate of sedimentation is quantitatively higher in the latter samples. By implication, the data suggest that the hydrothermal system in the proto-seamount environment is more active and

sedimentation rate is lower and hydrothermal input is diluted by authigenic, detrital and biogenic sources. This finding supports the theory put forward in the previous Section that the sediments of the As/Ls Group represent either (a) the relatively vent-proximal environment, or (b) the higher temperature, more vigorous hydrothermal system.

4.6 Linear Programming using local end-members

The end-members used in the literature have been adopted for the purpose of comparability. However, the next section applies local end-members, defined by factor analysis and partition experiments, because the results show that linear programming does not accurately model the hydrothermal end-members in a geologically realistic manner using end-members from the literature. Because the hydrothermal end-members were variable, the end-member components from the literature are not sufficiently similar to model hydrothermal processes. Using the results of factor analysis, it has been possible to approximate the end-member components from the bulk sediment analysis. By repeating the linear programming analysis using local end-members it was hoped to overcome the inadequacies of the original Dymond (1981) model.

4.6.1 End-member components

Quantitative estimates of the weight percent of distinct sediment-forming components have been calculated using factor analysis data from Chapter 2. The end-members calculated in Chapter 2 using factor analysis have been re-calculated, below, as elemental ratios for the purpose of linear programming (Table 4.16 to 4.24).

Table 4.16 End-member content calculated by factor analysis (As/Bu)

As/Bu	Hydrothermal Fe (P) oxide	Hydrothermal Mn oxide	Siliceous	Detritus	Biogenic carbonate
Al_2O_3 wt.%	0	0	0	3	0
SiO_2 wt.%	0	0	30	8	0
MnO wt.%	0	8	0	0	1
Fe_2O_3 wt.%	18	0	4	0	0
Ni ppm	165	36	0	0	12
Cu ppm	32	71	9	0	0
Zn ppm	3	144	0	0	8
Ba ppm	0	19	2	1	0

Table 4.17 End-member ratio coefficients calculated by factor analysis (As/Bu)

As/Bu	$(E/Fe)_H$	$(E/Mn)_{H2}$	$(E/Si)_B$	$(E/Al)_D$	$(E/Ni)_C$
Al_2O_3	0.000	0.000	0.009	1.000	0.021
SiO_2	0.000	0.000	1.000	2.367	0.000
MnO	0.002	1.000	0.000	0.001	0.044
Fe_2O_3	1.000	0.001	0.131	0.000	0.000
Ni	9.184	0.001	0.000	0.000	0.000
Cu	1.797	8.668	0.307	0.000	0.000
Zn	0.169	17.455	0.000	0.000	0.688
Ba	0.000	2.328	0.081	0.553	0.000

Table 4.18 End-member content calculated by factor analysis (Bu)

Bu	Hydrothermal Fe (P) oxide	Hydrothermal Fe + Mn oxide	Siliceous	Detritus	Biogenic Carbonate
Al_2O_3 wt.%	0	0	1	3	0
SiO_2 wt.%	0	0	27	15	0
MnO wt.%	0	8	0	0	0
Fe_2O_3 wt.%	14	4	3	1	0
Ni ppm	55	130	0	44	19
Cu ppm	0	0	1	3	0
Zn ppm	0	32	0	1	10
Ba ppm	0	0	28	28	0

Table 4.19 End-member ratio coefficients calculated by factor analysis (Bu)

Bu	$(E/Fe)_H$	$(E/Mn)_{H2}$	$(E/Si)_B$	$(E/Al)_D$	$(E/Ni)_C$
Al_2O_3	0.000	0.000	0.026	1.000	0.000
SiO_2	0.000	0.000	1.000	5.641	0.000
MnO	0.000	1.000	0.000	0.000	0.002
Fe_2O_3	1.000	0.530	0.113	0.254	0.000
Ni	3.726	0.530	0.000	16.871	0.000
Cu	0.000	0.035	0.017	1.002	0.000
Zn	0.000	4.007	0.000	0.408	0.541
Ba	0.000	0.000	1.021	10.755	0.000

The factor analysis results produced end-member components which are of slightly different composition for each of the sample Groups. Because the technique is so sensitive to the end-member composition that is used, it is suggested that the assumption that each component has a constant composition anywhere in the marine environment is inadequate for the purpose of this study. By calculating the local end-members for each sample Group it was hoped to overcome some of the inadequacies of the original methodology (Dymond, 1981; Leinen and Pisias, 1984).

Table 4.20 End-member content calculated by factor analysis (As/Ls)

As/Ls	Hydrothermal Fe oxide	Hydrothermal Fe Mn oxide	Siliceous	Detritus	Biogenic carbonate	Phosphate
Al_2O_3 wt.%	0	0	0	3	0	3
SiO_2 wt.%	2	0	39	0	0	0
MnO wt.%	0	1	0	0	0	0
Fe_2O_3 wt.%	25	0	0	0	0	0
Ni ppm	8	7	0	132	0	0
Cu ppm	23	5	5	0	0	155
Zn ppm	0	30	0	3	0	0
Ba ppm	0	11	1	0	0	0

Table 4.21 End-member ratio coefficients calculated by factor analysis (As/Ls)

As/Ls	(E/Fe)H	(E/Mn)H2	(E/Si)B	(E/Al)D	(E/Ni)C
Al_2O_3	0.000	0.029	0.002	1.000	0.000
SiO_2	0.095	0.000	1.000	0.000	0.000
MnO	0.001	1.000	0.000	0.000	1.146
Fe_2O_3	1.000	0.000	0.000	0.000	0.000
Ni	0.338	0.000	0.000	41.071	0.000
Cu	0.914	4.668	0.133	0.000	0.000
Zn	0.004	28.836	0.001	0.874	0.000
Ba	0.000	10.428	0.016	0.051	0.406

The principal drawback of calculating end-member components from factor analysis data is that in each FACTOR, two components may be represented in positive and negative vector space. Nevertheless, it has been possible to calculate approximate pure end-member sources using the assumption that the relative proportions of the sediment-forming minerals are directly related to the major element composition. The result is that each of the FACTORs containing any major element content has been used to represent an end-member. For each sample Group, five approximately comparable end-member components emerge, so that the element associations approximate to the pure source compositions.

In common to each sample Group there is a carbonate source, a detritus source and a siliceous source (Tables 4.16, 4.18, 4.20). The elemental ratios of the detrital source (Table 4.22) are comparable to those used by Dymond (1981). The elemental composition of the siliceous source is similar for each of the three sample Groups in this study (Tables 4.16, 4.18, 4.20), but the resultant elemental ratios (Tables 4.17, 4.19, 4.21) differ significantly from those of Dymond (1981), (Table 4.22). Because the Dymond (1981) model uses the bulk content of marine plankton for a biogenic component, the differences between the geochemistry of

plankton and the factor analysis derived "Siliceous component" suggest that Si is not principally or solely of biogenic origin. Probably the siliceous content of the Oman sediments reflects a combination of hydrothermal, detrital and biogenic sources.

Table 4.22 Comparison of Detrital Component element ratios

	Dymond (1981)	Leinen and Pisias (1983)	As/Bu	As/Ls	Bu
	$(E/Al)_D$	$(E/Al)_D$	$(E/Al)_D$	$(E/Al)_D$	$(E/Al)_D$
Al_2O_3	1.0000	1.000	1.000	1.000	1.000
SiO_2	3.0000	1.987	2.367	2.040	3.154
MnO	0.0160	0.192	0.010	0.023	0.015
Fe_2O_3	0.7000	0.776	0.000	0.000	0.000
Ni	0.0015	0.011	0.000	0.004	0.004
Cu	0.0012	0.0058	0.000	0.000	0.000
Zn	0.0014	0.0020	0.000	0.008	0.008

The carbonate component has been included instead of the authigenic component because there is evidence of the former but not of the latter in the Oman sediment.

The principal difference between the models used in the literature and this study is that two hydrothermal components have been included in this study. In each sample Group the end-member components differ slightly. In As/Bu and Bu Group samples there is (1) a hydrothermal Fe oxide component which includes P_2O_5 and (2) an hydrothermal ferromanganese oxide component. In the As/Ls Group samples there is a hydrothermal Fe oxide component and a pure hydrothermal Mn oxide component.

4.6.2 Calculated versus measured element content

The results of using the local end-members which have been calculated from factor analysis (Appendix B) have been calculated for the As/Bu, As/Ls and Bu sample Groups. The As and Ls samples are not included since there are too few samples on which to carry out factor analysis, and consequently it was not possible to calculate new end-end member compositions using this method.

The scatter plot (Figure 4.5) of measured versus calculated elemental contents illustrates the quality of the results of linear programming using (1) the modified Dymond (1981) end-members, against (2) the factor analysis end members. For each element, the measured versus the calculated bulk content has been plotted (Figure 4.6). All eight elements show statistically significant linear positive correlation.

4.6.3 Linear programming output

The results of linear programming using factor analysis-derived end-member components is fully documented in Appendix B. The product of each of the variables and the appropriate element ratio coefficients has been used to give the concentration of that element from each of the five sources. Furthermore, because factor analysis produces an approximate value for the concentration for each of the elements in each of the end-members, the weight fractions of each component may be calculated. By adopting, for each sample Group, the factor analysis values for Fe in pure Fe oxide, Mn in pure ferromanganese oxide, Al in pure detritus, Ca in pure carbonate, and Si in the pure siliceous component (Tables 4.16, 4.18 and 4.20), the concentration of each component in each sample has been computed (Appendix B). The results are summarised as pie charts for each sample Group, for comparison with the results of factor analysis (Figure 4.7).

4.7 Summary of results

The effect of using local end-members for linear programming is twofold: (1) the distribution of the elements is changed; and (2) the proportion of each end-member is different for each sample. The effect of using local end-member compositions and the comparability with factor analysis is described in the following section with the aid of plots of factor analysis versus linear programming. The carbonate source is not discussed since it was not previously calculated using linear programming.

4.7.1 Detrital component content and detrital elemental associations

The effect of using different detrital end-member components may be assessed from the comparison tabulated below (Table 4.23).

Table 4.23 Calculated detrital content using ;inear programming

Methodology	Sample Location			
	As	As/Bu	As/Ls	Bu
	(%)	(%)	(%)	(%)
Dymond (1981) Components	-	29.5	55.5	24.6
Modified Dymond (1981) Components	5.4	23.1	18.4	31.7
Factor Analysis Components	-	9.1	13.2	10.2

N.B. Factor analysis component has been recalculated to carbonate-free basis for comparability.

With one exception, the effect of refining the detrital end-member to match the local source has been to reduce its quantitative importance as a source. The conclusions reached from the results of applying the Dymond (1981) model to metalliferous sediment data was that due to oversimplification of the hydrothermal component, the output was an inaccurate representation of the rise-crest environment of Oman. By modification of this methodology to include two hydrothermal components, and by the use of average Oman lava composition for the pure detrital component, it was hoped to evaluate the source more accurately. However, the results showed that Si-content was likely to be controlled by different processes to those of the plate surface sediments which the Dymond (1981) model was intended to model. Consequently, the relative proportions of the components were still inaccurate as a result of overestimation of the biogenic content and underestimation of the hydrothermal content. By using the factor analysis components, the detrital content of the sediment is calculated by linear programming to be 10.8% with a range of 0.2% to 71.0%.

Table 4.24 r^2 values for calculated detrital component content

	As/Bu	Bu	As/Ls
	(r^2)	(r^2)	(r^2)
Modified Dymond (1981) Model Components	0.7962	0.9068	0.2646
Factor Analysis Components	0.7212	0.8386	0.7730

In comparison to using the detrital end-member of the modified Dymond (1981) method, the factor analysis-derived detrital end-member results in a closer fit between factor analysis and linear programming results (Figure 4.7 and Figure

4.8). The change in r^2 values is a reflection of the closer positive linear correlation between factor analysis and linear programming which is cause by using local end-members (Table 4.24).

The effect of discarding the Modified Dymond (1981) end-member component in favour of the end-member component calculated from factor analysis, has been to significantly increase the positive correlation with factor analysis results. The r^2 values for the As/Bu and Bu Group samples are slightly reduced by adopting factor analysis derived end-members. The good correlation of the Modified Dymond (1981) detrital component with factor analysis data resulted from the use of elemental ratios calculated from average Oman ophiolite lava data. The poor correlation, using the same elemental ratios, for As/Ls samples suggests that Al is incorporated into another component in a manner which was not taken into account in that Group. Alternatively, the problems of estimating the Si-component for the As/Ls samples may have resulted in inaccuracies in the detrital component, which would also be affected.

The change in correlation of factor analysis with linear programming, as a result of changing the end-member components, suggests that it is most useful to calculate elemental ratios from whole rock analysis of detritus rather than from factor analysis results. However, the similarity between the two methodologies confirms the general validity of using factor analysis-derived end-members when direct analysis of end-member components is not a possibility.

By using factor analysis end-members, the $(E/Al)_D$ ratios of Si, Al, Mn, Ni and Zn are comparable to those used in the literature (Dymond, 1981; Leinen and Pisias, 1984). The factor analysis technique unavoidably fails to take into consideration the Fe and Cu contents of the detrital source. This could be a source of error if detrital Fe was a significant contribution to the sediment.

4.7.2 Hydrothermal components and hydrothermal element associations

The effect of using two hydrothermal sources instead of one has already been assessed. The effect of using two local hydrothermal components, calculated using factor analysis, has been to improve the fit of the model to the data in terms of reducing the quantitative difference between (1) the measured Fe and Mn content of a given sample and (2) the sum of the concentrations of Fe and Mn from each of the sources (Figure 4.5).

Table 4.25 Hydrothermal component content

Component	As/Bu (%)	As/Ls (%)	Bu (%)
Dymond (1981)			
Hydrothermal	35.4	38.8	36.9
Modified Dymond (1981)			
Hydrothermal Fe	3.1	53.2	42.1
Hydrothermal Fe Mn	50.7	7.6	1.4
Total Hydrothermal	**53.8**	**60.8**	**43.5**
Factor Analysis Component			
Hydrothermal Fe	22.9	56.6	23.8
Hydrothermal (Fe) Mn	57.4	10.8	52.3
Total Hydrothermal	**80.3**	**67.4**	**76.1**

N.B. Factor analysis component has been recalculated to carbonate-free basis for comparability.

The different results obtained by using different initial element ratio coefficients illustrate (1) the shortcomings of the assumption that the hydrothermal component is invariant and (2) that these shortcomings may be minimized by the use of locally derived element ratio coefficients.

The correlation between linear programming and factor analysis is changed significantly by discarding the Modified Dymond (1981) end-members in favour of end-members calculated by factor analysis (Figure 4.9). The principal shortcoming of the linear programming method, using the Modified Dymond (1981) hydrothermal components, is the poor correlation of the results with factor analysis. Bivariate and ternary plots support the results of factor analysis which show that mixing of two hydrothermal end-members has probably occurred (see: Chapter 2). The sensitivity of linear programming to the end-member elemental ratio coefficients is overcome by using local end-members which have resulted in better correlation between the factor analysis and linear programming techniques (Table 4.26).

Table 4.26 r^2 values for calculated hydrothermal component content

	r^2		
	As/Bu	Bu	As/Ls
Modified Dymond (1981) Model Components			
Ferromanganese oxide	0.4758	-	0.0087
Iron oxide	-	0.5808	0.1194
Factor Analysis Components			
Ferromanganese oxide	0.9454	0.8364	0.9529
Iron oxide	0.8323	0.9277	0.9275

N.B. Factor analysis component has been recalculated to carbonate-free basis for comparability.

The geological implication is that two hydrothermal components are present in the majority of the samples. The Fe-rich component is present at >10% in all samples whereas the Fe-Mn-rich component is predominantly found in As/Bu and Bu Group samples rather than in As/Ls Group samples in which it has been very much diluted by other components.

4.7.3 Siliceous component and siliceous element associations

The effect of using a siliceous component calculated from factor analysis results has a profound effect on the results of linear programming. In the Dymond (1981) model and the Modified version, the Si-rich component is termed "Biogenic" and is calculated from marine plankton data. In contrast, the factor analysis Si-rich component may be derived from more than one source and is likely to be both biogenic and hydrothermal in origin. Linear programming using the Modified Dymond (1981) end-members correlates less closely with factor analysis (Figure 4.8) compared with using factor analysis-derived end-members (Figure 4.9) for the reason that, in the former, the silica is assumed to all be of biogenic origin. The differences between the elemental ratio coefficients, calculated (1) from average plankton and (2) from whole rock data by factor analysis, suggest that the Si-rich component of Oman sediments is not of entirely biogenic origin.

As a result of using the factor analysis-derived "Si-rich" end-member in linear programming, the problem has been minimized which was previously caused by attempting to differentiate pure Si into more than one source. By ignoring the origin of the Si, but by concentrating on the elemental associations of a multiple-

source, Si-rich component, the non-lattice → lattice transformations that may have affected some elements, e.g. during diagenesis, can be accommodated without affecting the accuracy of the model for the other components (Chester, 1990). The correlation between factor analysis and linear programming predictably improves, since both methods adopt the above assumption (Table 4.27).

Table 4.27 r^2 values for calculated silica-rich component content

	r^2		
	As/Bu	Bu	As/Ls
Modified Dymond (1981) Model Components	0.6477	0.1814	0.3226
Factor Analysis Components	0.9515	0.8388	0.8719

The effect of adopting the local Si-rich end-member has been to minimise the greatest source of error in the linear programming model, since Si, with Fe, is proportionately the largest constituent of the sediments. As a result, the other components, which all contain a proportion of Si, are more accurately estimated and the sum of the squares of the residuals has been reduced (Figure 4.8 and Figure 4.9).

4.7.4 Conclusions

The aim of using a linear programming model in this study has been to quantify the relationships that exist between the bulk sediment composition and the sediment-forming components, and to adapt a methodology which is suitable for application to the Oman metalliferous sediments. Previously in the literature, ancient metalliferous deposits have been classified as heterogeneous admixtures of phases which are derived from different sources. In this Chapter, by using selective chemical leaching and linear programming, the sediment-forming components have been identifiable and their composition calculated. From this information, it has also been possible to calculate the proportion of component in each sediment sample. The components not entirely dissimilar to measured components that are thought to comprise modern sediments from active rise-crest environments.

For the purpose of this study, factor analysis calculated that a five-fold component framework is necessary to explain the variation in the data-set. The

acceptance or rejection of the linear programming results is based on three criteria: (1) that measured bulk content, E_T(meas), is significantly correlated with calculated bulk content, E_T(calc); (2) that all of the resultant end-member source data are comparable to other published work and that there is compatibility between the results of the linear programming model and the conclusions already drawn in earlier Chapters of this study; and (3) that the conclusions drawn are geologically realistic.

By repeatedly running the linear programming method with different hydrothermal end-member elemental ratios, the optimum results were eventually obtained. For the elements Fe and Mn, the values for r^2 from the trend-lines on scatter plots of $E_{T(meas)}$ versus $E_{T(calc)}$ equalled 0.999, and r^2 values for Si and Al equalled 0.984 and 0.937 respectively. The fit of the Modified Dymond model has subsequently been improved by using local end-members. The improvement is in terms of (1) reducing the sum of the square of the residuals; and (2) improving the positive linear correlation between factor analysis results and linear programming. This means: (1) the measured chemical composition data have been converted by this model into quantitative estimates of the weight percent of five different components; (2) the distribution pattern of the elements has been quantified; and (3) the correlation between linear programming and factor analysis output supports the validity of both methodologies. On this basis of the statistical evaluation of the methods, and the comparability of the results presented in the previous chapters, the independent methodologies will now be interpreted in Chapter 5 with caution to model rise-crest sediment-forming processes

CHAPTER 5
Discussion and conclusions

5.1 Discussion

The aim of this chapter is to discuss a geological interpretation of the results which have been presented in the previous chapters. The high quality of the sample preparation and analytical procedures (Appendix A) has been relied upon in the subsequent application of linear programming modelling, factor analysis and chemical partitioning analysis. The overall objective of this project is to produce and present the data necessary to model the formation of the Oman metalliferous sediments. In the following sections, a model will be proposed which attempts to explain the geochemistry of the Oman metalliferous sediments in terms of sediment-forming processes and the evolution of the ophiolite.

5.1.1 Ocean-wide sediment-forming components

The component compositions which have been used in the literature to explain *plate-surface* sediments have used average values and have only attempted broadly to define the interaction of the components on a regional scale. This study has so far concentrated on the rise-crest environment because all of the possible sources which contribute to marine sediments are also found in rise-crest metalliferous sediments. The advantage of using rise-crest samples has been that the hydrothermal component was investigated in more detail. Each methodology used in this study has resulted in the subdivision of the "hydrothermal component". The redefinition of the hydrothermal system by this study is the principal development of the Dymond (1981) and Leinen and Pisias (1984) terminology. By using an average EPR sediment as representative of "hydrothermal" input, previous models have: (1) overlooked the non-hydrothermal contribution to rise-crest processes; and (2) ignored the variability in hydrothermal fluid compositions, physical homogenisation of the sediment, and non-uniform distribution of hydrothermal system in the rise-crest area. Using local end-member components derived from the paleorise-crest environment it has been possible to overcome these problems, and in doing so, it has been possible to explain

the volcanic stratigraphic differences in the Oman metalliferous sediment, which have previously not been identified.

What are termed *background* signals of the plate-surface sediments (i.e., authigenic minerals, carbonates, opaline silica and detritus), are the result of ocean-wide processes which occur irrespective of hydrothermal input. The results of linear programming have confirmed that, at the rise-crest, the background signals have been variably diluted by localised hydrothermal input. Hydrothermal input is termed a signal *spike*, since hydrothermal components are a relatively localized perturbation in the marine system.

Detrital background signal

The detrital background signal is incorporated into the sediments as particulate crystalline matrices of lithogenic minerals. XRD has identified a potential detrital component, and the composition of the detrital component has been calculated from chemical leaching experiments. Previously, models of the Oman ophiolite have discounted contribution to the metalliferous sediment composition from detrital sources (Karpoff *et al.,* 1988). Because of the very low amounts of detrital material present (Table 5.1), it is quite likely that this background signal results from the inclusion of volcanic glass associated with the contemporaneous magmatic events. The composition of the detrital end-members calculated by this study have been plotted on bivariate charts (Figure 5.1) with: (1) the Oman lava (Alabaster *et al.,* 1982; Alabaster and Pearce, 1985); and (2) the detrital end-member compositions used in previous linear programming studies (Dymond, 1981; Leinen & Pisias, 1983). By comparison with previous linear programming models, this study much more closely matches the proposed detrital end-member composition to the lava composition. From Figure 5.1, Fe and Mn content of the end-members in this study closely match the measured lava compositions. The factor analysis technique, which was used to calculate the compositions, has tended to underestimate the Al_2O_3 content by as much as 2 wt% and the SiO_2 content by as much as 15 wt%. Despite this, the factor analysis end-members are demonstrably a better fit for detrital component than are the average values used in the previous models (Figure 5.1).

Figure 5.1 Detrital end-member compositions

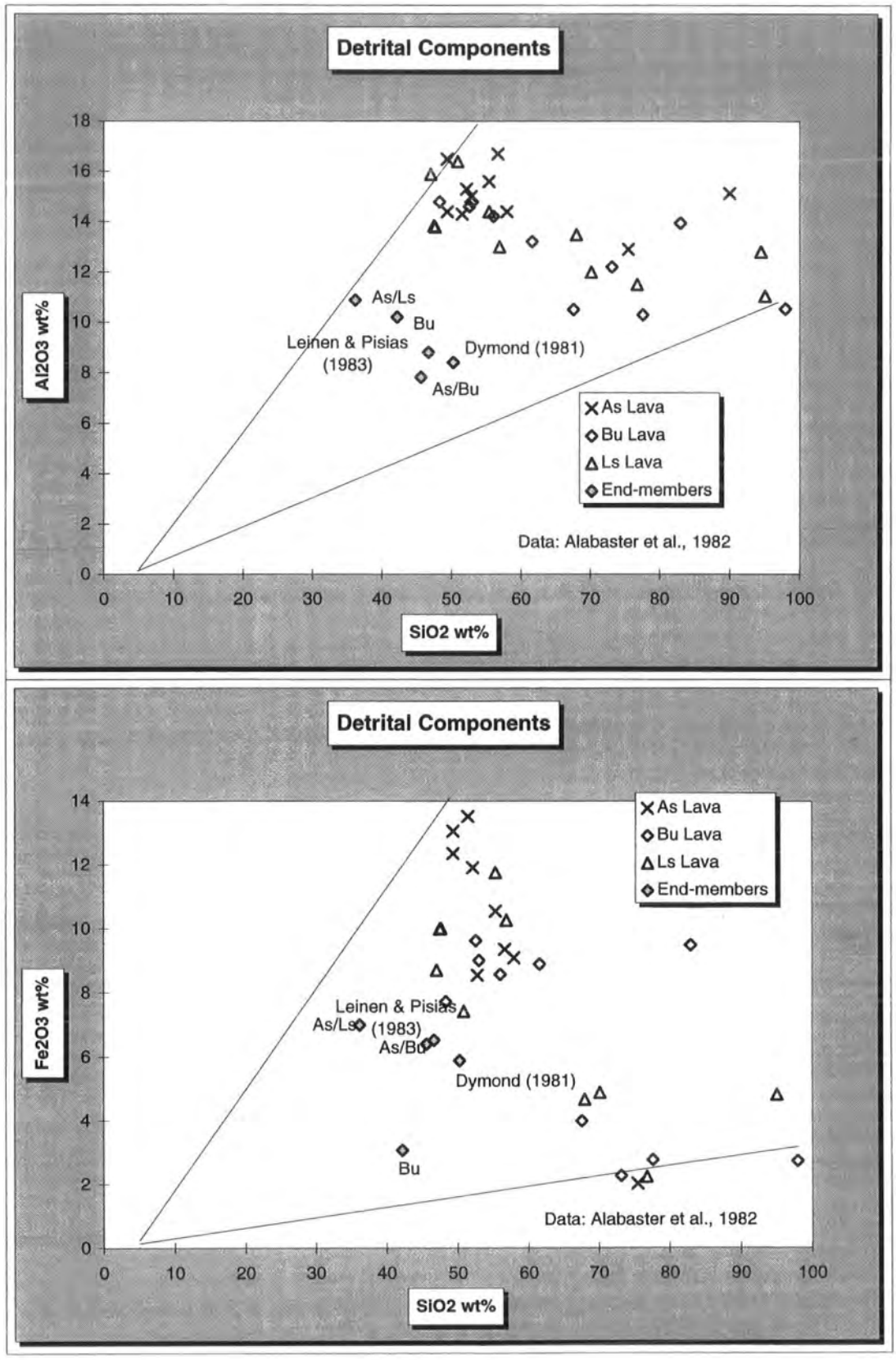

Figure 5.1 ctd. Detrital end-member compositions

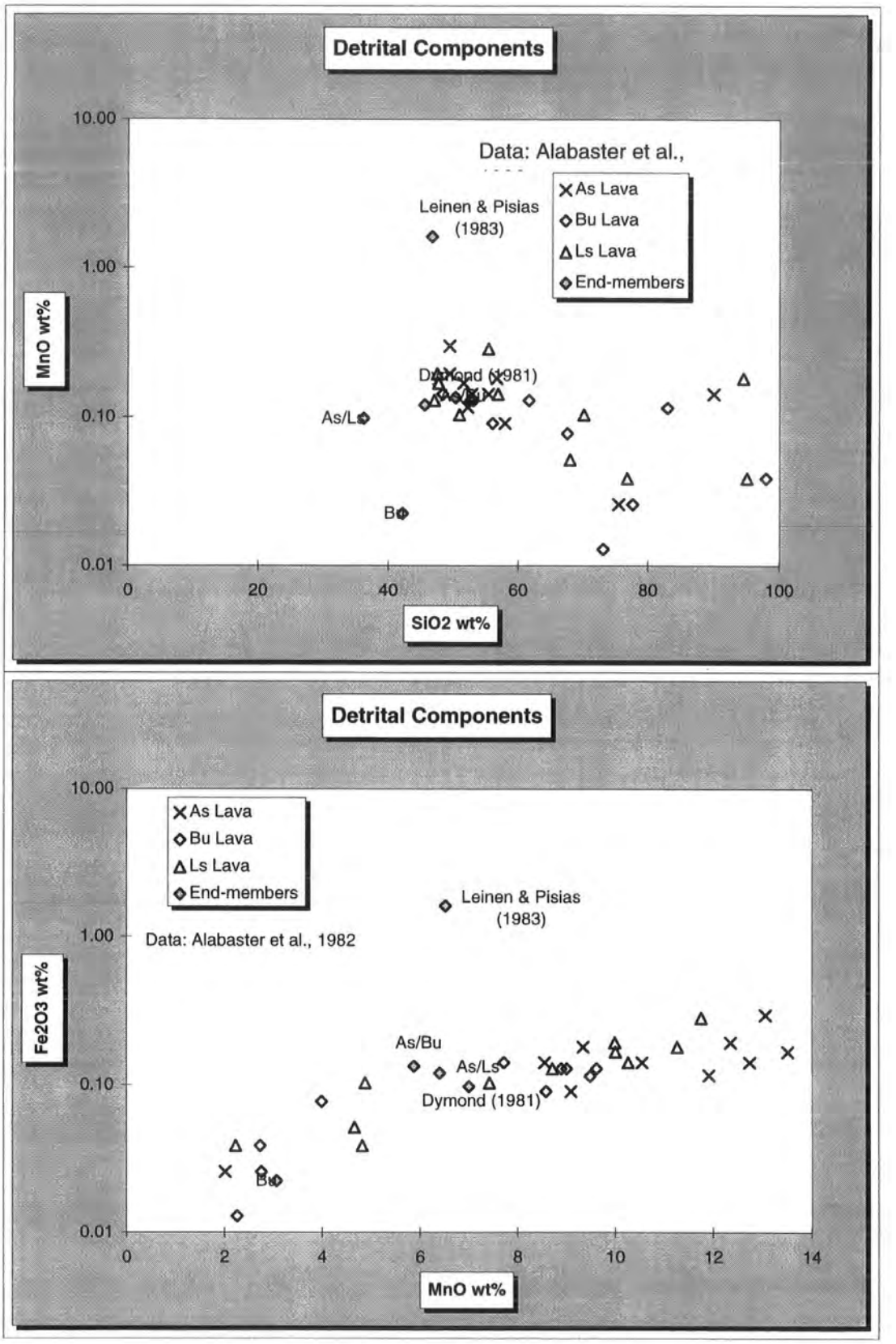

Siliceous background signal

The pure biogenic opal which has been used in previous models of recent sediments has not been recognised by factor analysis in this study (Figure 5.2). In contrast, a siliceous component has been identified, in this study, which is compatible with a combined hydrothermal and biogenic origin. The Fe_2O_3 and SiO_2 contents of the end-members that have been calculated by factor analysis (Figure 5.2) are compatible with: (1) the biogenic end-member measured from marine plankton (Martin and Knauer, 1973) and used in the linear programming model by Dymond (1981); and (2) the biogenic end-member calculated using factor analysis by Leinen and Pisias (1984). In contrast, the MnO and Al_2O_3 contents of the siliceous end-member, calculated in this study, are incompatible with solely biogenic origin. Hence, this study uses the term "siliceous component" to describe the Si-rich end-member. The siliceous component is, on average, as important a component of the sediments as the hydrothermal component (Table 5.1). Other studies have attributed the Si-content of the Oman metalliferous sediments to biogenic sources (e.g. Karpoff *et al.*, 1988), but it is more likely that Si-content is derived from both hydrothermal and biogenic sources, and has been affected by subsequent diagenetic reaction.

Carbonate background signal

The carbonate component was not used in the Dymond (1981) calculation, and for comparative purposes was also omitted from that of Leinen and Pisias (1984). In contrast, it has been included in this study for completeness. The proportion of carbonate component in the Oman metalliferous sediments is primarily a function of variable hydrothermal input, the effect of which is to swamp the carbonate background source in the vent proximal areas.

Hydrothermal signal spike

At the rise-crest depositional environment, the ocean-wide *background* signals are diluted by the effects of hydrothermal activity and diagenesis. The hydrothermal source locally superimposes a range of elements that have not been derived directly from seawater by pelagic sedimentation. In the ocean-wide context, the effects of diagenesis, hydrothermal activity, cosmogenous input, and anthropogenic contaminants may be termed perturbation spikes. In this study, the hydrothermal *spike* is the only such component directly recognised by factor analysis. The effects of diagenesis are implied by the difficulties in unscrambling the origin of the siliceous component. In previous models (Figure 5.2), a single hydrothermal component has

Figure 5.2 Comparison between hydrothermal end-member components

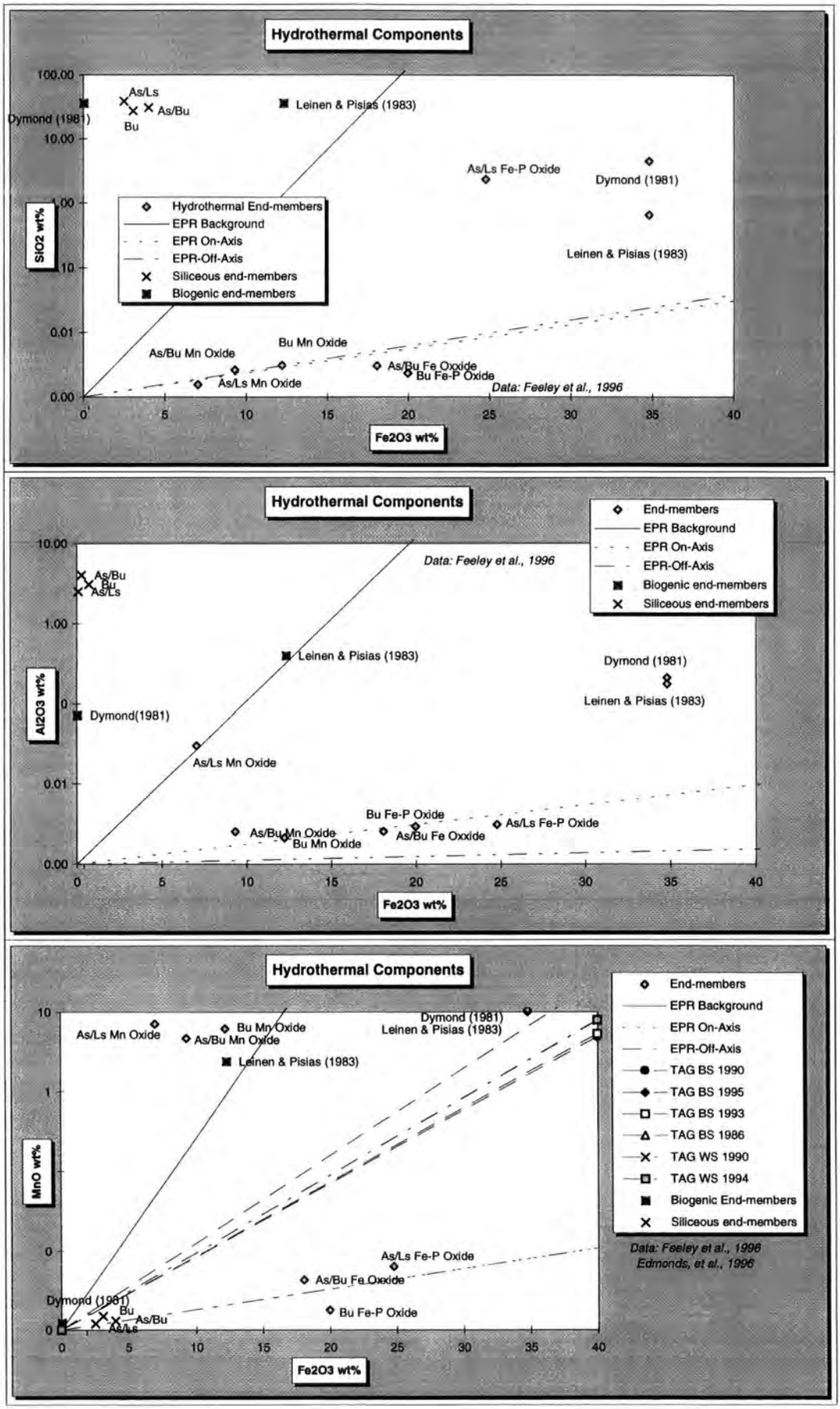

Figure 5.3 Detrital versus hydrothermal components

(a)

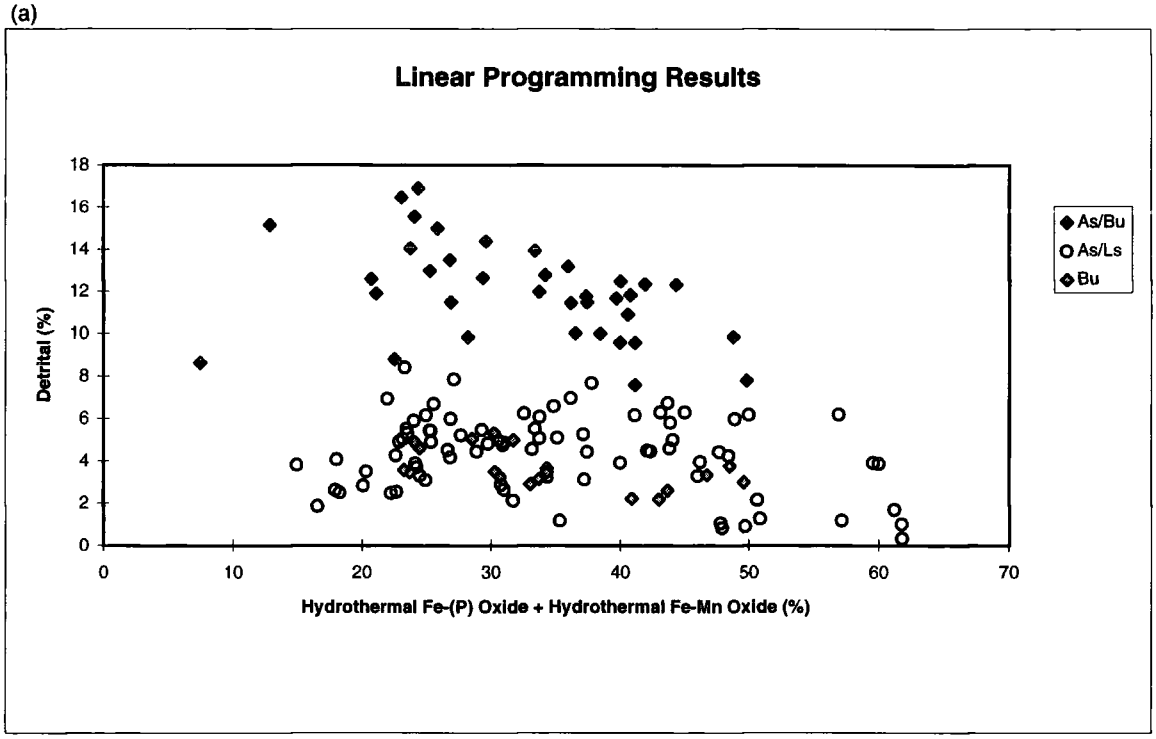

Carbonate versus hydrothermal components

(b)

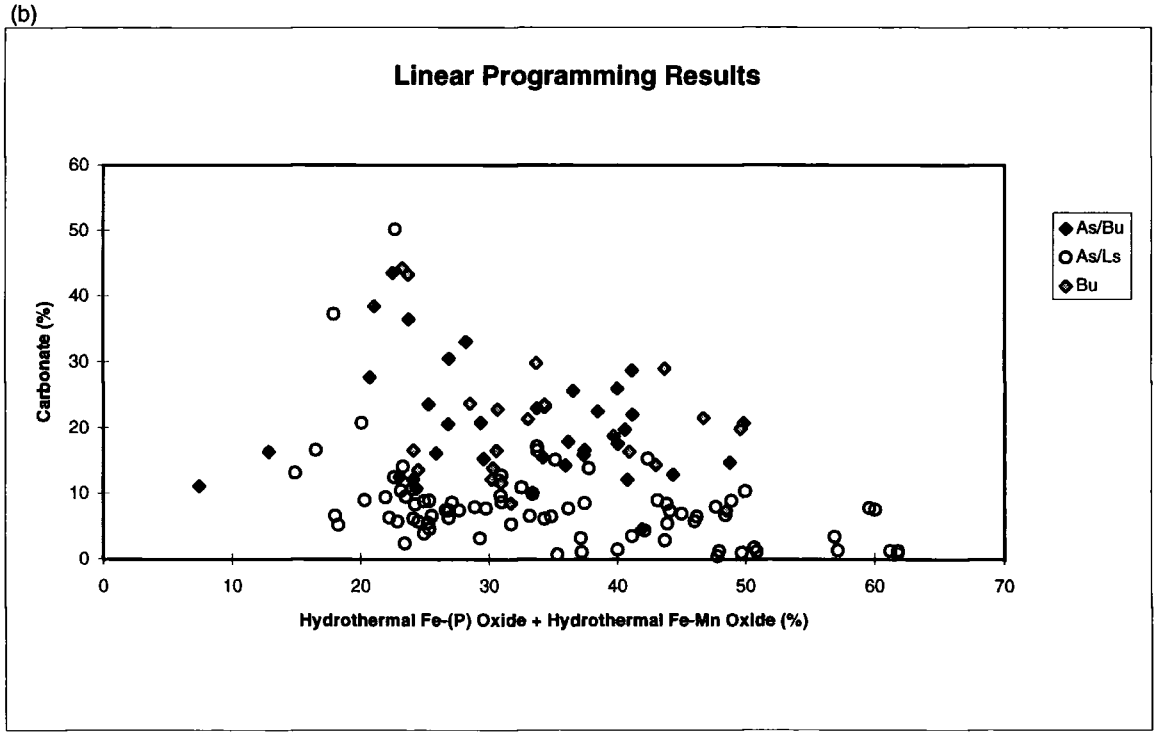

been used (Figure 5.2), approximating to the contemporary TAG hydrothermal end-member fluid composition (Dymond, 1981; Leinen & Pisias, 1984; Edmonds, *et al.,* 1996). In contrast, factor analysis output has suggested that separate ferrous and ferromanganese components have contributed to the sediment-forming process. The calculated hydrothermal *Fe-rich component* compositions (this study) very closely resemble the major element ratios of EPR suspended plume particulate composition (Feely *et al.,* 1994; Edmonds *et al.,* 1996). The plot of MnO/Fe_2O_3 (Figure 5.2) suggests that the *Mn-rich component* compositions also closely resemble EPR background particulate ratios. The geological implications of this are that (1) the Mn-rich component is probably largely of hydrothermal origin, and (2) its incorporation into sediment does not occur as physically close to the vent or as temporally close to the period of venting as the Fe-rich hydrothermal component.

In summary, the above discussion sets out a framework which enables the geochemistry of the Oman samples to be interpreted in terms geological processes which occurred at or near the Oman rise-crest during Cretaceous time, and which are currently occurring at the EPR. The usefulness of the methodology used is that a more representative set of samples may be obtained from the ophiolite than from active hydrothermal systems. The evidence of the calculated component compositions also suggests that the background signals were similar in composition to those incorporated into recent sediments.

In each volcanic stratigraphic position, similar component compositions have been calculated from the bulk-rock data by factor analysis (Figure 5.1 and Figure 5.2). This confirms one of the original propositions of this thesis, i.e. that geochemical variation in the Oman sediments may be explained by variable mixtures of fixed-composition end-member components. The exception to this is that the composition of the hydrothermal source is not fixed, and that compositional variation is a function of volcanic stratigraphic position.

5.1.2 Environmental variation in the rise-crest environment of deposition.

By using factor analysis-derived end-member components and linear programming, the broad distinctions between depositional environments represented in the Oman ophiolite have been described (Table 5.1). Volcanic stratigraphic position has been the underlying controlling factor on metalliferous sediment composition because it represents the different environments in which the sediments formed. On the upper

Figrue 5.4 Detrital versus Total Hydrothermal components

(a)

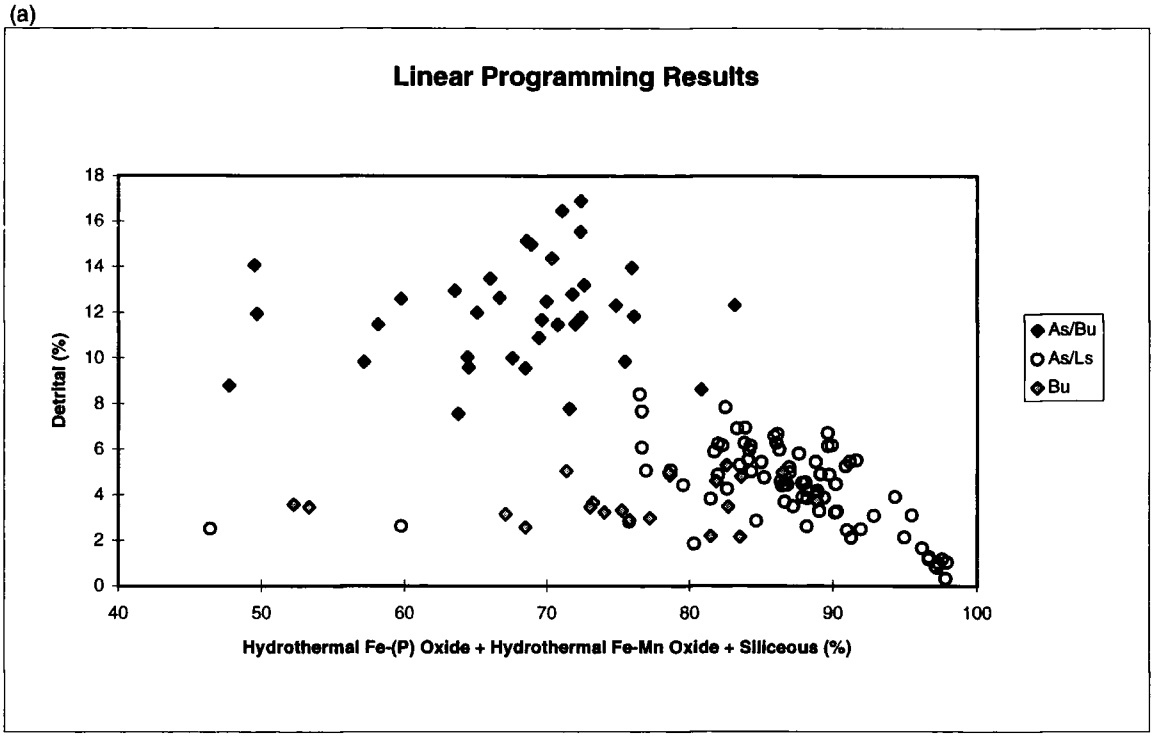

Carbonate versus total hydrothermal components

(b)

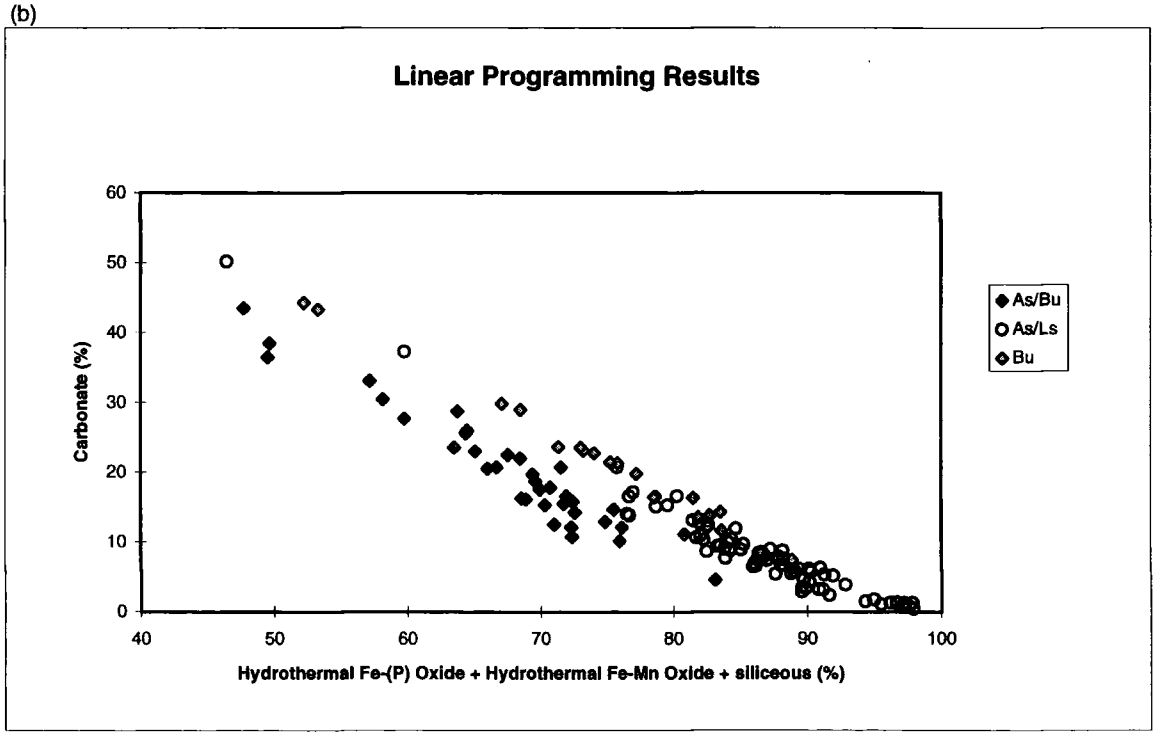

Figure 5.5 Fe-rich end-member versus total hydrothermal input

(a)

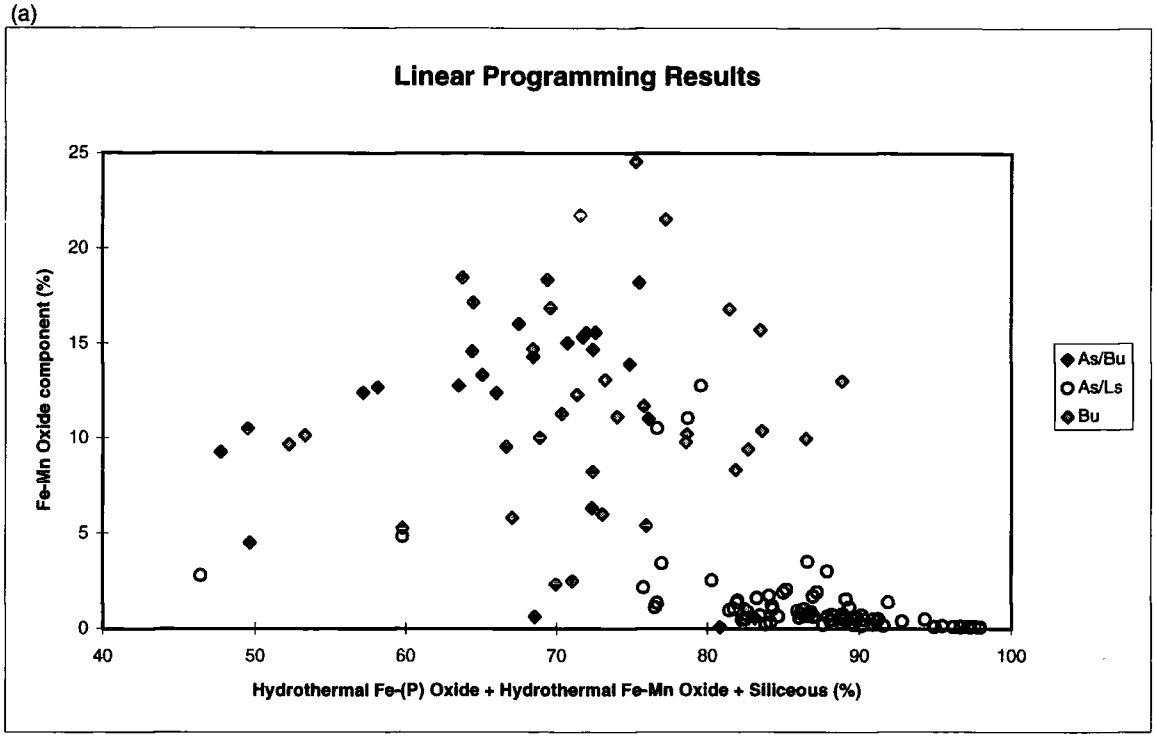

Fe-rich end-member versus total hydrothermal input

(b)

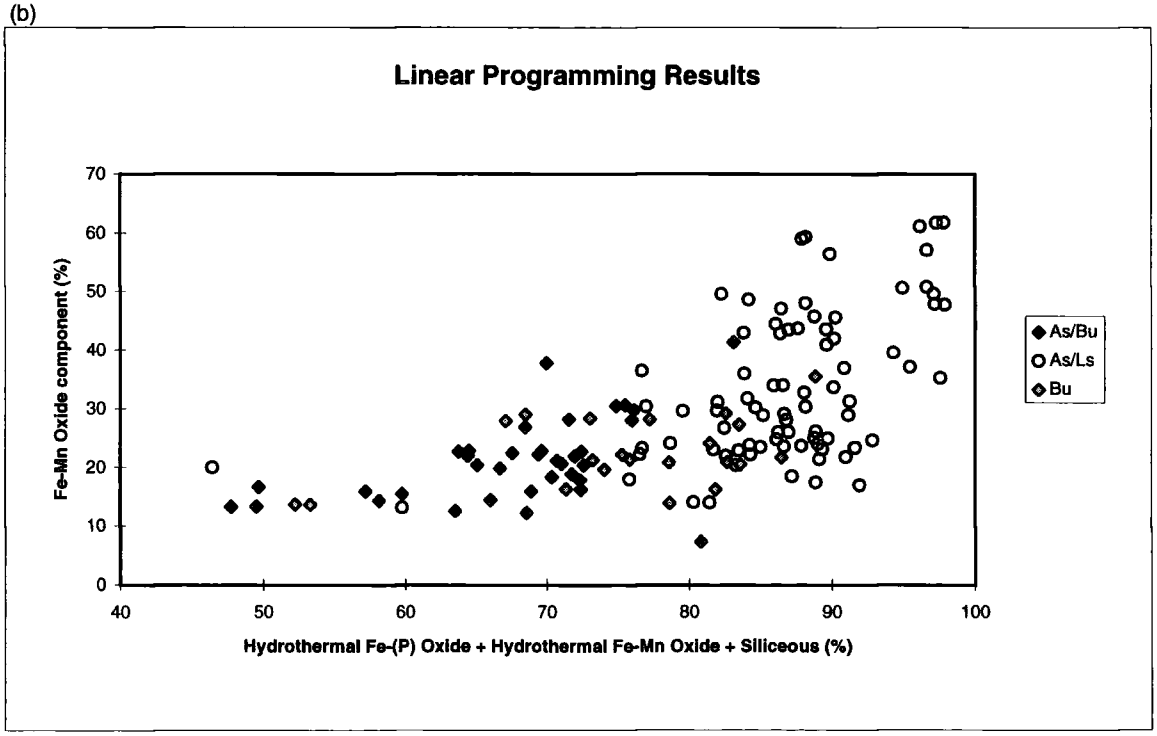

surface of the lower (As) lavas, there were at least two environments of deposition. The characteristic sediments have strongly suggested that two hydrothermal systems were in existence which have resulted in two broadly different types of metalliferous sediment being produced. One system mostly produced Mn-rich sediments, and the other produced mostly Fe-rich sediments. Individual samples illustrate the range of sediment-forming processes found in each of the broad environmental divisions recognised. The range of calculated sediment component contents was tabulated in Chapter 4.

The bimodality of whole-rock geochemistry defines the sphere of influence of two hydrothermal systems. The complex relationship between Fe_2O_3 and MnO, and the resulting complex relationship of the trace elements to Fe_2O_3 and MnO (Chapter 2), highlights the geochemical evidence for non-uniformity in the sediment-forming processes. In other words, the geochemistry is evidence of the presence, absence, or variable relative proportions of the main sediment-forming minerals which control the major element composition of the sediment. The output of the various methods employed in this study strongly suggests that different hydrothermal sediment-forming processes occurred penecontemporaneously, but at spatial separate locations, on the palaeo-rise crest. Using the end-member composition framework to infer geological processes that this study has adopted, it is now possible to explain the geochemical complexity of the Oman metalliferous sediment dataset.

Table 5.1 Average end-member source contribution

Component	As/Ls (%)	As/Bu (%)	Bu (%)
Hydrothermal Mn Oxide	1	11	-
Hydrothermal Fe-Mn Oxide	-	-	11
Hydrothermal Fe Oxide	33	21	22
Siliceous (hydrothermal/biogenic)	51	35	41
Detrital	4	12	3
Biogenic Carbonate	8	19	20
Phosphate	0	-	-

One of the principal findings of the previous chapters, after identifying the complexities in the geochemical data set, was that this may be caused by non-

uniformity in the hydrothermal contribution to rise-crest metalliferous sediments. Because the major element composition is controlled by the sediment-forming minerals, it has been possible to define the probable source of the major elements. Because there is less complexity in the components which formed the *background* signal, these will be dealt with initially, with emphasis on the uniformity of composition, and the processes controlling their relative abundance.

The Al_2O_3, MgO and TiO_2 content of the sediments seems, from the factor analysis distribution of those elements between the components, to have resulted almost exclusively from the inclusion in the sediments of rock detritus or volcanic glass in association with calcareous ooze (which is the predominant Ca source). Chemical separation of the sediments suggests that Al, Mg, and Ti have been concentrated in the insoluble residue. The chemical separation methodology has been designed to leave the aluminosilicates and more resistant silicates, made up of lava-derived lattice-held clay minerals, as an insoluble residuum (Balistrieri and Murray, 1986; Miller and Cronan, 1994). Factor analysis using Varimax rotation has also identified the presence of a relatively uniform detrital component made up of the following elements TiO_2 - Al_2O_3 - MgO - Zr - Ni - Sc. These end-members are calculated to be of relatively uniform composition throughout the study area. Moreover, the similarity with recent deposits suggests that biogenic calcareous ooze formed part of a uniform ocean-wide background source, and that the detrital content is derived from, and reflects geochemically, the variability of the local lava units with which it is related. Consequently, in Chapter 2, the relationship between the trace elements and the non-hydrothermal major elements was demonstrated to be a simple one in that there is no spatial control on the relationship of the trace elements to the non-hydrothermal major elements. The evidence clearly supports the detrital origin of the trace elements Sc, Ni and Zr. The minerals involved in the detrital content are plagioclase, clino-pyroxene and clay minerals.

The element Ca is consistently positively correlated with Cr in factor analysis data, and is not associated with any of the trace elements for which partition data are available. From partition analysis, the carbonate mineral constituents which are stripped from the sample in the acetic acid fraction include Mg, Cu, Co, Cu and Zn, which are all present at very low levels (3% - 4%). Some variety in the carbonate composition might be expected since calcite, huntite and ankerite were all detected in XRD analysis.

Figure 5.6 Geochemical variation by mine location

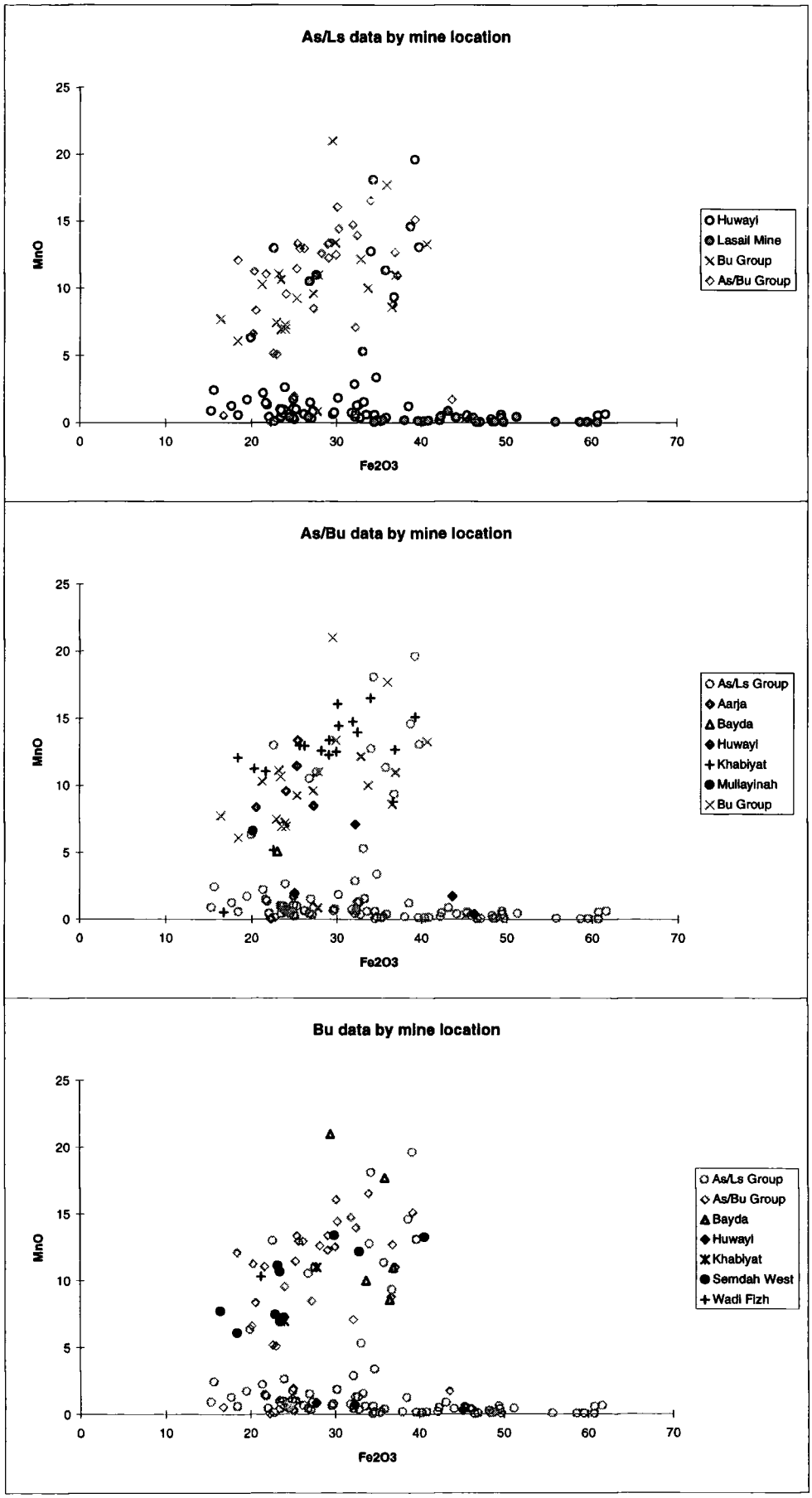

Figure 5.7 Al2O3 versus TiO2 evidence for detrital component in carbonate ooze

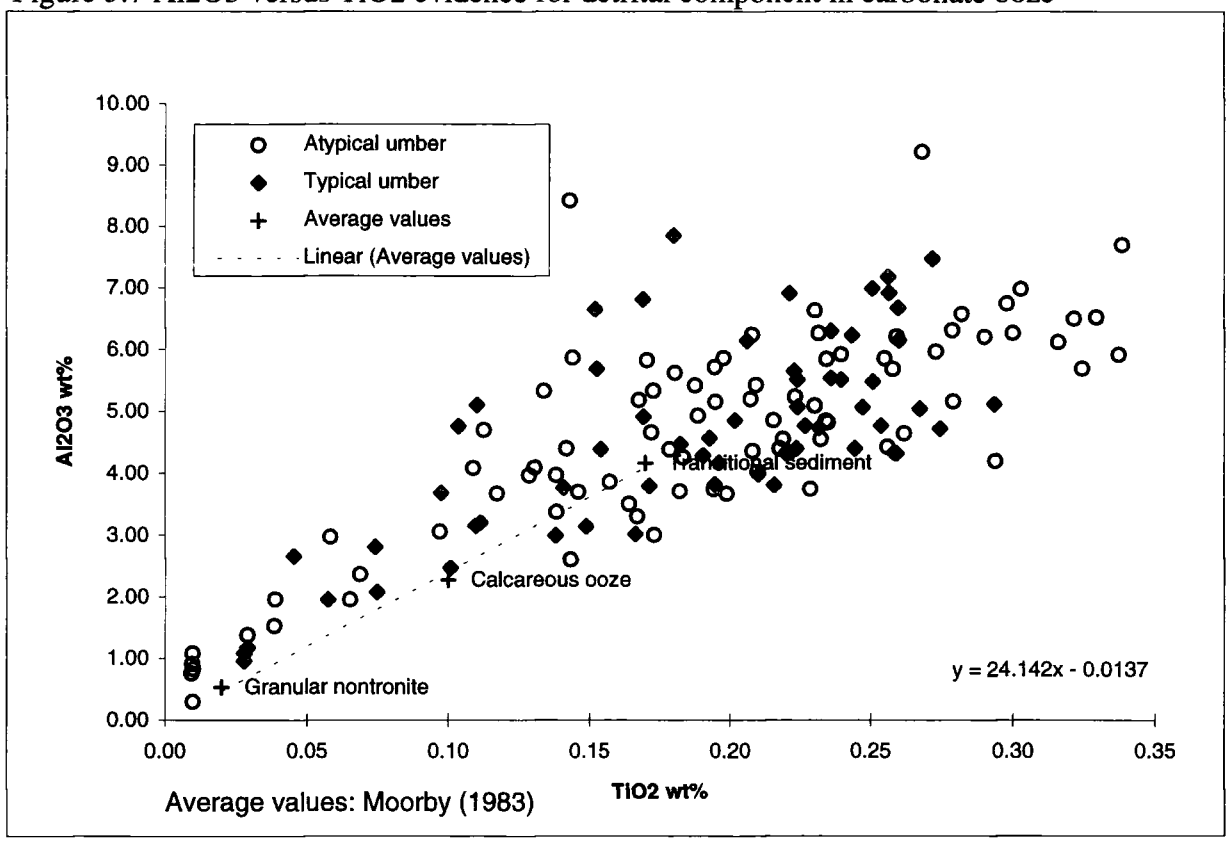

The abundance pattern of the two significant *background* signals from linear programming is summarised above in Table 5.1. The biogenic carbonate is more abundant in the As/Bu (19.8%) and Bu (20.6%) environments than the As/Ls environment (8.6%), whereas the detrital component is more abundant in the As/Bu locations (12.3%) than the As/Ls (4.32%) and Bu environments (5.72%). The linear programming results confirm the whole-rock data in that As/Bu and Bu group samples are more Ca-rich than the As/Ls Group samples. This is to be expected since factor analysis and partition analysis provide evidence of a single element source for Ca. Although the relationship between detrital content and Al content is not so clear, the particularly low levels of detritus in As/Ls Group samples are probably explained by the subgroup of 11 samples with unusually low Al content (<2 wt%). In order to explain these phenomena, geological sediment-supply mechanisms must have existed which explain the distribution observed pattern.

The plots of detrital component or carbonate component versus the Fe-rich + Fe-Mn-rich components (Figure 5.3), result in a poor negative correlation. When the siliceous component is added to the category axis (Figure 5.4), a negative linear correlation is observed when plotted against both detrital and carbonate components. This is important evidence to support the theory that a significant proportion of the siliceous component is of hydrothermal origin, and this at least confirms that increase in the silica component reduces the detrital and carbonate contents. Although the effects of closure should not be ruled out, it is likely that the siliceous component would positively correlate with the other *background* components if the processes controlling its incorporation into the sediment were entirely unrelated to hydrothermal activity. The diagrams are strong evidence of the effect of hydrothermal input swamping the background signal so that detritus and carbonate material, accumulating at similar rates on an ocean-wide scale, is relatively diluted where hydrothermal precipitation is greatest. Furthermore, evidence has been presented which clearly demonstrates the dissolution of carbonate by hydrothermal activity.

The geological implication of the plots of Total Hydrothermal Content versus background components is that there is evidence for variable hydrothermal activity at the rise-crest study area. This evidence supports the theory that metalliferous umber-type sediments are an admixture of components. The samples in which total hydrothermal input is greatest appear to be from the As/Ls Group, whereas total hydrothermal input is lower in samples mainly from the As/Bu and Bu Groups. Consequently, in the former samples, carbonate and detrital contents are much lower than in the latter samples, which is in indication of a slower rate of deposition and less intense hydrothermal activity. If bottom water currents were unsuitable for hydrothermal particulate matter to be deposited after precipitation from solution, then biogenic and detrital content would also be affected proportionately.

To clarify the role of siliceous sedimentation at the ancient paleoridge environment, it is useful to refer to the literature describing the restrictions on siliceous oozes in modern oceanic environments. Formation of siliceous ooze is controlled by fertility of the surface waters (i.e., nutrients), depth, temperature, time, and Ca + clay content (Kastner, 1981; Pisciotto, 1981). Because conditions of high fertility and high ocean water Si-content are highest in the equatorial belt, the formation of *biogenic* siliceous oozes is confined within the equatorial belt below the CCD. The axial zone of the Oman paleoridge was located within this fertile equatorial region throughout the

period during which the sediments in this study were formed (Thomas *et al.*, 1988). However, ocean spreading events and volcanic episodes often correspond to siliceous epochs (Adachi *et al.*, 1986) suggesting that the Si-content of sediments formed at a spreading ridge is also supplied by hydrothermal fluids or by halmyrolysis. Furthermore, in the Oman ophiolite, the normal pelagic sediment which is preserved above the last volcanic events is calcareous rather than siliceous (Fleet and Robertson, 1980); this is evidence supporting a *hydrothermal* siliceous source.

The linear programming evidence suggests, not only that the intensity of hydrothermal input is lower in some samples than others, but also that this affects which hydrothermal end-member predominates. In the samples where hydrothermal input is low, the hydrothermal component is of a different composition from samples in which hydrothermal content is high (Figure 5.5). The Mn-rich component dominates the hydrothermal input where total hydrothermal input is lowest, and the Fe-(P)-rich component dominates where total hydrothermal input is greatest. A spatial dimension to this pattern is evidence for the existence of different penecontemporaneous hydrothermal systems at different locations on the palaeo-rise-crest. The Axial lava surface, on which the principal deposits are located, has been defined in this study as a boundary between the spreading event lava below and seamount event lava (As/Ls) or rifting event lava (As/Bu) above (Pearce, 1980; Pearce *et al.*, 1981; Alabaster *et al.*, 1982; Alabaster and Pearce, 1985). The linear programming modelling suggests that the hydrothermal processes acting at the As/Ls boundary differed from those acting at the As/Bu boundary. The difference between the two approximately contemporary locations is defined by the intensity of and proximity to the active hydrothermal systems. It is therefore the hydrothermal processes which cause the greatest complexity in the data set, rather than the background processes which appear to constant throughout the study area from the evidence presented in this study.

5.1.3 The hydrothermal environment at the paleoridge

The use of the term "metalliferous sediment" to describe the Oman sediment, has no significance in terms of ascribing to them a hydrothermal origin. Deep sea red clays which form as a result of dissolution of biogenic oozes have a similar geochemistry to the Oman metalliferous sediment (Karpoff *et al.*, 1988), and so one of the principal aims of the project has been to re-examine the hypothetical hydrothermal contribution. Previously, the Oman umbers and ochres have been described as hydrothermal precipitates formed in an off-axis volcanic arc setting (Pearce *et al.*, 1981). Recent studies of active hydrothermal vents at spreading centres are characterised by non-uniform sub-seafloor processes, for which the evidence is the wide range of

temperatures, compositions, flow rates and precipitates (e.g., von Damm *et al.*, 1985; Alt *et al.*, 1987; Feely *et al.*,1994, 1996). The metalliferous sediments from Oman provide a convenient means of studying non-uniformity in the hydrothermal processes from a paleo-spreading centre.

The evidence of the partition analysis and linear programming in this study suggest that at least two hydrothermal end-member components are incorporated into the sediments. The simplest interpretation of the linear programming components and partition analysis components (Chapter 4) is that they represent end-members formed at variable distances from the late Cretaceous spreading centre. The two end-members which have been identified are: (1) a Mn-rich component with variable Fe-content; and (2) an Fe-rich component with insignificant Mn-content. The presence of apatite and carbonate apatite probably result from the hydrothermal supply of P.

The ferrous oxide component is associated with P and Ni (factor analysis and chemical partition analysis). A hydrothermal supply of phosphorous from fast spreading ridges has been established, (Kolodny, 1981), including the incorporation of P in solid solution in Fe oxyhydroxides at active hydrothermal sites (Fox, 1991). Bivariate plots against Fe_2O_3 of the elements Zn, Cu, Co and As closely resemble that of MnO versus Fe_2O_3. The trace elements do not correlate with Fe except in the circumstances in which Fe has a positive linear relationship with Mn. Consequently, the trace elements are associated with the ferromanganese component of the sediments whereas the Fe-rich component is relatively trace element depleted. The strong correlation between the REEs, Fe and P suggest that these were originally associated with the Fe oxyhydroxides, but may have been transferred to apatite during diagenesis. All of these findings are consistent with recent studies of the EPR metalliferous sediments (Barrett and Jarvis, 1988; Jarvis, 1995). The Fe-rich component dominates the hydrothermal contribution at the As/Ls boundary where the hydrothermal systems formed as precursors to seamount event volcanism. The evidence suggests that the geological environment of formation was proximal to vent deposits, and may originally have included Ba-Ca sulphates and Fe-Cu-Zn sulphide chimneys that subsequently underwent alteration to Fe oxyhydroxides.

The ferromanganese oxide component is associated with Cu, Co, Pb and V in the chemical leaching experiment, and with Zn, Pb, As, Co and Zr in factor analysis calculations. This component is consistent with a lower temperature hydrothermal origin at a greater distance from the site of hydrothermal discharge. The result is that,

Figure 5.8 Schematic block diagram illustratng the model of off-axis metalliferous sediment-formation which is derived from the evidence of the Semail ophiolite of Oman. The diagram is not intended to be to scale. The two hydrothermal systems define two mixing trends on the Fe-Mn-Si plot. Each mixing line between pure Si

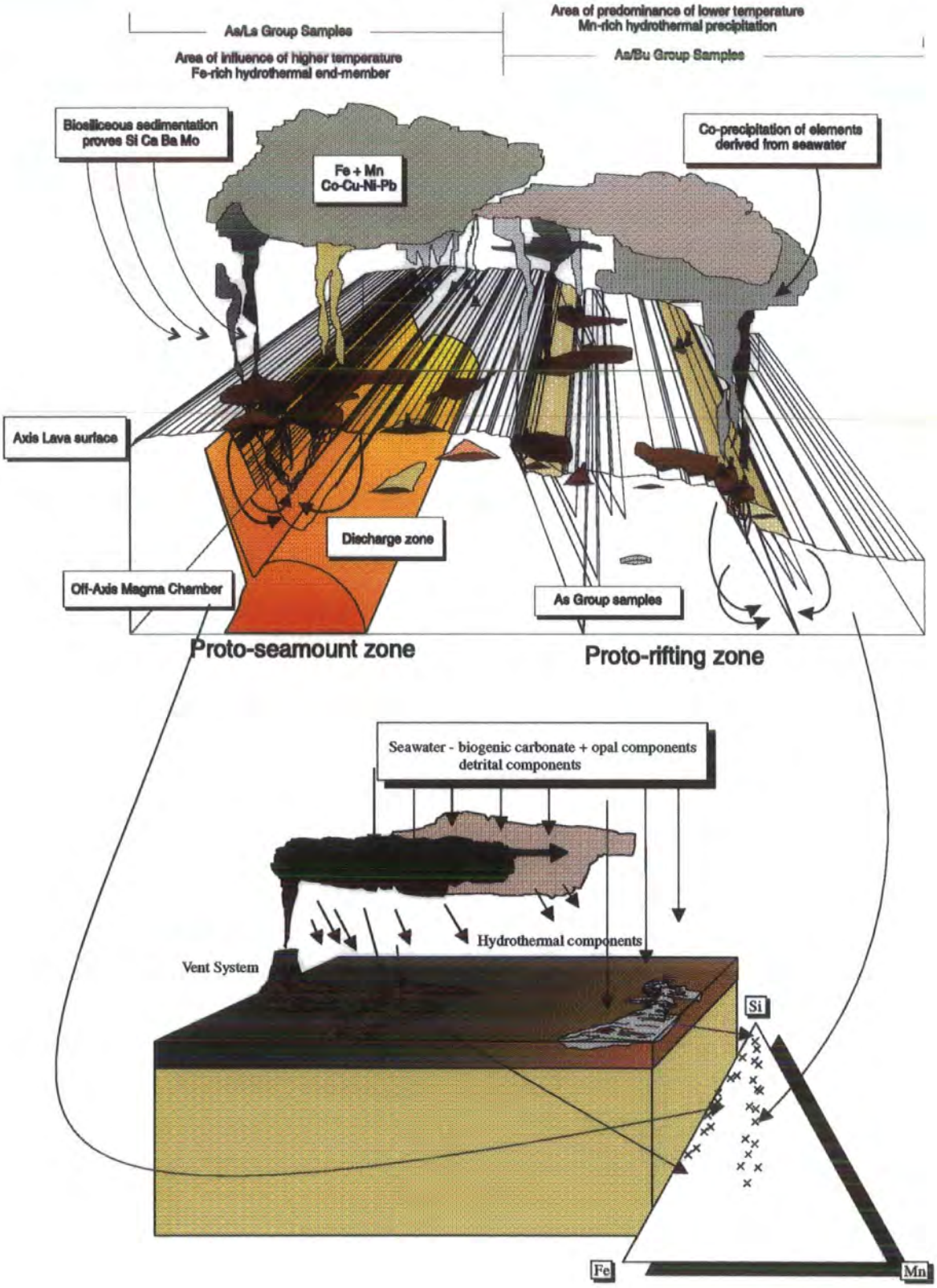

as a result of the greater time in suspension, hydrothermal Fe oxides accumulated Mn and other trace elements directly from seawater. This interpretation suggests that Fe reaching distal deposits has acted as a Mn scavenger.

Evidence was presented in the previous section supporting the role of hydrothermal fluids and halmyrolysis in siliceous sedimentation. Ternary plots of *Fe-Mn-Si* relationships show the overlap of the EPR rise-crest sediments with the As/Bu and Bu Group samples of the Oman paleoridge. By comparison, it is possible that pelagic silliceous input was as almost as important as the hydrothermal source in sediment formation.

5.1.4 Volcaniclastic supply or diagenetic alteration

The lack of detrital Al has been established (Chapter 2) in principal, in concurrance with other studies of the Oman sediments (e.g., Karpoff *et al.,* 1988). The association of Al, Ti, Mg and Sc in clays is one of the most clearly identifiable features of the factor analysis results. The clay content of the samples ranges between 0.0 and 8.0% from the linear programming data. Up to 66.3% Mg and 64.7% Al was reported in the residual fraction during chemical leaching. Although this evidence has been taken in pelagic sediments to represent detrital input, smectite clays, with similar compositions, may also result from hydrothermal transformation of the primary mineral assemblages during early diagenesis. The evidence in this study, which supports a diagenetic origin of clays, includes the very low content, and the highly crystalline form of the clay indicated by the factor analysis. However, the Al_2O_3/TiO_2 ratios very closely correspond to those of the local lava series, which strongly suggests that there may be a detrital component in the form of volcaniclastic material (e.g. hyaloclastic). The statistically significant positive linear correlation between Al and Ti falls on the mixing line between calcareous ooze and nontronite. Because the Al_2O_3/TiO_2 ratio is invariant and equal to that of calcareous ooze (~22) it is proposed that the nontronite-bearing sediments (XRD analysis, Chapter 2) are likely to have inherited the detrital content from the ooze. Mass loss caused by dissolution of the carbonate component has increased the relative Al_2O_3 and TiO_2 content beyond the content of carbonate ooze (Barrett, 1992). The evidence that dissolution has occurred thereby accounts for the diagenetic alteration of the detrital component suggested by factor analysis data and by other workers (Karpoff *et al.,* 1988). Nonetheless, the evidence clearly favours the inclusion of detrital clays, probably Al-smectite (Migdisov *et al.,* 1983), in carbonate ooze, and the concentration of the detrital component as a result of carbonate dissolution. This finding is not meant to imply

that the metalliferous sediments were in any way influenced by a proximal detrital source.

5.2 Conclusions

The evidence of the end-member components suggests that the hydrothermal environment of the Oman paleoridge was similar to that of the EPR at present. Although the chemistry of the sediments intercolated within the lava flows is non-uniform, there is a predictable correlation between geochemical composition and volcanic stratigraphic position. The most recent study of the Oman umbers by Karpoff *et al.,* (1988) recognises that there is some stratigraphic control, but fails to use a sufficient data-set to model the hydrothermal variation in detail accurately. The evidence provided by the interrelationship between magmatic and ore-forming processes (Alabaster and Pearce, 1985), suggests that at least two hydrothermal systems were active, one associated with the intrusion of the off-axis magma chambers which fed the Lasail Unit, and one associated with the intrusion of the Alley Unit magma chamber at a high level in the ocean crust (Alabaster and Pearce, 1985). The physical differences between the two hydrothermal systems may account for the differences in the hydrothermal end-members since the mineralogy, chemistry and paragenesis of the sulphide ores differ between the two systems. More recent data from the Landsat Thematic Mapper have confirmed that underlying some of the principal deposits are separate mappable discharge zones formed by upwelling hydrothermal fluids (Haymon *et al.,* 1989).

The earliest-formed metalliferous sediments in this study are found as rare, small, deposits within the spreading event (As) lava unit from Wadi Suq at a distance of 300m from the gossan. These deposits correspond in every respect to the As/Bu Group samples which are characterised by high Mn-content. The As Group samples in this study are not related to any gossans, and in no other study are ore bodies identified within the Axis lava. In this respect, this dissertation is consistent with other studies (e.g., Alabaster and Pearce, 1985) which suggest that the paleoridge was not the principal site of ore-forming hydrothermal processes.

Soon after the cessation of axial magmatism, off-axis magma chambers were emplaced at high levels within the still-hot basement. The local fracture zone and the near-surface heat source are thought to be the driving source of the hydrothermal system active prior to eruption of fresh lava onto the axial lava surface (Alabaster and Pearce, 1985). The As/Ls Group samples were taken from Lasail Mine, Huwayl and Mahab #2. The sediments at the Lasail mine outcrop within 25m of the gossan in a

50m exposure. At Mahab #2, the metalliferous sediments are located >500m from the gossan, and at Huwayl there is no evidence of a gossan at all. Despite the obvious differences, there is a striking similarity in the chemistry of the sediments which is irrespective of the variable distances from the principal discharge zones. On close examination of the Fe_2O_3 versus MnO plot (Figure 5.6), the Huwayl samples are the more Mn-rich and Fe-poor whilst still falling into the field defined by Fe-rich hydrothermal processes. In terms of the framework used, the Huwayl samples have probably undergone Mn-scavenging through longer residence in the water column than the Lasail samples. Six samples from Huwayl and two from the Lasail Mine exhibit the Mn-enrichment thought to occur with greater distance from the hydrothermal vent (Karpoff *et al*, 1988).

The As/Bu samples correspond to the Mn-rich Group and, in the simple classification system of Karpoff *et al.* (1988), represent distal facies of the same hydrothermal system that produced the As/Ls Group samples. The evidence in this study does not support this view, principally because of the field relationships of the samples to the gossans (Figure 5.6).

The As/Bu Group of samples no more exhibit a range of compositions analogous to the compositional aureoles found in the Atlantis II Deep (Cronan, 1980) than do the As/Ls Group samples. Because the outcrops of both sample Groups range from 25m to 1000m from the nearest gossans, it is only possible to conclude that two different hydrothermal systems existed. This confirms the Landsat data which suggests that each of the deposits is related to a separate discharge zone (Haymon *et al.*, 1989). Furthermore, the evidence presented has shown that the hydrothermal system which produced the As/Ls Group samples was of a more vigorous nature then the system which resulted in the As/Bu group samples. This is geologically reasonable, since the As/Ls system was the immediate precursor to proto-seamount magmatism, whereas the As/Bu system can only represent relatively minor hydrothermal circulation related to the beginning of inter-seamount rifting prior to the eruption of the Alley lava.

Having determined that there were at least two identifiable active hydrothermal systems, it is necessary to clarify some of their characteristics. The important point to note about the sediments is that they are principally a mixture of hydrothermal precipitates and biosiliceous sediments. The more (Fe + Mn)-rich sediments are the more hydrothermal rich, whereas the more (Si + Ca)-are the more biogenous. In Chapter 2, the SiO_2 versus Fe_2O_3 plot confirmed that the As/Bu Group samples are no less rich in hydrothermal content than the As/Ls Group samples which are described

above as resulting from a more vigourous hydrothermal system. Contrary to what might be expected, for a given Fe-content the As/Bu contain less Si than the As/Ls Group. In this Chapter, the range of Fe-content for both sample Groups is comparable (Figure 5.6), suggesting that, for both Groups, the full range from biosiliceous-rich to hydrothermal-rich sedimentation is represented. The linear programming data (Chapter 3) confirm that the full range of hydrothermal to siliceous sedimentation is present. Consequently, it is possible to conclude that, despite there being differences in the hydrothermal minerals precipitating, the two systems resulted in approximately equal rates of deposition. Of course, if higher temperature systems supplemented biogenic Si with hydrothermal Si, as the evidence has suggested, then the relative proportions of the components might remain approximately the same as in a lower temperature system.

The more Bu Group samples also exhibit Mn-enrichment characteristic of the As/Bu Group samples, but these formed at a time period after the volcanic hiatus during which sedimentation occurred on the Axis lava surface. The Semdah West deposits show the full range of biosiliceous to hydrothermal predominance. The Bayda samples are indicative of relatively more intense hydrothermal activity, which is in contrast to the Bayda sample from the younger As/Bu boundary that was one of the more biosiliceous. This may represent an intensification of hydrothermal activity in the inter-seamount region following the initial stages of Alley magmatism.

The metamorphic alteration phases which affected the lavas have also affected the metalliferous sediments (Pflumio, 1987; Karpoff *et al.*, 1988). The probability of diagenetic smectite clay formation has been discussed above. Other than this, the principal metamorphic facies is the epidotization of the samples, the evidence for which is presented in Chapter 2 from XRD analysis. Furthermore, XRD and factor analysis results show that the Mn oxide and "detrital" components are both well crystallized, probably as a result of burial diagenesis and early oxidative metamorphism. The XRD results from bulk samples revealed that quartz and hematite now dominate the sediments. Dissolution and recrystalization processes must be responsible for the conversion to hematite of the original Fe oxhydroxides that are prevalent in modern rise-crest metalliferous sediments.

5.3 Marine geochemistry at the Cretaceous Oman paleo-ridge: an overview

The first objective of this thesis was to present a reliable dataset on which discussion could be based. Having done this, this study has attempted to explain how metalliferous sediments of an ancient rise-crest environment fitted into the oceanic

chemical system. The second objective of this project has been to explore the range of techniques which have been previously applied to studies of metalliferous sediments, with a view to assessing the accuracy, comparability and value of each approach critically. Finally, the data has been interpreted to provide a new geological assessment of the sediment-forming environment. By applying numerical calculations and chemical leaching techniques, the questions posed in Chapter 1 have been discussed by identifying and quantifying the element pathways from source to sediment.

By comparison with ancient and modern sediments, this study proposes hypothetical physical, chemical and biogenic sediment-forming processes, and has compared the inferred processes to those which have been observed at sites of active hydrothermal systems on the ocean floor.

Essentially, the Oman paleo-ridge of the Cretaceous period was analogous in many ways to the hydrothermal sites which are currently being investigated on the EPR. The rise-crest environment is dominated by large fluxes of hydrothermal material from a number of vent fields which appear to be related to at least two approximately coeval hydrothermal systems. To attribute the geochemical variation of the Oman ophiolite merely to variable distances from the spreading centre, as most previous studies have done, is almost certainly an oversimplification which has been clarified using standard techniques which are more commonly applied to recent sediments (Figure 5.8). Moreover, the dominant role of the spreading centre in metalliferous sediment-forming processes is seriously called into doubt because of the relationship of the deposits to the lavas.

The domination of the system by hydrothermal fluxes of material is countered by an almost equivalent contribution of biosiliceous sedimentation. The varying ratio of biogenic to hydrothermal source contributions has determined the characteristics of the Oman sediments, which hitherto have all been inadequately termed *umber*. A broad spectrum of deposits have been studied, which range between the entirely hydrothermal to the more biosiliceous pelagic-like. The effect on geochemistry of spatial relationships between the sediment and the venting site have been identified operating in conjunction with the numerous hydrothermal systems (Figure 5.8). The paleo-environment of the Middle Cretaceous is depicted, from the evidence presented, as an off-axis region of discrete zones of variable hydrothermal discharge and black smoker fields, surrounded by metalliferous sediments where depositional conditions were favourable, and in which biogenic sedimentation competed as the second major

element flux. In the broadest terms, the findings of this study are not incompatible with any currently accepted model of oceanic sediment formation, or with any fundamental chemical principals. Specifically, the techniques employed have clarified the specific physical-chemical-biological processes that form ancient rise-crest sediments, and as a result, the processes which resulted in the Oman metalliferous sediments have now been more fully investigated than for any comparable ancient sediments.

References

Adachi, M., Koshi, Y. and Ryuichi, S., 1986: Hydrothermal chert and associated siliceous rocks from the northern Pacific: their geological significance as an indication of ocean ridge activity. *Sed. Geol.*, **47**, 125-148.

Alabaster, T. and Pearce, J.A. 1985: The interrelationship between magmatic and ore-forming hydrothermal processes in the Oman ophiolite. *Ec. Geol.*, **80**, 1-16.

Alabaster, T., Pearce, J.A. and Malpas, J., 1982: The volcanic stratigraphy of the Oman ophiolite complex. *Contrib. Mineral. Petrol.*, **81**, 168-183.

Alt, J.C., Honnorez, J., Laverne, C and Emmerman, R., 1986: Hydrothermal alteration of a 1km strip through the upper oceanic crust, deep Sea drilling Project Hole 504B: Mineralogy, chemistry and evolution of seawater-basalt interactions. *J. Geophys. Res.*, **91**, 10309-10335.

Anshutz, P. and Blanc, G. 1995: Chemical mass balance in metalliferous deposits from the Atlantis II Deep, Red Sea. *Geochim. Cosmochim. Acta,* **59**, 4205-4218.

Aplin, A.C. 1983: The geochemistry and environment of deposition of some ferro-manganese oxide deposits from the south Equatorial Pacific. *PhD Thesis*, Univ. London.

Aplin, A.C. and Cronan, D.S. 1985: Ferromanganese oxide deposits from the Central Pacific Ocean. 1. Encrustations from the Line Islands Archipeligo. *Geochimica. Cosmochim. Acta,* **49**, 427-436.

Bacon, M.P. and Rusholt, J.N. 1982: Accumulation rates of Th-220, Pa-331, and some transition metals on the Bermuda Rise. *Geochim. Cosmochim. Acta,* **46**, 651-666.

Balistrieri, L.S. and Murray, J.W. 1986: The surface chemistry of the sediments from the Pnanma Basin: the influence of Mn oxides on metal absorption. *Geochim. Cosmochim. Acta.* **50**, 2235-2243.

Barrett, T.J. 1992: Mass changes in the Galápagos hydrothermal mounds: near-axis sediment transformation and mineralization. *Geology,* **20**, 1075-1078.

Barrett, T.J. and Jarvis, I., 1988: Rare-earth element geochemistry of metalliferous sediments from DSDP Leg 92: the East Pacific Rise transect. *Chem. Geol.,* **67**, 243-259.

Barrett, T.J. and MacLean W.H. 1991: Chemical, mass and oxygen-isotopic changes during extreme hydrothermal alteration of an Archean rhyolite, Noranda. *Ec. Geol.,* **86**, 406-414.

Beurrier, M., Bourdillon de Grissac, C., Wever, P. and Lescuyer, J.L., 1987: Biostratigraphie des radiolarites associées aux volcanites ophiolitiques de la nappe de Samail (Sultanat d'Oman): conséqunces tectogénétiques. *C. R. Acad. Sci. Paris, Sér. 2,* **304**, 907-910.

Bischoff, J.L., 1969: Red Sea geothermal brine deposits: their mineralogy, chemistry and genesis. In: Degens, E.T. and Ross, A.D. (eds.*): Hot brines and recent heavy metal deposits in the Red Sea,* 368-401. Wiley, New York.

Bischoff J.L. and Rosenbauer, R.J., 1989: An empirical equation of state for hydrothermal sea water (3.2% NaCl). *Am. J. Sci.,* **285**, 725-763.

Blome, C.D. and Irwin, W.P., 1985: Equivalent radiolarian ages from ophiolitic terraines of Cyprus and Oman. *Geology,* **13**, 401-404.

Bonatti, E., Kraemer, T. and Rydell, H.S.: 1972: Classification and genesis of submarine iron-manganese deposits. In: Horn, D.R. (ed.): *Ferromanganese deposits on the ocean floor.* Natl. Sci. Found., Washington DC, 149-167.

Bonatti, E., 1975: Metallogenesis at oceanic spreading centres. *Ann. Rev. Earth Plan. Sci.*, **3**, 401-431.

Boström, K. and Peterson, M.N.A., 1966: Precipitates from hydrothermal exhalations on the East Pacific Rise. *Ec. Geol.*, **61**, 1258-1265.

Boström, K. and Peterson, M.N.A., 1969: The origin of aluminium-poor ferromanganoan sediments in areas of high heat flow on the East Pacific rise. *Mar. Geol.*, **7**, 427-447.

Boström, K., 1973: The origin and fate of ferromanganoan active ridge sediments. *Stokholm Contrib. Geol.*, **27**, 149-243.

Boström, K., Kraemer, T. and Gartner, S., 1973: Provenance and accumulation rates of opaline silica, Al, Ti, Fe, Mn, Cu, Ni and Co in Pacific pelagic sediments. *Chem. Geol.*, **11**, 123-148.

Bourdillion de Grissac, C., De Wever, P. and Bechennec, F., 1987: Nouvelles données biostratigraphiques des montagnes d'Oman, du Permian au Crétacé, á partir des radiolaires et des foraminifères. *Bur. Rech. Géol. Min. Soc. Géol. Fr., Scéance Spéc., Paris.* 10.

Boyle, J.F., 1990: The composition and origin of metalliferous sediments from the Troodos ophiolite, Cyprus. In: Malpas, J., Moores, E., Panayiotou, A. and

Xenophontos, C., (eds.), *Ophiolites, Oceanic Crustal Analogues. Proc. Symp. "Troodos, 1987"*. Cyprus Geological Survey Department, 705-718.

Bryan, W.B., Finger, L.W. and Chayes, F., 1969: Estimating proportions in petrographic mixing equations by least squares approximation. *Science,* **164**, 926-927.

Buser, W. and Grutter, A. 1956: Uber die Natur der Manganköllen. *Schweiz. Miner. Petrog. Mitt.,* **36**, 49-62.

Cann, J.R. and Strens M.R., 1982: Black smokers fuelled by freezing magma. *Nature,* 298 / July 8th, 147-149.

Chester, R, 1990: *Marine Geochemistry.* Unwin Hyman Ltd., London.

Chester, R. and Aston, S.R. 1976: The geochemistry of deep-sea sediments. In: Riley, J.P. and Chester, R (eds), *Chemical Oceanography.* London, Academic Press, 271-335.

Chester, R. and Hughes, M.J. 1967: A chemical technique for the separation of ferromanganese minerals, carbonate minerals and absorbed trace elements from pelagic sediments. *Chem. Geol.,* **2**, 249-262.

Chester, R. and Hughes, M.J., 1969: The trace element geochemistry of a North Pacific pelagic clay core. *Deep Sea Research,* **16**, 639-654.

Chester, R and Messiha-Hanna, R.G. 1970: Trace element partition patterns in North Atlantic deep-sea sediments. *Geochim. Cosmochim. Acta,* **34**, 1121-1128.

Cole, T.G. 1985: Composition, oxygen isotope geochemistry, and origin of smectite in the metalliferous sediments of the Bauer deep, southeast Pacific. *Geochim. Cosmochim. Acta,* **49**, 221-235.

Coleman, R.G. 1981: Tectonic setting for ophiolite obduction in Oman. *J. Geophysical Res.*, **86,** B4, 2497-2508.

Collier, R.W. and Edmond, J.M., 1984: The trace element geochemistry of marine biogenic particulate matter. *Progr. Oceanog.*, **13**, 113-199.

Constantinou, G. and Govett, G.J.S., 1972: Genesis of sulphide deposits, ochres and umbers of Cyprus. *Inst. Min. Metall.*, **81**, B34-B46.

Corliss, J.B., Grag, J.L., Skinner, B.J. and Hutchinson, R., (1972): Rare Earth data for iron and manganese sediments associated with sulphide ore bodies of the Troodos Massif, Cyprus. *Geol. Soc. Am. Abst. Prog.*, **4(7)**, 476.

Cronan, D.S., 1976: Basal metalliferous sediments from the eastern Pacific. *Geol. Soc. Am. Bull.*, **87**, 928-934.

Cronan, D.S., Galácz, A., Mindszenty, A., Moorby, S.A, and Polgari, M., 1991: Tethyan ferromanganese oxide deposits from Jurassic rocks in Hungary. *J. Geol. Soc. Lond.*, **148**, 655-668.

Dymond, J., Corliss, J.B., Heath, G.r., Field, C.W., Dasch, E.J. and Veeh, H.H., 1973: Origin of metalliferous sediments from the Pacific Ocean. *Geol. Soc. Am. Bull.*, **84**, 3355-337.

Dymond, J., Corliss, J.B. and Heath, G.R. 1977: History of metalliferous sedimentation at Deep Sea Drilling Site 319, in the south eastern Pacific. *Geochim. Cosmochim. Acta, **41***, 741-753.

Dymond, J., Corliss, J.B. and Stillinger, R., 1976: Chemical composition and metal accumulation rates in metalliferous sediments from sites 319, 320, 321. *Init. Rep. DSDP*, **34**, 575-588.

Dymond, J., 1981: Geochemistry of Nazca plate surface sediments: an evaluation of hydrothermal, biogenic, detrital, and hydrogenous sources. *Geol. Soc. Am. Mem.,* **154**, 133-173.

Dymond, J., Lyle, M., Finney, B., Piper, D.Z., Murphy, K.,Conrad, R. and Pisias, N. 1984: Ferromanganese nodules from MANOP Sites H, S and R - control of mineralogical and chemical composition by multiple accretionary processes. *Geochim Cosmochim. Acta,* **48**, 931-949.

Edmond, J.M., Measures, C.I., McDuff, R.E., Chan, L.H., Collier, R., Grant, B., Gordon, L.I., and Corliss, J.B., 1979: Crest hydrothermal activity and the balance of major and minor elements in the ocean: the Galapagos data. *Earth Plan. Sci. Lett.*, **46**, 1-18.

Edmond, J.M., Von Damm, K.L., McDuff, R.E., Measures, C.I. 1982: Chemistry of the hot springs of the east Pacific Rise and their effluent dispersal. *Nature,* **297**, 187-191.

Edmonds, H.N., German, C.R., Green, D.R.H., Huh, Y., Gamo, T. and Edmond, J.M. 1996: Continuation of the hydrothermal fluid chemistry time series at TAG, and the effects of ODP drilling. *Geophys. Res. Lett.*, **23**, 3487-3489.

El Wakeel, S.K. and Riley, J.P., 1961: Chemical and mineralogical studies of deep-sea sediments. *Geochim. Cosmochim. Acta,* **25**, 110-146.

Elderfield, H. Gass, I.G., Hammond, A. and Bear, L.M., 1972: The origin of ferromanganese sediments associated with the Troodos Massif of Cyprus. *Sedimentology*, **19**, 1-19.

Ernewein, M., Pflumio, C.and Whitechurch, H., 1988: The death of an accretion zone as evidenced by the magmatic history of the Sumail ophiolite (Oman). *Tectonophysics*, **151**, 247-274.

Feely, R.A., Grendon, J.F., Baker. E.T. and Lebon, G.T. 1994: Hydrotheermal plumes along the East Pacific Rise, 8°40' to 11°50' N: Particle distribution and composition. *E. Plan. Sci. Lett.,* **128**, 19-36.

Feely, R.A., Baker, E.T., Marumo, K., Urabe, T., Ishibashi, J., Gendron, J., Lebon, G.T. and Okamura, K. 1996: Hydrothermal plume particles and dissolved phosphate over the superfast-spreading southern East Pacific Rise. *Geochim. Cosmochim. Acta,* **60**, 2297-2323.

Fleet, A.J. and Robertson, A.H.F., 1980: Ocean ridge metalliferous sediments and pelagic sediments of the Semail Nappe, Oman. *J. Geol. Soc. London,* **137**, 403-422.

Fox, L.E. 1991: The chemical control of phosphate concentration in deep sea waters impacted by hydrothermal vents. *EOS, Trans. Amer. Geophys. Union,* **72**, 235.

Full, W.E., Ehrlich, R. and Kloven, J.E. 1981: EXTENDED QMODEL - objective definition of external end-members in the analysis of mixtures. *J. Math. Geology,* **13**, 331-344.

Full, W.E. and Ehrlich, R. 1986: Comment on "Objective technique for determining end-member compositions and for partitioning sediments according to their sources.". *Geochim. Cosmochim. Acta,* **50**, 1303.

Gill, J. and **Gorton M.,** 1973, A proposed Geological and Geochemical History of Eastern Melanesia. In: Coleman P.J. (ed.), *The Western Pacific: Island Arcs, Marginal Seas, Geochemistry*. Univ.W.Australia Press.

Glennie, K.W., Boeuf, M.G.A., Hughes-Clark, M.W., Moody-Stuart, M., Pilaar, W.F.H. and Reinhardt, B.M., 1974: Geology of the Oman mountains. Kon. Ned. Geol. Mijnbouwdk. Genoot. Verh., **31**, 423.

Goldberg, E.D. 1954: Marine geochemistry: chemical scavengers of the sea. *J. Geol.*, **62**, 249-255.

Hall, J.M., Walls, C.C. and Yang, J. 1988: Constructional features of the Troodos ophiolite and implications for the distribution of orebodies and the generation of oceanic crust. *Can. J. Earth Sci.*, **26**, 1172-1184.

Harder, H., 1976: Nontronite synthesis at low temperatures. *Chem. Geol.*, **18**, 169-180.

Hartmann, M. 1980:Atlantis II deep geothermal brine system. Hydrographic situation in 1977 and changes since 1965. *Deep Sea Res.*, **27A**, 161-171.

Hartmann, M. 1985: Atlantis II deep geothermal brine system. Chemical processes between hydrothermal brines and Red Sea deep water. *Mar. Geol.*, **64**, 157-177.

Haymon, R.M., Koski, R.A. and Abrams, M.J., 1989: Hydrothermal discharge zones beneath massive sulphide deposits mapped in the Oman ophiolite. *Geology,* **17,** 531-535

Haymon, R.M., Koski, R.A., and Sinclair, C. 1984: Fossils of hydrothermal vent worms from Cretaceous sulphide ores of the Samail ophiolite, Oman. *Science,* **223**, 1407-1409.

Haymon, R.M., Koski, R.A. and Stakes, S.D., 1990: Hydrothermalism and sulphide ore deposits at Bayda, Aarja and Lasail. In: *Symposium on ophiolite Genesis and evolution of Oceanic Lithosphere. Excursion E3, Sultanate of Oman.* Jan 1990, 21.

Heath, G.R. and Dymond, J.R. 1977: Genesis and diagenesis of metalliferous sediments from the East pacific Rise, Bauer Deep and Central Basin, north west Nazca plate. *Geol. Soc. Am. Bull.,* **88,** 723-733.

Hekinian, R., Fevrier, M., Bischoff, J.L., Picot, P. and Shanks W.C. 1980: Sulphide deposits from the East Pacific Rise near 21°N. *Science,* **207**, 1433-1444.

Hekinian, R. and Fouquet, Y. 1985: Volcanism and metallogenesis of Axial and Off-Axis structures on the East Pacific Rise near 13°N. *Bull. Soc. Ec. Geol,* **80**, 221-253.

Herzig, P.M. and Hanning, M.D. 1995: Polymetallic massive sulphides at the modern seafloor: A review. *Ore Geol. Rev.,* **10**, 95-115.

Hoffert, M., Perseil, A., Hekinian, R, Choukroune, P., needham, H.H., Francheteau, J. and Le Pichon, X. 1978: Hydrothermal deposits sampled by diving saucer in transform fault "A" near 37°N on the Mid-Atlantic ridge, FAMOUS Area. *Oceanol. Acta,* **1**, 73-86.

Honeyman, B.D., Balistrieri, L.S. and Murray, J.W., 1988: Oceanic trace metal scavenging: the importance of particle concentration. *Deep Sea Res.*, **35**, 227-246

Honnorez et al., 1981: Hydrothermal mounds and young ocean crust of the Galapagos: Preliminary Deep Sea Drilling results, Leg 70. *Geological Society of America Bulletin*, **Part I, 92**, 457-472, July.

Jannasch, H., Honeyman, B.D., Balistieri, L.S. and Murray, J.W., 1988: Kinetics of trace element uptake by marine particles. *Geochim. Cosmochim. Acta*, **52**, 567-577

Jarvis, I., 1995: Geochemistry and origin of Eocene-Oligocene metalliferous sediments from the central equatorial Pacific: Deep Sea Drilling Project Sites, 573 and 574. In: Mayer, L., Theyer, F. et al., (Eds.): *Initial reports of the Deep Sea Drilling Project.*, **85**, 781-804.

Jarvis, K.E. and Williams, J.G., 1989: The analysis of geological samples by slurry nebulisation inductively coupled plasma-mass spectrometry (ICP-MS). *Chem. Geol.*, **77**, 53-63.

Johnson R.W., 1982: Papua New Guinea. In: Thorpe R.S. (ed.), *Andesites*. Wiley, Chichester.

de Jongh, W.K., 1973: X-ray fluorescence analysis applying theoretical matrix corrections. Stainless Steel. *X-ray spectrom.*, **2**, 151-157.

Lippard, S.J., Shelton, A.W. and Gass, I.G., 1986: The ophiolite of northern Oman. *Geol. Soc. Lond. Mem.*, **11**, 178.

Martin, J.H. and Knauer, G.A., 1973: The elemental composition of plankton. *Geochim.Cosmochim.Acta*, **37**, 1639-1654.

Karpoff, A.M., Walter, A.V. and Pflumio, C., 1988: Metalliferous sediments within the lava sequences of the Sumail ophiolite (Oman): mineralogical and geochemical characterisation, origin and evolution. *Tectonophysics*, **151**, 223-245.

Kastner, M., 1981: Authigenic silicates in deep-sea sediments: formation and diagenesis. In Emiliani, C. (ed.): *The oceanic lithosphere.* Wiley, New York, 915-980.

Klein, E.M., 1991: Ocean ridge magmatism and hydrothermal geochemical processes. *Review of Geophysics, Supplement,* U.S. National report to International Union of Geodesy and Geophysics 1987-1990, 532-541.

Klinkhammer, G.P., Elderfield, H, Edmond, J.M. and Mitra, A. 1994: Geochemical implications of rare earth element patterns in hydrothermal fluids from mid-ocean ridges. *Geochim. Cosmochim. Acta,* **58**, 5105-5113.

Kolodny, Y., 1981: Phosphorites. In Emilani, C., (ed.): *The oceanic lithosphere.* Wiley, New York, 981-1024.

Krishnaswami, S. 1976: Authigenic transition elements in Pacific pelagic clays. *Geochem. Cosmochim. Acta,* **40**, 425-434.

Kurnosov, V.B., Chudaev, O.V. and Shevchenko, A. Y. 1983: Mineralogy and geochemistry of sediments from Galapagos hydrothermal mounds, Leg 70, Deep Sea Drilling Project. *Init. Rep. DSDP 70*, 225-229.

Lalou, C. 1983: Genesis of ferromanganese deposits: hydrothermal origin. In: Rona, P.A., Bostrom, K., Laubier, L. and Smith, K.L. (eds*): Hydrothermal processes at sea-floor spreading centres.* New York, Plenum.

Leckie, J.O., 1986: Adsorption and transformation of trace element species at sediment/water interface. In: Bernhard, M., Brinkman, F.E. and Sadler, P.J. (eds.*), The importance of chemical speciation in environmental processes.* 237-254

Leinen, M. and Pisias, N., 1984: An objective technique for determining end-member compositions and for partitioning sediments according to their sources. *Geochim. Cosmochim. Acta,* **48**, 47-62.

Li, T.-H., 1981: Ultimate removal mechanisms of elements from the ocean. *Geochim. Cosmochim. Acta*, **45**, 1659-1664.

Lowell, R.P., and Rona, P.A., 1985: Hydrothermal models for the generation of massive sulphide ore deposits. *J. Geophys. Res.*, **90**, 8769-8773.

Lowell, R.P. and Burrell, D.K., 1991: Mathematical modelling of conductive heat transfer from a freezing, convecting magma chamber to a single-pass hydrothermal system: implications for sea floor black-smokers. *E. Plan. Sci. Lett.*, **104**, 59-69.

Lyle, M., Dymond, J. and Heath, G.R. 1977: Copper-nickel enriched ferromanganese nodules and associated crusts from the Bauer Basin, Northwest Nazca Plate. *E. Plan. Sci. Lett,* **35**, 55-64.

MacLean, W.H. and Kranidiotis, P. 1987: Immobile elements as monitors of mass transfer in hydrothermal alteration: Phelps dodge massive sulphide deposit, Matagami, Quebec. *Ec. Geol.*, **82**, 951-962.

Marchig, V. and Gundlach, H., 1982: Iron-rich metalliferous sediments on the East Pacific Rise: prototype of undifferentiated metalliferous sediments on divergent plate boundaries. *E. Plan. Sci. Lett.*, **58**, 361-382.

Marchig, V., Gundlach, H., Möller, P. and Schley, F., 1982: Some geochemical indicator for discrimination between diagenetic and hydrothermal metalliferous sediments. *Mar. Geol.*, **50**, 241-258.

Migdisov, A.A., Gradusov, B.P., Bredanova, N.V., Bezrogova, E.V., Saveliev, B.V. and Smirnova, O.N. 1983: Major and minor elements in hydrothermal and pelagic sediments of the Galapagos Mounds area, Leg 70, Deep Sea Drilling Project. *Init. Rep. DSDP,* **70**, 277-295.

Miller, S. and Cronan, D.S., 1994: Element supply to surface sediments and interrelationships with nodules along the Aitutaki-Jarvis Transect, South Pacific. *J. Geol. Soc, Lond.*, **151**, 403-412.

Mills, R.A. and Elderfield, H. 1995: Rare earth element geochemistry of hydrothermal deposits from the active TAG Mound, 26°N Mid-Atlantic Ridge. *Geochim. Cosmochim. Acta,* **59**, 17, 3511-3524.

Mitra, A., Elderfield, H., and Greaves, M.J. 1994: Rare earth elements in submarine hydrothermal fluids and plumes from the Mid-Atlantic Ridge. *Mar. Chem.*, **47**, 217-236.

Moorby, S.A. 1983: The geochemistry of transitional sediments recovered from the Galapagos Hydrothermal Mounds Field dueing DSDP Leg 70 - Implications for mounds formation. *E. Plan. Sci. Lett.* **62**, 367-376.

Moorby, S.A. and D.S. Cronan 1983: The geochemistry of hydrothermal and pelagic sediments from the Galapagos hydrothermal mounds, DSDP Leg 70. *Mineralo. Mag.*, **47**, 291-300.

Moorby, S.A. and D.S. Cronan 1983: Chemical composition of sediments from the Galapagos hydrothermal mounds, Leg 70. *Init. Repts. DSDP*, 70, 269-275.

Moorby, S.A., D.S. Cronan and Glasby, G.P. 1984: Geochemistry of hydrothermal Mn-oxide deposits from the S.W. Pacific island arc. *Geochim. Cosmochim. Acta,* **48**, 433-441.

Moore, W.S. and Vogt, P.R. 1976: Hydrothermal manganese crust from two sites near the Galapagos spreading axis. *E. Plan. Sci. Lett.*, **29**, 349-356.

Nehlig, 1993: Interactions between magma chambers and hydrothermal systems: oceanic and ophiolitic constraints. *J. Geophys. Res.*,**98**, B11, 19,621-19,633.

Nehlig, P. Juteau, T., Bendel, V and Cotton, J., 1994: The root zones of oceanic hydrothermal systems: Constraints from the Samail ophiolite (Oman). *J. Geophys. Res.*, **99**, B3, 4703-4713.

Nyffeler, U.P., Li, Y.,-H and Santschi, P.S., 1984: A kinetic approach to describe trace element distribution between particles and solution in natural aquatic systems. *Geochim. Cosmochim. Acta*, **48**, 1513-1522.

Oudin, E. and Constantinou, G., 1984: Black smoker chimney fragments in Cyprus sulphide deposits. *Nature*, **308**, 349-353.

Pearce, J.A., 1980: Geochemical evidence for the genesis and eruptive setting of lavas from Tethyan ophiolites. In: Panayiotou, A. (ed.), *Ophiolites, Proc. Int. Ophiolite Symp.* (Cyprus 1979). Geol. Surv. Dept. Cyprus, Nicosia, 261-272.

Pearce, J.A., Alabaster, T., Shelton, A.W. and Searle, M.P., 1981: The Oman ophiolite as an arc-basin complex: evidence and implications. *Philos. Trans. R. Soc. Lond.*, **300**, 299-317.

Pearce, J.A. and Norry, M.J., 1979: Petrogenic implications of Ti, Zr, Y and Nb variations in volcanic rocks. *Contrib. Min. Pet.*, **69**, 33-47.

Perrin, M., Prevot, M. and Bruere, F. (1993): Rotation of the Oman ophiolite and initial location of the ridge in the hotspot reference frame. *Tectonophysics* **229**, 31-42.

Pflumio, C., 1987: Hydrothermalisme océanique dans la nappe de samail: emempl du Wadi Salahi. *Soc. Géol. Fr. Scéance Spéc., Paris.*

Pisciotto, K.A., 1981: Distribution, thermal histories, isotopic compositions and reflection characteristics of siliceous rocks recovered by the Deep Sea Drilling Project. *Soc. Econ. Paleontol. Min. Spec. Pub.,* **32**, 129-147.

Reuber, I., 1988: Complexity of the crustal sequence in the northern Oman ophiolite (Fizh and southern Aswad bloacks): The effect of early slicing? *Tectonophysics,* **151**, 137-165.

Riley, J.P. and Chester, R. 1971: *Introduction to marine chemistry.* London. Academic Press.

Robertson, A.H.F., 1975: Cyprus umbers: basalt sediment relatioships on a Mesozoic ocean ridge. *J. Geol. Soc. Lond.,* **131**, 511-531.

Robertson, A.H.F., 1976: Origin of ochres and umbers: evidence from Skouritissa, Troodos Massif, Cyprus. *Inst. Min. Metall.,* **95**, B122-146.

Robertson, A.H.F. and Fleet, A.J., 1986: Geochemistry and palaeo-oceanography of metalliferous and pelagic sediments from the Late Cretaceous Oman ophiolite. *Mar. Pet. Geol.,* **3**, 315-337.

Robertson A.H.F. and Hudson, J.D., 1973: Cyprus umbers: chemical precipitates on a Tethyan ocean ridge. *E. Plan. Sci. Lett.*, **18**, 93-101.

Robertson A.H.F. and Varnavas, 1993: The origin of hydrothermal metalliferous sediments associated with the early Mesozoic Othris and Pindos ophiolite, Mainland Greece. *Sed. Geol.*, **83**, 87-113.

Robertson, A.H.F., Varnavas, S.P. and Panagos, A.G. 1987: Ocean ridge origin and tectonic setting of mesozoic sulphide and oxide deposits of the Argolis Peninsula of the Peloponnesus, Greece. *Sed. Geol.*, **53**, 1-32.

Rona, P.A., Klinkhammer, G.A., Nelsen, T.A., Trefry, J.H. and Elderfield, H. 1986: Black smokers, massive sulphides and vent biota at the Mid Atlantic ridge. *Nature,* **321**, 33-37.

Rona, P.A., 1993: A special issue on hydrothermal mineralization at seafloor spreading centres. *Earth Sci. Rev.*, **20**, 1-104.

Rudnicki, M.D. and Elderfield, H. 1992: A chemical model of the buoyant plume above the TAG vent field, 26 degrees N, Mid-Atlantic Ridge. *Geochim. Cosmochim. Acta,* **57**, 2939-2957.

Scott, R.B., Rona, P.A., McGregor, B.A. and Scott, M.R., 1974: The TAG hydrothermal field. *Nature,* **251**, 301-302.

Scott, M.R., Scott, R.B., Rona, P.A., Butler, L.W. and Nalwak, A.J. 1974: Rapidly accumulating manganese deposit from the median valley of the Mid-Atlantic Ridge. *Geophys. Res. Lett,* **1**, 355-358.

Schwertmann, U. and Taylor, R.M., 1977: Iron oxides. In: Dixon, J.B. and Weeb, S.B. (eds.), Minerals in soil environments. *Soil Soc. Am.*, 145-176.

Spiess, F.N., MacDonald, K.C. and Atwater, T, 1980: East Pacific Rise: hot springs and geophysical experiments. *Science*, **207,** 1421.

Stepnova, T.V., Krasnov, S.G. and Cherkashev, G.A. 1996: Mineralogy, chemical composition and structure of the MIR mound, TAG hydrothermal field. *Geophys. Res. Lett.*, **23**, 3515-3518.

Terakado, Y., Fujitani, T. and akada, J., 1993: Experimental study on the sorption of rare-earth elements and other trace elements during rhyolite-hydrothermal water interactions. *Chem. Geol.*, **106**, 317-330.

Thomas, V., Pozzi, J.P. and Nicholas, A., 1988: Palaeomagnetic results from Omann ophiolites related to their emplacement. *Tectonophysics,* **151**, 297-321.

Thompson, G., Humphris, S.E., Schroeder, B., Sulanowska, M. and Rona, P.A. 1988: Active vents and massive sulphides at 26° (TAG) and 23°N (Snakepit) on the Mid-Atlantic ridge. *Can. Min.*, **26**, 697-711.

Thompson, J., Carpenter, M.S.N., Colley, S., Wilson, T.R.S., Elderfield, H. and Kennedy, H. 1984: Metal accumulation in northwest Atlantic pelagic sediments. *Geochim. Cosmochim. Acta,* **48**, 1935-1948.

Tilton, G.R., Hopson, C.A. and Wright, J.E., 1981: Uranium-lead isotope ages of the Samail ophiolite, Oman, with application to Tethyan ocean ridge tectonics. *J. Geophys. Res.*, **86**, 2763-2775.

Tippet, P.R., Pessagno, Jr, E.A. and Smewing, J.D., 1981: The biostratigraphy of sediments in the volcanic units of the Oman ophiolite. *J.Geophys. Res.*, **86**, 2756-2762.

Tivey, M.K., Humphris, S.E., Thompson, G., Hannington, M.D. and Rona, P.A. 1995: Deducing patterns of fluid flow and mixing within the active TAG mound using mineralogical and geochemical data. *J. Geophys. Res.*, **99**, 1135-1142.

Toth, J.R., 1980: Deposition of submarine crusts rich in manganese and iron. *Geol. Soc. Am. Bull.*, **91**, 44-55.

Toyoda, K. and Masuda, A, 1990: Sedimentary environments and chemical composition of Pacific pelagic sediments. *Chem. Geol.,* **88**, 127-141

Varentsov, B.A., Sakharov, B.A., Drits, V.A., Tsipursky, S.I., Choporov, D.B and Alexandrova, V.A. 1983: Hydrothermal deposits of the Galapagos Rift Zone, Leg 70: Mineralogy and Geochemistry of Major Components. *Init. Rep. DSDP,* **70**, 277-295.

Varnavas, S., 1981: Partition geochemical investigation on ferromanganese deposits from the Troodos massif, Cyprus. *Proceedings of UNESCO International Symposium on Metallogeny of Mafic and Ultramafic Complexes: The eastern Mediterranean-Western Asia Area and its comparisons with Similar Metallogenic Environments Around the World.* 391-410.

Varnavas, S.P., Moorby, S.A. and Cronan, D.S. 1983: Partition geochemistry of sediments from Holes 506 and 506B, Deep Sea Drilling Project, Leg 70. *Init. Rep. DSDP,* **70**, 297-302.

Varnavas, S.P. and Pangos, A.G., 1981: The genesis and preservation of fossil manganese nodules in the area of Panormo, Greece. *Proc. Of the International Symp. on the Hellenistic arc and Trench.*

Von Damm, K.L., Edmond, J.M., Measures, C.I. and Grant, R. 1985: Chemistry of submarine hydrothermal solutions at 21°N, East Pacific Rise. *Geochim. Cosmochim. Acta,* **49**, 2221-2237.

Von Damm, K.L., Grant, B., Edmond, J.M. 1983: Preliminary report on the chemistry of hydrothermal solutions at 21° north, East Pacific Rise. In Rona, P.A., Böstrom, K., Laubier, L. and Smith, K.L. (eds.): *Hydrothermal processes at seafloor spreading centres*, 369-390.

Von Damm, K.L., Edmond, J.M., Grant, B, Measures, C.I., Walden, B and Weiss, R.F., 1985: Chemistry of submarine hydrothermal solutions at Guaymas Basin, Gulf of California. *Geochim. Cosmochim.* Acta, **49**, 2197-2220.

Wilson, R.A.M., 1969: The geology of the Xeros-Troodos area with an account of the mineral resources. *Mem. Geol. Surv. Dept. Cyprus*, **I**, 18-19.

Wright, T.L., and Doherty, P.C., 1970: A linear programming and least squares computer method for solving petrologic mixing problems. *Geol. Soc. Am. Bull.*, **81**, 1995-2008.

Zierenberg, R.A., Shankes, W.C. and Bischoff, J.L. 1984: Massive sulphide deposits at 21°N, East pacific Rise: chemical composition, stable isotopes and phase equilibria. *Geol. Soc. Am. Bull.*, **95**, 922-929.

APPENDIX A

HARD ROCK ANALYTICAL TECHNIQUES

A.1 SAMPLE PREPARATION: METALLIFEROUS SEDIMENTS

The initial sample preparation was carried out in the same way for all of the samples used in this study. Because of the clay mineralogy and the very wide range in sediment compositions which are analysed in this study, metalliferous sediments are in particular danger of sample cross-contamination during the preparation stage. A number of measures have been employed to evaluate and minimise the effect of this. First, a number of individual samples were divided into three sub-samples prior to preparation and subsequently treated as separate samples, placed at random in each batch. Secondly, during preparation and processing of the samples, the samples were sub-divided into batches according to sample locality. The batches were then sorted for preparation into sub-batches of similar lithological type on the basis of colour, grain size and volcanic stratigraphic position. The cross-contamination data are tabulated below in the relevant analytical methodology.

Before the samples were crushed, they were dried in an oven. Prior to each batch being processed, the crushing machine was dismantled and cleaned using a wire brush and absolute alcohol to eliminate, as far as possible, any contamination from previous users. The jaws and sample collection box of the machine were also thoroughly cleaned between samples using the wire brush and absolute alcohol. During the crushing procedure, a dust extractor was used to help to reduce the build-up of dust within the machine. Samples were crushed in a Pulverisette jaw crusher.

After crushing, samples were milled in an agate ball mill for 20 minutes. Before and after use, and between each batch, the agate mill was cleaned using sharp sand before use. Between samples, the mill was cleaned under running water with a nylon brush, and then using absolute alcohol.

A.2 X-RAY FLUORESCENCE ANALYSIS

All samples were initially analysed for major and selected trace elements by X-Ray Fluorescence (XRF) at Durham. The major elements were analysed from fusion discs and the trace elements from pressed pellets.

The loss on ignition (LOI) for each sample was determined from milled sample powder prior to major element analysis. To do this, the powders were first dried at 105°C to remove the surface-adsorbed water, to derive the LOI.

To prepare fusion discs, the powders were first dried at 105° C to remove any adsorbed surface water, then heated at 900° C in porcelain crucibles for two hours. From each sample, 0.45 g ± 0.001 g of the dried powder was mixed with 2.25 g ± 0.001 g of dried lithium metaborate - lithium tetraborate flux (Spectroflux 100B) using an agate pestle and mortar. By ensuring careful mixing at this stage, it was possible to produce good totals when the samples were analysed. The measured powder was then placed in a furnace in a platinum crucible at 1050° C for 20 minutes. The molten material was then poured into metal moulds on a hot plate and quickly quenched with a metal plunger to ensure a planar analytical surface. Once cooled, the samples were labelled and bagged. After quenching the disc, care was taken not to touch the analytical surface to avoid Na contamination. Fusion discs were stored in a dessicator. As with other studies, Na was usually below the lower detection limit of the XRF and therfore not quoted (Karpoff *et al.*, 1988).

Pressed pellets were made by mixing approximately 10 g of sample with 4 to 8 drops of Mowiol binder in a glass beaker using a glass rod. The amount of Mowiol used varied significantly according to the properties of each sample, but in general less binding agent is used than for silicate rocks. The mix was pressed for 25 seconds at 10 bars. The pellets were labelled then dried overnight at 110° C. Again, contact with the analytical surface was avoided.

Discs and pellets were analysed using a Philips PW 2400 dispersive X-ray spectrometer with a rhodium tube, equipped with a PW1500/10 sample changer. The spectrometer was controlled by dedicated Phillips X41 software package. Following preliminary trials, count times were increased for those elements which appeared to be close to the detection limits of the XRF (Table A.1) above. Analytical runs consisted of up to 200 analyses, 15 of which were calibration standards. The major element data correction used influence coefficients to

reduce inter-element effects (de Jongh, 1973), and minor elements used the rhodium Compton scatter method.

Table A.1 Summary of final run count times (seconds) used in XRF analyses of Oman metalliferous sediments for pressed pellets and fusion discs.

Program: ROBIN		Program: ROBIN2	
	Measured Time		Measured Time
S	40	Rh3	40
S+	40	Zn	100
Mn	10	Zn+	100
Mn+	10	Cu	100
Fe	10	Cu+	100
Fe+	10	Ni	100
Ti-	10	Ni+	100
Ti	20	S	80
Ca	20	S+	100
Ca+	10	Co	100
K	20	Co+	100
K+	10	Cr	100
Si	40	Cr+	100
Si+	40	V-	100
Aal-	40	V	100
Al	40	Fe	10
P	80	Ti	40
P+	40	Sc-	100
Mg	100	Sc	100
Mg+	80	Ca	40
Na	100		
Na+	80		

The machine was calibrated using international standards. From published data and an initial preparatory XRF run, standards were selected with compositions close to those expected from

the unknowns to cover the range of data expected from the literature review, (e.g., Aplin, 1983; Aplin and Cronan, 1985; Karpoff *et al,* 1988; Boyle, 1990). No standards were used that were of sufficiently high concentrations to skew the calibration line at low levels. A sample, used as a drift monitor, was analysed every 10 samples. Had the variation of the monitor had exceeded the expected level (1% - major elements or 10% - trace elements) the analytical run would have been stopped and the XRF re-calibrated.

A.2.1 ERROR CONTROL

XRF error was monitored with regard to the following considerations:

(1) sample preparation precision,
(2) instrumental precision,
(3) accuracy compared to accepted values for international standards,
(4) XRF detection limit,

(1) *Sample preparation precision*:
Sample preparation precision refers to the repeatability of the sample preparation methodology. The purpose of measuring sample preparation precision was to identify and quantify the inherent errors due to: (a) sample collection and storage, (b) the disc and pellet making procedure, and (c) cross-sample contamination.

By taking three sub-samplings from a large sample at the point of collection, the error inherent in sampling and sample storage was determined for selected samples. The sub-samples were prepared separately at intervals during the subsequent sample preparation procedure. Having done this, each duplicate pellet was analysed repeatedly.

(2) *Instrumental precision*
Determination of instrumental precision, which refers to the repeatability of the measurement in terms of the XRD capability, which reflects the accurate re-positioning of the crystals. The values of Relative Standard Deviation (RSD), used to define precision, were calculated by repeated analysis of the same disc/pellet during the analytical run.

Table A.2 Relative Standard Deviations (RSD) calculated for instrument, sample preparation and duplicate sample precision.

Pellet	Relative Standard Deviations		
	Instrument Precision	Sample Precision	Average Duplicate
MnO	0.78	0.59	0.90
Fe_2O_3	0.41	0.65	0.55
CaO	1.12	1.09	0.45
SiO_2	0.21	0.24	0.53
Al_2O_3	1.58	3.12	2.93
MgO	0.18	0.35	0.34
Ni	0.37	0.34	0.40
Cr	73.1	87.2	21.0
V	4.10	3.60	3.50
Zn	2.61	0.51	1.78
Cu	1.16	0.89	0.69
Ni	0.23	0.54	0.54
Co	2.10	1.78	2.36
Cr	0.34	0.55	0.83
V	2.07	0.66	3.37
Ti	3.54	2.34	12.02
Sc	11.95	2.05	31.6

From the methods outlined above, the following RSD values were calculated: (1) the instrument precision and (2) the sample preparation precision. Instrument precision was calculated from the variation within each sub-sample whereas sample preparation precision was calculated from the variation between each sub-sample. For the sample preparation technique to be considered adequate, the *instrument precision* $\geq$ *sample preparation precision*. To separate the contamination that may result from the crushing procedure from that resulting from sample storage and collection, the samples were subdivided into two subsets prior to crushing/milling. Precision data, as defined by the RSD values obtained for the pellets, are given below (Table A.2), where RSD = 100 times the standard deviation divided by the mean (Jarvis and Williams, 1989).

(3) *Accuracy* - the calibration accuracy is routinely calculated from comparison between measured values and published accepted values of a range of international standards. Because of the extreme variability of the ferromanganese oxide samples, a range of international standard reference materials with accepted low level data were used. It was also necessary (a) to check accuracy with the same standards used in the calibration, and (b) to use standards other than ferromanganese oxides. The effect has been to slightly overestimate accuracy. The accuracy of the analyses of the international standards which were run as unknowns is presented below (Table A.3).

(4) *Detection Limit*

Using the following equation, the detection limit at the 3δ level was calculated for the less abundant trace elements. The calculated limits of detection are summarised in Table A.4.

Table A.3. Accuracy of international standard analyses for major elements and trace elements. N.B. n= number of repeat analyses, Meas. = Durham (XRF) analyses from this study; Rec. = recommended accepted values for the international standards. Oxide values in wt%, elemental values in ppm.

	SARM-11 (*n* = *4*)		BE-N (n=6)		SO-3 (n=5)	
	Meas.	Rec.	Meas.	Rec.	Meas.	Rec.
MnO	0.23	0.22	0.23	0.21	0.09	0.067
TiO_2	0.07	0.06	2.71	2.70	0.31	0.33
Fe_2O_3	94.44	94.59	13.33	13.27	2.16	2.16
CaO	0.07	0.05	14.17	14.33	20.49	20.47
SiO_2	2.99	3.10	40.01	39.48	32.99	33.93
Al_2O_3	1.33	1.38	10.40	10.41	5.69	5.76
MgO	0.12	0.02	13.47	13.59	8.31	8.26
Ni	27	30	275	276	15	14
Cr	41	41	312	372	27	27
V	39	40	236	243	38	36
Zn	26	23	118	120	45	50
Cu	9	11	78	72	18	17
Co	24	27	67	61	18	11
As	18	19	357	360	3.1	2.51
Sc		-	21	22	4.9	5.2

CALCULATING DETECTION LIMITS

Limit of detection $= 3\sqrt{2R_bT_b} * \frac{c}{R_pT_p}$

R_p = count rate on the peak,
R_b = count rate on the background,
T_p = time spent on the peak,
T_b = time spent on the background,
c = concentration of the element in question.

Table A.4 Selected XRF detection limits calculated from summary values obtained from the international standards SARM 11, BE-N and SO-3 which were run as unknowns.

	Detection limit (ppm)
Zn	0.5
Cu	0.2
Sc	0.5
Co	0.6
V	0.6

A.3 INDUCTIVELY-COUPLED PLASMA MASS SPECTROMETRY (ICP-MS) ANALYSIS

Rb, Sr, Y, Zr, Nb, Cs, Ba, La, Ce, Pr, Nd, Sm, Eu, Gd, Tb, Ho, Er, Y, Hf, Ta, Pb, Th and U were analysed by inductively-coupled plasma mass spectrometry at the British Nuclear Fuels Westlakes Laboratory, Cumbria, and also on a Perkin Elmer Sciex 6000 at Durham University. Silicate and oxide rock samples were dissolved in a suite of acids using Teflon screw-top bombs. The sample preparation for chemical partitioning analysis differed slightly from the whole rock analysis and will be described separately. The following clean techniques were used to prevent sample contamination.

A.3.1 WHOLE ROCK ANALYSIS

Samples were prepared in batches of 15, each batch including two blanks and one repeat sample. Prior to sample preparation, the equipment was very carefully cleaned to prevent cross-contamination. During the sample preparation, the batches from Oman were prepared separately, and the equipment was not used for any other samples.

Cleaning Procedure

The equipment used, which included 50 ml polypropylene volumetric flasks, funnels, polypropylene flasks, and screw-top (Savillex) Teflon bombs, was leached for 24 hours with 5% nitric acid. Taking adequate precautions, 2 ml of Analar Nitric acid was dispensed into each Savillex bomb and the lid hand-tightened. The bombs were then cleaned by heating them on a hot plate in a fume cupboard at 130°C - 150°C for 24 hours. The nitric acid refluxes within the vial, dissolving any metal species present. After 24 hours, the acid is emptied from the bombs, which are then thoroughly washed out with MilliQ water. The above process was repeated twice prior to using the bombs for the first time, and then once between each batch of samples.

Sample drying and weighing

Approximately 1 g of rock powder sample was transferred into a labelled glass vial. The glass vials were placed in an oven at 105°C overnight to remove trace moisture. From the glass vial, samples of 0.1 ± 0.001 g were placed into the previously cleaned, labelled Teflon bombs.

Acid digestion

Using the dispenser, 1 ml of Aristar HNO_3 was added to each previously prepared sample contained in a Teflon bomb. To allow the HNO_3 to react with any reactive species in the sample, five minutes was allowed before proceeding to the next step. Taking adequate precautions, 4ml of Aristar HF was added to each sample using the dispenser. The screw-caps were used to tightly close the bombs. The vials were placed on a hot-plate in a fume cupboard at 130°C - 150°C for 24 hours. During this phase, the acid mixture refluxes within the bomb, dissolving the sample. N.B. 24 hours proved adequate for acid digestion of silicate rocks from Savo volcano, but by experimentation, it was found that it required up to 48 hours to completely digest some of the metalliferous sediments. After completion of the appropriate digestion period, the bombs were allowed to cool, the screw-caps removed, and

the acid within evaporated at 130°C - 150°C. The sample was not allowed to evaporate completely, a few µl of liquid were allowed to remain to prevent oxidization of the sample.

Table A.5 Accuracy of international standard analyses for major elements and trace elements. N.B. n = number of repeat analyses, Meas. = BNFL (ICP-MS) analyses from this study; Rec. = recommended accepted values for the international standards (Potts *et al.*, 1992). Values are in ppm.

Table A.5 ICP-MS Accuracy

	AGV-1		BCR-1		MAG-1		W2	
	Meas.	Rec.	Meas.	Rec.	Meas.	Rec.	Meas.	Rec.
Rb	73	67	51	47	144	149	20	20
Sr	508	662	338	330	140	146	197	194
Y	21.0	21	38.9	38	26.7	28	-	-
Zr	228.1	225	188.0	190	-	-	90.6	94
Nb	13.54	16	12.91	14	-	-	7.71	7.9
Cs	1.36	1.26	1.04	-	8.61	8.6	0.93	0.99
Ba	1224	1221	0	0.51	487	479	183	182
La	37.21	38	24.64	24.9	-	-	10.05	11.4
Ce	67.32	66	56.23	53.7	86.13	88	23.66	24
Pr	-	-	7.23	6.8	9.72	9.3	4.94	5.9
Nd	31.13	34	27.87	28.8	36.95	38	11.93	14
Sm	6.51	5.9	7.04	6.59	7.73	7.5	3.43	3.25
Eu	1.87	1.66	2.11	1.95	1.65	1.55	1.14	1.1
Gd	6.14	5.20	7.02	6.68	6.03	5.8	3.97	3.6
Tb	0.63	.71	0.95	1.05	0.83	0.96	0.54	0.63
Dy	3.95	3.8	7.11	6.34	5.64	5.2	4.04	3.8
Ho	0.64	0.73	1.22	1.26	0.92	1.02	0.74	0.76
Er	1.93	1.61	3.75	3.63	2.85	3.0	-	-
Tm	0.32	0.32	-	-	0.43	0.43	-	-
Yb	1.67	1.67	3.54	3.38	2.63	2.61	2.14	2.05
Hf	5.03	5.12	4.79	4.95	3.46	3.7	2.67	2.56
Ta	1.01	0.92	0.95	0.81	1.57	1.11	-	-
Pb	35.15	36	12.92	13.6	21.87	24	9.18	9.3
Th	5.27	6.5	5.93	5.98	11.92	11.9	2.36	2.2
U	1.87	1.89	1.63	1.75	2.88	2.7	0.54	0.53

The sample was allowed to cool, and a further 1 ml of Aristar HNO_3 was added to each vial and the product evaporated to a moist residue. This process was repeated using HNO_3 one more time to fully eliminate all trace of HF from the bomb. The samples were allowed to cool. Finally, the sample was redissolved using 2.5 ml of Aristar HNO_3 and approximately 20 ml of deionised MilliQ water. The screw-cap was replaced and the sample boiled on a hot plate for 1 hour. At this stage, any samples in which undissolved material was apparent were discarded and the sample re-prepared. Using the automated dispenser, the samples were spiked with1.25 ml of a 2 ppm Rh, Re and Bi spike solution and made up accurately to 50 ml. The samples were now diluted to 50 ml in 3.5% HNO_3 with internal standards at 50 ppb. The samples were transferred to 60ml pre-cleaned bottles and at this stage were ready for analysis.

A.3.1.1 Accuracy

Calibration lines were constructed from analyses of international standards and in-house samples. The measured versus published recommended standard values are summarised in Table A.5, above.

As a further measure of the comparability of the ICP-MS methodology with other techniques, the values obtained for whole-rock analysis are presented for the elements Ba, Sr and Rb (Figure A.1).

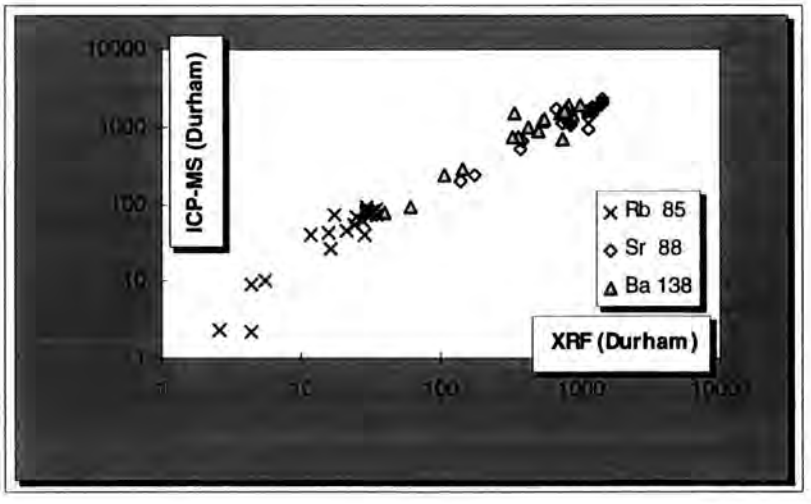

Figure A.1 Trace element data: ICP-MS versus XRF data for Ba, Sr and Rb. Values are in ppm.

A.3.1.2 Detection limit

Because the ICP-MS was often required to operate close to the detection limit for some samples, it was important to have good blank data in order to obtain reliable data for the unknowns. Previous in-house investigation has shown that the lowest blanks may be

achieved with Aristar HF and Romil Ultrapurity HNO_3. Although differences were still found between blanks made for each sample batch, the concentrations of the unknowns were not so low that it was only necessary to calculate a bulk average blank. The detection limit was assumed to be equal to 3 times the standard deviation of the average blank.

A.3.1.3 Precision

To evaluate the approximate precision of the ICP-MS technique, repeat measurements were made of an unknown, which was re-run throughout the analytical run. Two unknowns were used to measure precision: (a) a composite mixture made up from contributions from a number of samples, and (b) the international standard AGV-1. The standard deviation and relative standard calculated for AGV-1 from 5 measurements in one analytical run are shown in Table A.6.

		AGV - 1						
	Rec.	1	2	3	4	5	std.dev	RSD
Rb	67	64.4	65.2	66.6	64.6	66.5	1.0	1.6
Sr	662	658.7	659.0	661.9	664.3	661.2	2.3	0.3
Y	21	18.4	17.5	16.5	16.6	15.7	1.0	6.1
Zr	225	228.3	229.3	230.3	228.5	228.9	0.8	0.3
Nb	16	16.9	16.6	17.1	19.6	18.8	1.3	7.4
Cs	1.26	2.1	1.2	1.5	0.5	0.5	0.7	61.1
Ba	1221	1220.5	1218.7	1219.2	1217.2	1219.5	1.2	0.1
La	38	38.73	37.13	39.14	40.19	40.94	1.4	3.7
Ce	66	68.85	69.75	70.46	71.18	73.12	1.6	2.3
Nd	34	35.96	36.98	37.13	37.87	36.84	0.7	1.8
Sm	5.9	6.68	6.86	7.65	6.84	6.96	0.4	5.5
Eu	1.66	2.63	2.24	1.66	2.42	2.34	0.4	17.3
Gd	5.2	5.97	5.35	4.53	5.53	5.72	0.5	10.0
Tb	0.71	1.59	0.88	1.85	2.85	3.46	1.0	50.2
Dy	3.8	4.66	5.04	5.78	5.80	6.19	0.6	11.4
Ho	0.73	0.74	1.76	0.70	1.39	1.47	0.4	37.4
Er	1.61	1.53	1.48	1.64	2.47	3.25	0.8	37.9
Tm	0.32	0.95	1.25	0.23	1.23	1.53	0.5	48.5
Yb	1.67	1.57	1.48	1.35	2.36	1.55	0.4	25.5
Hf	5.12	4.53	4.56	4.37	4.03	4.58	0.2	5.0
Ta	0.92	0.46	0.54	0.93	0.65	0.59	0.2	32.3
Pb	36	37.48	35.65	36.36	37.03	35.30	0.9	2.5
Th	6.5	7.06	6.63	6.13	5.15	4.16	1.2	20.4
U	1.89	2.24	3.26	3.75	3.84	3.84	0.7	20.5

Table A.6 Summary of standard deviation and RSD values of the elements measured in standard AGV-1 from 5 replicate analyses of a single run. ; Recc. = recommended accepted values for the international standards. Values are in ppm.

Because the samples of each batch were run in a single analytical run using an ICP-MS auto sampler at the BNFL ICP-MS facility, it was possible to negate other possible sources of error, such as differences in inter-run calibration lines. This was possible because the

samples were run in a single day on the ICP-MS without changing the calibration lines. Future users of the methodology outlined above may find it useful, if attempting to determine accurate and precise low-level trace element values, to adopt a similar procedure to that employed in the XRF sample preparatory process: i.e. to emply multiple re-runs of replicate unknown samples.

A.3.2 SELECTIVE CHEMICAL LEACHING ANALYSIS

Leach solutions were analysed for Rb, Sr, Y, Zr, Nb, Cs, Ba, La, Ce, Pr, Nd, Sm, Eu, Gd, Tb, Ho, Er, Y, Hf, Ta, Pb, Th and U were analysed by inductively-coupled plasma mass spectrometry at the British Nuclear Fuels Westlakes Laboratory, Cumbria, and also on a Perkin Elmer Sciex 6000 at Durham University. Analysis of Fe, Mn, Al, Ca, Ti, Mg, Ni, Co, Cu, Zn, Pb and V using a Perkin Elmer 5000 Atomic Absorption Mass Spectrometer at Durham University.

This methodology is an adaptation of that supplied in personal communication from Rogers, T., (Marine Geochemistry Research, Dept. of Geology, Royal School of Mines). Partition analysis takes place in three stages using fresh 0.25 ± 0.001 g sub-samples that are leached with different agents. The final solutions are analyzed by ICP-MS. Chemical separation techniques have been widely used previously to determine pelagic sediment phases (e.g., Chester and Hughes, 1967; Aplin, 1983; Lyle *et al.*, 1984; Aplin and Cronan, 1985; Balistrieri and Murray, 1986; Miller & Cronan, 1994). In previous applications of this methodology, the (hot) HCl-soluble leachate has been known as the "iron oxide" fraction. The HCl attack principally dissolves the major elements Fe, Zn, Cu, Pb, Mg, Al and Ba (Cronan, 1976). Consequently, the HCl soluble leachate contains both the iron phase with associated elements bound in its structure (which are not soluble in hydroxylamine HCl), and the iron stripped from the insoluble clay minerals. The insoluble residuum made up of clay minerals has been termed the "aluminosilicate" fraction and represents lava-derived lattice-held detrital clay minerals stripped of adsorbed trace elements and quartz.

Cleaning procedures

The cleaning procedures for the apparatus used are the same as for whole rock analysis (refer to Appendix A.3.1).

Sample drying and weighing

Approximately 2 g of rock powder sample was transferred into a labelled glass vial. The glass vials were placed in an oven at 105°C overnight to remove trace moisture. From the

glass vial, three-sub-samples of 0.25 ± 0.0001 g were placed into three, previously cleaned, labelled Teflon bombs.

Acetic Acid Leach

The first 0.25g sub-sample of every sample was leached for 24 hours in 10ml 25% HNO_3 at room temperature. Using the pre-cleaned apparatus, each sample was then filtered using pre-weighed filter papers and the filtrate transferred to Savillex Teflon bombs. To each sample, 1 ml of Aristar HNO_3 was added and the product evaporated to a moist residue. This process was repeated twice using HNO_3, after which, the samples were allowed to cool. Finally, the sample was redissolved using 2.5 ml of Aristar HNO_3 and approximately 20 ml of deionised MilliQ water. The screw-cap was replaced and the sample boiled on a hot plate for 1 hour. At this stage, any samples in which undissolved material was apparent were discarded and the sample re-prepared. Using the automated dispenser, the samples were spiked with1.25 ml of a 2 ppm Rh, Re and Bi spike solution and made up accurately to 50 ml. The samples were now diluted to 50 ml in 3.5% HNO_3 with internal standards at 50 ppb. The samples were transferred to 60ml pre-cleaned bottles and at this stage were ready for analysis.

Acid Reducing Agent Leach

The second 0.25g sub-sample of every sample was then leached for 24 hours in screw-cap Teflon bombs with a 3:7 mixture of 35% Aristar HNO3 (v/v) and 25% Spectrosol hydroxylamine hydrochloride at room temperature. Using the pre-cleaned apparatus, each sample was then filtered using pre-weighed filter papers and the filtrate transferred to Savillex Teflon bombs. To each sample, 1 ml of Aristar HNO3 was added and the product evaporated to a moist residue. The resulting sample was subsequently filtered and prepared for ICP-MS analysis in exactly the same way as the acetic acid leachate.

Hot HCl Leach

The third and final 0.25g sub-sample of every sample was then leached for 24 hours in Teflon screw-cap bombs with 10ml of 50% (v/v) Analar HCl, on a hot plate for 6 hours at 90°C. Using the pre-cleaned apparatus, each sample was then filtered using pre-weighed filter papers and the filtrate transferred to Savillex Teflon bombs. To each sample, 1 ml of Aristar HNO3 was added and the product evaporated to a moist residue. The resulting sample was subsequently filtered and prepared for ICP-MS analysis in exactly the same way as the acetic acid leachate.

Limitations

A number of problems emerged with the application of this process, the worst being that leaches were not being mutually exclusive, e.g., some weathered material was removed in the

acid reducing leach. The results of the analysis clearly demonstrate this limitation, which has been drawn attention to in the text, and the data interpreted accordingly.

Precision, detection limits, and accuracy were determined for chemical leaching ICP-MS runs in the same way as for whole-rock analysis.

A.4 ATOMIC ABSORPTION SPECTROPHOTOMETRY (AA)

The elements Fe, Mn, Al, Ca, Ti, Mg, Ni, Co, Cu, Zn, Pb and V were analysed for the chemical separation experiment using a Perkin Elmer 5000 Atomic Absorption Mass Spectrometer at Durham University.

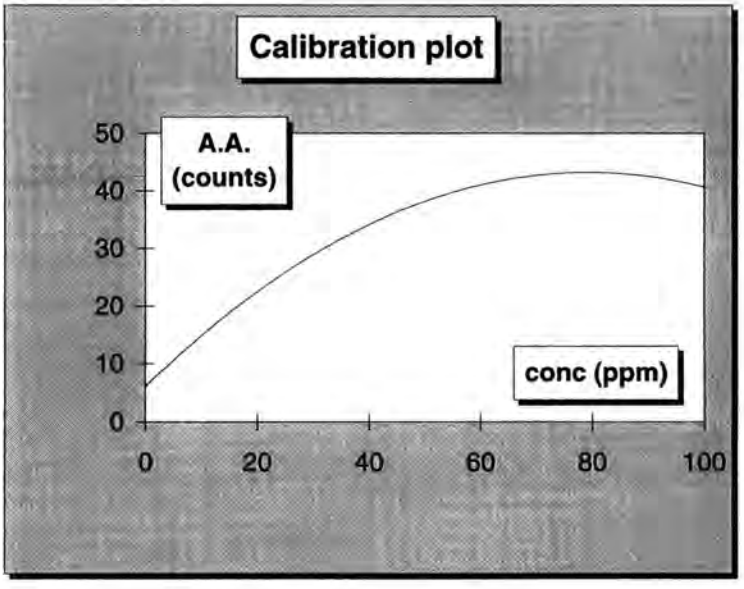

Figure A.2 Absorbance versus concentration showing a non-linear relationship >40ppm for K standard solutions.

A.4.1 Calculations

The equations below describe the determination of quantities required for the preparation of standard solutions and the determination of the concentration of the element of interest from its concentration in the sample solution.

Instrument calibration

The selection of the numbers and concentrations of calibration standards was very important, and it was essential that the range of concentrations of each element was already known for each sample from XRF whole-rock data. Quantitative measurements using AA are based on

Beer's Law, which states that concentration is proportional to absorbance (C=kA). However, at high concentrations, the relationship between concentration and absorbance deviates from Beer's law and becomes non-linear (Figure A.2). Using the Perkin-Elmer microprocessor-controlled instrument, an alogorithm is used which has the ability to calibrate and compute concentrations using absorbance from non-linear curves. The standard procedure uses three blanks and three standard solutions (calibration standards) in circumstances in which the unknown concentrations were thought to fall outside of the linear range. The first calibration standard falls at the top of the linear range, the second standard was approximately three times the concentration of the first, and the third standard was approximately twice the second standard.

A.4.2 Detection Limits

The AA detection limit is defined as the concentration of the element which will produce a signal/noise ratio of 2. Thus, the detection limit considers both the signal amplitude and the baseline noise, and is the lowest concentration which can clearly be differentiated from zero.

The standard procedure for establishing detection limits by flame AA is as follows: two concentrations of the element were prepared, with entirely separate pre-cleaned apparatus (refer to A.3.1) to remove the possibility of sample cross-contamination. The absorbance means of the two were established. This was done by making up the lower concentration standard to approximately five times the expected detection limit, and the second standard at twice the concnetration of the first. After establishing the optimum operating conditions, a reading was taken for each standard alternately twenty times. A blank reading was taken between each standard reading. Having obtained the data, the calculation to determine detection limit is as follows:

(1) the average of the blank readings before and after each standard are subtracted from the standard reading.
(2) the mean and standard deviation was calculated for the background-corrected standard readings. (At this stage, if the ratio of the concentrations prepared does not correspond to the ratio of the means, within statistical error, the data was rejected).
(3) detection limit was calculated from the following equation.

$$\text{Detection Limit} = \frac{(\text{Standard concentration})(2\ \text{Standard deviations})}{\text{Mean}}$$

The calculation was made independently for each standard concentration, and the detection limit equal to the average of the two results (Table A.7).

Element	Flame Atomic Absorption
Fe	0.003
Mn	0.001
Al	0.03
Ca	0.001
Ti	0.05
Mg	0.00001
Ni	0.004
Co	0.006
Cu	0.001
Zn	0.0008
Pb	0.01
V	0.04

Table A.7 Detection limits, $\mu g\ L^{-1}$

A.5 Percentage points of the *t*-Distribution

Table A.8 For a *t*-distribution with ν degrees of freedom, the table gives the values of t which are exceeded with probability α.

$\alpha =$	**0.05**	**0.025**	**0.01**
$\nu =$ *1*	6.314	12.706	31.821
2	2.920	4.303	6.965
3	2.353	3.182	4.541
4	2.132	2.776	3.747
5	2.015	2.571	3.365
6	1.943	2.447	3.143
7	1.895	2.365	2.998
8	1.860	2.306	2.896
9	1.833	2.262	2..821
10	1.812	2.228	2.764
20	1.721	2.086	2.528
25	1.708	2.060	2.485
30	1.697	2.042	2.457
40	1.684	2.021	2.423
60	1.671	2.000	2.390

APPENDIX B
MAJOR AND TRACE ELEMENT DATA

This appendix lists the geochemical data collected during the course of this study. The Rare Earth element normalising values used are from Boynton (1984).

B.1 XRF and ICP-MS data

All of the Oman samples are referred to by colour from the Munsell Soil Colour Chart, by location name, and by volcanic stratigraphic position (after Alabaster *et al.*, 1982)

As - sample from within the Axis lava unit
Bu - sample from within the Basal Upper (Alley) lava unit
Ls - sample from within the Lasail lava unit
As/Ls - sample from boundary of older As with younger Ls lava unit
As/Bu - sample from boundary of older As with younger Bu lava unit

Table B.1 Whole-rock data
Oman Metalliferous sediments

Appendix B

Sample	20681	U1	U10	U11	U13	U14	U14A	U15	U16	U17	U18
Sample Location	Lasail Mine (south)	Lasail Mine (south)	Lasail Mine (south)	Lasail Mine (south)	Lasail Mine (south)	Lasail Mine (south)	Lasail Mine (south)	Lasail Mine (south)	Lasail Mine (south)	Lasail Mine (south)	Lasail Mine (south)
Colour	greyish red	pale brown	dusky brown	greyish brown	moderate brown	olive grey	brownish grey	brownish grey	greyish red	greyish red	greyish brown
Colour Code	5 R 4/2	5 YR 5/2	5 YR 2/2	5 YR 3/2	5 YR 3/4	5 Y 4/1	5 YR 4/1	5 YR 4/1	10 R 4/2	10 R 4/2	5 YR 3/2
Horizon	As/Ls	As/Ls	As/Ls	As/Ls	As/Ls	As/Ls	As/Ls	As/Ls	As/Ls	As/Ls	As/Ls
SiO2	30.51	44.56	45.70	32.40	43.71	40.50	39.59	37.87	42.64	38.71	47.84
TiO2	0.23	0.33	0.01	0.01	0.11	0.17	0.17	0.14	0.21	0.19	0.11
Al2O3	5.84	6.52	0.75	0.91	4.08	2.99	5.82	5.86	5.42	5.15	4.70
Fe2O3	49.50	35.49	46.94	59.49	40.32	44.11	39.66	42.19	38.04	40.87	34.78
MnO	0.38	0.20	0.06	0.06	0.12	0.39	0.14	0.19	0.17	0.15	0.18
MgO	6.71	6.12	1.09	1.56	5.72	6.01	9.12	7.69	8.06	8.72	7.01
CaO	5.58	5.31	4.69	4.84	4.95	5.09	4.74	5.14	4.76	5.12	4.70
P2O5	1.24	1.47	0.76	0.74	0.99	0.73	0.76	0.92	0.70	1.08	0.68
CaCO3	2.90	0.70	1.51	1.00	0.05	0.75	0.00	0.00	0.00	0.79	0.00
Pb	1.0	16.0	1.0	1.0	1.0	1.0	1.0	1.0	1.0	1.0	1.0
Zn	48.4	97.6	40.4	29.4	35.7	62.3	51.8	45.1	46.9	36.7	43.0
Cu	127.8	32.7	1191.9	4966.7	35.6	23.2	12.3	530.3	62.7	29.7	68.1
Ni	444.5	332.1	43.9	36.1	187.1	351.9	262.6	253.8	197.4	264.0	215.0
Sr	138.0	100.1	262.6	96.7	81.3	197.7	181.7	97.6	73.6	269.5	
Co	122.0	123.0	121.0	187.0	93.0	92.0	80.0	93.0	104.0	95.0	92.0
Cr	59.7	33.4	43.4	35.5	5.3	38.7	24.6	39.0	21.1	27.7	29.8
V	352.0	174.7	276.9	422.1	486.4	306.4	252.0	184.6	232.4	149.2	244.1
Sc	18.7	11.7	5.2	0.4	16.2	12.5	8.2	8.7	11.2	10.3	11.6
Mo	15.0	13.0	60.0	32.0	17.0	12.0	16.0	17.0	12.0	18.0	22.0
As	69.0	150.0	26.0	18.0	32.0	10.0	19.0	12.0	17.0	36.0	16.0
Zr	21.7	45.7	4.8	3.8	21.8	29.2	24.7	18.5	25.0	24.8	24.2
Ba	18.0	10.0	3.1	0.8	25.8	13.5	15.1	7.8	2.9	13.9	17.5

Sample	U76	U77	U78	U8	U9	20647	20648	20660	20676	20686	20688
Sample Location	Lasail Mine (south)	Lasail Mine (south)	Lasail Mine (south)	Lasail Mine (south)	Lasail Mine (south)	Khabiyat (upper horizon)	Khabiyat (upper horizon)	Buriami Highway ii	Wadi Lasail	Huwayl	Semdah West
Colour	greyish brown	greyish red	brownish grey	greyish brown	moderate brown	moderate brown	dark yellowish brown	greyish red	moderate brown	dark yellowish brown	greyish brown
Colour Code	5 YR 3/2	5 R 4/2	5 YR 4/1	5 YR 3/2	5 YR 3/4	5 YR 3/4	10 YR 4/2	5 R 4/2	5 YR 3/4	10 YR 4/2	5 YR 3/2
Horizon	As/Ls	As/Ls	As/Ls	As/Ls	As/Ls	Bu/Bu	Bu/Bu	Bu/Bu	Bu/Bu	Bu/Bu	Bu/Bu
SiO2	46.76	47.21	62.72	42.43	59.89	55.21	46.67	50.09	51.37	53.12	46.28
TiO2	0.15	0.24	0.11	0.03	0.19	0.10	0.15	0.19	0.17	0.22	0.26
Al2O3	6.65	5.53	5.10	1.17	4.56	4.76	5.68	4.29	4.91	6.91	6.91
Fe2O3	26.79	27.61	22.73	49.70	24.54	24.00	27.79	27.22	25.31	32.31	23.23
MnO	10.51	10.99	0.12	0.06	0.41	6.95	10.98	9.59	9.23	0.71	11.10
MgO	1.97	0.88	3.69	0.85	4.81	3.10	1.75	1.68	1.84	0.44	3.12
CaO	6.33	6.20	5.01	4.85	4.81	5.76	6.35	6.34	6.51	5.52	8.55
P2O5	0.82	1.34	0.52	0.91	0.78	0.12	0.62	0.60	0.66	0.77	0.55
CaCO3	5.21	4.95	0.37	1.17	1.44	4.39	5.33	5.88	6.48	2.41	12.79
Pb	106.0	139.0	14.0	1.0	6.0	73.0	124.0	115.0	105.0	24.0	153.0
Zn	113.0	141.8	31.4	32.3	114.1	206.8	249.8	178.1	168.7	33.2	226.5
Cu	483.6	226.5	50.4	1258.6	7561.2	274.0	271.7	293.9	303.7	263.0	731.2
Ni	263.4	321.7	96.3	39.7	229.5	220.3	252.2	236.9	207.9	235.4	283.1
Sr	164.7	150.3	60.2	341.8	71.2	185.9	196.0	226.6	298.8	362.6	218.7
Co	230.0	283.0	37.0	116.0	77.0	169.0	201.0	181.0	188.0	131.0	126.0
Cr	47.6	40.8	18.9	63.1	84.6	24.9	61.6	87.0	65.8	305.4	1443.3
V	320.9	211.0	327.2	353.8	106.5	839.2	492.5	337.9	317.3	480.1	182.9
Sc	6.4	20.2	4.3	3.6	11.1	13.0	11.3	12.5	10.8	19.3	13.0
Mo	28.0	41.0	27.0	59.0	17.0	26.0	35.0	21.0	22.0	64.0	11.0
As	296.0	271.0	34.0	8.0	120.0	0.0	270.0	106.0	162.0	74.0	98.0
Zr	50.1	58.7	31.6	3.4	39.5	30.1	37.8	42.6	40.4	37.3	59.7
Ba	76.6	26.8	12.0	5.0	33.0	82.3	92.1	59.5	80.4	23.1	158.8

Table B.1 Whole-rock data
Oman Metalliferous sediments

Appendix B

Sample	U19	U2	U20	U21	U25	U26	U27	U28	U29	U3	U30
Sample Location	Lasail Mine (south)	Lasail Mine (south)	Lasail Mine (south)	Lasail Mine (south)	Huwayl (core)	Huwayl (core)	Huwayl (core)	Huwayl (core)	Huwayl (core)	Lasail Mine (south)	Huwayl (core)
Colour	greyish red	greyish brown	greyish red	greyish red	medium grey	medium dark grey	medium dark grey	medium dark grey	olive grey	greyish brown	dark grey
Colour Code	5 R 4/2	5 YR 3/2	5 R 4/2	10 R 4/2	N5	N4	N4	N4	5 Y 4/1	5 YR 3/2	N3
Horizon	As/Ls	As/Ls	As/Ls	As/Ls	As/Ls	As/Ls	As/Ls	As/Ls	As/Ls	As/Ls	As/Ls
SiO2	33.11	43.79	36.95	40.55	53.00	54.79	61.83	59.94	68.79	36.50	38.88
TiO2	0.18	0.01	0.32	0.18	0.14	0.17	0.12	0.13	0.14	0.01	0.34
Al2O3	5.62	0.83	5.69	4.38	8.42	4.65	3.67	5.32	3.96	1.08	7.70
Fe2O3	48.28	48.45	42.31	43.16	23.43	29.59	24.75	24.21	15.30	55.76	38.53
MnO	0.27	0.07	0.47	0.87	1.00	0.64	0.62	0.61	0.90	0.09	1.23
MgO	6.24	0.91	8.47	4.66	7.41	4.31	2.26	2.39	3.40	0.84	5.51
CaO	5.30	4.98	5.07	5.58	5.50	5.06	5.33	5.58	5.76	4.86	5.83
P2O5	1.00	0.98	0.72	0.61	1.10	0.79	1.42	1.81	1.75	0.86	1.97
CaCO3	1.27	2.23	0.10	2.90	2.36	0.00	1.57	1.67	2.84	1.02	2.12
Pb	1.0	1.0	1.0	1.0	16.0	10.0	18.0	18.5	21.0	1.0	5.0
Zn	40.7	38.7	95.1	65.4	46.3	40.0	36.2	39.3	45.8	31.5	49.0
Cu	40.4	1151.5	104.0	95.8	743.4	385.3	1302.4	2269.3	108.0	449.7	33.0
Ni	406.5	33.2	242.5	283.8	235.4	236.6	223.7	214.6	166.8	33.3	352.6
Sr	127.7	180.4	180.2	130.1	146.0	82.3	225.7	67.4	188.8	168.1	74.7
Co	114.0	133.0	125.0	89.0	71.0	83.0	69.0	53.0	52.0	126.0	152.0
Cr	30.9	39.5	28.7	56.7	141.2	56.4	66.6	73.0	90.2	48.1	76.8
V	332.9	376.8	246.6	199.0	383.3	250.1	173.8	161.4	354.8	405.8	407.5
Sc	10.8	3.5	21.7	14.3	14.3	13.4	9.9	5.9	12.4	0.5	24.9
Mo	10.0	48.0	9.0	23.0	48.0	72.0	99.0	103.0	130.0	50.0	41.0
As	46.0	6.0	36.0	60.0	84.0	78.0	87.0	105.0	76.0	4.0	198.0
Zr	16.5	3.4	26.8	32.5	60.0	40.0	39.9	43.3	48.5	2.9	54.8
Ba	11.7	9.3	8.9	30.5	14.7	15.0	20.2	19.9	15.7	6.6	27.6

Sample	20689	20690	20691	20692	20693	20694	20695	20696	20697	20698	20699
Sample Location	Semdah West	Semdah West	Semdah West	Semdah West	Semdah West	Ghayth	Ghayth	Ghayth	Ghayth	Ghayth	Semdah West
Colour	moderate brown	greyish brown	greyish brown	dusky brown	moderate brown	dusky brown	dusky brown	blackish red	greyish red	greyish red	greyish brown
Colour Code	5 YR 3/3	5 YR 3/2	5 YR 3/2	5 YR 2/2	5 YR 3/4	5YR 2/2	5 YR 2/2	5 R 2/2	10 R 4/2	5 R 4/2	5 YR 3/2
Horizon	Bu/Bu	Bu/Bu	Bu/Bu	Bu/Bu	Bu/Bu	Bu/Bu	Bu/Bu	Bu/Bu	Bu/Bu	Bu/Bu	Bu/Bu
SiO2	45.66	53.85	54.37	58.83	50.56	34.79	32.41	38.06	40.60	42.23	59.74
TiO2	0.26	0.24	0.24	0.17	0.26	0.27	0.26	0.22	0.25	0.23	0.21
Al2O3	7.18	6.23	6.30	6.81	6.67	5.04	4.32	4.40	4.77	4.73	6.13
Fe2O3	23.46	22.92	23.51	16.40	23.95	29.50	35.96	36.51	36.94	33.71	18.40
MnO	10.66	7.44	6.92	7.72	7.22	20.98	17.69	8.58	4.94	4.57	6.06
MgO	3.68	2.86	2.53	3.66	4.87	2.47	2.48	5.91	4.47	6.14	3.34
CaO	8.54	5.79	5.61	6.04	5.90	6.36	6.17	5.08	6.67	6.09	5.72
P2O5	0.56	0.66	0.52	0.37	0.55	0.59	0.73	1.24	1.36	2.30	0.40
CaCO3	13.89	2.72	0.26	4.45	3.43	5.75	5.14	0.17	5.48	4.05	3.61
Pb	143.0	150.0	146.0	135.0	163.0	46.3	144.0	1.0	14.0	10.0	120.0
Zn	221.1	206.2	183.4	154.7	211.9	241.1	268.5	120.2	88.6	96.3	174.9
Cu	528.1	528.3	462.6	614.2	446.2	376.0	653.2	69.9	33.4	53.1	367.2
Ni	262.7	245.4	243.2	219.4	285.8	376.3	421.2	381.0	382.4	343.2	208.4
Sr	237.6	189.2	202.3	157.8	171.2	186.1	181.7	91.0	157.6	133.1	154.6
Co	121.0	162.0	163.0	119.0	153.0	475.0	439.0	355.0	124.0	145.0	127.0
Cr	351.7	185.8	413.9	335.4	218.8	265.4	214.1	46.7	99.8	99.1	50.2
V	203.7	252.3	224.0	485.2	159.9	88.2	148.9	124.2	310.6	258.1	411.9
Sc	19.3	12.5	10.6	10.2	15.3	14.5	12.3	14.3	11.3	11.5	8.7
Mo	15.0	15.0	17.0	15.0	18.0	40.0	39.0	7.0	7.0	9.0	13.0
As	197.0	165.0	152.0	184.0	999.0	176.0	241.0	325.0	179.0	256.0	146.0
Zr	50.7	80.4	76.1	50.7	55.7	64.8	60.5	42.7	51.6	44.4	71.5
Ba	181.6	981.1	1215.1	325.6	94.5	41.9	57.4	556.6	26.0	17.2	991.7

Table B.1 Whole-rock data
Oman Metalliferous sediments

Appendix B

Sample	U19	U2	U20	U21	U25	U26	U27	U28	U29	U3	U30
Sample Location	Lasail Mine (south)	Lasail Mine (south)	Lasail Mine (south)	Lasail Mine (south)	Huwayl (core)	Huwayl (core)	Huwayl (core)	Huwayl (core)	Huwayl (core)	Lasail Mine (south)	Huwayl (core)
Colour	greyish red	greyish brown	greyish red	greyish red	medium grey	medium dark grey	medium dark grey	medium dark grey	olive grey	greyish brown	dark grey
Colour Code	5 R 4/2	5 YR 3/2	5 R 4/2	10 R 4/2	N5	N4	N4	N4	5 Y 4/1	5 YR 3/2	N3
Horizon	As/Ls	As/Ls	As/Ls	As/Ls	As/Ls	As/Ls	As/Ls	As/Ls	As/Ls	As/Ls	As/Ls
SiO2	33.11	43.79	36.95	40.55	53.00	54.79	61.83	59.94	68.79	36.50	38.88
TiO2	0.18	0.01	0.32	0.18	0.14	0.17	0.12	0.13	0.14	0.01	0.34
Al2O3	5.62	0.83	5.69	4.38	8.42	4.65	3.67	5.32	3.96	1.08	7.70
Fe2O3	48.28	48.45	42.31	43.16	23.43	29.59	24.75	24.21	15.30	55.76	38.53
MnO	0.27	0.07	0.47	0.87	1.00	0.64	0.62	0.61	0.90	0.09	1.23
MgO	6.24	0.91	8.47	4.66	7.41	4.31	2.26	2.39	3.40	0.84	5.51
CaO	5.30	4.98	5.07	5.58	5.50	5.06	5.33	5.58	5.76	4.86	5.83
P2O5	1.00	0.98	0.72	0.61	1.10	0.79	1.42	1.81	1.75	0.86	1.97
CaCO3	1.27	2.23	0.10	2.90	2.36	0.00	1.57	1.67	2.84	1.02	2.12
Pb	1.0	1.0	1.0	1.0	16.0	10.0	18.0	18.5	21.0	1.0	5.0
Zn	40.7	38.7	95.1	65.4	46.3	40.0	36.2	39.3	45.8	31.5	49.0
Cu	40.4	1151.5	104.0	95.8	743.4	385.3	1302.4	2269.3	108.0	449.7	33.0
Ni	406.5	33.2	242.5	283.8	235.4	236.6	223.7	214.6	166.8	33.3	352.6
Sr	127.7	180.4	180.2	130.1	146.0	82.3	225.7	67.4	188.8	168.1	74.7
Co	114.0	133.0	125.0	89.0	71.0	83.0	69.0	53.0	52.0	126.0	152.0
Cr	30.9	39.5	28.7	56.7	141.2	56.4	66.6	73.0	90.2	48.1	76.8
V	332.9	376.8	246.6	199.0	383.3	250.1	173.8	161.4	354.8	405.8	407.5
Sc	10.8	3.5	21.7	14.3	14.3	13.4	9.9	5.9	12.4	0.5	24.9
Mo	10.0	48.0	9.0	23.0	48.0	72.0	99.0	103.0	130.0	50.0	41.0
As	46.0	6.0	36.0	60.0	84.0	78.0	87.0	105.0	76.0	4.0	198.0
Zr	16.5	3.4	26.8	32.5	60.0	40.0	39.9	43.3	48.5	2.9	54.8
Ba	11.7	9.3	8.9	30.5	14.7	15.0	20.2	19.9	15.7	6.6	27.6

Sample	20689	20690	20691	20692	20693	20694	20695	20696	20697	20698	20699
Sample Location	Semdah West	Semdah West	Semdah West	Semdah West	Semdah West	Ghayth	Ghayth	Ghayth	Ghayth	Ghayth	Semdah West
Colour	moderate brown	greyish brown	greyish brown	dusky brown	moderate brown	dusky brown	dusky brown	blackish red	greyish red	greyish red	greyish brown
Colour Code	5 YR 3/3	5 YR 3/2	5 YR 3/2	5 YR 2/2	5 YR 3/4	5YR 2/2	5 YR 2/2	5 R 2/2	10 R 4/2	5 R 4/2	5 YR 3/2
Horizon	Bu/Bu	Bu/Bu	Bu/Bu	Bu/Bu	Bu/Bu	Bu/Bu	Bu/Bu	Bu/Bu	Bu/Bu	Bu/Bu	Bu/Bu
SiO2	45.66	53.85	54.37	58.83	50.56	34.79	32.41	38.06	40.60	42.23	59.74
TiO2	0.26	0.24	0.24	0.17	0.26	0.27	0.26	0.22	0.25	0.23	0.21
Al2O3	7.18	6.23	6.30	6.81	6.67	5.04	4.32	4.40	4.77	4.73	6.13
Fe2O3	23.46	22.92	23.51	16.40	23.95	29.50	35.96	36.51	36.94	33.71	18.40
MnO	10.66	7.44	6.92	7.72	7.22	20.98	17.69	8.58	4.94	4.57	6.06
MgO	3.68	2.86	2.53	3.66	4.87	2.47	2.48	5.91	4.47	6.14	3.34
CaO	8.54	5.79	5.61	6.04	5.90	6.36	6.17	5.08	6.67	6.09	5.72
P2O5	0.56	0.66	0.52	0.37	0.55	0.59	0.73	1.24	1.36	2.30	0.40
CaCO3	13.89	2.72	0.26	4.45	3.43	5.75	5.14	0.17	5.48	4.05	3.61
Pb	143.0	150.0	146.0	135.0	163.0	46.3	144.0	1.0	14.0	10.0	120.0
Zn	221.1	206.2	183.4	154.7	211.9	241.1	268.5	120.2	88.6	96.3	174.9
Cu	528.1	528.3	462.6	614.2	446.2	376.0	653.2	69.9	33.4	53.1	367.2
Ni	262.7	245.4	243.2	219.4	285.8	376.3	421.2	381.0	382.4	343.2	208.4
Sr	237.6	189.2	202.3	157.8	171.2	186.1	181.7	91.0	157.6	133.1	154.6
Co	121.0	162.0	163.0	119.0	153.0	475.0	439.0	355.0	124.0	145.0	127.0
Cr	351.7	185.8	413.9	335.4	218.8	265.4	214.1	46.7	99.8	99.1	50.2
V	203.7	252.3	224.0	485.2	159.9	88.2	148.9	124.2	310.6	258.1	411.9
Sc	19.3	12.5	10.6	10.2	15.3	14.5	12.3	14.3	11.3	11.5	8.7
Mo	15.0	15.0	17.0	15.0	18.0	40.0	39.0	7.0	7.0	9.0	13.0
As	197.0	165.0	152.0	184.0	999.0	176.0	241.0	325.0	179.0	256.0	146.0
Zr	50.7	80.4	76.1	50.7	55.7	64.8	60.5	42.7	51.6	44.4	71.5
Ba	181.6	981.1	1215.1	325.6	94.5	41.9	57.4	556.6	26.0	17.2	991.7

Table B.1 Whole-rock data
Oman Metalliferous sediments

Appendix B

Sample	U19	U2	U20	U21	U25	U26	U27	U28	U29	U3	U30
Sample Location	Lasail Mine (south)	Lasail Mine (south)	Lasail Mine (south)	Lasail Mine (south)	Huwayl (core)	Huwayl (core)	Huwayl (core)	Huwayl (core)	Huwayl (core)	Lasail Mine (south)	Huwayl (core)
Colour	greyish red	greyish brown	greyish red	greyish red	medium grey	medium dark grey	medium dark grey	medium dark grey	olive grey	greyish brown	dark grey
Colour Code	5 R 4/2	5 YR 3/2	5 R 4/2	10 R 4/2	N5	N4	N4	N4	5 Y 4/1	5 YR 3/2	N3
Horizon	As/Ls	As/Ls	As/Ls	As/Ls	As/Ls	As/Ls	As/Ls	As/Ls	As/Ls	As/Ls	As/Ls
SiO2	33.11	43.79	36.95	40.55	53.00	54.79	61.83	59.94	68.79	36.50	38.88
TiO2	0.18	0.01	0.32	0.18	0.14	0.17	0.12	0.13	0.14	0.01	0.34
Al2O3	5.62	0.83	5.69	4.38	8.42	4.65	3.67	5.32	3.96	1.08	7.70
Fe2O3	48.28	48.45	42.31	43.16	23.43	29.59	24.75	24.21	15.30	55.76	38.53
MnO	0.27	0.07	0.47	0.87	1.00	0.64	0.62	0.61	0.90	0.09	1.23
MgO	6.24	0.91	8.47	4.66	7.41	4.31	2.26	2.39	3.40	0.84	5.51
CaO	5.30	4.98	5.07	5.58	5.50	5.06	5.33	5.58	5.76	4.86	5.83
P2O5	1.00	0.98	0.72	0.61	1.10	0.79	1.42	1.81	1.75	0.86	1.97
CaCO3	1.27	2.23	0.10	2.90	2.36	0.00	1.57	1.67	2.84	1.02	2.12
Pb	1.0	1.0	1.0	1.0	16.0	10.0	18.0	18.5	21.0	1.0	5.0
Zn	40.7	38.7	95.1	65.4	46.3	40.0	36.2	39.3	45.8	31.5	49.0
Cu	40.4	1151.5	104.0	95.8	743.4	385.3	1302.4	2269.3	108.0	449.7	33.0
Ni	406.5	33.2	242.5	283.8	235.4	236.6	223.7	214.6	166.8	33.3	352.6
Sr	127.7	180.4	180.2	130.1	146.0	82.3	225.7	67.4	188.8	168.1	74.7
Co	114.0	133.0	125.0	89.0	71.0	83.0	69.0	53.0	52.0	126.0	152.0
Cr	30.9	39.5	28.7	56.7	141.2	56.4	66.6	73.0	90.2	48.1	76.8
V	332.9	376.8	246.6	199.0	383.3	250.1	173.8	161.4	354.8	405.8	407.5
Sc	10.8	3.5	21.7	14.3	14.3	13.4	9.9	5.9	12.4	0.5	24.9
Mo	10.0	48.0	9.0	23.0	48.0	72.0	99.0	103.0	130.0	50.0	41.0
As	46.0	6.0	36.0	60.0	84.0	78.0	87.0	105.0	76.0	4.0	198.0
Zr	16.5	3.4	26.8	32.5	60.0	40.0	39.9	43.3	48.5	2.9	54.8
Ba	11.7	9.3	8.9	30.5	14.7	15.0	20.2	19.9	15.7	6.6	27.6

Sample	20689	20690	20691	20692	20693	20694	20695	20696	20697	20698	20699
Sample Location	Semdah West	Semdah West	Semdah West	Semdah West	Semdah West	Ghayth	Ghayth	Ghayth	Ghayth	Ghayth	Semdah West
Colour	moderate brown	greyish brown	greyish brown	dusky brown	moderate brown	dusky brown	dusky brown	blackish red	greyish red	greyish red	greyish brown
Colour Code	5 YR 3/3	5 YR 3/2	5 YR 3/2	5 YR 2/2	5 YR 3/4	5YR 2/2	5 YR 2/2	5 R 2/2	10 R 4/2	5 R 4/2	5 YR 3/2
Horizon	Bu/Bu	Bu/Bu	Bu/Bu	Bu/Bu	Bu/Bu	Bu/Bu	Bu/Bu	Bu/Bu	Bu/Bu	Bu/Bu	Bu/Bu
SiO2	45.66	53.85	54.37	58.83	50.56	34.79	32.41	38.06	40.60	42.23	59.74
TiO2	0.26	0.24	0.24	0.17	0.26	0.27	0.26	0.22	0.25	0.23	0.21
Al2O3	7.18	6.23	6.30	6.81	6.67	5.04	4.32	4.40	4.77	4.73	6.13
Fe2O3	23.46	22.92	23.51	16.40	23.95	29.50	35.96	36.51	36.94	33.71	18.40
MnO	10.66	7.44	6.92	7.72	7.22	20.98	17.69	8.58	4.94	4.57	6.06
MgO	3.68	2.86	2.53	3.66	4.87	2.47	2.48	5.91	4.47	6.14	3.34
CaO	8.54	5.79	5.61	6.04	5.90	6.36	6.17	5.08	6.67	6.09	5.72
P2O5	0.56	0.66	0.52	0.37	0.55	0.59	0.73	1.24	1.36	2.30	0.40
CaCO3	13.89	2.72	0.26	4.45	3.43	5.75	5.14	0.17	5.48	4.05	3.61
Pb	143.0	150.0	146.0	135.0	163.0	46.3	144.0	1.0	14.0	10.0	120.0
Zn	221.1	206.2	183.4	154.7	211.9	241.1	268.5	120.2	88.6	96.3	174.9
Cu	528.1	528.3	462.6	614.2	446.2	376.0	653.2	69.9	33.4	53.1	367.2
Ni	262.7	245.4	243.2	219.4	285.8	376.3	421.2	381.0	382.4	343.2	208.4
Sr	237.6	189.2	202.3	157.8	171.2	186.1	181.7	91.0	157.6	133.1	154.6
Co	121.0	162.0	163.0	119.0	153.0	475.0	439.0	355.0	124.0	145.0	127.0
Cr	351.7	185.8	413.9	335.4	218.8	265.4	214.1	46.7	99.8	99.1	50.2
V	203.7	252.3	224.0	485.2	159.9	88.2	148.9	124.2	310.6	258.1	411.9
Sc	19.3	12.5	10.6	10.2	15.3	14.5	12.3	14.3	11.3	11.5	8.7
Mo	15.0	15.0	17.0	15.0	18.0	40.0	39.0	7.0	7.0	9.0	13.0
As	197.0	165.0	152.0	184.0	999.0	176.0	241.0	325.0	179.0	256.0	146.0
Zr	50.7	80.4	76.1	50.7	55.7	64.8	60.5	42.7	51.6	44.4	71.5
Ba	181.6	981.1	1215.1	325.6	94.5	41.9	57.4	556.6	26.0	17.2	991.7

Table B.1 Whole-rock data
Oman Metalliferous sediments

Appendix B

Sample	U31	U32	U33	U34	U35	U36
Sample Location	Huwayl (core)	Huwayl (core)	Huwayl (core)	Huwayl (core)	Huwayl (core)	Huwayl (outcrop)
Colour	medium dark grey	brownish black	medium dark grey	dark grey	dusky yellowish brown	greyish red
Colour Code	N4	5 YR 2/1	N4	N3	10 YR 2/2	10 R 4/2
Horizon	As/Ls	As/Ls	As/Ls	As/Ls	As/Ls	As/Ls
SiO2	46.60	59.64	45.27	39.93	58.77	54.78
TiO2	0.14	0.10	0.25	0.18	0.13	0.22
Al2O3	3.37	3.05	5.85	3.70	3.96	4.85
Fe2O3	35.87	23.51	31.81	45.33	26.22	27.08
MnO	0.38	0.42	0.73	0.43	0.62	0.32
MgO	8.72	6.49	10.22	4.58	4.68	7.86
CaO	4.61	4.86	4.90	5.06	4.95	4.68
P2O5	0.31	1.93	0.96	0.79	0.67	0.21
CaCO3	0.00	2.70	0.00	0.10	0.00	0.00
Pb	1.0	1.0	1.0	1.0	6.0	5.0
Zn	61.6	76.4	36.7	27.0	32.1	53.5
Cu	8.7	14.5	11.5	14.8	16.7	9.2
Ni	406.6	322.2	601.6	654.0	309.1	296.9
Sr	104.5	127.9	57.1	70.4	68.9	84.1
Co	121.0	89.0	142.0	65.0	87.0	106.0
Cr	120.7	92.7	78.2	46.8	51.1	97.1
V	439.5	364.9	431.6	238.1	250.7	384.9
Sc	11.4	8.6	17.2	11.8	8.3	6.2
Mo	58.0	63.0	35.0	39.0	80.0	40.0
As	63.0	225.0	144.0	117.0	105.0	2.0
Zr	24.1	38.3	49.9	20.4	44.5	41.3
Ba	8.7	11.6	11.5	6.4	14.8	21.3

Sample	20700	U22	U23	U24	U43	U44
Sample Location	Wadi Fizh (far E. horizon)	Semdah West	Semdah West	Semdah West	Huwayl (outcrop)	Huwayl (outcrop)
Colour	moderate brown	blackish red	blackish red	very dusky red	greyish brown	greyish red
Colour Code	5 YR 3/4	5 R 2/2	5 R 2/2	10 R 2/2	5 YR 3/2	5 R 4/2
Horizon	Bu/Bu	Bu/Bu	Bu/Bu	Bu/Bu	Ls/Ls	Ls/Ls
SiO2	51.27	46.10	44.78	31.96	41.74	54.19
TiO2	0.18	0.15	0.14	0.20	0.10	0.22
Al2O3	7.85	3.14	2.99	4.17	3.68	5.65
Fe2O3	21.25	29.89	32.87	40.65	45.16	27.74
MnO	10.29	13.38	12.16	13.25	0.31	0.84
MgO	2.37	1.14	0.57	1.23	3.72	5.88
CaO	6.43	5.72	5.75	6.53	4.88	5.06
P2O5	0.36	0.49	0.75	2.01	0.41	0.42
CaCO3	6.69	3.10	3.06	4.36	0.83	1.41
Pb		71.0	65.0	63.0	1.0	9.0
Zn	210.8	175.1	158.4	135.2	34.9	64.9
Cu	831.2	43.8	800.0	104.1	42.4	277.3
Ni	276.7	269.5	341.2	382.3	267.6	279.9
Sr	268.6	130.2	174.2	108.3	113.4	84.9
Co		302.0	438.0	406.0	126.0	111.0
Cr	88.9	72.8	28.8	69.1	28.8	30.1
V	667.0	225.1	479.3	530.3	351.2	286.8
Sc	23.5	11.9	12.5	18.0	9.1	8.7
Mo		20.0	20.0	17.0	33.0	15.0
As		305.0	305.0	377.0	16.0	90.0
Zr	49.3	73.8	48.8	67.1	7.1	51.9
Ba	180.4	19.6	37.5	16.2	9.4	31.5

Table B.1 Whole-rock data
Oman Metalliferous sediments

Appendix B

Sample	U31	U32	U33	U34	U35	U36
Sample Location	Huwayl (core)	Huwayl (core)	Huwayl (core)	Huwayl (core)	Huwayl (core)	Huwayl (outcrop)
Colour	medium dark grey	brownish black	medium dark grey	dark grey	dusky yellowish brown	greyish red
Colour Code	N4	5 YR 2/1	N4	N3	10 YR 2/2	10 R 4/2
Horizon	As/Ls	As/Ls	As/Ls	As/Ls	As/Ls	As/Ls
SiO2	46.60	59.64	45.27	39.93	58.77	54.78
TiO2	0.14	0.10	0.25	0.18	0.13	0.22
Al2O3	3.37	3.05	5.85	3.70	3.96	4.85
Fe2O3	35.87	23.51	31.81	45.33	26.22	27.08
MnO	0.38	0.42	0.73	0.43	0.62	0.32
MgO	8.72	6.49	10.22	4.58	4.68	7.86
CaO	4.61	4.86	4.90	5.06	4.95	4.68
P2O5	0.31	1.93	0.96	0.79	0.67	0.21
CaCO3	0.00	2.70	0.00	0.10	0.00	0.00
Pb	1.0	1.0	1.0	1.0	6.0	5.0
Zn	61.6	76.4	36.7	27.0	32.1	53.5
Cu	8.7	14.5	11.5	14.8	16.7	9.2
Ni	406.6	322.2	601.6	654.0	309.1	296.9
Sr	104.5	127.9	57.1	70.4	68.9	84.1
Co	121.0	89.0	142.0	65.0	87.0	106.0
Cr	120.7	92.7	78.2	46.8	51.1	97.1
V	439.5	364.9	431.6	238.1	250.7	384.9
Sc	11.4	8.6	17.2	11.8	8.3	6.2
Mo	58.0	63.0	35.0	39.0	80.0	40.0
As	63.0	225.0	144.0	117.0	105.0	2.0
Zr	24.1	38.3	49.9	20.4	44.5	41.3
Ba	8.7	11.6	11.5	6.4	14.8	21.3

Sample	20700	U22	U23	U24	U43	U44
Sample Location	Wadi Fizh (far E. horizon)	Semdah West	Semdah West	Semdah West	Huwayl (outcrop)	Huwayl (outcrop)
Colour	moderate brown	blackish red	blackish red	very dusky red	greyish brown	greyish red
Colour Code	5 YR 3/4	5 R 2/2	5 R 2/2	10 R 2/2	5 YR 3/2	5 R 4/2
Horizon	Bu/Bu	Bu/Bu	Bu/Bu	Bu/Bu	Ls/Ls	Ls/Ls
SiO2	51.27	46.10	44.78	31.96	41.74	54.19
TiO2	0.18	0.15	0.14	0.20	0.10	0.22
Al2O3	7.85	3.14	2.99	4.17	3.68	5.65
Fe2O3	21.25	29.89	32.87	40.65	45.16	27.74
MnO	10.29	13.38	12.16	13.25	0.31	0.84
MgO	2.37	1.14	0.57	1.23	3.72	5.88
CaO	6.43	5.72	5.75	6.53	4.88	5.06
P2O5	0.36	0.49	0.75	2.01	0.41	0.42
CaCO3	6.69	3.10	3.06	4.36	0.83	1.41
Pb		71.0	65.0	63.0	1.0	9.0
Zn	210.8	175.1	158.4	135.2	34.9	64.9
Cu	831.2	43.8	800.0	104.1	42.4	277.3
Ni	276.7	269.5	341.2	382.3	267.6	279.9
Sr	268.6	130.2	174.2	108.3	113.4	84.9
Co		302.0	438.0	406.0	126.0	111.0
Cr	88.9	72.8	28.8	69.1	28.8	30.1
V	667.0	225.1	479.3	530.3	351.2	286.8
Sc	23.5	11.9	12.5	18.0	9.1	8.7
Mo		20.0	20.0	17.0	33.0	15.0
As		305.0	305.0	377.0	16.0	90.0
Zr	49.3	73.8	48.8	67.1	7.1	51.9
Ba	180.4	19.6	37.5	16.2	9.4	31.5

Table B.1 Whole-rock data
Oman Metalliferous sediments

Appendix B

Sample	20681	U1	U10	U11	U13	U14	U14A	U15	U16	U17	U18
Sample Location	Lasail Mine (south)	Lasail Mine (south)	Lasail Mine (south)	Lasail Mine (south)	Lasail Mine (south)	Lasail Mine (south)	Lasail Mine (south)	Lasail Mine (south)	Lasail Mine (south)	Lasail Mine (south)	Lasail Mine (south)
Colour	greyish red	pale brown	dusky brown	greyish brown	moderate brown	olive grey	brownish grey	brownish grey	greyish red	greyish red	greyish brown
Colour Code	5 R 4/2	5 YR 5/2	5 YR 2/2	5 YR 3/2	5 YR 3/4	5 Y 4/1	5 YR 4/1	5 YR 4/1	10 R 4/2	10 R 4/2	5 YR 3/2
Horizon	As/Ls	As/Ls	As/Ls	As/Ls	As/Ls	As/Ls	As/Ls	As/Ls	As/Ls	As/Ls	As/Ls
SiO2	30.51	44.56	45.70	32.40	43.71	40.50	39.59	37.87	42.64	38.71	47.84
TiO2	0.23	0.33	0.01	0.01	0.11	0.17	0.17	0.14	0.21	0.19	0.11
Al2O3	5.84	6.52	0.75	0.91	4.08	2.99	5.82	5.86	5.42	5.15	4.70
Fe2O3	49.50	35.49	46.94	59.49	40.32	44.11	39.66	42.19	38.04	40.87	34.78
MnO	0.38	0.20	0.06	0.06	0.12	0.39	0.14	0.19	0.17	0.15	0.18
MgO	6.71	6.12	1.09	1.56	5.72	6.01	9.12	7.69	8.06	8.72	7.01
CaO	5.58	5.31	4.69	4.84	4.95	5.09	4.74	5.14	4.76	5.12	4.70
P2O5	1.24	1.47	0.76	0.74	0.99	0.73	0.76	0.92	0.70	1.08	0.68
CaCO3	2.90	0.70	1.51	1.00	0.05	0.75	0.00	0.00	0.00	0.79	0.00
Pb	1.0	16.0	1.0	1.0	1.0	1.0	1.0	1.0	1.0	1.0	1.0
Zn	48.4	97.6	40.4	29.4	35.7	62.3	51.8	45.1	46.9	36.7	43.0
Cu	127.8	32.7	1191.9	4966.7	35.6	23.2	12.3	530.3	62.7	29.7	68.1
Ni	444.5	332.1	43.9	36.1	187.1	351.9	262.6	253.8	197.4	264.0	215.0
Sr	138.0	100.1	262.6	96.7	81.3	197.7	181.7	97.6	73.6	269.5	
Co	122.0	123.0	121.0	187.0	93.0	92.0	80.0	93.0	104.0	95.0	92.0
Cr	59.7	33.4	43.4	35.5	5.3	38.7	24.6	39.0	21.1	27.7	29.8
V	352.0	174.7	276.9	422.1	486.4	306.4	252.0	184.6	232.4	149.2	244.1
Sc	18.7	11.7	5.2	0.4	16.2	12.5	8.2	8.7	11.2	10.3	11.6
Mo	15.0	13.0	60.0	32.0	17.0	12.0	16.0	17.0	12.0	18.0	22.0
As	69.0	150.0	26.0	18.0	32.0	10.0	19.0	12.0	17.0	36.0	16.0
Zr	21.7	45.7	4.8	3.8	21.8	29.2	24.7	18.5	25.0	24.8	24.2
Ba	18.0	10.0	3.1	0.8	25.8	13.5	15.1	7.8	2.9	13.9	17.5

Sample	U76	U77	U78	U8	U9	20647	20648	20660	20676	20686	20688
Sample Location	Lasail Mine (south)	Lasail Mine (south)	Lasail Mine (south)	Lasail Mine (south)	Lasail Mine (south)	Khabiyat (upper horizon)	Khabiyat (upper horizon)	Buriami Highway ii	Wadi Lasail	Huwayl	Semdah West
Colour	greyish brown	greyish red	brownish grey	greyish brown	moderate brown	moderate brown	dark yellowish brown	greyish red	moderate brown	dark yellowish brown	greyish brown
Colour Code	5 YR 3/2	5 R 4/2	5 YR 4/1	5 YR 3/2	5 YR 3/4	5 YR 3/4	10 YR 4/2	5 R 4/2	5 YR 3/4	10 YR 4/2	5 YR 3/2
Horizon	As/Ls	As/Ls	As/Ls	As/Ls	As/Ls	Bu/Bu	Bu/Bu	Bu/Bu	Bu/Bu	Bu/Bu	Bu/Bu
SiO2	46.76	47.21	62.72	42.43	59.89	55.21	46.67	50.09	51.37	53.12	46.28
TiO2	0.15	0.24	0.11	0.03	0.19	0.10	0.15	0.19	0.17	0.22	0.26
Al2O3	6.65	5.53	5.10	1.17	4.56	4.76	5.68	4.29	4.91	6.91	6.91
Fe2O3	26.79	27.61	22.73	49.70	24.54	24.00	27.79	27.22	25.31	32.31	23.23
MnO	10.51	10.99	0.12	0.06	0.41	6.95	10.98	9.59	9.23	0.71	11.10
MgO	1.97	0.88	3.69	0.85	4.81	3.10	1.75	1.68	1.84	0.44	3.12
CaO	6.33	6.20	5.01	4.85	4.81	5.76	6.35	6.34	6.51	5.52	8.55
P2O5	0.82	1.34	0.52	0.91	0.78	0.12	0.62	0.60	0.66	0.77	0.55
CaCO3	5.21	4.95	0.37	1.17	1.44	4.39	5.33	5.88	6.48	2.41	12.79
Pb	106.0	139.0	14.0	1.0	6.0	73.0	124.0	115.0	105.0	24.0	153.0
Zn	113.0	141.8	31.4	32.3	114.1	206.8	249.8	178.1	168.7	33.2	226.5
Cu	483.6	226.5	50.4	1258.6	7561.2	274.0	271.7	293.9	303.7	263.0	731.2
Ni	263.4	321.7	96.3	39.7	229.5	220.3	252.2	236.9	207.9	235.4	283.1
Sr	164.7	150.3	60.2	341.8	71.2	185.9	196.0	226.6	298.8	362.6	218.7
Co	230.0	283.0	37.0	116.0	77.0	169.0	201.0	181.0	188.0	131.0	126.0
Cr	47.6	40.8	18.9	63.1	84.6	24.9	61.6	87.0	65.8	305.4	1443.3
V	320.9	211.0	327.2	353.8	106.5	839.2	492.5	337.9	317.3	480.1	182.9
Sc	6.4	20.2	4.3	3.6	11.1	13.0	11.3	12.5	10.8	19.3	13.0
Mo	28.0	41.0	27.0	59.0	17.0	26.0	35.0	21.0	22.0	64.0	11.0
As	296.0	271.0	34.0	8.0	120.0	0.0	270.0	106.0	162.0	74.0	98.0
Zr	50.1	58.7	31.6	3.4	39.5	30.1	37.8	42.6	40.4	37.3	59.7
Ba	76.6	26.8	12.0	5.0	33.0	82.3	92.1	59.5	80.4	23.1	158.8

Table B.2 Whole-rock REE data
Oman Metalliferous sediments

Sample	20635	20639	20641	20643	20653	20654	20668	20669	U82
Sample Location	Khabiyat (main horizon)	Khabiyat (main horizon)	Khabiyat (main horizon)	Khabiyat (main horizon)	Wadi Suq	Wadi Suq	Khabiyat (Sthn hoizon)	Khabiyat (Sthn hoizon)	Aarja Mine
Horizon	As/Bu	As/Bu	As/Bu	As/Bu	As/Bu	As/Bu	As/Bu	As/Bu	As/Bu
Colour	dusky brown	dusky brown	greyish red	pale red	greyish brown	moderate brown	greyish red	moderate reddish brown	moderate brown
Colour Code	5 YR 2/2	5 YR 2/2	10 R 4/2	5 R 6/2	5 YR 3/2	5 YR 3/4	5 R 4/2	10 R 4/6	5 YR 4/4
La	1761.00	2408.58	2882.44	2696.25	2909.11	2721.20	3756.30	3197.13	3756.30
Ce	783.66	822.48	1282.70	1112.05	2612.92	1611.11	1800.90	1867.60	1934.30
Pr	51.05	51.52	59.43	61.09	117.49	65.31	120.78	78.89	65.92
Nd	1032.46	1023.00	1190.90	1308.80	2290.20	1425.19	2791.73	1643.89	1081.12
Sm	125.58	143.12	160.21	174.46	296.28	181.01	397.83	215.13	158.75
Eu	26.08	28.14	27.66	35.12	59.47	38.04	76.79	43.88	30.92
Gd	86.77	92.55	106.75	109.74	197.86	136.57	227.70	154.00	101.71
Tb	14.60	15.29	16.20	17.31	32.02	20.34	38.32	24.57	15.57
Dy	85.61	92.37	115.75	106.54	191.65	127.50	217.02	155.12	96.94
Ho	13.93	14.89	16.07	18.71	30.90	23.93	35.97	26.30	15.92
Er	46.05	49.23	52.63	60.56	120.01	78.38	144.95	91.70	53.61
Tm	12.79	14.06	14.76	17.34	34.28	22.80	39.17	29.99	15.17
Yb	50.02	53.97	60.98	66.40	124.22	83.40	151.42	98.90	62.83
SH.NORM.									
La	56.62	77.45	92.68	86.70	93.54	87.50	120.78	102.80	120.78
Ce	11.75	12.33	19.23	16.67	39.17	24.15	27.00	28.00	29.00
Pr	51.05	51.52	59.43	61.09	117.49	65.31	120.78	78.89	65.92
Nd	33.96	33.65	39.17	43.05	75.34	46.88	91.83	54.08	35.56
Sm	21.00	23.93	26.79	29.17	49.55	30.27	66.53	35.97	26.55
Eu	22.10	23.85	23.44	29.76	50.40	32.24	65.08	37.19	26.21
Gd	15.78	16.83	19.41	19.95	35.97	24.83	41.40	28.00	18.49
Tb	17.18	17.99	19.05	20.37	37.67	23.93	45.08	28.91	18.32
Dy	15.45	16.67	20.89	19.23	34.59	23.01	39.17	28.00	17.50
Ho	13.93	14.89	16.07	18.71	30.90	23.93	35.97	26.30	15.92
Er	14.06	15.03	16.07	18.49	36.64	23.93	44.26	28.00	16.37
Tm	12.79	14.06	14.76	17.34	34.28	22.80	39.17	29.99	15.17
Yb	16.07	17.34	19.59	21.33	39.90	26.79	48.64	31.77	20.18

Table B.2 Whole-rock REE data
Oman Metalliferous sediments

Sample	20635	20639	20641	20643	20653	20654	20668	20669	U82
Sample Location	Khabiyat (main horizon)	Khabiyat (main horizon)	Khabiyat (main horizon)	Khabiyat (main horizon)	Wadi Suq	Wadi Suq	Khabiyat (Sthn hoizon)	Khabiyat (Sthn hoizon)	Aarja Mine
Horizon	As/Bu	As/Bu	As/Bu	As/Bu	As/Bu	As/Bu	As/Bu	As/Bu	As/Bu
Colour	dusky brown	dusky brown	greyish red	pale red	greyish brown	moderate brown	greyish red	moderate reddish brown	moderate brown
Colour Code	5 YR 2/2	5 YR 2/2	10 R 4/2	5 R 6/2	5 YR 3/2	5 YR 3/4	5 R 4/2	10 R 4/6	5 YR 4/4
La	1761.00	2408.58	2882.44	2696.25	2909.11	2721.20	3756.30	3197.13	3756.30
Ce	783.66	822.48	1282.70	1112.05	2612.92	1611.11	1800.90	1867.60	1934.30
Pr	51.05	51.52	59.43	61.09	117.49	65.31	120.78	78.89	65.92
Nd	1032.46	1023.00	1190.90	1308.80	2290.20	1425.19	2791.73	1643.89	1081.12
Sm	125.58	143.12	160.21	174.46	296.28	181.01	397.83	215.13	158.75
Eu	26.08	28.14	27.66	35.12	59.47	38.04	76.79	43.88	30.92
Gd	86.77	92.55	106.75	109.74	197.86	136.57	227.70	154.00	101.71
Tb	14.60	15.29	16.20	17.31	32.02	20.34	38.32	24.57	15.57
Dy	85.61	92.37	115.75	106.54	191.65	127.50	217.02	155.12	96.94
Ho	13.93	14.89	16.07	18.71	30.90	23.93	35.97	26.30	15.92
Er	46.05	49.23	52.63	60.56	120.01	78.38	144.95	91.70	53.61
Tm	12.79	14.06	14.76	17.34	34.28	22.80	39.17	29.99	15.17
Yb	50.02	53.97	60.98	66.40	124.22	83.40	151.42	98.90	62.83
SH.NORM.									
La	56.62	77.45	92.68	86.70	93.54	87.50	120.78	102.80	120.78
Ce	11.75	12.33	19.23	16.67	39.17	24.15	27.00	28.00	29.00
Pr	51.05	51.52	59.43	61.09	117.49	65.31	120.78	78.89	65.92
Nd	33.96	33.65	39.17	43.05	75.34	46.88	91.83	54.08	35.56
Sm	21.00	23.93	26.79	29.17	49.55	30.27	66.53	35.97	26.55
Eu	22.10	23.85	23.44	29.76	50.40	32.24	65.08	37.19	26.21
Gd	15.78	16.83	19.41	19.95	35.97	24.83	41.40	28.00	18.49
Tb	17.18	17.99	19.05	20.37	37.67	23.93	45.08	28.91	18.32
Dy	15.45	16.67	20.89	19.23	34.59	23.01	39.17	28.00	17.50
Ho	13.93	14.89	16.07	18.71	30.90	23.93	35.97	26.30	15.92
Er	14.06	15.03	16.07	18.49	36.64	23.93	44.26	28.00	16.37
Tm	12.79	14.06	14.76	17.34	34.28	22.80	39.17	29.99	15.17
Yb	16.07	17.34	19.59	21.33	39.90	26.79	48.64	31.77	20.18

Table B.2 Whole-rock REE data
Oman Metalliferous sediments

Appendix B

Sample	20635	20639	20641	20643	20653	20654	20668	20669	U82
Sample Location	Khabiyat (main horizon)	Khabiyat (main horizon)	Khabiyat (main horizon)	Khabiyat (main horizon)	Wadi Suq	Wadi Suq	Khabiyat (Sthn hoizon)	Khabiyat (Sthn hoizon)	Aarja Mine
Horizon	As/Bu	As/Bu	As/Bu	As/Bu	As/Bu	As/Bu	As/Bu	As/Bu	As/Bu
Colour	dusky brown	dusky brown	greyish red	pale red	greyish brown	moderate brown	greyish red	moderate reddish brown	moderate brown
Colour Code	5 YR 2/2	5 YR 2/2	10 R 4/2	5 R 6/2	5 YR 3/2	5 YR 3/4	5 R 4/2	10 R 4/6	5 YR 4/4
La	1761.00	2408.58	2882.44	2696.25	2909.11	2721.20	3756.30	3197.13	3756.30
Ce	783.66	822.48	1282.70	1112.05	2612.92	1611.11	1800.90	1867.60	1934.30
Pr	51.05	51.52	59.43	61.09	117.49	65.31	120.78	78.89	65.92
Nd	1032.46	1023.00	1190.90	1308.80	2290.20	1425.19	2791.73	1643.89	1081.12
Sm	125.58	143.12	160.21	174.46	296.28	181.01	397.83	215.13	158.75
Eu	26.08	28.14	27.66	35.12	59.47	38.04	76.79	43.88	30.92
Gd	86.77	92.55	106.75	109.74	197.86	136.57	227.70	154.00	101.71
Tb	14.60	15.29	16.20	17.31	32.02	20.34	38.32	24.57	15.57
Dy	85.61	92.37	115.75	106.54	191.65	127.50	217.02	155.12	96.94
Ho	13.93	14.89	16.07	18.71	30.90	23.93	35.97	26.30	15.92
Er	46.05	49.23	52.63	60.56	120.01	78.38	144.95	91.70	53.61
Tm	12.79	14.06	14.76	17.34	34.28	22.80	39.17	29.99	15.17
Yb	50.02	53.97	60.98	66.40	124.22	83.40	151.42	98.90	62.83
SH.NORM.									
La	56.62	77.45	92.68	86.70	93.54	87.50	120.78	102.80	120.78
Ce	11.75	12.33	19.23	16.67	39.17	24.15	27.00	28.00	29.00
Pr	51.05	51.52	59.43	61.09	117.49	65.31	120.78	78.89	65.92
Nd	33.96	33.65	39.17	43.05	75.34	46.88	91.83	54.08	35.56
Sm	21.00	23.93	26.79	29.17	49.55	30.27	66.53	35.97	26.55
Eu	22.10	23.85	23.44	29.76	50.40	32.24	65.08	37.19	26.21
Gd	15.78	16.83	19.41	19.95	35.97	24.83	41.40	28.00	18.49
Tb	17.18	17.99	19.05	20.37	37.67	23.93	45.08	28.91	18.32
Dy	15.45	16.67	20.89	19.23	34.59	23.01	39.17	28.00	17.50
Ho	13.93	14.89	16.07	18.71	30.90	23.93	35.97	26.30	15.92
Er	14.06	15.03	16.07	18.49	36.64	23.93	44.26	28.00	16.37
Tm	12.79	14.06	14.76	17.34	34.28	22.80	39.17	29.99	15.17
Yb	16.07	17.34	19.59	21.33	39.90	26.79	48.64	31.77	20.18

Table B.2 Whole-rock REE data
Oman Metalliferous sediments

Appendix B

Sample	20662	20669	20684	20687	20665	20663		20660	20691	20694
Sample Location	Plant Site	Khabiyat (S.horizon)	Huwayl	Mulayyinah	Aarja Mine	Plant Site		Buriami Highway ii	Semdah West	Ghayth
Horizon	As/Bu	As/Bu	As/Bu	As/Bu	As/Bu	As/Bu		Bu/Bu	Bu/Bu	Bu/Bu
Colour	greyish brown	moderate reddish brown	dusky red	greyish brown	greyish brown	pale brown		greyish red	greyish brown	dusky brown
Colour Code	5 YR 3/2	10 R 4/6	5 R 3/4	5 YR 3/2	5 YR 3/2	5 YR 5/2		5 R 4/2	5 YR 3/2	5YR 2/2
La	1638.99	2335.57	4911.13	5531.61	6673.05	7609.62		3410.05	6731.59	3704.76
Ce	603.60	681.37	1888.69	3105.63	2146.68	2871.98		2061.23	2784.36	2535.86
Pr	45.58	45.35	72.21	103.49	109.01	122.81		90.61	98.89	96.61
Nd	983.60	974.71	1484.54	2040.39	2930.04	2516.18		1818.51	2042.68	1909.30
Sm	123.61	132.65	186.51	270.94	421.41	314.88		292.91	261.64	275.08
Eu	24.29	25.55	36.33	50.66	80.59	66.31		57.01	51.92	49.19
Gd	78.05	88.38	123.13	169.34	238.98	220.14		195.59	180.04	189.83
Tb	13.53	14.15	20.53	27.11	39.33	34.73		31.43	28.60	30.93
Dy	75.08	80.71	124.12	164.63	228.59	207.16		199.13	178.45	189.46
Ho	12.33	13.03	22.18	28.12	40.73	32.02		32.54	29.99	30.83
Er	44.36	44.41	74.00	99.06	159.11	139.50		128.89	105.49	113.03
Tm	11.49	12.05	21.33	33.34	42.82	37.47		35.97	33.04	34.51
Yb	45.52	48.10	75.89	116.19	166.33	137.96		127.11	112.25	119.45
SH.NORM.										
La	52.70	75.10	157.91	177.87	214.57	244.68		109.65	216.45	119.12
Ce	9.05	10.22	28.32	46.56	32.18	43.06		30.90	41.74	38.02
Pr	45.58	45.35	72.21	103.49	109.01	122.81		90.61	98.89	96.61
Nd	32.36	32.06	48.83	67.12	96.38	82.77		59.82	67.19	62.81
Sm	20.67	22.18	31.19	45.31	70.47	52.65		48.98	43.75	46.00
Eu	20.59	21.65	30.79	42.93	68.30	56.19		48.31	44.00	41.69
Gd	14.19	16.07	22.39	30.79	43.45	40.03		35.56	32.73	34.51
Tb	15.92	16.65	24.15	31.89	46.27	40.86		36.97	33.65	36.39
Dy	13.55	14.57	22.40	29.72	41.26	37.39		35.94	32.21	34.20
Ho	12.33	13.03	22.18	28.12	40.73	32.02		32.54	29.99	30.83
Er	13.54	13.56	22.59	30.25	48.58	42.59		39.36	32.21	34.51
Tm	11.49	12.05	21.33	33.34	42.82	37.47		35.97	33.04	34.51
Yb	14.62	15.45	24.38	37.33	53.43	44.32		40.83	36.06	38.37

Table B.2 Whole-rock REE data
Oman Metalliferous sediments

Appendix B

Sample	20662	20669	20684	20687	20665	20663		20660	20691	20694
Sample Location	Plant Site	Khabiyat (S.horizon)	Huwayl	Mulayyinah	Aarja Mine	Plant Site		Buriami Highway ii	Semdah West	Ghayth
Horizon	As/Bu	As/Bu	As/Bu	As/Bu	As/Bu	As/Bu		Bu/Bu	Bu/Bu	Bu/Bu
Colour	greyish brown	moderate reddish brown	dusky red	greyish brown	greyish brown	pale brown		greyish red	greyish brown	dusky brown
Colour Code	5 YR 3/2	10 R 4/6	5 R 3/4	5 YR 3/2	5 YR 3/2	5 YR 5/2		5 R 4/2	5 YR 3/2	5YR 2/2
La	1638.99	2335.57	4911.13	5531.61	6673.05	7609.62		3410.05	6731.59	3704.76
Ce	603.60	681.37	1888.69	3105.63	2146.68	2871.98		2061.23	2784.36	2535.86
Pr	45.58	45.35	72.21	103.49	109.01	122.81		90.61	98.89	96.61
Nd	983.60	974.71	1484.54	2040.39	2930.04	2516.18		1818.51	2042.68	1909.30
Sm	123.61	132.65	186.51	270.94	421.41	314.88		292.91	261.64	275.08
Eu	24.29	25.55	36.33	50.66	80.59	66.31		57.01	51.92	49.19
Gd	78.05	88.38	123.13	169.34	238.98	220.14		195.59	180.04	189.83
Tb	13.53	14.15	20.53	27.11	39.33	34.73		31.43	28.60	30.93
Dy	75.08	80.71	124.12	164.63	228.59	207.16		199.13	178.45	189.46
Ho	12.33	13.03	22.18	28.12	40.73	32.02		32.54	29.99	30.83
Er	44.36	44.41	74.00	99.06	159.11	139.50		128.89	105.49	113.03
Tm	11.49	12.05	21.33	33.34	42.82	37.47		35.97	33.04	34.51
Yb	45.52	48.10	75.89	116.19	166.33	137.96		127.11	112.25	119.45
SH.NORM.										
La	52.70	75.10	157.91	177.87	214.57	244.68		109.65	216.45	119.12
Ce	9.05	10.22	28.32	46.56	32.18	43.06		30.90	41.74	38.02
Pr	45.58	45.35	72.21	103.49	109.01	122.81		90.61	98.89	96.61
Nd	32.36	32.06	48.83	67.12	96.38	82.77		59.82	67.19	62.81
Sm	20.67	22.18	31.19	45.31	70.47	52.65		48.98	43.75	46.00
Eu	20.59	21.65	30.79	42.93	68.30	56.19		48.31	44.00	41.69
Gd	14.19	16.07	22.39	30.79	43.45	40.03		35.56	32.73	34.51
Tb	15.92	16.65	24.15	31.89	46.27	40.86		36.97	33.65	36.39
Dy	13.55	14.57	22.40	29.72	41.26	37.39		35.94	32.21	34.20
Ho	12.33	13.03	22.18	28.12	40.73	32.02		32.54	29.99	30.83
Er	13.54	13.56	22.59	30.25	48.58	42.59		39.36	32.21	34.51
Tm	11.49	12.05	21.33	33.34	42.82	37.47		35.97	33.04	34.51
Yb	14.62	15.45	24.38	37.33	53.43	44.32		40.83	36.06	38.37

	Al calc	Al meas	Si calc	Si meas	Mn calc	Mn meas	Fe calc	Fe meas	Ni calc	Ni meas	Cu calc	Ba calc	Ba meas
Axis													
20655	34931	15189	156284	156320	40303	29275	160957	165629	176	767	618	1167	369
20656	15609	15613	147203	147205	70696	70709	201510	201511	765	622	1079	1355	674
20657	19790	19794	120652	120653	83242	83256	228650	228649	998	755	1276	1466	957
20658	16292	16301	126401	126402	93058	93092	223268	223264	1399	667	1442	1490	614
As/Ls													
20601	28870	8362	154434	154450	109631	542	395186	426943	380	101	1615	2253	9
20602	22583	1588	159202	159218	111979	310	399190	431699	379	49	1644	2264	221
20679	33442	19476	161031	161042	77043	2788	286198	307827	286	784	1148	1764	291
20680	35171	29373	141700	137855	94230	3485	346360	373225	341	546	1397	2014	245
20681	33638	27732	130694	127898	77623	2633	288327	310485	287	889	1155	1714	270
U1	56913	32442	190899	195961	53091	1471	219077	233545	246	664	823	1570	150
U10	60540	4234	213641	227562	83852	465	327076	349794	346	88	1271	2135	47
U11	36883	4975	152610	156554	109204	465	398899	430090	389	72	1615	2289	12
U12	11702	2276	88871	83162	139359	155	486236	527383	445	26	2027	2506	0
U13	57597	21805	198220	206245	66742	929	266406	284675	289	374	1021	1810	387
U14A	55204	32548	192016	195400	69230	1162	273410	292859	293	525	1055	1824	227
U15	48013	30167	170343	172120	68850	1394	267466	286913	281	508	1042	1733	117
U16	59593	30167	203530	209518	65019	1394	261776	279639	286	395	998	1804	44
U17	49209	26621	173028	176561	66537	1162	260292	278940	276	528	1010	1708	209
U18	68416	26462	227259	237986	58066	1471	243584	258865	278	430	906	1789	263
U19	38965	28050	147096	145896	78796	1936	295794	318319	299	813	1177	1796	176
U2	54112	4393	193825	205591	82372	542	317846	340351	332	66	1244	2035	140
U20	47258	29690	168724	170438	70518	3563	272707	292019	285	485	1066	1753	134
U21	46660	20799	164869	169923	65172	6041	253960	270616	268	568	988	1655	458
U25	68725	40487	216911	225178	28886	7048	143553	148982	188	471	484	1297	221
U26	74140	24345	238525	253132	42874	4879	195093	204518	239	473	692	1598	225
U27	80052	18206	251494	270989	30633	4492	156857	162272	210	447	521	1460	303
U28	74983	25245	235511	250982	28538	4260	146394	151710	196	429	485	1365	299
U29	84310	18206	256841	279123	11477	6041	93805	92887	158	334	248	1184	236
U3	43477	5875	168919	175393	100319	697	372634	400923	371	67	1493	2215	99
U30	44818	34930	155376	155759	54870	8132	217385	230958	234	705	837	1458	414
U31	66717	19317	223719	236163	62074	3175	256255	272015	288	813	962	1838	131
U32	84589	16618	265480	286930	31670	3330	163349	169196	220	644	540	1530	174
U33	62944	31596	208031	215875	50700	5731	214751	226971	247	1203	794	1600	173
U34	62944	19370	208031	184415	50700	3253	214751	313213	247	1308	794	1600	96
U35	81742	21170	258829	277534	36519	4879	178167	185284	231	618	607	1579	222
U36	80749	27415	257577	273373	40970	2633	192816	202210	243	594	671	1643	320
U37	80749	27785	257577	285247	40970	1859	192816	177869	243	426	671	1643	429
U38	81181	31225	257554	272672	37568	6660	181409	188711	233	558	622	1591	372
U39	44222	21381	162549	165623	78060	4182	296655	317829	304	532	1172	1846	218
U4	53086	11061	193331	202038	89049	620	340120	364902	351	127	1339	2136	6
U40	78031	30749	245984	260611	32025	7745	160339	165769	212	742	539	1460	492
U41	52090	24927	184066	188949	72779	4027	283591	303071	299	765	1103	1848	75
U41A	92054	16142	288380	312407	33099	2556	173072	179268	235	249	568	1642	351
U42	78826	32919	248676	262622	32837	5266	163639	170106	215	622	551	1483	141
U45	90657	18047	279788	304086	21684	13011	132961	132755	198	635	401	1432	1299
U46	99275	21540	304309	330030	18367	4492	127127	128279	200	204	362	1477	489
U47	92465	12702	287329	313108	27197	3408	153063	157096	218	349	483	1547	375
U48	61412	30167	201812	210125	46477	9371	199258	209135	232	680	732	1510	300
U49	90683	25562	282076	303291	27405	10610	152628	155137	216	633	484	1529	468
U5	81983	6139	267104	289501	56072	542	245487	259145	291	138	890	1915	534
U50	83658	35406	260434	275991	25822	10843	142661	145275	201	460	454	1420	614
U51	69262	23657	224048	237752	43201	13476	193070	200182	233	620	692	1547	405
U52	79208	26727	251663	267951	37606	11462	180268	186053	230	654	621	1568	365
U53	69987	13654	218003	236771	21934	13863	120486	120725	169	372	385	1194	336
U54	81282	23075	256239	275337	33378	20446	167081	168707	221	663	561	1521	254
U55	27858	18682	122384	119297	100905	3950	364569	393159	351	778	1486	2042	78
U56A	27890	18682	123201	120045	102766	4569	370985	399944	356	662	1513	2074	263
U56B	68471	14342	222637	238500	45679	4182	201069	211373	240	559	727	1580	656
U56C	24158	10479	83228	87089	28223	15412	112528	115828	122	110	432	763	146
U57	74194	22069	237650	253272	40190	5576	185908	194237	231	511	653	1553	209
U58	70904	27521	223401	236818	28804	6428	144675	149682	191	301	485	1321	233
U59	72321	19582	226605	243269	26118	4414	136365	140799	185	423	448	1292	246
U6	70686	37841	225650	234761	36315	3098	170335	178989	214	469	594	1446	417
U60	100432	12913	307287	336761	17115	9526	123572	122473	198	324	345	1469	374
U61	87345	19899	273261	294877	30456	7512	160954	165209	220	646	525	1542	483
U62	64112	27362	210749	220924	48689	11230	208599	218367	243	633	766	1580	411
U63	79884	27732	251735	268325	32558	12856	163363	167238	216	625	548	1490	342
U64	75235	16036	248051	264585	59046	929	251347	266420	291	395	927	1886	170
U65	70468	22916	230313	243549	50075	2711	217458	229768	256	937	792	1678	384
U66	72526	16671	237691	253693	53219	4647	229587	241939	269	644	840	1755	267
U67	80383	25139	251699	269213	28592	6815	150061	154438	204	575	491	1429	368
U68	81147	8997	248165	273046	13527	16341	98807	95195	159	806	274	1182	230
U69	49630	23128	165958	173476	44971	20756	186487	192698	210	539	698	1347	228
U7	62319	5451	219027	233125	84011	387	328770	351542	349	74	1275	2159	89
U70	55605	20058	185731	196055	49853	21143	207108	214311	234	884	775	1500	788
U71	60972	22757	198836	209751	42186	8442	184235	192838	218	796	669	1432	236
U72	72847	10267	235417	254160	44850	3098	201047	211093	244	514	719	1617	258
U73	11323	11326	159638	159639	27951	27958	79245	79247	351	379	438	754	200

	Al calc	Al meas	Si calc	Si meas	Mn calc	Mn meas	Fe calc	Fe meas	Ni calc	Ni meas	Cu calc	Ba calc	Ba meas
U74	21023	12384	237512	237519	50208	4260	185965	199343	191	501	754	1409	285
U75	20368	20376	150335	150337	78345	78377	189063	189061	1221	699	1224	1369	528
U76	27780	27785	172588	172588	64255	64281	147939	147933	1163	527	1026	1236	1149
U77	23596	23604	177915	177917	68582	68618	155700	155697	1216	643	1088	1278	402
U78	33693	26938	292626	292633	36849	929	148240	158705	169	193	574	1374	180
U8	23658	6404	204642	204656	92230	465	332027	358747	321	79	1362	2040	75
U9	32426	25086	290757	290763	42510	3330	166870	178219	184	459	655	1455	495
As/Bu													
20617	15291	15295	113921	113921	47223	47243	94499	94495	959	559	767	816	803
20634	17202	17200	127105	127104	74889	74892	196969	196964	983	868	1154	1323	2196
20635	20639	20640	127526	127524	98261	98281	230897	230888	1554	941	1530	1557	2501
20636	66263	22228	208660	224149	26609	33070	134144	130517	178	576	449	1229	1458
20637	25977	25986	173570	173570	83127	83178	152352	152340	1821	708	1340	1331	1485
20638	23545	23551	183715	183714	65481	65520	106958	106946	1594	636	1072	1109	1667
20639	23327	23340	134489	134490	96516	96577	163334	163321	2196	822	1554	1342	944
20640	21742	21752	178431	178431	67252	67302	92550	92537	1793	560	1110	1050	1149
20641	21954	21963	114528	114529	90489	90536	168368	168357	1904	833	1445	1287	1076
20642	19574	19582	131076	131077	77418	77447	162905	162901	1445	814	1225	1235	477
20643	37355	46044	117606	114622	52887	52742	93066	93446	1363	582	883	922	893
20644	43020	26356	140588	146316	69869	70245	150925	150171	1466	687	1137	1262	1439
20645	17354	17359	136361	136359	84695	84727	165710	165699	1676	779	1344	1279	1890
20646	16296	16301	132854	132853	64176	64204	114788	114779	1405	655	1032	1003	1275
20649	18675	18682	166090	166090	84305	84340	165988	165979	1669	812	1340	1342	1325
20650	19686	19688	167775	167773	79206	79229	171445	171435	1428	759	1251	1345	2397
20651	20005	19635	170998	170999	62143	60177	226328	226901	223	970	922	1464	1241
20652	26348	26356	138931	138930	88248	88290	167110	167098	1868	754	1415	1337	1490
20653	11475	11485	99945	99944	92106	92162	158090	158075	1987	714	1466	1193	1544
20654	14701	14713	99852	99850	112846	112918	204258	204239	2331	710	1788	1455	2063
20659	29955	29955	143838	143839	73972	73962	226409	226411	750	858	1135	1499	1227
20662	18040	18047	162771	162771	79735	79771	157035	157026	1582	675	1269	1283	1305
20663	22855	22863	143185	143184	65552	65598	103111	103099	1629	565	1073	1013	1241
20664	27618	27626	197736	197737	61697	61726	140242	140239	1144	586	989	1248	338
20665	21220	21223	175392	175393	50641	50651	147094	147094	602	472	787	1155	725
20666	27197	27203	202504	202506	53190	53206	118070	118067	1043	539	861	1142	533
20668	30124	29108	128646	128646	28160	22770	116148	117717	131	725	438	887	1164
20669	11624	7992	261356	261359	22572	3253	84950	90578	94	407	348	953	216
20671	17842	17518	176422	176421	28589	26874	109667	110163	118	586	436	918	1535
20682	33923	29426	231484	231488	37308	13398	149990	156956	168	633	578	1262	498
20683	35760	29585	131898	130610	64298	11307	243924	259495	249	1006	965	1512	447
20684	56436	21064	187496	198345	47978	28346	201204	205707	229	944	749	1477	305
20685	53707	13443	190084	199187	75827	2943	295102	315311	311	602	1149	1919	138
20687	31702	31702	227470	227468	43983	43990	120939	120934	700	466	709	1176	1856
U82	10390	7515	409030	409031	15670	387	60390	64839	77	16	255	1128	1227
U83	22325	22334	181145	181142	83349	83411	143544	143527	1891	345	1346	1304	2372
Bu													
20647	21857	21858	223962	223962	46697	46701	145695	145695	473	441	724	1231	1235
20648	23652	23657	171653	171653	66881	66914	152977	152969	1179	504	1061	1249	1382
20660	17884	17888	184601	184602	58529	58550	150104	150101	845	474	915	1207	893
20676	19949	19952	184462	184461	54889	54910	135978	135973	867	416	866	1149	1206
20686	41200	33078	224703	224710	48150	4957	191938	204518	211	471	740	1466	347
20688	21383	21381	126499	126496	50261	50263	94995	94985	1118	566	817	878	2382
20689	22231	22228	124957	124953	48321	48327	96046	96034	1040	525	784	873	2724
20690	28520	28473	217491	217464	49855	49799	138539	138491	719	491	791	1232	14717
20691	29689	29690	226487	226487	47777	47785	146536	146534	667	486	1016	18224	18227
20692	29844	29849	227749	227749	49467	49489	94992	94985	1180	439	878	4885	4884
20693	29902	29902	200215	200215	47399	47398	141918	141918	602	572	752	1420	1418
20694	20933	20958	127803	127805	127585	127711	162157	162132	3371	753	2078	1455	629
20695	18509	18523	122802	122803	110994	111059	203902	203889	2295	842	1763	1505	861
20696	23519	22916	175219	175206	68542	65443	250578	251451	248	762	1018	1597	8349
20697	22948	18894	142152	142156	50211	28656	187255	193537	190	765	751	1230	390
20698	24472	20535	162066	162070	49979	29043	187435	193537	192	686	750	1275	258
20699	28365	28367	244063	244063	41033	41047	112474	112471	728	417	875	14872	14876
20700	32330	32337	186518	186518	62012	62035	115697	115689	1451	553	1042	2711	2706
U22	14486	14501	188339	188341	90463	90536	182704	182696	1701	539	1428	1457	294
U23	13753	13760	182029	182031	81844	81862	199904	199902	1192	682	1268	1462	563
U24	16876	16883	114386	114389	78504	78532	217666	217668	907	765	1199	1384	243
Ls													
U43	34735	19952	200016	200028	81078	2478	300879	323774	302	535	1209	1914	141
U44	36891	29532	250228	250234	45561	6428	180251	191649	198	560	701	1450	473

TABLE B.4 Measured versus calculated values
(Factor analysis end-members)

Group	Sample	Al				
		detrital	hydrothermal Fe	h/t FeMn	biogenic	authigenic
As/As	20657	664.5	0.0	13635.5	93.4	5405.4
As/As	20658	16492.8	0.0	7756.2	202.0	4242.8
AVERAGE		**8579**	**0**	**10696**	**148**	**4824**
As/Bu	20617	4660.6	0.0	13098.7	106.9	4681.4
As/Bu	20634	5377.6	0.0	13552.4	61.8	5598.3
As/Bu	20635	16695.6	0.0	8026.6	327.2	1883.5
As/Bu	20636	18632.7	0.0	7706.8	177.4	4808.2
As/Bu	20637	21520.0	0.0	5365.6	264.6	4185.8
As/Bu	20638	15200.8	0.0	8823.2	105.1	5987.6
As/Bu	20639	21139.3	0.0	4324.4	286.0	4506.4
As/Bu	20640	14357.6	0.0	10477.3	64.5	6138.5
As/Bu	20641	11480.5	0.0	10544.4	128.8	5175.8
As/Bu	20642	63447.0	0.0	5984.7	0.0	5268.4
As/Bu	20643	23721.1	0.0	4704.7	0.0	2574.2
As/Bu	20644	16072.0	0.0	4570.9	0.0	2657.1
As/Bu	20645	20021.8	0.0	2747.6	0.0	2030.6
As/Bu	20646	8541.5	24.4	9202.5	205.1	4965.9
As/Bu	20649	9384.1	0.0	9861.0	197.9	4638.8
As/Bu	20650	4924.7	0.0	13918.4	157.1	3213.7
As/Bu	20651	18826.0	0.0	9120.0	88.3	5365.3
As/Bu	20652	0.0	0.0	10887.1	122.0	6740.1
As/Bu	20653	0.0	0.0	12700.9	59.8	7299.2
As/Bu	20654	0.0	0.0	29281.7	265.3	8553.1
As/Bu	20659	0.0	0.0	16176.3	442.8	8280.8
As/Bu	20662	24234.0	0.0	5845.3	189.1	4838.2
As/Bu	20663	22019.4	0.0	7400.3	225.3	3538.5
As/Bu	20664	14787.8	0.0	9387.7	225.2	3118.6
As/Bu	20665	23744.3	0.0	6054.7	253.5	3095.4
As/Bu	20666	37289.8	0.0	9671.2	71.2	1760.1
As/Bu	20668	2454.2	0.0	7150.8	566.6	153.5
As/Bu	20669	15177.5	0.0	8314.8	306.1	1845.0
As/Bu	20671	22310.6	0.0	9637.0	253.6	643.8
As/Bu	20682	11453.8	0.0	18357.1	0.0	531.1
As/Bu	20683	19099.9	0.0	5292.4	0.0	607.7
As/Bu	20684	6428.2	0.0	5571.8	0.0	0.0
As/Bu	20685	33968.5	0.0	2123.0	0.0	1108.4
As/Bu	20687	7456.3	458.9	476.7	508.1	0.0
As/Bu	U82	15084.0	0.0	7394.5	232.6	4991.0
As/Bu	U83	0.0	0.0	10000.0	0.0	0.0
Average		**15264**	**13**	**8993**	**164**	**3633**
As/Ls	20601	0.0	0.0	3000.0	0.0	0.0
As/Ls	20602	1883.2	31.6	20104.4	63.1	0.0
As/Ls	20679	0.0	0.0	22258.7	0.0	49.8
As/Ls	20680	0.0	0.0	21880.1	0.0	0.0
As/Ls	20681	15552.1	101.1	20435.7	211.2	0.0
As/Ls	U1	0.0	4377.8	0.0	105.8	0.0
As/Ls	U10	0.0	5246.7	0.0	0.0	214.3
As/Ls	U11	17995.3	3591.9	0.0	36.9	4.4
As/Ls	U13	11757.5	3989.5	0.0	14.5	107.7
As/Ls	U14	19853.3	3491.0	0.0	0.0	41.0
As/Ls	U14A	22367.7	5803.1	0.0	0.0	129.2
As/Ls	U15	25922.6	3304.3	0.0	0.0	18.3
As/Ls	U16	16655.3	3634.8	0.0	0.0	45.1

TABLE B.4 Measured versus calculated values
(Factor analysis end-members)

Group	Sample	Al				
		detrital	hydrothermal Fe	h/t FeMn	biogenic	authigenic
As/Ls	U17	27507.1	2192.9	0.0	0.0	0.0
As/Ls	U18	1995.5	22187.8	0.0	0.0	816.7
As/Ls	U19	5089.5	1810.5	0.0	0.0	0.0
As/Ls	U2	16507.3	1154.3	12427.0	0.0	70.4
As/Ls	U20	17170.2	3267.0	2658.1	0.0	272.7
As/Ls	U21	38785.9	1049.2	0.0	0.0	164.8
As/Ls	U25	24304.1	1065.3	0.0	0.0	30.5
As/Ls	U26	14812.4	387.6	0.0	0.0	0.0
As/Ls	U27	25735.1	1987.9	0.0	258.7	214.4
As/Ls	U28	19034.6	1204.2	0.0	438.6	315.2
As/Ls	U29	0.0	5084.8	0.0	0.0	75.3
As/Ls	U3	22845.4	14303.3	0.0	329.8	2121.5
As/Ls	U30	14420.1	3196.0	0.0	113.8	108.0
As/Ls	U31	13661.6	2045.1	0.0	324.7	131.7
As/Ls	U32	28040.1	2673.8	0.0	57.3	232.3
As/Ls	U33	12441.7	4087.0	0.0	0.0	132.6
As/Ls	U34	21032.8	663.0	0.0	0.0	4.2
As/Ls	U35	23255.0	2296.5	0.0	203.4	84.4
As/Ls	U36	25015.8	2096.7	0.0	258.3	54.4
As/Ls	U37	28847.9	2233.6	0.0	212.3	292.9
As/Ls	U38	12107.6	8550.9	0.0	0.0	441.4
As/Ls	U39	7875.5	4473.9	0.0	0.0	0.0
As/Ls	U4	23842.9	657.1	0.0	0.0	0.0
As/Ls	U40	16884.1	4061.9	0.0	0.0	0.0
As/Ls	U41	17468.9	431.1	0.0	0.0	0.0
As/Ls	U41A	30768.6	1944.2	0.0	194.7	215.9
As/Ls	U42	15929.2	1581.8	0.0	408.7	625.7
As/Ls	U45	19526.2	1507.8	0.0	434.3	194.7
As/Ls	U46	10001.2	1944.6	0.0	412.1	142.0
As/Ls	U47	29777.7	2710.2	0.0	79.2	455.5
As/Ls	U48	22638.8	1760.4	0.0	329.6	478.5
As/Ls	U49	2236.8	3192.9	0.0	290.9	0.0
As/Ls	U5	34658.0	1634.4	0.0	245.4	468.7
As/Ls	U50	21611.4	2524.4	0.0	182.6	665.1
As/Ls	U51	24104.1	2213.7	0.0	232.1	531.7
As/Ls	U52	13991.2	1751.1	0.0	368.9	816.9
As/Ls	U53	19790.8	1919.7	0.0	281.5	958.4
As/Ls	U54	0.0	17812.6	0.0	0.0	1687.4
As/Ls	U55	0.0	19250.6	0.0	0.0	1949.4
As/Ls	U56A	17125.6	1041.9	0.0	12.4	20.1
As/Ls	U56B	18608.3	3038.8	0.0	42.3	1628.5
As/Ls	U56C	20645.8	2548.0	0.0	230.5	257.0
As/Ls	U57	29940.8	2032.0	0.0	228.7	336.2
As/Ls	U58	20670.3	1997.5	0.0	304.3	239.8
As/Ls	U59	37217.2	2130.6	0.0	110.2	112.6
As/Ls	U6	10602.6	1485.0	0.0	504.0	448.3
As/Ls	U60	17388.3	2010.6	0.0	340.5	340.2
As/Ls	U61	25755.6	2790.1	0.0	108.3	543.3
As/Ls	U62	26118.6	2000.6	0.0	253.1	621.3
As/Ls	U63	11509.6	3183.3	0.0	187.7	7.5
As/Ls	U64	19799.3	2862.0	0.0	157.1	95.5
As/Ls	U65	13190.8	3068.8	0.0	200.6	192.8
As/Ls	U66	24301.7	1924.4	0.0	285.1	320.4
As/Ls	U67	7713.1	1263.4	0.0	483.1	898.4
As/Ls	U68	25032.0	2837.7	0.0	71.1	1233.2

TABLE B.4 Measured versus calculated values
(Factor analysis end-members)

Group	Sample	Al				
		detrital	hydrothermal Fe	h/t FeMn	biogenic	authigenic
As/Ls	U69	607.9	4333.2	0.0	109.8	0.0
As/Ls	U7	17340.7	2706.5	0.0	103.0	980.0
As/Ls	U70	23455.5	2744.9	0.0	148.4	446.5
As/Ls	U71	7625.2	2911.1	0.0	282.0	143.5
As/Ls	U72	15861.0	1392.1	0.0	350.1	2370.5
As/Ls	U73	10693.0	2883.2	0.0	261.3	212.6
As/Ls	U74	18561.4	2365.6	0.0	65.2	4776.9
As/Ls	U75	29537.8	1697.3	0.0	111.8	3929.8
As/Ls	U76	23296.0	1807.6	0.0	144.2	4111.3
As/Ls	U77	24814.1	1885.1	0.0	299.0	11.9
As/Ls	U78	1541.6	4621.4	0.0	48.1	0.0
As/Ls	U8	21838.1	2083.2	0.0	276.0	0.0
As/Ls	U9	20703.6	1697.7	0.0	251.8	2591.8
Average		**17002**	**3183**	**1269**	**149**	**521**
Bu/Bu	20647	24088.8	1817.9	0.0	133.6	4107.5
Bu/Bu	20648	17067.5	1898.9	0.0	204.9	3588.4
Bu/Bu	20660	20678.6	1705.1	0.0	210.3	3451.8
Bu/Bu	20676	33593.4	2669.6	0.0	97.7	222.4
Bu/Bu	20686	31057.4	1320.8	0.0	124.5	4154.8
Bu/Bu	20688	32615.1	1350.1	0.0	108.2	3985.7
Bu/Bu	20689	28551.2	1499.2	0.0	205.5	2775.9
Bu/Bu	20690	29031.6	1576.1	0.0	203.0	2578.8
Bu/Bu	20691	32107.9	843.1	0.0	278.2	2880.9
Bu/Bu	20692	30935.1	1584.9	0.0	154.6	2690.0
Bu/Bu	20693	17321.8	1535.9	0.0	61.3	7886.0
Bu/Bu	20694	13976.9	2336.0	0.0	7.7	6643.2
Bu/Bu	20695	17301.1	2816.0	0.0	26.1	3200.3
Bu/Bu	20696	20412.6	3010.9	0.0	25.0	1823.6
Bu/Bu	20697	20588.4	2726.0	0.0	61.0	1685.7
Bu/Bu	20698	28830.1	1143.5	0.0	288.0	2257.0
Bu/Bu	20699	21920.2	676.4	0.0	92.8	2310.6
Bu/Bu	20700	9437.9	2027.8	0.0	195.4	5018.4
Bu/Bu	U22	8801.5	2372.8	0.0	164.3	4562.6
Bu/Bu	U23	8399.8	3034.2	0.0	0.0	4985.3
Bu/Bu	U24	15306.4	4058.8	0.0	0.0	76.4
Average		**22001**	**2000**	**0**	**126**	**3376**
Ls/Ls	U43	55016.1	2114.7	0.0	0.0	155.3
Ls/Ls	U44	16118.7	0.0	901.7	0.0	0.0
Average		**35567**	**1057**	**451**	**0**	**78**

Group Value %	Sample	Al detrital	Al hydrothermal	Al FeMn	Al biogenic	Al authigenic
Average	As	65.4	0.0	14.1	0.6	19.9
Average	As/Bu	74.4	0.0	12.0	0.6	12.9
Average	As/Ls	76.8	14.4	5.7	0.7	2.4
Average	Bu	80.0	7.3	0.0	0.5	12.3
Average	Ls	95.7	2.8	1.2	0.0	0.2
Average		78.5	4.9	6.6	0.5	9.5
Standard Deviation		11.1	6.1	6.3	0.3	8.1

TABLE B.4 Measured versus calculated values
(Factor analysis end-members)

Group	Sample	Si				
		detrital	hydrothermal Fe	h/t FeMn	biogenic	authigenic
As/As	20657	1993.6	0.0	88452.4	46693.0	16216.1
As/As	20658	49478.3	0.0	50313.7	101002.2	12728.4
AVERAGE		**25736**	**0**	**69383**	**73848**	**14472**
As/Bu	20617	13981.9	0.0	84970.4	53443.7	14044.3
As/Bu	20634	16132.8	0.0	87913.5	30917.8	16794.9
As/Bu	20635	50086.9	0.0	52067.8	163576.6	5650.4
As/Bu	20636	55898.1	0.0	49993.7	88720.6	14424.5
As/Bu	20637	64560.1	0.0	34806.3	132298.9	12557.3
As/Bu	20638	45602.5	0.0	57235.2	52564.8	17962.8
As/Bu	20639	63417.8	0.0	28051.8	142981.3	13519.1
As/Bu	20640	43072.8	0.0	67965.6	32226.5	18415.4
As/Bu	20641	34441.5	0.0	68400.8	64386.6	15527.3
As/Bu	20642	149011.1	0.0	30392.6	0.0	12373.2
As/Bu	20643	124614.6	0.0	53442.1	0.0	13523.0
As/Bu	20644	98428.5	0.0	60529.8	0.0	16272.4
As/Bu	20645	140466.4	0.0	41681.8	0.0	14246.0
As/Bu	20646	25624.4	896.7	59696.0	102573.5	14897.7
As/Bu	20649	28152.2	0.0	63967.8	98974.8	13916.4
As/Bu	20650	14774.2	0.0	90287.6	78573.6	9641.1
As/Bu	20651	56477.9	0.0	59160.6	44152.9	16095.8
As/Bu	20652	0.0	0.0	70623.6	61010.0	20220.3
As/Bu	20653	0.0	0.0	82389.4	29917.6	21897.6
As/Bu	20654	0.0	0.0	90106.3	62914.5	12172.1
As/Bu	20659	0.0	0.0	62712.8	132322.0	14846.8
As/Bu	20662	72701.9	0.0	37917.8	94525.7	14514.6
As/Bu	20663	66058.1	0.0	48004.9	112634.0	10615.6
As/Bu	20664	44363.5	0.0	60897.0	112620.9	9355.7
As/Bu	20665	71232.8	0.0	39276.3	126764.8	9286.2
As/Bu	20666	111869.4	0.0	62736.2	35585.4	5280.2
As/Bu	20668	7362.7	0.0	46386.4	283320.5	460.4
As/Bu	20669	45532.5	0.0	53937.4	153042.5	5534.9
As/Bu	20671	66931.8	0.0	62514.5	126822.3	1931.5
As/Bu	20682	34361.5	0.0	119080.9	0.0	1593.2
As/Bu	20683	126235.7	0.0	75635.1	0.0	4016.3
As/Bu	20684	67521.7	0.0	126551.9	0.0	0.0
As/Bu	20685	214426.2	0.3	28978.6	15.4	6996.7
As/Bu	20687	29792.5	22437.6	4118.7	338359.8	0.0
As/Bu	U82	45251.9	0.0	47967.3	116318.0	14973.0
As/Bu	U83	0.0	0.0	164579.4	0.0	0.0
Average		**56344**	**648**	**63194**	**79766**	**10932**
As/Ls	20601	0.0	0.0	170631.7	0.0	0.0
As/Ls	20602	5649.6	1159.7	130415.9	31536.9	0.0
As/Ls	20679	0.0	0.0	144390.1	0.0	149.3
As/Ls	20680	0.0	0.0	141934.5	0.0	0.0
As/Ls	20681	33816.1	2689.4	96081.8	76526.8	0.0
As/Ls	U1	0.0	160720.4	0.0	52889.6	0.0
As/Ls	U10	0.0	192621.2	0.0	0.0	642.9
As/Ls	U11	53985.8	131869.6	0.0	18447.9	13.3
As/Ls	U13	35272.6	146465.4	0.0	7260.9	323.2
As/Ls	U14	59560.0	128164.2	0.0	0.0	123.1
As/Ls	U14A	43476.6	138034.9	0.0	0.0	251.2
As/Ls	U15	77767.9	121308.2	0.0	0.0	54.9
As/Ls	U16	49966.0	133441.5	0.0	0.0	135.4

TABLE B.4 Measured versus calculated values
(Factor analysis end-members)

Group	Sample	Si				
		detrital	hydrothermal Fe	h/t FeMn	biogenic	authigenic
As/Ls	U17	110402.8	107709.9	0.0	0.0	0.0
As/Ls	U18	1193.0	162325.3	0.0	0.0	488.3
As/Ls	U19	37363.2	162658.9	0.0	0.0	0.0
As/Ls	U2	49521.8	42377.4	80613.2	0.0	211.1
As/Ls	U20	51510.5	119941.6	17242.8	0.0	818.0
As/Ls	U21	180645.0	59802.2	0.0	0.0	767.8
As/Ls	U25	159112.0	85351.0	0.0	0.0	199.9
As/Ls	U26	204666.0	65543.1	0.0	0.0	0.0
As/Ls	U27	77205.4	72980.4	0.0	129348.6	643.3
As/Ls	U28	57103.9	44210.7	0.0	219302.6	945.7
As/Ls	U29	0.0	186675.4	0.0	0.0	225.8
As/Ls	U3	16569.9	126955.1	0.0	39864.6	1538.7
As/Ls	U30	43260.3	117334.8	0.0	56919.2	324.0
As/Ls	U31	40984.8	75079.3	0.0	162348.8	395.2
As/Ls	U32	84120.3	98161.9	0.0	28641.4	696.9
As/Ls	U33	37325.0	150042.8	0.0	0.0	397.7
As/Ls	U34	186605.0	71981.7	0.0	1.2	37.7
As/Ls	U35	69765.1	84310.8	0.0	101705.7	253.1
As/Ls	U36	75047.3	76974.2	0.0	129132.9	163.3
As/Ls	U37	86543.8	81999.8	0.0	106169.2	878.7
As/Ls	U38	19087.9	164970.9	0.0	0.0	695.9
As/Ls	U39	23626.5	164250.0	0.0	0.0	0.0
As/Ls	U4	195616.2	65975.6	0.0	0.0	0.0
As/Ls	U40	50652.2	149122.0	0.0	0.0	0.0
As/Ls	U41	216884.5	65492.4	0.0	0.0	0.0
As/Ls	U41A	92305.7	71375.9	0.0	97328.8	647.7
As/Ls	U42	47787.7	58073.7	0.0	204349.1	1877.2
As/Ls	U45	58578.6	55354.8	0.0	217129.9	584.2
As/Ls	U46	30003.6	71393.1	0.0	206032.0	426.0
As/Ls	U47	89333.2	99498.8	0.0	39576.0	1366.5
As/Ls	U48	67916.4	64630.6	0.0	164787.7	1435.5
As/Ls	U49	6710.3	117220.3	0.0	145468.3	0.0
As/Ls	U5	103974.0	60003.6	0.0	122710.0	1406.0
As/Ls	U50	64834.3	92677.2	0.0	91314.9	1995.2
As/Ls	U51	72312.4	81271.4	0.0	116043.9	1595.0
As/Ls	U52	41973.7	64289.1	0.0	184452.8	2450.8
As/Ls	U53	59372.3	70478.9	0.0	140739.8	2875.3
As/Ls	U54	0.0	190580.6	0.0	0.0	1475.3
As/Ls	U55	0.0	192931.3	0.0	0.0	1596.5
As/Ls	U56A	136177.9	101385.2	0.0	16466.3	159.9
As/Ls	U56B	55825.0	111561.8	0.0	21142.3	4885.6
As/Ls	U56C	61937.4	93543.0	0.0	115253.2	771.1
As/Ls	U57	89822.4	74599.1	0.0	114325.1	1008.6
As/Ls	U58	62010.8	73333.7	0.0	152149.3	719.5
As/Ls	U59	111651.6	78218.2	0.0	55076.9	337.9
As/Ls	U6	31807.9	54519.4	0.0	251992.6	1345.0
As/Ls	U60	52164.8	73815.3	0.0	170232.9	1020.5
As/Ls	U61	77266.8	102430.3	0.0	54154.0	1629.8
As/Ls	U62	78355.8	73448.1	0.0	126569.9	1863.9
As/Ls	U63	34528.7	116866.1	0.0	93825.4	22.4
As/Ls	U64	59397.9	105071.8	0.0	78531.3	286.5
As/Ls	U65	39572.3	112663.8	0.0	100312.5	578.4
As/Ls	U66	72905.0	70649.6	0.0	142547.3	961.2
As/Ls	U67	23139.3	46382.3	0.0	241525.6	2695.2
As/Ls	U68	75096.0	104181.1	0.0	35530.1	3699.7

TABLE B.4 Measured versus calculated values (Factor analysis end-members)

Group	Sample	Si				
		detrital	hydrothermal Fe	h/t FeMn	biogenic	authigenic
As/Ls	U69	1823.6	159082.3	0.0	54901.1	0.0
As/Ls	U7	52022.0	99364.5	0.0	51483.2	2940.1
As/Ls	U70	70366.4	100771.8	0.0	74224.1	1339.4
As/Ls	U71	22875.6	106875.1	0.0	140987.6	430.6
As/Ls	U72	47582.9	51105.8	0.0	175042.9	7111.4
As/Ls	U73	32079.0	105850.7	0.0	130664.1	637.9
As/Ls	U74	55684.3	86847.8	0.0	32607.0	14330.7
As/Ls	U75	88613.3	62311.0	0.0	55891.4	11789.3
As/Ls	U76	69888.1	66360.8	0.0	72091.9	12334.0
As/Ls	U77	74442.4	69205.8	0.0	149501.2	35.6
As/Ls	U78	4624.9	169662.8	0.0	24043.7	0.0
As/Ls	U8	65514.2	76479.4	0.0	137986.1	0.0
As/Ls	U9	62110.8	62328.2	0.0	125875.1	7775.4
Average		**60231**	**94536**	**9646**	**72654**	**1380**
Bu/Bu	20647	72266.5	66740.3	0.0	66816.5	12322.5
Bu/Bu	20648	51202.5	69712.9	0.0	102474.4	10765.3
Bu/Bu	20660	62035.9	62598.5	0.0	105162.4	10355.4
Bu/Bu	20676	100780.2	98008.0	0.0	48847.5	667.3
Bu/Bu	20686	93172.1	48488.2	0.0	62238.0	12464.5
Bu/Bu	20688	97845.3	49567.4	0.0	54093.0	11957.1
Bu/Bu	20689	85653.5	55040.2	0.0	102729.3	8327.8
Bu/Bu	20690	87094.7	57862.0	0.0	101485.9	7736.4
Bu/Bu	20691	96323.7	30950.6	0.0	139091.6	8642.7
Bu/Bu	20692	92805.2	58186.7	0.0	77292.3	8070.1
Bu/Bu	20693	51965.5	56385.3	0.0	30629.9	23658.0
Bu/Bu	20694	41930.7	85759.2	0.0	3861.5	19929.6
Bu/Bu	20695	51903.3	103381.7	0.0	13040.6	9601.0
Bu/Bu	20696	61237.8	110537.5	0.0	12522.6	5470.8
Bu/Bu	20697	61765.1	100079.7	0.0	30523.9	5057.2
Bu/Bu	20698	86490.2	41980.0	0.0	144011.9	6771.1
Bu/Bu	20699	109522.3	41357.2	0.0	77250.5	11544.8
Bu/Bu	20700	28313.7	74447.6	0.0	97686.6	15055.3
Bu/Bu	U22	26404.5	87112.2	0.0	82125.9	13687.9
Bu/Bu	U23	25199.3	111394.5	0.0	0.0	14956.0
Bu/Bu	U24	45919.3	149010.1	0.0	0.0	229.1
Average		**68087**	**74219**	**0**	**64375**	**10346**
Ls/Ls	U43	165048.3	77635.5	0.0	0.0	466.0
Ls/Ls	U44	48356.2	0.0	5849.2	0.0	0.0
Average		**106702**	**38818**	**2925**	**0**	**233**

Group Value %	Sample	Si detrital	Si hydrothermal	Si FeMn	Si biogenic	Si authigenic
Average	As	14.0	0.0	37.8	40.3	7.9
Average	As/Bu	26.7	0.3	30.0	37.8	5.2
Average	As/Ls	25.3	39.6	4.0	30.5	0.6
Average	Bu	31.4	34.2	0.0	29.7	4.8
Average	Ls	71.8	26.1	2.0	0.0	0.2
Average		33.8	20.1	14.8	27.6	3.7
Standard Deviation		22.1	18.8	17.7	16.1	3.3

TABLE B.4 Measured versus calculated values
(Factor analysis end-members)

Group	Sample	Fe				
		detrital	hydrothermal Fe	h/t FeMn	biogenic	authigenic
As/As	20657	10.6	0.0	1898.1	1.1	108107.6
As/As	20658	263.9	0.0	1079.7	2.3	84856.0
AVERAGE		**137**	**0**	**1489**	**2**	**96482**
As/Bu	20617	74.6	0.0	1823.4	1.2	93628.9
As/Bu	20634	86.0	0.0	1886.6	0.7	111966.2
As/Bu	20635	267.1	0.0	1117.3	3.8	37669.2
As/Bu	20636	298.1	0.0	1072.8	2.0	96163.4
As/Bu	20637	344.3	0.0	746.9	3.0	83715.5
As/Bu	20638	243.2	0.0	1228.2	1.2	119752.2
As/Bu	20639	338.2	0.0	602.0	3.3	90127.4
As/Bu	20640	229.7	0.0	1458.5	0.7	122769.1
As/Bu	20641	183.7	0.0	1467.8	1.5	103515.5
As/Bu	20642	794.7	0.0	652.2	0.0	82488.2
As/Bu	20643	664.6	0.0	1146.8	0.0	90153.2
As/Bu	20644	525.0	0.0	1298.9	0.0	108483.0
As/Bu	20645	749.2	0.0	894.5	0.0	94973.1
As/Bu	20646	136.7	2.3	1281.0	2.4	99318.0
As/Bu	20649	150.1	0.0	1372.7	2.3	92776.0
As/Bu	20650	78.8	0.0	1937.5	1.8	64273.9
As/Bu	20651	301.2	0.0	1269.6	1.0	107305.3
As/Bu	20652	0.0	0.0	1515.5	1.4	134801.8
As/Bu	20653	0.0	0.0	1768.0	0.7	145983.7
As/Bu	20654	0.0	0.0	1933.6	1.4	81147.4
As/Bu	20659	0.0	0.0	1345.8	3.0	98978.8
As/Bu	20662	387.7	0.0	813.7	2.2	96764.0
As/Bu	20663	352.3	0.0	1030.2	2.6	70770.8
As/Bu	20664	236.6	0.0	1306.8	2.6	62371.5
As/Bu	20665	379.9	0.0	842.8	2.9	61908.0
As/Bu	20666	596.6	0.0	1346.3	0.8	35201.2
As/Bu	20668	39.3	0.0	995.4	6.5	3069.4
As/Bu	20669	242.8	0.0	1157.5	3.5	36899.3
As/Bu	20671	357.0	0.0	1341.5	2.9	12876.4
As/Bu	20682	183.3	0.0	2555.4	0.0	10621.2
As/Bu	20683	673.3	0.0	1623.1	0.0	26775.5
As/Bu	20684	360.1	0.0	2715.7	0.0	0.0
As/Bu	20685	1143.6	0.0	621.9	0.0	46644.7
As/Bu	20687	158.9	57.5	88.4	7.8	0.0
As/Bu	U82	241.3	0.0	1029.4	2.7	99820.2
As/Bu	U83	0.0	0.0	3531.8	0.0	0.0
Average		**301**	**2**	**1356**	**2**	**72881**
As/Ls	20601	0.0	0.0	3661.7	0.0	0.0
As/Ls	20602	30.1	3.0	2798.7	0.7	0.0
As/Ls	20679	0.0	0.0	3098.5	0.0	995.0
As/Ls	20680	0.0	0.0	3045.8	0.0	0.0
As/Ls	20681	180.4	6.9	2061.9	1.8	0.0
As/Ls	U1	0.0	412.0	0.0	1.2	0.0
As/Ls	U10	0.0	493.8	0.0	0.0	4286.1
As/Ls	U11	287.9	338.0	0.0	0.4	88.5
As/Ls	U13	188.1	375.5	0.0	0.2	2154.5
As/Ls	U14	317.7	328.5	0.0	0.0	820.6
As/Ls	U14A	231.9	353.8	0.0	0.0	1674.5
As/Ls	U15	414.8	311.0	0.0	0.0	366.3
As/Ls	U16	266.5	342.1	0.0	0.0	902.7

TABLE B.4 Measured versus calculated values
(Factor analysis end-members)

Group	Sample	Fe				
		detrital	hydrothermal Fe	h/t FeMn	biogenic	authigenic
As/Ls	U17	588.8	276.1	0.0	0.0	0.0
As/Ls	U18	6.4	416.1	0.0	0.0	3255.1
As/Ls	U19	199.3	417.0	0.0	0.0	0.0
As/Ls	U2	264.1	108.6	1729.9	0.0	1407.3
As/Ls	U20	274.7	307.5	370.0	0.0	5453.1
As/Ls	U21	963.4	153.3	0.0	0.0	5118.5
As/Ls	U25	848.6	218.8	0.0	0.0	1332.5
As/Ls	U26	1091.6	168.0	0.0	0.0	0.0
As/Ls	U27	411.8	187.1	0.0	3.0	4288.8
As/Ls	U28	304.6	113.3	0.0	5.0	6304.7
As/Ls	U29	0.0	478.5	0.0	0.0	1505.1
As/Ls	U3	88.4	325.4	0.0	0.9	10258.3
As/Ls	U30	230.7	300.8	0.0	1.3	2160.0
As/Ls	U31	218.6	192.5	0.0	3.7	2634.9
As/Ls	U32	448.6	251.6	0.0	0.7	4646.0
As/Ls	U33	199.1	384.6	0.0	0.0	2651.6
As/Ls	U34	995.2	184.5	0.0	0.0	251.1
As/Ls	U35	372.1	216.1	0.0	2.3	1687.4
As/Ls	U36	400.3	197.3	0.0	3.0	1088.7
As/Ls	U37	461.6	210.2	0.0	2.4	5857.9
As/Ls	U38	101.8	422.9	0.0	0.0	4639.7
As/Ls	U39	126.0	421.1	0.0	0.0	0.0
As/Ls	U4	1043.3	169.1	0.0	0.0	0.0
As/Ls	U40	270.1	382.3	0.0	0.0	0.0
As/Ls	U41	1156.7	167.9	0.0	0.0	0.0
As/Ls	U41A	492.3	183.0	0.0	2.2	4318.0
As/Ls	U42	254.9	148.9	0.0	4.7	12514.9
As/Ls	U45	312.4	141.9	0.0	5.0	3894.4
As/Ls	U46	160.0	183.0	0.0	4.7	2839.8
As/Ls	U47	476.4	255.1	0.0	0.9	9110.2
As/Ls	U48	362.2	165.7	0.0	3.8	9570.3
As/Ls	U49	35.8	300.5	0.0	3.3	0.0
As/Ls	U5	554.5	153.8	0.0	2.8	9373.2
As/Ls	U50	345.8	237.6	0.0	2.1	13301.1
As/Ls	U51	385.7	208.3	0.0	2.7	10633.1
As/Ls	U52	223.9	164.8	0.0	4.2	16338.6
As/Ls	U53	316.7	180.7	0.0	3.2	19168.8
As/Ls	U54	0.0	488.5	0.0	0.0	9835.2
As/Ls	U55	0.0	494.6	0.0	0.0	10643.3
As/Ls	U56A	726.3	259.9	0.0	0.4	1065.9
As/Ls	U56B	297.7	286.0	0.0	0.5	32570.6
As/Ls	U56C	330.3	239.8	0.0	2.7	5140.5
As/Ls	U57	479.1	191.2	0.0	2.6	6723.7
As/Ls	U58	330.7	188.0	0.0	3.5	4796.7
As/Ls	U59	595.5	200.5	0.0	1.3	2252.9
As/Ls	U6	169.6	139.8	0.0	5.8	8966.3
As/Ls	U60	278.2	189.2	0.0	3.9	6803.2
As/Ls	U61	412.1	262.6	0.0	1.2	10865.3
As/Ls	U62	417.9	188.3	0.0	2.9	12425.7
As/Ls	U63	184.2	299.6	0.0	2.2	149.3
As/Ls	U64	316.8	269.3	0.0	1.8	1909.9
As/Ls	U65	211.1	288.8	0.0	2.3	3856.0
As/Ls	U66	388.8	181.1	0.0	3.3	6407.8
As/Ls	U67	123.4	118.9	0.0	5.6	17968.1
As/Ls	U68	400.5	267.1	0.0	0.8	24664.4

TABLE B.4 Measured versus calculated values (Factor analysis end-members)

Group	Sample	Fe				
		detrital	hydrothermal Fe	h/t FeMn	biogenic	authigenic
As/Ls	U69	9.7	407.8	0.0	1.3	0.0
As/Ls	U7	277.5	254.7	0.0	1.2	19600.9
As/Ls	U70	375.3	258.3	0.0	1.7	8929.5
As/Ls	U71	122.0	274.0	0.0	3.2	2870.4
As/Ls	U72	253.8	131.0	0.0	4.0	47409.0
As/Ls	U73	171.1	271.3	0.0	3.0	4252.5
As/Ls	U74	297.0	222.6	0.0	0.7	95538.1
As/Ls	U75	472.6	159.7	0.0	1.3	78595.0
As/Ls	U76	372.7	170.1	0.0	1.7	82226.8
As/Ls	U77	397.0	177.4	0.0	3.4	237.5
As/Ls	U78	24.7	434.9	0.0	0.6	0.0
As/Ls	U8	349.4	196.1	0.0	3.2	0.0
As/Ls	U9	331.3	159.8	0.0	2.9	51835.9
Average		**321**	**242**	**207**	**2**	**9203**
Bu/Bu	20647	385.4	171.1	0.0	1.5	82150.1
Bu/Bu	20648	273.1	178.7	0.0	2.4	71768.6
Bu/Bu	20660	330.9	160.5	0.0	2.4	69036.3
Bu/Bu	20676	537.5	251.2	0.0	1.1	4448.7
Bu/Bu	20686	496.9	124.3	0.0	1.4	83096.6
Bu/Bu	20688	521.8	127.1	0.0	1.2	79713.7
Bu/Bu	20689	456.8	141.1	0.0	2.4	55518.7
Bu/Bu	20690	464.5	148.3	0.0	2.3	51576.2
Bu/Bu	20691	513.7	79.3	0.0	3.2	57618.1
Bu/Bu	20692	495.0	149.2	0.0	1.8	53800.9
Bu/Bu	20693	277.1	144.5	0.0	0.7	157720.1
Bu/Bu	20694	223.6	219.8	0.0	0.1	132863.8
Bu/Bu	20695	276.8	265.0	0.0	0.3	64006.7
Bu/Bu	20696	326.6	283.4	0.0	0.3	36471.8
Bu/Bu	20697	329.4	256.6	0.0	0.7	33714.9
Bu/Bu	20698	461.3	107.6	0.0	3.3	45140.8
Bu/Bu	20699	584.1	106.0	0.0	1.8	76965.1
Bu/Bu	20700	151.0	190.8	0.0	2.2	100368.9
Bu/Bu	U22	140.8	223.3	0.0	1.9	91252.4
Bu/Bu	U23	134.4	285.6	0.0	0.0	99706.9
Bu/Bu	U24	244.9	382.0	0.0	0.0	1527.5
Average		**363**	**190**	**0**	**1**	**68975**
Ls/Ls	U43	880.3	199.0	0.0	0.0	3106.5
Ls/Ls	U44	257.9	0.0	125.5	0.0	0.0
Average		**569**	**100**	**63**	**0**	**1553**

Group Value %	Sample	Fe detrital	Fe hydrothermal	Fe FeMn	Fe biogenic	Fe authigenic
Average	As	0.1	98.3	1.5	0.0	0.0
Average	As/Bu	0.4	1.8	97.8	0.0	0.0
Average	As/Ls	3.2	92.3	2.1	0.0	2.4
Average	Bu	0.5	99.2	0.0	0.0	0.3
Average	Ls	24.9	68.0	2.7	0.0	4.4
Average		5.8	71.9	20.8	0.0	1.4
Standard Deviation		10.7	41.2	43.0	0.0	1.9

TABLE B.4 Measured versus calculated values (Factor analysis end-members)

Group	Sample	Mn				
		detrital	hydrothermal Fe	h/t FeMn	biogenic	authigenic
As/As	20657	465.2	0.0	216272.2	46.7	54053.8
As/As	20658	11544.9	0.0	123020.5	101.0	42428.0
AVERAGE		**6005**	**0**	**169646**	**74**	**48241**
As/Bu	20617	3262.4	0.0	207758.4	53.4	46814.4
As/Bu	20634	3764.3	0.0	214954.6	30.9	55983.1
As/Bu	20635	11687.0	0.0	127309.3	163.6	18834.6
As/Bu	20636	13042.9	0.0	122238.1	88.7	48081.7
As/Bu	20637	15064.0	0.0	85103.7	132.3	41857.7
As/Bu	20638	10640.6	0.0	139944.0	52.6	59876.1
As/Bu	20639	14797.5	0.0	68588.5	143.0	45063.7
As/Bu	20640	10050.3	0.0	166180.6	32.2	61384.5
As/Bu	20641	8036.3	0.0	167244.7	64.4	51757.8
As/Bu	20642	34769.3	0.0	74311.9	0.0	41244.1
As/Bu	20643	29076.7	0.0	130669.7	0.0	45076.6
As/Bu	20644	22966.6	0.0	147999.5	0.0	54241.5
As/Bu	20645	32775.5	0.0	101915.0	0.0	47486.5
As/Bu	20646	5979.0	1831.2	145960.9	102.6	49659.0
As/Bu	20649	6568.9	0.0	156405.7	99.0	46388.0
As/Bu	20650	3447.3	0.0	220759.5	78.6	32136.9
As/Bu	20651	13178.2	0.0	144651.7	44.2	53652.6
As/Bu	20652	0.0	0.0	172679.6	61.0	67400.9
As/Bu	20653	0.0	0.0	201447.8	29.9	72991.9
As/Bu	20654	0.0	0.0	220316.1	62.9	40573.7
As/Bu	20659	0.0	0.0	153337.1	132.3	49489.4
As/Bu	20662	16963.8	0.0	92711.6	94.5	48382.0
As/Bu	20663	15413.6	0.0	117375.4	112.6	35385.4
As/Bu	20664	10351.5	0.0	148897.5	112.6	31185.7
As/Bu	20665	16621.0	0.0	96033.2	126.8	30954.0
As/Bu	20666	26102.8	0.0	153394.3	35.6	17600.6
As/Bu	20668	1718.0	0.0	113418.0	283.3	1534.7
As/Bu	20669	10624.3	0.0	131880.7	153.0	18449.6
As/Bu	20671	15617.4	0.0	152852.2	126.8	6438.2
As/Bu	20682	8017.7	0.0	291161.0	0.0	5310.6
As/Bu	20683	29455.0	0.0	184933.0	0.0	13387.8
As/Bu	20684	15755.1	0.0	309428.3	0.0	0.0
As/Bu	20685	50032.8	0.7	70854.6	0.0	23322.4
As/Bu	20687	6951.6	45821.8	10070.4	338.4	0.0
As/Bu	U82	10558.8	0.0	117283.4	116.3	49910.1
As/Bu	U83	0.0	0.0	402408.0	0.0	0.0
Average		**13147**	**1324**	**154513**	**80**	**36440**
As/Ls	20601	0.0	0.0	417206.3	0.0	0.0
As/Ls	20602	1318.2	2368.3	318876.0	31.5	0.0
As/Ls	20679	0.0	0.0	353043.8	0.0	497.5
As/Ls	20680	0.0	0.0	347039.8	0.0	0.0
As/Ls	20681	7890.4	5492.3	234926.5	76.5	0.0
As/Ls	U1	0.0	328220.4	0.0	52.9	0.0
As/Ls	U10	0.0	393367.7	0.0	0.0	2143.1
As/Ls	U11	12596.7	269301.7	0.0	18.4	44.2
As/Ls	U13	8230.3	299109.1	0.0	7.3	1077.2
As/Ls	U14	13897.3	261734.7	0.0	0.0	410.3
As/Ls	U14A	10144.5	281892.5	0.0	0.0	837.3
As/Ls	U15	18145.9	247733.6	0.0	0.0	183.2
As/Ls	U16	11658.7	272511.9	0.0	0.0	451.3

TABLE B.4 Measured versus calculated values (Factor analysis end-members)

Group	Sample	Mn				
		detrital	hydrothermal Fe	h/t FeMn	biogenic	authigenic
As/Ls	U17	25760.6	219963.2	0.0	0.0	0.0
As/Ls	U18	278.4	331498.0	0.0	0.0	1627.6
As/Ls	U19	8718.1	332179.1	0.0	0.0	0.0
As/Ls	U2	11555.1	86542.3	197105.0	0.0	703.6
As/Ls	U20	12019.1	244942.5	42159.7	0.0	2726.5
As/Ls	U21	42150.5	122127.1	0.0	0.0	2559.2
As/Ls	U25	37126.1	174302.4	0.0	0.0	666.2
As/Ls	U26	47755.4	133850.9	0.0	0.0	0.0
As/Ls	U27	18014.6	149039.4	0.0	129.3	2144.4
As/Ls	U28	13324.2	90286.3	0.0	219.3	3152.4
As/Ls	U29	0.0	381225.3	0.0	0.0	752.5
As/Ls	U3	3866.3	259265.4	0.0	39.9	5129.1
As/Ls	U30	10094.1	239619.2	0.0	56.9	1080.0
As/Ls	U31	9563.1	153325.7	0.0	162.3	1317.4
As/Ls	U32	19628.1	200464.5	0.0	28.6	2323.0
As/Ls	U33	8709.2	306414.7	0.0	0.0	1325.8
As/Ls	U34	43541.2	146999.7	0.0	0.0	125.6
As/Ls	U35	16278.5	172178.0	0.0	101.7	843.7
As/Ls	U36	17511.0	157195.4	0.0	129.1	544.3
As/Ls	U37	20193.5	167458.6	0.0	106.2	2929.0
As/Ls	U38	4453.9	336900.7	0.0	0.0	2319.8
As/Ls	U39	5512.9	335428.5	0.0	0.0	0.0
As/Ls	U4	45643.8	134734.2	0.0	0.0	0.0
As/Ls	U40	11818.9	304534.3	0.0	0.0	0.0
As/Ls	U41	50606.4	133747.5	0.0	0.0	0.0
As/Ls	U41A	21538.0	145762.7	0.0	97.3	2159.0
As/Ls	U42	11150.5	118597.0	0.0	204.3	6257.5
As/Ls	U45	13668.3	113044.5	0.0	217.1	1947.2
As/Ls	U46	7000.8	145797.7	0.0	206.0	1419.9
As/Ls	U47	20844.4	203194.6	0.0	39.6	4555.1
As/Ls	U48	15847.2	131987.6	0.0	164.8	4785.1
As/Ls	U49	1565.7	239385.2	0.0	145.5	0.0
As/Ls	U5	24260.6	122538.4	0.1	122.7	4686.6
As/Ls	U50	15128.0	189263.8	0.1	91.3	6650.5
As/Ls	U51	16872.9	165971.0	0.1	116.0	5316.5
As/Ls	U52	9793.9	131290.1	0.1	184.5	8169.3
As/Ls	U53	13853.5	143930.8	0.1	140.7	9584.4
As/Ls	U54	0.0	389200.3	0.1	0.0	4917.6
As/Ls	U55	0.0	394000.8	0.1	0.0	5321.6
As/Ls	U56A	31774.8	207047.0	0.0	16.5	533.0
As/Ls	U56B	13025.8	227829.5	0.0	21.1	16285.3
As/Ls	U56C	14452.1	191031.9	0.0	115.3	2570.2
As/Ls	U57	20958.6	152345.0	0.0	114.3	3361.9
As/Ls	U58	14469.2	149760.9	0.0	152.1	2398.3
As/Ls	U59	26052.0	159735.9	0.0	55.1	1126.4
As/Ls	U6	7421.8	111338.5	0.0	252.0	4483.2
As/Ls	U60	12171.8	150744.3	0.0	170.2	3401.6
As/Ls	U61	18028.9	209181.3	0.0	54.2	5432.6
As/Ls	U62	18283.0	149994.5	0.0	126.6	6212.8
As/Ls	U63	8056.7	238661.9	0.0	93.8	74.6
As/Ls	U64	13859.5	214575.8	0.0	78.5	954.9
As/Ls	U65	9233.5	230080.0	0.0	100.3	1928.0
As/Ls	U66	17011.2	144279.3	0.0	142.5	3203.9
As/Ls	U67	5399.2	94721.2	0.0	241.5	8984.1
As/Ls	U68	17522.4	212756.7	0.0	35.5	12332.2

TABLE B.4 Measured versus calculated values (Factor analysis end-members)

Group	Sample	Mn				
		detrital	hydrothermal Fe	h/t FeMn	biogenic	authigenic
As/Ls	U69	425.5	324875.1	0.0	54.9	0.0
As/Ls	U7	12138.5	202920.4	0.0	51.5	9800.4
As/Ls	U70	16418.8	205794.4	0.0	74.2	4464.7
As/Ls	U71	5337.6	218258.5	0.0	141.0	1435.2
As/Ls	U72	11102.7	104367.4	0.0	175.0	23704.5
As/Ls	U73	7485.1	216166.4	0.0	130.7	2126.2
As/Ls	U74	12993.0	177359.0	0.0	32.6	47769.1
As/Ls	U75	20676.4	127250.5	0.0	55.9	39297.5
As/Ls	U76	16307.2	135520.9	0.0	72.1	41113.4
As/Ls	U77	17369.9	141330.8	0.0	149.5	118.8
As/Ls	U78	1079.1	346482.4	0.0	24.0	0.0
As/Ls	U8	15286.6	156184.9	0.0	138.0	0.0
As/Ls	U9	14492.5	127285.6	0.0	125.9	25918.0
Average		**14054**	**193059**	**23585**	**73**	**4601**
Bu/Bu	20647	16862.2	136296.0	0.0	66.8	41075.0
Bu/Bu	20648	11947.2	142366.5	0.0	102.5	35884.3
Bu/Bu	20660	14475.0	127837.5	0.0	105.2	34518.2
Bu/Bu	20676	23515.4	200150.2	0.0	48.8	2224.3
Bu/Bu	20686	21740.2	99021.8	0.0	62.2	41548.3
Bu/Bu	20688	22830.6	101225.7	0.0	54.1	39856.9
Bu/Bu	20689	19985.8	112402.1	0.0	102.7	27759.3
Bu/Bu	20690	20322.1	118164.8	0.0	101.5	25788.1
Bu/Bu	20691	22475.5	63206.7	0.0	139.1	28809.1
Bu/Bu	20692	21654.6	118828.0	0.0	77.3	26900.5
Bu/Bu	20693	12125.3	115149.0	0.0	30.6	78860.0
Bu/Bu	20694	9783.8	175135.9	0.0	3.9	66431.9
Bu/Bu	20695	12110.8	211124.3	0.0	13.0	32003.4
Bu/Bu	20696	14288.8	225737.7	0.0	12.5	18235.9
Bu/Bu	20697	14411.9	204381.0	0.0	30.5	16857.5
Bu/Bu	20698	20181.0	85730.8	0.0	144.0	22570.4
Bu/Bu	20699	25555.2	84459.0	0.0	77.3	38482.5
Bu/Bu	20700	6606.5	152035.6	0.0	97.7	50184.4
Bu/Bu	U22	6161.1	177899.0	0.0	82.1	45626.2
Bu/Bu	U23	5879.8	227487.9	0.0	0.0	49853.4
Bu/Bu	U24	10714.5	304305.8	0.0	0.0	763.8
Average		**15887**	**151569**	**0**	**64**	**34487**
Ls/Ls	U43	38511.3	158545.8	0.0	0.0	1553.2
Ls/Ls	U44	11283.1	0.0	14301.6	0.0	0.0
Average		**24897**	**79273**	**7151**	**0**	**777**

Group Value %	Sample	Mn detrital	Mn hydrothermal	Mn FeMn	Mn biogenic	Mn authigenic
Average	As	2.7	75.8	0.0	0.0	21.5
Average	As/Bu	6.4	0.6	75.2	0.0	17.7
Average	As/Ls	6.0	82.0	10.0	0.0	2.0
Average	Bu	7.9	75.0	0.0	0.0	17.1
Average	Ls	22.2	70.7	6.4	0.0	0.7
Average		9.0	60.8	18.3	0.0	11.8
Standard Deviation		7.6	33.9	32.1	0.0	9.7

TABLE B.4 Measured versus calculated values
(Factor analysis end-members)

Group	Sample	Ni				
		detrital	hydrothermal Fe	h/t FeMn	biogenic	authigenic
As/As	20657	0.1	0.0	18.2	0.2	360.4
As/As	20658	2.5	0.0	10.3	0.4	282.9
AVERAGE		**1**	**0**	**14**	**0**	**322**
As/Bu	20617	0.7	0.0	17.5	0.2	312.1
As/Bu	20634	0.8	0.0	18.1	0.1	373.2
As/Bu	20635	2.5	0.0	10.7	0.7	125.6
As/Bu	20636	2.8	0.0	10.3	0.4	320.5
As/Bu	20637	3.2	0.0	7.2	0.5	279.1
As/Bu	20638	2.3	0.0	11.8	0.2	399.2
As/Bu	20639	3.2	0.0	5.8	0.6	300.4
As/Bu	20640	2.2	0.0	14.0	0.1	409.2
As/Bu	20641	1.7	0.0	14.1	0.3	345.1
As/Bu	20642	7.5	0.0	6.2	0.0	275.0
As/Bu	20643	6.2	0.0	11.0	0.0	300.5
As/Bu	20644	4.9	0.0	12.4	0.0	361.6
As/Bu	20645	7.0	0.0	8.6	0.0	316.6
As/Bu	20646	1.3	0.0	12.3	0.4	331.1
As/Bu	20649	1.4	0.0	13.2	0.4	309.3
As/Bu	20650	1.5	0.0	37.6	0.6	434.2
As/Bu	20651	2.8	0.0	12.2	0.2	357.7
As/Bu	20652	0.0	0.0	14.5	0.2	449.3
As/Bu	20653	0.0	0.0	16.9	0.1	486.6
As/Bu	20654	0.0	0.0	18.5	0.3	270.5
As/Bu	20659	0.0	0.0	12.9	0.5	329.9
As/Bu	20662	3.6	0.0	7.8	0.4	322.5
As/Bu	20663	3.3	0.0	9.9	0.5	235.9
As/Bu	20664	2.2	0.0	12.5	0.5	207.9
As/Bu	20665	3.6	0.0	8.1	0.5	206.4
As/Bu	20666	14.3	0.0	33.0	0.4	300.3
As/Bu	20668	3.7	0.0	95.4	11.3	102.3
As/Bu	20669	5.2	0.0	25.5	1.4	282.9
As/Bu	20671	19.1	0.0	73.3	2.9	244.7
As/Bu	20682	17.2	0.0	244.9	0.0	354.0
As/Bu	20683	25.7	0.0	63.4	0.0	363.9
As/Bu	20684	33.8	0.0	260.2	0.0	0.0
As/Bu	20685	10.7	0.0	6.0	0.0	155.5
As/Bu	20687	14.9	4.6	8.5	13.5	0.0
As/Bu	U82	1.2	0.0	5.2	0.2	175.4
As/Bu	U83	0.0	0.0	33.8	0.0	0.0
Average		**6**	**0**	**33**	**1**	**279**
As/Ls	20601	0.0	0.0	35.1	0.0	0.0
As/Ls	20602	2.8	0.2	268.2	1.3	0.0
As/Ls	20679	0.0	0.0	296.9	0.0	33.2
As/Ls	20680	0.0	0.0	291.9	0.0	0.0
As/Ls	20681	16.9	0.5	197.6	3.1	0.0
As/Ls	U1	0.0	32.9	0.0	2.1	0.0
As/Ls	U10	0.0	8.0	0.0	0.0	29.0
As/Ls	U11	92.7	92.6	0.0	2.5	10.1
As/Ls	U13	51.4	87.3	0.0	0.8	209.4
As/Ls	U14	91.5	80.5	0.0	0.0	84.0
As/Ls	U14A	21.7	28.2	0.0	0.0	55.8
As/Ls	U15	106.0	67.6	0.0	0.0	33.3
As/Ls	U16	94.6	103.4	0.0	0.0	114.0

TABLE B.4 Measured versus calculated values
(Factor analysis end-members)

Group	Sample	Ni				
		detrital	hydrothermal Fe	h/t FeMn	biogenic	authigenic
As/Ls	U17	153.7	61.3	0.0	0.0	0.0
As/Ls	U18	1.7	93.3	0.0	0.0	305.0
As/Ls	U19	18.7	33.3	0.0	0.0	0.0
As/Ls	U2	24.8	8.7	165.8	0.0	46.9
As/Ls	U20	25.8	24.5	35.5	0.0	181.8
As/Ls	U21	90.3	12.2	0.0	0.0	170.6
As/Ls	U25	79.6	17.5	0.0	0.0	44.4
As/Ls	U26	102.3	13.4	0.0	0.0	0.0
As/Ls	U27	38.6	14.9	0.0	5.2	143.0
As/Ls	U28	28.6	9.0	0.0	8.8	210.2
As/Ls	U29	0.0	38.2	0.0	0.0	50.2
As/Ls	U3	8.3	26.0	0.0	1.6	341.9
As/Ls	U30	70.5	78.2	0.0	7.4	234.8
As/Ls	U31	54.5	40.8	0.0	17.3	233.5
As/Ls	U32	42.1	20.1	0.0	1.1	154.9
As/Ls	U33	89.8	147.7	0.0	0.0	425.5
As/Ls	U34	229.3	36.2	0.0	0.0	20.6
As/Ls	U35	81.3	40.2	0.0	9.5	131.1
As/Ls	U36	72.1	30.2	0.0	9.9	69.7
As/Ls	U37	43.3	16.8	0.0	4.2	195.3
As/Ls	U38	9.5	33.7	0.0	0.0	154.7
As/Ls	U39	11.8	33.6	0.0	0.0	0.0
As/Ls	U4	302.3	41.7	0.0	0.0	0.0
As/Ls	U40	25.3	30.5	0.0	0.0	0.0
As/Ls	U41	108.4	13.4	0.0	0.0	0.0
As/Ls	U41A	46.2	14.6	0.0	3.9	143.9
As/Ls	U42	23.9	11.9	0.0	8.2	417.2
As/Ls	U45	29.3	11.3	0.0	8.7	129.8
As/Ls	U46	15.0	14.6	0.0	8.2	94.7
As/Ls	U47	44.7	20.3	0.0	1.6	303.7
As/Ls	U48	34.0	13.2	0.0	6.6	319.0
As/Ls	U49	3.4	24.0	0.0	5.8	0.0
As/Ls	U5	33.2	7.8	0.0	3.1	199.8
As/Ls	U50	19.5	11.4	0.0	2.2	266.9
As/Ls	U51	36.2	16.6	0.0	4.6	354.4
As/Ls	U52	8.1	5.1	0.0	2.9	210.9
As/Ls	U53	17.0	8.2	0.0	3.2	365.6
As/Ls	U54	0.0	39.0	0.0	0.0	327.8
As/Ls	U55	0.0	39.4	0.0	0.0	354.8
As/Ls	U56A	68.1	20.7	0.0	0.7	35.5
As/Ls	U56B	2.8	2.3	0.0	0.1	108.6
As/Ls	U56C	31.0	19.1	0.0	4.6	171.3
As/Ls	U57	27.2	9.2	0.0	2.8	135.8
As/Ls	U58	31.0	15.0	0.0	6.1	159.9
As/Ls	U59	55.8	16.0	0.0	2.2	75.1
As/Ls	U6	8.1	5.7	0.0	5.1	152.1
As/Ls	U60	26.1	15.1	0.0	6.8	226.8
As/Ls	U61	38.6	20.9	0.0	2.2	362.2
As/Ls	U62	26.6	10.2	0.0	3.4	281.7
As/Ls	U63	58.8	81.4	0.0	12.8	17.0
As/Ls	U64	101.7	73.6	0.0	10.8	218.0
As/Ls	U65	19.8	23.0	0.0	4.0	128.5
As/Ls	U66	36.5	14.4	0.0	5.7	213.6
As/Ls	U67	7.6	6.2	0.0	6.3	391.0
As/Ls	U68	12.1	6.9	0.0	0.5	264.6

TABLE B.4 Measured versus calculated values
(Factor analysis end-members)

Group	Sample	Ni				
		detrital	hydrothermal Fe	h/t FeMn	biogenic	authigenic
As/Ls	U69	0.9	32.5	0.0	2.2	0.0
As/Ls	U7	16.6	12.9	0.0	1.3	416.2
As/Ls	U70	35.2	20.6	0.0	3.0	297.6
As/Ls	U71	11.4	21.9	0.0	5.6	95.7
As/Ls	U72	2.4	1.0	0.0	0.7	158.0
As/Ls	U73	16.0	21.6	0.0	5.2	141.7
As/Ls	U74	2.8	1.8	0.0	0.1	318.5
As/Ls	U75	4.4	1.3	0.0	0.2	262.0
As/Ls	U76	3.5	1.4	0.0	0.3	274.1
As/Ls	U77	37.2	14.2	0.0	6.0	7.9
As/Ls	U78	2.3	34.7	0.0	1.0	0.0
As/Ls	U8	123.3	58.9	0.0	20.8	0.0
As/Ls	U9	3.1	1.3	0.0	0.5	172.8
Average		**41**	**27**	**16**	**3**	**151**
Bu/Bu	20647	3.6	1.4	0.0	0.3	273.8
Bu/Bu	20648	2.6	1.4	0.0	0.4	239.2
Bu/Bu	20660	3.1	1.3	0.0	0.4	230.1
Bu/Bu	20676	50.4	20.0	0.0	2.0	148.3
Bu/Bu	20686	4.7	1.0	0.0	0.2	277.0
Bu/Bu	20688	4.9	1.0	0.0	0.2	265.7
Bu/Bu	20689	4.3	1.1	0.0	0.4	185.1
Bu/Bu	20690	4.4	1.2	0.0	0.4	171.9
Bu/Bu	20691	4.8	0.6	0.0	0.6	192.1
Bu/Bu	20692	4.6	1.2	0.0	0.3	179.3
Bu/Bu	20693	2.6	1.2	0.0	0.1	525.7
Bu/Bu	20694	2.1	1.8	0.0	0.0	442.9
Bu/Bu	20695	2.6	2.1	0.0	0.1	213.4
Bu/Bu	20696	10.3	7.6	0.0	0.2	407.0
Bu/Bu	20697	8.4	5.6	0.0	0.3	305.7
Bu/Bu	20698	4.3	0.9	0.0	0.6	150.5
Bu/Bu	20699	5.5	0.8	0.0	0.3	256.6
Bu/Bu	20700	1.4	1.5	0.0	0.4	334.6
Bu/Bu	U22	1.3	1.8	0.0	0.3	304.2
Bu/Bu	U23	1.3	2.3	0.0	0.0	332.4
Bu/Bu	U24	23.0	30.5	0.0	0.0	50.9
Average		**7**	**4**	**0**	**0**	**261**
Ls/Ls	U43	82.5	15.9	0.0	0.0	103.5
Ls/Ls	U44	24.2	0.0	12.0	0.0	0.0
Average		**53**	**8**	**6**	**0**	**52**

Group Value %	Sample	Ni detrital	Ni hydrothermal	Ni FeMn	Ni biogenic	Ni authigenic
Average	As	0.4	40.0	4.2	0.1	45.3
Average	As/Bu	1.8	0.0	50.2	0.3	47.6
Average	As/Ls	0.1	38.5	16.7	1.3	43.4
Average	Bu	2.6	41.5	0.0	0.1	55.7
Average	Ls	24.8	46.7	15.1	0.0	33.5
Average		6.0	33.3	17.2	0.4	45.1
Standard Deviation		10.6	18.9	19.7	0.5	8.0

TABLE B.4 Measured versus calculated values
(Factor analysis end-members)

Group	Sample	Cu				
		detrital	hydrothermal Fe	h/t FeMn	biogenic	authigenic
As/As	20657	0.0	0.0	2.1	0.1	720.7
As/As	20658	0.4	0.0	0.6	0.1	282.9
AVERAGE		**0**	**0**	**1**	**0**	**502**
As/Bu	20617	0.1	0.0	1.0	0.1	312.1
As/Bu	20634	0.1	0.0	1.0	0.0	373.2
As/Bu	20635	1.6	0.0	2.4	0.7	502.3
As/Bu	20636	0.4	0.0	0.6	0.1	320.5
As/Bu	20637	0.5	0.0	0.4	0.1	279.1
As/Bu	20638	0.4	0.0	0.7	0.1	399.2
As/Bu	20639	0.5	0.0	0.3	0.1	300.4
As/Bu	20640	0.3	0.0	0.8	0.0	409.2
As/Bu	20641	0.6	0.0	1.6	0.1	690.1
As/Bu	20642	1.2	0.0	0.4	0.0	275.0
As/Bu	20643	2.0	0.0	1.2	0.0	601.0
As/Bu	20644	1.6	0.0	1.4	0.0	723.2
As/Bu	20645	1.1	0.0	0.5	0.0	316.6
As/Bu	20646	0.4	0.3	1.4	0.2	662.1
As/Bu	20649	0.5	0.0	1.5	0.2	618.5
As/Bu	20650	0.5	0.0	4.2	0.3	857.0
As/Bu	20651	0.9	0.0	1.4	0.1	715.4
As/Bu	20652	0.0	0.0	0.8	0.1	449.3
As/Bu	20653	0.0	0.0	1.0	0.0	486.6
As/Bu	20654	0.0	0.0	4.2	0.3	1082.0
As/Bu	20659	0.0	0.0	1.5	0.3	659.9
As/Bu	20662	0.6	0.0	0.4	0.1	322.5
As/Bu	20663	1.1	0.0	1.1	0.2	471.8
As/Bu	20664	0.7	0.0	1.4	0.2	415.8
As/Bu	20665	1.1	0.0	0.9	0.3	412.7
As/Bu	20666	0.4	0.0	0.4	0.0	58.7
As/Bu	20668	0.0	0.0	0.3	0.1	5.1
As/Bu	20669	0.7	0.0	1.3	0.3	246.0
As/Bu	20671	0.3	0.0	0.4	0.1	21.5
As/Bu	20682	13.7	0.0	69.6	0.0	1770.2
As/Bu	20683	0.5	0.0	0.4	0.0	44.6
As/Bu	20684	27.0	0.0	73.9	0.0	0.0
As/Bu	20685	6.0	0.0	1.2	0.0	542.8
As/Bu	20687	11.9	215.3	2.4	16.9	0.0
As/Bu	U82	0.4	0.0	0.6	0.1	332.7
As/Bu	U83	0.0	0.0	3076.0	0.0	0.0
Average		**2**	**6**	**91**	**1**	**435**
As/Ls	20601	0.0	0.0	3189.1	0.0	0.0
As/Ls	20602	2.3	11.1	76.2	1.6	0.0
As/Ls	20679	0.0	0.0	84.3	0.0	165.8
As/Ls	20680	0.0	0.0	82.9	0.0	0.0
As/Ls	20681	13.5	25.8	56.1	3.8	0.0
As/Ls	U1	0.0	1542.0	0.0	2.6	0.0
As/Ls	U10	0.0	3696.1	0.0	0.0	1428.7
As/Ls	U11	0.9	53.4	0.0	0.0	0.6
As/Ls	U13	0.1	13.4	0.0	0.0	3.4
As/Ls	U14	0.2	11.5	0.0	0.0	1.3
As/Ls	U14A	8.0	611.3	0.0	0.0	128.8
As/Ls	U15	3.8	142.2	0.0	0.0	7.5
As/Ls	U16	2.8	176.5	0.0	0.0	20.7

TABLE B.4 Measured versus calculated values
(Factor analysis end-members)

Group	Sample	Cu				
		detrital	hydrothermal Fe	h/t FeMn	biogenic	authigenic
As/Ls	U17	4.4	102.6	0.0	0.0	0.0
As/Ls	U18	0.0	15.6	0.0	0.0	5.4
As/Ls	U19	14.9	1560.6	0.0	0.0	0.0
As/Ls	U2	6.5	134.3	15.6	0.0	77.5
As/Ls	U20	0.9	51.5	0.5	0.0	40.7
As/Ls	U21	72.3	573.8	0.0	0.0	853.1
As/Ls	U25	63.6	818.9	0.0	0.0	222.1
As/Ls	U26	81.9	628.8	0.0	0.0	0.0
As/Ls	U27	30.9	700.2	0.0	6.5	714.8
As/Ls	U28	3.2	59.7	0.0	1.5	147.9
As/Ls	U29	0.0	228.1	0.0	0.0	31.9
As/Ls	U3	0.1	12.2	0.0	0.0	17.1
As/Ls	U30	0.2	11.3	0.0	0.0	3.6
As/Ls	U31	0.2	7.2	0.0	0.1	4.4
As/Ls	U32	0.3	9.4	0.0	0.0	7.7
As/Ls	U33	0.1	14.4	0.0	0.0	4.4
As/Ls	U34	2.8	26.0	0.0	0.0	1.6
As/Ls	U35	0.3	8.1	0.0	0.1	2.8
As/Ls	U36	7.1	173.7	0.0	1.5	42.7
As/Ls	U37	5.5	125.8	0.0	0.8	156.2
As/Ls	U38	1.5	308.0	0.0	0.0	150.5
As/Ls	U39	1.7	278.3	0.0	0.0	0.0
As/Ls	U4	12.5	100.8	0.0	0.0	0.0
As/Ls	U40	2.7	190.5	0.0	0.0	0.0
As/Ls	U41	86.8	628.4	0.0	0.0	0.0
As/Ls	U41A	1.0	19.2	0.0	0.1	20.1
As/Ls	U42	0.8	22.9	0.0	0.4	85.9
As/Ls	U45	23.4	531.1	0.0	10.9	649.1
As/Ls	U46	2.3	132.9	0.0	2.0	91.8
As/Ls	U47	1.4	38.0	0.0	0.1	60.5
As/Ls	U48	2.5	57.9	0.0	0.8	148.8
As/Ls	U49	0.3	114.3	0.0	0.7	0.0
As/Ls	U5	7.2	100.1	0.0	1.1	271.6
As/Ls	U50	11.1	379.9	0.0	2.0	947.1
As/Ls	U51	2.7	72.3	0.0	0.5	164.4
As/Ls	U52	3.0	110.0	0.0	1.6	485.4
As/Ls	U53	0.2	6.8	0.0	0.1	31.9
As/Ls	U54	0.0	18.3	0.0	0.0	16.4
As/Ls	U55	0.0	18.5	0.0	0.0	17.7
As/Ls	U56A	0.5	9.7	0.0	0.0	1.8
As/Ls	U56B	0.2	10.7	0.0	0.0	54.3
As/Ls	U56C	1.6	59.1	0.0	0.4	56.4
As/Ls	U57	10.3	205.8	0.0	1.6	322.2
As/Ls	U58	24.8	703.6	0.0	7.6	799.4
As/Ls	U59	0.4	7.5	0.0	0.0	3.8
As/Ls	U6	1.0	40.9	0.0	1.0	116.7
As/Ls	U60	1.2	42.1	0.0	0.5	67.4
As/Ls	U61	1.7	55.6	0.0	0.2	102.5
As/Ls	U62	6.7	150.3	0.0	1.3	441.7
As/Ls	U63	0.1	11.2	0.0	0.0	0.2
As/Ls	U64	0.2	10.1	0.0	0.0	3.2
As/Ls	U65	0.2	10.8	0.0	0.1	6.4
As/Ls	U66	0.3	6.8	0.0	0.1	10.7
As/Ls	U67	0.1	4.5	0.0	0.1	29.9
As/Ls	U68	1.8	58.3	0.0	0.1	239.8

TABLE B.4 Measured versus calculated values
(Factor analysis end-members)

Group	Sample	Cu				
		detrital	hydrothermal Fe	h/t FeMn	biogenic	authigenic
As/Ls	U69	0.5	1071.6	0.0	1.9	0.0
As/Ls	U7	0.2	9.5	0.0	0.0	32.7
As/Ls	U70	1.8	62.2	0.0	0.2	95.7
As/Ls	U71	9.2	1025.4	0.0	7.0	478.4
As/Ls	U72	0.2	4.9	0.0	0.1	79.0
As/Ls	U73	12.8	1015.6	0.0	6.5	708.7
As/Ls	U74	0.2	8.3	0.0	0.0	159.2
As/Ls	U75	1.2	20.9	0.0	0.1	457.8
As/Ls	U76	0.3	6.4	0.0	0.0	137.0
As/Ls	U77	29.8	664.0	0.0	7.5	39.6
As/Ls	U78	1.8	1627.8	0.0	1.2	0.0
As/Ls	U8	26.2	733.8	0.0	6.9	0.0
As/Ls	U9	1.1	25.8	0.0	0.3	372.8
Average		**8**	**276**	**43**	**1**	**149**
Bu/Bu	20647	0.3	6.4	0.0	0.0	136.9
Bu/Bu	20648	0.2	6.7	0.0	0.1	119.6
Bu/Bu	20660	0.2	6.0	0.0	0.1	115.1
Bu/Bu	20676	3.5	80.7	0.0	0.2	63.6
Bu/Bu	20686	1.2	14.9	0.0	0.1	443.8
Bu/Bu	20688	1.9	22.7	0.0	0.1	635.3
Bu/Bu	20689	2.5	38.2	0.0	0.4	669.0
Bu/Bu	20690	2.1	33.2	0.0	0.3	514.4
Bu/Bu	20691	5.2	40.0	0.0	0.9	1293.9
Bu/Bu	20692	2.0	29.8	0.0	0.2	478.1
Bu/Bu	20693	0.2	5.4	0.0	0.0	262.9
Bu/Bu	20694	0.7	36.2	0.0	0.0	973.1
Bu/Bu	20695	0.2	9.9	0.0	0.0	106.7
Bu/Bu	20696	2.6	111.0	0.0	0.1	636.3
Bu/Bu	20697	2.9	113.4	0.0	0.2	663.5
Bu/Bu	20698	2.0	22.7	0.0	0.4	424.9
Bu/Bu	20699	3.6	32.6	0.0	0.3	1053.5
Bu/Bu	20700	0.1	7.1	0.0	0.0	167.3
Bu/Bu	U22	0.7	53.1	0.0	0.3	966.0
Bu/Bu	U23	0.1	10.7	0.0	0.0	166.2
Bu/Bu	U24	1.2	96.9	0.0	0.0	17.2
Average		**2**	**37**	**0**	**0**	**472**
Ls/Ls	U43	66.0	744.9	0.0	0.0	517.7
Ls/Ls	U44	1.0	0.0	0.2	0.0	0.0
Average		**34**	**372**	**0**	**0**	**259**

Group Value %	Sample	Cu detrital	Cu hydrothermal	Cu FeMn	Cu biogenic	Cu authigenic
Average	As	0.0	99.7	0.3	0.0	0.0
Average	As/Bu	0.4	81.4	16.9	0.1	1.1
Average	As/Ls	1.6	57.9	9.1	0.2	31.2
Average	Bu	0.3	92.4	7.3	0.0	0.0
Average	Ls	5.0	56.0	0.0	0.0	38.9
Average		1.5	77.5	6.7	0.1	14.3
Standard Deviation		2.1	19.9	7.0	0.1	19.2

TABLE B.4 Measured versus calculated values
(Factor analysis end-members)

Group	Sample	Zn				
		detrital	hydrothermal Fe	h/t FeMn	biogenic	authigenic
As/As	20657	0.9	0.0	21.4	3.7	360.4
As/As	20658	23.1	0.0	12.2	8.1	282.9
AVERAGE		**12**	**0**	**17**	**6**	**322**
As/Bu	20617	6.5	0.0	20.6	4.3	312.1
As/Bu	20634	7.5	0.0	21.3	2.5	373.2
As/Bu	20635	23.4	0.0	12.6	13.1	125.6
As/Bu	20636	26.1	0.0	12.1	7.1	320.5
As/Bu	20637	30.1	0.0	8.4	10.6	279.1
As/Bu	20638	21.3	0.0	13.9	4.2	399.2
As/Bu	20639	29.6	0.0	6.8	11.4	300.4
As/Bu	20640	20.1	0.0	16.5	2.6	409.2
As/Bu	20641	16.1	0.0	16.6	5.2	345.1
As/Bu	20642	69.5	0.0	7.4	0.0	275.0
As/Bu	20643	58.2	0.0	12.9	0.0	300.5
As/Bu	20644	45.9	0.0	14.7	0.0	361.6
As/Bu	20645	65.6	0.0	10.1	0.0	316.6
As/Bu	20646	12.0	0.2	14.5	8.2	331.1
As/Bu	20649	13.1	0.0	15.5	7.9	309.3
As/Bu	20650	6.9	0.0	21.9	6.3	214.2
As/Bu	20651	26.4	0.0	14.3	3.5	357.7
As/Bu	20652	0.0	0.0	17.1	4.9	449.3
As/Bu	20653	0.0	0.0	20.0	2.4	486.6
As/Bu	20654	0.0	0.0	21.8	5.0	270.5
As/Bu	20659	0.0	0.0	15.2	10.6	329.9
As/Bu	20662	33.9	0.0	9.2	7.6	322.5
As/Bu	20663	30.8	0.0	11.6	9.0	235.9
As/Bu	20664	20.7	0.0	14.8	9.0	207.9
As/Bu	20665	33.2	0.0	9.5	10.1	206.4
As/Bu	20666	52.2	0.0	15.2	2.8	117.3
As/Bu	20668	3.4	0.0	11.2	22.7	10.2
As/Bu	20669	21.2	0.0	13.1	12.2	123.0
As/Bu	20671	31.2	0.0	15.1	10.1	42.9
As/Bu	20682	16.0	0.0	28.9	0.0	35.4
As/Bu	20683	58.9	0.0	18.3	0.0	89.3
As/Bu	20684	31.5	0.0	30.7	0.0	0.0
As/Bu	20685	100.1	0.0	7.0	0.0	155.5
As/Bu	20687	13.9	4.1	1.0	27.1	0.0
As/Bu	U82	21.1	0.0	11.6	9.3	332.7
As/Bu	U83	0.0	0.0	39.9	0.0	0.0
Average		**26**	**0**	**15**	**6**	**243**
As/Ls	20601	0.0	0.0	41.3	0.0	0.0
As/Ls	20602	2.6	0.2	31.6	2.5	0.0
As/Ls	20679	0.0	0.0	35.0	0.0	3.3
As/Ls	20680	0.0	0.0	34.4	0.0	0.0
As/Ls	20681	15.8	0.5	23.3	6.1	0.0
As/Ls	U1	0.0	29.3	0.0	4.2	0.0
As/Ls	U10	0.0	35.1	0.0	0.0	14.3
As/Ls	U11	25.2	24.0	0.0	1.5	0.3
As/Ls	U13	16.5	26.7	0.0	0.6	7.2
As/Ls	U14	27.8	23.4	0.0	0.0	2.7
As/Ls	U14A	20.3	25.2	0.0	0.0	5.6
As/Ls	U15	36.3	22.1	0.0	0.0	1.2
As/Ls	U16	23.3	24.3	0.0	0.0	3.0

TABLE B.4 Measured versus calculated values
(Factor analysis end-members)

Group	Sample	Zn				
		detrital	hydrothermal Fe	h/t FeMn	biogenic	authigenic
As/Ls	U17	51.5	19.6	0.0	0.0	0.0
As/Ls	U18	0.6	29.6	0.0	0.0	10.9
As/Ls	U19	17.4	29.6	0.0	0.0	0.0
As/Ls	U2	23.1	7.7	19.5	0.0	4.7
As/Ls	U20	24.0	21.9	4.2	0.0	18.2
As/Ls	U21	84.3	10.9	0.0	0.0	17.1
As/Ls	U25	74.3	15.6	0.0	0.0	4.4
As/Ls	U26	95.5	11.9	0.0	0.0	0.0
As/Ls	U27	36.0	13.3	0.0	10.3	14.3
As/Ls	U28	26.6	8.1	0.0	17.5	21.0
As/Ls	U29	0.0	34.0	0.0	0.0	5.0
As/Ls	U3	7.7	23.1	0.0	3.2	34.2
As/Ls	U30	20.2	21.4	0.0	4.6	7.2
As/Ls	U31	19.1	13.7	0.0	13.0	8.8
As/Ls	U32	39.3	17.9	0.0	2.3	15.5
As/Ls	U33	17.4	27.3	0.0	0.0	8.8
As/Ls	U34	87.1	13.1	0.0	0.0	0.8
As/Ls	U35	32.6	15.4	0.0	8.1	5.6
As/Ls	U36	35.0	14.0	0.0	10.3	3.6
As/Ls	U37	40.4	14.9	0.0	8.5	19.5
As/Ls	U38	8.9	30.1	0.0	0.0	15.5
As/Ls	U39	11.0	29.9	0.0	0.0	0.0
As/Ls	U4	91.3	12.0	0.0	0.0	0.0
As/Ls	U40	23.6	27.2	0.0	0.0	0.0
As/Ls	U41	101.2	11.9	0.0	0.0	0.0
As/Ls	U41A	43.1	13.0	0.0	7.8	14.4
As/Ls	U42	22.3	10.6	0.0	16.3	41.7
As/Ls	U45	27.3	10.1	0.0	17.4	13.0
As/Ls	U46	14.0	13.0	0.0	16.5	9.5
As/Ls	U47	41.7	18.1	0.0	3.2	30.4
As/Ls	U48	31.7	11.8	0.0	13.2	31.9
As/Ls	U49	3.1	21.4	0.0	11.6	0.0
As/Ls	U5	48.5	10.9	0.0	9.8	31.2
As/Ls	U50	30.3	16.9	0.0	7.3	44.3
As/Ls	U51	33.7	14.8	0.0	9.3	35.4
As/Ls	U52	19.6	11.7	0.0	14.8	54.5
As/Ls	U53	27.7	12.8	0.0	11.3	63.9
As/Ls	U54	0.0	34.7	0.0	0.0	32.8
As/Ls	U55	0.0	35.2	0.0	0.0	35.5
As/Ls	U56A	63.5	18.5	0.0	1.3	3.6
As/Ls	U56B	26.1	20.3	0.0	1.7	108.6
As/Ls	U56C	28.9	17.0	0.0	9.2	17.1
As/Ls	U57	41.9	13.6	0.0	9.1	22.4
As/Ls	U58	28.9	13.4	0.0	12.2	16.0
As/Ls	U59	52.1	14.3	0.0	4.4	7.5
As/Ls	U6	14.8	9.9	0.0	20.2	29.9
As/Ls	U60	24.3	13.4	0.0	13.6	22.7
As/Ls	U61	36.1	18.7	0.0	4.3	36.2
As/Ls	U62	36.6	13.4	0.0	10.1	41.4
As/Ls	U63	16.1	21.3	0.0	7.5	0.5
As/Ls	U64	27.7	19.1	0.0	6.3	6.4
As/Ls	U65	18.5	20.5	0.0	8.0	12.9
As/Ls	U66	34.0	12.9	0.0	11.4	21.4
As/Ls	U67	10.8	8.5	0.0	19.3	59.9
As/Ls	U68	35.0	19.0	0.0	2.8	82.2

TABLE B.4 Measured versus calculated values
(Factor analysis end-members)

Group	Sample	Zn				
		detrital	hydrothermal Fe	h/t FeMn	biogenic	authigenic
As/Ls	U69	0.9	29.0	0.0	4.4	0.0
As/Ls	U7	24.3	18.1	0.0	4.1	65.3
As/Ls	U70	32.8	18.4	0.0	5.9	29.8
As/Ls	U71	10.7	19.5	0.0	11.3	9.6
As/Ls	U72	22.2	9.3	0.0	14.0	158.0
As/Ls	U73	15.0	19.3	0.0	10.5	14.2
As/Ls	U74	26.0	15.8	0.0	2.6	318.5
As/Ls	U75	41.4	11.4	0.0	4.5	262.0
As/Ls	U76	32.6	12.1	0.0	5.8	274.1
As/Ls	U77	34.7	12.6	0.0	12.0	0.8
As/Ls	U78	2.2	30.9	0.0	1.9	0.0
As/Ls	U8	30.6	13.9	0.0	11.0	0.0
As/Ls	U9	29.0	11.4	0.0	10.1	172.8
Average		**28**	**17**	**2**	**6**	**31**
Bu/Bu	20647	33.7	12.2	0.0	5.3	273.8
Bu/Bu	20648	23.9	12.7	0.0	8.2	239.2
Bu/Bu	20660	29.0	11.4	0.0	8.4	230.1
Bu/Bu	20676	47.0	17.9	0.0	3.9	14.8
Bu/Bu	20686	43.5	8.8	0.0	5.0	277.0
Bu/Bu	20688	45.7	9.0	0.0	4.3	265.7
Bu/Bu	20689	40.0	10.0	0.0	8.2	185.1
Bu/Bu	20690	40.6	10.5	0.0	8.1	171.9
Bu/Bu	20691	45.0	5.6	0.0	11.1	192.1
Bu/Bu	20692	43.3	10.6	0.0	6.2	179.3
Bu/Bu	20693	24.3	10.3	0.0	2.5	525.7
Bu/Bu	20694	19.6	15.6	0.0	0.3	442.9
Bu/Bu	20695	24.2	18.8	0.0	1.0	213.4
Bu/Bu	20696	28.6	20.1	0.0	1.0	121.6
Bu/Bu	20697	28.8	18.2	0.0	2.4	112.4
Bu/Bu	20698	40.4	7.6	0.0	11.5	150.5
Bu/Bu	20699	51.1	7.5	0.0	6.2	256.6
Bu/Bu	20700	13.2	13.6	0.0	7.8	334.6
Bu/Bu	U22	12.3	15.9	0.0	6.6	304.2
Bu/Bu	U23	11.8	20.3	0.0	0.0	332.4
Bu/Bu	U24	21.4	27.2	0.0	0.0	5.1
Average		**32**	**14**	**0**	**5**	**230**
Ls/Ls	U43	77.0	14.1	0.0	0.0	10.4
Ls/Ls	U44	7.0	0.0	0.4	0.0	0.0
Average		**42**	**7**	**0**	**0**	**5**

Group Value %	Sample	Zn detrital	Zn hydrothermal	Zn FeMn	Zn biogenic	Zn authigenic
Average	As	3.4	90.3	4.7	1.7	0.0
Average	As/Bu	9.0	5.3	83.5	2.2	0.0
Average	As/Ls	33.4	20.5	36.5	6.9	2.8
Average	Bu	11.3	82.0	0.0	1.8	4.8
Average	Ls	13.0	77.1	0.4	0.0	9.5
Average		14.0	55.0	25.0	2.5	3.4
Standard Deviation		11.4	39.1	36.0	2.6	4.0

TABLE B.4 Measured versus calculated values
(Factor analysis end-members)

Group	Sample	Ba				
		detrital	hydrothermal Fe	h/t FeMn	biogenic	authigenic
As/As	20657	8.0	0.0	7.0	93.4	720.7
As/As	20658	197.9	0.0	4.0	202.0	565.7
AVERAGE		**103**	**0**	**5**	**148**	**643**
As/Bu	20617	55.9	0.0	6.7	106.9	624.2
As/Bu	20634	64.5	0.0	7.0	61.8	746.4
As/Bu	20635	200.3	0.0	4.1	327.2	251.1
As/Bu	20636	223.6	0.0	4.0	177.4	641.1
As/Bu	20637	258.2	0.0	2.8	264.6	558.1
As/Bu	20638	182.4	0.0	4.5	105.1	798.3
As/Bu	20639	253.7	0.0	2.2	286.0	600.8
As/Bu	20640	172.3	0.0	5.4	64.5	818.5
As/Bu	20641	137.8	0.0	5.4	128.8	690.1
As/Bu	20642	596.0	0.0	2.4	0.0	549.9
As/Bu	20643	498.5	0.0	4.2	0.0	601.0
As/Bu	20644	393.7	0.0	4.8	0.0	723.2
As/Bu	20645	561.9	0.0	3.3	0.0	633.2
As/Bu	20646	102.5	0.0	4.7	205.1	662.1
As/Bu	20649	112.6	0.0	5.1	197.9	618.5
As/Bu	20650	59.1	0.0	7.1	157.1	428.5
As/Bu	20651	225.9	0.0	4.7	88.3	715.4
As/Bu	20652	0.0	0.0	5.6	122.0	898.7
As/Bu	20653	0.0	0.0	6.5	59.8	973.2
As/Bu	20654	0.0	0.0	7.1	125.8	541.0
As/Bu	20659	0.0	0.0	5.0	264.6	659.9
As/Bu	20662	290.8	0.0	3.0	189.1	645.1
As/Bu	20663	264.2	0.0	3.8	225.3	471.8
As/Bu	20664	177.5	0.0	4.8	225.2	415.8
As/Bu	20665	284.9	0.0	3.1	253.5	412.7
As/Bu	20666	447.5	0.0	5.0	71.2	234.7
As/Bu	20668	29.5	0.0	3.7	566.6	20.5
As/Bu	20669	182.1	0.0	4.3	306.1	246.0
As/Bu	20671	267.7	0.0	4.9	253.6	85.8
As/Bu	20682	137.4	0.0	9.4	0.0	70.8
As/Bu	20683	504.9	0.0	6.0	0.0	178.5
As/Bu	20684	270.1	0.0	10.0	0.0	0.0
As/Bu	20685	857.7	0.0	2.3	0.0	311.0
As/Bu	20687	119.2	0.7	0.3	676.7	0.0
As/Bu	U82	181.0	0.0	3.8	232.6	665.5
As/Bu	U83	0.0	0.0	13.0	0.0	0.0
Average		**225**	**0**	**5**	**160**	**486**
As/Ls	20601	0.0	0.0	13.5	0.0	0.0
As/Ls	20602	22.6	0.0	10.3	63.1	0.0
As/Ls	20679	0.0	0.0	11.4	0.0	6.6
As/Ls	20680	0.0	0.0	11.2	0.0	0.0
As/Ls	20681	135.3	0.1	7.6	153.1	0.0
As/Ls	U1	0.0	5.1	0.0	105.8	0.0
As/Ls	U10	0.0	6.1	0.0	0.0	28.6
As/Ls	U11	215.9	4.2	0.0	36.9	0.6
As/Ls	U13	141.1	4.6	0.0	14.5	14.4
As/Ls	U14	238.2	4.0	0.0	0.0	5.5
As/Ls	U14A	173.9	4.4	0.0	0.0	11.2
As/Ls	U15	311.1	3.8	0.0	0.0	2.4
As/Ls	U16	199.9	4.2	0.0	0.0	6.0

TABLE B.4 Measured versus calculated values
(Factor analysis end-members)

Group	Sample	Ba				
		detrital	hydrothermal Fe	h/t FeMn	biogenic	authigenic
As/Ls	U69	7.3	5.0	0.0	109.8	0.0
As/Ls	U7	208.1	3.1	0.0	103.0	130.7
As/Ls	U70	281.5	3.2	0.0	148.4	59.5
As/Ls	U71	91.5	3.4	0.0	282.0	19.1
As/Ls	U72	190.3	1.6	0.0	350.1	316.1
As/Ls	U73	128.3	3.3	0.0	261.3	28.3
As/Ls	U74	222.7	2.7	0.0	65.2	636.9
As/Ls	U75	354.5	2.0	0.0	111.8	524.0
As/Ls	U76	279.6	2.1	0.0	144.2	548.2
As/Ls	U77	297.8	2.2	0.0	299.0	1.6
As/Ls	U78	18.5	5.3	0.0	48.1	0.0
As/Ls	U8	262.1	2.4	0.0	276.0	0.0
As/Ls	U9	248.4	2.0	0.0	251.8	345.6
Average		**241**	**3**	**1**	**145**	**61**
Bu/Bu	20647	289.1	2.1	0.0	133.6	547.7
Bu/Bu	20648	204.8	2.2	0.0	204.9	478.5
Bu/Bu	20660	248.1	2.0	0.0	210.3	460.2
Bu/Bu	20676	403.1	3.1	0.0	97.7	29.7
Bu/Bu	20686	372.7	1.5	0.0	124.5	554.0
Bu/Bu	20688	391.4	1.6	0.0	108.2	531.4
Bu/Bu	20689	1028.1	5.2	0.0	616.6	1110.7
Bu/Bu	20690	348.4	1.8	0.0	203.0	343.8
Bu/Bu	20691	851.5	2.2	0.0	614.8	848.9
Bu/Bu	20692	371.2	1.8	0.0	154.6	358.7
Bu/Bu	20693	207.9	1.8	0.0	61.3	1051.5
Bu/Bu	20694	167.7	2.7	0.0	7.7	885.8
Bu/Bu	20695	740.1	11.6	0.0	93.0	1521.2
Bu/Bu	20696	245.0	3.5	0.0	25.0	243.1
Bu/Bu	20697	247.1	3.2	0.0	61.0	224.8
Bu/Bu	20698	1308.1	5.0	0.0	1089.0	1137.9
Bu/Bu	20699	438.1	1.3	0.0	154.5	513.1
Bu/Bu	20700	113.3	2.3	0.0	195.4	669.1
Bu/Bu	U22	105.6	2.7	0.0	164.3	608.3
Bu/Bu	U23	100.8	3.5	0.0	0.0	664.7
Bu/Bu	U24	183.7	4.7	0.0	0.0	10.2
Average		**398**	**3**	**0**	**206**	**609**
Ls/Ls	U43	660.2	2.4	0.0	0.0	20.7
Ls/Ls	U44	22.9	0.0	0.1	0.0	0.0
Average		**342**	**1**	**0**	**0**	**10**

Group Value %	Sample	Ba detrital	Ba hydrothermal	Ba FeMn	Ba biogenic	Ba authigenic
Average	As	11.4	71.5	0.6	16.4	0.0
Average	As/Bu	25.7	0.6	55.5	18.2	0.0
Average	As/Ls	33.4	30.7	0.2	32.2	13.6
Average	Bu	32.8	50.1	0.0	16.9	0.3
Average	Ls	36.7	60.3	0.0	0.0	2.9
Average		28.0	42.6	11.3	16.7	3.4
Standard Deviation		10.1	27.9	24.7	11.4	5.9

TABLE B.4 Measured versus calculated values
(Factor analysis end-members)

Group	Sample	Ba				
		detrital	hydrothermal Fe	h/t FeMn	biogenic	authigenic
As/Ls	U17	441.6	3.4	0.0	0.0	0.0
As/Ls	U18	4.8	5.1	0.0	0.0	21.7
As/Ls	U19	149.5	5.1	0.0	0.0	0.0
As/Ls	U2	198.1	1.3	6.4	0.0	9.4
As/Ls	U20	206.0	3.8	1.4	0.0	36.4
As/Ls	U21	722.6	1.9	0.0	0.0	34.1
As/Ls	U25	636.4	2.7	0.0	0.0	8.9
As/Ls	U26	818.7	2.1	0.0	0.0	0.0
As/Ls	U27	308.8	2.3	0.0	258.7	28.6
As/Ls	U28	228.4	1.4	0.0	438.6	42.0
As/Ls	U29	0.0	5.9	0.0	0.0	10.0
As/Ls	U3	66.3	4.0	0.0	79.7	68.4
As/Ls	U30	173.0	3.7	0.0	113.8	14.4
As/Ls	U31	163.9	2.4	0.0	324.7	17.6
As/Ls	U32	336.5	3.1	0.0	57.3	31.0
As/Ls	U33	149.3	4.7	0.0	0.0	17.7
As/Ls	U34	746.4	2.3	0.0	0.0	1.7
As/Ls	U35	279.1	2.7	0.0	203.4	11.2
As/Ls	U36	300.2	2.4	0.0	258.3	7.3
As/Ls	U37	346.2	2.6	0.0	212.3	39.1
As/Ls	U38	76.4	5.2	0.0	0.0	30.9
As/Ls	U39	94.5	5.2	0.0	0.0	0.0
As/Ls	U4	782.5	2.1	0.0	0.0	0.0
As/Ls	U40	202.6	4.7	0.0	0.0	0.0
As/Ls	U41	867.5	2.1	0.0	0.0	0.0
As/Ls	U41A	369.2	2.2	0.0	194.7	28.8
As/Ls	U42	191.2	1.8	0.0	408.7	83.4
As/Ls	U45	234.3	1.7	0.0	434.3	26.0
As/Ls	U46	120.0	2.3	0.0	412.1	18.9
As/Ls	U47	357.3	3.1	0.0	79.2	60.7
As/Ls	U48	271.7	2.0	0.0	329.6	63.8
As/Ls	U49	26.8	3.7	0.0	290.9	0.0
As/Ls	U5	415.9	1.9	0.0	245.4	62.5
As/Ls	U50	259.3	2.9	0.0	182.6	88.7
As/Ls	U51	289.2	2.6	0.0	232.1	70.9
As/Ls	U52	167.9	2.0	0.0	368.9	108.9
As/Ls	U53	237.5	2.2	0.0	281.5	127.8
As/Ls	U54	0.0	6.0	0.0	0.0	65.6
As/Ls	U55	0.0	6.1	0.0	0.0	71.0
As/Ls	U56A	544.7	3.2	0.0	32.9	7.1
As/Ls	U56B	223.3	3.5	0.0	42.3	217.1
As/Ls	U56C	247.7	2.9	0.0	230.5	34.3
As/Ls	U57	359.3	2.4	0.0	228.7	44.8
As/Ls	U58	248.0	2.3	0.0	304.3	32.0
As/Ls	U59	446.6	2.5	0.0	110.2	15.0
As/Ls	U6	127.2	1.7	0.0	504.0	59.8
As/Ls	U60	208.7	2.3	0.0	340.5	45.4
As/Ls	U61	309.1	3.2	0.0	108.3	72.4
As/Ls	U62	313.4	2.3	0.0	253.1	82.8
As/Ls	U63	138.1	3.7	0.0	187.7	1.0
As/Ls	U64	237.6	3.3	0.0	157.1	12.7
As/Ls	U65	158.3	3.6	0.0	200.6	25.7
As/Ls	U66	291.6	2.2	0.0	285.1	42.7
As/Ls	U67	92.6	1.5	0.0	483.1	119.8
As/Ls	U68	300.4	3.3	0.0	71.1	164.4

TABLE B.5 Linear programming and factor analysis reults

		Linear Prog (Modified Dymond, 1981)					Factor Analysis							Linear Prog (Factor Analysis end-members)				
Sample	Horizon	detrital %	h/t Fe %	h/t FeMn %	bioge-nic %	auth-igenic %	carb-onate %	detrital %	h/t Fe %	h/t FeMn %	bioge-nic %	auth-igenic %	carb-onate %	Hydroth-ermal Fe oxide %	Hydroth-ermal Mn Oxide %	Silic-eous %	Detr-itus %	Bioge-nic Carbo-nate %
20655	As	0.5	0.0	82.3	10.3	0.9	6.0											
20656	As	4.2	0.0	84.0	4.9	2.3	4.6											
20657	As	0.6	0.0	81.9	9.4	2.6	5.5											
20658	As	16.3	0.0	53.2	23.3	2.3	4.9											
20617	As/Bu	4.0	0.0	78.3	10.7	2.3	4.7	7.0	21.9	44.9	10.5	0.1	15.6	20.5	50.6	1.0	3.6	24.4
20634	As/Bu	4.7	0.0	81.9	6.3	2.7	4.4	8.3	25.3	47.5	10.4	0.1	8.4	23.5	55.7	1.5	2.1	17.2
20635	As/Bu	14.3	0.0	47.8	32.8	0.9	4.2	9.5	21.3	34.4	25.0	0.1	9.8	17.8	46.9	9.1	5.3	20.9
20636	As/Bu	18.7	0.0	53.8	20.8	2.7	3.9	11.9	19.0	45.9	16.2	0.1	7.0	20.2	62.4	5.7	9.0	2.6
20637	As/Bu	22.5	0.0	39.0	32.3	2.5	3.7	14.6	18.2	34.1	23.2	0.1	9.7	14.1	47.1	6.3	11.3	21.2
20638	As/Bu	15.9	0.0	64.2	12.9	3.5	3.5	10.1	19.4	50.5	11.9	0.1	8.1	19.5	59.5	2.0	5.7	13.3
20639	As/Bu	23.5	0.0	33.4	37.1	2.8	3.2	14.1	16.4	35.2	23.6	0.1	10.6	13.2	48.4	6.8	10.8	20.9
20640	As/Bu	14.2	0.0	72.0	7.4	3.4	3.0	10.0	21.0	49.9	10.7	0.1	8.3	22.5	61.2	1.3	4.8	10.2
20641	As/Bu	10.9	0.0	69.4	14.2	2.7	2.7	9.5	21.7	45.5	13.0	0.1	10.1	20.7	54.9	3.0	6.4	14.9
20642	As/Bu	63.0	0.0	32.3	0.0	2.3	2.5	17.1	17.4	37.6	15.9	0.1	11.9	13.8	55.0	4.0	8.1	19.1
20643	As/Bu	27.8	0.0	67.0	0.0	3.0	2.2	12.7	19.8	40.8	14.3	0.1	12.3	15.4	48.7	4.0	11.4	20.5
20644	As/Bu	18.8	0.0	75.7	0.0	3.6	2.0	8.2	21.3	48.1	13.1	0.1	9.3	14.9	61.3	3.2	1.0	19.6
20645	As/Bu	29.3	0.0	65.1	0.0	3.9	1.7	13.4	17.9	44.2	15.5	0.1	8.8	16.7	54.4	4.8	3.2	20.9
20646	As/Bu	8.5	0.4	63.2	23.7	2.8	1.5	8.2	20.1	45.0	15.0	0.1	11.6	21.4	58.2	2.9	4.0	13.6
20649	As/Bu	9.0	0.0	65.3	22.0	2.5	1.2	9.2	22.0	44.8	16.0	0.1	8.0	15.4	52.3	5.7	5.4	21.2
20650	As/Bu	4.0	0.0	77.5	14.7	2.9	0.9	8.0	25.4	44.6	14.3	0.1	7.6	31.9	50.6	3.0	3.3	11.3
20651	As/Bu	19.6	0.0	65.9	10.7	3.1	0.7	11.9	20.7	48.2	12.8	0.1	6.3	17.4	54.8	2.4	8.4	17.1
20652	As/Bu	0.0	0.0	80.4	15.2	4.0	0.4	5.7	21.5	55.3	10.1	0.1	7.2	15.2	61.9	1.4	0.7	20.8
20653	As/Bu	0.0	0.0	88.7	7.0	4.1	0.2	6.0	22.6	55.2	8.2	0.1	7.8	18.1	67.8	0.4	2.4	11.2
20654	As/Bu	0.0	0.0	85.0	13.0	2.0	0.0	6.1	24.4	49.2	11.6	0.1	8.6	22.5	59.9	2.3	0.3	15.0
20659	As/Bu	0.0	0.0	66.6	30.6	2.8	0.0	8.8	21.0	47.0	16.2	0.1	7.0	18.2	54.0	4.6	3.8	19.4
20662	As/Bu	27.0	0.0	45.3	24.6	3.0	0.1	14.8	18.2	38.1	18.9	0.1	9.9	18.7	47.1	6.0	12.0	16.2
20663	As/Bu	21.6	0.0	50.5	25.8	1.9	0.1	13.4	18.6	36.0	19.5	0.1	12.5	16.0	45.6	9.0	7.6	21.8
20664	As/Bu	13.7	0.0	60.3	24.3	1.6	0.1	9.4	22.8	38.7	20.3	0.1	8.7	18.3	47.5	6.0	8.6	19.7
20665	As/Bu	24.4	0.0	43.2	30.4	1.8	0.1	14.7	17.5	34.8	22.3	0.1	10.6	15.7	48.3	6.7	11.6	17.8
20666	As/Bu	32.3	0.0	58.1	7.2	2.2	0.2	16.0	21.6	36.5	17.6	0.1	8.3	20.0	46.8	5.7	12.2	15.3
20668	As/Bu	2.1	0.0	41.6	55.4	0.7	0.2	5.6	17.5	25.7	37.5	0.0	13.7	10.4	41.7	17.2	0.7	30.1
20669	As/Bu	13.6	0.0	51.9	32.1	2.1	0.2	9.8	22.9	35.3	19.2	0.1	12.6	24.6	41.4	4.4	4.5	25.1
20671	As/Bu	18.4	0.0	55.2	24.4	1.7	0.2	9.5	22.1	32.4	24.3	0.1	11.6	17.0	48.5	10.3	3.5	20.8
20682	As/Bu	8.1	0.0	89.6	0.0	2.1	0.3	5.4	33.3	42.2	12.5	0.1	6.6	34.2	49.0	3.2	2.3	11.4
20683	As/Bu	18.5	0.0	78.3	0.0	3.0	0.3	10.0	26.8	35.9	19.2	0.1	8.0	28.3	42.1	7.4	6.3	16.5
20684	As/Bu	4.5	0.0	95.2	0.0	0.0	0.3	5.6	36.0	35.3	16.9	0.1	6.1	31.6	48.3	4.9	1.0	14.2
20685	As/Bu	51.1	0.0	46.6	0.0	2.0	0.4	23.7	16.6	30.8	23.3	0.1	5.6	14.5	51.6	14.6	12.6	6.7
20687	As/Bu	7.3	10.8	4.3	77.2	0.0	0.4	6.1	14.5	0.4	67.9	0.0	11.0	11.0	0.5	43.6	1.6	43.2
U82	As/Bu	15.8	0.0	53.8	28.5	1.5	0.4	11.6	20.4	44.1	19.2	0.1	4.6	17.0	47.5	5.8	8.9	20.9
U83	As/Bu	0.0	0.0	99.6	0.0	0.0	0.4	2.9	40.2	38.2	10.8	0.0	7.9	47.4	42.1	1.4	1.7	8.2
20601	As/Ls	0.0	0.0	99.5	0.0	0.0	0.5	1.4	60.1	0.2	32.7	0.0	5.5	81.5	0.2	11.2	0.1	7.4
20602	As/Ls	1.3	0.4	93.0	4.9	0.0	0.5	11.3	54.7	8.3	21.9	0.2	3.6	67.9	8.6	6.7	6.1	12.7
20679	As/Ls	0.0	0.0	99.3	0.0	0.2	0.5	21.9	44.2	2.4	24.1	0.2	7.3	57.2	1.9	6.9	13.0	21.0
20680	As/Ls	0.0	0.0	99.5	0.0	0.0	0.5	23.8	42.4	2.1	25.8	0.3	5.6	54.4	4.4	10.4	16.0	14.8
20681	As/Ls	11.2	1.0	74.3	12.9	0.0	0.6	25.5	29.1	1.1	36.1	0.2	8.0	36.8	1.3	20.2	17.3	24.5
U1	As/Ls	0.0	86.0	0.0	13.4	0.0	0.6	3.5	45.7	0.3	43.9	0.0	6.5	70.5	0.8	18.7	0.5	9.5
U10	As/Ls	0.0	99.1	0.0	0.0	0.3	0.6	4.3	58.6	0.4	31.5	0.1	5.2	80.0	0.1	11.0	0.6	8.6
U11	As/Ls	20.5	73.9	0.0	4.9	0.1	0.6	11.9	67.7	0.8	13.6	0.1	5.9	84.8	0.6	1.3	3.7	9.6
U13	As/Ls	13.4	82.1	0.0	1.9	2.0	0.7	13.2	40.9	2.3	37.1	0.2	6.3	50.5	3.3	19.5	11.2	15.5
U14	As/Ls	23.5	74.9	0.0	0.0	0.8	0.7	24.1	34.5	0.8	34.0	0.2	6.5	42.6	1.1	19.4	14.7	23.2
U14A	As/Ls	24.4	74.3	0.0	0.0	0.5	0.7	24.2	36.6	1.0	32.4	0.2	5.6	58.9	1.6	12.4	17.2	9.9
U15	As/Ls	29.9	69.0	0.0	0.0	0.3	0.7	22.6	33.3	1.0	36.9	0.1	6.1	59.2	2.1	16.9	14.6	7.2
U16	As/Ls	19.8	78.3	0.0	0.0	1.1	0.8	22.0	36.7	0.9	34.4	0.2	5.8	46.6	1.6	14.9	14.8	22.1
U17	As/Ls	33.9	65.4	0.0	0.0	0.0	0.8	20.0	31.0	1.0	42.2	0.1	5.7	41.1	0.6	25.5	14.8	18.0
U18	As/Ls	2.3	93.8	0.0	0.0	3.0	0.8	23.0	41.6	1.5	28.2	0.2	5.5	50.4	2.6	10.1	16.6	20.4
U19	As/Ls	5.9	93.2	0.0	0.0	0.0	0.8	3.8	46.5	0.4	41.5	0.0	7.8	77.5	1.3	15.9	0.3	5.1
U2	As/Ls	13.2	16.7	68.9	0.0	0.3	0.9	18.4	48.6	3.4	23.6	0.2	5.8	72.9	3.9	6.3	10.8	6.1
U20	As/Ls	17.7	60.9	19.0	0.0	1.6	0.9	11.0	31.8	22.4	29.5	0.1	5.1	51.1	27.3	10.0	5.8	5.7
U21	As/Ls	55.1	41.9	0.0	0.0	2.0	0.9	26.4	18.7	5.1	41.8	0.2	7.8	19.6	7.7	23.3	20.6	28.9
U25	As/Ls	36.1	62.4	0.0	0.0	0.6	0.9	18.6	24.8	3.4	45.3	0.1	7.8	32.6	6.7	23.5	17.4	19.7
U26	As/Ls	31.1	67.9	0.0	0.0	0.0	1.0	15.3	21.7	3.4	53.5	0.1	6.0	31.2	6.1	28.7	15.8	18.1
U27	As/Ls	27.4	38.3	0.0	32.1	1.3	1.0	20.9	20.0	3.2	48.8	0.1	7.0	30.5	6.2	30.3	24.1	8.9
U28	As/Ls	20.1	23.0	0.0	54.0	1.9	1.0	16.1	13.1	4.9	58.1	0.2	7.6	12.8	7.3	42.0	13.8	24.1
U29	As/Ls	0.0	98.5	0.0	0.0	0.5	1.1	4.8	51.8	0.5	33.5	0.1	9.3	73.6	0.5	12.5	0.1	14.0
U3	As/Ls	23.2	63.4	0.0	9.4	2.9	1.1	8.8	56.3	6.2	23.8	0.2	4.7	85.9	0.6	7.2	4.2	2.1
U30	As/Ls	16.3	65.4	0.0	15.0	2.2	1.1	14.6	32.6	2.2	41.8	0.2	8.7	44.2	3.9	20.8	9.0	23.1
U31	As/Ls	14.9	40.4	0.0	41.4	2.1	1.1	13.7	22.2	2.5	55.5	0.2	5.9	28.1	3.5	33.8	13.0	22.6
U32	As/Ls	32.8	56.7	0.0	7.8	1.5	1.2	24.5	28.0	4.1	39.3	0.2	4.0	37.4	2.0	30.0	16.7	13.9
U33	As/Ls	13.7	81.2	0.0	0.0	3.9	1.2	15.7	40.4	2.4	35.2	0.3	5.9	50.2	3.5	16.3	10.5	19.5
U34	As/Ls	36.7	61.8	0.0	0.0	0.3	1.2	16.5	22.9	3.5	50.8	0.2	6.1	32.3	3.0	36.1	14.7	13.8
U35	As/Ls	25.6	45.8	0.0	26.1	1.2	1.2	20.4	23.9	1.8	47.8	0.2	5.9	22.3	2.8	34.2	14.2	26.5
U36	As/Ls	26.4	40.0	0.0	31.8	0.6	1.3	21.0	21.4	1.3	50.7	0.1	5.4	32.5	2.8	34.0	16.1	14.6
U37	As/Ls	29.8	41.7	0.0	25.6	1.7	1.3	22.2	21.4	4.3	45.6	0.1	6.2	32.0	8.5	26.8	22.3	10.4
U38	As/Ls	12.6	84.7	0.0	0.0	1.4	1.3	17.4	41.0	3.1	31.6	0.2	6.7	61.6	4.2	13.4	10.9	9.9
U39	As/Ls	8.7	89.9	0.0	0.0	0.0	1.3	8.8	45.9	0.4	37.6	0.0	7.3	66.1	0.7	16.9	5.0	11.4
U4	As/Ls	41.7	56.9	0.0	0.0	0.0	1.4	14.1	54.5	5.9	21.5	0.2	3.7	67.2	8.1	5.5	9.3	9.9
U40	As/Ls	18.5	80.7	0.0	0.0	0.0	0.8	19.2	37.1	2.8	34.2	0.2	6.4	54.2	3.5	13.6	11.4	17.3
U41	As/Ls	34.7	64.2	0.0	0.0	0.0	1.1	12.5	22.0	1.8	56.7	0.1	7.0	28.4	5.3	28.1	12.9	26.1
U41A	As/Ls	33.9	38.7	0.0	25.0	1.3	1.1	24.4	20.0	3.6	45.7	0.2	6.1	22.7	6.6	30.2	18.9	21.5
U42	As/Ls	16.6	29.9	0.0	49.8	3.7	0.0	13.9	16.2	9.1	54.9	0.2	5.6	17.2	13.9	37.4	13.6	18.0

TABLE B.5 Linear programming and factor analysis reults

Appendix B

Sample	Horizon	Linear Prog (Modified Dymond, 1981)					Factor Analysis							Linear Prog (Factor Analysis end-members)				
		detrital %	h/t Fe %	h/t FeMn %	bioge-nic %	auth-igenic %	carb-onate %	detrital %	h/t Fe %	h/t FeMn %	bioge-nic %	auth-igenic %	carb-onate %	Hydroth-ermal Fe oxide %	Hydroth-ermal Mn Oxide %	Silic-eous %	Detr-itus %	Bioge-nic Carbo-nate %
U45	As/Ls	19.2	26.9	0.0	49.9	1.1	3.0	16.1	15.2	3.1	57.9	0.1	7.7	13.3	4.8	38.5	12.9	30.5
U46	As/Ls	10.5	36.8	0.0	50.3	0.8	1.6	10.3	20.2	2.5	59.5	0.1	7.4	24.4	4.4	35.8	9.8	25.7
U47	As/Ls	32.2	53.1	0.0	10.0	2.8	2.0	23.2	25.6	6.6	38.0	0.2	6.4	29.9	8.9	20.4	17.1	23.7
U48	As/Ls	23.3	32.8	0.0	39.6	2.8	1.6	18.1	17.5	6.9	50.5	0.2	6.9	23.0	9.8	34.6	14.2	18.5
U49	As/Ls	2.4	60.7	0.0	35.7	0.0	1.3	4.9	32.9	0.4	54.4	0.0	7.3	60.6	0.2	22.6	1.0	15.7
U5	As/Ls	36.6	31.2	0.0	30.2	1.8	0.1	5.9	68.8	8.3	12.1	0.2	4.7	86.5	0.9	0.9	1.0	10.7
U50	As/Ls	23.2	48.9	0.0	22.8	2.4	2.7	10.7	25.8	10.0	45.4	0.2	7.9	29.6	16.7	22.5	4.4	27.4
U51	As/Ls	25.0	41.6	0.0	28.1	3.1	2.1	19.1	21.2	7.5	45.1	0.2	6.9	25.5	13.2	24.1	20.6	16.5
U52	As/Ls	15.2	34.5	0.0	46.9	1.9	1.4	12.6	17.7	11.7	51.3	0.1	6.6	21.4	31.8	28.8	11.9	6.0
U53	As/Ls	20.3	35.6	0.0	33.6	3.1	7.4	14.5	16.8	11.7	46.7	0.2	10.2	13.3	16.5	29.6	13.4	27.3
U54	As/Ls	0.0	94.4	0.0	0.0	2.8	2.8	15.3	51.1	3.0	22.9	0.2	7.6	66.5	3.7	6.9	8.3	17.1
U55	As/Ls	0.0	94.7	0.0	0.0	3.0	2.4	15.0	51.1	3.4	22.7	0.2	7.6	66.4	3.0	5.8	8.4	19.0
U56A	As/Ls	23.5	68.5	0.0	5.3	0.4	2.3	14.4	33.8	3.8	38.5	0.2	9.2	44.4	5.0	19.4	12.0	19.7
U56B	As/Ls	22.7	67.1	0.0	6.0	1.1	3.1	6.7	29.6	22.6	32.9	0.1	8.0	40.4	29.5	13.7	2.1	14.3
U56C	As/Ls	18.4	41.1	0.0	24.0	1.3	15.2	15.0	20.9	3.5	40.3	0.1	20.2	23.1	4.7	18.4	9.7	44.2
U57	As/Ls	31.1	38.2	0.0	27.7	1.2	1.9	11.7	22.4	5.5	52.4	0.1	7.8	23.5	11.2	37.5	5.7	22.1
U58	As/Ls	21.8	38.1	0.0	37.4	1.4	1.3	17.5	20.0	3.6	51.1	0.1	7.6	30.9	7.7	30.9	19.7	10.7
U59	As/Ls	40.0	41.4	0.0	13.8	0.7	4.1	27.7	20.8	2.1	40.4	0.1	8.8	23.5	2.2	25.5	16.5	32.3
U6	As/Ls	10.8	27.4	0.0	59.9	1.3	0.7	10.5	49.2	7.1	26.3	0.1	6.8	67.6	12.1	10.9	2.0	7.4
U60	As/Ls	18.0	37.6	0.0	41.0	2.0	1.5	15.1	20.0	5.2	52.7	0.2	6.7	25.6	8.2	35.2	17.2	13.8
U61	As/Ls	28.0	54.9	0.0	13.7	3.3	0.0	20.8	26.4	7.8	39.4	0.2	5.4	47.6	7.4	17.8	15.6	11.6
U62	As/Ls	27.0	37.5	0.0	30.5	2.4	2.5	19.9	19.1	8.4	45.3	0.2	7.1	26.4	14.2	24.1	20.6	14.7
U63	As/Ls	12.4	62.3	0.0	23.7	0.2	1.5	12.2	32.2	0.6	47.3	0.1	7.5	43.6	1.7	27.7	8.6	19.3
U64	As/Ls	21.6	56.5	0.0	20.0	2.0	0.0	18.1	28.9	2.0	45.3	0.2	5.6	35.4	2.4	30.4	12.6	19.2
U65	As/Ls	14.2	59.6	0.0	25.1	1.2	0.0	13.1	30.3	3.3	47.0	0.2	6.0	39.8	3.7	29.5	12.4	14.6
U66	As/Ls	25.8	37.0	0.0	35.3	1.9	0.0	19.9	19.4	4.9	50.0	0.2	5.6	25.9	6.5	29.8	18.3	19.5
U67	As/Ls	8.2	24.2	0.0	59.8	3.5	4.3	7.9	13.3	13.2	56.2	0.2	9.1	14.2	18.5	33.4	5.0	28.9
U68	As/Ls	28.2	57.9	0.0	9.3	2.5	2.0	19.0	25.1	15.5	33.4	0.2	6.8	29.5	22.6	15.4	14.5	18.1
U69	As/Ls	0.6	81.5	0.0	13.3	0.0	4.6	4.2	42.6	0.3	41.8	0.0	11.2	67.4	0.3	13.9	0.9	17.5
U7	As/Ls	21.2	59.7	0.0	14.7	4.3	0.2	16.1	27.3	15.5	36.9	0.3	4.1	37.9	22.8	19.6	13.2	6.6
U70	As/Ls	25.0	52.9	0.0	18.4	2.7	1.1	19.3	25.9	6.5	41.7	0.2	6.4	38.3	7.4	20.0	14.6	19.7
U71	As/Ls	7.8	54.0	0.0	33.7	0.8	3.7	8.7	28.4	2.4	50.6	0.2	9.7	34.3	3.8	28.0	4.7	29.3
U72	As/Ls	19.0	30.3	0.0	49.0	1.6	0.1	12.4	13.7	27.9	40.9	0.1	5.0	13.9	37.5	29.2	10.1	9.3
U73	As/Ls	9.9	48.2	0.0	28.2	1.1	12.7	9.8	25.0	3.1	44.1	0.1	17.8	38.5	4.1	21.3	2.4	33.8
U74	As/Ls	25.1	58.0	0.0	10.3	3.6	2.9	12.2	18.0	43.0	21.2	0.2	5.3	17.8	58.1	9.2	9.5	5.4
U75	As/Ls	37.1	38.6	0.0	16.4	2.8	5.2	17.1	14.5	36.2	25.0	0.2	6.9	13.6	53.9	11.8	18.1	2.6
U76	As/Ls	29.5	41.4	0.0	21.3	2.9	5.0	14.4	15.0	38.1	25.4	0.2	6.9	13.4	55.3	12.6	7.2	11.6
U77	As/Ls	25.2	34.6	0.0	35.4	0.1	4.7	19.9	18.6	0.6	50.8	0.1	10.0	20.9	1.7	32.1	18.6	26.6
U78	As/Ls	1.7	92.1	0.0	6.2	0.0	0.0	5.4	47.7	0.4	40.3	0.0	6.3	76.7	0.2	17.3	1.4	4.2
U8	As/Ls	23.8	41.0	0.0	35.1	0.0	0.1	19.1	21.5	2.3	51.9	0.1	5.0	30.9	4.6	35.0	14.5	15.1
U9	As/Ls	25.1	37.3	0.0	35.7	1.8	0.1	15.0	15.9	29.3	36.1	0.2	3.6	16.7	41.7	21.1	8.3	12.3
20647	Bu	30.8	42.1	0.0	19.9	2.9	4.2	9.4	18.2	42.8	21.5	0.1	8.0	16.9	55.1	8.6	6.3	13.1
20648	Bu	20.9	42.2	0.0	29.3	2.5	5.1	7.5	18.8	39.5	24.4	0.1	9.6	17.2	48.7	13.8	2.8	17.4
20660	Bu	25.0	37.4	0.0	29.7	2.3	5.6	8.7	17.6	38.3	25.2	0.1	10.0	14.4	48.8	12.9	7.6	16.4
20676	Bu	33.4	48.0	0.0	11.3	1.2	6.1	14.1	31.1	4.1	36.1	0.1	14.6	27.8	5.0	14.6	11.1	41.5
20686	Bu	42.2	32.5	0.0	19.7	3.2	2.4	15.2	14.9	42.4	20.9	0.1	6.6	15.1	58.5	8.0	10.9	7.5
20688	Bu	40.2	30.1	0.0	15.6	2.8	11.3	14.2	14.1	38.2	19.3	0.1	14.1	13.0	46.1	6.5	10.1	24.3
20689	Bu	30.9	29.3	0.0	25.9	1.7	12.2	10.9	15.8	30.5	26.1	0.1	16.7	13.7	40.6	9.8	8.0	27.9
20690	Bu	34.2	33.6	0.0	27.9	1.7	2.6	12.3	18.1	31.7	29.5	0.1	8.4	16.7	47.8	14.2	8.2	13.1
20691	Bu	39.3	18.7	0.0	39.7	2.0	0.3	13.3	12.6	35.4	31.9	0.1	6.6	13.3	52.6	11.7	7.8	14.5
20692	Bu	37.4	34.7	0.0	21.8	1.8	4.3	12.8	18.1	32.5	26.9	0.1	9.6	17.4	46.9	11.8	8.1	15.7
20693	Bu	29.5	47.4	0.0	12.2	7.5	3.3	9.8	13.9	59.0	11.6	0.2	5.5	11.4	69.2	3.0	8.6	7.8
20694	Bu	21.7	65.7	0.0	1.4	5.8	5.4	7.8	18.5	54.3	11.8	0.2	7.4	17.0	65.6	2.8	3.4	11.2
20695	Bu	22.5	66.3	0.0	4.0	2.3	4.9	8.0	26.2	36.7	19.3	0.1	9.7	37.6	41.8	6.2	3.6	10.8
20696	Bu	25.1	67.1	0.0	3.6	4.2	0.0	10.6	32.2	25.7	24.9	0.1	6.5	38.7	36.6	8.3	5.2	11.2
20697	Bu	24.5	58.7	0.0	8.5	3.1	5.2	10.2	28.7	23.2	25.4	0.1	12.4	31.6	37.6	10.5	8.7	11.5
20698	Bu	32.8	23.6	0.0	38.3	1.4	3.9	12.5	14.7	28.9	33.7	0.1	10.0	15.2	43.3	16.4	10.0	15.1
20699	Bu	33.9	31.5	0.0	27.8	3.3	3.5	13.3	14.1	40.8	24.0	0.1	7.7	14.0	56.8	9.4	10.7	9.1
20700	Bu	12.3	47.9	0.0	29.8	3.7	6.3	4.8	18.1	48.2	19.6	0.1	9.2	17.4	58.1	9.0	2.4	13.2
U22	Bu	11.6	56.7	0.0	25.3	3.4	3.0	4.9	21.1	46.5	20.3	0.1	7.1	18.7	59.1	9.4	0.8	12.0
U23	Bu	12.3	80.6	0.0	0.0	4.1	3.0	6.5	24.8	48.1	13.7	0.1	6.8	24.8	63.3	4.9	3.4	3.6
U24	Bu	16.4	78.9	0.0	0.0	0.5	4.2	7.9	46.2	1.9	30.1	0.2	13.7	60.0	4.1	12.4	4.7	18.8

TABLE B.6 Partition Analysis data:
Major and Trace Elements

Sample	20635	20639	20641	20643	20653	20654	20668	20669	U82	20662
Sample Location	Khabiyat (main horizon)	Khabiyat (main horizon)	Khabiyat (main horizon)	Khabiyat (main horizon)	Wadi Suq	Wadi Suq	Khabiyat (Sthn hoizon)	Khabiyat (Sthn hoizon)	Aarja Mine	Plant Site
Horizon	As/Bu	As/Bu	As/Bu	As/Bu	As/Bu	As/Bu	As/Bu	As/Bu	As/Bu	As/Bu
Colour	dusky brown	dusky brown	greyish red	pale red	greyish brown	moderate brown	greyish red	moderate reddish brown	moderate brown	greyish brown
Colour Code	5 YR 2/2	5 YR 2/2	10 R 4/2	5 R 6/2	5 YR 3/2	5 YR 3/4	5 R 4/2	10 R 4/6	5 YR 4/4	5 YR 3/2
Mn AA	0.31	0.43	0.41	0.19	0.54	0.33	0.14	0.02	0.00	0.12
Mn ARA	6.85	6.83	7.84	4.42	9.76	9.47	1.79	0.20	0.03	3.99
Mn HCl	7.63	8.54	8.05	6.15	7.59	9.31	2.94	0.31	0.02	3.75
Mn Res	0.31	0.28	0.21	0.29	0.18	0.49	0.05	0.01	0.00	0.12
Mn	**15.10**	**16.07**	**16.50**	**11.05**	**18.08**	**19.60**	**4.92**	**0.54**	**0.05**	**7.98**
Fe AA	0.00	0.00	0.00	0.00	0.00	0.00	0.00	0.00	0.00	0.00
Fe ARA	0.71	3.34	2.19	0.85	1.16	2.62	2.59	1.98	0.90	0.89
Fe HCl	32.30	26.76	31.79	20.83	33.18	36.63	25.27	14.75	8.08	14.81
Fe Res	0.00	0.00	0.00	0.00	0.00	0.00	0.32	0.00	0.00	0.00
Fe	**33.01**	**30.10**	**33.98**	**21.68**	**34.34**	**39.25**	**28.19**	**16.72**	**8.98**	**15.70**
Al AA	0.15	0.56	0.19	0.38	0.32	0.40	0.12	0.19	0.03	0.19
Al ARA	0.68	0.67	0.64	1.88	0.48	0.60	1.58	0.27	0.14	0.31
Al HCl	1.21	1.28	1.59	4.52	0.82	0.95	2.91	0.52	0.39	0.54
Al Res	2.61	3.18	3.44	7.34	1.68	1.79	4.61	0.97	0.82	0.76
Al	**4.64**	**5.68**	**5.86**	**14.12**	**3.30**	**3.74**	**9.21**	**1.95**	**1.38**	**1.80**
Ca AA	4.53	5.10	5.26	6.36	6.00	5.12	6.22	4.81	3.77	7.37
Ca ARA	0.74	0.74	1.00	1.09	0.88	0.90	1.36	1.01	0.78	1.05
Ca HCl	0.62	0.47	0.73	0.67	0.72	0.64	0.72	0.57	0.29	1.15
Ca Res	0.06	0.13	0.07	0.00	0.00	0.06	0.08	0.06	0.00	0.10
Ca	**5.95**	**6.45**	**7.06**	**8.12**	**7.60**	**6.72**	**8.37**	**6.46**	**4.84**	**9.66**
Ti AA	0.01	0.01	0.01	0.01	0.01	0.02	0.01	0.00	0.00	0.00
Ti ARA	0.02	0.01	0.00	0.01	0.00	0.01	0.01	0.00	0.00	0.00
Ti HCl	0.16	0.17	0.13	0.09	0.11	0.15	0.19	0.03	0.02	0.05
Ti Res	0.07	0.06	0.05	0.04	0.04	0.06	0.06	0.01	0.01	0.01
Ti	**0.26**	**0.26**	**0.20**	**0.15**	**0.17**	**0.23**	**0.27**	**0.04**	**0.03**	**0.07**
Mg AA	0.09	0.29	0.15	0.20	0.05	0.10	0.04	0.20	0.00	0.03
Mg ARA	0.19	0.47	0.20	0.86	0.09	0.12	0.40	0.24	-0.02	0.10
Mg HCl	0.48	0.64	0.39	1.06	0.25	0.27	0.65	0.53	-0.04	0.17
Mg Res	0.92	1.70	0.59	2.27	0.32	0.50	0.82	0.89	-0.06	0.23
Mg	**1.68**	**3.10**	**1.33**	**4.39**	**0.71**	**0.98**	**1.92**	**1.86**	**-0.13**	**0.53**
Ni AA	12.19	15.24	8.09	10.88	11.40	5.15	17.87	7.26	0.08	11.69
Ni ARA	143.63	116.14	135.22	90.64	134.08	108.79	147.12	70.77	3.06	145.49
Ni HCl	308.15	273.73	266.89	185.18	208.17	237.58	191.98	122.99	4.87	173.75
Ni Res	6.53	6.10	6.15	4.46	3.30	3.33	5.32	2.63	0.09	6.50
Ni	**470.50**	**411.20**	**416.35**	**291.15**	**356.95**	**354.85**	**362.30**	**203.65**	**8.10**	**337.43**
Co AA	0.84	2.63	2.97	4.68	3.29	1.93	1.25	0.00	0.64	6.64
Co ARA	43.55	47.01	45.22	109.12	46.75	48.34	41.88	0.00	10.63	175.54
Co HCl	16.23	16.48	18.46	42.13	18.17	18.23	20.17	0.00	4.43	59.78
Co Res	0.89	0.98	0.86	3.07	0.89	0.81	0.70	0.00	0.31	4.03
Co	**61.50**	**67.10**	**67.50**	**159.00**	**69.10**	**69.30**	**64.00**		**16.00**	**246.00**
Cu AA	29.41	28.68	26.34	6.24	9.16	23.12	1.28	0.73	4.05	27.74
Cu ARA	501.55	377.27	400.32	194.70	325.15	361.25	23.64	13.94	58.60	410.76
Cu HCl	187.31	136.63	128.10	51.67	101.67	109.24	7.73	5.19	17.70	136.02
Cu Res	10.84	5.62	7.23	4.49	7.33	6.80	0.46	0.33	1.16	13.53
Cu	**729.10**	**548.20**	**562.00**	**257.10**	**443.30**	**500.40**	**33.10**	**20.20**	**81.50**	**588.05**
Zn AA	18.02	11.73	6.41	8.50	7.98	10.20	2.02	2.00	0.49	8.45
Zn ARA	215.30	234.57	195.19	186.14	219.51	222.21	48.00	29.51	14.41	187.69
Zn HCl	78.09	75.76	65.06	65.08	69.23	64.05	15.06	7.38	4.36	60.17
Zn Res	5.69	5.39	4.58	2.93	3.83	4.53	0.86	0.71	0.24	2.82
Zn	**317.10**	**327.45**	**271.25**	**262.65**	**300.55**	**301.00**	**65.95**	**39.60**	**19.50**	**259.13**
Pb AA	2.63	3.30	2.69	1.83	1.45	2.53	2.45	1.89	2.17	0.21
Pb ARA	71.80	81.53	74.49	51.43	40.21	89.30	61.75	56.99	59.95	6.03
Pb HCl	20.59	32.45	26.95	13.81	12.92	37.24	19.74	17.69	20.08	2.19
Pb Res	0.98	23.72	23.87	10.93	5.42	12.92	1.06	19.43	16.79	0.85
Pb	**96.0**	**141.0**	**128.0**	**78.0**	**60.0**	**142.0**	**85.0**	**96.0**	**99.0**	**9.28**
V AA	0.23	0.17	0.30	5.17	0.39	0.41	1.01	7.38	1.28	7.83
V ARA	6.70	5.28	9.36	158.49	8.13	8.71	24.72	145.09	39.34	233.45
V HCl	5.92	4.07	5.79	118.75	7.20	6.44	16.82	121.48	23.59	163.88
V Res	0.25	0.38	0.15	7.99	0.98	1.04	3.16	11.56	2.38	7.83
V	**13.10**	**9.90**	**15.60**	**290.40**	**16.70**	**16.60**	**45.70**	**285.50**	**66.60**	**413.00**

TABLE B.6 Partition Analysis data:
Major and Trace Elements

Sample	20669	20684	20687	20665	20663		20660	20691	20694	20695
Sample Location	Khabiyat (S.horizon)	Huwayl	Mulayyinah	Aarja Mine	Plant Site		Buriami Highway ii	Semdah West	Ghayth	Ghayth
Horizon	As/Bu	As/Bu	As/Bu	As/Bu	As/Bu		Bu/Bu	Bu/Bu	Bu/Bu	Bu/Bu
Colour	moderate reddish brown	dusky red	greyish brown	greyish brown	pale brown		greyish red	greyish brown	dusky brown	dusky brown
Colour Code	10 R 4/6	5 R 3/4	5 YR 3/2	5 YR 3/2	5 YR 5/2		5 R 4/2	5 YR 3/2	5YR 2/2	5 YR 2/2
Mn AA	0.01	0.04	0.08	0.24	0.09		0.06	0.19	0.17	0.26
Mn ARA	0.14	1.49	1.44	2.50	3.72		2.99	1.74	8.49	3.97
Mn HCl	0.17	1.20	2.79	2.14	2.66		2.74	2.78	11.99	6.70
Mn Res	0.00	0.11	0.08	0.18	0.09		0.06	0.07	0.33	0.18
Mn	**0.33**	**2.83**	**4.40**	**5.07**	**6.56**		**5.86**	**4.78**	**20.98**	**11.11**
Fe AA	0.00	0.00	0.00	0.00	0.00		0.00	0.00	0.00	0.00
Fe ARA	0.90	0.23	0.80	1.14	1.33		1.67	1.70	1.82	1.27
Fe HCl	8.16	20.34	11.29	13.57	8.98		13.34	12.96	27.68	19.11
Fe Res	0.00	0.00	0.00	0.00	0.00		0.00	0.00	0.00	0.00
Fe	**9.06**	**20.57**	**12.09**	**14.71**	**10.31**		**15.01**	**14.65**	**29.50**	**20.39**
Al AA	0.05	0.22	0.14	0.14	0.17		0.02	0.30	0.11	0.25
Al ARA	0.09	0.26	0.45	0.20	0.28		0.35	0.45	0.66	0.29
Al HCl	0.21	0.44	1.00	0.60	0.67		0.45	0.90	1.48	0.49
Al Res	0.45	1.18	1.59	1.19	1.17		0.96	1.32	2.79	0.83
Al	**0.80**	**2.11**	**3.17**	**2.12**	**2.29**		**1.79**	**2.97**	**5.04**	**1.85**
Ca AA	6.84	4.21	4.87	8.44	13.23		6.99	2.72	4.90	6.55
Ca ARA	1.24	0.55	0.62	1.71	1.84		1.52	0.46	0.89	1.06
Ca HCl	0.71	0.55	0.37	0.85	1.00		0.63	0.25	0.57	0.98
Ca Res	0.00	0.11	0.00	0.21	0.00		0.00	0.07	0.00	0.16
Ca	**8.80**	**5.42**	**5.86**	**11.21**	**16.07**		**9.14**	**3.50**	**6.36**	**8.76**
Ti AA	0.00	0.00	0.01	0.00	0.01		0.01	0.01	0.02	0.01
Ti ARA	0.00	0.00	0.01	0.01	0.00		0.01	0.00	0.01	0.00
Ti HCl	0.01	0.09	0.10	0.06	0.06		0.05	0.09	0.18	0.09
Ti Res	0.00	0.02	0.04	0.03	0.02		0.02	0.03	0.06	0.03
Ti	**0.02**	**0.11**	**0.16**	**0.10**	**0.09**		**0.09**	**0.13**	**0.27**	**0.13**
Mg AA	0.03	0.36	0.09	0.05	0.01		0.11	0.11	0.13	0.07
Mg ARA	0.18	0.57	0.25	0.22	0.10		0.10	0.21	0.29	0.21
Mg HCl	0.24	1.05	0.34	0.53	0.25		0.23	0.32	0.63	0.35
Mg Res	0.42	1.42	0.82	0.68	0.39		0.37	0.71	1.42	0.59
Mg	**0.87**	**3.40**	**1.50**	**1.48**	**0.75**		**0.80**	**1.36**	**2.47**	**1.21**
Ni AA	6.08	7.71	4.72	3.05	9.23		8.62	10.69	12.67	6.84
Ni ARA	74.79	145.23	79.80	98.68	98.06		75.59	96.43	136.22	135.70
Ni HCl	120.60	314.88	145.08	130.36	169.59		149.45	131.41	223.19	275.01
Ni Res	2.18	4.28	3.40	3.86	5.77		3.20	4.62	4.22	3.60
Ni	**203.65**	**472.10**	**233.00**	**235.95**	**282.65**		**236.85**	**243.15**	**376.30**	**421.15**
Co AA	2.41	4.91	5.63	5.23	3.55		6.16	6.78	7.10	12.89
Co ARA	114.72	101.90	88.35	109.90	109.11		121.58	108.07	177.03	307.22
Co HCl	47.12	48.25	37.46	46.02	38.56		50.52	46.53	78.14	113.91
Co Res	2.75	2.94	2.56	1.85	1.78		2.74	1.62	3.13	4.99
Co	**167.00**	**158.00**	**134.00**	**163.00**	**153.00**		**181.00**	**163.00**	**265.40**	**439.00**
Cu AA	0.92	1.46	7.22	6.78	19.06		7.28	10.76	13.99	24.39
Cu ARA	15.03	32.94	223.48	238.19	229.75		219.93	353.30	266.93	480.68
Cu HCl	4.01	11.70	79.07	72.52	71.29		63.60	90.37	88.62	137.42
Cu Res	0.24	0.70	6.14	5.01	6.00		3.08	8.18	6.46	10.71
Cu	**20.20**	**46.80**	**315.90**	**322.50**	**326.10**		**293.90**	**462.60**	**376.00**	**653.20**
Zn AA	1.52	2.66	10.12	5.75	7.59		6.30	9.21	10.06	11.91
Zn ARA	28.19	63.05	117.47	74.98	157.57		133.32	125.27	176.78	187.03
Zn HCl	9.44	19.55	37.84	28.51	56.00		35.08	46.23	50.76	66.58
Zn Res	0.45	1.25	3.37	1.56	3.08		3.41	2.69	3.50	2.98
Zn	**39.60**	**86.50**	**168.80**	**110.80**	**224.25**		**178.10**	**183.40**	**241.10**	**268.50**
Pb AA	0.34	2.55	1.98	1.68	2.64		3.03	3.95	0.97	3.00
Pb ARA	10.26	74.09	60.43	59.76	74.39		83.76	99.67	30.99	101.49
Pb HCl	3.19	20.80	19.61	20.91	20.96		26.02	39.67	10.76	42.40
Pb Res	2.46	28.65	2.05	2.96	9.91		10.77	12.28	3.57	23.12
Pb	**16.25**	**126.09**	**84.06**	**85.32**	**107.90**		**123.59**	**155.58**	**46.30**	**170.01**
V AA	4.56	7.54	7.46	7.24	7.39		7.31	4.93	0.34	4.27
V ARA	169.79	189.17	204.02	159.66	247.76		187.23	120.37	8.38	79.15
V HCl	101.78	142.17	172.23	123.72	160.81		132.55	95.69	5.40	61.92
V Res	9.36	25.82	18.49	9.47	11.75		10.81	3.00	0.38	3.56
V	**285.50**	**364.70**	**402.20**	**300.10**	**427.70**		**337.90**	**224.00**	**14.50**	**148.90**

TABLE B.6 Partition Analysis data:
Major and Trace Elements

Sample	**20695**	**U24**		**20601**	**20602**	**20680**	**U11**	**U3**	**U55**	**U56A**
Sample Location	Ghayth	Semdah West		Lasail Mine (south)	Lasail Mine (south)	Lasail Mine (south)	Lasail Mine (south)	Lasail Mine (south)	Huwayl (outcrop)	Huwayl (outcrop)
Horizon	Bu/Bu	Bu/Bu		As/Ls	As/Ls	As/Ls	As/Ls	As/Ls	As/Ls	As/Ls
Colour	dusky brown	very dusky red		greyish brown	moderate brown	moderate brown	greyish brown	greyish brown	blackish red	blackish red
Colour Code	5 YR 2/2	10 R 2/2		5 YR 3/2	5 YR 3/4	5 YR 3/4	5 YR 3/2	5 YR 3/2	5 R 2/2	5 R 2/2
Mn AA	0.56	0.13		0.01	0.00	0.05	0.00	0.01	0.04	0.03
Mn ARA	6.14	4.03		0.00	0.00	0.02	0.00	0.00	0.01	0.03
Mn HCl	10.43	8.83		0.06	0.03	0.34	0.04	0.06	0.42	0.52
Mn Res	0.56	0.26		0.00	0.00	0.02	0.01	0.01	0.08	0.06
Mn	**17.69**	**13.25**		**0.07**	**0.04**	**0.43**	**0.06**	**0.09**	**0.55**	**0.64**
Fe AA	0.00	0.00		0.00	0.00	0.00	0.00	0.00	0.00	0.00
Fe ARA	0.37	4.97		0.00	0.00	0.00	0.00	0.00	0.00	0.00
Fe HCl	35.58	35.68		52.00	52.37	45.65	56.93	53.08	56.13	57.61
Fe Res	0.00	0.00		6.65	8.33	5.57	2.56	2.68	4.62	4.03
Fe	**35.96**	**40.65**		**58.65**	**60.71**	**51.22**	**59.49**	**55.76**	**60.75**	**61.64**
Al AA	0.59	0.10		0.02	0.01	0.15	0.02	0.05	0.12	0.16
Al ARA	0.83	0.74		0.05	0.00	0.00	0.01	0.05	0.04	0.04
Al HCl	1.13	1.03		0.47	0.08	1.33	0.23	0.40	1.14	0.97
Al Res	1.77	2.30		0.98	0.20	3.84	0.65	0.57	2.52	2.64
Al	**4.32**	**4.17**		**1.52**	**0.30**	**5.33**	**0.91**	**1.08**	**3.82**	**3.81**
Ca AA	4.51	4.93		3.76	3.97	3.45	3.75	3.76	4.14	4.21
Ca ARA	1.07	0.86		0.67	0.65	0.81	0.59	0.50	0.55	0.67
Ca HCl	0.59	0.68		0.10	0.05	0.00	0.10	0.10	0.11	0.11
Ca Res	0.00	0.06		0.29	0.25	0.54	0.39	0.50	0.61	0.39
Ca	**6.17**	**6.53**		**4.80**	**4.92**	**4.80**	**4.84**	**4.86**	**5.40**	**5.39**
Ti AA	0.01	0.02		0.00	0.00	0.00	0.00	0.00	0.00	0.00
Ti ARA	0.00	0.01		0.00	0.00	0.00	0.00	0.00	0.00	0.00
Ti HCl	0.16	0.12		0.03	0.01	0.12	0.01	0.01	0.13	0.15
Ti Res	0.08	0.05		0.01	0.00	0.05	0.00	0.00	0.05	0.06
Ti	**0.26**	**0.20**		**0.04**	**0.01**	**0.17**	**0.01**	**0.01**	**0.19**	**0.22**
Mg AA	0.13	0.10		0.05	0.00	0.09	0.06	0.06	0.07	0.01
Mg ARA	0.34	0.14		0.02	0.00	0.00	0.04	0.00	0.03	0.01
Mg HCl	0.57	0.42		0.71	-0.02	2.68	0.61	0.34	0.36	0.08
Mg Res	1.44	0.58		1.52	-0.05	6.44	0.84	0.44	0.85	0.13
Mg	**2.48**	**1.23**		**2.31**	**-0.08**	**9.22**	**1.56**	**0.84**	**1.31**	**0.23**
Ni AA	5.39	17.52		0.87	0.93	5.41	1.07	1.17	4.97	17.39
Ni ARA	165.30	140.13		6.21	4.58	47.48	3.82	3.84	76.91	35.84
Ni HCl	243.52	218.96		41.44	18.86	211.25	25.76	27.44	271.83	256.58
Ni Res	6.94	5.69		2.09	0.28	9.01	5.39	0.80	35.14	21.29
Ni	**421.15**	**382.30**		**50.60**	**24.65**	**273.15**	**36.05**	**33.25**	**388.85**	**331.10**
Co AA	6.81	2.62		0.00	2.79	5.55	1.77	1.72	4.23	6.44
Co ARA	147.15	48.18		0.00	32.81	54.54	16.56	15.61	18.02	27.86
Co HCl	56.64	17.40		0.00	107.05	174.95	137.80	99.49	139.79	144.75
Co Res	3.50	0.90		0.00	12.35	27.96	30.87	9.18	18.96	29.95
Co	**214.10**	**69.10**			**155.00**	**263.00**	**187.00**	**126.00**	**181.00**	**209.00**
Cu AA	40.16	2.19		32.20	84.08	0.73	197.96	10.75	0.13	0.75
Cu ARA	435.47	74.40		469.22	377.31	11.62	492.71	67.32	1.11	3.57
Cu HCl	163.48	25.74		1715.87	1496.96	43.17	3638.14	320.25	6.65	15.40
Cu Res	14.09	1.77		128.81	176.35	7.59	637.88	51.38	1.31	1.78
Cu	**653.20**	**104.10**		**2346.10**	**2134.70**	**63.10**	**4966.70**	**449.70**	**9.20**	**21.50**
Zn AA	12.40	6.97		1.53	1.61	3.60	0.61	1.66	0.90	0.81
Zn ARA	201.49	90.09		16.65	22.14	44.59	22.62	23.05	16.21	15.62
Zn HCl	51.98	35.29		5.92	5.62	12.28	5.65	6.18	4.19	5.14
Zn Res	2.62	2.85		7.35	0.39	0.98	0.47	0.57	0.36	0.48
Zn	**268.50**	**135.20**		**31.45**	**29.75**	**61.45**	**29.35**	**31.45**	**21.65**	**22.05**
Pb AA	2.83	1.56		0.06	0.03	0.04	0.05	0.05	0.04	0.05
Pb ARA	93.75	39.38		0.26	0.24	0.26	0.26	0.26	0.25	0.24
Pb HCl	34.40	11.97		0.55	0.54	0.58	0.58	0.51	0.62	0.61
Pb Res	13.02	10.09		0.13	0.18	0.12	0.12	0.18	0.10	0.09
Pb	**144.00**	**63.00**		**1.00**	**1.00**	**1.00**	**1.00**	**1.00**	**1.00**	**1.00**
V AA	0.23	0.37		20.89	9.13	19.52	28.61	6.20	3.66	1.42
V ARA	7.32	9.41		208.87	209.57	109.48	189.07	165.52	56.51	68.11
V HCl	4.24	7.33		225.25	304.78	143.42	194.31	229.18	81.90	79.20
V Res	0.51	0.89		8.60	6.52	4.88	10.12	4.90	1.83	3.27
V	**12.30**	**18.00**		**463.60**	**530.00**	**277.30**	**422.10**	**405.80**	**143.90**	**152.00**

TABLE B.6 Partition Analysis data:
Major and Trace Elements

Sample	U10	U2	U3	U7	U46	U60	U12	U29	U30	U34
Sample Location	Lasail Mine (south)	Lasail Mine (south)	Lasail Mine (south)	Lasail Mine (south)	Huwayl (outcrop)	Huwayl (outcrop)	Lasail Mine (south)	Huwayl (core)	Huwayl (core)	Huwayl (core)
Horizon	As/Ls	As/Ls	As/Ls	As/Ls	As/Ls	As/Ls	As/Ls	As/Ls	As/Ls	As/Ls
Colour	dusky brown	greyish brown	greyish brown	greyish red	greyish red	brownish grey	greyish red	olive grey	dark grey	dark grey
Colour Code	5 YR 2/2	5 YR 3/2	5 YR 3/2	5 R 4/2	5 R 4/2	5 YR 4/1	10 R 4/2	5 Y 4/1	N3	N3
Mn AA	0.00	0.01	0.01	0.00	0.06	0.12	0.00	0.06	0.11	0.04
Mn ARA	0.00	0.00	0.00	0.00	0.01	0.06	0.00	0.03	0.05	0.01
Mn HCl	0.04	0.06	0.06	0.03	0.47	0.89	0.01	0.44	0.60	0.22
Mn Res	0.01	0.00	0.01	0.01	0.04	0.17	0.00	0.07	0.06	0.05
Mn	**0.06**	**0.07**	**0.09**	**0.05**	**0.58**	**1.24**	**0.02**	**0.60**	**0.81**	**0.33**
Fe AA	0.00	0.00	0.00	0.00	0.00	0.00	0.00	0.00	0.00	0.00
Fe ARA	0.00	0.00	0.00	0.00	0.00	0.00	0.00	0.00	0.00	0.00
Fe HCl	45.23	42.25	49.50	42.07	16.40	15.31	45.93	8.28	21.41	29.26
Fe Res	1.72	6.20	6.26	4.45	2.03	2.35	6.80	1.01	1.69	2.07
Fe	**46.94**	**48.45**	**55.76**	**46.53**	**18.43**	**17.66**	**52.74**	**9.29**	**23.10**	**31.32**
Al AA	0.01	0.04	0.01	0.03	0.17	0.07	0.00	0.07	0.04	0.05
Al ARA	0.02	0.04	0.02	0.04	0.11	0.09	0.01	0.05	0.17	0.09
Al HCl	0.20	0.23	0.31	0.34	1.68	0.60	0.07	0.49	1.15	0.59
Al Res	0.52	0.52	0.73	0.54	2.13	1.70	0.14	1.21	2.13	1.22
Al	**0.75**	**0.83**	**1.08**	**0.95**	**4.09**	**2.46**	**0.23**	**1.82**	**3.49**	**1.94**
Ca AA	3.67	4.00	3.53	3.37	3.95	3.93	0.91	6.67	6.62	3.29
Ca ARA	0.64	0.67	0.78	0.78	0.72	0.61	0.14	1.04	1.03	0.62
Ca HCl	0.05	0.00	0.00	0.09	0.10	0.00	0.02	0.00	0.00	0.08
Ca Res	0.34	0.31	0.55	0.39	0.26	0.50	0.10	0.69	0.77	0.29
Ca	**4.69**	**4.98**	**4.86**	**4.63**	**5.02**	**5.04**	**1.18**	**8.40**	**8.43**	**4.27**
Ti AA	0.00	0.00	0.00	0.00	0.00	0.00	0.00	0.00	0.00	0.00
Ti ARA	0.00	0.00	0.00	0.00	0.00	0.00	0.00	0.00	0.00	0.00
Ti HCl	0.01	0.01	0.01	0.02	0.10	0.07	0.00	0.05	0.13	0.08
Ti Res	0.00	0.00	0.00	0.01	0.03	0.03	0.00	0.02	0.05	0.03
Tl	**0.01**	**0.01**	**0.01**	**0.03**	**0.13**	**0.10**	**0.01**	**0.07**	**0.17**	**0.11**
Mg AA	0.01	0.01	0.02	0.03	0.00	0.01	0.00	0.08	0.15	0.05
Mg ARA	0.02	0.00	0.01	0.03	0.01	0.00	0.00	0.00	0.00	0.11
Mg HCl	0.29	0.21	0.23	0.25	0.12	0.09	0.05	0.75	0.93	0.78
Mg Res	0.77	0.69	0.58	0.71	0.14	0.27	0.08	0.95	1.78	1.79
Mg	**1.09**	**0.91**	**0.84**	**1.01**	**0.28**	**0.37**	**0.14**	**1.78**	**2.85**	**2.73**
Ni AA	1.61	0.54	0.75	1.05	3.29	1.53	0.26	5.14	12.01	16.09
Ni ARA	3.70	3.41	6.08	6.96	11.11	21.48	2.56	19.48	65.09	132.40
Ni HCl	32.87	27.51	22.23	26.91	71.98	116.47	8.89	119.45	238.54	497.42
Ni Res	5.72	1.72	4.19	2.23	15.82	22.32	1.09	22.73	36.97	8.04
Ni	**43.90**	**33.18**	**33.25**	**37.15**	**102.20**	**161.80**	**12.80**	**166.80**	**352.60**	**653.95**
Co AA	2.63	4.65	4.70	1.17	1.58	1.50	0.00	0.89	5.33	2.81
Co ARA	20.12	27.11	20.08	13.51	9.88	12.42	0.00	9.54	27.11	7.96
Co HCl	83.80	99.49	84.78	84.37	46.41	49.42	0.00	39.74	101.21	48.49
Co Res	14.46	1.75	16.44	18.95	2.13	10.67	0.00	1.83	18.35	5.74
Co	**121.00**	**133.00**	**126.00**	**118.00**	**60.00**	**74.00**		**52.00**	**152.00**	**65.00**
Cu AA	21.71	25.59	13.66	18.72	9.48	0.95	57.81	3.30	1.31	0.35
Cu ARA	157.40	216.95	41.74	68.79	44.32	13.72	790.04	21.48	4.63	1.90
Cu HCl	903.15	891.16	329.78	339.28	173.04	46.30	3930.92	66.56	24.78	11.66
Cu Res	109.64	17.80	64.51	77.21	31.55	6.14	399.84	16.66	2.28	0.89
Cu	**1191.90**	**1151.50**	**449.70**	**504.00**	**258.40**	**67.10**	**5178.60**	**108.00**	**33.00**	**14.80**
Zn AA	1.98	1.08	0.59	1.04	1.76	1.72	1.05	1.95	1.40	0.62
Zn ARA	29.06	28.35	23.74	24.60	19.00	21.44	27.58	31.83	36.79	20.45
Zn HCl	8.98	8.68	6.81	6.37	6.98	6.04	10.80	11.20	10.04	5.66
Zn Res	0.38	0.61	0.31	0.55	0.41	0.60	0.87	0.76	0.77	0.27
Zn	**40.40**	**38.73**	**31.45**	**32.55**	**28.15**	**29.80**	**40.30**	**45.75**	**49.00**	**27.00**
Pb AA	0.04	0.04	0.04	0.04	0.91	0.28	0.72	0.64	0.85	0.28
Pb ARA	0.24	0.25	0.29	0.25	6.93	1.79	4.06	3.73	5.06	1.71
Pb HCl	0.55	0.61	0.57	0.56	14.69	4.15	9.59	8.26	10.76	4.27
Pb Res	0.17	0.10	0.10	0.14	2.47	0.78	3.25	2.67	3.91	0.96
Pb	**1.00**	**1.00**	**1.00**	**1.00**	**25.00**	**7.00**	**17.63**	**15.31**	**20.58**	**7.21**
V AA	18.31	30.24	15.88	19.67	8.53	13.41	14.90	4.49	8.84	14.83
V ARA	101.63	152.14	184.55	141.51	112.00	78.54	253.74	157.19	157.15	94.49
V HCl	153.39	185.78	195.84	196.41	165.46	104.84	280.74	183.82	234.36	124.50
V Res	3.58	8.64	9.53	3.82	3.92	1.72	6.52	9.30	7.14	4.29
V	**276.90**	**376.80**	**405.80**	**361.40**	**289.90**	**198.50**	**555.90**	**354.80**	**407.50**	**238.10**

TABLE B.6 Partition Analysis data:
Major and Trace Elements

Sample	U35	U40	U51	U54	U6	U77
Sample Location	Huwayl (core)	Huwayl (outcrop)	Huwayl (outcrop)	Huwayl (outcrop)	Lasail Mine (south)	Lasail Mine (south)
Horizon	As/Ls	As/Ls	As/Ls	As/Ls	As/Ls	As/Ls
Colour	dusky yellowish brown	greyish brown	dusky red	dusky red	moderate brown	greyish red
Colour Code	10 YR 2/2	5 YR 3/2	5 R 3/4	5 R 3/4	5 YR 3/4	5 R 4/2
Mn AA	0.06	0.06	0.14	0.15	0.02	0.40
Mn ARA	0.01	0.04	0.07	0.07	0.01	0.33
Mn HCl	0.38	0.59	0.99	1.57	0.25	5.06
Mn Res	0.04	0.09	0.15	0.26	0.04	1.07
Mn	**0.49**	**0.77**	**1.35**	**2.04**	**0.31**	**6.86**
Fe AA	0.00	0.00	0.00	0.00	0.00	0.00
Fe ARA	0.00	0.00	0.00	0.00	0.00	0.00
Fe HCl	16.84	15.83	17.69	16.17	16.21	14.69
Fe Res	1.68	0.75	2.33	0.70	1.69	0.88
Fe	**18.53**	**16.58**	**20.02**	**16.87**	**17.90**	**15.57**
Al AA	0.07	0.12	0.10	0.09	0.11	0.03
Al ARA	0.02	0.00	0.03	0.04	0.00	0.03
Al HCl	0.67	1.05	0.93	0.66	0.93	0.75
Al Res	1.35	1.90	1.30	1.52	2.75	1.56
Al	**2.12**	**3.07**	**2.37**	**2.31**	**3.78**	**2.36**
Ca AA	3.30	4.72	4.91	3.98	4.13	7.11
Ca ARA	0.66	0.61	0.64	0.77	0.75	1.46
Ca HCl	0.00	0.06	0.13	0.10	0.11	0.09
Ca Res	0.31	0.49	0.77	0.26	0.59	0.73
Ca	**4.27**	**5.89**	**6.44**	**5.10**	**5.57**	**9.38**
Ti AA	0.00	0.00	0.00	0.00	0.00	0.00
Ti ARA	0.00	0.00	0.00	0.00	0.00	0.00
Ti HCl	0.06	0.13	0.11	0.11	0.12	0.07
Ti Res	0.02	0.05	0.04	0.04	0.04	0.04
Ti	**0.08**	**0.18**	**0.16**	**0.16**	**0.16**	**0.11**
Mg AA	0.09	0.03	0.09	0.03	0.17	0.01
Mg ARA	0.06	0.06	0.05	0.03	0.10	0.01
Mg HCl	0.76	0.45	0.47	0.81	1.00	0.16
Mg Res	1.94	1.01	1.47	2.27	2.38	0.26
Mg	**2.85**	**1.56**	**2.08**	**3.15**	**3.66**	**0.43**
Ni AA	14.21	10.51	10.36	13.97	9.03	11.25
Ni ARA	49.09	54.23	48.52	54.55	49.57	42.41
Ni HCl	235.10	253.55	207.18	242.13	140.68	255.01
Ni Res	10.66	52.81	43.89	20.95	35.12	12.98
Ni	**309.05**	**371.10**	**309.95**	**331.60**	**234.40**	**321.65**
Co AA	3.10	1.89	2.28	3.51	2.51	3.33
Co ARA	12.18	22.25	19.98	18.35	14.51	40.19
Co HCl	58.34	73.92	73.07	68.65	45.98	206.22
Co Res	13.37	0.94	6.66	14.49	6.00	33.26
Co	**87.00**	**99.00**	**102.00**	**105.00**	**69.00**	**283.00**
Cu AA	0.36	0.50	31.41	0.10	0.82	2.14
Cu ARA	3.42	5.96	217.79	2.22	3.89	22.89
Cu HCl	12.68	19.31	749.71	7.14	16.58	192.28
Cu Res	0.24	3.53	110.99	0.63	3.91	9.20
Cu	**16.70**	**29.30**	**1109.90**	**10.10**	**25.20**	**226.50**
Zn AA	1.63	3.81	1.94	4.45	5.81	3.01
Zn ARA	22.00	46.40	46.96	50.54	76.78	104.28
Zn HCl	7.93	15.92	17.70	18.06	21.17	31.90
Zn Res	0.54	1.12	1.01	1.54	1.04	2.56
Zn	**32.10**	**67.25**	**67.60**	**74.60**	**104.80**	**141.75**
Pb AA	0.49	0.50	0.35	0.65	0.37	0.49
Pb ARA	2.75	2.20	2.57	3.21	1.86	2.21
Pb HCl	6.12	5.70	5.81	6.66	4.97	5.59
Pb Res	1.24	1.38	1.12	1.15	0.77	1.37
Pb	**10.60**	**9.79**	**9.85**	**11.67**	**7.97**	**9.66**
V AA	14.91	5.05	4.18	10.63	6.27	10.73
V ARA	106.98	63.92	91.03	70.23	101.11	98.35
V HCl	126.00	85.65	123.75	92.62	123.14	98.88
V Res	2.81	2.38	5.05	3.92	5.18	3.04
V	**250.70**	**157.00**	**224.00**	**177.40**	**235.70**	**211.00**

TABLE B.7 Partition Data: REE

Sample	20635	20639	20641	20643	20653	20654	20668	20669	U82	20662	20669	20684
Sample Location	Khabiyat (main horizon)	Khabiyat (main horizon)	Khabiyat (main horizon)	Khabiyat (main horizon)	Wadi Suq	Wadi Suq	Khabiyat (Sthn hoizon)	Khabiyat (Sthn hoizon)	Aarja Mine	PDynt Site	Khabiyat (S.horizon)	Huwayl
Horizon	As/Bu	As/Bu	As/Bu	As/Bu	As/Bu	As/Bu	As/Bu	As/Bu	As/Bu	As/Bu	As/Bu	As/Bu
Colour	dusky brown	dusky brown	greyish red	pale red	greyish brown	moderate brown	greyish red	moderate reddish brown	moderate brown	greyish brown	moderate reddish brown	dusky red
Colour Code	5 YR 2/2	5 YR 2/2	10 R 4/2	5 R 6/2	5 YR 3/2	5 YR 3/4	5 R 4/2	10 R 4/6	5 YR 4/4	5 YR 3/2	10 R 4/6	5 R 3/4
La AA	0.9	1.5	1.4	0.2	0.7	1.8	3.0	1.2	1.4	0.4	0.2	1.9
La ARA	1.0	0.9	3.1	1.6	7.4	0.9	1.5	1.4	1.9	1.3	3.0	2.9
La HCl	45.0	48.6	53.3	59.4	107.1	75.0	135.0	91.8	55.0	41.4	41.8	64.9
La Res	3.2	3.0	3.2	5.3	9.0	5.7	11.9	4.5	4.5	2.4	3.0	6.2
La	50.0	54.0	61.0	66.4	124.2	83.4	151.4	98.9	62.8	45.5	48.1	75.9
Ce AA	1.12	1.88	2.55	0.17	0.67	1.94	1.81	1.35	2.86	0.40	0.22	3.92
Ce ARA	1.12	0.94	5.55	2.14	6.22	1.01	1.21	1.97	4.53	1.27	4.95	7.84
Ce HCl	51.07	70.86	79.31	78.31	79.32	78.08	108.45	94.49	103.97	47.87	66.02	134.99
Ce Res	3.31	3.76	5.28	6.08	7.32	6.48	9.31	4.98	9.42	3.16	3.91	11.16
Ce	**56.62**	**77.45**	**92.68**	**86.70**	**93.54**	**87.50**	**120.78**	**102.80**	**120.78**	**52.70**	**75.10**	**157.91**
Pr AA	0.22	0.32	0.51	0.03	0.26	0.52	0.40	0.36	0.73	0.07	0.04	0.72
Pr ARA	0.23	0.16	1.06	0.38	2.45	0.26	0.25	0.54	1.10	0.20	0.68	1.37
Pr HCl	10.62	11.22	16.65	15.06	33.34	21.60	24.40	25.78	25.01	8.24	8.94	24.24
Pr Res	0.68	0.63	1.01	1.20	3.12	1.77	1.94	1.31	2.17	0.54	0.56	1.99
Pr	**11.75**	**12.33**	**19.23**	**16.67**	**39.17**	**24.15**	**27.00**	**28.00**	**29.00**	**9.05**	**10.22**	**28.32**
Nd AA	1.03	1.32	1.71	0.17	0.74	1.36	1.95	1.14	1.70	0.31	0.16	1.81
Nd ARA	1.03	0.63	3.45	1.35	6.85	0.65	1.19	1.49	2.44	1.06	3.15	3.63
Nd HCl	45.79	46.87	51.09	55.27	100.24	58.66	108.60	72.66	56.70	41.59	39.58	61.30
Nd Res	3.20	2.70	3.18	4.31	9.66	4.64	9.05	3.60	5.07	2.63	2.45	5.47
Nd	**51.05**	**51.52**	**59.43**	**61.09**	**117.49**	**65.31**	**120.78**	**78.89**	**65.92**	**45.58**	**45.35**	**72.21**
Sm AA	0.71	0.87	1.20	0.12	0.46	1.04	1.45	0.78	0.88	0.21	0.15	1.24
Sm ARA	0.67	0.42	2.27	0.93	4.31	0.48	0.92	1.12	1.31	0.79	2.24	2.34
Sm HCl	30.43	30.58	33.60	39.06	64.39	42.10	82.78	49.62	30.83	29.51	27.82	41.66
Sm Res	2.15	1.78	2.10	2.95	6.18	3.27	6.69	2.56	2.55	1.84	1.85	3.60
Sm	**33.96**	**33.65**	**39.17**	**43.05**	**75.34**	**46.88**	**91.83**	**54.08**	**35.56**	**32.36**	**32.06**	**48.83**
Eu AA	0.43	0.64	0.81	0.07	0.28	0.68	1.11	0.51	0.62	0.13	0.10	0.74
Eu ARA	0.41	0.31	1.58	0.65	2.75	0.30	0.66	0.72	0.93	0.52	1.52	1.40
Eu HCl	18.92	21.77	22.94	26.39	42.46	27.17	59.87	33.12	23.15	18.81	19.23	26.67
Eu Res	1.25	1.22	1.47	2.06	4.04	2.12	4.88	1.63	1.85	1.21	1.33	2.37
Eu	**21.00**	**23.93**	**26.79**	**29.17**	**49.55**	**30.27**	**66.53**	**35.97**	**26.55**	**20.67**	**22.18**	**31.19**
Gd AA	0.44	0.65	0.65	0.07	0.26	0.70	1.05	0.51	0.64	0.13	0.09	0.71
Gd ARA	0.44	0.34	1.32	0.71	2.76	0.30	0.69	0.72	0.85	0.50	1.53	1.41
Gd HCl	19.85	21.57	20.22	26.87	43.26	29.16	58.46	34.19	22.87	18.78	18.74	26.39
Gd Res	1.37	1.28	1.25	2.10	4.12	2.09	4.88	1.77	1.85	1.18	1.29	2.27
Gd	**22.10**	**23.85**	**23.44**	**29.76**	**50.40**	**32.24**	**65.08**	**37.19**	**26.21**	**20.59**	**21.65**	**30.79**
Tb AA	0.28	0.45	0.51	0.05	0.17	0.57	0.70	0.39	0.45	0.10	0.07	0.51
Tb ARA	0.31	0.22	1.04	0.48	2.00	0.24	0.45	0.51	0.57	0.35	1.14	1.05
Tb HCl	14.21	15.25	16.84	17.94	30.95	22.32	37.37	25.74	16.16	12.99	13.92	19.08
Tb Res	0.97	0.91	1.02	1.48	2.85	1.70	2.88	1.37	1.32	0.76	0.94	1.74
Tb	**15.78**	**16.83**	**19.41**	**19.95**	**35.97**	**24.83**	**41.40**	**28.00**	**18.49**	**14.19**	**16.07**	**22.39**
Dy AA	0.30	0.49	0.49	0.05	0.20	0.55	0.77	0.41	0.44	0.10	0.06	0.55
Dy ARA	0.32	0.26	1.03	0.47	2.08	0.22	0.47	0.49	0.56	0.40	1.08	1.11
Dy HCl	15.55	16.23	16.53	18.35	32.57	21.65	40.72	26.64	15.99	14.50	14.52	20.52
Dy Res	1.01	1.01	1.01	1.50	2.82	1.52	3.12	1.36	1.33	0.92	0.98	1.97
Dy	**17.18**	**17.99**	**19.05**	**20.37**	**37.67**	**23.93**	**45.08**	**28.91**	**18.32**	**15.92**	**16.65**	**24.15**
Ho AA	0.28	0.46	0.51	0.04	0.21	0.52	0.72	0.37	0.46	0.10	0.07	0.55
Ho ARA	0.29	0.24	1.07	0.44	2.02	0.23	0.42	0.45	0.52	0.36	0.94	1.01
Ho HCl	13.94	15.03	18.26	17.39	29.65	20.73	35.21	25.84	15.22	12.31	12.67	18.91
Ho Res	0.93	0.94	1.05	1.35	2.72	1.54	2.82	1.34	1.30	0.78	0.90	1.93
Ho	**15.45**	**16.67**	**20.89**	**19.23**	**34.59**	**23.01**	**39.17**	**28.00**	**17.50**	**13.55**	**14.57**	**22.40**
Er AA	0.23	0.40	0.40	0.04	0.20	0.51	0.72	0.32	0.39	0.10	0.06	0.57
Er ARA	0.24	0.22	0.84	0.41	1.86	0.24	0.38	0.39	0.48	0.31	0.84	0.96
Er HCl	12.66	13.48	14.00	16.86	26.53	21.58	32.15	24.30	13.90	11.21	11.32	18.74
Er Res	0.79	0.79	0.83	1.40	2.32	1.60	2.73	1.28	1.15	0.72	0.81	1.91
Er	**13.93**	**14.89**	**16.07**	**18.71**	**30.90**	**23.93**	**35.97**	**26.30**	**15.92**	**12.33**	**13.03**	**22.18**
Tm AA	0.25	0.40	0.38	0.04	0.21	0.55	0.95	0.38	0.38	0.12	0.07	0.60
Tm ARA	0.26	0.25	0.80	0.40	2.13	0.25	0.45	0.42	0.48	0.37	0.90	0.93
Tm HCl	12.69	13.57	14.09	16.58	31.71	21.55	39.48	25.88	14.35	12.30	11.71	19.07
Tm Res	0.85	0.81	0.81	1.47	2.58	1.58	3.37	1.33	1.15	0.76	0.88	1.99
Tm	**14.06**	**15.03**	**16.07**	**18.49**	**36.64**	**23.93**	**44.26**	**28.00**	**16.37**	**13.54**	**13.56**	**22.59**
Yb AA	0.23	0.38	0.34	0.05	0.22	0.50	0.81	0.37	0.35	0.11	0.06	0.52
Yb ARA	0.24	0.22	0.72	0.41	2.12	0.24	0.39	0.44	0.48	0.32	0.79	0.85
Yb HCl	11.51	12.69	12.94	15.42	29.44	20.64	34.86	27.79	13.27	10.45	10.42	18.11
Yb Res	0.82	0.76	0.76	1.46	2.50	1.42	3.12	1.39	1.07	0.61	0.78	1.84
Yb	**12.79**	**14.06**	**14.76**	**17.34**	**34.28**	**22.80**	**39.17**	**29.99**	**15.17**	**11.49**	**12.05**	**21.33**
La AA	0.28	0.47	0.44	0.06	0.23	0.58	0.96	0.38	0.45	0.13	0.07	0.61
La ARA	0.31	0.29	0.99	0.50	2.37	0.28	0.49	0.45	0.62	0.40	0.97	0.94
La HCl	14.45	15.62	17.12	19.07	34.41	24.10	43.36	29.48	17.66	13.31	13.43	20.84
La Res	1.03	0.96	1.03	1.70	2.89	1.83	3.83	1.46	1.45	0.78	0.97	2.00

TABLE B.7 Partition Data: REE

Sample	20687	20665	20663	Average	20660	20691	20694	20695	20695	U24	Average	20601	20602
Sample Location	MuDyyyinah	Aarja Mine	PDynt Site		Buriami Highway li	Semdah West	Ghayth	Ghayth	Ghayth	Semdah West		Dysail Mine (south)	Dysail Mine (south)
Horizon	As/Bu	As/Bu	As/Bu		Bu/Bu	Bu/Bu	Bu/Bu	Bu/Bu	Bu/Bu	Bu/Bu		As/Ls	As/Ls
Colour	greyish brown	greyish brown	pale brown		greyish red	greyish brown	dusky brown	dusky brown	dusky brown	very dusky red		greyish brown	moderate brown
Colour Code	5 YR 3/2	5 YR 3/2	5 YR 5/2		5 R 4/2	5 YR 3/2	5YR 2/2	5 YR 2/2	5 YR 2/2	10 R 2/2		5 YR 3/2	5 YR 3/4
La AA	1.9	2.0	1.9	1.4	2.0	0.7	3.0	3.0	3.3	1.2	2.2	4.5	3.8
La ARA	8.7	2.1	3.2	2.7	9.2	5.9	8.2	5.5	9.6	15.9	9.1	3.5	4.9
La HCl	98.7	149.0	121.8	79.2	107.0	100.5	101.9	119.2	122.6	162.3	118.9	159.8	155.1
La Res	6.9	13.3	11.0	6.2	8.9	5.2	6.3	12.3	13.2	14.2	10.0	7.1	16.9
La	116.2	166.3	138.0	89.5	127.1	112.2	119.4	140.0	148.7	193.7	140.2	174.9	180.7
Ce AA	2.78	3.63	4.77	2.0	1.21	0.64	3.34	6.93	6.92	1.27	3.4	3.79	4.48
Ce ARA	12.94	2.95	6.92	4.1	7.68	11.60	9.17	13.47	17.19	22.90	13.7	4.74	7.78
Ce HCl	153.63	188.48	211.06	103.1	90.55	194.76	100.90	308.25	206.06	284.69	197.5	178.96	206.36
Ce Res	8.52	19.51	21.94	8.3	10.21	9.45	5.72	26.17	21.01	22.27	15.8	10.43	20.99
Ce	**177.87**	**214.57**	**244.68**	117.4	**109.65**	**216.45**	**119.12**	**354.81**	**251.19**	**331.13**	230.4	**197.92**	**239.61**
Pr AA	0.72	0.55	0.86	0.4	0.34	0.16	1.07	1.46	1.47	0.35	0.8	0.51	0.87
Pr ARA	3.24	0.42	1.22	0.9	2.17	2.23	2.74	2.84	3.80	5.41	3.2	0.60	1.43
Pr HCl	40.39	28.28	37.18	22.1	25.53	37.43	32.43	65.93	48.13	68.00	46.2	23.96	39.30
Pr Res	2.20	2.94	3.79	1.7	2.86	1.91	1.78	5.62	4.55	5.13	3.6	1.32	3.98
Pr	**46.56**	**32.18**	**43.06**	25.1	**30.90**	**41.74**	**38.02**	**75.86**	**57.94**	**78.89**	53.9	**26.39**	**45.58**
Nd AA	1.51	1.77	2.51	1.3	0.99	0.47	2.89	2.96	3.14	0.58	1.8	2.06	2.22
Nd ARA	7.51	1.46	3.48	2.6	6.35	5.43	6.65	5.60	8.00	9.83	7.0	2.32	3.80
Nd HCl	89.41	95.50	105.96	68.6	74.94	88.48	82.56	130.13	98.81	115.63	98.4	96.93	104.81
Nd Res	5.06	10.27	10.86	5.5	8.33	4.51	4.52	11.72	9.17	8.86	7.8	4.88	10.70
Nd	**103.49**	**109.01**	**122.81**	78.0	**90.61**	**98.89**	**96.61**	**150.41**	**119.12**	**134.90**	115.1	**106.18**	**121.53**
Sm AA	1.00	1.51	1.63	0.9	0.70	0.36	1.91	1.97	2.74	0.42	1.4	1.47	1.43
Sm ARA	5.11	1.25	2.23	1.8	4.25	3.49	4.22	3.86	7.09	7.23	5.0	1.64	2.53
Sm HCl	57.84	84.72	72.21	47.8	49.39	60.29	53.80	83.95	89.55	93.68	71.8	70.21	69.95
Sm Res	3.16	8.89	6.71	3.8	5.47	3.04	2.88	8.04	8.01	6.81	5.7	3.39	7.43
Sm	**67.12**	**96.38**	**82.77**	54.2	**59.82**	**67.19**	**62.81**	**97.82**	**107.40**	**108.14**	83.9	**76.71**	**81.33**
Eu AA	0.66	1.00	0.95	0.6	0.61	0.28	1.36	1.19	1.79	0.31	0.9	1.03	1.02
Eu ARA	3.45	0.90	1.39	1.2	3.54	2.26	2.92	2.32	4.45	5.78	3.5	1.20	1.82
Eu HCl	39.19	62.01	46.08	32.5	40.42	39.19	39.67	52.58	56.25	69.17	49.5	51.62	51.07
Eu Res	2.00	6.55	4.24	2.5	4.41	2.02	2.04	5.39	5.43	5.10	4.1	2.36	5.58
Eu	**45.31**	**70.47**	**52.65**	36.8	**48.98**	**43.75**	**46.00**	**61.47**	**67.92**	**80.35**	58.1	**56.21**	**59.48**
Gd AA	0.65	0.96	0.98	0.6	0.63	0.30	1.20	1.10	1.80	0.27	0.9	1.23	1.23
Gd ARA	3.18	0.87	1.55	1.1	3.48	2.25	2.70	2.22	4.40	5.29	3.4	1.30	1.97
Gd HCl	37.11	60.53	48.90	32.5	39.86	39.42	35.82	53.80	53.18	60.68	47.1	58.03	60.99
Gd Res	2.00	5.94	4.76	2.5	4.35	2.02	1.96	5.47	5.18	4.56	3.9	2.55	6.10
Gd	**42.93**	**68.30**	**56.19**	36.7	**48.31**	**44.00**	**41.69**	**62.59**	**64.57**	**70.79**	55.3	**63.11**	**70.29**
Tb AA	0.45	0.56	0.65	0.4	0.46	0.25	0.95	0.81	1.41	0.21	0.7	0.81	0.87
Tb ARA	2.31	0.55	1.06	0.8	2.47	1.74	2.12	1.54	3.33	4.60	2.6	0.85	1.34
Tb HCl	26.60	38.51	35.07	22.9	29.58	29.16	29.83	38.58	40.51	50.58	36.4	37.06	40.38
Tb Res	1.43	3.83	3.25	1.8	3.05	1.58	1.61	3.87	4.29	3.63	3.0	1.75	4.05
Tb	**30.79**	**43.45**	**40.03**	25.8	**35.56**	**32.73**	**34.51**	**44.80**	**49.55**	**59.02**	42.7	**40.47**	**46.63**
Dy AA	0.50	0.58	0.69	0.4	0.50	0.25	0.93	0.91	1.33	0.28	0.7	0.93	1.02
Dy ARA	2.27	0.62	1.01	0.8	2.49	1.71	2.20	1.63	3.25	5.12	2.7	0.89	1.47
Dy HCl	27.65	41.08	35.74	23.9	30.91	30.10	31.50	40.37	41.28	54.40	38.1	42.08	44.12
Dy Res	1.47	4.00	3.43	1.8	3.08	1.59	1.76	4.12	4.48	4.03	3.2	1.97	4.68
Dy	**31.89**	**46.27**	**40.86**	27.0	**36.97**	**33.65**	**36.39**	**47.03**	**50.35**	**63.83**	44.7	**45.87**	**51.29**
Ho AA	0.46	0.50	0.62	0.4	0.52	0.23	0.84	0.83	1.06	0.25	0.6	0.86	0.84
Ho ARA	2.14	0.57	0.96	0.8	2.63	1.67	2.19	1.35	2.81	4.63	2.5	0.78	1.23
Ho HCl	25.69	36.56	32.75	22.0	29.87	28.71	29.40	35.31	34.66	50.40	34.7	38.15	37.98
Ho Res	1.42	3.62	3.06	1.7	2.92	1.59	1.76	3.44	3.74	3.74	2.9	1.72	3.83
Ho	**29.72**	**41.26**	**37.39**	24.9	**35.94**	**32.21**	**34.20**	**40.94**	**42.27**	**59.02**	40.8	**41.51**	**43.88**
Er AA	0.47	0.46	0.49	0.4	0.50	0.21	0.79	0.76	0.93	0.26	0.6	0.78	0.82
Er ARA	2.04	0.53	0.79	0.7	2.55	1.60	2.11	1.23	2.35	4.37	2.4	0.72	1.16
Er HCl	24.18	36.31	28.03	20.3	26.86	26.76	26.37	29.79	31.41	43.62	30.8	35.11	35.01
Er Res	1.42	3.42	2.70	1.6	2.63	1.43	1.56	3.07	3.32	3.51	2.6	1.64	3.54
Er	**28.12**	**40.73**	**32.02**	23.0	**32.54**	**29.99**	**30.83**	**34.84**	**38.02**	**51.76**	36.3	**38.25**	**40.54**
Tm AA	0.49	0.55	0.68	0.4	0.55	0.21	0.85	1.05	1.15	0.28	0.7	1.14	1.08
Tm ARA	2.33	0.57	0.97	0.8	2.94	1.69	2.30	1.68	3.02	4.72	2.7	0.97	1.47
Tm HCl	25.79	43.56	37.53	22.7	32.84	28.85	29.63	38.68	41.45	47.34	36.5	46.33	45.59
Tm Res	1.63	3.90	3.42	1.8	3.02	1.46	1.73	3.84	4.27	4.15	3.1	2.15	4.71
Tm	**30.25**	**48.58**	**42.59**	25.6	**39.36**	**32.21**	**34.51**	**45.26**	**49.89**	**56.49**	43.0	**50.60**	**52.84**
Yb AA	0.55	0.46	0.55	0.4	0.54	0.23	0.83	0.91	0.96	0.29	0.6	0.95	0.83
Yb ARA	2.50	0.52	0.88	0.7	2.60	1.69	2.34	1.50	2.63	4.27	2.5	0.78	1.06
Yb HCl	28.47	38.53	33.03	21.2	30.23	29.62	29.61	35.65	35.35	42.94	33.9	36.04	32.81
Yb Res	1.82	3.31	3.01	1.6	2.60	1.50	1.73	3.43	3.72	3.79	2.8	1.66	3.30
Yb	**33.34**	**42.82**	**37.47**	23.9	**35.97**	**33.04**	**34.51**	**41.50**	**42.66**	**51.29**	39.8	**39.43**	**38.00**
La AA	0.62	0.64	0.62	0.4	0.63	0.23	0.96	0.95	1.05	0.39	0.7	1.45	1.23
La ARA	2.78	0.66	1.02	0.9	2.95	1.88	2.63	1.76	3.10	5.12	2.9	1.11	1.58
La HCl	31.70	47.87	39.14	25.4	34.38	32.29	32.75	38.31	39.38	52.15	38.2	51.34	49.81
La Res	2.22	4.27	3.54	2.0	2.86	1.66	2.03	3.96	4.23	4.57	3.2	2.28	5.41

TABLE B.7 Partition Data: REE

Sample	20680	U11	U3	U55	U56A	U10	U2	U3	U7	U46	U60	U12
Sample Location	Dysail Mine (south)	Dysail Mine (south)	Dysail Mine (south)	Huwayl (outcrop)	Huwayl (outcrop)	Dysail Mine (south)	Dysail Mine (south)	Dysail Mine (south)	Dysail Mine (south)	Huwayl (outcrop)	Huwayl (outcrop)	Dysail Mine (south)
Horizon	As/Ls	As/Ls	As/Ls	As/Ls	As/Ls	As/Ls	As/Ls	As/Ls	As/Ls	As/Ls	As/Ls	As/Ls
Colour	moderate brown	greyish brown	greyish brown	bDyckish red	bDyckish red	dusky brown	greyish brown	greyish brown	greyish red	greyish red	brownish grey	greyish red
Colour Code	5 YR 3/4	5 YR 3/2	5 YR 3/2	5 R 2/2	5 R 2/2	5 YR 2/2	5 YR 3/2	5 YR 3/2	5 R 4/2	5 R 4/2	5 YR 4/1	10 R 4/2
La AA	5.6	3.2	0.3	5.2	1.5	0.1	0.2	0.2	0.1	4.3	3.1	0.0
La ARA	3.4	4.6	5.2	2.7	8.6	0.6	0.7	0.8	1.0	11.6	6.0	0.5
La HCl	153.4	112.0	151.3	163.1	109.5	11.9	10.2	11.9	14.4	130.8	137.4	13.4
La Res	16.4	9.5	21.3	14.1	10.8	0.7	1.3	1.0	1.3	8.5	12.5	0.9
La	178.9	129.4	178.2	185.1	130.4	13.4	12.4	13.9	16.8	155.3	159.0	14.8
Ce AA	8.03	3.61	0.23	6.26	3.03	0.20	0.28	0.14	0.14	7.33	6.13	0.02
Ce ARA	5.26	5.13	6.29	4.96	17.69	1.20	0.71	0.98	1.47	18.69	9.34	0.69
Ce HCl	238.91	125.02	214.45	225.59	218.83	18.21	11.13	12.93	26.88	209.18	249.53	22.03
Ce Res	24.08	12.63	22.38	20.08	23.05	1.14	1.19	1.29	1.87	11.87	20.43	1.34
Ce	**276.28**	**146.39**	**243.36**	**256.89**	**262.60**	**20.74**	**13.30**	**15.34**	**30.37**	**247.07**	**285.43**	**24.09**
Pr AA	1.92	0.48	0.05	1.39	0.51	0.05	0.09	0.04	0.02	1.13	1.19	0.01
Pr ARA	1.21	0.67	1.51	1.11	2.77	0.27	0.24	0.24	0.24	2.89	1.88	0.18
Pr HCl	58.36	16.71	49.81	48.80	34.11	4.43	4.04	3.15	3.84	31.78	50.24	5.61
Pr Res	5.61	1.66	5.03	4.26	3.56	0.28	0.41	0.31	0.27	1.65	4.09	0.37
Pr	**67.10**	**19.52**	**56.40**	**55.56**	**40.95**	**5.04**	**4.79**	**3.73**	**4.36**	**37.46**	**57.40**	**6.17**
Nd AA	4.40	1.99	0.11	3.73	1.67	0.11	0.26	0.10	0.09	4.00	3.10	0.01
Nd ARA	2.99	2.57	3.41	3.05	9.53	0.61	0.66	0.65	0.90	10.38	5.10	0.43
Nd HCl	133.15	67.73	111.05	125.15	115.51	10.15	10.60	9.11	13.80	114.52	134.84	13.78
Nd Res	12.90	6.25	12.09	11.76	12.79	0.64	1.06	0.85	1.05	6.39	10.42	0.90
Nd	**153.45**	**78.54**	**126.66**	**143.69**	**139.51**	**11.52**	**12.59**	**10.72**	**15.83**	**135.29**	**153.46**	**15.14**
Sm AA	2.82	1.42	0.07	2.31	1.10	0.08	0.17	0.07	0.06	2.58	1.83	0.01
Sm ARA	1.85	1.76	2.38	1.89	5.82	0.37	0.45	0.43	0.57	7.00	3.29	0.26
Sm HCl	86.04	49.22	72.08	79.60	74.52	6.57	7.38	6.35	8.88	71.50	85.63	8.16
Sm Res	8.39	4.34	7.90	7.48	8.32	0.42	0.72	0.56	0.70	4.34	6.62	0.49
Sm	**99.10**	**56.74**	**82.44**	**91.29**	**89.77**	**7.44**	**8.71**	**7.41**	**10.22**	**85.41**	**97.37**	**8.91**
Eu AA	2.30	1.13	0.06	1.76	0.81	0.06	0.12	0.05	0.04	2.39	1.56	0.01
Eu ARA	1.51	1.33	1.86	1.39	4.47	0.26	0.30	0.33	0.43	6.49	2.75	0.19
Eu HCl	63.50	35.98	59.52	60.51	59.54	4.92	5.24	4.70	6.52	62.99	70.29	6.03
Eu Res	6.21	3.13	6.25	5.43	6.49	0.28	0.50	0.41	0.53	3.79	5.86	0.36
Eu	**73.53**	**41.58**	**67.68**	**69.08**	**71.31**	**5.52**	**6.17**	**5.50**	**7.53**	**75.66**	**80.47**	**6.59**
Gd AA	2.45	1.24	0.06	1.73	0.74	0.08	0.21	0.08	0.07	2.11	1.41	0.01
Gd ARA	1.61	1.36	1.90	1.26	4.12	0.38	0.46	0.46	0.70	6.01	2.72	0.25
Gd HCl	71.76	40.66	61.06	59.15	54.17	6.90	8.44	6.79	10.52	56.70	63.60	8.06
Gd Res	7.33	3.41	6.54	5.18	5.84	0.38	0.81	0.56	0.92	3.63	5.68	0.47
Gd	**83.15**	**46.68**	**69.56**	**67.31**	**64.88**	**7.74**	**9.93**	**7.89**	**12.21**	**68.46**	**73.41**	**8.78**
Tb AA	1.61	0.79	0.04	1.27	0.51	0.04	0.10	0.04	0.03	1.42	1.02	0.01
Tb ARA	1.02	0.87	1.42	0.85	2.81	0.20	0.21	0.23	0.28	3.83	2.09	0.16
Tb HCl	48.41	26.10	43.34	41.04	36.91	3.74	3.77	3.60	4.40	38.81	47.98	4.67
Tb Res	4.63	2.17	4.58	3.53	3.98	0.20	0.39	0.29	0.37	2.43	4.00	0.29
Tb	**55.67**	**29.93**	**49.38**	**46.69**	**44.20**	**4.18**	**4.47**	**4.17**	**5.08**	**46.49**	**55.10**	**5.13**
Dy AA	1.75	0.88	0.04	1.53	0.61	0.05	0.10	0.05	0.03	1.61	1.07	0.01
Dy ARA	1.13	1.06	1.55	0.95	3.51	0.20	0.24	0.26	0.33	4.40	2.06	0.18
Dy HCl	51.16	29.50	47.37	50.32	45.67	3.99	4.02	4.24	4.92	44.84	51.33	4.79
Dy Res	5.25	2.49	5.11	4.15	4.87	0.21	0.42	0.34	0.44	2.82	4.13	0.32
Dy	**59.29**	**33.93**	**54.08**	**56.94**	**54.65**	**4.45**	**4.79**	**4.90**	**5.73**	**53.67**	**58.58**	**5.29**
Ho AA	1.69	0.77	0.04	1.24	0.53	0.04	0.08	0.06	0.03	1.50	0.94	0.01
Ho ARA	0.98	0.96	1.38	0.84	2.82	0.18	0.19	0.28	0.29	4.02	1.82	0.14
Ho HCl	46.71	26.74	42.31	43.05	38.70	3.64	3.35	4.53	4.23	39.09	43.87	3.88
Ho Res	4.60	2.23	4.95	3.43	3.90	0.19	0.36	0.38	0.39	2.64	3.56	0.26
Ho	**53.99**	**30.70**	**48.68**	**48.56**	**45.95**	**4.05**	**3.98**	**5.25**	**4.94**	**47.25**	**50.19**	**4.29**
Er AA	1.43	0.76	0.08	1.17	0.53	0.04	0.07	0.05	0.04	1.29	0.74	0.01
Er ARA	0.88	0.92	1.21	0.70	2.86	0.16	0.17	0.24	0.28	3.50	1.48	0.13
Er HCl	42.38	24.48	35.85	39.45	36.21	3.26	2.89	3.88	3.90	36.57	37.24	3.78
Er Res	3.89	2.14	4.31	2.93	3.60	0.18	0.33	0.30	0.37	2.51	2.92	0.24
Er	**48.58**	**28.29**	**41.45**	**44.26**	**43.21**	**3.65**	**3.47**	**4.47**	**4.59**	**43.87**	**42.38**	**4.17**
Tm AA	1.55	0.86	0.10	1.52	0.46	0.04	0.08	0.05	0.04	1.64	0.98	0.01
Tm ARA	1.08	1.17	1.44	0.94	2.55	0.19	0.21	0.23	0.31	4.26	1.85	0.13
Tm HCl	47.74	28.85	44.49	49.34	31.45	3.68	3.38	3.52	4.07	44.95	44.17	3.74
Tm Res	4.69	2.46	5.53	4.05	3.21	0.22	0.40	0.27	0.41	3.02	3.80	0.25
Tm	**55.06**	**33.34**	**51.57**	**55.85**	**37.67**	**4.13**	**4.07**	**4.07**	**4.82**	**53.86**	**50.80**	**4.13**
Yb AA	1.43	0.73	0.09	1.38	0.40	0.04	0.08	0.05	0.04	1.35	0.84	0.01
Yb ARA	0.88	1.06	1.45	0.79	2.28	0.19	0.21	0.23	0.30	3.51	1.47	0.13
Yb HCl	40.61	25.29	41.80	44.24	29.00	3.71	3.15	3.43	3.90	39.35	35.10	3.83
Yb Res	4.22	2.09	5.47	3.81	2.83	0.23	0.36	0.27	0.36	2.49	3.07	0.25
Yb	**47.14**	**29.16**	**48.82**	**50.22**	**34.51**	**4.17**	**3.80**	**3.98**	**4.60**	**46.70**	**40.48**	**4.22**
La AA	1.81	1.03	0.11	1.66	0.48	0.04	0.08	0.06	0.05	1.37	1.01	0.01
La ARA	1.10	1.48	1.67	0.88	2.76	0.21	0.23	0.27	0.33	3.73	1.93	0.15
La HCl	49.29	35.99	48.62	52.39	35.18	3.83	3.26	3.83	4.63	42.03	44.13	4.31
La Res	5.28	3.06	6.84	4.54	3.45	0.23	0.41	0.31	0.40	2.75	4.02	0.30

TABLE B.7 Partition Data: REE

Sample	U29	U30	U34	U35	U40	U51	U54	U6	U77	Average
Sample Location	Huwayl (core)	Huwayl (core)	Huwayl (core)	Huwayl (core)	Huwayl (outcrop)	Huwayl (outcrop)	Huwayl (outcrop)	Dysail Mine (south)	Dysail Mine (south)	
Horizon	As/Ls	As/Ls	As/Ls	As/Ls	As/Ls	As/Ls	As/Ls	As/Ls	As/Ls	
Colour	olive grey	dark grey	dark grey	dusky yellowish brown	greyish brown	dusky red	dusky red	moderate brown	greyish red	
Colour Code	5 Y 4/1	N3	N3	10 YR 2/2	5 YR 3/2	5 R 3/4	5 R 3/4	5 YR 3/4	5 R 4/2	
La AA	3.1	2.7	2.4	1.9	1.5	3.3	0.5	1.4	2.9	2.2
La ARA	6.7	11.1	3.5	8.4	9.8	10.2	13.2	10.5	8.9	6.7
La HCl	109.4	172.8	125.4	118.9	150.4	113.4	159.7	138.4	135.3	113.0
La Res	11.9	12.2	7.5	6.2	18.8	7.1	9.7	14.9	10.3	9.7
La	131.1	198.7	138.7	135.4	180.5	134.1	183.1	165.3	157.3	131.6
Ce AA	2.55	5.78	2.94	1.95	1.30	6.08	0.47	1.74	4.56	3.2
Ce ARA	6.43	26.74	6.77	9.06	11.21	15.63	16.61	19.69	15.03	10.3
Ce HCl	109.36	307.46	236.18	161.27	209.55	176.44	206.93	258.58	214.91	174.0
Ce Res	10.79	30.71	13.84	7.28	24.50	8.90	12.58	25.48	15.83	14.4
Ce	**129.12**	**370.68**	**259.74**	**179.56**	**246.56**	**207.04**	**236.59**	**305.49**	**250.33**	201.9
Pr AA	0.41	0.94	0.46	0.36	0.30	1.50	0.10	0.30	0.71	0.6
Pr ARA	1.00	4.21	1.10	1.79	2.65	3.87	3.88	3.61	2.33	2.1
Pr HCl	16.79	47.79	36.81	30.54	48.49	42.76	48.21	48.39	32.51	35.0
Pr Res	1.58	4.57	2.14	1.47	5.71	2.16	2.76	4.47	2.40	2.9
Pr	**19.78**	**57.51**	**40.50**	**34.15**	**57.14**	**50.28**	**54.95**	**56.78**	**37.95**	40.6
Nd AA	1.77	2.92	1.57	1.06	0.64	3.47	0.25	0.92	2.66	1.7
Nd ARA	4.06	13.55	3.57	4.86	6.21	8.95	9.95	9.39	8.94	5.5
Nd HCl	67.35	150.51	125.72	81.37	108.18	97.79	124.24	129.17	117.00	91.7
Nd Res	6.40	14.24	7.13	3.79	13.31	4.79	7.69	12.30	8.47	7.5
Nd	**79.57**	**181.23**	**137.99**	**91.07**	**128.33**	**114.99**	**142.13**	**151.79**	**137.07**	106.5
Sm AA	1.29	1.91	1.08	0.72	0.51	2.25	0.25	0.67	1.71	1.2
Sm ARA	2.82	8.32	2.31	3.05	4.12	6.01	6.81	6.29	5.42	3.7
Sm HCl	48.76	94.03	80.67	54.74	70.26	62.85	78.46	81.27	73.80	61.4
Sm Res	4.62	8.72	4.73	2.44	8.63	3.16	4.77	8.09	5.60	5.1
Sm	**57.49**	**112.98**	**88.79**	**60.95**	**83.52**	**74.27**	**90.29**	**96.31**	**86.53**	71.4
Eu AA	0.99	1.66	0.88	0.56	0.48	1.56	0.18	0.61	1.43	0.9
Eu ARA	2.08	6.93	1.71	2.39	3.57	4.40	5.31	5.41	4.69	2.9
Eu HCl	37.02	80.84	64.44	39.76	57.47	46.83	59.29	66.72	65.63	46.9
Eu Res	3.66	7.18	3.50	1.87	7.04	2.31	3.54	6.85	4.92	3.9
Eu	**43.75**	**96.61**	**70.53**	**44.57**	**68.57**	**55.10**	**68.33**	**79.59**	**76.66**	54.6
Gd AA	1.04	1.51	0.82	0.71	0.49	1.74	0.17	0.60	1.37	0.9
Gd ARA	2.23	6.12	1.46	3.07	3.88	4.93	5.33	4.67	4.02	2.8
Gd HCl	41.90	75.08	58.68	49.24	58.95	53.14	57.85	60.92	59.31	47.1
Gd Res	4.08	6.41	3.20	2.24	7.15	2.51	3.24	6.42	4.66	3.9
Gd	**49.25**	**89.13**	**64.17**	**55.26**	**70.48**	**62.32**	**66.58**	**72.61**	**69.36**	54.7
Tb AA	0.74	1.04	0.56	0.49	0.40	1.13	0.11	0.43	0.87	0.6
Tb ARA	1.48	4.52	1.00	2.10	2.80	3.07	3.79	3.64	2.66	2.0
Tb HCl	26.87	54.24	39.99	32.99	41.78	35.79	39.97	45.81	40.61	33.1
Tb Res	2.53	4.61	2.17	1.49	5.05	1.73	2.32	4.62	2.97	2.7
Tb	**31.62**	**64.42**	**43.72**	**37.07**	**50.03**	**41.72**	**46.18**	**54.50**	**47.11**	38.4
Dy AA	0.82	1.19	0.74	0.59	0.42	1.10	0.12	0.51	1.00	0.7
Dy ARA	1.71	4.89	1.28	2.22	3.13	3.22	4.27	3.91	3.00	2.2
Dy HCl	30.13	60.74	49.31	34.96	45.64	38.24	49.04	48.23	46.92	36.6
Dy Res	2.83	5.45	2.72	1.58	5.76	1.87	2.89	5.29	3.45	3.0
Dy	**35.48**	**72.28**	**54.05**	**39.36**	**54.95**	**44.43**	**56.32**	**57.94**	**54.38**	42.5
Ho AA	0.75	0.90	0.67	0.51	0.43	1.01	0.10	0.48	0.86	0.6
Ho ARA	1.56	3.88	1.11	2.12	2.78	3.11	3.70	3.31	2.58	1.9
Ho HCl	27.07	50.00	41.21	30.74	41.12	34.53	41.59	40.89	41.44	32.3
Ho Res	2.54	4.24	2.46	1.47	5.00	1.80	2.64	4.96	2.99	2.7
Ho	**31.92**	**59.02**	**45.45**	**34.83**	**49.32**	**40.46**	**48.03**	**49.64**	**47.87**	37.5
Er AA	0.66	0.80	0.66	0.44	0.35	0.88	0.09	0.37	0.82	0.6
Er ARA	1.48	3.65	1.08	1.92	2.34	2.75	3.32	2.65	2.45	1.8
Er HCl	24.16	48.07	38.72	28.17	34.98	31.03	37.99	34.80	38.27	29.1
Er Res	2.37	3.98	2.27	1.38	4.32	1.75	2.38	4.10	2.91	2.4
Er	**28.66**	**56.49**	**42.74**	**31.92**	**41.99**	**36.41**	**43.78**	**41.92**	**44.45**	33.8
Tm AA	0.75	0.88	0.62	0.45	0.46	0.92	0.11	0.42	0.99	0.7
Tm ARA	1.80	3.89	0.97	2.06	2.78	2.80	4.29	3.27	3.01	2.0
Tm HCl	28.22	51.81	35.40	29.29	43.66	32.14	47.77	41.78	46.96	33.8
Tm Res	2.88	3.95	2.09	1.55	5.34	1.80	3.07	4.79	3.62	2.9
Tm	**33.65**	**60.53**	**39.08**	**33.34**	**52.24**	**37.67**	**55.24**	**50.25**	**54.57**	39.3
Yb AA	0.66	0.73	0.59	0.36	0.41	0.85	0.14	0.35	0.91	0.6
Yb ARA	1.44	3.19	0.95	1.74	2.70	2.76	3.74	2.42	2.57	1.8
Yb HCl	22.88	46.66	31.90	25.12	41.27	29.88	43.23	33.65	40.72	29.8
Yb Res	2.51	3.51	2.03	1.25	5.09	1.84	2.57	3.62	3.12	2.5
Yb	**27.48**	**54.08**	**35.48**	**28.48**	**49.46**	**35.33**	**49.67**	**40.04**	**47.32**	34.7
La AA	1.01	0.86	0.76	0.61	0.47	1.07	0.16	0.45	0.92	0.7
La ARA	2.14	3.55	1.13	2.70	3.16	3.29	4.24	3.37	2.86	2.1
La HCl	35.14	55.50	40.27	38.18	48.32	36.44	51.30	44.47	43.45	36.3
La Res	3.81	3.91	2.41	1.99	6.04	2.27	3.11	4.80	3.31	3.1

Table B.8 Factor Analysis Results for REEs

	AL	BA	CA	CE	CO	CR	CS	CU	DY	ER	EU	FE	GD	HF	HO	LA	MG	MN	NB
AL	1.000																		
BA	0.215	1.000																	
CA	0.032	-0.237	1.000																
CE	0.822	0.045	0.002	1.000															
CO	-0.262	0.034	0.274	-0.147	1.000														
CR	0.142	0.847	-0.032	0.051	0.326	1.000													
CS	-0.128	-0.052	0.176	-0.413	0.240	0.014	1.000												
CU	-0.519	-0.050	-0.413	-0.421	0.180	-0.069	0.018	1.000											
DY	0.706	-0.156	0.194	0.859	-0.137	-0.074	-0.382	-0.518	1.000										
ER	0.662	-0.105	0.259	0.785	-0.137	-0.016	-0.409	-0.551	0.951	1.000									
EU	0.709	-0.145	0.177	0.832	-0.114	-0.052	-0.362	-0.446	0.980	0.918	1.000								
FE	-0.282	-0.133	-0.619	-0.100	0.042	-0.207	-0.076	0.725	-0.112	-0.262	-0.049	1.000							
GD	0.756	-0.099	0.157	0.899	-0.117	-0.017	-0.412	-0.485	0.989	0.937	0.978	-0.092	1.000						
HF	0.421	0.297	0.371	0.515	0.072	0.257	-0.213	-0.121	0.244	0.233	0.260	-0.238	0.316	1.000					
HO	0.682	-0.151	0.183	0.825	-0.151	-0.087	-0.380	-0.502	0.993	0.953	0.977	-0.084	0.973	0.203	1.000				
LA	0.718	0.016	0.186	0.903	0.004	0.114	-0.442	-0.503	0.945	0.892	0.925	-0.098	0.966	0.418	0.928	1.000			
MG	0.446	-0.043	-0.427	0.474	-0.540	-0.259	-0.300	-0.290	0.410	0.349	0.417	0.201	0.434	-0.039	0.412	0.409	1.000		
MN	-0.032	0.156	0.536	-0.021	0.821	0.394	0.356	-0.105	-0.046	0.019	-0.076	-0.291	-0.034	0.289	-0.049	0.105	-0.562	1.000	
NB	0.650	0.029	0.258	0.873	-0.182	0.027	-0.437	-0.375	0.813	0.772	0.776	-0.101	0.847	0.655	0.787	0.881	0.372	0.044	1.000
ND	0.736	-0.070	0.222	0.898	-0.005	0.052	-0.344	-0.524	0.958	0.897	0.947	-0.125	0.972	0.392	0.941	0.985	0.398	0.100	0.856
NI	0.222	-0.040	0.020	0.378	0.052	-0.074	0.065	-0.507	0.416	0.288	0.366	0.109	0.390	0.069	0.420	0.480	0.373	0.117	0.371
P	0.315	-0.145	0.015	0.104	-0.133	-0.152	-0.086	-0.064	0.348	0.373	0.439	0.159	0.367	-0.057	0.363	0.278	0.278	-0.233	0.128
PB	0.042	0.555	0.234	0.077	0.489	0.635	-0.172	-0.093	-0.090	-0.012	-0.103	-0.212	-0.029	0.486	-0.092	0.161	-0.209	0.646	0.168
PR	0.728	-0.092	0.200	0.905	0.003	0.024	-0.354	-0.509	0.959	0.889	0.941	-0.104	0.971	0.369	0.941	0.984	0.401	0.096	0.851
RB	0.280	0.697	-0.217	0.065	-0.023	0.424	-0.105	-0.096	-0.262	-0.237	-0.254	-0.179	-0.197	0.413	-0.252	-0.076	0.073	0.143	-0.041
SC	0.757	-0.053	0.265	0.672	-0.009	-0.075	-0.065	-0.524	0.716	0.668	0.729	-0.262	0.738	0.396	0.690	0.686	0.215	0.113	0.590
SI	0.141	0.052	-0.365	0.090	-0.671	-0.117	-0.220	-0.320	0.000	0.094	-0.059	-0.361	-0.018	-0.246	-0.016	-0.119	0.377	-0.618	-0.092
SM	0.699	-0.205	0.188	0.829	-0.090	-0.105	-0.348	-0.480	0.985	0.911	0.971	-0.066	0.974	0.196	0.978	0.931	0.385	-0.035	0.767
SR	0.440	0.120	-0.106	0.556	-0.141	0.080	-0.267	-0.303	0.643	0.687	0.680	-0.101	0.632	0.086	0.656	0.561	0.355	-0.197	0.427
TA	0.059	0.023	0.628	0.148	0.001	0.028	-0.083	-0.066	0.073	0.089	0.070	-0.234	0.108	0.778	0.044	0.194	-0.200	0.258	0.526
TB	0.692	-0.167	0.168	0.847	-0.132	-0.086	-0.375	-0.506	0.994	0.935	0.980	-0.074	0.982	0.217	0.990	0.946	0.451	-0.060	0.800
TH	0.721	0.138	-0.145	0.789	-0.162	0.120	-0.413	-0.462	0.760	0.748	0.703	-0.071	0.776	0.260	0.748	0.789	0.467	-0.038	0.654
TI	0.881	0.096	-0.007	0.925	-0.143	0.048	-0.205	-0.520	0.790	0.733	0.761	-0.202	0.815	0.420	0.766	0.797	0.464	0.032	0.717
TM	0.688	-0.076	0.273	0.832	-0.037	-0.001	-0.379	-0.492	0.955	0.962	0.935	-0.222	0.942	0.343	0.950	0.902	0.288	0.075	0.786
U	0.195	-0.015	-0.334	0.394	-0.128	-0.009	-0.421	0.347	0.366	0.292	0.392	0.536	0.406	0.087	0.369	0.419	0.436	-0.260	0.441
V	-0.195	-0.093	0.240	-0.490	-0.098	-0.205	0.303	0.305	-0.441	-0.436	-0.339	0.068	-0.433	0.131	-0.406	-0.468	-0.204	-0.014	-0.301
Y	0.706	0.013	0.320	0.848	0.006	0.106	-0.443	-0.586	0.933	0.914	0.921	-0.238	0.944	0.461	0.919	0.965	0.352	0.128	0.846
YB	0.687	-0.067	0.217	0.830	-0.130	0.016	-0.427	-0.523	0.957	0.981	0.935	-0.210	0.948	0.290	0.958	0.909	0.374	0.015	0.796
ZN	0.119	0.258	0.506	0.031	0.672	0.468	0.453	-0.119	-0.096	-0.051	-0.124	-0.358	-0.056	0.416	-0.122	0.070	-0.514	0.930	0.096
ZR	0.414	0.323	0.302	0.594	0.143	0.412	-0.534	-0.406	0.398	0.424	0.385	-0.481	0.449	0.701	0.355	0.546	0.013	0.241	0.555

ND	NI	P	PB	PR	RB	SC	SI	SM	SR	TA	TB	TH	TI	TM	U	V	Y	YB	ZN
1.000																			
0.478	1.000																		
0.314	0.082	1.000																	
0.061	0.062	-0.221	1.000																
0.997	0.480	0.278	0.042	1.000															
-0.134	0.021	-0.111	0.574	-0.146	1.000														
0.745	0.384	0.537	-0.030	0.728	0.093	1.000													
-0.109	-0.166	-0.138	-0.413	-0.107	0.054	-0.085	1.000												
0.954	0.402	0.371	-0.139	0.961	-0.285	0.716	-0.063	1.000											
0.586	0.165	0.305	-0.245	0.574	-0.141	0.495	0.328	0.588	1.000										
0.175	0.009	-0.044	0.276	0.152	0.038	0.150	-0.329	0.043	-0.145	1.000									
0.965	0.432	0.357	-0.114	0.967	-0.268	0.700	-0.015	0.991	0.646	0.057	1.000								
0.755	0.343	0.193	0.143	0.762	0.135	0.531	0.138	0.743	0.410	-0.069	0.750	1.000							
0.815	0.434	0.163	0.078	0.817	0.199	0.760	0.136	0.754	0.546	-0.031	0.769	0.745	1.000						
0.906	0.280	0.296	0.032	0.903	-0.190	0.699	-0.007	0.921	0.684	0.114	0.933	0.761	0.785	1.000					
0.382	-0.125	0.085	-0.089	0.405	-0.211	-0.074	-0.146	0.410	0.190	0.050	0.418	0.396	0.144	0.301	1.000				
-0.421	-0.351	0.273	0.032	-0.452	0.211	-0.057	-0.346	-0.410	-0.450	0.308	-0.431	-0.450	-0.418	-0.413	-0.167	1.000			
0.948	0.421	0.314	0.215	0.938	-0.052	0.713	-0.102	0.902	0.569	0.244	0.920	0.776	0.768	0.939	0.289	-0.370	1.000		
0.904	0.299	0.309	0.054	0.897	-0.187	0.646	0.059	0.910	0.667	0.085	0.936	0.794	0.770	0.978	0.325	-0.420	0.940	1.000	
0.077	0.032	-0.257	0.635	0.067	0.244	0.158	-0.537	-0.086	-0.291	0.353	-0.115	-0.023	0.091	0.007	-0.241	0.079	0.079	-0.046	1.000
0.487	0.061	-0.208	0.593	0.475	0.363	0.327	0.055	0.331	0.264	0.356	0.360	0.415	0.508	0.507	-0.013	-0.297	0.626	0.493	0.257

Table B.8 Factor Analysis Results for REEs

Factor pattern Matrix

	Factor 1	Factor 2	Factor 3	Factor 4	Factor 5	Factor 6	Factor 7
GD	0.988	-0.068	-0.078	0.059	-0.012	-0.006	0.038
DY	0.978	-0.111	-0.136	-0.001	-0.045	-0.043	0.027
ND	0.977	0.063	-0.100	0.074	-0.043	0.030	-0.047
LA	0.974	0.096	-0.015	0.147	-0.039	-0.019	-0.063
PR	0.974	0.043	-0.103	0.092	-0.065	0.009	-0.079
TB	0.971	-0.141	-0.147	0.032	-0.056	-0.022	0.010
Y	0.966	0.164	-0.035	0.020	0.035	-0.044	0.028
HO	0.963	-0.134	-0.146	0.010	-0.056	-0.024	0.050
EU	0.958	-0.125	-0.157	0.054	-0.006	0.029	0.126
YB	0.956	-0.026	-0.040	-0.027	-0.026	-0.125	0.128
SM	0.952	-0.131	-0.202	0.040	-0.069	-0.003	0.030
TM	0.952	0.029	-0.100	-0.024	-0.032	-0.117	0.152
ER	0.942	-0.052	-0.096	-0.094	-0.037	-0.133	0.169
CE	0.921	0.034	0.192	0.093	0.039	0.007	-0.163
NB	0.865	0.152	0.018	0.166	0.312	-0.078	-0.197
TI	0.856	0.062	0.219	-0.113	-0.092	0.225	-0.126
TH	0.809	-0.038	0.276	0.097	-0.124	0.070	-0.058
AL	0.782	0.077	0.257	-0.152	0.069	0.365	0.079
SC	0.751	0.133	-0.148	-0.243	0.062	0.433	0.128
SR	0.647	-0.250	0.141	-0.107	-0.179	-0.084	0.356
ZN	-0.018	0.895	-0.186	0.018	-0.190	0.116	-0.046
MN	0.002	0.856	-0.308	0.067	-0.332	0.002	-0.024
PB	0.037	0.811	0.301	0.257	-0.040	-0.016	-0.028
CO	-0.124	0.614	-0.359	0.312	-0.484	-0.057	0.076
HF	0.386	0.609	0.173	0.142	0.554	0.047	-0.104
CR	0.021	0.583	0.485	0.183	-0.308	-0.031	0.330
CA	0.179	0.577	-0.566	-0.374	0.282	-0.204	0.047
MG	0.450	-0.539	0.342	0.036	0.093	0.263	-0.297
ZR	0.522	0.535	0.388	-0.038	0.180	-0.342	-0.006
BA	-0.032	0.428	0.731	0.136	-0.128	0.166	0.243
RB	-0.095	0.429	0.707	-0.013	0.126	0.421	-0.028
SI	0.024	-0.497	0.561	-0.561	0.019	-0.267	0.020
FE	-0.176	-0.456	-0.113	0.787	-0.079	0.242	-0.135
U	0.352	-0.322	0.057	0.740	0.138	-0.136	0.022
CU	-0.559	-0.179	-0.094	0.693	0.120	-0.023	0.189
TA	0.140	0.505	-0.205	0.060	0.712	-0.119	-0.161
V	-0.441	0.119	-0.255	-0.009	0.590	0.460	0.221
P	0.320	-0.278	-0.259	0.009	0.151	0.532	0.488
CS	-0.415	0.190	-0.370	-0.295	-0.297	0.434	-0.070
NI	0.426	0.028	-0.089	-0.070	-0.307	0.320	-0.626

Varimax Rotated Factor Pattern Matrix

	Factor 1	Factor 2	Factor 3	Factor 4	Factor 5	Factor 6	Factor 7
GD	0.990	-0.048	-0.041	0.060	0.033	0.020	0.037
DY	0.986	-0.050	-0.126	0.018	-0.013	0.002	0.034
TB	0.980	-0.056	-0.141	0.001	0.029	0.010	0.058
HO	0.975	-0.053	-0.133	-0.009	0.004	0.028	0.026
EU	0.973	-0.044	-0.107	0.016	0.046	0.118	-0.019
ND	0.972	0.070	-0.004	0.111	0.015	-0.005	0.129
PR	0.970	0.067	-0.023	0.096	0.037	-0.041	0.146
SM	0.968	-0.011	-0.171	-0.009	0.035	0.046	0.052
LA	0.966	0.065	0.074	0.137	0.071	-0.081	0.110
TM	0.965	0.031	-0.033	0.056	-0.087	-0.013	-0.109
YB	0.964	-0.044	-0.016	0.040	-0.073	-0.042	-0.095
ER	0.956	-0.043	-0.076	0.006	-0.131	-0.008	-0.127
Y	0.954	0.071	0.076	0.196	-0.071	-0.029	0.017
CE	0.885	-0.131	0.185	0.175	0.049	-0.137	0.193
TI	0.818	-0.111	0.263	0.016	-0.144	0.022	0.318
NB	0.815	-0.053	0.054	0.488	0.094	-0.111	0.111
TH	0.793	-0.143	0.268	-0.045	0.071	-0.099	0.166
AL	0.741	-0.174	0.356	0.077	-0.176	0.264	0.198
SC	0.731	0.055	0.066	0.093	-0.271	0.456	0.195
SR	0.683	-0.217	0.076	-0.300	-0.087	0.035	-0.243
ZR	0.469	0.076	0.466	0.436	-0.235	-0.378	-0.170
CS	-0.399	0.396	-0.150	-0.235	-0.293	0.344	0.337
MN	0.024	0.921	0.167	0.122	-0.197	-0.083	0.078
CO	-0.056	0.906	0.063	-0.116	0.097	-0.105	-0.035
ZN	-0.024	0.819	0.289	0.237	-0.241	0.000	0.135
SI	-0.011	-0.781	0.088	-0.267	-0.413	-0.273	-0.121
MG	0.401	-0.635	0.058	-0.078	0.208	0.026	0.401
BA	-0.053	0.049	0.908	-0.051	-0.006	-0.039	-0.081
RB	-0.173	-0.089	0.856	0.191	-0.103	0.118	0.236
CR	0.040	0.369	0.767	-0.112	-0.032	-0.147	-0.228
PB	0.008	0.508	0.640	0.328	0.001	-0.205	0.013
TA	0.066	0.171	-0.047	0.906	-0.067	0.033	-0.064
HF	0.302	0.132	0.395	0.790	-0.030	0.023	0.029
FE	-0.131	-0.052	-0.151	-0.186	0.910	0.115	0.187
U	0.380	-0.163	-0.023	0.086	0.777	-0.110	-0.144
CU	-0.506	0.079	-0.058	-0.006	0.729	0.099	-0.279
CA	0.163	0.487	-0.314	0.518	-0.532	0.080	-0.169
P	0.355	-0.111	-0.098	-0.122	0.102	0.778	-0.109
V	-0.470	0.016	-0.056	0.419	0.024	0.691	-0.070
NI	0.385	0.106	-0.073	-0.072	-0.052	-0.106	0.775

	Mean	Std Dev
AL	2.2	0.8
BA	145.1	345.3
CA	7.2	3.4
CE	30.0	13.2
CO	158.2	90.3
CR	89.3	88.8
CS	17.6	74.8
CU	503.7	1118.8
DY	11.5	4.7
ER	8.3	3.2
EU	3.2	1.3
FE	18.1	8.0
GD	9.4	3.9
HF	1.2	1.3
HO	2.3	1.0
LA	62.2	25.0
MG	1.8	1.0
MN	3.3	3.2
NB	5.3	2.9
ND	41.9	15.8
NI	302.8	128.5
P	0.3	0.2
PB	52.2	57.9
PR	13.0	5.1
RB	7.3	15.0
SC	12.5	5.6
SI	20.7	5.0
SM	10.3	4.4
SR	602.4	461.8
TA	0.3	0.8
TB	1.9	0.8
TH	4.2	2.5
TI	0.1	0.1
TM	1.1	0.5
U	1.2	0.5
V	293.8	94.9
Y	54.5	18.9
YB	8.7	3.4
ZN	113.6	79.0
ZR	66.7	29.2

Factor	Eigenvalue		
1	18.517	46.3	46.3
2	5.779	14.4	60.7
3	3.340	8.3	69.1
4	2.647	6.6	75.7
5	2.227	5.6	81.3
6	1.844	4.6	85.9
7	1.381	3.5	89.3
8	0.997	2.5	91.8
9	0.820	2	93.9
10	0.763	1.9	95.8
11	0.404	1	96.8
12	0.342	0.9	97.6
13	0.317	0.8	98.4
14	0.221	0.6	99
15	0.185	0.5	99.5
16	0.100	0.3	99.7
17	0.075	0.2	99.9
18	0.043	0.1	100
19	0	0	100
20	0	0	100
21	0	0	100
22	0	0	100
23	0	0	100
24	0	0	100
25	0	0	100
26	0	0	100
27	0	0	100
28	0	0	100
29	0	0	100
30	0	0	100
31	0	0	100
32	0	0	100
33	0	0	100
34	0	0	100
35	0	0	100
36	0	0	100
37	0	0	100
38	0	0	100
39	0	0	100
40	0	0	100